STEREOSELECTIVE ALLYLIC CYCLIZATIONS AND REARRANGEMENTS

by

Ksenia Sergeyevna Stankevich

A dissertation submitted in partial fulfillment
of the requirements for the degree

of

Doctor of Philosophy

in

Chemistry

MONTANA STATE UNIVERSITY
Bozeman, Montana

December 2022

DEDICATION

To my family, which kept me grounded in these turbulent times.

ACKNOWLEDGEMENTS

I am deeply grateful to my advisor, Dr. Matthew Cook, for sending me on a challenging yet successful scientific journey and providing help, support, and advice throughout. I appreciate the level of independency balanced by the guidance and support I was given by Dr. Cook, which allowed me to pursue my own ideas as well as learn new skills while working on the projects in the lab. These recent years were not easy for multiple reasons and without Dr. Cook's kindness, flexibility, and our shared passion for science and allylic chemistry, this work would not be possible.

I would like to thank my committee members Dr. Thomas Livinghouse, Dr. Michael Mock, Dr. Mary Cloninger, and Dr. Sharon Neufeldt for their support and valuable input and Dr. Mary Cloninger and Dr. Sharon Neufeldt for stepping in as advisors towards the end of my Ph.D. I would also like to acknowledge Dr. Brian Tripet for all the help with NMR.

I am grateful to my family, especially my parents Sergey and Olga, and to my friends Semen, Anastasia, and Valeria, who supported me over these years. I would also like to thank all members of the Cook group, including Aoife, Veronika, and Oliver, and my friends and colleagues from the Chemistry and Biochemistry Department.

I would like to acknowledge the financial support from Montana State University and the National Science Foundation.

TABLE OF CONTENTS

TABLE OF CONTENTS CONTINUED

LIST OF TABLES

Table Page

LIST OF TABLES CONTINUED

Table Page

LIST OF TABLES CONTINUED

Table Page

LIST OF FIGURES

Figure Page

LIST OF FIGURES CONTINUED

Figure Page

LIST OF FIGURES CONTINUED

Figure Page

LIST OF FIGURES CONTINUED

Figure Page

LIST OF SCHEMES

Scheme Page

LIST OF SCHEMES CONTINUED

Scheme Page

LIST OF SCHEMES CONTINUED

Scheme Page

LIST OF SCHEMES CONTINUED

Scheme Page

LIST OF SCHEMES CONTINUED

Scheme Page

LIST OF SCHEMES CONTINUED

Scheme Page

LIST OF SCHEMES CONTINUED

Scheme Page

LIST OF SCHEMES CONTINUED

Scheme Page

LIST OF SCHEMES CONTINUED

Scheme Page

LIST OF SCHEMES CONTINUED

Scheme Page

LIST OF SCHEMES CONTINUED

Scheme Page

LIST OF SCHEMES CONTINUED

Scheme Page

ABSTRACT

Herein, we aim to explore the unique reactivity of allyl groups in two different areas: synthesis of densely functionalized five-membered ring systems and mechanistic studies of Pd-catalyzed formation of complex quaternary nitriles. The first part addresses the paucity of methods available for the formation of highly substituted five-membered rings, which are a common motif in natural compounds and pharmaceuticals. We developed a method that provides access to cyclopentenols and methylene cyclopentenols *via* the union of the Claisen rearrangement and Sakurai allylation. In this instance, the Claisen rearrangement allows for the stereospecific generation of the carbon framework, whereas the intramolecular Sakurai allylation provides a stereoselective cyclization reaction. For 1,2,5-trisubstituted cyclopenten-1-ols this approach has proven to be highly general and stereoselective, furnishing a library of cyclized products in good and very good yields and >20:1 diastereomeric ratio. For 1,2,5-trisubstituted 3-methylene cyclopentan-1-ols, we have developed a stereodivergent method whereby the one-pot stepwise Claisen-Sakurai reaction provided *anti*-, *anti*- product and the cascade Claisen-Sakurai reaction furnished *syn*-, *anti*- product as a major diastereomer with good yield. In both cases reaction mechanism was investigated to uncover the origin of diastereoselectivity using density functional theory. The second part of this research covers investigating the mechanism of a Pd-catalyzed double rearrangement to form quaternary nitriles, which are molecules of synthetic interest. We studied the mechanism of recently developed highly complex auto-tandem catalytic double allylic rearrangement of *N*-alloc-*N*-allyl ynamides to complex quaternary nitriles using density functional theory. This reaction proceeds through two separate and distinct catalytic cycles with both decarboxylative Pd-π-allyl and Pd(0)-promoted aza-Claisen rearrangements occurring. We discovered previously unreported concomitant decarboxylation/C-C bond formation, reversible C-N ionization and a Pd(0) catalyzed [3,3]-rearrangement along with its stepwise variant. These catalytic cycles are characterized by the highly dynamic nature of the catalyst systems with large degrees of conformational flexibility and a flat potential energy surface. Our studies have rationalized the reactivity observed and can be further developed into predictive models for ligand and catalyst screening.

CHAPTER ONE

CLAISEN-SAKURAI APPROACHES TO DENSELY FUNCTIONALIZED FIVE-MEMBERED RING SYSTEMS

Introduction

Densely functionalized five-membered ring systems are prevalent in many natural products and have become increasingly sought after by the pharmaceutical industry (Figure 1).[1,2] These types of compounds are ideal scaffolds for drug discovery due their rigid nature while retaining a high sp^3:sp^2 atom ratio which can provide enhanced pharmacokinetic properties.[3–5] This motif is especially prevalent in virology with compounds with carbocyclic nucleoside analogue reverse transcriptase inhibitors, such as abacavir, licensed to combat HIV and HBV.[6] The neuraminidase inhibitor peramivir also contains a stereochemically dense cyclopentane core.[7] Complex cyclopentanes are found in numerous natural products, including terpenes,[8] polyketides,[9] and alkaloids,[10] such as Palau'amine.[11] Therefore, new stereoselective methods and strategies for cyclopentane syntheses are needed.

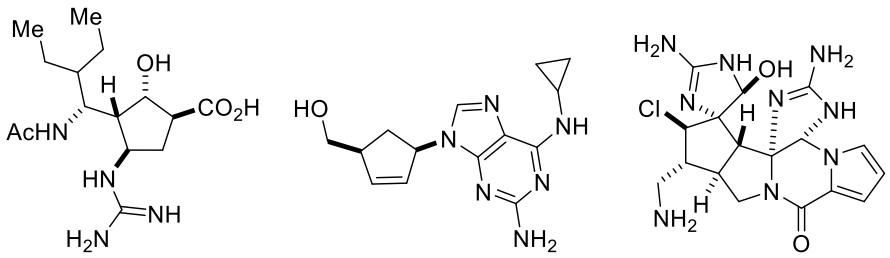

Peramivir ***Abacavir*** ***Palau'amine***

Figure 1. Cyclopentane pharmaceuticals and natural products.

The stereoselective synthesis of five-membered ring systems can be problematic due to their dynamic conformational nature leading to both thermodynamic and kinetic selectivity issues.[12] Indeed, the pioneering prostaglandin research from the 1970's onwards highlighted the inherent challenges producing these systems in a stereodefined manner.[13–15] Currently available methods for the synthesis of cyclopentanes suffer from a lack of flexibility in both the substitution tolerated and stereochemistry of the product possible.[16,17] These methods include ring opening of bicyclic structures,[18–22] multistep conversion of carbohydrates,[23,24] functionalization of cyclopentenones,[25–29] allylic functionalization of cyclopentenes,[30,31] Nazarov cyclizations,[32] [2,3]-dipolar cycloadditions,[33–37] and ring closing metathesis strategies.[38–40]

We envisaged that a method for the synthesis of functionalized cyclopentenols could be developed through the union of the Claisen and Sakurai reactions which would harness the stereoelectronics of these reactions to provide high levels of stereocontrol (Scheme 1). This proposal was further strengthened by preliminary studies conducted in the Cook group.[41] In this instance, the Claisen rearrangement would allow for the stereospecific generation of the carbon framework, whereas the intramolecular Sakurai allylation will provide a stereoselective cyclization reaction. Given that the Claisen rearrangement proceeds *via* a well-defined cyclic

transition state, one can employ substrate control (alkene geometry) to tune the relative stereochemical outcome.[42] Additionally, reagent control can be utilized to modulate the resulting alkene geometry (*Z*-selectivity[43]) as well as relative stereochemistry (*syn*-selectivity[44,45]). Notably, this overall transformation can be conducted in either a stepwise or a cascade fashion since each reaction is known to be promoted by Lewis or Brønsted acids. Depending on the silylated allyl vinyl ether structure, these reactions can provide access to cyclopentenols or methylene cyclopentanols (Scheme 1).

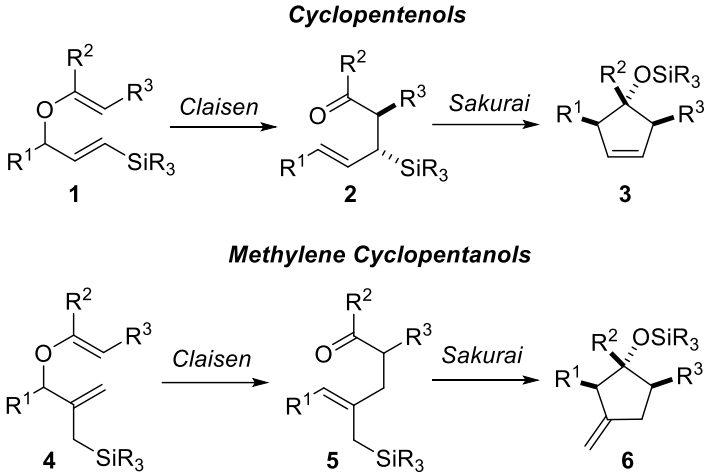

Scheme 1. Claisen-Sakurai approach as a stereoselective route to complex cyclopentanes.

Isolated reports of Claisen and Sakurai reactions being combined in a single synthetic sequence have been previously described. Based on Nakai's pioneering work,[46] Paquette demonstrated that a Sakurai ring-closure could be achieved following a thermal Claisen (Scheme 2, Eq. 1), alongside a single report of a Lewis acid mediated cascade Claisen-Sakurai reaction (Scheme 2, Eq. 2).[47,48] Panek reported the use of an intramolecular Sakurai allylation to form more substituted cyclopentenols with up to three contiguous stereocenters with high levels of stereocontrol.[49] Although effective, this method was generally limited to simple alkyl

substituents and required long synthetic schemes to form the allylsilane aldehyde prior to cyclization (Scheme 2, Eq. 3).

Our approach was to utilize readily synthesized silylated allyl vinyl ethers (**1**) and (**4**),[45,50,51] and perform a Claisen-Sakurai sequence in either a one-pot stepwise or a cascade fashion (Scheme 1). The result is a very modular synthesis of 1,2,5-trisubstituted cyclopent-3-en-1-ols (**3**) and 1,2,5-trisubstituted 3-methylene cyclopentan-1-ols (**6**), which can utilize the stereospecificity of both Claisen and intramolecular Sakurai reactions.

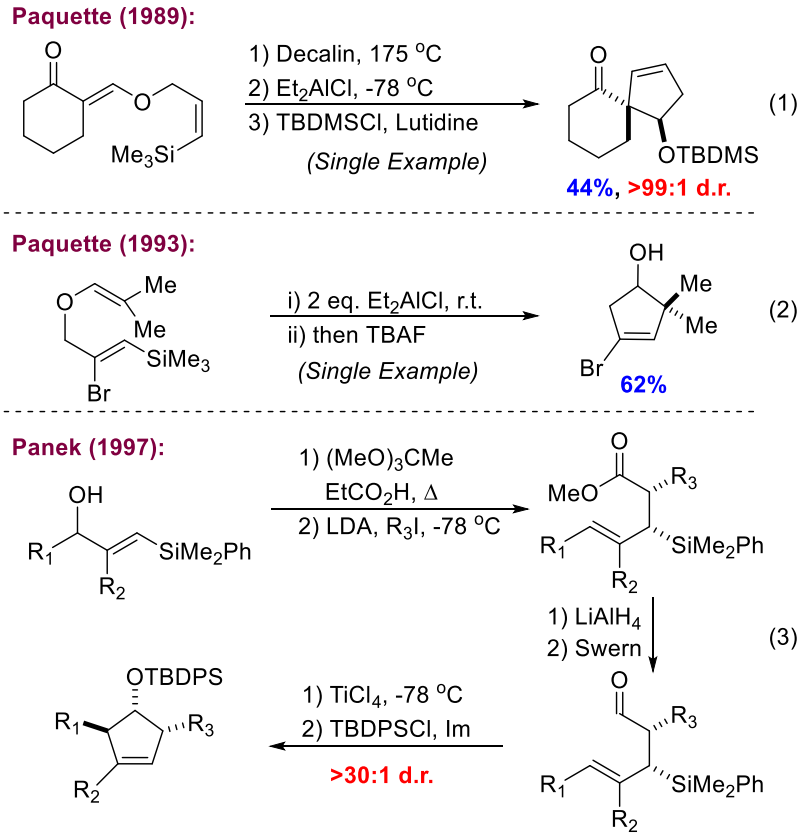

Scheme 2. Previous Claisen-Sakurai approaches.

In this chapter, we describe the realization of the Claisen-Sakurai reaction pathway to produce highly substituted cyclopentenols[52,53] and methylene cyclopentanols. The background

with the focus on aliphatic Claisen rearrangement and Sakurai-carbocyclization will first be covered followed by experimental results in the development of Claisen-Sakurai methodology.

Claisen Rearrangement

The thermal rearrangement of aliphatic allyl vinyl ethers first published in 1912 by Ludwig Claisen[54] (Scheme 3) has become one of the most versatile synthetic methods for the stereoselective formation of C-C bond.[42,55,56] This reaction converts allyl vinyl ethers into the corresponding γ,δ-unsaturated carbonyl compounds by breaking C-O bond and forming C-C bond in a pericyclic process classified as [3,3]-sigmatropic rearrangement (Scheme 3).[42,55,56]

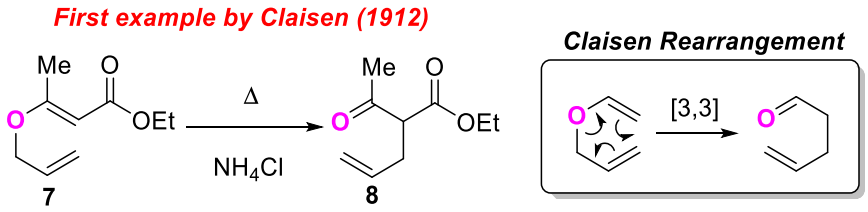

Scheme 3. Claisen rearrangement of aliphatic allyl vinyl ethers.

Considering that Claisen rearrangement is suprafacial, there are two possible transition state (TS) structures, that are often described as chair and boat conformations (Scheme 4).[42] Both theoretical and experimental mechanistic studies showed that in thermal aliphatic Claisen rearrangement chair transition state is favored over competing boat variant due to steric considerations.[57–61]

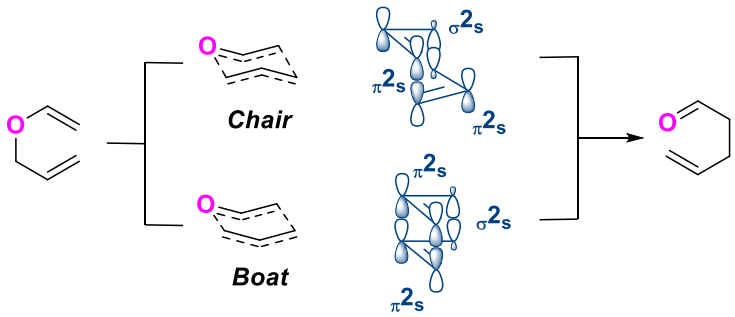

Scheme 4. Possible transition states in aliphatic Claisen rearrangement.

There are several variations in the transition state of the Claisen rearrangement depending on the electronic environment of the substrate. These include aromatic (synchronous), diradical or ion-pair forms (Scheme 5).[42,55] The type of transition state is important for reaction optimization and catalysis applications.[55] Further details on the reaction mechanism and catalysis can be found in comprehensive reviews by Castro[42] and Hiersemann[55,56].

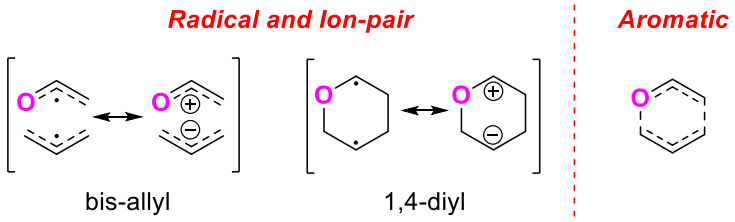

Scheme 5. Nature of transition state in aliphatic Claisen rearrangement.

Herein, we will focus on the examples demonstrating how one can utilize substrate and reagent control to tailor the relative stereochemistry of the Claisen rearrangement of allyl vinyl ethers.

Substrate Control While converting allyl vinyl ethers into γ,δ-unsaturated carbonyl compounds, the Claisen rearrangement produces up to two new stereogenic centers as well as defines the geometry of the alkene.[56] Both outcomes could potentially be tailored *via* the

substrate design. Since Claisen rearrangement proceeds *via* a well-defined cyclic transition state,[42] the relative stereochemistry between novel stereogenic centers (X and Y in Scheme 6) can be controlled by the double bond configuration of the allyl vinyl ether. In this case, *(E,E)*- and *(Z,Z)*- allyl vinyl ethers would provide *syn* configuration, whereas *(Z,E)*- and *(E,Z)* – *anti* variant (Scheme 6). For chiral secondary allyl vinyl ethers this concept could be further extended to self immolative 1,n-chirality transfer.[55]

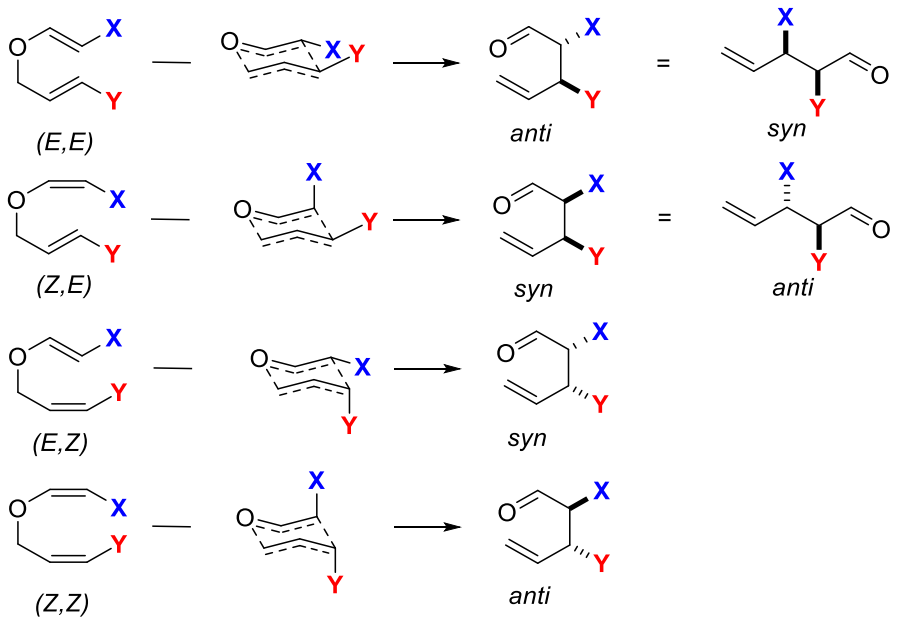

Scheme 6. Reagent control of diastereochemical outcome in Claisen rearrangement.

This approach relies on the established preference of Claisen rearrangement to occur *via* a concerted chair transition state,[57–61] which sometimes is not the case. For example, in recently reported total synthesis of diterpenoid (+)-mutilin the thermal Claisen rearrangement utilized to furnish the 6,9-bicycle (**10**) from (**9**) was believed to proceed *via* a boat transition state due to the transannular nature of the rearrangement (Scheme 7).[62]

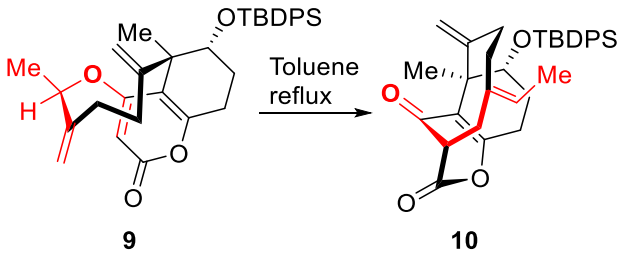

Scheme 7. Claisen rearrangement in the synthesis of diterpenoid (+)-mutilin.

The geometry of the alkene produced in the Claisen rearrangement arises from the stereospecific cyclic transition state, which in most cases has a chair configuration.[42] The thermal Claisen rearrangement of secondary allyl vinyl ethers (**11**) almost exclusively results in *(E)*-olefinic aldehyde (**13**) with *(Z)*-isomer (**12**) only being obtained when special constraints are present. This selectivity originates from the two competing chair transition states where the R group is either in an axial or equatorial position with the latter being more favorable (Scheme 8).[42]

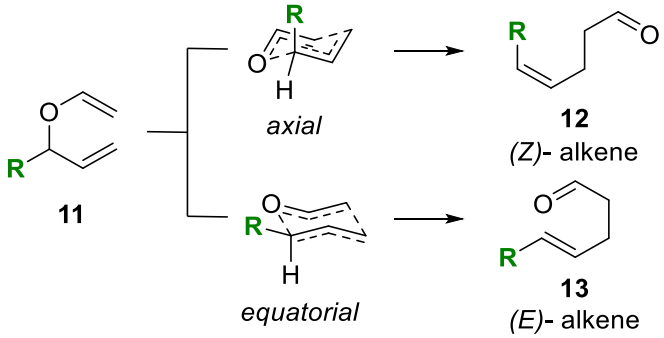

Scheme 8. *(E)*/*(Z)* selectivity of the Claisen rearrangement.

Reagent Control It is possible to use reagent control to dictate both the relative and absolute stereochemistry, alongside the alkene geometry. In many cases these are complementary and can be used on a single substrate to provide stereodivergence in one step.

Chiral transition metal catalysis can provide a great tool for reagent control over both relative and absolute configuration between stereogenic centers in Claisen rearrangement. Nelson *et al*. reported Ru-catalyzed Claisen rearrangement furnishing *anti*- products (**15**) from *(E,E)*- allyl vinyl ethers (**14**) with high enantioselectivity.[63] Both diastereoselectivity and regioselectivity depended on the R^1 and R^2 substituents with alkyl variant (R^1=Me, R^2=Cy) providing exclusively [1,3] product (Scheme 9).[63]

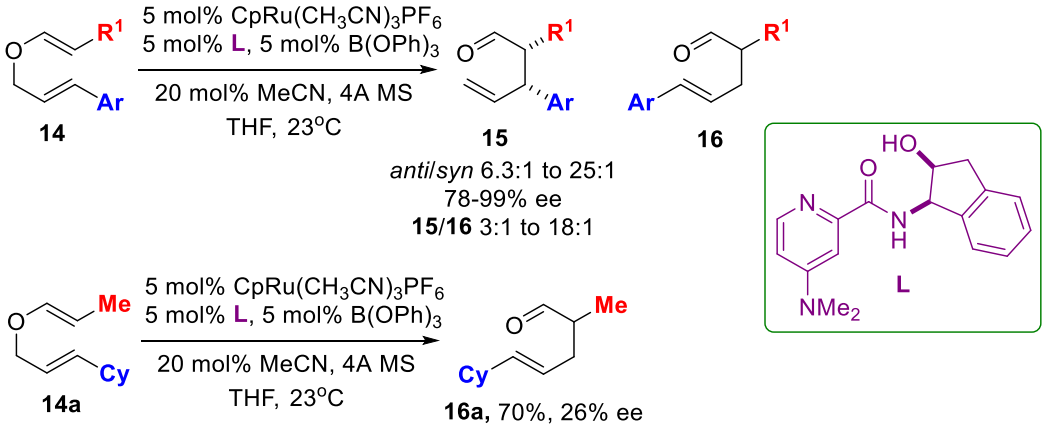

Scheme 9. Ru-catalyzed Claisen rearrangement of (*E*,*E*)-allyl vinyl ethers.

When *(Z,E)*- and *(E,Z)*- allyl vinyl ethers were subjected to the reaction conditions, *syn*-products were formed with moderate d.r. (Scheme 10).When the *(Z)*- vinyl ether (**17**) was used, an isomerization to the more thermodynamically favored *(E)*- enolate occurred providing the *syn*-product. Likewise, the *(Z)*-allyl ether (**20**) also isomerized, *via* a π-σ-π mechanism to provide the same isomer. In both these cases the d.r. was reduced suggesting partial isomerization, and the competing 1,3-rearrangement became a more significant byproduct.[63]

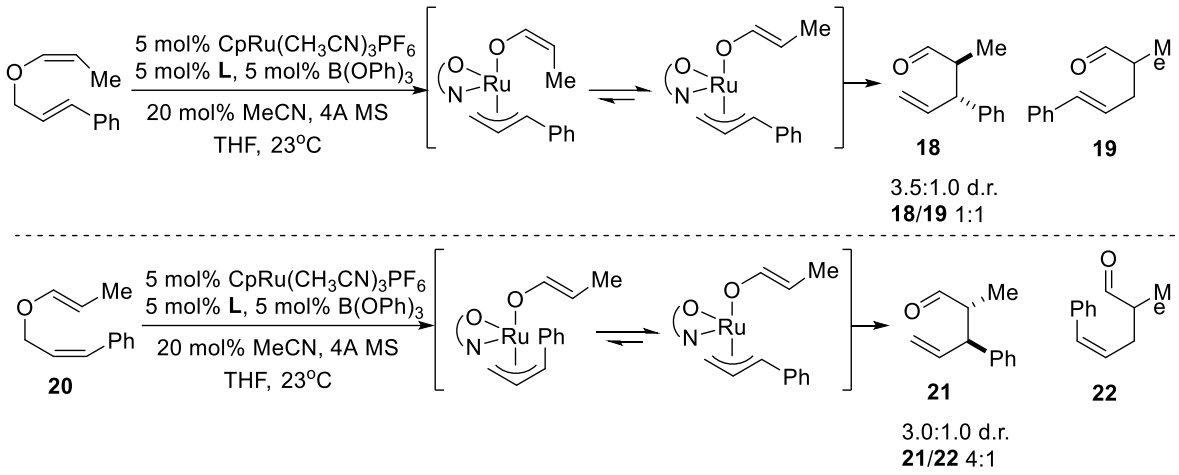

Scheme 10. Ru-catalyzed Claisen rearrangement of *(Z,E)*- and *(Z,E)*-allyl vinyl ethers.

The geometry of the alkene product in the Claisen can be tailored using Al Lewis acids. Yamamoto *et al.* utilized bulky organoaluminum reagents to achieve high levels of control over *(E)*/*(Z)*- diastereoselectivity of Claisen rearrangement of secondary allyl vinyl ethers (**11**) (Scheme 11).[43] They showed that reagent A provides *(Z)*- isomer (**12**), while reagent B produces *(E)*- isomer (**13**) with very good to excellent d.r. (Scheme 11). Upon examination of other Lewis acids structurally similar to reagent A, authors concluded that to achieve (*Z*)-selectivity in this reaction, it is nessesary for phenoxy ligands to bear sterically hindered *tert*-butyl group. In contrast, the origin of *(E)*-selectivity with reagent B was unclear and was attributed to both electronics and sterics of organoaluminum reagent.[43]

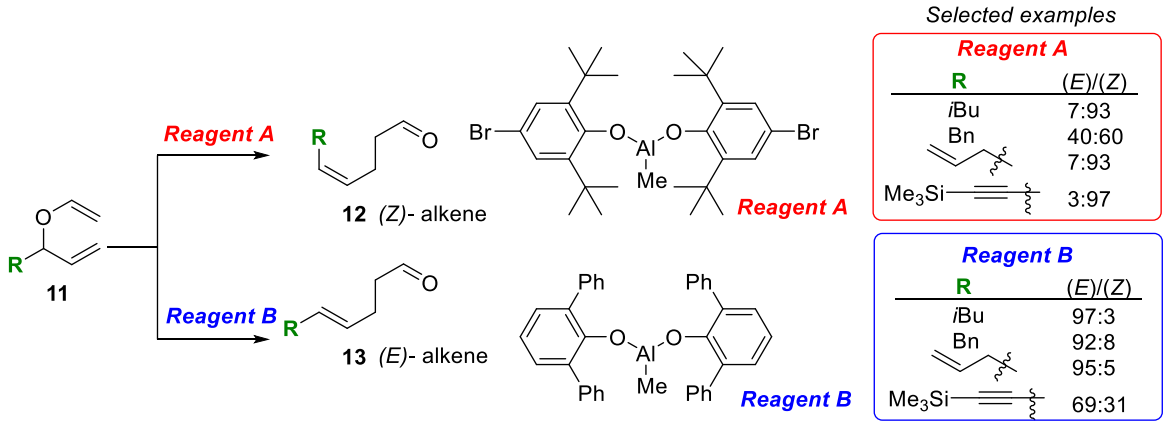

Scheme 11. Organoaluminum-catalyzed Claisen rearrangement.

Tandem Isomerization-Claisen Rearrangements Chemo- and stereo- selective isomerization of di(allyl) ethers followed by Claisen rearrangement is another strategy that allows to achieve high stereoselectivity in Claisen rearrangement. This approach provides control over the substrate generated for Claisen rearrangement and allows to avoid potential limitations associated with the stability of aliphatic allyl vinyl ethers.

Nelson *et al.* developed Ir(I)-catalyzed alkene isomerization-Claisen rearrangement protocol that transforms di(allyl) ethers (**23**) into *syn*- products (**25**) with high yield and diastereoselectivity (Scheme 12).[44] In this reaction, Ir performs isomerization at the less substituted allyl group in (**23**), selectively furnishing *(E,E)*-allyl vinyl ethers (**24**) that then undergo thermal Claisen rearrangement.[44]

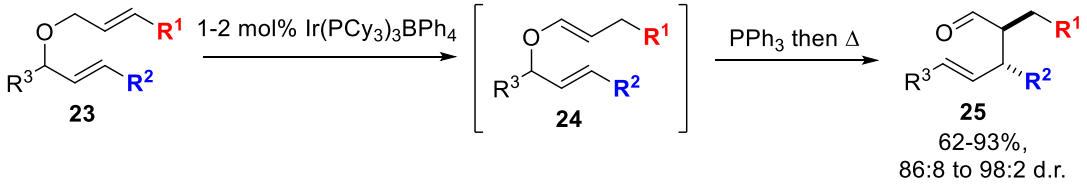

Scheme 12. Ir(I)-catalyzed tandem isomerization-Claisen rearrangement of di(allyl) ethers.

They further expanded this methodology to access α,α-disubstituted pentenals (**28**) with high diastereoselectivity (Scheme 13).[64] The mechanism of this reaction involves the formation of Ir π-allyl complex that undergoes hapticity change to less strained η^1-isomer which upon reductive elimination provides either (*Z*)- or (*E*)-vinyl ethers with high selectivity (Scheme 13).[64]

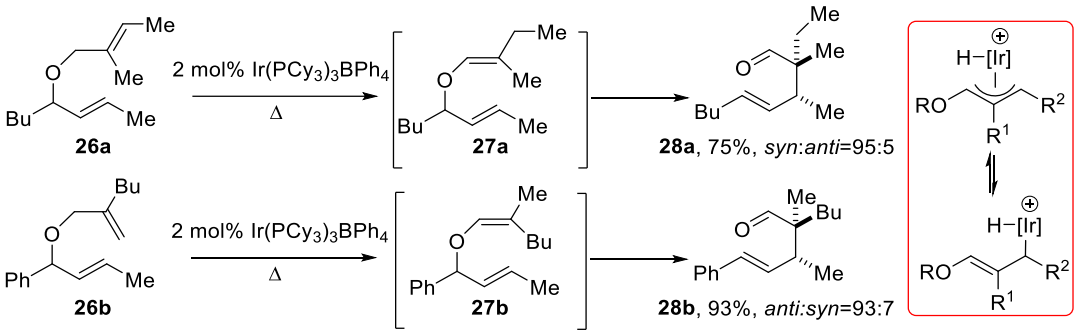

Scheme 13. Ir(I)-catalyzed tandem isomerization-Claisen rearrangement providing α,α-disubstituted pentenals.

Cook *et al*. utilized similar strategy to furnish allylsilanes (**30**) in high yield and diastereoselectivity with *syn*-isomer being the major product (Scheme 14).[45] It was shown that this reaction tolerates allyl vinyl ethers derived from both secondary and tertiary alcohols with alkyl and aryl substituents at the allylic position. Additionally, authors demonstrated that when (E)/(Z) mixtures of allyl crotyl ethers (**29-1**) were subjected to reaction conditions, products (**30-1**) were still isolated with high d.r. (Scheme 14).[45]

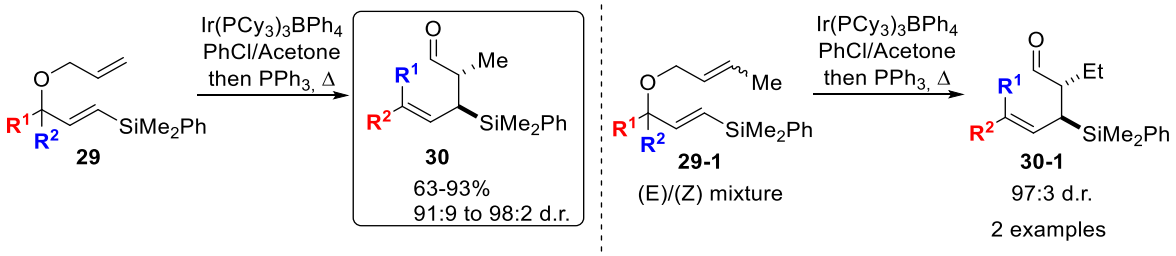

Scheme 14. Ir(I)-catalyzed tandem isomerization-Claisen rearrangement of monosilylated di(allyl) ethers.

When asymmetrical tertiary substrates were used, in some cases authors were able to control *(E)*/*(Z)*- ratio of the product by changing the temperature during Claisen rearrangement. For example, under optimized conditions phenyl methyl substrate (**29a**) provided 55:45 mixture of *(E)*/*(Z)*- isomers, while at lower temperature this ratio was improved to 80:20 (Scheme 15).[45] The observed effect was rationalized by a larger A value of the phenyl group comparing to methyl, which results in the preference towards transition state conformer with phenyl group in equatorial position (Scheme 15, **A**) and explains selectivity increase at lower temperature.[45]

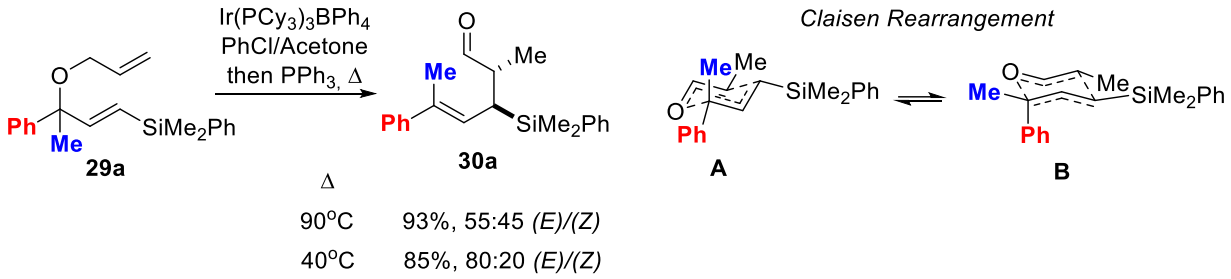

Scheme 15. Ir(I)-catalyzed tandem isomerization-Claisen rearrangement of asymmetrical tertiary allyl vinyl ether.

Overall, high levels of stereochemical control can be achieved in Claisen rearrangement of aliphatic allyl vinyl through both substrate design and metal catalysis providing access to a variety of stereochemical outcomes.

Sakurai-Carbocyclization

The formation of carbon-carbon bonds *via* the Lewis acid mediated addition of allylsilanes to aldehydes has become a highly useful tool for synthetic organic chemists. The first examples of this transformation utilized activated α-halo carbonyl compounds with reactions occuring under both Lewis-acidic[65–67] and uncatalyzed thermal conditions.[67] The following report by Hosomi and Sakurai provided more general and efficient synthetic route involving

$TiCl_4$-promoted addition of allylsilane (**32**) to unactivated aldehydes and ketones (**31**) that has been later named Hosomi-Sakurai allylation (Scheme 16).[68]

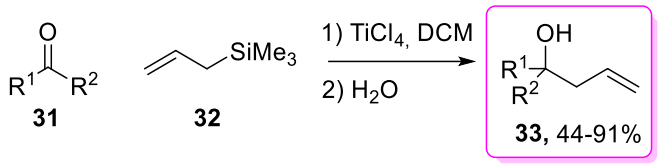

Scheme 16. Hosomi-Sakurai allylation.

The basis of allylsilane reactivity is the β-silicon effect, whereby, hyperconjugation of the C-Si σ-bond into the C-C π*-orbital increases the nucleophilicity of the alkene.[69–73] As a result, allylsilanes can react with activated electrophiles through an open transition state to form a new C-C bond. This same effect stabilizes the intermediate β-carbocation formed in a stepwise mechanism. In this reaction, activation of either the silane, as an "ate" complex, or the electrophile with a protic or Lewis acid, lowers the HOMO-LUMO gap allowing carbon-carbon bond formations to occur.[74] Following original Hosomi-Sakurai report, additional reactions appeared where this approach was used to add allylsilanes to enones,[75–77] nitroalkenes,[78] acid chlorides,[77,79] acetals,[80] epoxides,[79] imines,[81] and ketoimines.[82] This area has been extensively reviewed in the past,[83–91] however herein we will the focus on the recent use of Sakurai-type transformations in carbocyclization reactions.

Carbonyl Addition Cyclizations The first example of an intramolecular Sakurai reaction was reported in 1978 by Andersen (Scheme 17).[92] The study examined the use of a Hosomi-Sakurai approach to the synthesis of 5,6-fused ring systems, a motif commonly found in terpenoid natural products, through the cyclization of allylsilane (**34**).[92,93] In their studies, some interesting trends in the stereochemical outcome were found. When $SnCl_4$ was used as the Lewis

acidic mediator, very little stereocontrol was observed with the silyl ether (**34a**) being obtained. When the Lewis acid was changed to $BF_3 \cdot OEt_2$, good diastereoselectivity was obtained, providing the free alcohol (**34b**) with the axial R-isomer (anti to C-7 Me group) predominating. Interestingly, when fluoride mediated conditions were used, the reaction proceeded *via* an antiperiplanar transition state to afford the equatorial S-isomer (**34c**) (*syn*- to C-7 Me group). The complementary selectivity for these two conditions is an impressive example of reagent controlled stereoselectivity and represent the opposite "pull" and "push" mechanisms for the Hosomi-Sakurai allylation. The Lewis acidic "pull" mechanism provides the *syn*- clinal (R)-stereoisomer, whereas the fluoride mediated "push" mechanism affords the *anti*- periplanar (S)-product.[92,93]

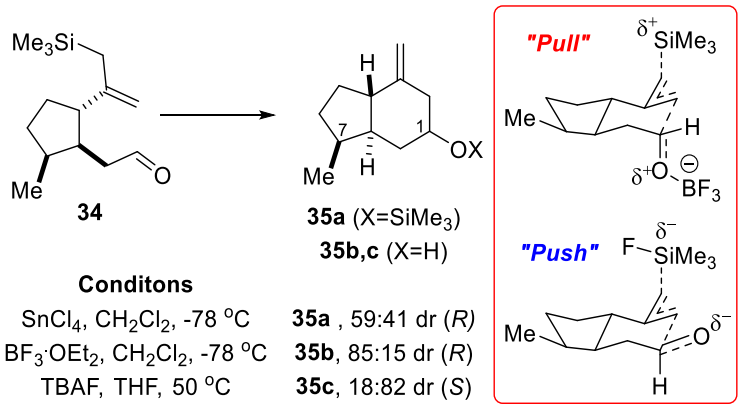

Scheme 17. First examples of the Sakurai-cyclization.

A year later Oshima provided another example of intramolecular Sakurai reaction (Scheme 18).[94] This report utilized an aldehyde with a pendant sulfide-containing allylsilane (**36**) which following cyclization furnished (**37**). This highly stereospecific reaction provides the *syn*-diastereomer (***syn*-37**) from *(E)*- allylsilane (***E*-36**), whereas the *anti*-product (***anti*-37**) yields

from (***Z*-36**). The stereochemical outcome of these reactions was confirmed by converting them to known products with well-established configurations.[94]

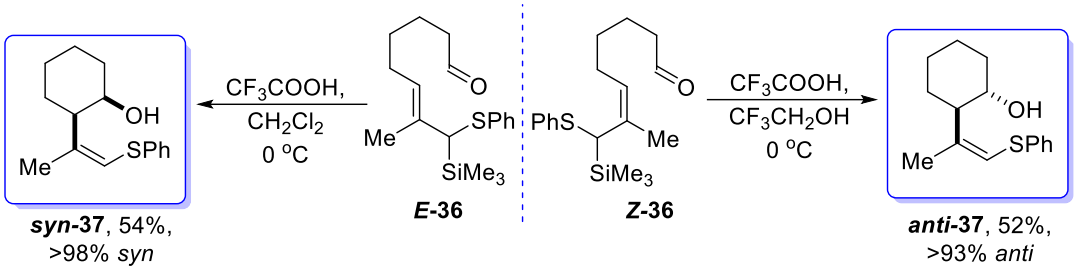

Scheme 18. Sakurai stereospecificity.

The formation of bridged bicyclic systems could be achieved using a Sakurai-cyclization. Trost reported the cyclization of allyl silanes (**38**) to form [2.2.1] (**39a**) and [3.2.1]-systems (**39b**) in excellent yields (Scheme 19).[95] The starting allylsilanes (**38**) are readily synthesized from the corresponding enone through a copper catalyzed conjugate addition of the corresponding allylsilane Grignard reagent which provides a facile two-step approach to the bicyclic frameworks (**39**).[95]

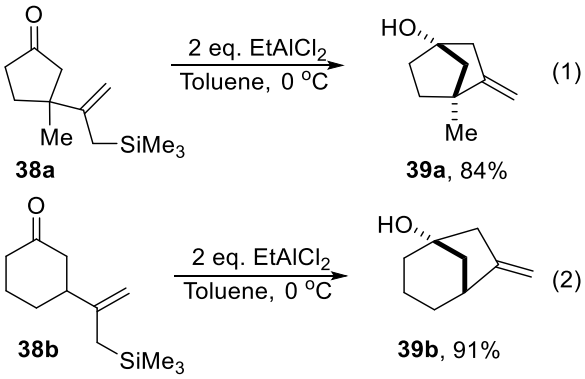

Scheme 19. Formation of [2.2.1] and [3.2.1]-bicycles using Sakurai-cyclization.

This strategy was applied by Baran in the total synthesis of (-)-maoecrystal V. They utilized an intramolecular Sakurai reaction of (**40**) to form [3.2.1] bicycle (**41**) – a key

intermediate in their synthesis with the Sakurai cyclization performed on a 20-gram scale (Scheme 20).[96]

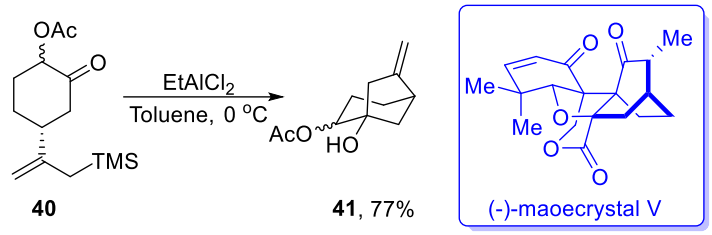

40 **41**, 77%

Scheme 20. Application of Sakurai cyclization in the total synthesis of (-)-maoecrystal V.

Denmark designed mechanistic probes to investigate the formation of [2.2.2]-bicycles through a Sakurai cyclization. To achieve this, they utilized stereochemically pure deuterated allylsilane (**42**) (Scheme 21),[97,98] analogous to their previous findings with the non-deuterated variant.[99,100] They analyzed the product distribution of this cyclization with synclinal (proximal) and antiperiplanar (distal) diastereoisomers, alongside their *(E)*- and *(Z)*- alkene isomers possible. Their hypothesis was to use the defined stereochemistry at the allylic position to identify whether nucleofuge was reacting through an *anti*- or *syn*- S_E' reaction, or whether the C-Si bond was freely rotating and independent of the C-C bond being formed. They discovered the preference for the synclinal (**43a**) over the antiperiplanar (**43b**) diastereomer with both Lewis and Brønsted acids. In almost all cases, the *(Z)*- isomer was formed as a single product, which provides good evidence for *anti*- S_E' reactivity under acidic activation. When fluoride activation of the allylsilane was used, the distal product (**43b**) was the major product with mixtures of *(E)*/*(Z)*- isomers suggesting C-C bond formation is independent from C-Si cleavage. Control experiments with the opposite diastereomer provided almost identical results observed with the *(E)*- isomer predominating in this series.[97,98]

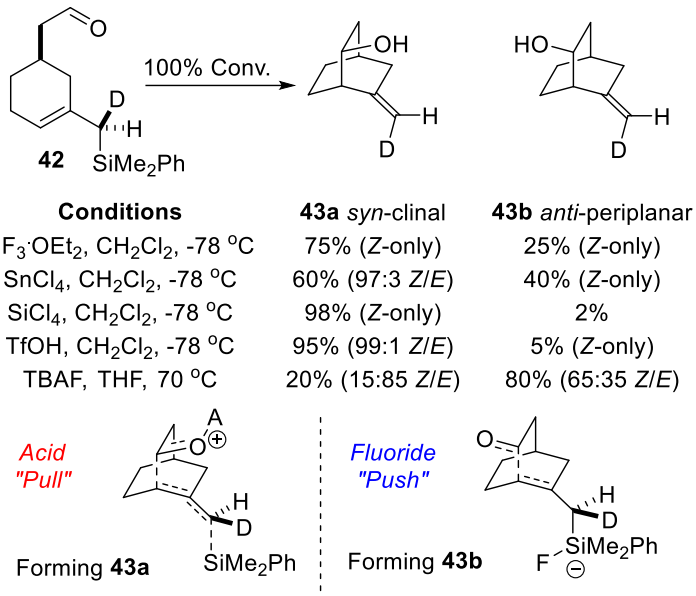

Scheme 21. Denmark's mechanistic studies of the formation of [2.2.2]-bicycles through a Sakurai cyclization.

Panek employed the Sakurai reaction to form stereochemically dense cyclopentenols and cyclohexenols that contain up to three contiguous stereogenic centers (Scheme 22).[49] In this report, the aldehyde precursor was generated *via* a Johnson-Claisen rearrangement of a silylated allylic alcohol, followed by a diastereoselective α-alkylation and modulation of the ester oxidation state to the requisite aldehyde (**44**) and (**46**)[101–105] The one carbon homolog was formed through a Wittig/hydrolysis sequence using a methoxy substituted phosphorane. These aldehydes underwent a cyclization reaction to form the corresponding 5 and 6-membered carbocycles (**45**) and (**47**) exclusively as the *anti*, *syn*-distereoisomer. In these examples, it was necessary to protect the corresponding as a silyl ether for isolation purposes.[49]

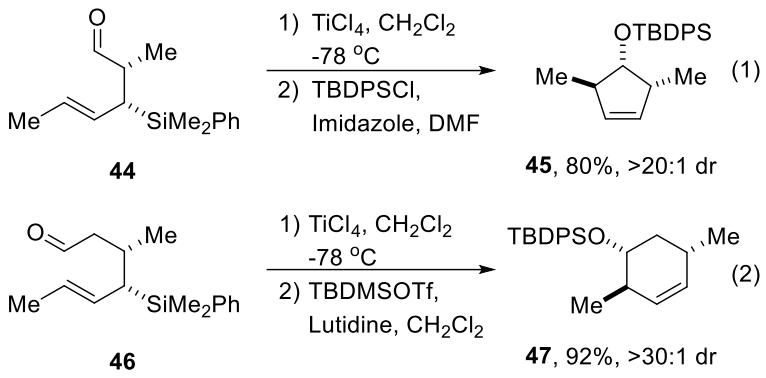

Scheme 22. Stereoselectivity and stereospecificity in Sakurai-cyclization.

More recently, the Panek group have described a cyclization of a γ,γ-disubstituted allylsilanes (**48**) which provide an exocyclic alkene and generate an all-carbon quaternary stereocenter in both five-membered and six-membered systems (Scheme 23).[106] This cyclization is highly stereoselective providing the *anti*-product (**49**). In addition, the stereogenicity of the allylsilane determines the stereochemical outcome on the ring formed. Substitution on the ring is tolerated and does not change the stereochemical outcome of the cyclization. For example, an ethyl group adjacent to the allylsilane does not change the diastereoselectivity of the cyclization reaction and provides the corresponding trisubstituted cyclopentanol as a single distereoisomer in slightly reduced yield compared to the parent compound. When a 1:1 mixture of diastereoisomers is present on the ring, there is no kinetic resolution, and both cyclize at similar rates providing a 1:1 mix of stereoisomers in the product.[106]

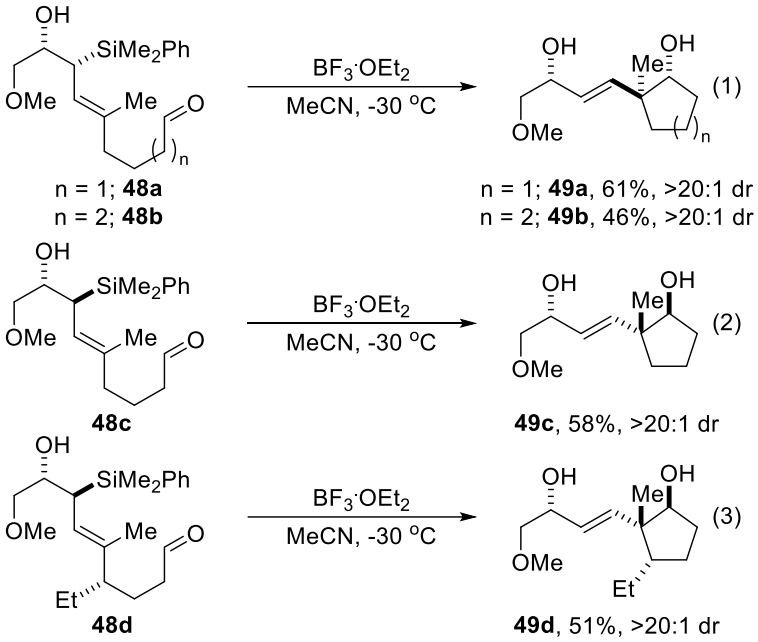

Scheme 23. Exocyclic allylsilane cyclization.

Claisen-Sakurai Sequences The Sakurai cyclization can be used in conjunction with the Claisen rearrangement to provide a powerful approach to the synthesis of cyclopentanes. Kuwajima first reported a sequential Claisen-Sakurai sequence, where a γ-silylated allylic alcohol could undergo an acid catalyzed condensation with concomitant Claisen rearrangement to form allylsilane substituted aldehyde (**53**). This could then be cyclized under Lewis acidic conditions to form the corresponding cyclopentene in good yield (Scheme 24).[107]

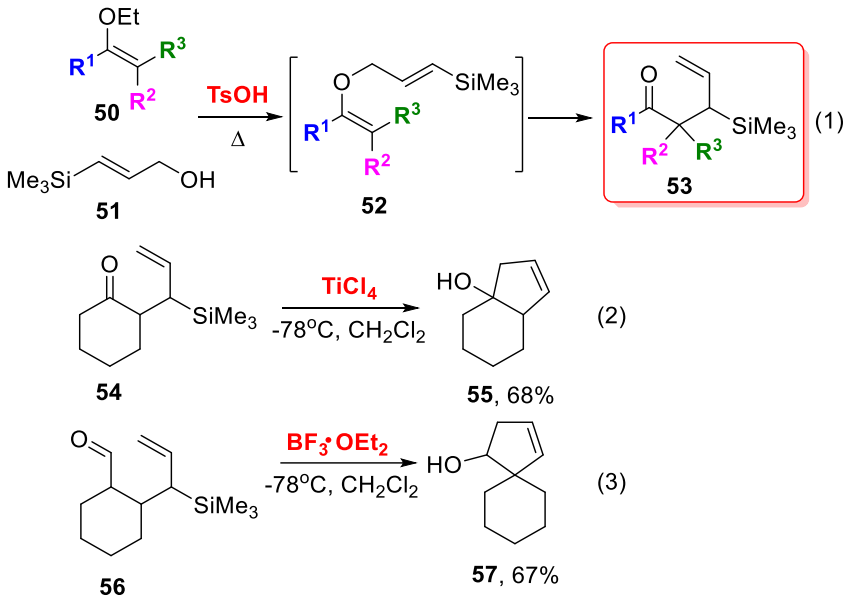

Scheme 24. Sequential Claisen-Sakurai reactions.

Paquette later utilized a similar Claisen-Sakurai approach, with allyl vinyl ether (**58**), during their efforts towards the kaurene natural products (Scheme 25, Eq. 1).[48,108] The only example of a cascade Claisen-Sakurai reaction was published by Paquette.[47] In this report, an isolated example of a silylated allyl vinyl (**60**) which can undergo both reactions under a unified set of conditions was disclosed (Scheme 25, Eq. 2). The Et_2AlCl Lewis acid was efficient for the Claisen, without ionization, and strong enough to activate the ensuing aldehyde to cyclize. The product of the reaction contains only one stereocenter and is racemic, therefore, no insight into any stereoselectivity could be gained.[47]

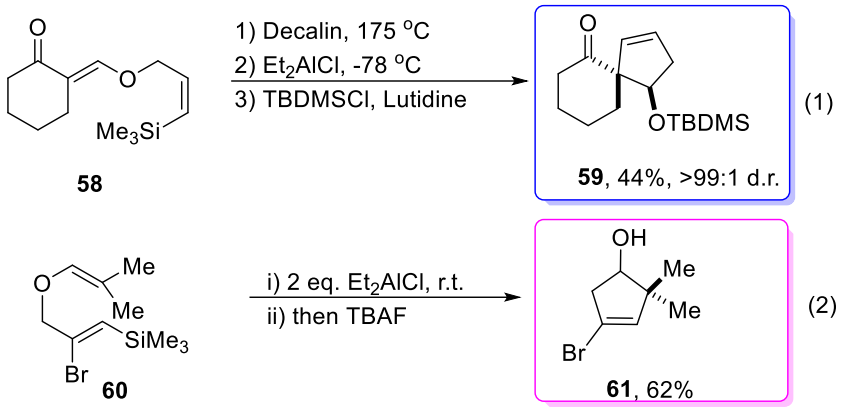

Scheme 25. One-pot and cascade Claisen-Sakurai cyclizations.

In Situ Carbocation Cyclizations Allylsilanes can also react with other activated electrophilic sites, including *in situ* generated carbocation intermediates. Nakada employed this approach to perform a spirocyclization in total synthesis of (+)-ophiobolin A.[109] This strategy utilized allylsilane hemiacetal (**62**) to form the spirocyclic tetrahydrofuran (**63**) which can provide four possible diastereomers (Scheme 26). Their ratio was found to be dependent on both Lewis acid and solvent utilized. Thus, when (**62**) was treated with $BF_3{\cdot}OEt_2$ in CH_2Cl_2, the desired diastereomer (**63a**) was obtained in 45% yield alongside the other two stereoisomers, while the use of $TiCl(OiPr)_3$ resulted exclusively in the formation of unanticipated diastereomer (**63d**) in 84% yield. In the latter case, the epimerization at C15 was proposed to occur *via* reversible deprotonation by ($iPrO^-$) prior to cyclization. When $BF_3{\cdot}OEt_2$ in ether/toluene (1:1) mixture was used for cyclization, the target product (**63a**) was obtained in 68% yield. While authors were able to provide transition state models to explain preference towards (**63a**) between (**63a-c**), the observed solvent effect was harder to rationalize.[109]

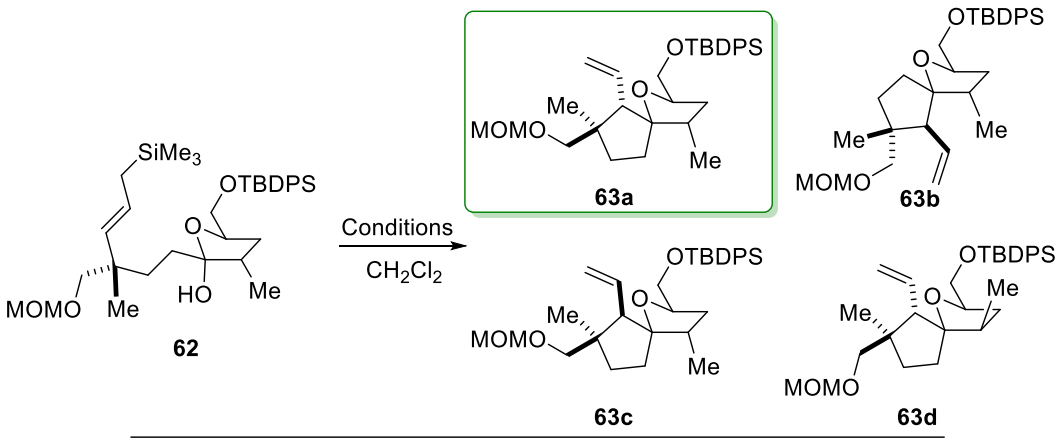

Conditions	63a	63b	63c	63d
$BF_3{\cdot}OEt_2$, CH_2Cl_2, -78 °C	45%	25%	27%	0%
$EtAlCl_2$, CH_2Cl_2, -78 °C	20%	40%	40%	0%
$TiCl(O\textit{i}Pr)_3$, CH_2Cl_2, -78 °C	0%	0%	0%	**84%**
$BF_3{\cdot}OEt_2$, Et_2O/PhMe (1:1), -60 °C	**68%**	17%	trace	0%

Scheme 26. Oxocarbenium ion spirocyclizations.

A Nazarov/Hosomi−Sakurai cascade proved to be a pivotal step in the total synthesis of (-)-oridonin reported by Luo.[110] The premise of this approach was to intercept intermediate oxyallyl cation with a pendant allylsilane (Scheme 27). When a 1:1 mixture of diastereomeric ketones (**64**) (C16) was treated with $EtAlCl_2$, a highly efficient kinetic resolution was observed with only one diastereomer (shown) converting to the desired product (**65**). As (**64**) can be prepared as a single enantiomer, this crucial finding laid foundation for the synthesis of (**65**) with control of absolute stereochemistry. Importantly, this cascade allows stereoselectively form three contiguous stereocenters in a single step, which could be performed on a 2 g scale.[110]

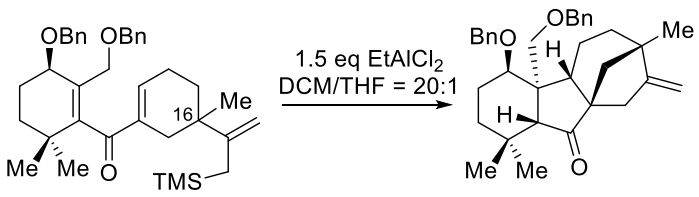

Scheme 27. Sakurai terminated Nazarov cyclizations.

Reisman utilized their method the stereoselective formation of chiral allylsilanes (**66**) and (**68**) to perform a ring closure with an *in situ* generated carbocation (Scheme 28).[111] Interestingly, the stereochemistry of the major diastereomer in each case differs with the formation of 5-membred ring (**67**) proceeding *via* antiperiplanar *anti*- S_E' transition state, whereas the formation of 6-membred ring (**69**) occurs *via* synclinal *anti*- S_E' pathway.[111]

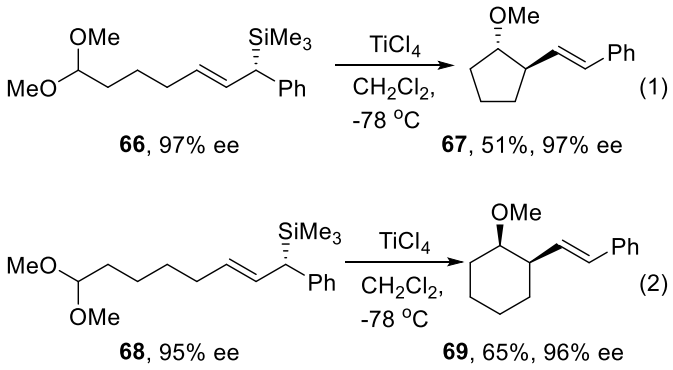

Scheme 28. Allyl silane stereospecificity.

Enone Conjugate Addition Cyclizations The formation of bicyclic systems using the enone Hosomi-Sakurai reaction was developed in the early 1980's and has been utilized in numerous total syntheses. Majetich developed a number of methods to form terpene and steroid-like structures using this method. These included reactions which could form three contiguous all-carbon stereocenters in a single step with good stereocontrol.[112] They also found a divergence in product selectivity between the Lewis acid activation of an aldehyde and the fluoride activation of the silane (Scheme 29).[113] In this case, they were investigating the 1,6-addition in to vinyligous enones which provided a rapid entry in to the natural product nootkanone (**71**). They found that a "softer" Lewis acid such as Et_2AlCl, provided much higher yields for (**71**), by limiting protodesilyation products. When fluoride activation was used, an eight-membered product (**72**) was formed which corresponds to a S_E2 reaction instead of the normal S_E2' route.

More recently, the Lewis acid has been found to be critical in the stereocehmical outcome of these reactions with Et_2AlCl and catalytic $InCl_3$ providing opposite stereoisomers.[114]

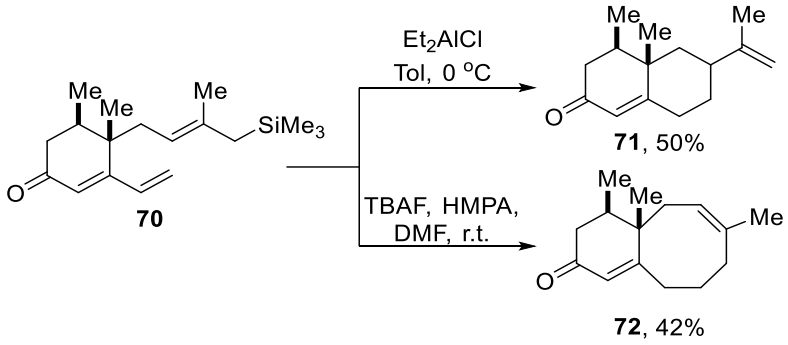

Scheme 29. S_E versus S_E' 1,6-enone cyclization.

Due to the high levels of predictable stereoselectivity and stereospecificity, the enone Sakurai cyclization is an attractive approach to form polycarbocyclic natural product targets. Many of these terpenoid natural products contain dense stereochemical features with few or no polar functional groups, making them formidable targets for synthesis. One such class of natural products are the clerodanes, whose members include both *cis*- and *trans*- decalins alongside numerous all carbon quaternary stereocenters. Tokoroyama was the first to use this approach in the syntheses of the clerodanes and linaridial.[115] In this report, they utilized an allylsilane conjugate addition – enolate trapping method to set three contiguous stereocenters, two of which were all-carbon quaternary (Scheme 30). They discovered that highly reactive electrophiles, such as an α-chlorosulfide, could be used as an *in situ* enolate trap which provided the *cis*-decalin structure. Remarkably, the product (**74**) is formed as a single diastereoisomer which is directed by a single methyl group providing enough conformational bias to set the remaining stereocenters. Although this report was using a racemic substrate, Anderson later used the enantiopure starting in their studies towards 6′-hydroxyarenarol and popolohuanone E.[116,117]

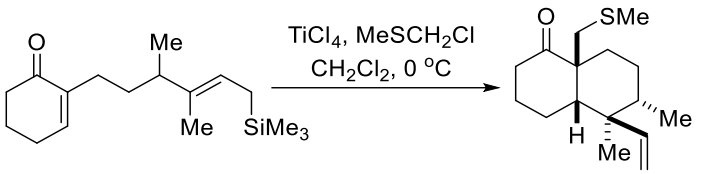

73 **74**, 77%, >20:1 dr

Scheme 30. Alkylative enone Sakurai additions.

Schauss demonstrated an extension of their substituted *H*$_8$-BINOL catalyzed enantioselective Morita-Bayliss-Hilman methodology.[118] They were able to derivatize a product of this reaction to form an allylsilane (**75**) which could undergo an enone Sakurai cyclization thus forming the *trans*-decalin core of the clerodane natural products (**76**) (Scheme 31).[118] In this report, they used $BF_3{\cdot}OEt_2$ as a Lewis acid which was very efficient at closing the second ring to form a *trans*-decalin structure (**76**) and generating three new stereogenic centers, including an all-carbon quaternary center, with almost complete stereocontrol. The formation of the *trans*-decalin core, which is opposite to the chemistry described by Tokoroyama, is proposed to be due to a chelation of the β-hydroxy group. This chelation, either through the Lewis acid or by hydrogen bonding of the OH group, directs the allylsilane addition on the upper face of the enone with the enolate being protonated form the upper more accessible face to provide the *trans*- structure.[118]

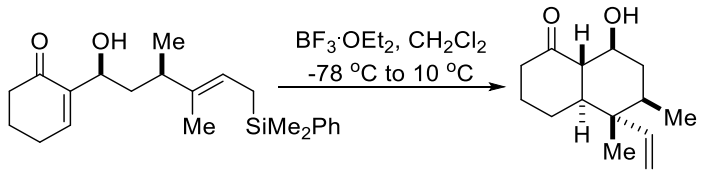

75 **76**, 81%, 99:1 d.r.

Scheme 31. Alcohol directed Sakurai cyclization.

Aside from simple enolate trapping, the enone Sakurai reaction can be combined with a variety of other reactions. Tietze was able to successfully combine the allylation with a carbonyl-ene reaction (Scheme 32).[119] In this remarkable reaction, an α,β-unsaturated aldehyde and a methyl substitiuted allyl silane could react to generate two rings and four contiguous stereocenters in a single transformation as a single diastereoisomer. Due to the moderate yield obtained it is possible that other stereoisomers are formed but do not perform the ene reaction to form (**78**). Interestingly, when the Lewis acid is change to Et_2AlCl, the stereochemical outcome of the reaction is modulated at C6/7. In this case, a 3:1 mixture of diastereomers was obtained with no traces of (**78**) being formed. The two stereoisomers formed in the 3:1 ratio are the C-6/7 double epimer and the C-6 single epimer respectively.[119]

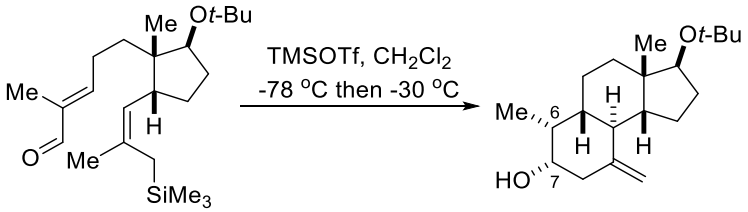

77 **78**, 52%, >20:1 dr

Scheme 32. Enone Sakurai-ene polycyclization.

Nelson also demonstrated the power of the Sakurai-cyclization to multiply stereogenicity in a molecule. In their report, they were able to perform a cascade reaction which combined the enone Sakurai allylation with an aldol reaction (Scheme 33).[120] They examined the use of tethered allylsilane-enone substrates and investigated the use of both external and internal aldehydes for the aldol reaction. The most impressive example is where they utilize (**79**), a molecule that contains an allylsilane, an enone and an aldehyde, which performs a cascade double cyclization to form a [5.6.6]-fused tricyclic system (**80**). The reaction proceeded with

good levels of chemoselectivity and stereocontrol forming two new carbon-carbon bonds and four stereocenters in a single reaction. The polycyclized product (**80**) was 83% stereochemically pure with the remainder a mixture of the other possible diastereoisomers.[120]

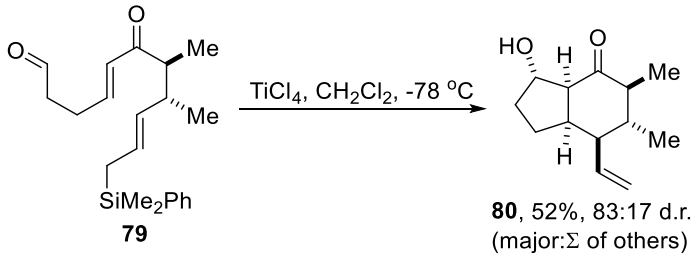

Scheme 33. Enone Sakurai-aldol polycyclization.

The formation of cyclopropanes was reported by Gimazetdinov using the conjugate addition variant of the Sakurai allylation.[121] In this reaction, a cyclic allylsilane with a pendant enoate ester (**81**) was activated with fluoride and underwent 1,4-addition to the acrylate functionality to form (**82**) (Scheme 34).[121] This report is notable due to the S_E nature of this reaction, as opposed to the S_E' observed in most allylsilane additions. Reaction occurs with inversion of stereochemistry at the silylated position, therefore, conventional mechanisms that are commonly proposed cannot be in operation. This approach can also form cyclopropanes using enones and nitroalkenes.[121]

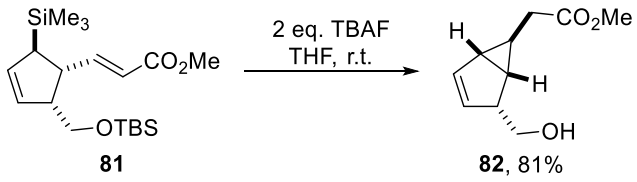

Scheme 34. [3.1.0]-Ring systems *via* S_E enone additions.

<u>Imine and Iminium Addition Cyclizations</u> Aside from allylations of C=O and C=C bond systems, the nitrogenous analogs can also be a powerful tool in synthetic routes. Since imines are

not as electrophilic as their carbonyl cousins, for an imine to react, it must be either activated with a strong electron withdrawing group or ionized into an iminium ion. *In situ* generated iminium ions from eliminations or sigmatropic processes are particularly attractive. Overman described the first iminium Sakurai reaction (or aza-Sakurai) which could be combined with a 2-aza-Claisen rearrangement to form complex cyclic systems present in many alkaloids.[122–124] However, the focus of this review is the formation of carbocycles using the Sakurai allylation, therefore, the many recently published approaches to nitrogen heterocycles will not be discussed.[125–132]

Weinreb has utilized the aza-Sakurai to form both fused and spirocyclic products which were used in the synthesis of several polycyclic alkaloid natural products. An example of the formation of spirocyclic *N*-heterocycles was reported in their synthesis of lepadiformine (Scheme 35).[133] In this report, they demonstrated the synthesis and reaction of the allylsilane precursor to form a 5,6-spiropyrrolidine structure. The allylsilane was formed through base mediated alkylation chemistry of dihydropyrrolidine (**83**) and iodide (**84**) followed by acylation to form (**85**) as a mixture of enamine isomers. This was treated with TFA to form an acyl iminium ion which cyclized to form the spirocyclic product (**86**) as a single diastereoisomer.[133]

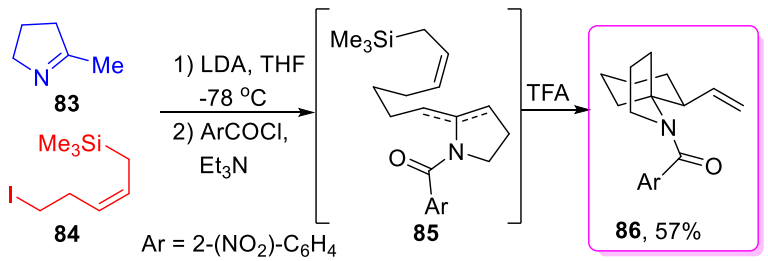

Scheme 35. Imine alkylation-Aza-Sakurai sequence.

More recently, the Weinreb group reported a one-pot reduction – elimination – iminium Sakurai allylation sequence in their synthesis of (±)-myrioneurinol (Scheme 36).[134] In this reaction, they used DIBAL-*H* to reduce *N*-tosyl lactam (**87**) to the corresponding aluminum alkoxide, which upon treatment with $FeCl_3$ eliminated the oxygen atom to form an iminium ion which could undergo cyclization in good overall yield. Due to the existing architecture of the molecule, there is only one stereochemical outcome that is possible, however, this is an impressive example of the power of the aza-Sakurai reaction.[134]

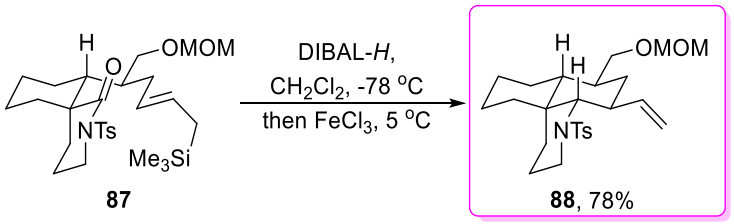

87 **88**, 78%

Scheme 36. Lactam reduction-aza-Sakurai cyclization.

Outside of acyl iminium-type chemistry, the aza-Sakurai can be used to form carbocycles through the reaction of imines. Many imines are unstable and difficult to handle, therefore, methods for in situ generation and cyclization of imines have been established. Although the acyclic variant has been widely reported, the formation of carbocyclic structures is much less developed.

In Panek's original Sakurai cyclization paper, they reported a subset of reactions whereby the aldehyde (**89**) could be condensed with a sulfonamide to form the corresponding imine, which cyclized to form the requisite cyclopentylsulfonamide (**90**) (Scheme 37).[49] To circumvent any chemoselectivity issues that could arise from the straight cyclization on to the aldehyde, they used a milder Lewis acid ($BF_3.OEt_2$) at low temperature to mediate the imine formation, which was then warmed to -35 °C at which point cyclization occurred. The stereochemical outcome of

this reaction is the same as the aldehyde cyclization reaction with the products being formed as a single diastereoisomer.[49]

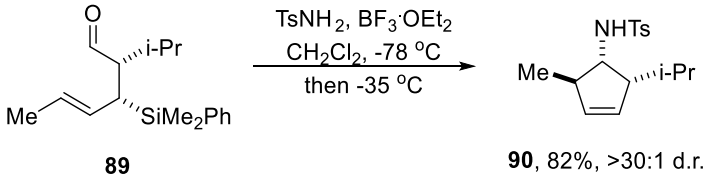

89 **90**, 82%, >30:1 d.r.

Scheme 37. Imine formation-aza-Sakurai reaction.

Chida employed Sakurai allylation to assemble diazatricyclic scaffold (**93**) commonly found in madangamine alkaloids (Scheme 38).[135] In this reaction they utilized N-Boc-enamine (**91**) that upon treatment with $BF_3 \cdot Et_2O$ in the presence of EtOH formed N-acyliminium ion (**92**). The latter underwent cyclization with pendant allylsilane to form a 6-membered ring finalizing the assembly of tricyclic core. Authors showed that this transformation can be also done in a stepwise manner where (**91**) is first transformed to *N*,*O*-acetal, which then participates in Sakurai ring closure. However, this route resulted in lower yield due to acetal instability.[135]

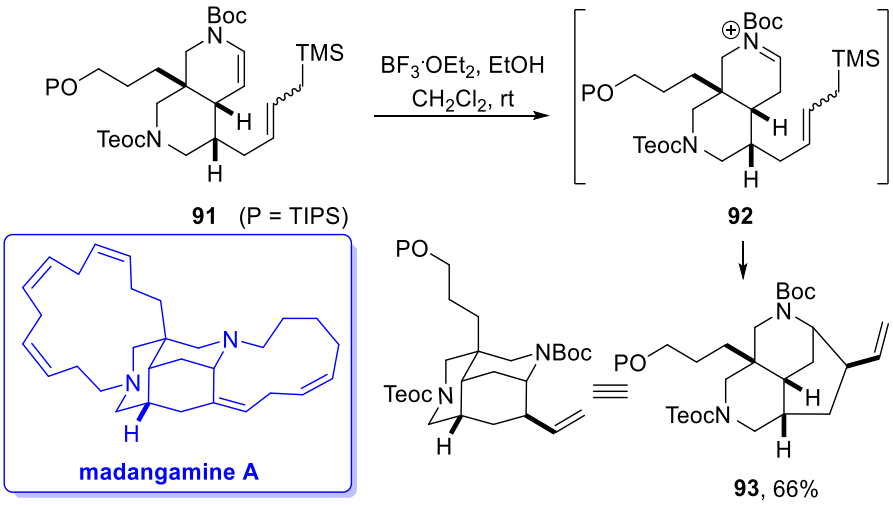

91 (P = TIPS) **92**

Scheme 38. Enamide protonation-aza-Sakurai cyclization.

Other Reactions While not technically a Hosomi-Sakurai allylation, the addition of allylsilanes to activated π-systems is an analogous reaction. In particular, a carbocyclization reaction that proceeds *via* the outer-sphere attack of an allylsilane to an electrophilic π-system that has been activated by a transition metal is in many ways a similar reaction. Echavarran demonstrated that alkynes activated by a π-Lewis acidic Pt(II) catalyst can form cyclic skipped dienes (**95**) (Scheme 39).[136]

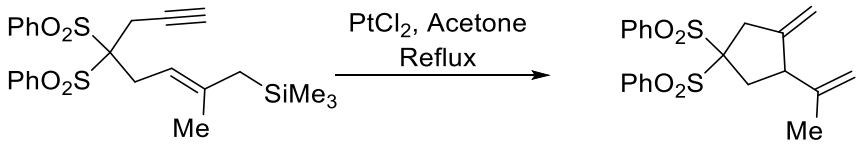

94 **95**

Scheme 39. Allylsilane addition to activated alkynes.

Chang has shown that allyl silyl ethers (**96**) and (**99**) can undergo Lewis acid-mediated condensative carbocyclization with silyl nucleophiles (**97**) (Scheme 40).[137] This reaction can result in either cyclopropane (**98**) or cyclobutane (**100**) product with selectivity being dictated by the substituent in the C3-position of the silyl ether. In particular, having aryl group at this position was found to be necessary for cyclobutanation. In this case, the use of bulkier nucleophiles resulted in improved diastereoselectivity.[137]

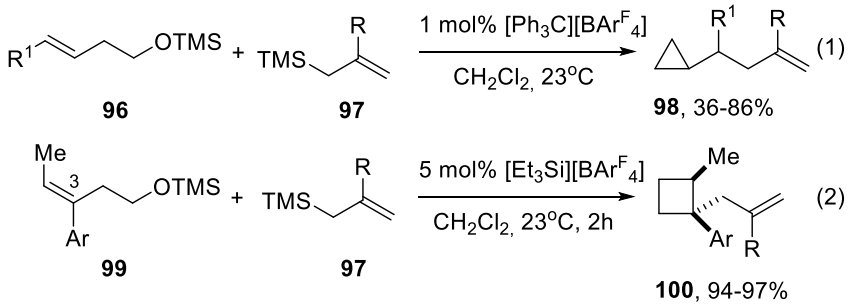

96 **97** **98**, 36-86%

99 **97** **100**, 94-97%

Scheme 40. Allylsilane terminated carbocyclization.

Over the past four decades, the Hosomi-Sakurai reaction has been applied to many carbocyclizations that afford products of impressive complexity. The versatility of these allylsilane additions come from the ease of synthesis, stability, and their reactivity with a wide range of carbocations (or formal carbocations). Indeed, these reactions provide facile access to the rings of various size including bicyclic, tricyclic and spirocyclic systems. Notably, these reactions can exhibit high diastereoselectivity and stereospecificity with the outcome being determined by the choice of promotor. The differing mechanisms for the Hosomi-Sakurai allylation (S_E vs. S_E', and synclinal vs. antiperiplanar) provide the synthetic practitioner with a diverse range of tools to modulate both regio and stereoselectivity. The wide array of reactions available, combined with the ease in which stereo and regiochemical modulation can occur, makes the Hosomi-Sakurai carbocyclization a preeminent method for the synthesis of complex carbocyclic frameworks.

To summarize, both Claisen rearrangement and Sakurai-carbocyclization offer a significant degree of control over reaction stereochemical outcome. In each case this outcome can be predicted beforehand as reactions proceed *via* organized transition states. Since the relative stereochemistry of Claisen rearrangement can be controlled by substrate[42] and the reaction does not require promotor (other than heat) and can be performed in a variety of solvents, it is an excellent candidate for one-pot methodology. One the other hand, both Claisen rearrangement and Sukurai-carbocyclization are catalyzed by organoaluminum reagents furnishing corresponding products with high selectivities, which makes it a promising platform for a cascade process.

A Highly Stereospecific Claisen-Sakurai Approach to Densely Functionalized Cyclopentenols

Herein, we describe the realization of the Claisen-Sakurai reaction pathway to produce highly substituted cyclopentenols. As was alluded earlier, our approach was to utilize readily synthesized silylated allyl vinyl ethers (**101**),[41,45,50,51,138] and perform a Claisen-Sakurai sequence in either a one-pot stepwise or a cascade fashion (Scheme 41). As a result, a very modular synthesis of 1,2,5-trisubstituted cyclopent-3-en-1-ols (**103**) has been achieved, which utilizes the stereospecificity of both Claisen and intramolecular Sakurai reactions.[52,53]

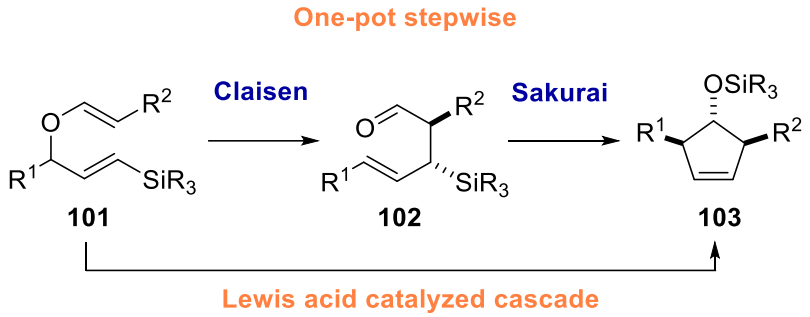

Scheme 41. Claisen-Sakurai approach to stereochemically dense 1,2,5-trisubstituted cyclopent-3-en-1-ols.

Starting Material Preparation

The Claisen-Sakurai approach to stereochemically dense cyclopentenols utilizes silylated allyl vinyl ethers (**101**). We utilized divergent synthetic routes to these substrates which allow for the introduction of various silyl groups, alongside alternative substituents at the allylic position.

Depending on which silyl group is required, one of two synthetic pathways (Route 1 and Route 2) were employed.

When a silyl group other than $SiMe_3$ is required, Route 1, developed in the Cook group previously (Scheme 42),[41,45,50,51,138] is utilized whereby ethynylmagnesium bromide is added to an aldehyde,[139] followed by platinum catalyzed hydrosilylation to install the requisite silane.[50,51] *O*-Allylation[45,138,140] can be performed under basic conditions and finally iridium(I) catalyzed isomerization[45] furnishes (**101**).

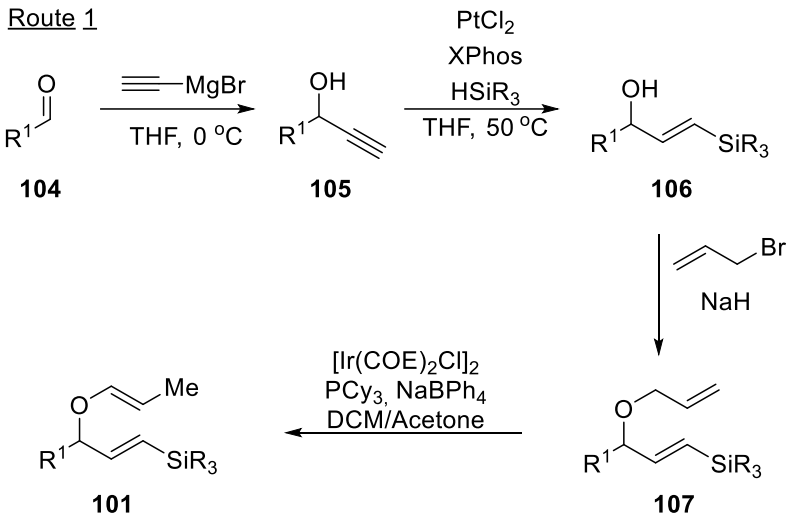

Scheme 42. Synthetic Route 1 to monosilylated allyl-vinyl ethers (**101**).

Alternatively, the $SiMe_3$ substituted variant can be produced *via* a modified synthetic scheme (Route 2, Scheme 43) that entails the nucleophilic addition of lithiated TMS acetylene,[141] followed by a highly *E*-selective Red-Al reduction,[142] and the allylation[45,138,140]/isomerization[45] pathway alluded to above. Notably, propargyl and allylic alcohols can be readily synthesized as a single enantiomer if needed.[143,144]

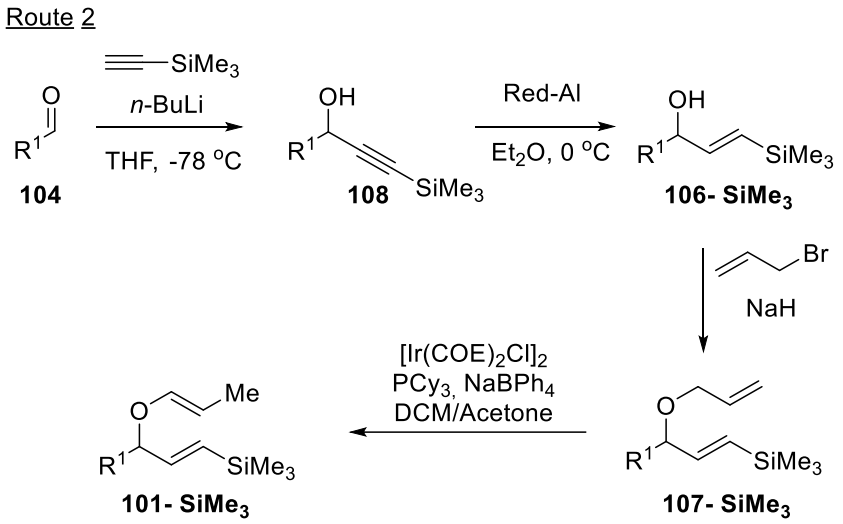

Scheme 43. Synthetic Route 2 to monosilylated allyl-vinyl ethers (**101- SiMe$_3$**) bearing TMS group.

These protocols provide a rapid and tolerant approach to a wide variety of substrates, including alkyl and aryl substituted variants, two of which are exemplified below (Scheme 44 and 45). The only experimental difference in the synthesis of alkyl and aryl substituted allyl vinyl ethers is the allylation step. In the case of alkyl substituted substrates, more forcing allylation conditions are needed with the addition of 15-crown-5 to activate the nucleophile and Bu_4NI to activate the electrophile (Scheme 44).[140] In contrast, aryl substituted alcohols are efficiently allylated with no additive in cold DMF (Scheme 45).[45,138]

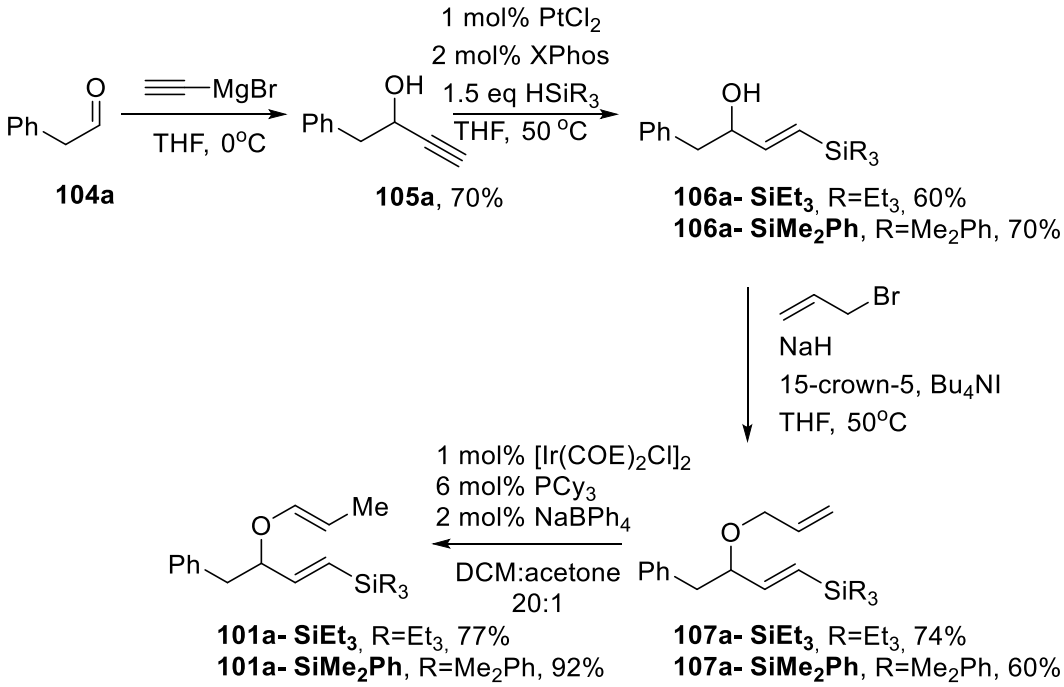

Scheme 44. Selected examples of synthesis of monosilylated allyl-vinyl ethers with alkyl substituent at the allylic position. Average yields are shown.

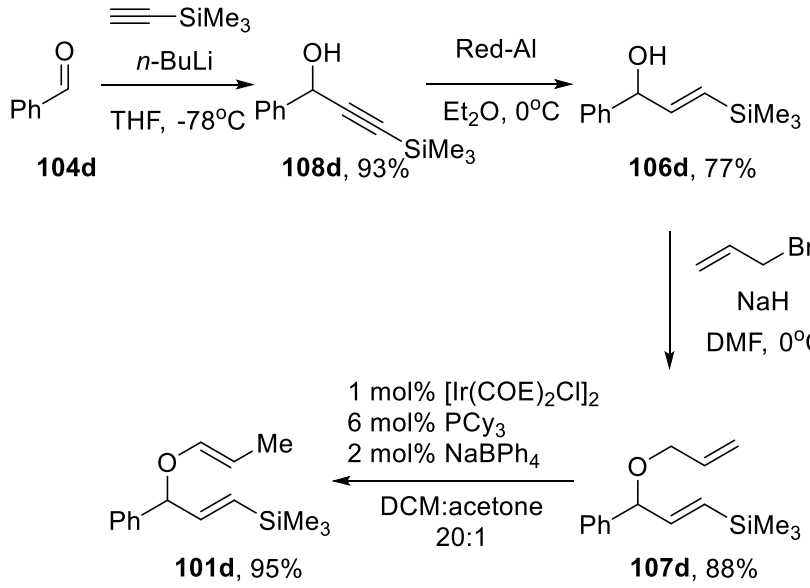

Scheme 45. Selected example of synthesis of monosilylated allyl-vinyl ethers with aryl substituent at the allylic position. Average yields are shown.

To further diversify the reaction scope and include 1,1-disubstituted vinyl ethers, we adopted olefin isomerization-Claisen rearrangement conditions previously reported by Nelson.[64] First, phenyl substituted allylic alcohol (**106d**) was reacted with methylallyl bromide in the presence of NaH in DMF at room temperature to produce 1,1-dimethyl allyl ether (**107p**), which was then subjected to an isomerization-Claisen rearrangement, using a cationic Ir(I) catalyst at 90 °C, to access 2,2-dimethyl-4-pentenal (**109**) (Scheme 46).

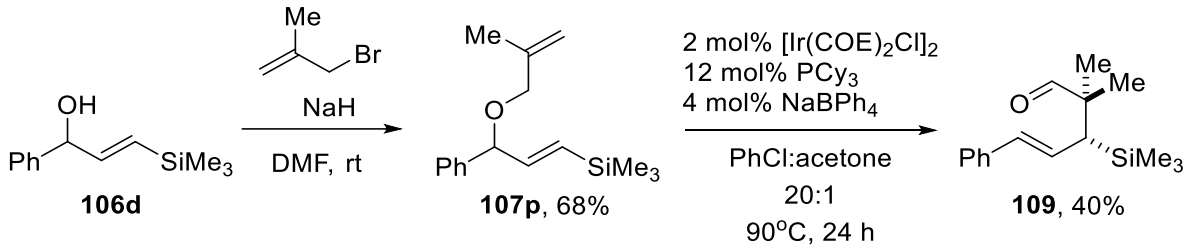

Scheme 46. Synthesis of monosilylated 1,1-dimethyl allyl-allyl ether (**107p**) and corresponding 2,2-dimethyl-4-pentenal (**109**).

Enantioenrichment (86% ee) of allylic alcohol (**106d**) was achieved *via* a Sharpless kinetic resolution.[145] The allylic alcohol (**106d**) was further subjected to the developed reaction sequence. This provided the corresponding monosilylated allyl-vinyl ether was obtained in 88% ee demonstrating that no stereochemical erosion had occured.

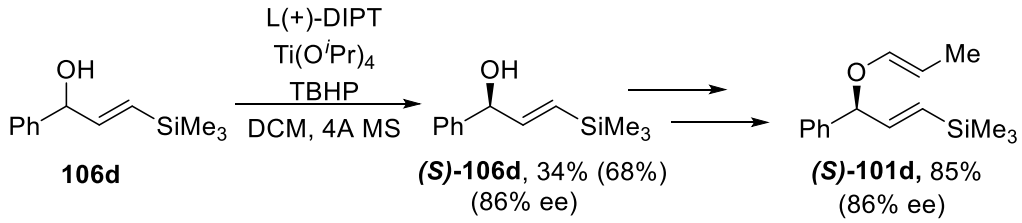

Scheme 47. Synthesis of enantioenriched monosilylated allyl-vinyl ether.

Stepwise Claisen-Sakurai Reaction

With these results in hand, we embarked on synthesis of stereochemically dense cyclopentenols *via* Claisen-Sakurai approach. We commenced our studies by examining the Claisen-Sakurai reaction as a one-pot, stepwise transformation. Our optimization studies examined the conversion of benzyl substituted allyl vinyl ether (**101a**) to the corresponding cyclopentenol (**110a**). A thermal Claisen rearrangement was performed on (**101a**) in chlorobenzene at 110 °C, followed by cooling to ambient temperature, and the addition of a Lewis acid to affect the Sakurai-cyclization. A range of Lewis acids were tested; however, aluminum reagents were most effective (Table 1). No cyclized product was observed with $AlMe_3$, with significant amounts of aldehyde alkylation detected (Entry 1). The more Lewis acidic reagents (Et_2AlCl, $EtAlCl_2$, $AlCl_3$) provided the cyclized product (**110a**) in good yields and excellent diastereoselectivity (Entries 2-4). $AlCl_3$ provided the cleanest reactions due to the absence of any alkylation reaction, with 1.5 equivalents of Lewis acid proving optimal (Entries 4-7).

The reactions are clean, as judged by the crude reaction mixtures, therefore the mass balance can be accounted for by competing decomposition. Alternative silanes, other than $SiMe_3$, were also tested, however $SiEt_3$ and $SiMe_2Ph$ groups had a deleterious effect on the reactivity and stereochemical outcome (Entries 8 and 9). High levels of stereocontrol with >20:1 d.r. were observed in all cases except with the less nucleophilic and more sterically encumbered $SiMe_2Ph$

variant (Entry 9). The stereochemical outcome was assigned as the *anti, anti*-isomer shown by NMR and computational methods (*vide infra*). Interestingly, the use of $SnCl_4$ (Entry 11) led to poor stereocontrol and $BF_3.OEt_2$ (Entry 10) led to a reversal of stereoselectivity.

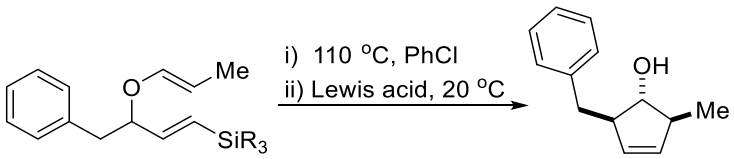

101a **110a**

Entry	R_3Si	Lewis Acid	Yield[a]	d.r.[b]
1	$SiMe_3$	1.5 equiv. $AlMe_3$	0%	n.a.
2	$SiMe_3$	1.5 equiv. Et_2AlCl	59%	>20:1
3	$SiMe_3$	1.5 equiv. $EtAlCl_2$	45%	>20:1
4	$SiMe_3$	1.5 equiv. $AlCl_3$	65%	>20:1
5[c]	$SiMe_3$	1.5 equiv. $AlCl_3$[c]	59%	>20:1
6	$SiMe_3$	1 equiv. $AlCl_3$	34%	>20:1
7	$SiMe_3$	2 equiv. $AlCl_3$	47%	>20:1
8	$SiEt_3$	1.5 equiv. $AlCl_3$	47%	>20:1
9	$SiMe_2Ph$	1.5 equiv. $AlCl_3$	37%[d]	8:1
10	$SiMe_3$	1.5 equiv. $BF_3{\cdot}OEt_2$	61%	1:2
11	$SiMe_3$	1.5 equiv. $SnCl_4$	65%	2:1

Table 1. Optimization studies for stepwise synthesis of cyclopentenols. [a] Determined by ^{1}H NMR against an internal standard (1,3,5-triisoproylbenzene); [b] Determined by ^{1}H NMR analysis; [c] Lewis acid reaction performed at 0 °C. [d] Product formed as a mixture of *O*-silylated and free OH.

With the optimized conditions in hand, we examined the scope of this reaction (Scheme 48). The optimized conditions described above (Table 1, Entry 4) were applied to other alkyl substituted allyl vinyl ethers (**101a-c**). Cyclohexyl (**101b**) and benzyloxyethyl (**101c**) substituted variants provided (**110b**) and (**110c**) in good to moderate yields and excellent stereoselectivity >20:1 d.r. Aryl substituted allyl vinyl ethers (**101d-o**) were also examined. These substrates exhibited an accelerated Claisen rearrangement, compared to (**101a-c**), allowing the initial reaction to occur at 90 °C or below.[42] This transformation was very general and relatively insensitive to functionality and substitution pattern. Good yields of the cyclopentenol products

(**110d-o**) and high levels of stereocontrol (>20:1) were obtained in all cases. Although σ-withdrawing groups do not significantly influence the reaction efficiency, mesomeric electron-donating groups provide slightly higher overall yields and faster reaction times. This is exemplified by examining 4-substitution on the benzene ring where OMe (**110e**), CF_3 (**110f**), OCF_3 (**110g**) and F (**110h**) all provide similar reactivity with **110e** being formed more efficiently. We also examined the effect of the substitution position by comparing the formation of 4-F (**110h**), 3-F (**110i**), and 2-F (**110j**) cyclopentenols. There were minimal differences in reaction efficiency between these regioisomers (**110h-j**), demonstrating no clear electronic sensitivity. More complex arene substitution was also examined. 2-Naphthyl cyclopentenol (**110k**) was produced in excellent yield, and 2,4-disubstituted groups were well tolerated. Specifically, 2-fluoro-4-methoxy (**110l**), 2,4-difluoro (**110m**), and 2-fluoro-4-chloro (**110n**) products could be isolated in good yields. Finally, we demonstrated the use of heteroaromatic groups in this reaction with *N*-tosyl indole derivative (**110o**) being isolated with high efficiency. To further demonstrate the synthetic utility of this reaction, we performed the rearrangement of (**101d**) on a one millimole scale with comparable results. Formation of the allyl vinyl ethers (**101**) containing groups other than methyl groups was more challenging using the Ir(I) isomerization approach. This limitation could be surmounted by converting 1,1-di- and trisubstituted allyl ethers to corresponding aldehydes using alkene isomerization-Claisen rearrangement conditions reported by Nelson.[64] Utilizing this strategy, we were able to access 2,2-dimethyl-4-pentenal (**109**) which upon cyclization provided (**110p**) with >20:1 d.r. This example demonstrates that the developed reaction allows for the construction of all-carbon quaternary centers alongside multiple contiguous stereocenters.

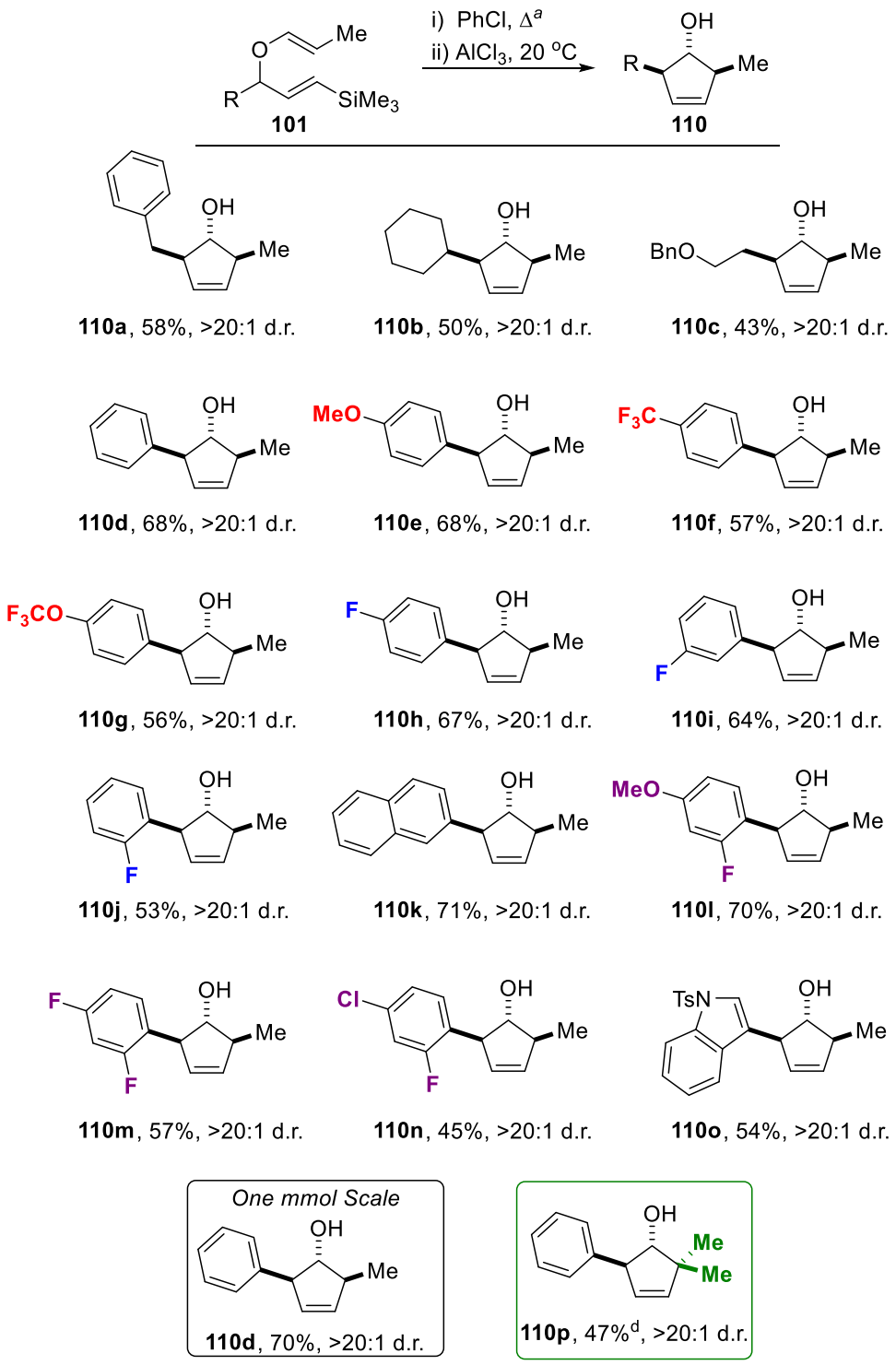

Scheme 48. Substrate Scope.[a-d a] (**101a-c**) 110 °C, (**101d-n**) 90 °C, (**101o**) 70 °C; [b] Isolated yields; [c] Determined by ^{1}H NMR analysis; [d] Yield over cyclization step.

This transformation converts allyl vinyl ethers (**101**), which contains a single stereogenic center, into cyclopentenols (**110**) that contain three contiguous stereocenters. We therefore examined whether the absolute stereochemistry of enantioenriched allyl vinyl ethers could be transferred to the products (**110**) providing a new enantioselective route to these structures. Enantiospecificity would render this reaction even more impactful due to the abundance of methods of enantiocontrolled allylic and propargylic alcohol synthesis.[143,144] To test this hypothesis, we prepared a sample of allyl vinyl ether (***(S)*-101d**) in 86% ee from the corresponding allylic alcohol[145] with no erosion of stereochemistry. When (***(S)*-101d**) was subjected to identical reaction conditions to those described in Scheme 48, the corresponding cyclopentenol (***(1S,2R,5R)*-110d**) was produced with no loss of enantioenrichment (Scheme 49). This stereospecificity is evidence of the concerted nature of the Claisen rearrangement and that Sakurai cyclization is significantly faster than any epimerization mechanism.[52,53]

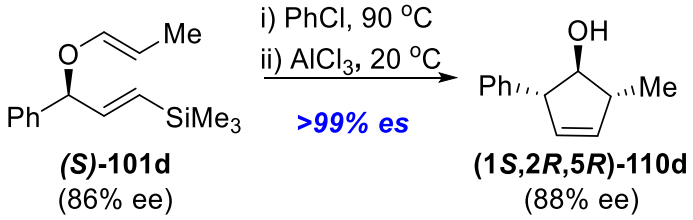

***(S)*-101d**
(86% ee)

(1*S*,2*R*,5*R*)-110d
(88% ee)

Scheme 49. Enantiospecificity of Claisen-Sakurai reaction.

Mechanistic Studies

Reprinted (adapted) with permission from Stankevich, K. S.; Cook, M. J. A Highly Stereospecific Claisen–Sakurai Approach to Densely Functionalized Cyclopentenols. *J. Org. Chem.* **2022**, *87* (18), 12250–12256. DOI: 10.1021/acs.joc.2c01397. Copyright 2022 American Chemical Society. http://pubs.acs.org/articlesonrequest/AOR-VKSAE6YWPREVKNJDRRJT

To investigate the origin of high levels of stereospecificity, we conducted DFT calculations. We commenced our studies by looking at the mechanism of thermal Claisen rearrangement utilizing (**101d**) as a model.

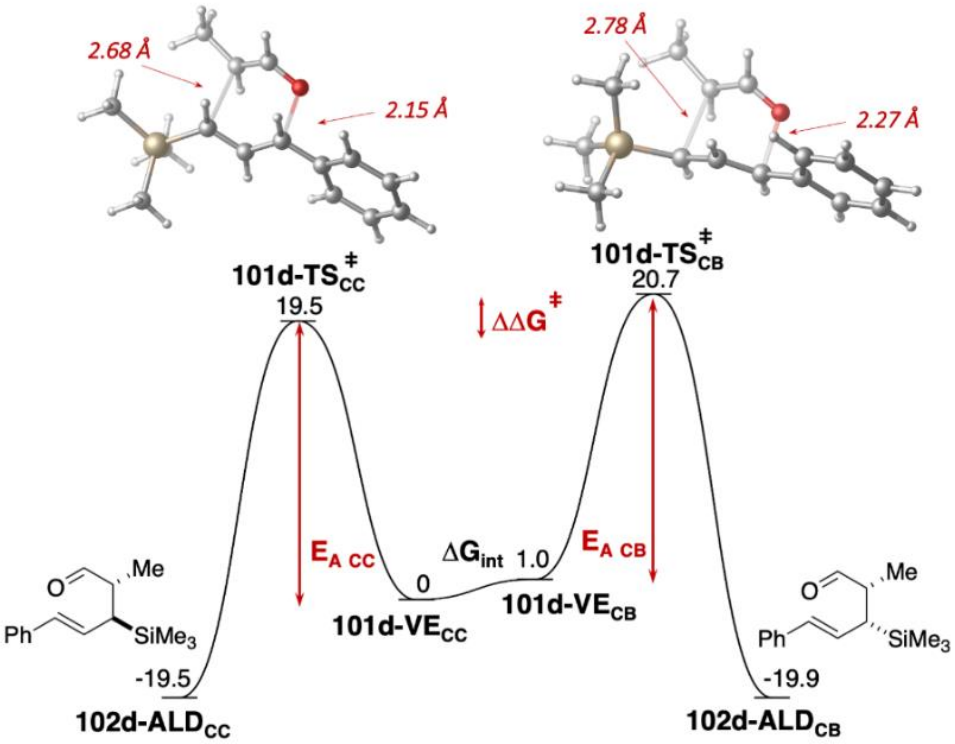

Figure 2. Potential energy surface of the thermal Claisen rearrangement showing Curtin-Hammett equilibrium between two conformations of the allyl vinyl ether (**101d**) leading to the chair and boat transition states. Calculations were performed at C-PCM (chlorobenzene)-M11L/6-311++G(2d,2p)//C-PCM (chlorobenzene)-B3LYP/6-31+G(d). The quasi-harmonic Gibbs Free energies are reported at 363.15 K and 1 mol/L standard state.

It is well established that the Claisen rearrangement proceeds *via* either a boat or a chair transition state.[42] Each of these would be preceded by a corresponding reactive ground-state conformation of the monosilylated allyl-vinyl ether (**101d**). According to our calculations, the interconversion gap between the two reactive (chair and boat) conformers is small comparing to the activation energies and lies within the range of 2.2 kcal/mol (Figure 2).

We further examined the effect of substituent at the allylic position on the reaction potential energy surface (Table 2). Alkyl variants are characterized by higher TS_{CC} energies comparing to aryl one, which can be explained by lower ability of the former to stabilize developing positive charge. It correlates with experimental observation that alkyl substituted vinyl-ethers required higher temperatures during the Claisen rearrangement step. For a substrate (**101a**) the predicted $\Delta\Delta G^{\ddagger}$ between TS_{CC} and TS_{CB} is 2.1 kcal/mol, which at 110 °C would result in relative rates of 16:1. This is close to the >20:1 d.r. selectivity observed experimentally, when the corresponding aldehyde was isolated. For (**101d**) the predicted $\Delta\Delta G^{\ddagger}$ of 1.2 kcal/mol at 90 °C would result in relative rates of 5.3:1, while experimental d.r. for isolated aldehyde is 10:1 by ^{1}H NMR.

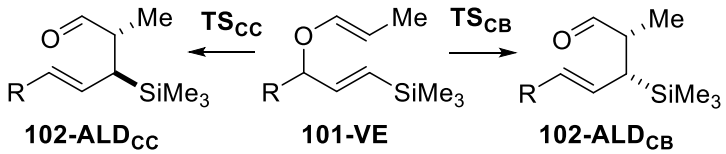

R	ΔG_{int}, kcal/mol	$E_{A\ CC}$, kcal/mol	$E_{A\ CB}$, kcal/mol	$\Delta\Delta G_{CB\text{-}CC}$, kcal/mol
Me[a] (**101q**)	1.5	24.2	24.9	2.2
Bn[a] (**101a**)	1.5	24.9	25.5	2.1
Ph[b] (**101d**)	1.0	19.5	19.7	1.2

Table 2. Activation energies of the thermal Claisen rearrangement calculated at C-PCM (chlorobenzene)-M11L/6-311++G(2d,2p)//C-PCM (chlorobenzene)-B3LYP/6-31+G(d). [a] The quasi-harmonic Gibbs Free energies are reported at 383.15 K and 1 mol/L standard state. [b] The quasi-harmonic Gibbs Free energies are reported at 363.15 K and 1 mol/L standard state.

When one considers *para*-substituted aromatic ring at the allylic position, it is observed that as π-donating ability of the substituent increases, the TS_{CC} energy becomes lower. In attempt to quantitatively describe this trend, we built a Hammett plot. The rate constants of the rearrangement of *para*-substituted (k_X) and unsubstituted (k_H) aryl allyl-vinyl ethers were calculated using Eyring–Polanyi Equation taking TS_{CC} energies as activation energies (Table 3).

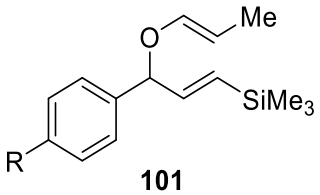

101

R	σ_{p+}	k_X/k_H
OMe (**101e**)	-0.78	5.97
Me (**101r**)	-0.31	4.20
F (**101h**)	-0.07	1.74
Cl (**101s**)	0.11	1.50
CF_3 (**101f**)	0.61	0.23

Table 3. Rate constants predicted using activation energies calculated at CPCM (Chlorobenzene)-B3LYP/6-31+G(d) and Hammett plot.

When $\log(k_X/k_H)$ were plotted against the Hammett σ_p^+ values,[146] a moderately sensitive negative ρ value was found (ρ = -1.0, R^2 = 0.916), pointing to a resonance stabilization of developing positive charge. The predicted ρ value points to an early character of the TS_{CC} and/or the remote position of the charge buildup on the aromatic system.

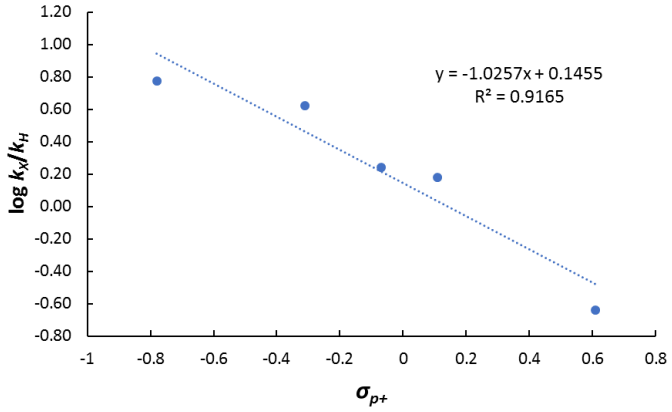

Figure 3. Hammet Plot for thermal Claisen rearrangement of monosilylated allyl-vinyl ethers.

We continued our mechanistic studies by focusing on investigating the origin of the Sakurai selectivity. The stereochemical outcome of the Sakurai-cyclization is determined by two factors: the internal diastereoselection; and relative asymmetric induction (Scheme 50). The former describes the relative disposition between the aldehyde group and *trans*-alkene and can be defined as antiperiplanar (*AP*) and synclinal (*SC*) which determines the relative stereochemistry between the R and OH groups. The latter refers to the direction of electrophilic attack of the $AlCl_3$-bound carbonyl which can approach the alkene from the same side as silicon electrofuge (*syn*-S_E') or from the opposite side (*anti*-S_E') dictating the diastereomer between the OH and Me groups.[97,147,148] Therefore, the possible transition states (and consequently, reaction pathways) can be limited to four combinations: *AP syn*-S_E' (**TS$_{AP1}$**); *AP anti*-S_E' (**TS$_{AP2}$**); *SC syn*-S_E' (**TS$_{SC1}$**); and *SC anti*-S_E' (**TS$_{SC2}$**) (Scheme 50).

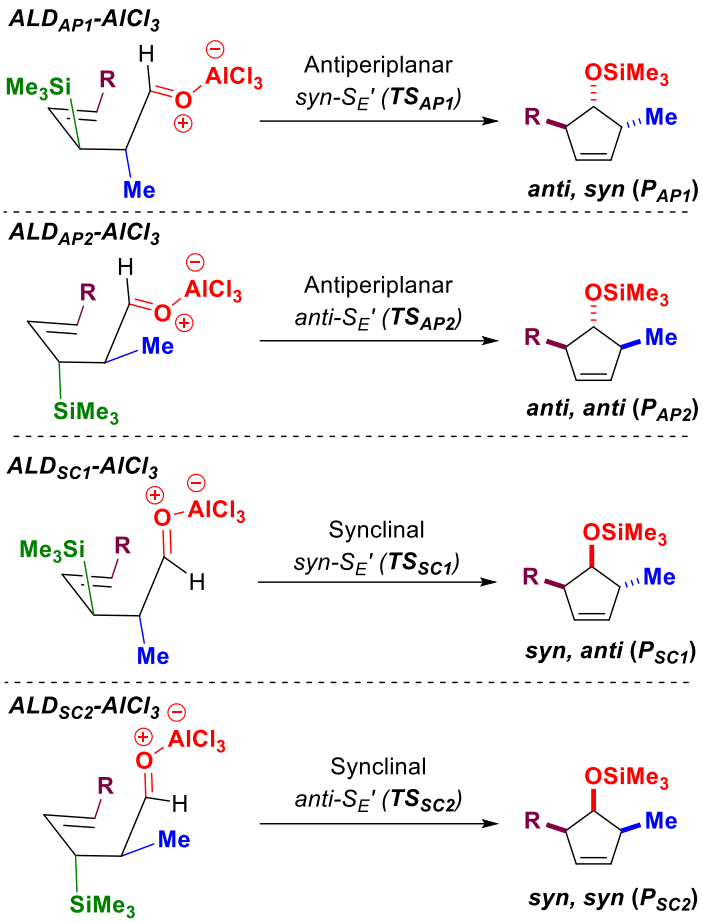

Scheme 50. Origin of Sakurai stereoselectivity in synthesis of cyclopentenols.

Calculations were conducted for the formation of four diastereomeric silylated alcohols (**P**$_{AP1}$, **P**$_{AP2}$, **P**$_{SC1}$ and **P**$_{SC2}$) (Figure 4), with all four of the transition-state structures described above considered. These computations showed that the ground-state energies of all four $AlCl_3$-bound aldehyde reactive conformations (**ALD-AlCl$_3$**) are within 1.0 kcal/mol, therefore these conformers are easily interconvertible. In contrast, the corresponding TS energies for the Sakurai cyclization are in the range of 10.1-16.9 kcal/mol (Figure 4). This Curtin-Hammett scenario proceeds *via* the lowest overall transition state (**TS**$_{AP2}$), with the antiperiplanar *anti*-S_E' pathway providing the *anti, anti*-isomer **P**$_{AP2}$. The $\Delta\Delta G^{\ddagger}$ between the two lowest transition states (**TS**$_{AP2}$ and **TS**$_{SC2}$) is 2.3 kcal/mol, corresponding to >50:1 relative rates and is in agreement with

experimentally derived data. Alternative conformations of $AlCl_3$-carbonyl binding were also considered; values quoted represent the energies corrected using accessible conformations based on the Boltzmann-weighted energies of the conformers.

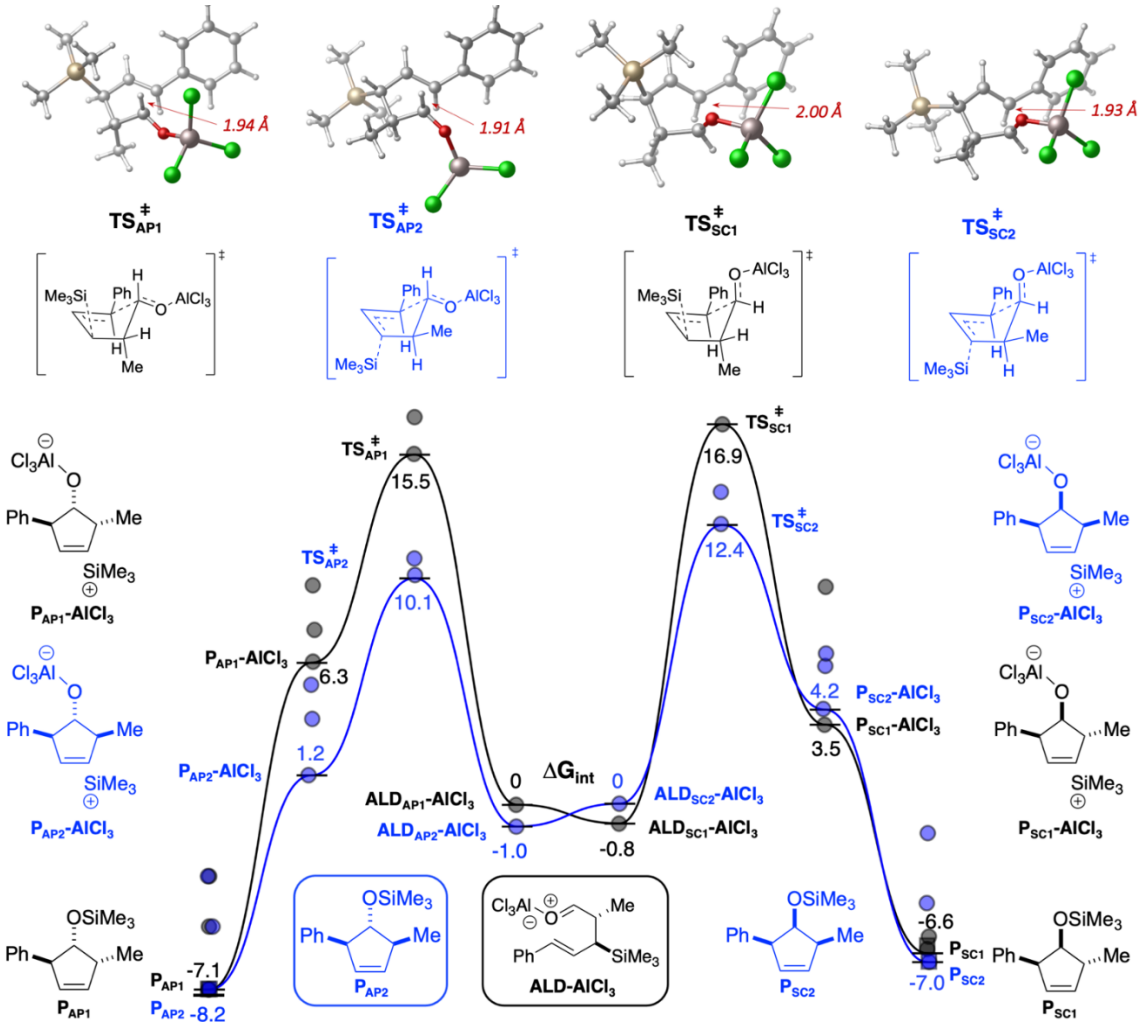

Figure 4. Potential energy surface of intramolecular $AlCl_3$-mediated Sakurai allylation. Calculations were performed at C-PCM (chlorobenzene)-M11L/6-311++G(2d,2p)//C-PCM (chlorobenzene)-B3LYP/6-31+G(d). The quasi-harmonic Gibbs Free energies are reported at 293.15 K and 1 mol/L standard state. The energies were corrected using accessible conformations based on the Boltzmann-weighted energies of the conformers. Individual conformers are shown as dots. Structures of the lowest energy TS conformer are shown.

Importantly, our computations are in agreement with stereochemical outcomes stated in other Sakurai-cyclization methods by Paquette[47,48] and Panek[49] (Scheme 2). Both reports show structures of products from antiperiplanar-*anti* S_E' cyclization, which provides further credence to our computational models. Although products were experimentally isolated as the corresponding alcohols (**110**), we observed the *O*-silylated products with alternative workup procedures. We therefore believe the aqueous NaOH cleaves the TMS during work-up.

The stereochemical outcome appears to be dictated by two deleterious steric interactions (Figure 5). Firstly, the relative asymmetric induction is controlled through conformational effects resulting from a destabilizing *syn*-pentane interaction. Steric interference between the *pseudo*-axial substituents increases torsional strain in the *syn*-S_E' variants ($\mathbf{TS_{AP1}}$ and $\mathbf{TS_{CS1}}$) which results in a significant twisting of the structure during the C-C bond forming step. Secondly, the internal diastereoselection is determined by Gauche interactions as the new bond is produced. The synclinal transition states ($\mathbf{TS_{SC1}}$ and $\mathbf{TS_{SC2}}$) proceed through orientations where the Lewis acid-bound carbonyl experiences two Gauche interactions, whereas the antiperiplanar ($\mathbf{TS_{AP1}}$ and $\mathbf{TS_{AP2}}$) variants only experience one such interaction. The molecular orbitals were also examined, however there was no significant stereoelectronic effects observed, such as the increased orbital mixing reported by Denmark, therefore we believe that steric arguments alone rationalize the stereochemical outcome.[97,147,148] The *syn*-pentane interaction is destabilizing by 4.5-5.4 kcal/mol, whereas the effects of the Gauche interacts are more moderate (1.4-2.3 kcal/mol). As a result, the antiperiplanar *anti*-S_E' conformation ($\mathbf{TS_{AP2}}$) is the preferred transition state structure, as can be observed in the *anti, anti*-stereochemistry of the cyclopentenol products (**110**) (Scheme 48).[149,150]

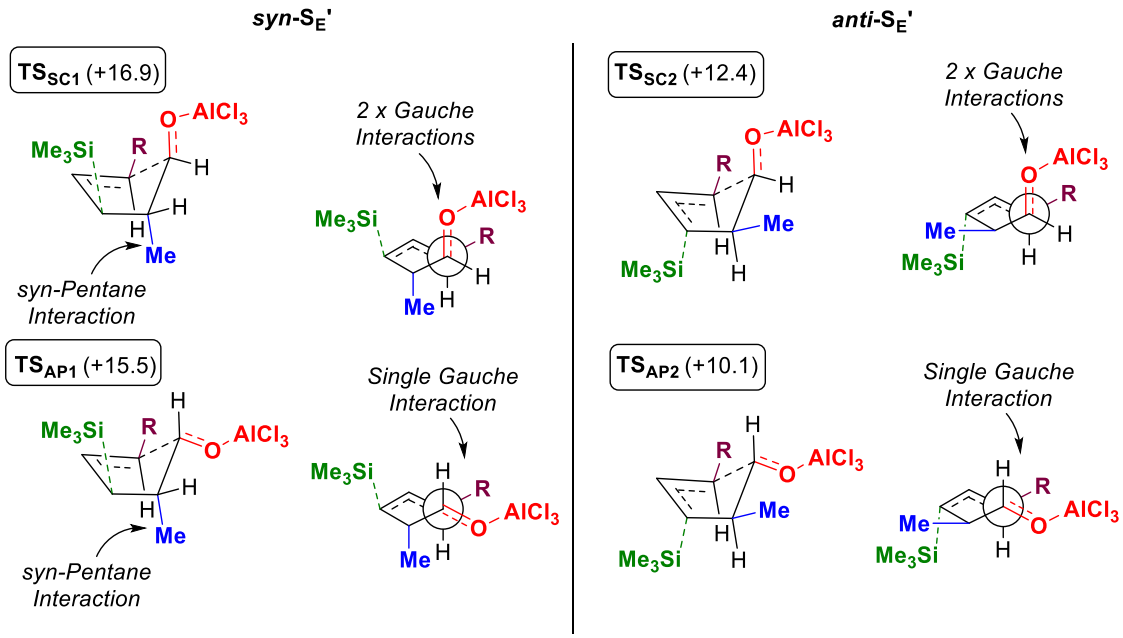

Figure 5. Steric considerations for stereocontrol.

To elucidate the relative stereochemistry of the cyclopentenol products (**110**) experimentally, we conducted NMR studies. Compound (**110j**) was chosen because of optimal peak resolution. 1D-NOESY experiments showed weak correlations (0.5-0.6%) between all three of the sp^3-bound hydrogen atoms (H_a, H_b and H_c, Scheme 51).[151] The magnitude and similarity of these through-space spin-spin polarizations suggest relatively distant, yet similar, spatial positioning from each other, implying all *pseudo*-axial (**110j-a**) or *pseudo*-equatorial (**110j-b**) orientation. These represent the two ring-flipped conformations of *anti*, *anti*-product (**110j**) (Scheme 51). DFT calculations predict a conformational mixture of 7.8:1 at equilibrium between (**110j-a**) and (**110j-b**) ($\Delta\Delta G^0$ = 1.2 kcal/mol), which interconvert much faster than the NMR timescale. We are therefore observing an average correlation based on this conformational makeup. When one examines the average H-H distances of (**110j**), we find that all three hydrogen atoms (H_a-H_c) are close to equidistant from each other with 3.01 Å (H_a-H_b), 3.07 Å

(H_a-H_c), and 3.01 Å (H_b-H_c). Importantly, this is the only stereoisomer that provides such similar average H-H distances and is consistent with both the magnitude and similarity of the correlations measured (Table 4). By combining the NMR and DFT data, we have a high degree of confidence in our stereochemical assignment of the *anti*, *anti*-isomer.[52,53]

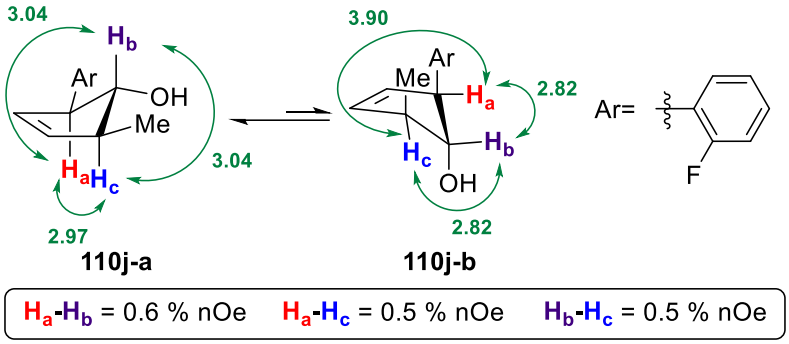

Scheme 51. Stereochemical Assignment by 1D-NOESY NMR Spectroscopy.

TS	Diastereomer[a]	H_a-H_b (Å)	H_b-H_c (Å)	H_a-H_c (Å)	$\Delta\Delta G^{0b}$	Av. H_a-H_b (Å)	Av. H_b-H_c (Å)	Av. H_a-H_c (Å)
AP2	110j-a	3.04	3.04	2.97	1.2	3.01	3.07	3.01
	110j-b	2.82	2.82	3.9	(7.8:1)[c]			
AP1	110j-c	3.04	2.34	3.97	0.1	2.91	2.36	3.95
	110j-d	2.78	2.38	3.93	(1.2:1)[c]			
SC2	110j-e	2.38	2.38	2.83	1.3	2.33	2.34	3.40
	110j-f	2.27	2.29	3.97	(9.3:1)[c]			
SC1	110j-g	2.36	2.78	3.95	-0.5	2.34	2.91	3.98
	110j-h	2.31	3.03	4.00	(1:2.4)[c]			

Table 4. Interproton distances in different stereoisomers and conformers of (**110j**). [a] Structures *a* and *b*, *c* and *d*, *e* and *f*, and *g* and *h* are ring flipped forms; [b] Difference in quasi-harmonic solvent and temperature (293.15 K) corrected Gibbs free energies at 1 mol/L standard state; [c] Ratio between the conformers calculated based on $\Delta\Delta G^0$.

Functionalization of Cyclopentenols

With an efficient route towards 1,2,5-trisubstituted cyclopent-3-en-1-ols at hand, we were able to demonstrate further synthetic utility of these compounds. For example, (**110d**) undergoes

epoxidation when treated with *m*-CBPA[152] providing *trans*-product (**111a**) (compared to the alcohol) as the major diastereomer with moderate yield (Scheme 52). The stereochemistry of the major product was determined *via* NOE experiments and provided additional support towards *anti*-, *anti*- assignment of the initial cyclopentenol (**110d**). Notably, the stereochemical outcome of epoxidation in similar systems has been controlled by installing various protecting groups on OH[152], and the cyclopenten-3-ol can be converted into an amide *via* Mitsunobu inversion[153]. One can envision that with the variety of methods available for nucleophilic epoxide opening, these compounds provide an avenue towards the synthesis of novel carbocyclic nucleoside analogues[153] and other pharmaceutically relevant applications.

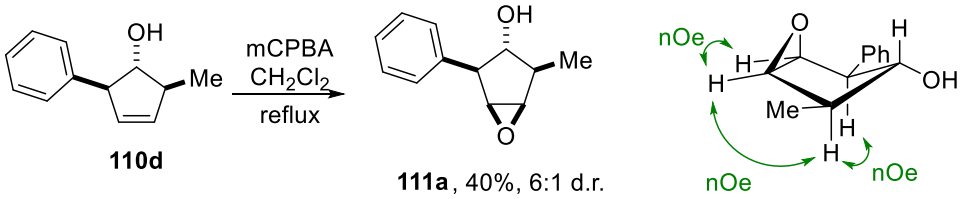

Scheme 52. Epoxidation of (**110d**).

Compound (**110d**) can also be converted to the corresponding sulfamate ester (**112**) that further undergoes C-H bond insertion under Rh(II)-catalyzed conditions[154] providing a 3:1 mixture of regioisomers (**113a**) and (**113b**) with good yield. These compounds have a potential to be used for the synthesis of bicycloproline analogues.[154]

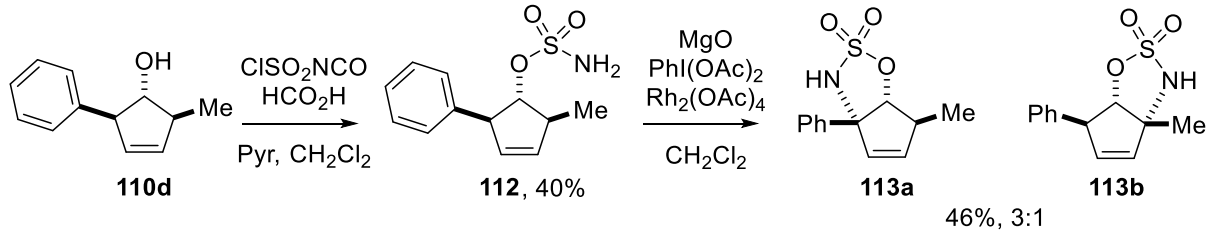

Scheme 53. Conversion of (**110d**) to bicyclic sulfamate (**113**).

Lastly, one can utilize the fact that depending on the work-up (**110d**) can be isolated as OTMS derivative (**114**), which can be then directly subjected to catalytic hydrogenation[155] furnishing cyclopentanol (**115**).

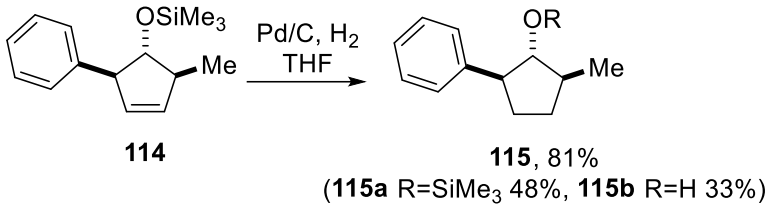

114

115, 81%
(**115a** R=$SiMe_3$ 48%, **115b** R=H 33%)

Scheme 54. Catalytic reduction of (**114**).

Overall, these few examples demonstrate high synthetic potential of 1,2,5-trisubstituted cyclopent-3-en-1-ols (**110**) as stereodefined building blocks (containing 3 pre-installed contiguous stereocenters) for use in both total synthesis and drug discovery applications.

Cascade Claisen-Sakurai Reaction: Optimization and Mechanistic Studies

As was mentioned earlier, the Claisen-Sakurai sequence can be performed as a cascade utilizing Lewis acid as a promotor.[52,53] In attempt to optimize this cascade transformation and taking into account earlier efforts in the Cook group[41,156] as well as conditions reported by Paquette,[47] we subjected monosilylated allyl vinyl ethers to Lewis acidic conditions. It was found that for (**101- $SiMe_2Ph$**) the reaction was not efficient and provided mostly degradation products as well as by-products with trace amounts of the desired cyclopentenols (**103-$SiMe_2Ph$**) (Scheme 55). This outcome was observed for substrates with both alkyl and aryl groups at the allylic position. Allyl vinyl ethers (**101**) bearing $SiMe_3$ group provided similar results outside a single example that will be discussed later.[52,53]

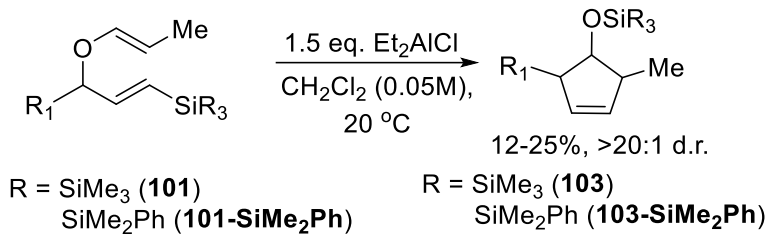

Scheme 55. Cascade Claisen-Sakurai reaction catalyzed by Et_2AlCl.

Further optimization studies that included temperature screening (-78°C, -30°C, -15°C and 0°C) and solvent screening (CH_2Cl_2, DCE, toluene, chlorobenzene, trifluorotoluene and p-xylene) did not result in improved reactivity. Modulation of the Lewis acid also did not prove beneficial, and often resulted in complete decomposition and/or an absence of desired product. Lewis acids tested included: $EtAlCl_2$, $AlCl_3$, $AlMe_3$, $BF_3{\cdot}OEt_2$, TMSOTf, $AlMe_2OTf$, $AlMe_2OCOCF_3$, $AlMe(2,6\text{-}tBuOPh)_2$, $AlMe_2OCOPh$, $AlMe_2(p\text{-}CH_3PhSO_2NH)$, $AlCl(4\text{-}MeOPh)_2$, $Al(OiPr)_3$, and $(i\text{-}Bu_2Al)_2O$.

To rationalize the observed results, we investigated the mechanism of the cascade catalyzed by Et_2AlCl using DFT with (**101q- $SiMe_2Ph$)** as a model substrate. Possible transformations that might occur within the cascade were considered based on the crude NMR and isolated by-products.

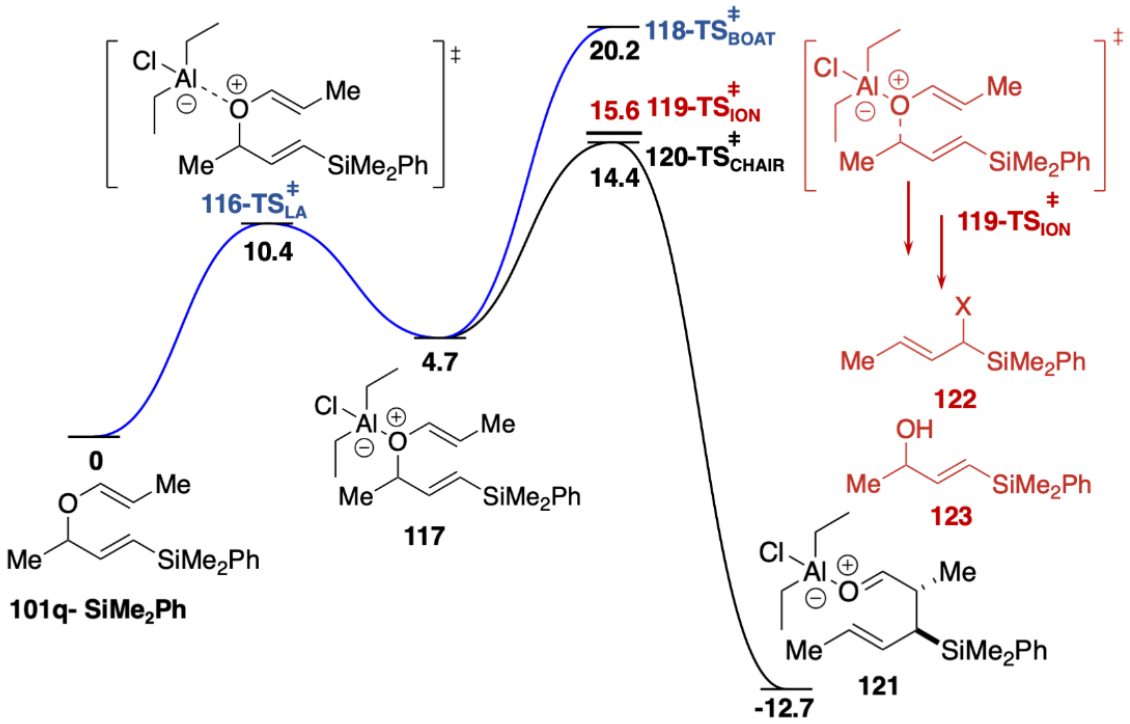

Figure 6. Potential energy surface showing the mechanism of the Claisen rearrangement calalyzed by Et_2AlCl and other competing pathways. Calculations were done at C-PCM (dichloromethane)-B3LYP/6-31+G(d). Energies are in kcal/mol.

It was found that the main competitive pathway during the Claisen rearrangement is allyl vinyl ether ionization. Although, the transition state for ionization **119-TS$_{ION}$** was predicted to be 1.2 kcal/mol higher than **120-TS$_{CHAIR}$** (Figure 6), the corresponding allylic alcohol (**123**) could be clearly identified in crude reaction mixture.

Another by-product that manifests up to 50% of the crude material (NMR data) is ethylated alcohol (**130**). Indeed, it was reported by Nozaki *et al.* that allyl vinyl ethers can undergo [3,3] sigmatropic rearrangement followed by methylation, alkynylation, alkenylation, and reduction when treated with R_3Al Lewis acids.[157,158] Originally, it was suggested that this by-product is formed as a result of aldehyde alkylation by Et_2AlCl *via* **124-TS$_{ALK}$** and represents a competing pathway to carbocyclization **125-128-TS**. However, DFT predicted a significant

difference between transition state energies for these transformations and the Sakurai ring-closures described previously ($\Delta\Delta G^{\ddagger}$ = 7.6 kcal/mol) (Figure 7). Another possible route leading to the formation of this by-product could be a concomitant [3,3] sigmatropic rearrangement/nucleophile addition as proposed by Nozaki *et al.*[158]

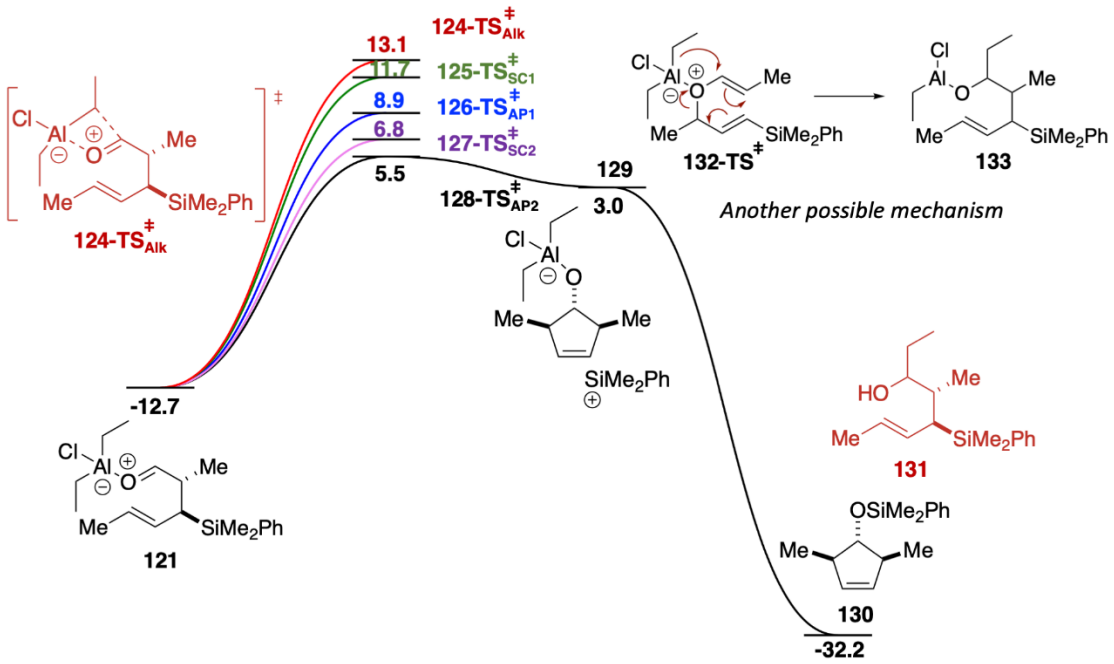

Figure 7. Potential energy surface showing the mechanism of Sakurai intramolecular allylation catalyzed by Et_2AlCl and other competing pathways. Calculations were done at C-PCM (dichloromethane)-B3LYP/6-31+G(d). Energies are in kcal/mol.

To circumvent this issue, we tested *iso*-butyl substituted aluminum Lewis acids which have lower alkylation ability, however, in these cases reduction by-products were produced. Less nucleophilic (Bn_2AlCl) was synthesized and tested, however no carbocyclization product was observed.

In attempt to elucidate why some Lewis acids performed better than the others we analyzed the structures of complexes of allyl vinyl ether (**101q- $SiMe_2Ph$)** with $AlMe_3$, Et_2AlCl, $EtAlCl_2$, $AlCl_3$ optimized by DFT.

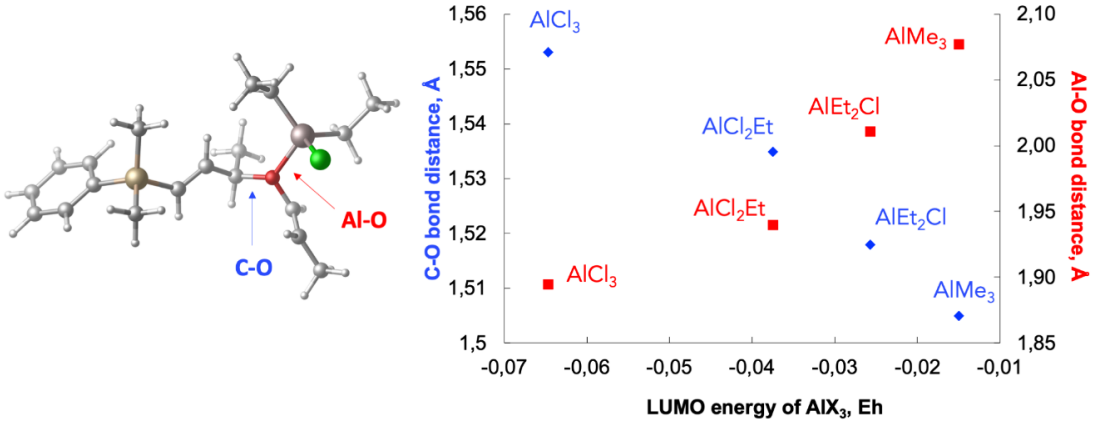

Figure 8. The relationship between LUMO energies of AlX_3 complexes and C-O and Al-O bond distances. Calculations were performed at C-PCM (dichloromethane)-B3LYP/6-31+G(d).

When C-O and Al-O bond distances measured in allyl vinyl ether-AlX_3 complexes were plotted against corresponding LUMO energies of AlX_3 complexes, it was found that as the LUMO energy decreases, C-O bond becomes shorter while Al-O becomes longer (Figure 8). Lewis acids leading to complexes with longer C-O bonds ($AlCl_3$, $AlCl_2Et$) experimentally resulted in starting material decomposition, while the use of $AlMe_3$ provided no cyclization product. We hypothesized that by calculating LUMO energies we could identify Al-based Lewis acid that would be an efficient promoter of the cascade Claisen-Sakurai reaction by comparing it with Et_2AlCl. Given that an array of Al-based Lewis acids were already tested experimentally, we explored Lewis acid-Lewis base pair adducts of the $AlCl_3$ as $AlCl_3$ was found to be the most efficient for promoting Sakurai cyclization in a stepwise reaction. Taking into account previous efforts in the Cook group,[41] various phosphine ligands, including mono- and bidentate variants

were tested as Lewis bases. Possible coordination modes were considered based on experimentally reported structures.[159] We calculated and tested experimentally several adducts and while proposed model based on LUMO energies did not show sighnificant predictive power, we identifyed $AlCl_3$-PPh_3 pair that was able to catalyze Claisen-Sakurai cascade (Scheme 56). Although full conversion was not achieved during the Sakurai step, the alkylation by-product was eliminated. Interestingly, the combination of $AlEt_2Cl$ and PPh_3 was previously reported to promote Claisen rearrangement of aliphatic allyl vinyl ethers without the deleterious alkylation step alluded to above.[158] Although the combination of the Lewis acid and Lewis base clearly has a pronounced effect on reactivity, no rationale was proposed by the authors. A possible explanation is that the reaction proceeds *via* transition state **134-TS** similar to one proposed by Nozaki *et al*.[158] with concomitant phosphine migration instead of the alkyl group (Scheme 56). The resulting intermediate (**135**) provides aldehyde (**102- $SiMe_2Ph$)**.

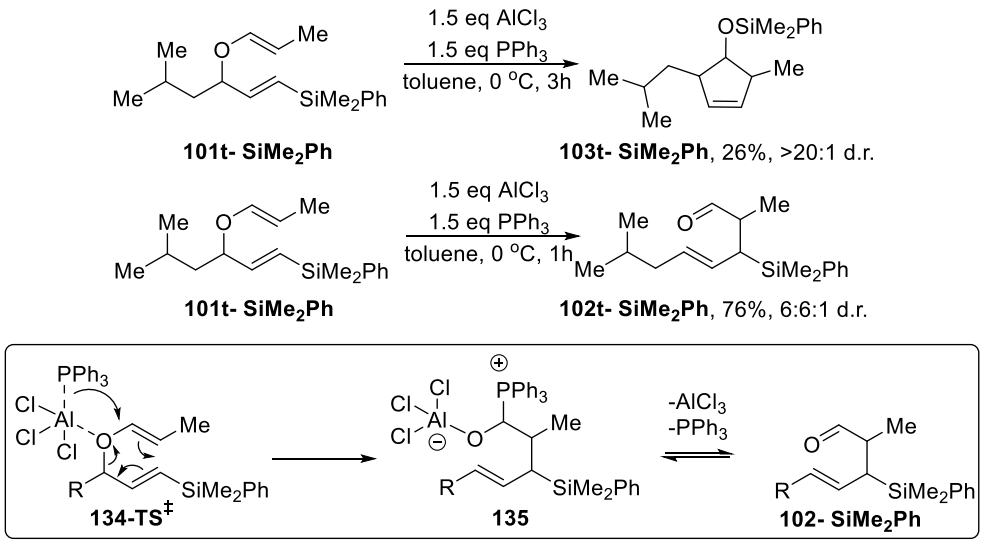

Scheme 56. The use of Lewis acid-Lewis base pair $AlCl_3$-PPh_3 as a catalyst for the cascade Claisen-Sakurai reaction. Yields were measured by 1H NMR. For aldehyde d.r. represents [3.3]:[3.3]:[1.3] product ratio.

Cascade Claisen-Sakurai Reaction: Example of Successful Cascade Transformation

Reprinted (adapted) with permission from Stankevich, K. S.; Cook, M. J. A Highly Stereospecific Claisen–Sakurai Approach to Densely Functionalized Cyclopentenols. *J. Org. Chem.* **2022**, *87* (18), 12250–12256. DOI: 10.1021/acs.joc.2c01397. Copyright 2022 American Chemical Society. http://pubs.acs.org/articlesonrequest/AOR-VKSAE6YWPREVKNJDRRJT

As was alluded earlier, the silylated allyl vinyl ethers (**101**) proved unstable under Lewis acidic conditions resulting in numerous degradation products. These decomposition pathways occurring during the cascade were problematic for both alkyl and aryl substituents providing only trace amounts of cyclized products. Nevertheless, when OBn substituted allyl vinyl ether (**101c**) was treated with Et_2AlCl at 0 °C, a cascade Claisen-Sakurai reaction was observed providing the product (**110c**) in 52% yield (Scheme 57).

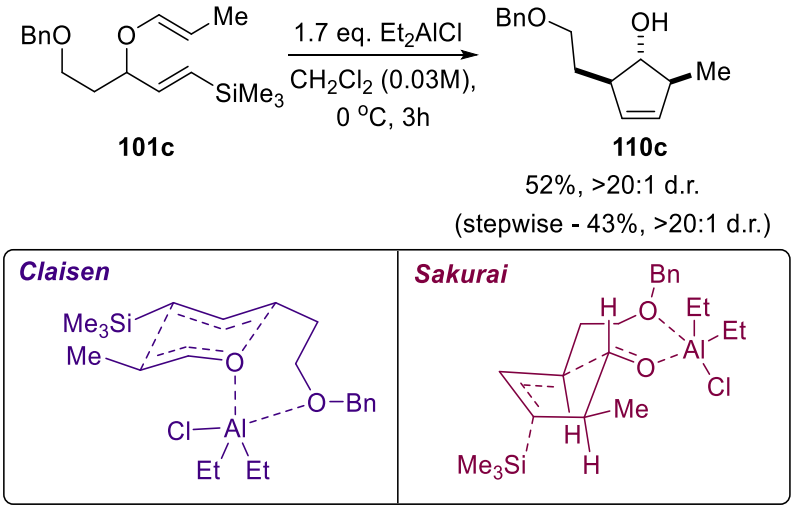

Scheme 57. Cascade Claisen-Sakurai of benzyl ether (**101c**).

Furthermore, this reaction resulted in both the same stereochemical ratio and major diastereoisomer. Indeed, this reaction was more efficient than the stepwise procedure described

in Scheme 48, with minimal degradation observed. The dichotomy between (**101c**) and other vinyl ethers can be rationalized *via* an internal Lewis acid-base interaction between the aluminum and the benzyl ether. This interaction provides a two-point binding that both lowers the Lewis acidity, and thus, prevents ionization, and pre-organizes the substrate closer to the reactive conformation. A similar two-point binding motif can also be invoked for the Sakurai ring-closure, providing the same (*anti, anti*) stereoisomer of (**110c**).[52,53]

Conclusions

In conclusion, we have developed a highly stereoselective and general method for the synthesis of substituted cyclopentenols. This reaction can tolerate a wide range of electronic and steric environments, producing the cyclized products in >20:1 d.r. Alongside the scope and synthetic utility, we also investigated the mechanism of this reaction, with the origin of the stereoselectivity of particular interest. Our findings highlight a complex dynamic equilibrium which is under Curtin-Hammett control. Computations and experimental findings suggest the major stereoisomer is the *anti*, *anti*-isomer which results from an antiperiplanar *anti*-S_E' mechanism. We also demonstrated the first example of a Claisen-Sakurai cascade reaction where multiple stereocenters are formed with excellent levels of stereocontrol. This example is mediated by an internal Lewis acid-base interaction that provides high reactivity and selectivity. We also demonstrated a rational approach towards Lewis acid search that resulted in finding

Lewis acid – Lewis base pair that provided the desired product in a cascade fashion albeit full conversion wasn't achieved. The potential applications of these methods are numerous in both synthetic and medicinal chemistry as was demonstrated by examples of further functionalization of 1,2,5-trisubstituted cyclopent-3-en-1-ols.[52,53]

The future directions in this area could include further investigation of the reaction scope (Scheme 58). For example, one could explore disubstitution at the allylic position (preliminary studies done in the Cook group[41]) as well as attempt to introduce various substituents at positions 1, 2 and 5 to access cyclopent-3-en-1-ols with all-carbon quaternary stereocenters (**137**) (Scheme 58).

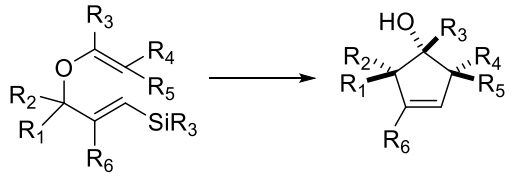

136 **137**

Scheme 58. Introducing further substitution in the ring.

Routes that allow to install various substituents on the allyl group include titanium–zinc methylenation (olefination),[160] reacting allylic alcohol with dimethyl acetal in refluxing benzene containing a catalytic quantity of p-toluenesulfonic acid[47] and Wittig reaction.[161] Vinyl moiety can be functionalized *via* Cu-catalyzed C-C coupling of 3-(trimethylsilyl)-2-propyn-1-ol with Grignard reagent with subsequent alcohol oxidation and Grignard addition.[162,163]

In addition, the formation of spirocycles (**140**), which was attempted in the Cook group previously,[41,156] could be further developed. Substrate variants (**141**-**144**)[164] leading to bicyclic product (**145**) could also be explored (Scheme 59).

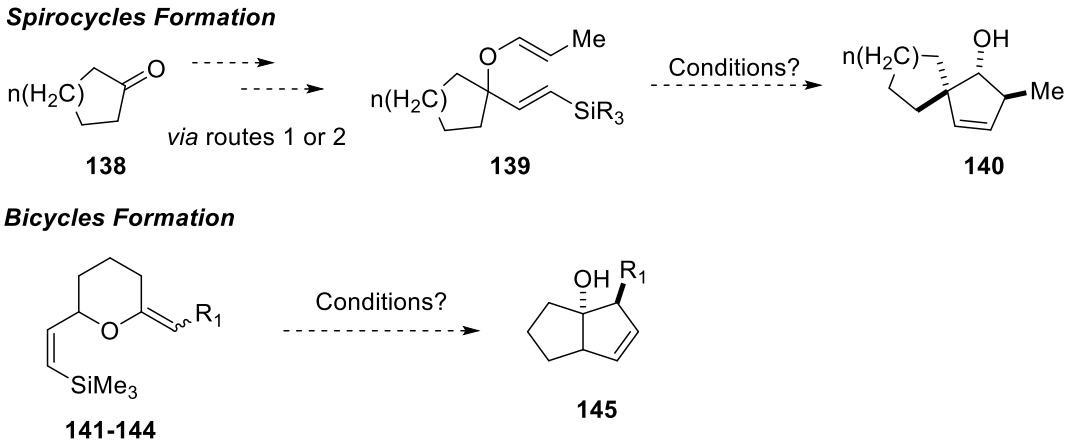

Scheme 59. Formation of spirocycles and bicycles.

Stereodivergent Approach to Methylene Cyclopentanols

Herein, the development of Claisen-Sakurai methodology to access 1,2,5-trisubstituted 3-methylene cyclopentan-1-ols is described. To form these products, we utilized allyl vinyl ethers containing a methylene silane group at the 5-positon (**146**). Analogous to transformation described earlier, these substrates were subjected to either a one-pot stepwise or a cascade Claisen-Sakurai reaction (Scheme 60).[52,53] This methodology provides a stereodivergent route to 1,2,5-trisubstituted 3-methylene cyclopentan-1-ols (**148-149**), with the stereochemical outcome controlled by both Claisen rearrangement and Sakurai-carbocyclization.

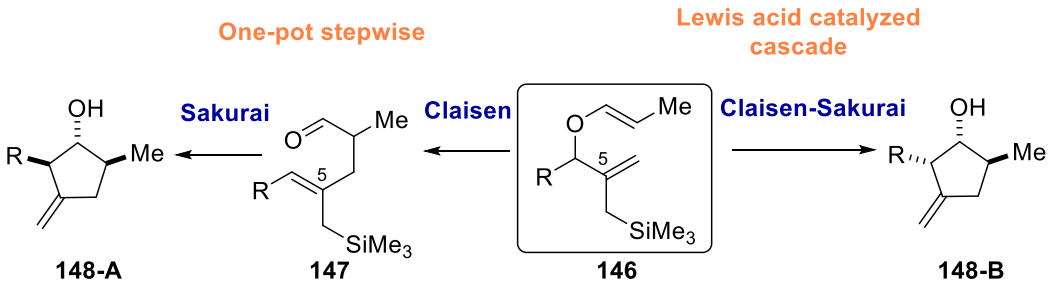

Scheme 60. Stereodivergent Claisen-Sakurai approach to stereochemically dense methylene cyclopentanols.

Starting Material Preparation

The Claisen-Sakurai approach to methylene cyclopentanols utilizes an allyl vinyl ether containing a methylene silane group at the 5-positon (**146**). We envisaged two distinct synthetic routes to these substrates (Scheme 61-62). First route entails iodination of propargyl alcohol (**105**)[165] followed by O-allylation[45,138] which provides mono-iodo-diallyl ether (**150**) that further undergoes Kumada-type coupling[166] followed by iridium(I) catalyzed isomerization[45] furnishing the allyl vinyl ether (**146**) (Scheme 61).

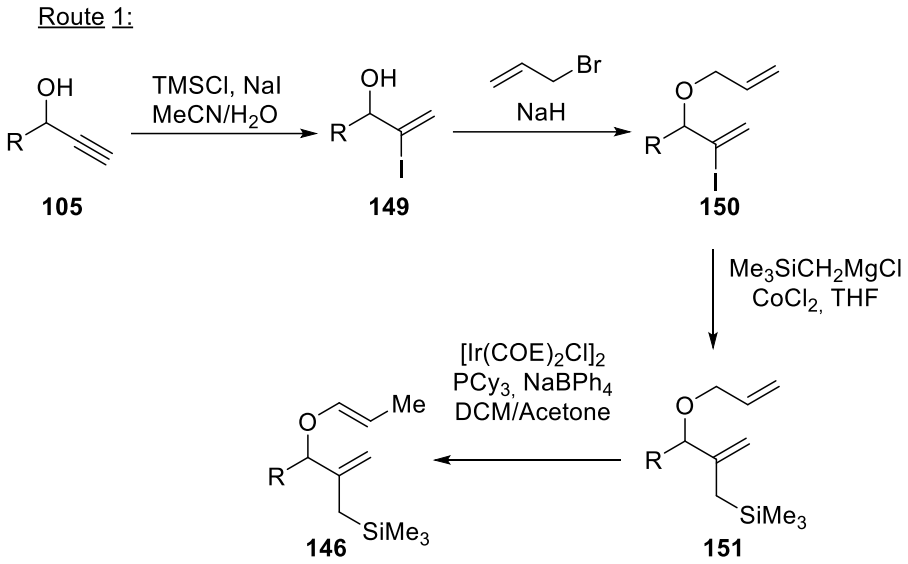

Scheme 61. Route 1 to allyl vinyl ether containing a methylene silane group at the 5-positon.

Alternatively, these allyl vinyl ethers can be prepared via a routes described by Trost (Scheme 62).[167–169] In this case, the requisite 2-bromo-3-(trimethylsilyl)-l-propene (**155**) can be obtained from 2,3-dibromopropene *via* Cu-catalyzed conjugate S_N2' addition of the $SiCl_3$ group, followed by exchange of Cl for CH_3 group using a methyl Grignard reagent.[170] The following O-allylation can be performed using two distinctive protocols[44,45,138,172] and, ultimately iridium(I) catalyzed isomerization[45] would provide the desired product (**146**)

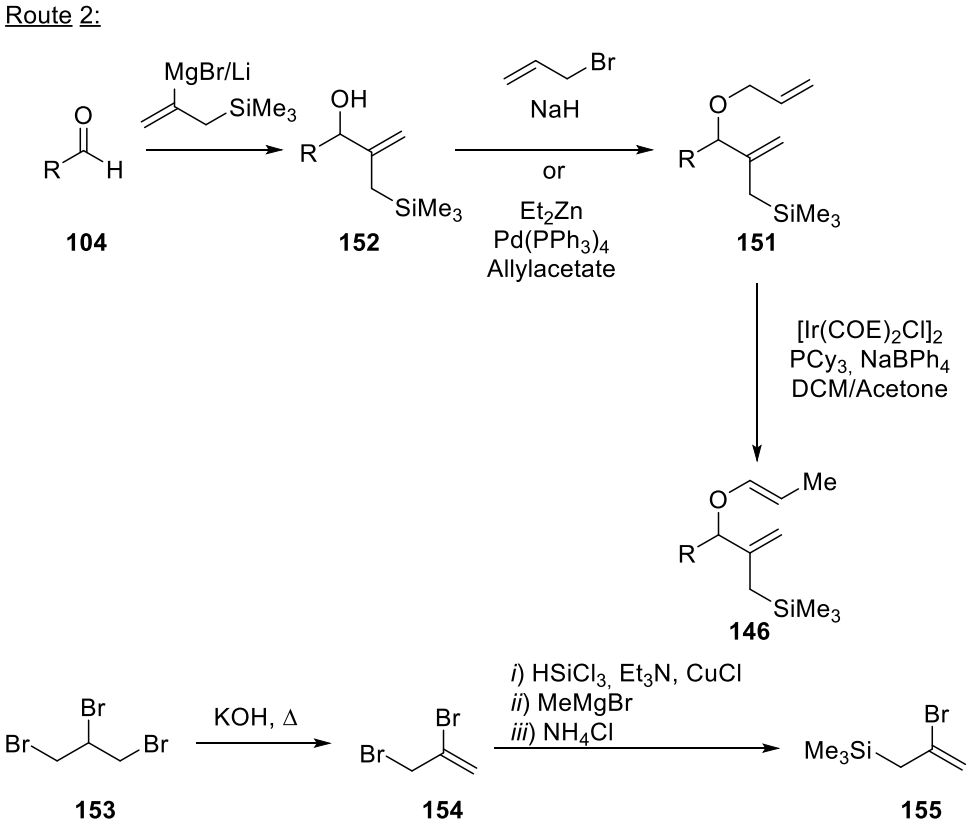

Scheme 62. Route 2 to allyl vinyl ether containing a methylene silane group at the 5-positon.

Experimental efforts have proven route 1 impractical (Scheme 63). Iodination[165] of alkyl substituted propargyl alcohol (**105s**) resulted in moderate yields due to competing iodination of the alcohol. Allylation[45,138] of (**149a**) also suffered from competing side reactions, such as the concomitant HI elimination to form an alkyne. Cobalt (II) chloride catalyzed Kumada-type coupling produced only trace amounts of product (**152a**), presumably, due to a steric hindrance derived from the substituent at the 3-position comparing to the reported examples.[166] Aryl substituted variant was not accessible *via* this route as corresponding iodopropenol (**149d**) was unstable and readily decomposed.

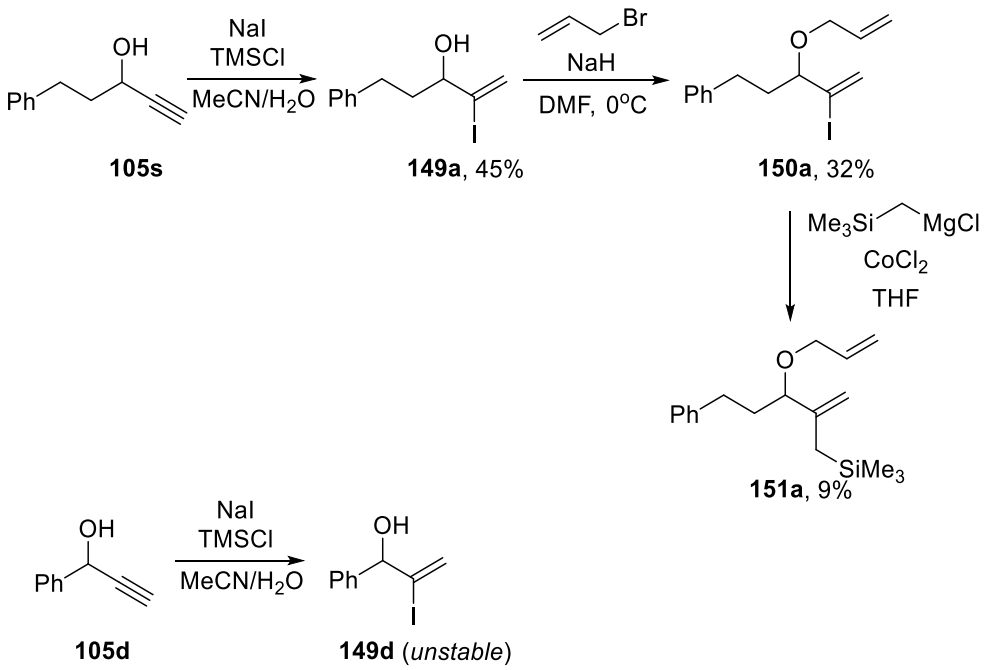

Scheme 63. Synthesis of allyl vinyl ethers containing a methylene silane moiety at the 5-positon *via* route 1 (selected examples).

In contrast, route 2 was found to be efficient in producing the requisite allyl vinyl ethers (**146**) with both alkyl and aryl substituents at the allylic position (Scheme 64-65). The synthetic sequence entailed the addition of β-lithiated allylsilane to an aldehyde to form allylic alcohol[170,171] followed by Pd-catalyzed O-allylation of corresponding Zn(II) alkoxide with allyl acetate[44,172] and iridium(I) catalyzed isomerization.[45] In this case, allylation *via* Williamson ether synthesis was impractical as strong basic conditions led to silane elimination.

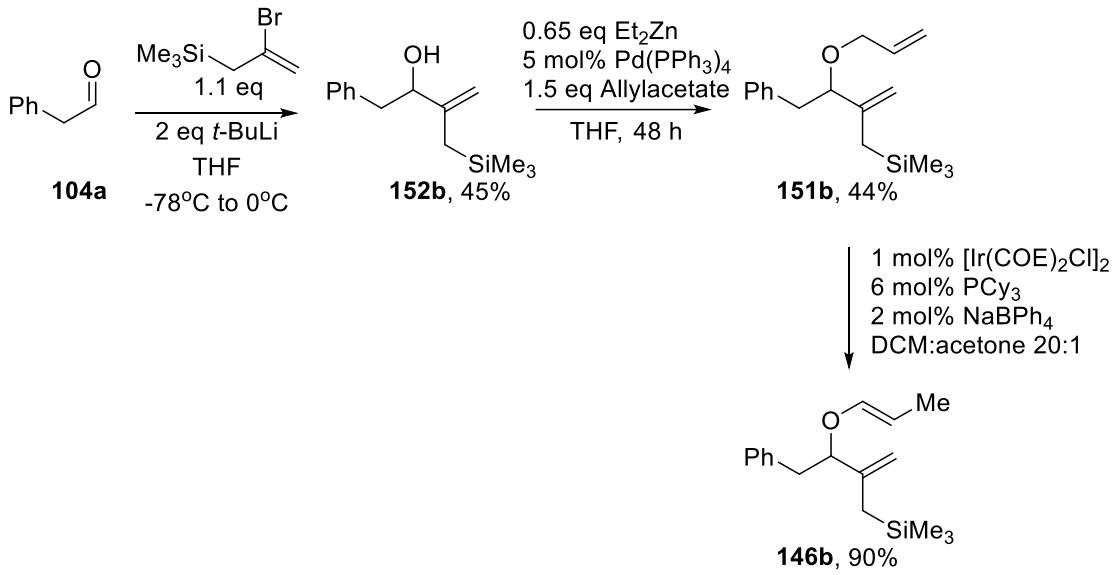

Scheme 64. Selected example of synthesis of allyl vinyl ethers containing a methylene silane moiety at the 5-positon with alkyl substituent at the allylic position. Average yields are shown.

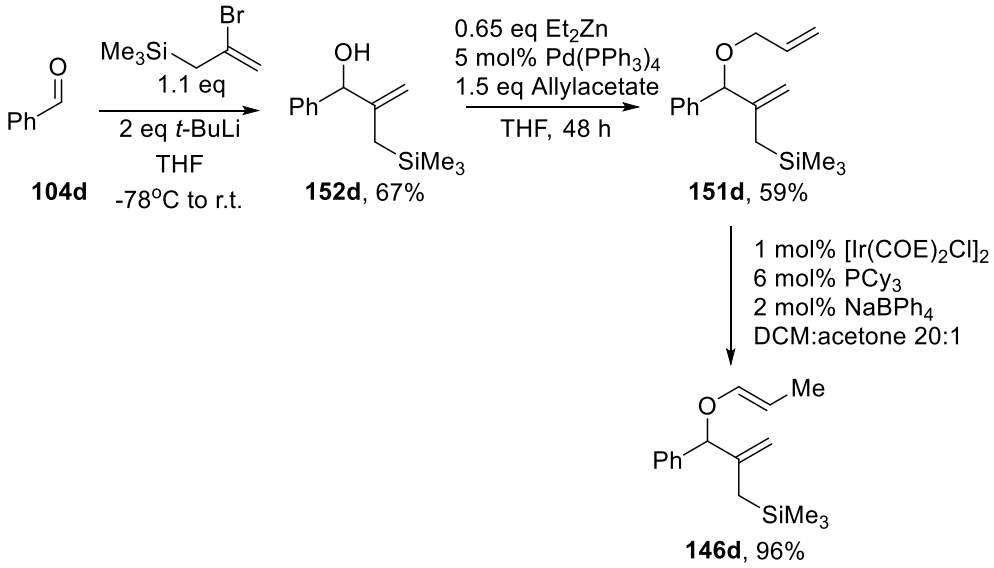

Scheme 65. Selected example of synthesis of allyl vinyl ethers containing a methylene silane moiety at the 5-positon with aryl substituent at the allylic position. Average yields are shown.

With these results in hand, we commenced our studies towards synthesis of stereochemically dense methylene cyclopentanols *via* Claisen-Sakurai approach.

Claisen-Sakurai Reaction: Stepwise and Cascade Methodology

We initially attempted to optimize Claisen-Sakurai reaction furnishing methylene cyclopentanols in a stepwise fashion utilizing phenyl substituted allyl vinyl ether (**146d**) as a substrate. We subjected (**146d**) to a thermal Claisen rearrangement at 90 °C, followed by the Lewis acid-promoted Sakurai-cyclization at a lower temperature. We examined a number of Lewis acids, solvents and temperatures to identify optimal conditions (Table 5). These reactions produce three diastereomeric products with moderate levels of selectivity. Unlike in previous transformation leading to cyclopentenols (**110**),[52,53] aluminum reagents were no longer the most effective Lewis acids (Entries 1-5). Among them, $EtAlCl_2$ showed the best performance providing only moderate yield of the cyclized product (Entry 2). Reactions mediated by TMSOTf and $InCl_3$ were ineffective: the former led to starting material decomposition while the latter resulted in no conversion (Entries 6, 7 and 9). Among the Lewis acids tested, optimal yields were observed with $SnCl_4$ and $BF_3{\cdot}OEt_2$, with $BF_3{\cdot}OEt_2$ providing better diastereoselectivity (Entries 8 and 12). Screening of other BF_3 adducts identified that $BF_3{\cdot}MeCN$ furnished cyclization product with similar yield to $BF_3{\cdot}OEt_2$ (Entries 18-20). Upon consideration of these results, we further focused our efforts on optimizing reaction efficiency and diastereochemical outcome with $BF_3{\cdot}OEt_2$ as a Lewis acid. Unfortunately, both temperature and solvent polarity variation did not result in further improvement of diastereoselectivity or yield (Entries 10-17). Therefore, we considered 1.5 eq $BF_3{\cdot}OEt_2$ at -20 to -5 °C optimal (Entry 12). With these results in hand, we embarked on optimizing this transformation as a cascade.

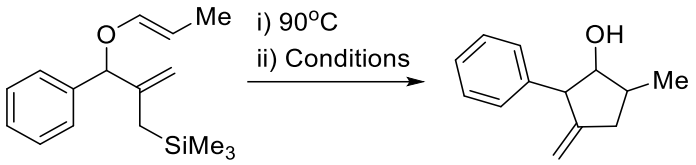

146d **148d**

Entry	Lewis acid	Eq.	Solvent	T, °C	Yield, %	d.r. (A:B:C) [c]
1	Et_2AlCl	1.5	Chlorobenzene	20 [a]	14 [c]	3.4:(0.0):1.0
2	$EtAlCl_2$	1.5	Chlorobenzene	20 [a]	34 [d]	3.6:1.2:1.0
3	$EtAlCl_2$	1.5	Chlorobenzene	0 [a]	31 [c]	3.8:1.9:1.0
4	$EtAlCl_2$	1.5	Chlorobenzene	-15 [a]	38 [c]	2.4:1.6:1.0
5	$AlCl_3$	1.5	Chlorobenzene	20 [a]	23 [c]	3.6:2.7:1.0
6	$InCl_3$	1.5	Chlorobenzene	20	0 [f]	n/a
7	$InCl_3$/TMSCl	5 mol%	Chlorobenzene	20	0 [f]	n/a
8	$SnCl_4$	1.5	Chlorobenzene	-20 to -5 [b]	50 [d]	4.5:4.5:1.0
9	TMSOTf	1.5	Chlorobenzene	-20	0 [g]	n/a
10	$BF_3{\cdot}OEt_2$	1.5	Chlorobenzene	20 [a]	42 [c]	3.5:1.6:1.0
11	$BF_3{\cdot}OEt_2$	1.0	Chlorobenzene	-20 to -5 [b]	52 [d]	4.7:1.6:1.0
12	$BF_3{\cdot}OEt_2$	1.5	Chlorobenzene	-20 to -5 [b]	54 [d]	5.5:2.0:1.0
13	$BF_3{\cdot}OEt_2$	1.5	Chlorobenzene	-42 [h]	40 [d]	5.6:2.7:1.0
14	$BF_3{\cdot}OEt_2$	1.5	Toluene	-20 to -5 [b]	40 [c]	3.1:1.7:1.0
15	$BF_3{\cdot}OEt_2$	1.5	Trifluorotoluene	-20 to -5 [b]	40 [c]	5.0:2.5:1.0
16	$BF_3{\cdot}OEt_2$	1.5	Acetonitrile [e]	-20 to -5 [b]	38 [c]	3.2:1.0:(0.0)
17	$BF_3{\cdot}OEt_2$	1.5	Chlorobenzene/Acetone	-20 to -5 [b]	20 [c]	3.4:1.6:1.0
18	$BF_3{\cdot}SMe_2$	1.5	Chlorobenzene	-20 to -5 [b]	22 [c]	2.6:1.9:1.0
19	$BF_3{\cdot}MeCN$	1.5	Chlorobenzene	-20 to -5 [b]	58 [d]	5.8:2.7:1.0
20	$BF_3{\cdot}NH_2Et$	1.5	Chlorobenzene	-20 to -5 [b]	0 [f,i]	n/a

Table 5. Optimization studies for stepwise synthesis of methylene cyclopentanols.[a] 30 min; [b] 1h; [c] determined by ^{1}H NMR; [d] isolated yield; [e] Claisen rearrangement done at 70 °C; [f] starting material recovered; [g] starting material decomposed; [h] 2.5 h; [i] $BF_3{\cdot}NH_2Et$ is not soluble in PhCl.

To optimize cascade rearrangement of (**146d**) we utilized data-driven approach. Thus, we compared the Lewis acids that showed the best performance during optimization studies of the Sakurai-cyclization step (Table 5, Entries 2, 8, 12 and 19) with the Lewis acids known to efficiently promote Claisen rearrangement of similar substrates described in literature. This allowed us to identify $EtAlCl_2$ and $BF_3{\cdot}OEt_2$ as the most promising candidates. While $BF_3{\cdot}OEt_2$

was found to be inefficient for this transformation (Table 6, Entry 7), 1.5 eq $EtAlCl_2$ furnished the desired product with good yield and moderate d.r. (Entry 1). Notably, the cascade transformation resulted in a switch of diastereoselectivity providing (**148d-B**) as a major product. Decreasing solvent polarity resulted in slight improvement of both yield and d.r. ratio (Entry 2). Temperature screening revealed clear dependence of diastereochemical outcome on reaction temperature, with -78 °C proven to be optimal (Entry 2-5). At 20 °C the formation of equal amounts of diastereomers (**148d-A**) and (**148d-B**) was observed (Entry 5). The use of basic additives deteriorated d.r. and the yield due to the limited conversion (Entry 6).

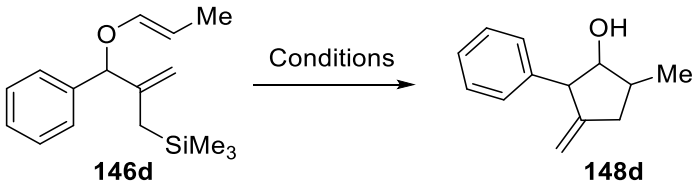

146d **148d**

Entry	Lewis acid	Eq.	Solvent	T, °C	Yield, %	d.r. (A:B:C) [a]
1	$EtAlCl_2$	1.5	DCM	-78 [b]	43 [c]	2.0:5.5:1.0
2	$EtAlCl_2$	1.5	Toluene	-78 [b]	49 [c]	1.9:6.4:1.0
3	$EtAlCl_2$	1.5	Toluene	-42 [d]	44 [c]	1.4:3.7:1.0
4	$EtAlCl_2$	1.5	Toluene	0 [e]	60 [c]	1.3:1.9:1.0
5	$EtAlCl_2$	1.5	Toluene	20 [f]	46 [c]	7.1:7.1:5.3:1.0
6	$EtAlCl_2{\cdot}PPh_3$	1.5	Toluene	-78 [g]	18 [h]	1.2:1.0:1.0
7	$BF_3{\cdot}OEt_2$	1.5	DCM	-78 [g]	0 [i]	n/a

Table 6. Optimization studies for cascade synthesis of methylene cyclopentanols.[a] Determined by ^1H NMR; [b] 50 min; [c] isolated yield; [d] 30 min; [e] 15 min; [f] 5 min; [g] 3 h, [h] conversion not full, remaining aldehyde isolated (27%, d.r. > 20:1), [i] starting material recovered.

Inspired by the discovered stereodivergent transformation, we attempted to elucidate the relative stereochemistry of two major diastereomers **A** and **B**. We were able to separate **A** and **B** using column chromatography and conducted NMR studies (Figure 9).

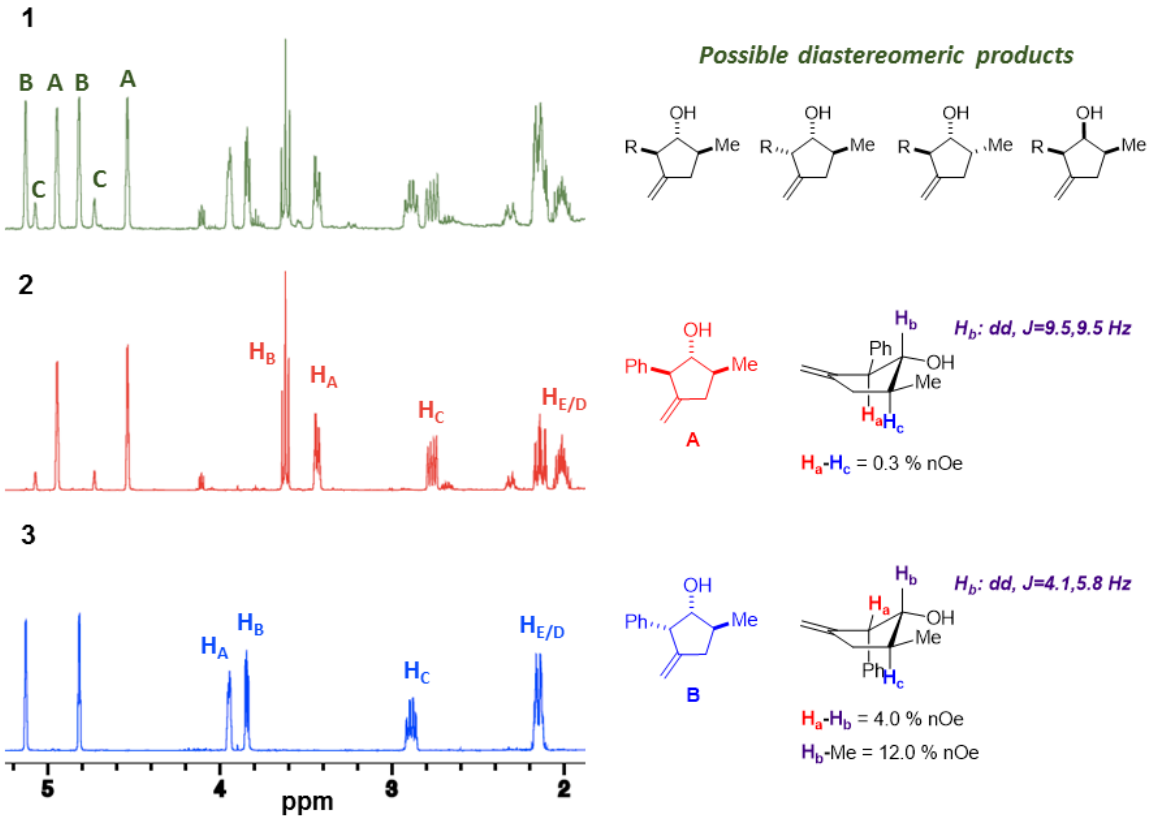

Figure 9. NMR spectra and results of 1D-NOESY experiment: 1) NMR spectrum of a mixture of diastereomers A, B and C; 2) NMR spectrum of diastereomer A and stereochemical assignment based on 1D-NOESY experiment; 3) NMR spectrum of diastereomer B and stereochemical assignment based on 1D-NOESY experiment.

In the case of diastereomer **A**, 1D-NOESY experiments showed very weak correlation between H_a and H_c (Figure 9) and no correlation between H_a and H_b, and H_b and H_c. Similarly, to the cyclopentenol product (**110j**), a lack of interaction between the protons suggests distant spatial positioning, which can be achieved within 5-membred ring in *anti-*, *anti-* configuration.[52,53,151] In contrast, for diastereomer **B** a strong correlation between H_a and H_b and H_b and Me was observed indicating that H_a, H_b and Me are on the same side of the ring (Figure 9).[151] Therefore, diastereomer **B** was assigned as *syn-*, *anti-*.

With these results in hand, we continued our studies by investigating the effect of substituent at the allylic position of the allyl vinyl ether on the reaction outcome.

First, we probed the substrate scope for a stepwise rearrangement (Scheme 66). The obtained results revealed strong effect of both steric and electronic environments on the reaction stereochemical outcome. A certain trend could be observed among alkyl variants; in particular, less bulky CH_2CH_2Ph (**148a-A**) and Bn (**148b-A**) groups result in moderate selectivity comparing to bulkier Cy (**148c-A**). In case of aryl substituted compounds, electronic effects seem to play a major role as having π-donating σ-withdrawing group at the *ortho*-position in (**148e-A**) resulted in significant d.r. improvement.

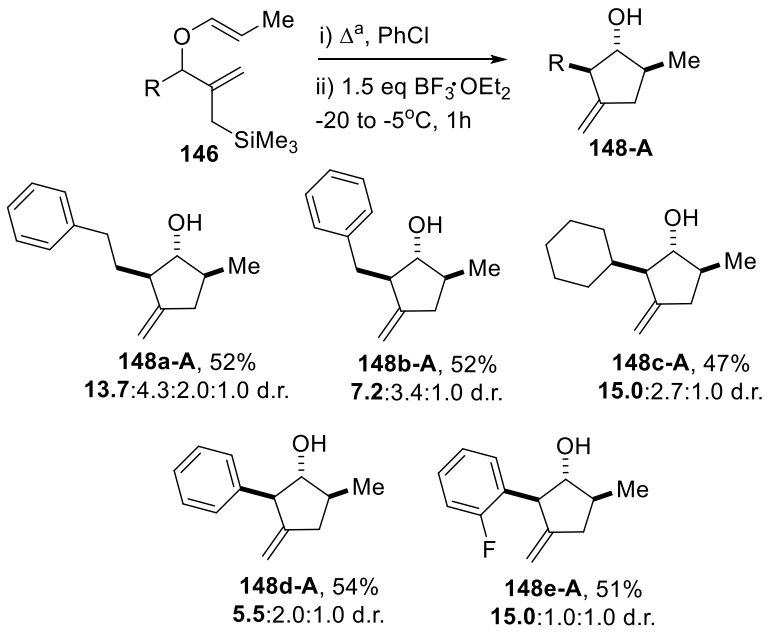

Scheme 66. Substrate scope for stepwise approach to methylene cyclopentanols.[a-c a] (**148a-c-A**) 110 °C, (**148d-e-A**) 90 °C; [b] Isolated combined yields; [c] Determined by ^{1}H NMR analysis.

The cascade transformation was also found to be sensitive to the substituent at the allylic position of (**146**). Similar to stepwise approach, for the alkyl substituted variants diastereochemical outcome was mainly dependent on the sterics of R group with bulkier

substituents leading to products with improved d.r. When aryl substitued compounds were subjected to the reaction, allyl vinyl ether (**146e**) bearing *ortho*-substitued phenyl ring furnished the product (**148e-B**) with lower d.r. suggesting that in this case electronic effects were prevalent in determining the diastereochemical outcome. Notably, Cy substituted substrate provided the same major product in both stepwise and cascade rerrangement.

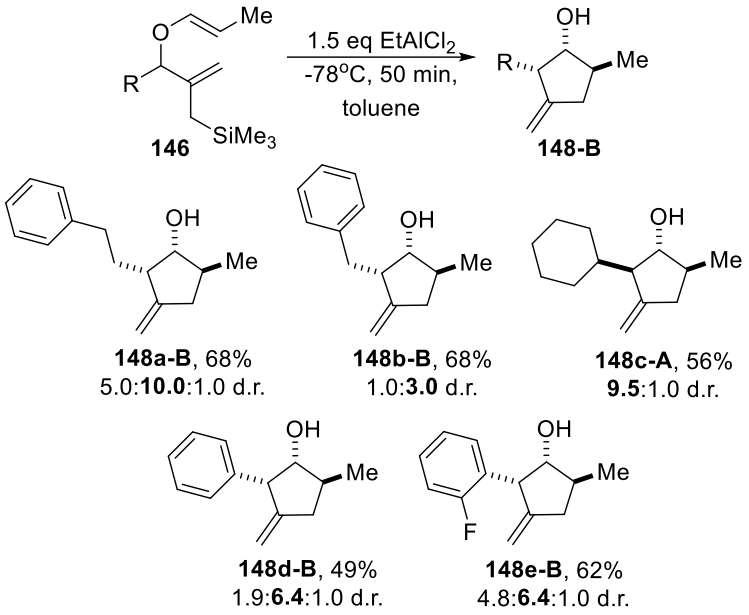

Scheme 67. Substrate scope for cascade approach to methylene cyclopentanols.

To further illustrate the substituent effect on the diastereochemical outcome of the reaction, we conducted cascade trasformation of (**146d**) and (**146e**) at higher temperature (Scheme 68). As was alluded earlier, reaction temperature has a pronounced effect on diastereomeric ratio. While (**146d**) still provided excess of **B** at 0 °C albeit with lower d.r., (**146e**) demonstrated a flip in diastereoselectivity furnishing **A** as a major product.

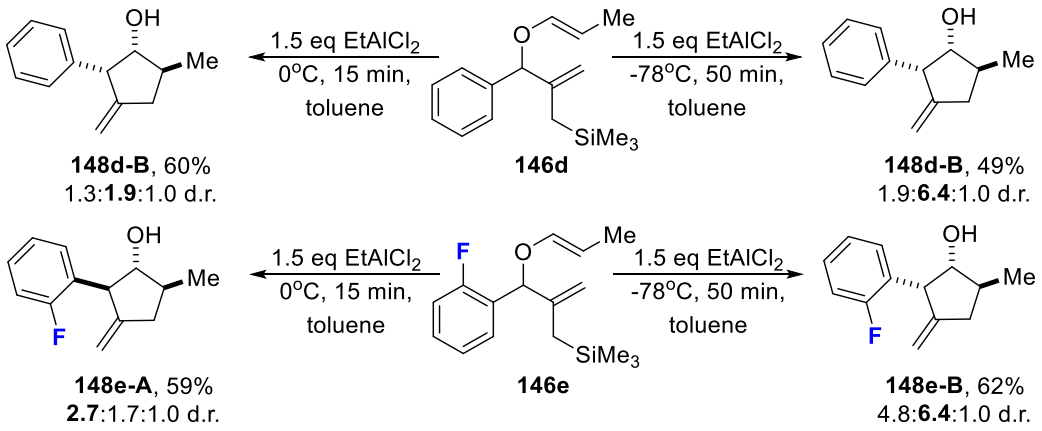

Scheme 68. Effect of temperature and substrate electronics on for cascade synthesis of methylene cyclopentanols.

The results obtained were both promising and intriguing which led us towards investigation of the mechanism of this trasformation in attempt to elucidate the origin of diastereoselectivity in each case.

Mechanistic Studies

We first investigated the mechanism of thermal Claisen rearrangement. In this case, alongside with chair and boat transition states where R group is equatorial, we need to consider their conformers where R group is axial (Scheme 69). The former would result in (*Z*)-alkene, whereas the latter would provide the (*E*)-alkene.[42] These (*E*) and (*Z*) isomers will produce diastereomers during the Sakurai cyclization (if they react *via* the same mechanism), therefore understanding the factors that control their formation is important.

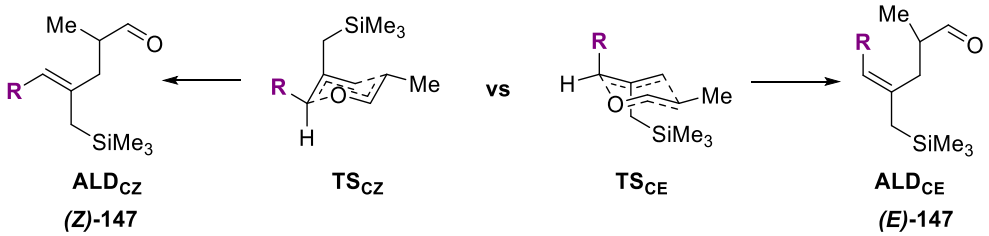

Scheme 69. Competing chair transition states and corresponding products.

The potential energy surface of the thermal Claisen rearrangement of (**146d**) demonstrates that the reaction is also under Curtin-Hammett control, and therefore would proceed *via* the overall lowest TS, which is the chair with an equatorial R group **TS$_{CZ}$** (Figure 10). The boat transition states (**TS$_{BZ}$, TS$_{BE}$**) were higher in energy, compared to chair transition states in all cases (**TS$_{CZ}$, TS$_{CE}$**), which is in agreement with previous reports on the thermal allyl-vinyl ethers rearrangement.[57–61] Therefore, we focused our studies on examining competing chair transition states for compounds (**146a-e**) (Table 7).

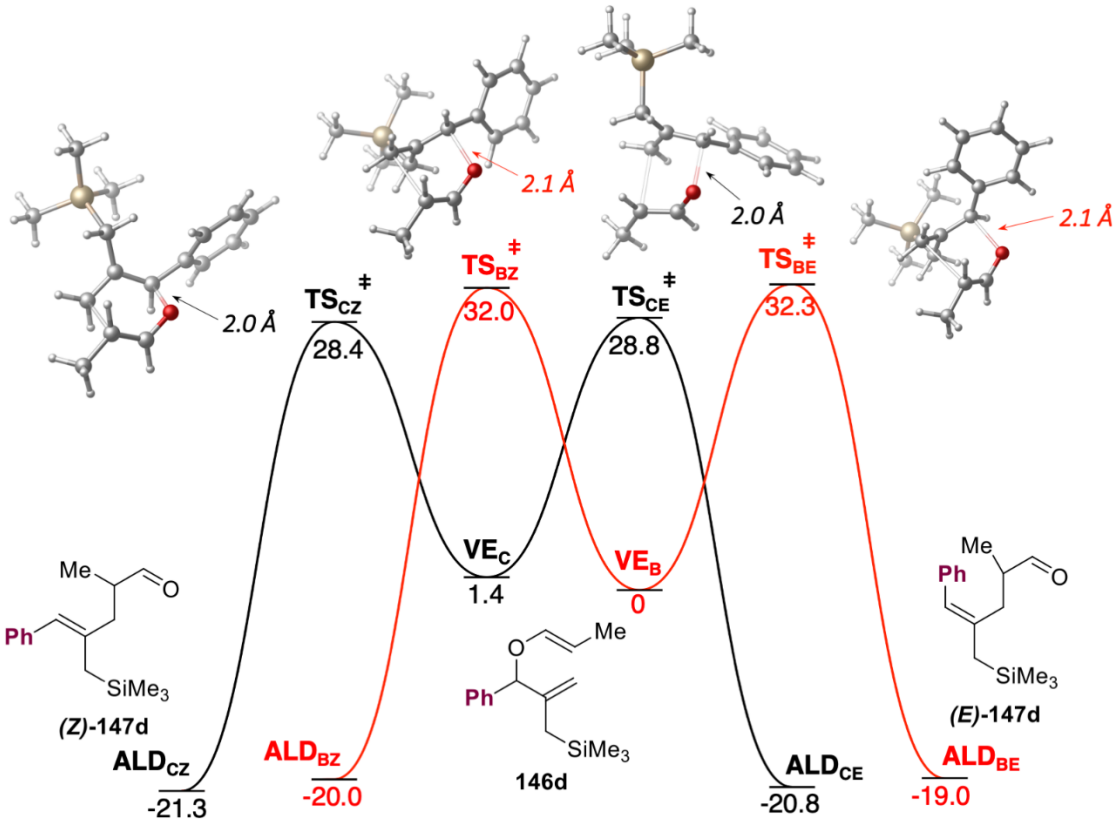

Figure 10. Potential energy surface of the thermal Claisen rearrangement showing Curtin-Hammett equilibrium between two conformations of the allyl vinyl ether (**146d**) leading to the chair and boat transition states. Calculations were performed at C-PCM (chlorobenzene)-ωB97XD/6-311++G(2d,2p)//C-PCM (chlorobenzene)-B3LYP/6-31+G(d). The quasi-harmonic Gibbs Free energies are reported at 363.15 K and 1 mol/L standard state.

The computational results mirror the trend observed experimentally, with (*Z*)-isomer being the major product in most cases, albeit with moderate selectivity (Table 7). Indeed, in this transformation one could envision a preference towards (*Z*)-product as it allows to put R in equatorial position in corresponding transition state, thus avoiding $A^{1,3}$-strain. It was observed that the sterics of R group has a major effect on diastereochemical outcome among alkyl substituted variants. While both CH_2CH_2Ph (**146a**) and Bn (**146b**) provide (*Z*)-isomer as a major product, bulky Cy results in a switch of diastereoselectivity furnishing (*E*)-alkene. This can be rationalized by considering the increasing $A^{1,2}$-strain between Cy and methylene silane moiety destabilizing TS_{CZ}, leading to a preference for TS_{CE}.

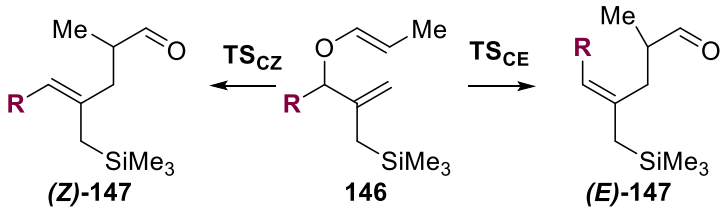

Allyl Vinyl Ether	$\Delta\Delta G_{E/Z}$ pred.[c], kcal/mol	(E)/(*Z*) ratio pred.	$\Delta\Delta G_{E/Z}$ obs.[c], kcal/mol	(*E*)/(*Z*) ratio obs.
146a (R=CH_2CH_2Ph)[a]	-0.9	1:3.3[d]	-0.5	1:2
146b (R=Bn)[a]	-1.1	1:4.2[d]	-0.5	1:2
146c (R=Cy)[a]	+1.0	3.7:1[d]	+0.5	2:1
146d (R=Ph)[b]	-0.4	1:1.7[e]	-0.1	1:1.1
147e (R=2-FPh)[b]	-1.6	1:9.2[e]	-1.1	1:4

Table 7. Energy differences ($\Delta\Delta G_{E/Z}$) between competing chair transition states in thermal Claisen rearrangement of (**146a-e**) calculated at C-PCM (chlorobenzene)-ωB97XD/6-311++G(2d,2p)//C-PCM (chlorobenzene)-B3LYP/6-31+G(d) and experimentally observed (*E*)/(*Z*) ratio.s [a] The quasi-harmonic Gibbs Free energies are reported at 383.15 K and 1 mol/L standard state; [b] The quasi-harmonic Gibbs Free energies are reported at 363.15 K and 1 mol/L standard state; [c] $\Delta\Delta G_{E/Z} = \Delta G(TS_Z) - \Delta G(TS_E)$; [d] At 383.15 K; [e] At 363.15 K.

The enhanced selectivity observed for the rearrangement of 2F-Ph (**146e**), compared to Ph (**146d**), can be rationalized by a difference in overall dipole moments of TS_{CZ} and TS_{CE}. In case of Ph (**146d**), computations predict similar dipole moments (3.4 *D*) for both TS_{CZ} and TS_{CE}, whereas for 2F-Ph (**146e**) calculated dipole moments of TS_{CZ} and TS_{CE} are 3.0 *D* and 5.0 *D*, respectively. This is due to the polarized C-F bond being roughly anti-parallel to the C-O bond, minimizing the overall dipole moment. Since Claisen rearrangement is conducted in chlorobenzene (ε = 5.7), which is non-polar, polarization effects will influence the energy of transition state significantly, resulting in improved selectivity.

Overall, both computational and experimental data show that thermal Claisen rearrangement does not provide high levels of geometric control, suggesting that both (*E*) and (*Z*) alkene isomers undergo Sakurai-carbocyclization.

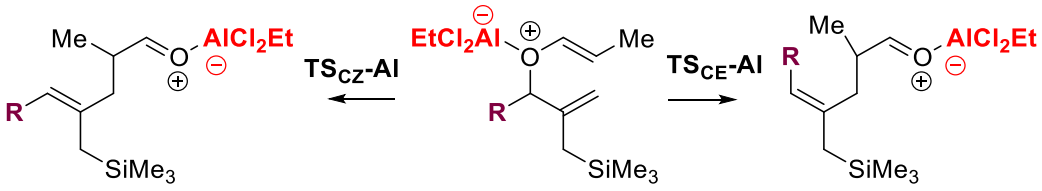

(Z)-147-EtAlCl$_2$ 146-EtAlCl$_2$ *(E)*-147-EtAlCl$_2$

Allyl Vinyl Ether	$\Delta\Delta G_{E/Z}$[b], kcal/mol	(E)/(*Z*) ratio pred.[c]
146a-EtAlCl$_2$ (R=CH_2CH_2Ph)[a]	2.7	1060:1
146b-EtAlCl$_2$ (R=Bn)[a]	2.7	1060:1
146c-EtAlCl$_2$ (R=Cy)[a]	3.8	18100:1
146d-EtAlCl$_2$ (R=Ph)[a]	3.0	2298:1
146e-EtAlCl$_2$ (R=2-FPh)[a]	0.6	4.7:1

Table 8. Energy differences ($\Delta\Delta G_{E/Z}$) between competing chair transition states in $EtAlCl_2$-catalyzed Claisen rearrangement calculated at C-PCM (toluene)-ωB97XD/6-311++G(2d,2p)//C-PCM (toluene)-B3LYP/6-31+G(d). [a] The quasi-harmonic Gibbs Free energies are reported at 195.15 K and 1 mol/L standard state; [b] $\Delta\Delta G_{E/Z} = \Delta G(TS_Z) - \Delta G(TS_E)$; [c] At 195.15 K.

In contrast, $EtAlCl_2$-catalyzed Claisen rearrangement occurring during the cascade Claisen-Sakurai reaction is predicted to be highly selective. Computations suggest (*E*)-alkene to be a major product in all cases with >1000:1 selectivity in all but one case (Table 8).

It has been previously reported that Al-based Lewis acids can provide both *(Z)*- and *(E)*-selective Claisen rearrangements with very good discrimination of the two forms.[43] The preference towards *(Z)*- or *(E)*-alkene was shown to be dependent on both sterics and electronics of organoaluminum reagent. In our case, the predicted selectivity can be rationalized by destabilizing 1,2-steric interaction[43] between the R and $EtAlCl_2$ groups in **TSCZ-Al**, leading to a higher energy transition state (Scheme 70).

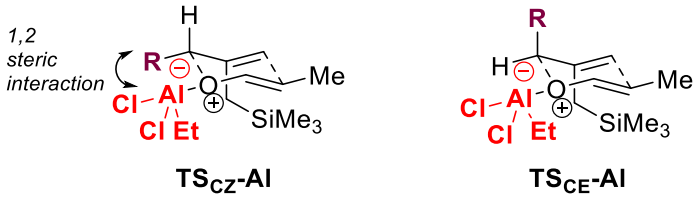

TS_{CZ}-Al TS_{CE}-Al

Scheme 70. Steric considerations for $EtAlCl_2$-catalyzed Claisen rearrangement.

With these results in hand, we further investigated the Sakurai-cyclization step. Analogous to the mechanism for endocyclic cyclopentenol formation,[52] two factors define the the stereochemical outcome of the Sakurai-cyclization: the internal diastereoselection and relative asymmetric induction (Scheme 71).[97,147,148] Since aldehyde moiety and the alkene can be in either antiperiplanar (AP) or synclinal (SC) orientations, internal diastereoselection would set the relative stereochemistry between the substituent R and OH functional group in the product.[52] The distinctive feature of this transformation is that both *(Z)*- and *(E)*- alkenes undergo cyclization, therefore four possible transition states leading to different stereochemical outcomes need to be considered (Scheme 71).

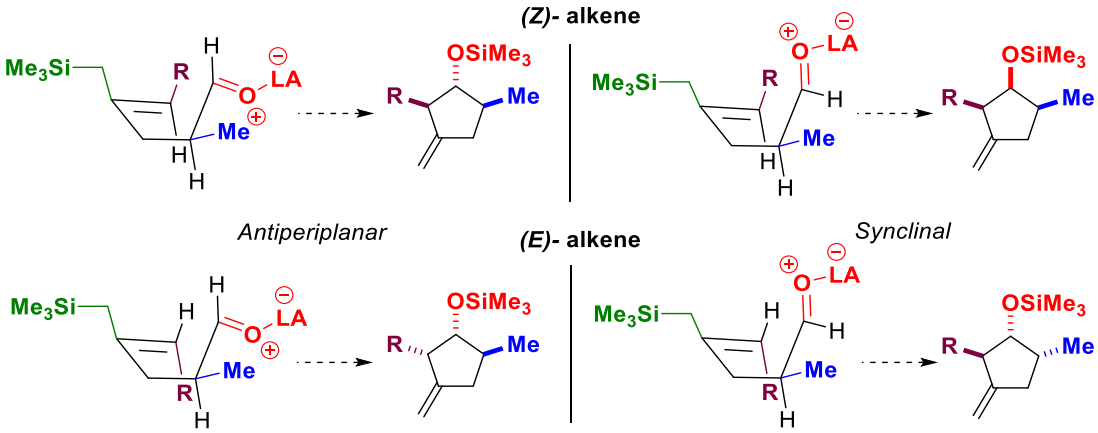

Scheme 71. Internal diastereoselection for *(Z)*- and *(E)*- alkene: conformers of LA-bound aldehyde and corresponding products.

The direction of Lewis acid-bound carbonyl attack on the alkene is described by the relative asymmetric induction. Thus, the alkene can be approached by electrophilic carbonyl either from the same (*syn*-S_E') or the opposite (*anti*-S_E') side as silicon electrofuge.[52 97,147,148] In this transformation, the position of silicon electrofuge is not determined by the direction of electrophilic attack since in methylene silane moiety TMS group can freely rotate around a single bond. Therefore, the relative stereochemistry between the OH and Me groups is determined by the direction of electrophilic attack during which silane can be both *syn*- and *anti*- (Scheme 72).

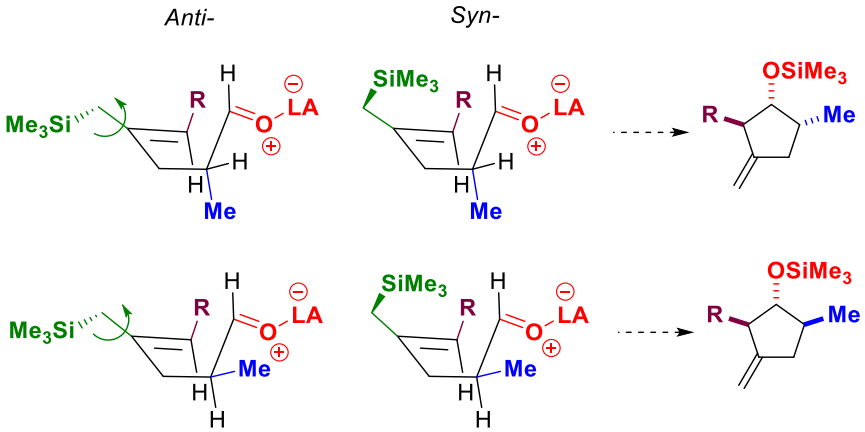

Scheme 72. Considerations for relative asymmetric induction: conformers and rotamers of LA-bound aldehyde.

One can envision that *syn*- orientations would result in very sterically hindered transition states (Scheme 72), while transition states with a *pseudo*-axial methyl group would suffer from a destabilizing *syn*-pentane interaction.[52] Indeed, DFT calculations predict these variants to be 3-7 kcal/mol higher in energy.

Therefore, the stereochemical outcome of the Sakurai-carbocyclization would be determined by internal diastereoselection and the possible transition states can be narrowed down to two combinations: *AP anti-S_E'* and *SC anti-S_E'*. When applied to *(Z)*- and *(E)*-alkene, this would result in four transition states providing four mechanistic routes (Scheme 73).

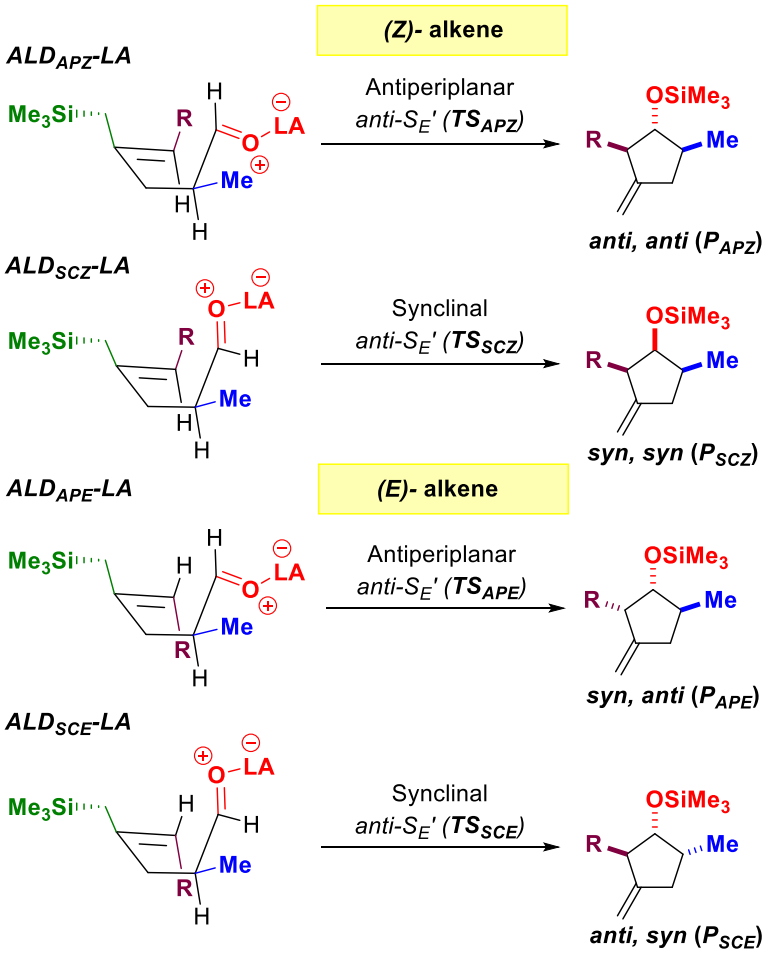

Scheme 73. Origin of stereoselectivity in methylene cyclopentanol synthesis.

We first considered the BF_3-mediated cyclization (*vide supra*) in the stepwise Claisen-Sakurai reaction using phenyl-substituted substrate (**147d-BF$_3$**) as a model. We performed calculations for transition states outlined earlier that lead to the formation of four diastereomeric products from *(Z)*- and *(E)*-alkenes (Scheme 73). It was found that the interconversion energy gaps between the BF_3-bound aldehyde reactive conformations (**ALD-BF$_3$**) of *(Z)*- and *(E)*-alkenes are within 2.1 kcal/mol and 0.4 kcal/mol, respectively. The transition state energies for the Sakurai-carbocyclization are significantly higher (9.7-12.0 kcal/mol) (Figure 11). According to Curtin-Hammett principle, the reaction would proceed *via* the lowest transition state for each alkene isomer, which in both cases is antiperiplanar *anti*-S_E' pathway. Therefore, *(Z)*-alkene would provide *anti, anti*-isomer **P$_{APZ}$** and *(E)*-alkene would provide *syn, anti*-isomer **P$_{APE}$**.

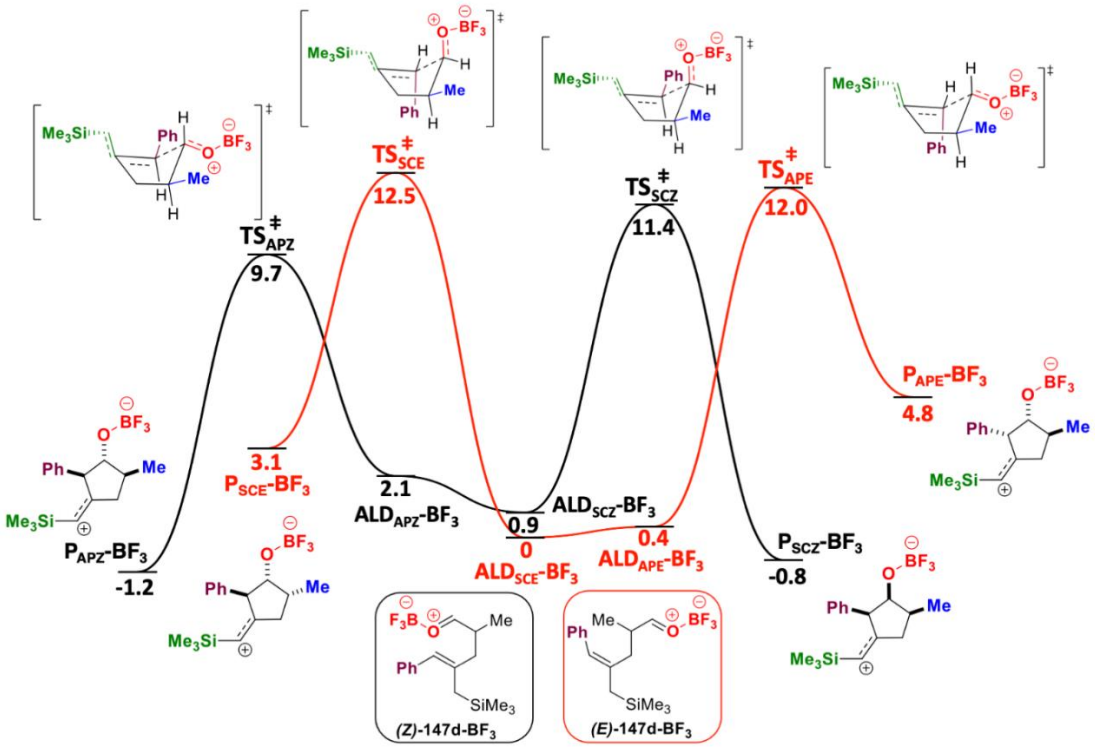

Figure 11. Potential energy surface of intramolecular BF_3-mediated Sakurai-carbocyclization of Ph-substituted variant. Calculations were performed at C-PCM (chlorobenzene)-ωB97XD/6-

311++G(2d,2p)//C-PCM (chlorobenzene)-B3LYP/6-31+G(d). The quasi-harmonic Gibbs Free energies are reported at 253.15 K and 1 mol/L standard state.

Analysis of transition state structures showed that internal diastereoselection is guided by steric interactions (Figure 12). When (Z)-alkene undergoes Sakurai-cyclization, the Lewis acid bound carbonyl experiences only one Gauche interaction in the antiperiplanar transition state (**TS_{APZ}**) and two Gauche interactions in the synclinal transition state (**TS_{SCZ}**). As a result, antiperiplanar transition state is less sterically hindered and 1.7 kcal/mol lower in energy. In contrast, there are two Gauche interactions in both synclinal (**TS_{SCE}**) and antiperiplanar (**TS_{APE}**) transition state orientations of *(E)*-alkene: one coming from the Lewis acid-bound carbonyl and the other coming from the phenyl group (Figure 12). Same number of Gauche interactions albeit between different groups results in lower energy difference (0.5 kcal/mol) between **TS_{SCE}** and **TS_{APE}**.

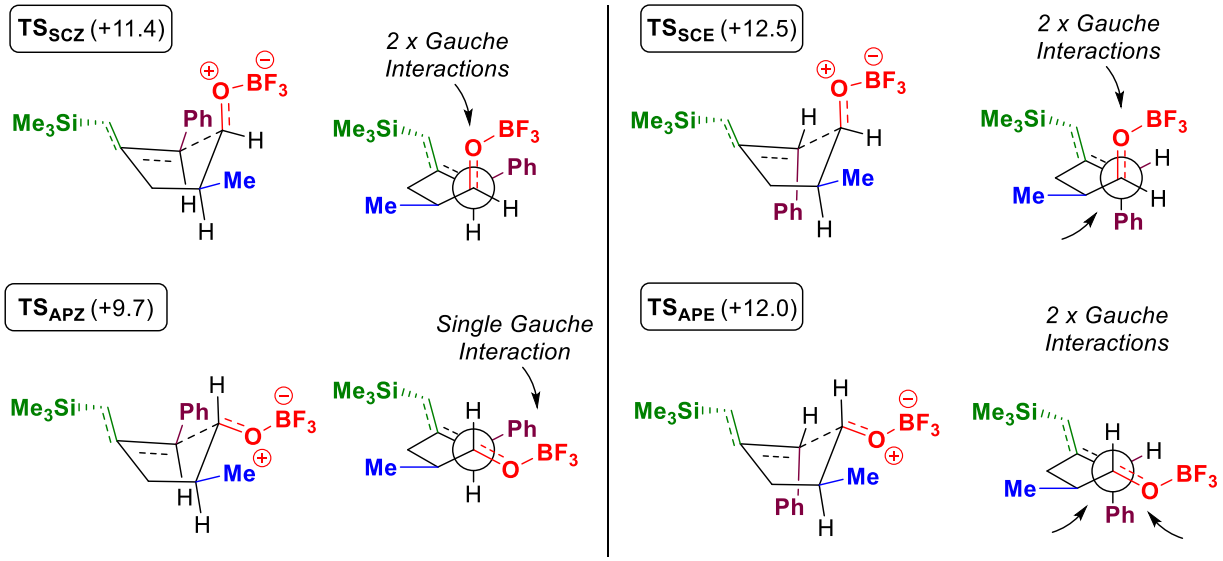

Figure 12. Steric effects guiding stereocontrol in Sakurai-cyclization.

The predicted diastereochemical outcome for the cyclization each alkene isomer matches the experimentally determined relative stereochemistry for diastereomers **A** and **B**, whereby **A** is **P**$_{APZ}$ and **B** is **P**$_{APE}$ (Scheme 74). The proposed mechanism is further supported by the fact that **TS**$_{APZ}$ is the lowest overall transition state leading to thermodynamic product **P**$_{APZ}$**-BF**$_3$, and diastereomer A (**P**$_{APZ}$) is the major product of stepwise transformation of (**146d**). Additionally, **TS**$_{APZ}$ is on PES of *(Z)*-alkene cyclization, and *(Z)*-alkene is the major product of thermal Claisen rearrangement of (**146d**) (Table 7). When other substituents were examined, the similar trend was observed in most cases except Cy-substituted variant (**147c-BF**$_3$) (Table 9).

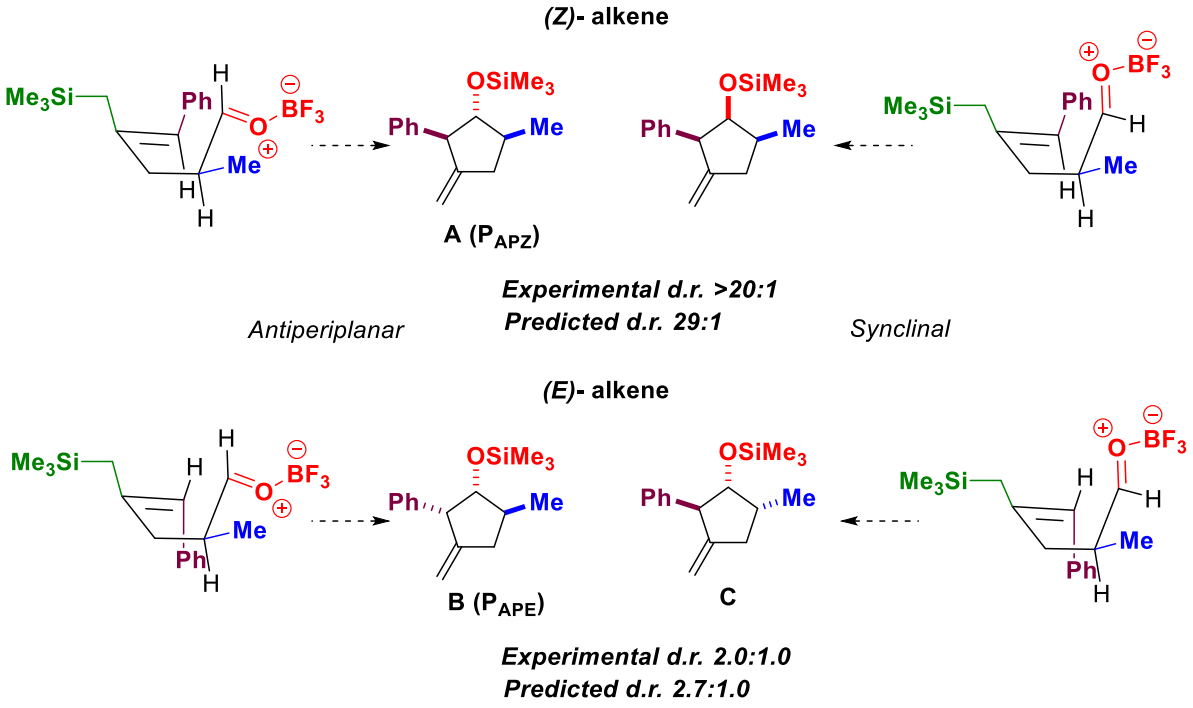

Scheme 74. Internal diastereoselection for *(Z)*- and *(E)*- alkene: comparison between experimental and computational data.

Aldehyde	Experimental d.r. (P_{AP}:P_{SC})		Predicted d.r. (P_{AP}:P_{SC})[a]	
	(Z)-alkene	*(E)*-alkene	*(Z)*-alkene	*(E)*-alkene
147a-BF_3 (R=CH_2CH_2Ph)	13.7:1	2.2:1	1.5:1	7.3:1
147b-BF_3 (R=Bn)	> 20:1	3.4:1	19.8:1	10.9:1
147c-BF_3 (R=Cy)	> 20:1	2.7:1	1:1	1:4
147d-BF_3 (R=Ph)	> 20:1	2:1	29:1	2.7:1
147e-BF_3 (R=2-FPh)	> 20:1	1:1	24:1	6:1

Table 9. Experimental and predicted selectivity in BF_3-mediated Sakurai-carbocyclization. [a] C-PCM (chlorobenzene)- ωB97XD/6-311++G(2d,2p)//C-PCM (chlorobenzene)-B3LYP/6-31+G(d). Selectivity calculated using the quasi-harmonic Gibbs Free energies are reported at 353.15 K and 1 mol/L standard state.

For Cy-substituted aldehyde (**147c-BF_3**) computations predict same energetic barrier for **TS_{APZ}** and **TS_{SCZ}** for the cyclization of (*Z*)-alkene. However, the opposite selectivity was observed for the cyclization of (*E*)-alkene, with the synclinal TS being favored by 0.7 kcal/mol (Figure 13). Considering that internal diastereoselection is determined by steric interactions and Cy is the bulkiest substituent in the scope, this result is not surprising. As was alluded earlier, cyclization of (*E*)-alkene proceeds *via* transition states experiencing two Gauche interactions. Since one of these interactions comes from R group (in this case Cy), changing the sterics of R group would alter the energetic preference towards synclinal or antiperiplanar orientation. In particular, if the Gauche interaction between Lewis acid-bound carbonyl and Cy is more destabilizing than other Gauche interactions, it would increase the energy of antiperiplanar transition states (**TS_{APZ}** and **TS_{APE}**). Considering experimentally observed preference towards (*E*)-alkene in thermal Claisen rearrangement of Cy variant (Table 7), one would expect **P_{SCE}** as the major diastereomer.

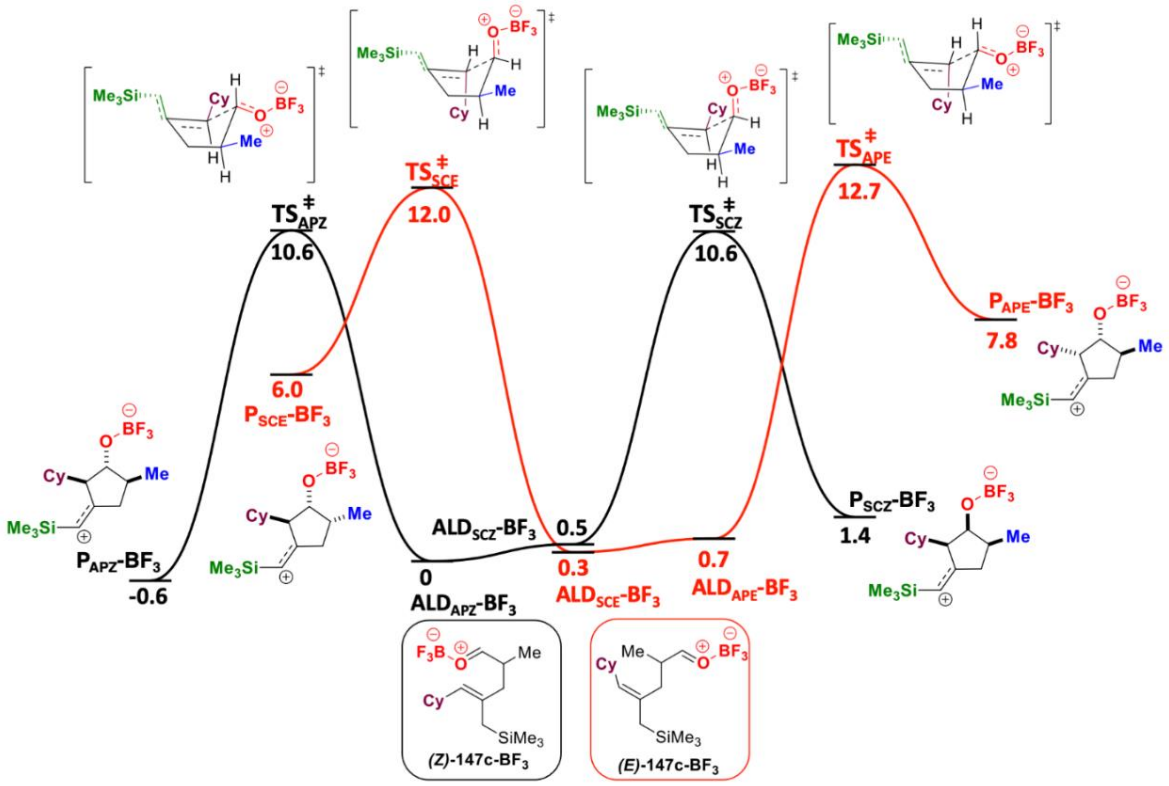

Figure 13. Potential energy surface of intramolecular BF_3-mediated Sakurai-carbocyclization of Cy-substituted variant. Calculations were performed at C-PCM (chlorobenzene)- ωB97XD/6-311++G(2d,2p)//C-PCM (chlorobenzene)-B3LYP/6-31+G(d). The quasi-harmonic Gibbs Free energies are reported at 253.15 K and 1 mol/L standard state.

This prediction does not match experimentally observed d.r. for (**148c-A**) with **P_{APZ}** being a major product. Further examination of potential energy surface, however, demonstrates that Sakurai-cyclization of (**147c- BF_3**) is endergonic and therefore potentially reversible in all cases except **TS_{APZ}** pathway. Consequently, one can argue that cyclization of *(Z)*-alkene is under thermodynamic control and, thus, provides **P_{APZ}-BF_3** intermediate as a major product. It might also be possible that during the ring opening of BF_3-adducts **P_{APE}-BF_3** and **P_{APE}-BF_3**, alkene undergoes partial isomerization leading to the formation of ALD_Z-BF_3 and ultimately giving **P_{APZ}-BF_3** (Scheme 75).

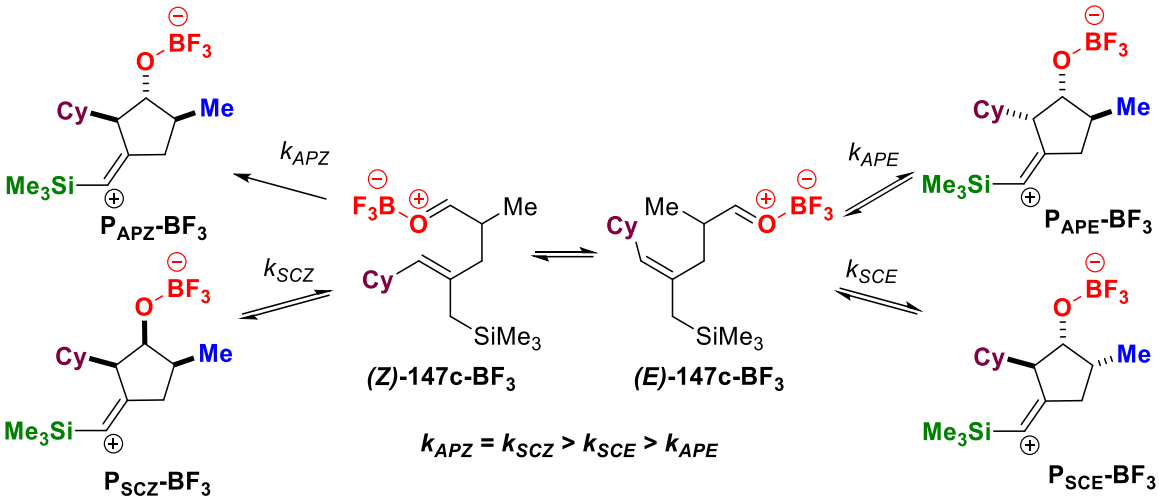

Scheme 75. Potential reversibility and dynamic kinetic resolution in cyclization of (**147c- BF_3**).

We next examined Sakurai-cyclization portion of $EtAlCl_2$-mediated Claisen-Sakurai cascade reaction using phenyl-substituted substrate (**147d-$EtAlCl_2$**) as a model. Same as above, calculations were performed for four transition state structures, which are *AP anti-S_E'* and *SC anti-S_E'* conformations of *(Z)*- and *(E)*-alkene (Scheme 73). The discovered PES that is similar to the one calculated for the BF_3-promoted cyclization. Thus, the interconversion energy gaps between the $EtAlCl_2$-bound aldehyde reactive conformations (**ALD-$EtAlCl_2$**) of *(Z)*- and *(E)*-alkenes are within 1.5 kcal/mol and 0.8 kcal/mol, respectively. The corresponding transition state energies for the Sakurai-carbocyclization are significantly higher (7.3-12.0 kcal/mol) (Figure 14). According to Curtin-Hammett principle, the reaction would proceed *via* the lowest transition state for each alkene isomer, which in both cases again is antiperiplanar *anti*-S_E' pathway. As a result, the *(Z)*-alkene would provide *anti, anti*-isomer **P_{APZ}** and *(E)*-alkene would provide *syn, anti*-isomer **P_{APE}**. The **TS_{APZ}** pathway is the only exergonic pathway leading to both kinetic and thermodynamic intermediate **P_{APZ}- $EtAlCl_2$**, whereas all other cyclization pathways are potentially reversible.

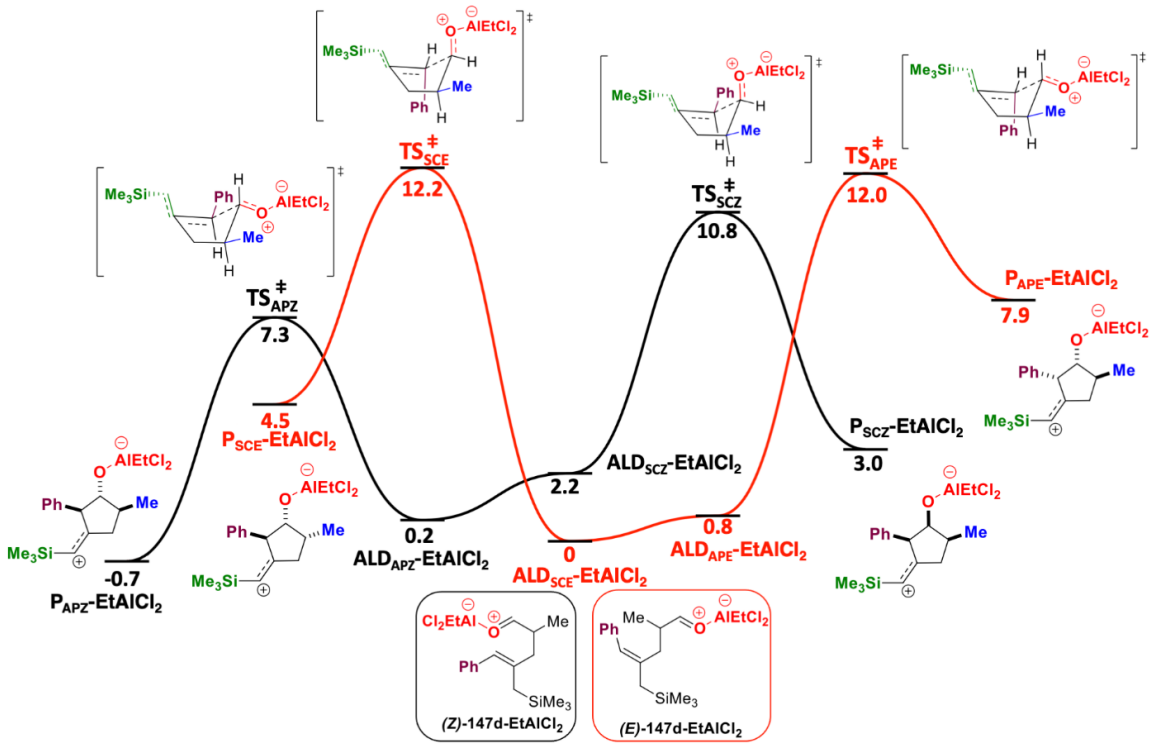

Figure 14. Potential energy surface of intramolecular $EtAlCl_2$-mediated Sakurai-carbocyclization of phenyl variant calculated at C-PCM (toluene)-M11L/6-311++G(2d,2p)//C-PCM (toluene)-B3LYP/6-31+G(d). The quasi-harmonic Gibbs Free energies are reported at 195.15 K and 1 mol/L standard state.

Considerations for stereocontrol in $EtAlCl_2$-mediated Sakurai-carbocyclization are identical to ones described above (Figure 12). Consequently, the predicted diastereochemical outcome for the cyclization of each alkene isomer is similar to the BF_3-promoted cyclization. Thus, the *(Z)*-alkene is expected to provide **P**$_{\mathbf{APZ}}$ product (diastereomer **A**), whereas *(E)*-alkene - **P**$_{\mathbf{APE}}$ (diastereomer **B**). These data match the experimental observation regarding stereochemical outcome: both stepwise and cascade Claisen-Sakurai reactions result in the same pair of major diastereomers, albeit at opposite ratios. Specifically, the cascade rearrangement furnishes **P**$_{\mathbf{APE}}$ (diastereomer **B**) as a major product in almost all cases. This product (diastereomer **B**) is on PES of *(E)*-alkene cyclization, and *(E)*-alkene is predicted to be the major product of $EtAlCl_2$-

catalyzed Claisen rearrangement of (**146d-EtAlCl$_2$**) (Table 8). Preference towards **P$_{APE}$** (diastereomer **B**) in the cascade observed experimentally demonstrate that the reaction is under kinetic control and potential reversibility is not occurring. Indeed, better selectivity towards **B** is observed at lower temperatures (Table 10).

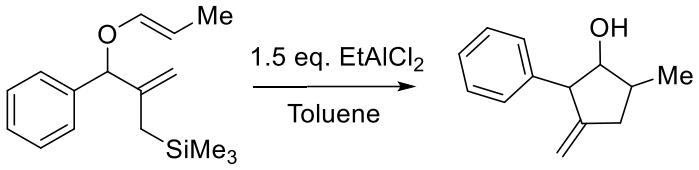

146d **148d-B**

Entry	T, °C	Yield [a], %	d.r. (A:B:C) [b]
1	-78	49	1.9:6.4:1.0
2	-42	44	1.4:3.7:1.0
3	0	60	1.3:1.9:1.0
4	20	46	7.1:7.1:5.3:1.0

Table 10. Reaction selectivity at different temperatures.[a] Isolated yield; [b] determined by ^{1}H NMR.

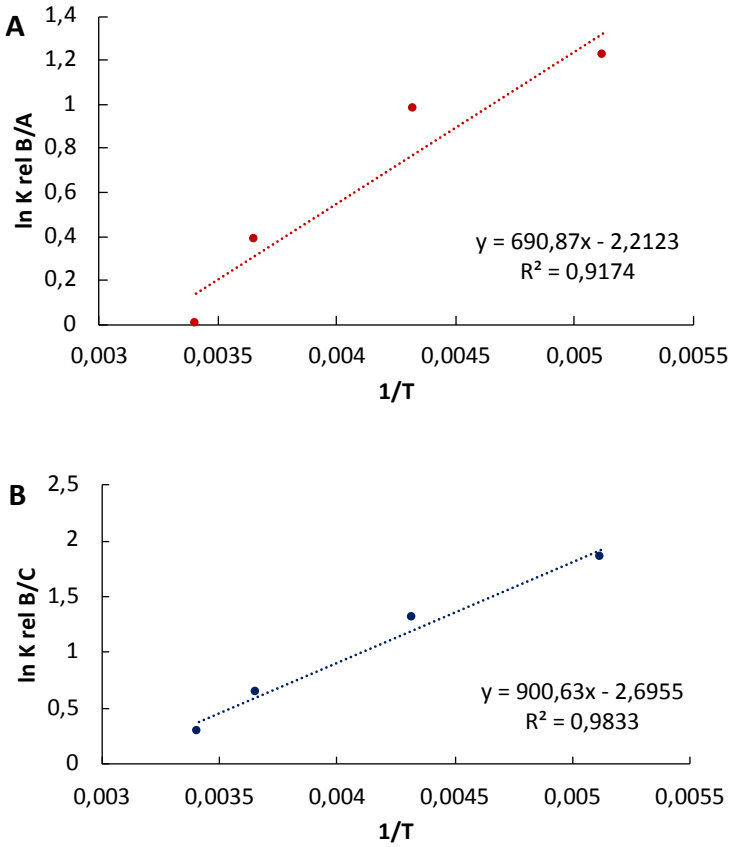

Figure 15. Eyring plots showing experimental differences in activation parameters for competing pathways A) formation of diastereomer **A** versus **B** and B) formation of diastereomer **B** versus **C**.

We built Eyring plot to determine experimental differences in activation parameters for competing pathways in $EtAlCl_2$-mediated Sakurai-carbocyclization of (**147d**). While computations predict 4.7 kcal/mol difference between $\mathbf{TS_{APZ}}$ and $\mathbf{TS_{APE}}$, experimental data provides ΔΔG of 0.5 kcal/mol. On the other hand, experimental ΔΔG between $\mathbf{TS_{APE}}$ and $\mathbf{TS_{SCE}}$ is -0.7 kcal/mol, while calculated is -0.2 kcal/mol. It suggests that in the cascade competition between pathways involving (*E*)- and (*Z*)- alkene cyclization might be more complex and include crossover between the pathways, reversibility, or even alternative cyclization routes.

A similar trend was observed for allyl vinyl ethers with other substituents except Cy variant (**147c-EtAlCl$_2$**) (Table 11). When one examines PES of *(E)*-alkene rearrangement, calculations predict **TS$_{SCE}$** pathway to be lower in energy. Considering the predicted preference towards the *(E)*-alkene in EtAlCl$_2$-catalyzed Claisen rearrangement of Cy variant (Table 11), one would expect **P$_{SCE}$** as a major diastereomer. Overall, computations suggest that both BF_3 and EtAlCl$_2$ mediated cyclization provide **P$_{SCE}$** as a major diastereomer. That is also supported by the fact that both thermal and EtAlCl$_2$-catalyzed Claisen rearrangement of Cy favor *(E)*-alkene. Indeed, the same major product is observed experimentally when Cy variant undergoes stepwise and cascade rearrangement. However, NOE experiment provides evidence towards **P$_{APZ}$** being the product in both cases.

It is worth noting that although in several cases trend in ΔΔG depended on functional used for single point calculations, both M11L and ωB97XD predicted **TS$_{SCE}$** to be lower in energy.

Aldehyde	Experimental d.r. (P_{AP}:P_{SC})		Predicted d.r. (P_{AP}:P_{SC})[a]	
	(Z)-alkene	*(E)*-alkene	*(Z)*-alkene	*(E)*-alkene
147a-EtAlCl$_2$ (R=CH_2CH_2Ph)[a]	> 20:1	10:1	1:17	104:1
147b-EtAlCl$_2$ (R=Bn)[a]	> 20:1	> 20:1	23436:1	489:1
147c-EtAlCl$_2$ (R=Cy)[a]	> 20:1	> 20:1	80:1	1:48
147d-EtAlCl$_2$ (R=Ph)[a]	> 20:1	6.4:1	8350:1	1.7:1
147e-EtAlCl$_2$ (R=2-FPh)[a]	> 20:1	6.4:1	80:1	1.3:1

Table 11. Experimental and predicted selectivity in EtAlCl$_2$-mediated Sakurai-carbocyclization. [a] Calculated at C-PCM (toluene)-M11L/6-311++G(2d,2p)//C-PCM (toluene)-B3LYP/6-31+G(d). Selectivity calculated using the quasi-harmonic Gibbs Free energies are reported at 195.15 K and 1 mol/L standard state.

The proposed model allows us to explain changes in selectivity observed during the cascade rearrangement of (**146d**) and (**146e**) upon the temperature increase (Scheme 76). Since $EtAlCl_2$-catalyzed Sakurai-cyclization was predicted to be reversible in all cases except antiperiplanar *anti*-S_E' pathway, under thermodynamic conditions the formation of *anti*-, *anti*-product (**P$_{APZ}$**) could be expected. Computations suggest that $EtAlCl_2$-catalyzed Claisen rearrangement favors *(E)*-alkene over *(Z)*, however predicted $\Delta\Delta G^{\ddagger}$ for Ph variant is 3 kcal/mol, while for 2-FPh $\Delta\Delta G^{\ddagger}$ is only 0.6 kcal/mol (Table 8). High selectivity during Claisen step would allow diastereomer **B** (**P$_{APE}$**) to remain the major product of the carbocyclization at 0°C. At the same time, low selectivity of Claisen rearrangement of 2-FPh would account for larger amounts of *anti*-, *anti*- product (**P$_{APZ}$**) due to the low initial *(E)*/*(Z)* ratio. Equilibration under thermodynamic conditions could result in diastereoselectivity switch providing (**P$_{APZ}$**) as a major diastereomer. Low selectivity of Claisen step would also explain poor diastereoselectivity in the cascade at -78°C observed for 2-FPh (Scheme 76).

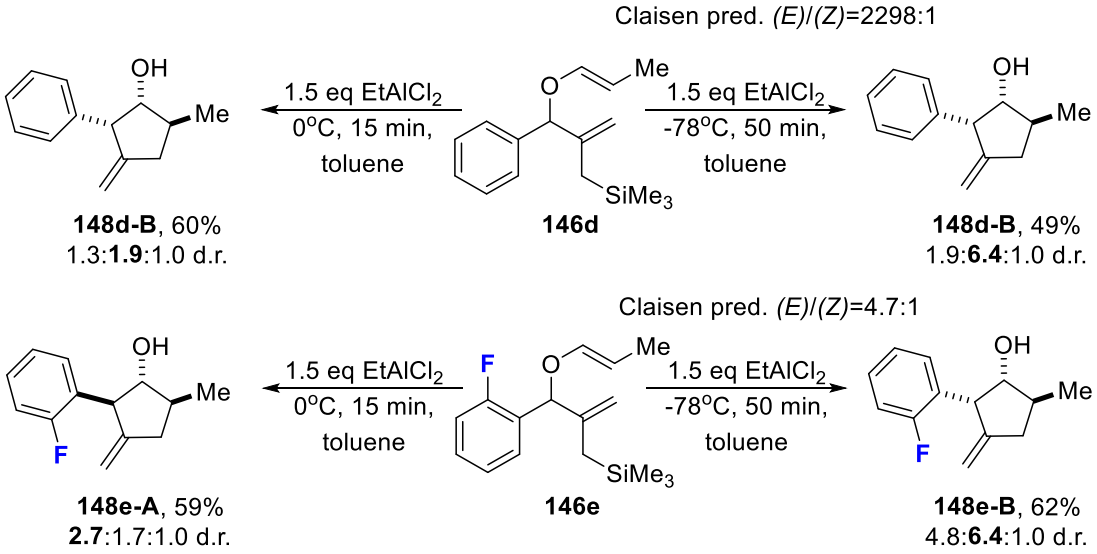

Scheme 76. Effect of temperature and substrate electronics on reaction outcome.

Conclusions

In conclusion, a stereodivergent method for the synthesis of substituted methylene cyclopentanols has been developed. We have shown that one-pot Claisen-Sakurai reaction provides *anti*-, *anti*- product, whereas cascade Claisen-Sakurai reaction furnishes *syn*-, *anti*-product as a major diastereomer with moderate to good stereoselectivity and yield. The reaction was found to be sensitive to both sterics and electronics of the substituent at the allylic position with cyclohexyl variant providing best selectivity in a cascade reaction and *ortho*-fluorophenyl variant showing best selectivity in a stepwise transformation. Mechanistic studies showed that in this transformation both Claisen and Sakurai step determine the stereochemical outcome. In the stepwise transformation thermal Claisen rearrangement in most cases favors (*Z*)-alkene, which upon cyclization *via* antiperiplanar *anti*-S_E' mechanism provides *anti*, *anti*-isomer. In a cascade reaction, Lewis acid-catalyzed Claisen rearrangement favors (*E*)-alkene, which upon cyclization *via* antiperiplanar *anti*-S_E' mechanism results in *syn*-, *anti*-product.

Further investigation of the reaction scope is a major development avenue in this area as the reaction was found to be sensitive to substitution. As such, one could investigate substitution across aromatic ring as well as cyclohexyl analogues.

Another area that can be explored is Claisen-Sakurai stepwise rearrangement that utilizes F^--mediated Sakurai-carbocyclization. Our preliminary data show that both alkyl and aryl-substituted aldehydes undergo TBAF-mediated ring closure with alkyl variant (**146b**) providing access to other regioisomers of methylene cyclopentanol (**156**) (Scheme 77). Interestingly, our initial studies have shown both the S_E and S_E' pathways are accessible when alkyl substituents are present. Controlling access to both pathways would further extend this methodology to a stereo and regiodivergent transformation.

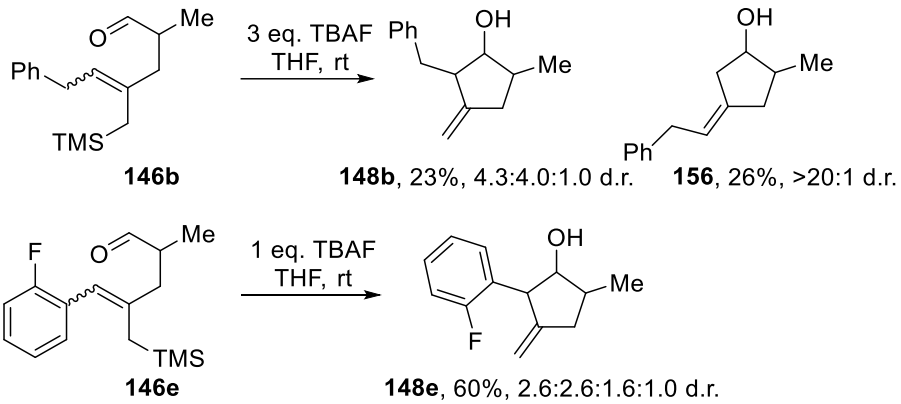

Scheme 77. TBAF catalyzed Sakurai-cyclization.

Conclusions and Future Work

In summary, we developed an efficient and stereoselective Claisen-Sakurai reaction that transforms silylated allyl vinyl ethers (**101**) and (**146**) into 1,2,5-trisubstituted cyclopent-3-en-1-ols (**110**)[52] and 1,2,5-trisubstituted 3-methylene cyclopentan-1-ols (**148**), respectively (Scheme 78). This can be achieved in either a one-pot stepwise or a cascade fashion.[52]

In case of 1,2,5-trisubstituted cyclopenten-1-ols (**110**), the reaction has proven to be general and highly stereoselective, furnishing a library of cyclized products in good and very good yields and >20:1 diastereomeric ratio. The stereochemical outcome of the reaction is defined by a combination of chair-like transition state for the Claisen step and *anti*-S_E' antiperiplanar transition state for the Sakurai cyclization that results in the formation of *anti*, *anti*-isomer. We have also shown for the first time that 1,2,5-trisubstituted cyclopenten-1-ols can be obtained with high levels of stereocontrol *via* Claisen-Sakurai cascade methodology.[52,53]

For the synthesis of 1,2,5-trisubstituted 3-methylene cyclopentan-1-ols (**148**), we have developed a stereodivergent method whereby the one-pot stepwise Claisen-Sakurai reaction provided *anti-anti*- product and the cascade Claisen-Sakurai reaction furnished *syn*-, *anti*-

product as a major diastereomer in good yield. Both sterics and electronics of the substituent at the allylic position influenced the observed stereoselectivity levels. Mechanistic studies showed that in the stepwise transformation, the thermal Claisen rearrangement, in most cases, favors *(Z)*-alkene, which upon cyclization *via* antiperiplanar *anti*-S_E' mechanism provides the *anti*, *anti*-isomer. In contrast, the cascade reaction mediated by a single Lewis acid-catalyzed favors the *(E)*-alkene Claisen product, which upon cyclization *via* antiperiplanar *anti*-S_E' mechanism furnishes *syn*-, *anti*-product.

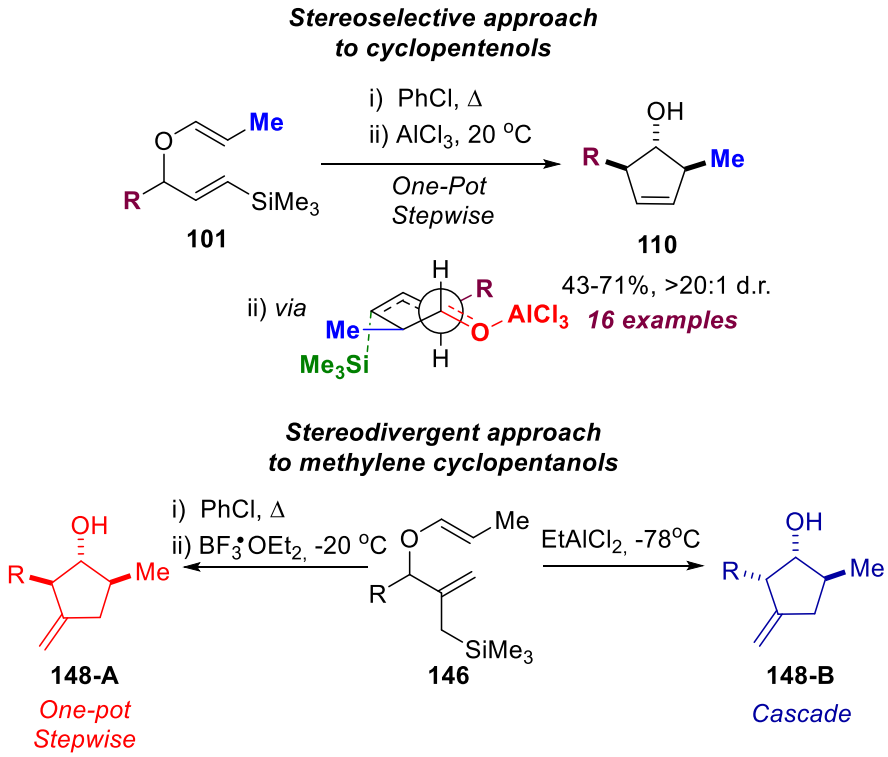

Scheme 78. Summary of developed Claisen-Sakurai approaches.

Although, our results highlight the power of Claisen-Sakurai approach, certain challenges and limitations need to be addressed. In particular, one can notice that silylated allyl vinyl ethers (**146**) undergo both stepwise and cascade reaction with high chemical efficiency whereas

silylated allyl vinyl ethers (**101**) are only amenable to stepwise approach and decompose in a cascade (except one specific example).[52] This observation leads us to consideration of electronics of the substrates utilized in these two processes (Scheme 79).

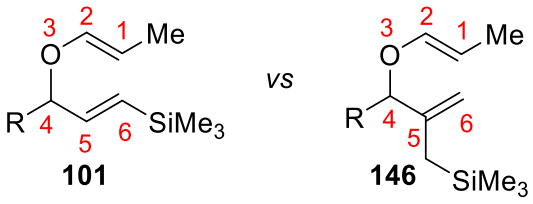

Scheme 79. Considerations for substrate electronics.

Cyclopentenol synthesis employs silylated allyl vinyl ethers (**101**) with methyl group at C1, R group at C4 and silyl group C6-position. It is known that having electron-donating groups in C1 or C6 and either electron-donating or withdrawing group at C4 accelerates Claisen rearrangement.[42] Therefore, one would expect Claisen to be fast. In contrast, Sakurai cyclization would be slow. High reactivity of the substrate would result in decomposition during aluminum catalyzed Claisen rearrangement, whereas slow Sakurai cyclization would compete with other non-productive pathways, which overall would result in low efficiency in a cascade.

Methylene cyclopentanol variant utilizes an allyl vinyl ether (**146**) containing a methylene silane moiety at the C5-position and unsubstituted C6-position. Thus, comparing to (**101**), the Claisen rearrangement of (**146**) is expected to be slower.[42] However, given that allyl vinyl ethers (**146**) contain internally substituted allyl silane, the Sakurai reaction should be more facile.[173] Therefore, these substrates would be less prone to ionization during Claisen rearrangement while Sakurai cyclization would be faster than other competing non-productive pathways providing product with high chemical efficiency in a cascade.

Substitution across allyl vinyl ethers has a major effect on the diastereoselectivity of Claisen rearrangement and ultimately overall transformation. Thus, silylated allyl vinyl ethers (**101**) used in cyclopentenol synthesis provide olefinic aldehydes with high d.r. as in this case it is determined by chair versus boat transition states with the former being much lower in energy. In contrast, having C5 and C6-substituion in allyl vinyl ether (**146**) leads to two competing chair transition states with small energy gap resulting in moderate d.r. Based on that, one can envision that introducing substituent at C2-position could improve d.r. in both cases due to 1,3-diaxial interaction in chair configuration where groups at C4 and C2 are both axial.[42]

Issues with diastereoselectivity in methylene cyclopentanol synthesis could also be addressed by utilizing bulky aluminum Lewis acids similar to ones reported by Yamamoto.[43] If one can identify or design such promotor that would catalyze both Claisen and Sakurai reactions, it would provide the product in a cascade fashion with high d.r.

The developed methodology could be further extended to the synthesis of vinyl cyclobutanes (**158**) providing access to even more challenging four-membered rings with up to four contiguous stereocenters (Scheme 80).

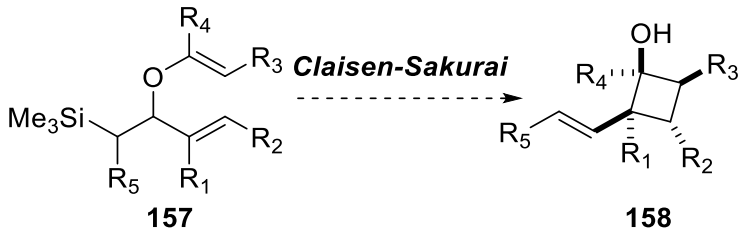

Scheme 80. Future directions for methodogy development.

Experimental Section

General Information

All reactions were carried out under an atmosphere of nitrogen in oven-dried glassware with a magnetic stirring bar. All reactions were monitored by thin layer chromatography (TLC) using Merck TLC silica gel 60 sheets, which were visualized with ultraviolet light and then developed with acidic p-anisaldehyde solution.

Flash chromatography was performed on Silacycle silica gel 60 as the stationary phase and the solvents employed were of analytical grade. Base-washed silica gel was obtained by stirring commercially obtained SiO_2 with 10% Et_3N in CH_2Cl_2 for one hour followed by vacuum filtration in on a glass frit and extensive drying *in vacuo* and stored until needed.
^1H NMR spectra were recorded at 400 MHz or 500 MHz at ambient temperature. Data are reported as follows: chemical shift in parts per million (ppm) from deuterated chloroform ($CDCl_3$) taken as 7.26 ppm, integration, multiplicity (s = singlet, d = doublet; t = triplet; dd = double doublets, dt = double triplets, dq = double quartets, qt = quartet triplets, ddd = double double doublets, ddt = double double triplets, dddd = double double double doublets, tq = triplet quartets, dtq = double triplet quartets, dqt = double quartet triplets, m = multiplet, br = broad), and coupling constant (Hz). ^{13}C NMR spectra were recorded at 100 MHz or 125 MHz. Chemical shifts are reported in ppm from $CDCl_3$ taken as 77.16 ppm. Mass spectra were recorded with a UPLC Q-TOF mass spectrometer using electrospray ionization (ESI).

Unless stated otherwise, all commercially available reagents were used as received. When necessary, commonly used organic solvents were dried prior to use according to standard laboratory practices.[52]

General Procedures

General Procedure A: Isomerization of Diallyl Ethers To an oven dried 5 mL reaction vial, equipped with a magnetic stirrer bar, was added chlorobis(cyclooctene)iridium(I) dimer (1 mol%), tricyclohexylphosphine (6 mol%) and sodium tetraphenylborate (2 mol%) under a nitrogen atmosphere. A 20:1 mixture of dichloromethane-acetone (0.8 M) was added, and the resulting yellow solution stirred at room temperature for 30 minutes followed by addition of the corresponding diallyl ether (1.00 equiv.) via syringe. The mixture was stirred at room temperature until isomerization was shown to be complete by TLC, after which the solvent was evaporated under reduced pressure. The crude mixture was purified by flash column chromatography on based-washed silica to afford the requisite allyl vinyl ether.[52]

General Procedure B: Stepwise Stereoselective Claisen-Sakurai Reaction To an oven dried round bottom flask equipped with reflux condenser and magnetic stirrer bar and purged with nitrogen was added desired allyl vinyl ether (1.00 equiv.). Dry chlorobenzene was added (0.05 M) and the temperature was raised to 70, 90 or 110 ºC depending on the substrate using heating mantle. Once reaction was complete by TLC, the reaction mixture was cooled to 20 ºC and aluminum trichloride (1.50 equiv.) was added in a single portion. The reaction was allowed to stir for 30 minutes at 20 ºC. The reaction mixture was diluted with ether and cooled to 0 ºC. Water (0.04*x* mL) was added and stirred for 5 minutes, followed by the sequential addition of NaOH ($15\%_{(aq)}$, 0.04*x* mL) and water (0.1*x* mL) [where *x* is amount of mmol of aluminum trichloride]. The mixture was warmed to room temperature, stirred for 45 min, the white precipitate was filtered, and the filtrate concentrated *in vacuo*. The crude product was purified by column chromatography.[52]

General Procedure C: Stepwise Stereodivergent Claisen-Sakurai Reaction To an oven dried round bottom flask equipped with reflux condenser and magnetic stirrer bar and purged with nitrogen was added desired allyl vinyl ether (1.00 equiv.). Dry chlorobenzene was added (0.05 M) and the temperature was raised to 90 or 110 ºC depending on the substrate using heating mantle. Once reaction was complete by TLC, the reaction mixture was cooled to -20 ºC and $BF_3{\cdot}OEt_2$ (1.50 equiv.) was added dropwise. The reaction was allowed to warm up to -5 ºC stir over 1 hour. The reaction mixture was quenched with saturated aqueous solution of $NaHCO_3$ (3 mL) and extracted with Et_2O (3 × 5 mL). Combined organic layers were dried over $MgSO_4$, filtered and the filtrate concentrated *in vacuo*. The crude product was purified by column chromatography.

General Procedure D: Cascade Stereodivergent Claisen-Sakurai Reaction To an oven dried round bottom flask equipped with magnetic stirrer bar and purged with nitrogen was added desired allyl vinyl ether (1.00 equiv.). Dry toluene was added (0.05 M) and the reaction mixture was cooled to -78 ºC using acetone/dry ice cooling bath. Ethyl aluminuim dichloride (1.50 equiv.) was added dropwise. The reaction was allowed to stir for 50 minutes at -78 ºC. The reaction mixture was diluted with ether at -78 ºC. Water (0.04*x* mL) was added and stirred for 5 minutes, followed by the sequential addition of NaOH ($15\%_{(aq)}$, 0.04*x* mL) and water (0.1*x* mL) [where *x* is amount of mmol of aluminum trichloride]. The mixture was warmed to room temperature, stirred for 45 min, the white precipitate was filtered and the filtrate concentrated *in vacuo*. The crude product was purified by column chromatography.

Synthesis of Allyl Vinyl Ethers (**101**)

((*E*)-4-Phenyl-3-(((*E*)-prop-1-en-1-yl)oxy)but-1-en-1-yl)trimethylsilane (**101a**).

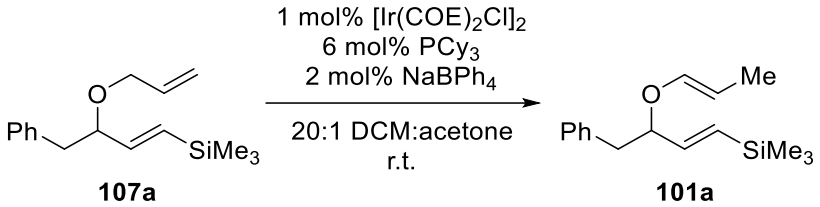

Scheme 81. Synthesis of ((*E*)-4-Phenyl-3-(((*E*)-prop-1-en-1-yl)oxy)but-1-en-1-yl)trimethylsilane (**101a**).

The title compound was prepared by general procedure A from diallyl ether (**107a**)[45,140] (177.6 mg, 0.68 mmol), $[Ir(COE)_2Cl]_2$ (6.1 mg, 0.0068 mmol), PCy_3 (11.5 mg, 0.0409 mmol) and $NaBPh_4$ (4.6 mg, 0.0136 mmol) (Scheme 81). Isomerization was complete after 2 h. The crude product was purified *via* flash column chromatography (Hexanes/Ethyl acetate 98:2) on based-washed silica to afford (**1a**) (159.0 mg, 89%) as a light-yellow oil.

R_f (Hexanes/Ethyl acetate 95:5) = 0.71. ^{1}H-NMR (400 MHz, $CDCl_3$) δ 7.29-7.27 (2H, m), 7.22-7.16 (3H, m), 6.05 (1H, dq, *J* = 12.3, 1.5 Hz), 5.91 (1H, dd, *J* = 18.8, 5.9 Hz), 5.72 (1H, dd, *J* = 18.8, 1.0 Hz), 4.88 (1H, dq, *J* = 12.4, 6.8 Hz), 4.21 (1H, dddd, *J* = 6.7, 6.3, 5.9, 1.0 Hz), 2.97 (1H, dd, *J* = 13.7, 6.7 Hz), 2.79 (1H, dd, *J* = 13.7, 6.3 Hz), 1.51 (3H, dd, *J* = 6.8, 1.6 Hz), 0.03 (9H, s, ^{29}Si isotopomers *J* = 6.6 Hz). ^{13}C{1H}-NMR (100 MHz, $CDCl_3$) δ 145.3, 144.9, 137.9, [134.0, 133.8 and 129.9 rotamers], 132.6, [128.9, 128.7 and 128.2 rotamers], 128.6 and 126.4 rotamers, 101.3, 83.7, 41.7, 12.6, -1.3. HRMS (ESI-TOF) *m/z*: $[M - Me]^+$ Calcd. for $C_{15}H_{21}OSi$ 245.1356 found 245.1364.

((*E*)-4-Phenyl-3-(((*E*)-prop-1-en-1-yl)oxy)but-1-en-1-yl)triethylsilane (**101a- SiEt$_3$**).

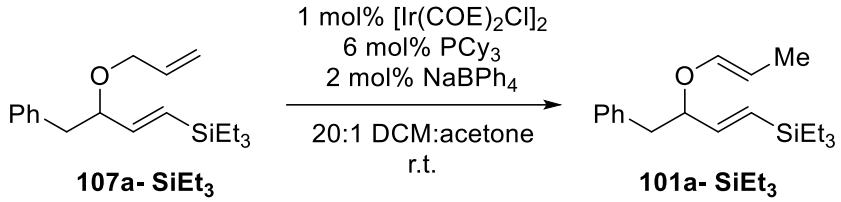

Scheme 82. Synthesis of ((*E*)-4-Phenyl-3-(((*E*)-prop-1-en-1-yl)oxy)but-1-en-1-yl)triethylsilane (**101a- SiEt$_3$**).

The title compound was prepared by general procedure A from diallyl ether (**107a-SiEt$_3$**)[45,140] (91.4 mg, 0.30 mmol), $[Ir(COE)_2Cl]_2$ (2.7 mg, 0.003 mmol), PCy_3 (5.0 mg, 0.018 mmol) and $NaBPh_4$ (2.0 mg, 0.006 mmol) (Scheme 82). Isomerization was complete after 2.5 h. The crude product was purified *via* flash column chromatography (Hexanes/Ethyl acetate 98:2) on based-washed silica to afford (**101a- SiEt$_3$**) (70.6 mg, 77%) as a light-yellow oil.

R_f (Hexanes/Ethyl acetate 95:5) = 0.68. ^{1}H-NMR (400 MHz, $CDCl_3$) δ 7.35-7.24 (2H, m), 7.22-7.16 (3H, m), 6.06 (1H, dq, *J* = 12.3, 1.5 Hz), 5.91 (1H, dd, *J* = 19.0, 6.2 Hz), 5.65 (1H, dd, *J* = 19.0, 0.7 Hz), 4.88 (1H, dq, *J* = 12.4, 6.8 Hz), 4.21 (1H, dddd, *J* = 6.7, 6.5, 6.2, 0.7 Hz), 2.99 (1H, dd, *J* = 13.7, 6.7 Hz), 2.80 (1H, dd, *J* = 13.7, 6.5 Hz), 1.50 (3H, dd, *J* = 6.8, 1.5 Hz), 0.89 (9H, t, *J* = 7.9 Hz), 0.53 (6H, q, *J* = 7.9 Hz). ^{13}C{1H}-NMR (100 MHz, $CDCl_3$) δ 146.3, 145.2, 137.8, [134.0, 133.8 and 129.8 rotamers], 129.2, [128.9, 128.7 and 128.3 rotamers], 128.6 and 126.4 rotamers, 101.4, 83.9, 41.8, 12.6, 7.4, 3.5. HRMS (ESI-TOF) *m/z*: $[M + Na]^+$ Calcd. for $C_{19}H_{30}NaOSi$ 325.1958 found 325.1961.

((*E*)-4-Phenyl-3-(((*E*)-prop-1-en-1-yl)oxy)but-1-en-1-yl)dimethylphenylsilane (**101a-SiMe$_2$Ph**).

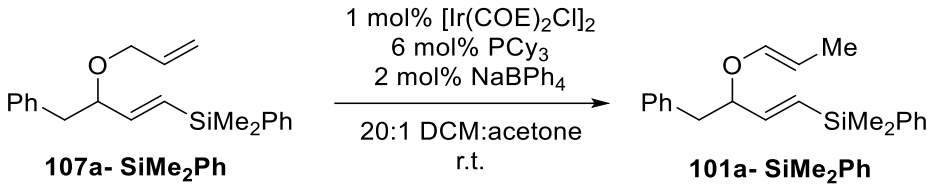

Scheme 83. Synthesis of ((E)-4-Phenyl-3-(((E)-prop-1-en-1-yl)oxy)but-1-en-1-yl)dimethylphenylsilane (**101a- SiMe$_2$Ph**).

The title compound was prepared by general procedure A from diallyl ether (**107a-SiMe$_2$Ph**)[45,140] (147.6 mg, 0.46 mmol), $[Ir(COE)_2Cl]_2$ (4.1 mg, 0.0046 mmol), PCy_3 (7.7 mg, 0.0275 mmol) and $NaBPh_4$ (3.1 mg, 0.0092 mmol) (Scheme 83). Isomerization was complete after 3 h. The crude product was purified *via* flash column chromatography (Hexanes/Ethyl acetate 98:2) on based-washed silica to afford (**101a- SiMe$_2$Ph**) (136.5 mg, 92%) as a light-yellow oil.

R_f (Hexanes/Ethyl acetate 95:5) = 0.68. ^{1}H-NMR (400 MHz, $CDCl_3$) δ 7.44-7.27 (6H, m), 7.25-7.15 (4H, m), 6.07 (1H, dq, *J* = 12.4, 1.5 Hz), 6.00 (1H, dd, *J* = 18.9, 5.8 Hz), 5.86 (1H, d, *J* = 18.9 Hz), 4.90 (1H, dq, *J* = 12.4, 6.8 Hz), 4.28 (1H, ddd, *J* = 6.6, 6.4, 5.8 Hz), 2.99 (1H, dd, *J* = 13.7, 6.6 Hz), 2.81 (1H, dd, *J* = 13.7, 6.4 Hz), 1.52 (3H, dd, *J* = 6.8, 1.5 Hz), 0.31 (3H, s), 0.30 (3H, s). ^{13}C{1H}-NMR (100 MHz, $CDCl_3$) δ 146.8, 145.3, 138.5, 137.7, 134.0, [133.8, 133.7 and 129.9 rotamers], 130.4, 129.1, [128.9, 128.7 and 128.3 rotamers], 128.6 and 126.4 rotamers, 127.9, 101.5, 83.5, 41.6, 12.6, -2.49, -2.55. HRMS (ESI-TOF) *m/z*: $[M + H]^+$ Calcd. for $C_{21}H_{27}OSi$ 323.1826 found 323.1832.

((*E*)-3-Cyclohexyl-3-(((*E*)-prop-1-en-1-yl)oxy)prop-1-en-1-yl)trimethylsilane (**101b**).

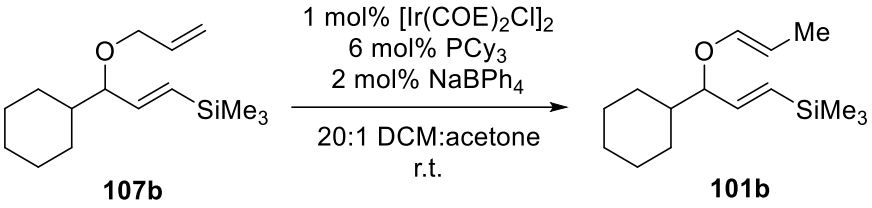

Scheme 84. Synthesis of ((*E*)-3-Cyclohexyl-3-(((*E*)-prop-1-en-1-yl)oxy)prop-1-en-1-yl)trimethylsilane (**101b**).

The title compound was prepared by general procedure A from diallyl ether (**107b**)[45,140] (126.0 mg, 0.50 mmol), $[Ir(COE)_2Cl]_2$ (4.5 mg, 0.005 mmol), PCy_3 (8.4 mg, 0.03 mmol) and $NaBPh_4$ (3.4 mg, 0.01 mmol) (Scheme 84). Isomerization was complete after 2 h. The crude product was purified *via* flash column chromatography (Hexanes/Ethyl acetate 99:1) on based-washed silica to afford (**101b**) (98.3 mg, 78%) as a light-yellow oil.

R_f (Hexanes/Ethyl acetate 95:5) = 0.89. ^{1}H-NMR (400 MHz, $CDCl_3$) δ 6.05 (1H, dq, *J* = 12.3, 1.4 Hz), 5.87 (1H, dd, *J* = 18.9, 6.1 Hz), 5.78 (1H, d, *J* = 19.1 Hz), 4.86 (1H, dq, *J* = 12.4, 6.8 Hz), 3.70 (1H, dd, *J* = 6.1, 6.1 Hz), 1.86-1.59 (5H, m), 1.53-1.43 (1H, m), 1.51 (3H, dd, *J* = 6.7, 1.5 Hz), 1.28-1.05 (3H, m), 1.05-0.90 (2H, m), 0.07 (9H, s, ^{29}Si isotopomers *J* = 6.7 Hz). ^{13}C{1H}-NMR (100 MHz, $CDCl_3$) δ 146.1, 144.5, 133.2, 100.5, 88.1, 42.31, 28.9, 28.9, 26.7, 26.3, 26.3, 12.6, -1.1. HRMS (ESI-TOF) *m/z*: $[M - Me]^+$ Calcd. for $C_{14}H_{25}OSi$ 237.1669 found 237.1670.

((*E*)-5-(Benzyloxy)-3-(((*E*)-prop-1-en-1-yl)oxy)pent-1-en-1-yl)trimethylsilane (**101c**).

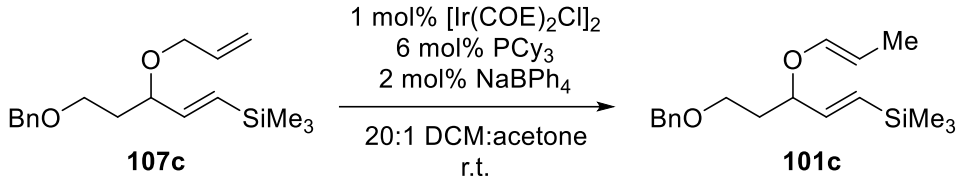

Scheme 85. Synthesis of ((*E*)-5-(Benzyloxy)-3-(((*E*)-prop-1-en-1-yl)oxy)pent-1-en-1-yl)trimethylsilane (**101c**).

The title compound was prepared by general procedure A from diallyl ether (**107c**)[45,140] (145.0 mg, 0.48 mmol), $[Ir(COE)_2Cl]_2$ (4.3 mg, 0.0048 mmol), PCy_3 (8.1 mg, 0.0288 mmol) and $NaBPh_4$ (3.3 mg, 0.0096 mmol) (Scheme 85). Isomerization was complete after 2 h. The crude product was purified *via* flash column chromatography (Hexanes/Ethyl acetate 95:5) on based-washed silica to afford (**101c**) (118.6 mg, 82%) as a light-yellow oil.

R_f (Hexanes/Ethyl acetate 95:5) = 0.50. ^{1}H-NMR (400 MHz, $CDCl_3$) δ 7.37-7.27 (5H, m), 6.07 (1H, dq, *J* = 12.3, 1.6 Hz), 5.91 (1H, dd, *J* = 18.8, 5.3 Hz), 5.83 (1H, d, *J* = 18.9 Hz), 4.88 (1H, dq, *J* = 12.3, 6.7 Hz), 4.52-4.46 (2H, m), 4.23 (1H, ddd, *J* = 7.6, 5.3, 5.3 Hz), 3.61-3.48 (2H, m), 1.96-1.78 (2H, m), 1.52 (3H, dd, *J* = 6.8, 1.6 Hz), 0.05 (9H, s, ^{29}Si isotopomers *J* = 6.6 Hz). ^{13}C{1H}-NMR (100 MHz, $CDCl_3$) δ 145.7 and 145.5 rotamers, 145.4 and 144.6 rotamers, 138.6 and 138.7 rotamers, [134.0, 133.8 and 128.5 rotamers], [132.3, 132.2, 132.2 and 132.2 rotamers], [129.2, 128.9, 128.7, 128.7, 127.8 and 127.8 rotamers], [128.6, 128.6, 127.7 and 127.7 rotamers], 101.0 and 101.0 rotamers, 81.0 and 80.0 rotamers, 73.5 and 73.1 rotamers, 66.5 and 66.5 rotamers, 35.4 and 35.4 rotamers, 12.6, -1.2 and -1.2 rotamers. HRMS (ESI-TOF) *m/z*: $[M - H]^+$ Calcd. for $C_{18}H_{27}O_2Si$ 303.1775 found 303.1785.

((*E*)-3-(Phenyl)-3-(((E)-prop-1-en-1-yl)oxy)prop-1-en-1-yl)trimethylsilane (**101d**).

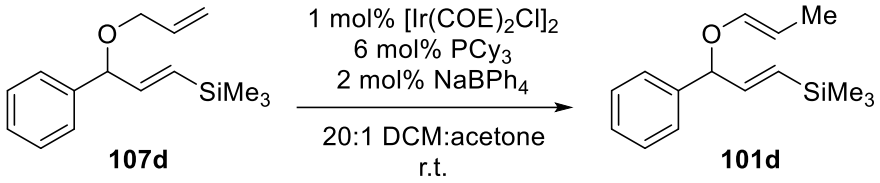

107d **101d**

Scheme 86. Synthesis of ((*E*)-3-(Phenyl)-3-(((E)-prop-1-en-1-yl)oxy)prop-1-en-1-yl)trimethylsilane (**101d**).

The title compound was prepared by general procedure A from diallyl ether (**107d**)[45] (147.6 mg, 0.60 mmol), $[Ir(COE)_2Cl]_2$ (5.4 mg, 0.006 mmol), PCy_3 (10.1 mg, 0.036 mmol) and $NaBPh_4$ (4.1 mg, 0.012 mmol) (Scheme 86). Isomerization was complete after 1.5 h. The crude product was purified *via* flash column chromatography (Hexanes/Ethyl acetate 98:2) on based-washed silica to afford (**101d**) (138.5 mg, 94%) as an amber oil.

R_f (Hexanes/Ethyl acetate 95:5) = 0.82. ^{1}H-NMR (400 MHz, $CDCl_3$) δ 7.38-7.33 (2H, m), 7.32-7.27 (3H, m), 6.14 (1H, dq, *J* = 12.4, 1.6 Hz), 6.11 (1H, dd, *J* = 18.7, 5.6 Hz), 5.92 (1H, dd, *J* = 18.7, 1.2 Hz), 5.07 (1H, dd, *J* = 5.5, 1.2 Hz), 4.95 (1H, dq, *J* = 12.2, 6.8 Hz), 1.50 (3H, dd, *J* = 6.8, 1.6 Hz), 0.06 (9H, s, ^{29}Si isotopomers *J* = 6.8 Hz). ^{13}C{1H}-NMR (100 MHz, $CDCl_3$) δ 145.1, 144.9, 140.5, 132.1, 128.6, 127.8, 127.1, 102.0, 84.6, 12.7, -1.3. HRMS (ESI-TOF) *m/z*: $[M - H]^+$ Calcd. for $C_{15}H_{21}OSi$ 245.1356 found 245.1361.

((*E*)-3-(4-Methoxyphenyl)-3-(((E)-prop-1-en-1-yl)oxy)prop-1-en-1-yl)trimethylsilane (**101e**).

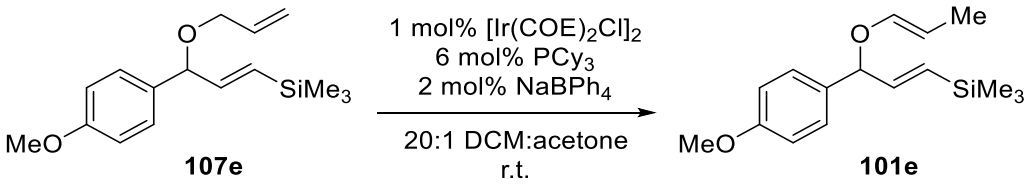

Scheme 87. Synthesis of ((*E*)-3-(4-Methoxyphenyl)-3-(((E)-prop-1-en-1-yl)oxy)prop-1-en-1-yl)trimethylsilane (**101e**).

The title compound was prepared by general procedure A from diallyl ether (**107e**)[45] (165.6 mg, 0.60 mmol), $[Ir(COE)_2Cl]_2$ (5.4 mg, 0.006 mmol), PCy_3 (10.1 mg, 0.036 mmol) and $NaBPh_4$ (4.1 mg, 0.012 mmol) (Scheme 87). Isomerization was complete after 2 h. The crude product was purified *via* flash column chromatography (Hexanes/Ethyl acetate 95:5) on based-washed silica to afford (**101e**) (110.2 mg, 67%) as an amber oil.

R_f (Hexanes/Ethyl acetate 95:5) = 0.60. ^{1}H-NMR (400 MHz, $CDCl_3$) δ 7.22 (2H, AA'XX' system, $J_{AA'}$ = 2.5 Hz, J_{AX} = 8.8 Hz, $J_{XX'}$ = 2.5 Hz, $J_{AX'}$ = 0.0 Hz), 6.89 (2H, AA'XX' system, $J_{AA'}$ = 2.5 Hz, J_{AX} = 8.8 Hz, $J_{XX'}$ = 2.5 Hz, $J_{AX'}$ = 0.0 Hz), 6.12 (1H, dq, *J* = 12.4, 1.5 Hz), 6.11(1H, dd, *J* = 18.6, 5.4 Hz), 5.89 (1H, dd, *J* = 18.7, 1.3 Hz), 5.02 (1H, dd, *J* = 5.6, 1.3 Hz), 4.93 (1H, dq, *J* = 12.5, 6.8 Hz), 3.81 (3H, s), 1.49 (3H, dd, *J* = 6.8, 1.6 Hz), 0.06 (9H, s, ^{29}Si isotopomers *J* = 6.9 Hz). ^{13}C{1H}-NMR (100 MHz, $CDCl_3$) δ 159.3, 145.1, 145.1, 132.6, 131.8, 128.4, 114.0, 101.9, 84.2, 55.4, 12.7, -1.2. HRMS (ESI-TOF) *m/z*: $[M - H]^+$ Calcd. for $C_{16}H_{23}O_2Si$ 275.1462 found 275.1471.

A background Claisen rearrangement occurred at room temperature during the ^{13}C-NMR in $CDCl_3$ leading to small amounts of aldehyde contaminant with the mixture used directly in the next step.

((*E*)-3-(4-Trifluoromethylphenyl)-3-(((*E*)-prop-1-en-1-yl)oxy)prop-1-en-1-yl)trimethylsilane (**101f**).

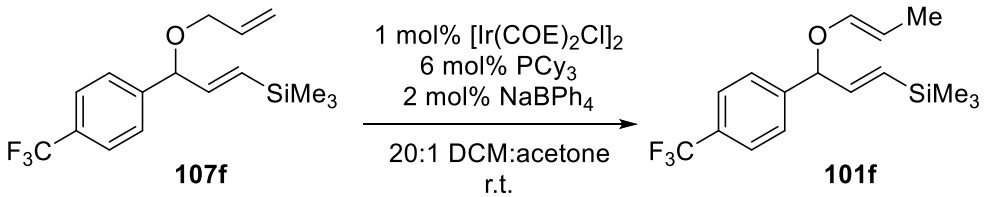

Scheme 88. Synthesis of ((*E*)-3-(4-Trifluoromethylphenyl)-3-(((*E*)-prop-1-en-1-yl)oxy)prop-1-en-1-yl)trimethylsilane (**101f**).

The title compound was prepared by general procedure A from diallyl ether (**107f**)[45] (85.0 mg, 0.27 mmol), $[Ir(COE)_2Cl]_2$ (2.4 mg, 0.0027 mmol), PCy_3 (4.5 mg, 0.0162 mmol) and $NaBPh_4$ (1.8 mg, 0.0054 mmol) (Scheme 88). Isomerization was complete after 1.5 h. The crude product was purified *via* flash column chromatography (Hexanes/Ethyl acetate 98:2) on based-washed silica to afford (**101f**) (73.7 mg, 87%) as an amber oil.

R_f (Hexanes/Ethyl acetate 95:5) = 0.84. ^{1}H-NMR (400 MHz, $CDCl_3$) δ 7.61 (2H, d, J = 8.1 Hz), 7.42 (2H, d, J = 8.1 Hz), 6.13 (1H, dq, J = 12.3, 1.6 Hz), 6.07 (1H, dd, J = 18.7, 5.5 Hz), 5.94 (1H, dd, J = 18.7, 1.1 Hz), 5.11 (1H, dd, J = 5.5, 1.1 Hz), 4.94 (1H, dq, J = 12.4, 6.8 Hz), 1.5 (3H, dd, J = 6.8, 1.6 Hz), 0.06 (9H, s, ^{29}Si isotopomers J = 6.8 Hz). ^{13}C{1H}-NMR (100 MHz, $CDCl_3$) δ 144.8, 144.5, 144.1, 133.3, 130.0 (q, $^2J_{CF}$ = 32.1 Hz), 127.2, 125.6 (q, $^3J_{CF}$ = 3.8 Hz), 124.3 (q, $^1J_{CF}$ = 253.1 Hz), 102.6, 83.9, 12.6, -1.3. HRMS (ESI-TOF) *m/z*: $[M - H]^+$ Calcd. for $C_{16}H_{20}F_3OSi$ 313.1230 found 313.1236.

((*E*)-3-(4-Trifluoromethoxyphenyl)-3-(((*E*)-prop-1-en-1-yl)oxy)prop-1-en-1-yl)trimethylsilane (**101g**).

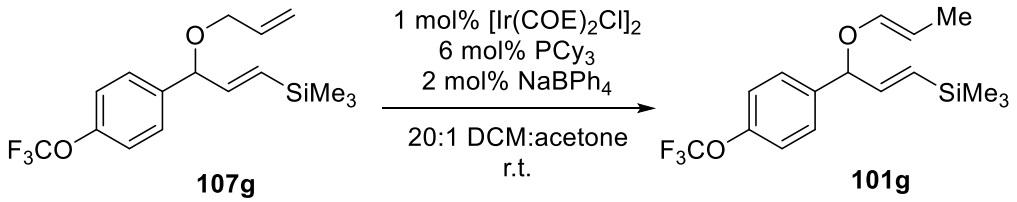

Scheme 89. Synthesis of ((*E*)-3-(4-Trifluoromethoxyphenyl)-3-(((*E*)-prop-1-en-1-yl)oxy)prop-1-en-1-yl)trimethylsilane (**101g**).

The title compound was prepared by general procedure A from diallyl ether (**107g**)[45] (112.5 mg, 0.34 mmol), $[Ir(COE)_2Cl]_2$ (3.0 mg, 0.0034 mmol), PCy_3 (5.7 mg, 0.0204 mmol) and $NaBPh_4$ (2.3 mg, 0.0068 mmol) (Scheme 89). Isomerization was complete after 2 h. The crude product was purified *via* flash column chromatography (Hexanes/Ethyl acetate 98:2) on based-washed silica to afford (**101g**) (77.2 mg, 69%) as an amber oil.

R_f (Hexanes/Ethyl acetate 95:5) = 0.82. ^{1}H-NMR (400 MHz, $CDCl_3$) δ 7.33 (2H, AA'BB' system, $J_{AA'}$ =2.2 Hz, J_{AB} =8.6 Hz, $J_{BB'}$ =2.2 Hz, $J_{AB'}$ = 0.0 Hz), 7.19 (2H, AA'BB' system, $J_{AA'}$ =2.2 Hz, J_{AB} =8.6 Hz, $J_{BB'}$ =2.2 Hz, $J_{AB'}$ = 0.0 Hz), 6.12 (1H, dq, *J* = 12.4, 1.6 Hz), 6.06 (1H, dd, *J* = 18.6, 5.5 Hz), 5.93 (1H, dd, *J* = 18.7, 1.2 Hz), 5.06 (1H, dd, *J* = 5.6, 1.2 Hz), 4.94 (1H, dq, *J* = 12.4, 6.8 Hz), 1.5 (3H, dd, *J* = 6.8, 1.6 Hz), 0.07 (9H, s, ^{29}Si isotopomers *J* = 6.8 Hz). ^{13}C{1H}-NMR (100 MHz, $CDCl_3$) δ 148.8, 144.8, 144.3, 139.2, 132.9, 128.4, 121.1, 120.7 (q, $^1J_{CF}$ = 258.3 Hz), 102.5, 83.8, 12.6, -1.3. HRMS (ESI-TOF) *m/z*: $[M + H_2O + Na]^+$ Calcd. for $C_{16}H_{23}F_3NaO_3Si$ 371.1261 found 371.1264.

((*E*)-3-(4-Fluorophenyl)-3-(((*E*)-prop-1-en-1-yl)oxy)prop-1-en-1-yl)trimethylsilane (**101h**).

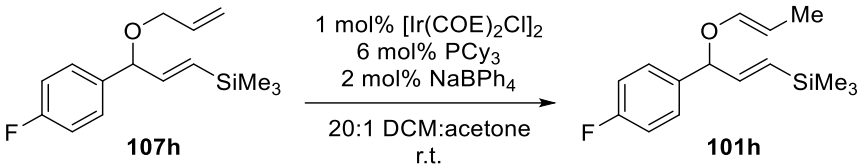

Scheme 90. Synthesis of ((*E*)-3-(4-Fluorophenyl)-3-(((*E*)-prop-1-en-1-yl)oxy)prop-1-en-1-yl)trimethylsilane (**101h**).

The title compound was prepared by general procedure A from diallyl ether (**107h**)[45] (158.4 mg, 0.60 mmol), $[Ir(COE)_2Cl]_2$ (5.4 mg, 0.006 mmol), PCy_3 (10.1 mg, 0.036 mmol) and $NaBPh_4$ (4.1 mg, 0.012 mmol) (Scheme 90). Isomerization was complete after 1.5 h. The crude product was purified *via* flash column chromatography (Hexanes/Ethyl acetate 98:2) on based-washed silica to afford (**101h**) (110.2 mg, 70%) as an amber oil.

R_f (Hexanes/Ethyl acetate 95:5) = 0.83. ^{1}H-NMR (400 MHz, $CDCl_3$) δ 7.27 (2H, AA'XX' system, $J_{AA'}$ = 2.8 Hz, J_{AX} = 8.6 Hz, $J_{XX'}$ = 1.8 Hz, $J_{AX'}$ = 0.0 Hz; J_{HF} = 5.4 Hz), 7.04 (2H, AA'XX' system, $J_{AA'}$ = 2.8 Hz, J_{AX} = 8.6 Hz, $J_{XX'}$ = 1.8 Hz, $J_{AX'}$ = 0.0 Hz; J_{HF} = 8.6 Hz), 6.12 (1H, dq, *J* = 12.3, 1.6 Hz), 6.07 (1H, dd, *J* = 18.7, 5.4 Hz), 5.89 (1H, dd, *J* = 18.7, 1.3 Hz), 5.04 (1H, dd, *J* = 5.5, 1.3 Hz), 4.93 (1H, dq, *J* = 12.5, 6.8 Hz), 1.5 (3H, dd, *J* = 6.8, 1.6 Hz), 0.06 (9H, s, ^{29}Si isotopomers *J* = 6.9 Hz). ^{13}C{1H}-NMR (100 MHz, $CDCl_3$) δ 162.4 (d, $^1J_{CF}$ = 245.7 Hz), 144.9, 144.7, 136.2 (d, $^4J_{CF}$ = 3.0 Hz), 132.5, 128.7 (d, $^3J_{CF}$ = 8.0 Hz), 115.6, 115.4, 102.3, 83.9, 12.6, -1.3. HRMS (ESI-TOF) *m/z*: $[M - H]^+$ Calcd. for $C_{15}H_{20}FOSi$ 263.1262 found 263.1269.

((*E*)-3-(3-Fluorophenyl)-3-(((*E*)-prop-1-en-1-yl)oxy)prop-1-en-1-yl)trimethylsilane (**101i**).

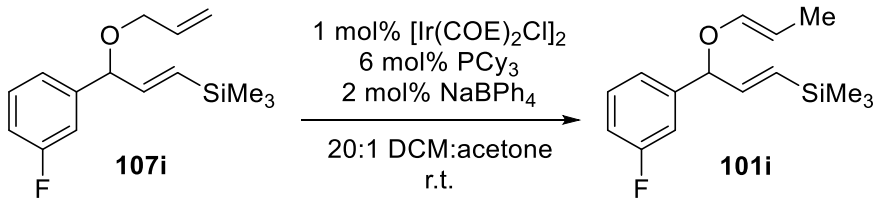

Scheme 91. Synthesis of ((*E*)-3-(3-Fluorophenyl)-3-(((*E*)-prop-1-en-1-yl)oxy)prop-1-en-1-yl)trimethylsilane (**101i**).

The title compound was prepared by general procedure A from diallyl ether (**107i**)[45] (105.7 mg, 0.40 mmol), $[Ir(COE)_2Cl]_2$ (3.6 mg, 0.004 mmol), PCy_3 (6.7 mg, 0.024 mmol) and $NaBPh_4$ (2.7 mg, 0.008 mmol) (Scheme 91). Isomerization was complete after 2 h. The crude product was purified *via* flash column chromatography (Hexanes/Dichloromethane 4:1) on based-washed silica to afford (**101i**) (85.2 mg, 78%) as an amber oil.

R_f (Hexanes/Dichloromethane 4:1) = 0.72. ^{1}H-NMR (400 MHz, $CDCl_3$) δ 7.31 (1H, ddd, J = 7.9, 7.9 Hz; $^4J_{HF}$ = 5.9 Hz), 7.08 (1H, d, J = 7.7 Hz), 7.03 (1H, ddd, J = 2.3, 2.3 Hz; $^3J_{HF}$ = 9.8 Hz), 6.97 (1H, dddd, J = 8.5, 2.6, 0.8 Hz; $^3J_{HF}$ = 8.5 Hz), 6.13 (1H, dq, J = 12.3, 1.6 Hz), 6.07 (1H, dd, J = 18.7, 5.5 Hz), 5.93 (1H, dd, J = 18.7, 1.2 Hz), 5.05 (1H, dd, J = 5.5, 1.2 Hz), 4.95 (1H, dq, J = 12.3, 6.8 Hz), 1.50 (3H, dd, J = 6.8, 1.6 Hz), 0.06 (9H, s, ^{29}Si isotopomers J = 6.7 Hz). ^{13}C{1H}-NMR (100 MHz, $CDCl_3$) δ 163.1 (d, $^1J_{CF}$ = 245.8 Hz), 144.8, 144.3, 143.2 (d, $^3J_{CF}$ = 7.1 Hz), 132.9, 130.1 (d, $^3J_{CF}$ = 8.1 Hz), 122.5 (d, $^4J_{CF}$ = 2.8 Hz), 114.7 (d, $^2J_{CF}$ = 21.3 Hz), 113.9 (d, $^2J_{CF}$ = 22.2 Hz), 102.4, 83.9 (d, $^4J_{CF}$ = 1.8 Hz), 12.6, -1.3. HRMS (ESI-TOF) *m/z*: $[M + H_2O + NH_4]^+$ Calcd. for $C_{15}H_{27}FNO_2Si$ 300.1790 found 300.1800.

((*E*)-3-(2-Fluorophenyl)-3-(((*E*)-prop-1-en-1-yl)oxy)prop-1-en-1-yl)trimethylsilane (**101j**).

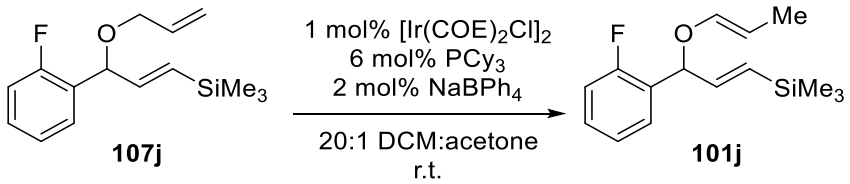

Scheme 92. Synthesis of ((*E*)-3-(2-Fluorophenyl)-3-(((*E*)-prop-1-en-1-yl)oxy)prop-1-en-1-yl)trimethylsilane (**101j**).

The title compound was prepared by general procedure A from diallyl ether (**107j**)[45] (158.4 mg, 0.60 mmol), $[Ir(COE)_2Cl]_2$ (5.4 mg, 0.006 mmol), PCy_3 (10.1 mg, 0.036 mmol) and $NaBPh_4$ (4.1 mg, 0.012 mmol) (Scheme 92). Isomerization was complete after 1.5 h. The crude product was purified *via* flash column chromatography (Hexanes/Ethyl acetate 98:2) on based-washed silica to afford (**101j**) (155.2 mg, 98%) as an amber oil.

R_f (Hexanes/Ethyl acetate 95:5) = 0.83. ^{1}H-NMR (400 MHz, $CDCl_3$) δ 7.37 (1H, ddd, J = 7.5, 7.5, 1.8 Hz), 7.30-7.24 (1H, m), 7.15 (1H, ddd, J = 7.5, 1.1 Hz; $^4J_{HF}$ = 7.5 Hz) 7.04 (1H, ddd, J = 8.2, 1.1 Hz; $^3J_{HF}$ = 10.0 Hz), 6.13 (1H, dq, J = 12.3, 1.5 Hz), 6.11 (1H, dd, J = 18.6, 5.1 Hz), 5.94 (1H, ddd, J = 18.7, 1.0, 1.0 Hz), 5.44 (1H, dd, J = 5.1, 1.0 Hz), 4.93 (1H, dq, J = 12.4, 6.8 Hz), 1.5 (3H, dd, J = 6.8, 1.6 Hz), 0.05 (9H, s, ^{29}Si isotopomers J = 6.8 Hz). ^{13}C{1H}-NMR (100 MHz, $CDCl_3$) δ 160.2 (d, $^1J_{CF}$ = 246.4 Hz), 144.9, 143.3, 132.1, 129.3 (d, $^3J_{CF}$ = 8.1 Hz), 128.4 (d, $^3J_{CF}$ = 3.8 Hz), 127.7 (d, $^2J_{CF}$ = 13.7 Hz), 124.5 (d, $^4J_{CF}$ = 3.4 Hz), 115.4 (d, $^2J_{CF}$ = 21.7 Hz), 102.1, 77.4 (d, $^4J_{CF}$ = 2.0 Hz), 12.7, -1.3. HRMS (ESI-TOF) *m/z*: $[M - H]^+$ Calcd. for $C_{15}H_{20}FOSi$ 263.1262 found 263.1264.

((*E*)-3-(Naphthalen-2-yl)-3-(((*E*)-prop-1-en-1-yl)oxy)prop-1-en-1-yl)trimethylsilane (**101k**).

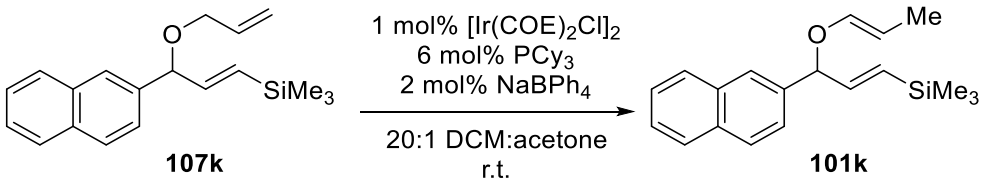

107k **101k**

Scheme 93. Synthesis of ((*E*)-3-(Naphthalen-2-yl)-3-(((*E*)-prop-1-en-1-yl)oxy)prop-1-en-1-yl)trimethylsilane (**101k**).

The title compound was prepared by general procedure A from diallyl ether (**107k**)[45] (177.8 mg, 0.60 mmol), $[Ir(COE)_2Cl]_2$ (5.4 mg, 0.006 mmol), PCy_3 (10.1 mg, 0.036 mmol) and $NaBPh_4$ (4.1 mg, 0.012 mmol) (Scheme 93). Isomerization was complete after 2 h. The crude product was purified *via* flash column chromatography (Hexanes/Dichloromethane 4:1) on based-washed silica to afford (**101k**) (137.4 mg, 77%) as a brown oil.

R_f (Hexanes/Dichloromethane 4:1) = 0.63. ^{1}H-NMR (400 MHz, $CDCl_3$) δ 7.87-7.82 (3H, m), 7.78 (1H, s), 7.52-7.46 (2H, m), 7.43 (1H, dd, *J* = 8.5, 1.7 Hz), 6.20 (1H, dd, *J* = 18.7, 5.5 Hz), 6.20 (1H, dq, *J* = 12.4, 1.6 Hz), 5.97 (1H, dd, *J* = 18.7, 1.3 Hz), 5.24 (1H, dd, *J* = 5.4, 1.3 Hz), 5.00 (1H, dq, *J* = 12.4, 6.8 Hz), 1.50 (3H, dd, *J* = 6.8, 1.6 Hz), 0.07 (9H, s, ^{29}Si isotopomers *J* = 6.7 Hz). ^{13}C{1H}-NMR (100 MHz, $CDCl_3$) δ 145.0, 144.9, 137.9, 133.4, 133.2, 132.3, 128.5, 128.2, 127.9, 126.3, 126.1, 126.0, 125.0, 102.2, 84.7, 12.7, -1.3. HRMS (ESI-TOF) *m/z*: $[M + NH_4]^+$ Calcd. for $C_{19}H_{28}NOSi$ 314.1935 found 314.1927.

((*E*)-3-(2-Fluoro-4-methoxyphenyl)-3-(((*E*)-prop-1-en-1-yl)oxy)prop-1-en-1-yl)trimethylsilane (**101l**).

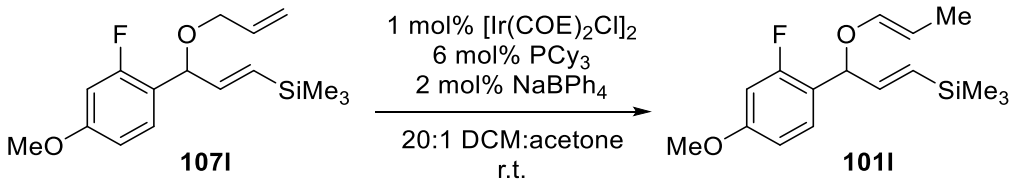

Scheme 94. Synthesis of ((*E*)-3-(2-Fluoro-4-methoxyphenyl)-3-(((*E*)-prop-1-en-1-yl)oxy)prop-1-en-1-yl)trimethylsilane (**101l**).

The title compound was prepared by general procedure A from diallyl ether (**107l**)[45] (176.4 mg, 0.60 mmol), $[Ir(COE)_2Cl]_2$ (5.4 mg, 0.006 mmol), PCy_3 (10.1 mg, 0.036 mmol) and $NaBPh_4$ (4.1 mg, 0.012 mmol) (Scheme 94). Isomerization was complete after 2 h. The crude product was purified *via* flash column chromatography (Hexanes/Ethyl acetate 95:5) on based-washed silica to afford (**101l**) (165.0 mg, 94%) as an amber oil.

R_f (Hexanes/Ethyl acetate 95:5) = 0.60. ^{1}H-NMR (400 MHz, $CDCl_3$) δ 7.24 (1H, dd, J = 8.5 Hz; $^4J_{HF}$ = 8.5 Hz), 6.71 (1H, dd, J = 8.6, 2.4 Hz), 6.60 (1H, dd, J = 2.5 Hz; $^3J_{HF}$ = 11.9 Hz), 6.12 (1H, dq, J = 12.4, 1.6 Hz), 6.11 (1H, ddd, J = 18.8, 5.0, 0.4 Hz), 5.91 (1H, ddd, J = 18.7, 1.1, 1.1 Hz), 5.36 (1H, dd, J = 5.1, 1.1 Hz), 4.92 (1H, dq, J = 12.4, 6.8 Hz), 3.79 (3H, s), 1.50 (3H, dd, J = 6.8, 1.6 Hz), 0.05 (9H, s, ^{29}Si isotopomers J = 6.8 Hz). ^{13}C{1H}-NMR (100 MHz, $CDCl_3$) δ 160.9 (d, $^1J_{CF}$ = 246.2 Hz), 160.6 (d, $^3J_{CF}$ = 11.2 Hz), 144.9, 143.6, 131.8, 129.1 (d, $^3J_{CF}$ = 6.0 Hz), 119.6 (d, $^2J_{CF}$ = 14.3 Hz), 110.4 (d, $^4J_{CF}$ = 2.9 Hz), 101.9, 101.5 (d, $^2J_{CF}$ = 25.7 Hz), 77.2 (d, $^3J_{CF}$ = 1.6 Hz), 55.7, 12.7, -1.3. HRMS (ESI-TOF) *m/z*: $[M - H]^+$ Calcd. for $C_{16}H_{22}FO_2Si$ 293.1368 found 293.1372.

((*E*)-3-(2,4-Difluorophenyl)-3-(((*E*)-prop-1-en-1-yl)oxy)prop-1-en-1-yl)trimethylsilane (**101m**).

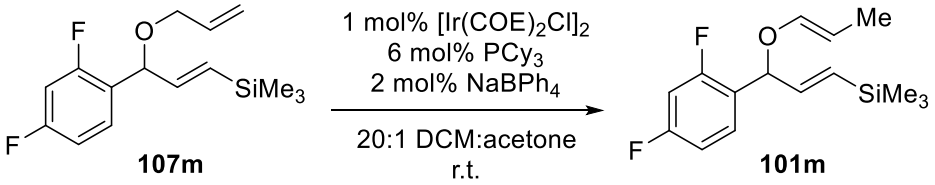

Scheme 95. Synthesis of ((*E*)-3-(2,4-Difluorophenyl)-3-(((*E*)-prop-1-en-1-yl)oxy)prop-1-en-1-yl)trimethylsilane (**101m**).

The title compound was prepared by general procedure A from diallyl ether (**107m**)[45] (141.0 mg, 0.60 mmol), $[Ir(COE)_2Cl]_2$ (5.4 mg, 0.006 mmol), PCy_3 (10.1 mg, 0.036 mmol) and $NaBPh_4$ (4.1 mg, 0.012 mmol) (Scheme 95). Isomerization was complete after 2 h. The crude product was purified *via* flash column chromatography (Hexanes/Ethyl acetate 98:2) on based-washed silica to afford (**101m**) (140.0 mg, 99%) as an amber oil.

R_f (Hexanes/Ethyl acetate 95:5) = 0.84. ^{1}H-NMR (400 MHz, $CDCl_3$) δ 7.33 (1H, ddd, J = 6.6 Hz; $^4J_{HF}$ = 8.4, 8.4 Hz), 6.91-6.86 (1H, m), 6.79 (1H, ddd, J = 2.5 Hz; $^3J_{HF}$ = 10.1, 9.0 Hz), 6.11 (1H, dq, J = 12.4, 1.5 Hz), 6.08 (1H, dd, J = 18.7, 5.0 Hz), 5.92 (1H, ddd, J = 18.7, 1.2, 1.2 Hz), 5.38 (1H, dd, J = 5.1, 1.2 Hz), 4.92 (1H, dq, J = 12.5, 6.8 Hz), 1.5 (3H, dd, J = 6.8, 1.6 Hz), 0.06 (9H, s, ^{29}Si isotopomers J = 6.6 Hz). ^{13}C{1H}-NMR (100 MHz, $CDCl_3$) δ 162.5 (dd, $^1J_{CF}$ = 248.5 Hz, $^3J_{CF}$ = 12.2 Hz), 160.3 (dd, $^1J_{CF}$ = 248.8 Hz, $^3J_{CF}$ = 12.1 Hz), 144.8, 143.1, 132.4, 129.4 (dd, $^3J_{CF}$ = 9.7, 5.5 Hz), 123.7 (dd, $^2J_{CF}$ = 13.9 Hz, $^4J_{CF}$ = 3.7 Hz), 111.8 (dd, $^2J_{CF}$ = 21.1 Hz, $^4J_{CF}$ = 3.7 Hz), 103.8 (dd, $^2J_{CF}$ = 25.7, 25.7 Hz), 102.4, 77.0 (d, $^3J_{CF}$ = 1.3 Hz), 12.6, -1.3. HRMS (ESI-TOF) *m/z*: $[M + H_3O]^+$ Calcd. for $C_{15}H_{23}F_2O_2Si$ 301.1430 found 301.1437.

((*E*)-3-(4-Dichloro-2-fluorophenyl)-3-(((*E*)-prop-1-en-1-yl)oxy)prop-1-en-1-yl)trimethylsilane (**101n**).

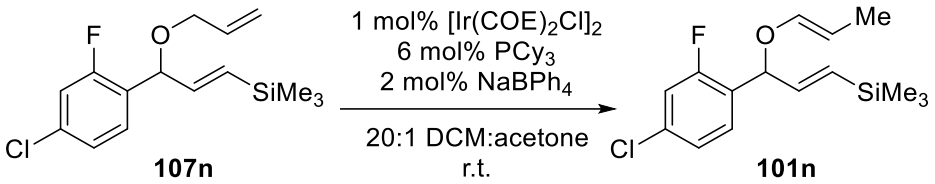

Scheme 96. Synthesis of ((*E*)-3-(4-Dichloro-2-fluorophenyl)-3-(((*E*)-prop-1-en-1-yl)oxy)prop-1-en-1-yl)trimethylsilane (**101n**).

The title compound was prepared by general procedure A from diallyl ether (**107n**)[45] (179.3 mg, 0.60 mmol), $[Ir(COE)_2Cl]_2$ (5.4 mg, 0.006 mmol), PCy_3 (10.1 mg, 0.036 mmol) and $NaBPh_4$ (4.1 mg, 0.012 mmol) (Scheme 96). Isomerization was complete after 2 h. The crude product was purified *via* flash column chromatography (Hexanes/Ethyl acetate 98:2) on based-washed silica to afford (**101n**) (137.1 mg, 76%) as an amber oil.

R_f (Hexanes/Ethyl acetate 95:5) = 0.84. ^{1}H-NMR (400 MHz, $CDCl_3$) δ 7.31 (1H, dd, J = 8.0 Hz; $^4J_{HF}$ = 8.0 Hz), 7.15 (1H, dd, J = 8.4, 1.9 Hz), 7.08 (1H, dd, J = 1.9 Hz; $^3J_{HF}$ = 9.8 Hz), 6.10 (1H, dq, J = 12.3, 1.6 Hz), 6.06 (1H, ddd, J = 18.7, 5.1, 0.4 Hz), 5.93 (1H, ddd, J = 18.7, 1.1, 1.1 Hz), 5.38 (1H, dd, J = 5.1, 1.1 Hz), 4.92 (1H, dq, J = 12.6, 6.8 Hz), 1.5 (3H, dd, J = 6.8, 1.6 Hz), 0.05 (9H, s, ^{29}Si isotopomers J = 6.7 Hz). ^{13}C{1H}-NMR (100 MHz, $CDCl_3$) δ 159.9 (d, $^1J_{CF}$ = 249.8 Hz), 144.7, 142.8, 134.3 (d, $^3J_{CF}$ = 10.4 Hz), 132.6, 129.3 (d, $^3J_{CF}$ = 5.0 Hz), 126.5 (d, $^2J_{CF}$ = 14.0 Hz), 125.0 (d, $^4J_{CF}$ = 3.6 Hz), 116.3 (d, $^2J_{CF}$ = 25.3 Hz), 102.5, 76.9 (d, $^3J_{CF}$ = 1.2 Hz), 12.6, -1.3. HRMS (ESI-TOF) *m/z*: $[M - H]^+$ Calcd. for $C_{15}H_{19}{}^{35}ClFOSi$ 297.0872 found 297.0865.

3-((*E*)-1-(((*E*)-Prop-1-en-1-yl)oxy)-3-(trimethylsilyl)allyl)-1-tosyl-1*H*-indole (**101o**).

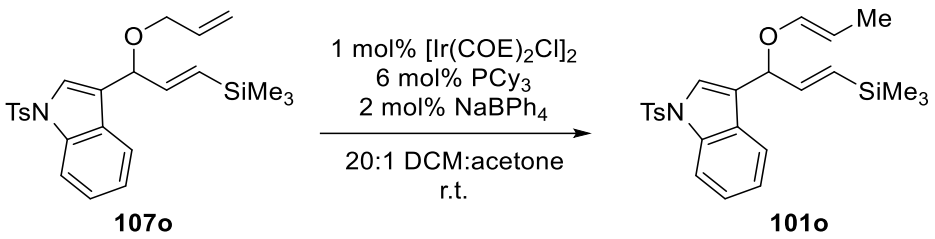

107o **101o**

Scheme 97. Synthesis of 3-((*E*)-1-(((*E*)-Prop-1-en-1-yl)oxy)-3-(trimethylsilyl)allyl)-1-tosyl-1*H*-indole (**101o**).

The title compound was prepared by general procedure A from diallyl ether (**107o**)[45] (94.8 mg, 0.20 mmol), $[Ir(COE)_2Cl]_2$ (1.8 mg, 0.002 mmol), PCy_3 (3.4 mg, 0.012 mmol) and $NaBPh_4$ (1.4 mg, 0.004 mmol) (Scheme 97). Isomerization was complete after 2.5 h. The crude product was purified *via* flash column chromatography (Hexanes/Ethyl acetate 9:1) on based-washed silica to afford (**101o**) (77.2 mg, 81%) as an amber oil.

R_f (Hexanes/Ethyl acetate 95:5) = 0.31. ^{1}H-NMR (400 MHz, $CDCl_3$) δ 7.96 (1H, ddd, *J* = 8.3, 0.8, 0.8 Hz), 7.75 (2H, AA'XX' system, $J_{AA'}$ = 1.9 Hz, J_{AX} = 8.4 Hz, $J_{XX'}$ = 1.9 Hz, $J_{AX'}$ = 0.0 Hz), 7.54 (1H, ddd, *J* = 7.8, 1.0, 1.0 Hz), 7.50 (1H, d, *J* = 0.3 Hz), 7.30 (1H, ddd, *J* = 8.3, 7.3, 1.1 Hz), 7.23-7.19 (3H, m), 6.17 (1H, dd, *J* = 18.7, 5.5 Hz), 6.14 (1H, dq, *J* = 12.3, 1.6 Hz), 6.0 (1H, dd, *J* = 18.7, 1.2 Hz), 5.27 (1H, ddd, *J* = 5.5, 1.2, 1.2 Hz), 4.96 (1H, dq, *J* = 12.5, 6.8 Hz), 2.34 (3H, s), 1.50 (3H, dd, *J* = 6.8, 1.6 Hz), 0.06 (9H, s, ^{29}Si isotopomers *J* = 6.5 Hz). ^{13}C{1H}-NMR (100 MHz, $CDCl_3$) δ 145.1, 144.7, 142.8, 135.7, 135.3, 133.7, 130.0, 129.1, 127.0, 124.9, 124.3, 123.4, 121.8, 120.8, 113.8, 102.4, 78.3, 21.7, 12.6, -1.3. HRMS (ESI-TOF) *m/z*: $[M - H]^+$ Calcd. for $C_{24}H_{28}NO_3SSi$ 438.1554 found 438.1559.

(*E*)-2,2-Dimethyl-5-phenyl-3-(trimethylsilyl)pent-4-enal (**109**): Isomerization-Claisen rearrangement .

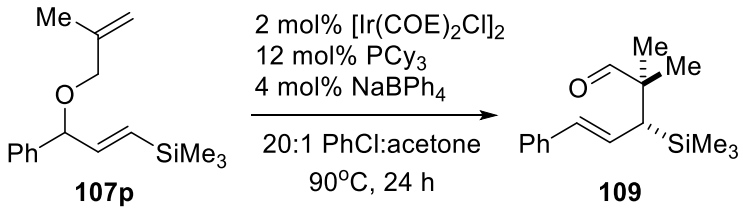

Scheme 98. Synthesis of (*E*)-2,2-Dimethyl-5-phenyl-3-(trimethylsilyl)pent-4-enal (**109**).

A solution of chlorobis(cyclooctene)iridium(I) dimer (2 mol%, 12.2 mg, 0.0136 mmol) and tricyclohexylphosphine (12 mol%, 22.9 mg, 0.0816 mmol) in anhydrous chlorobenzene (0.5 mL) was added to a solution of sodium tetraphenylborate (4 mol%, 9.3 mg, 0.0272 mmol) in a 20:1 mixture of chlorobenzene-acetone (0.5 mL, 0.68 M final concentration in substrate) (Scheme 98).[64] The resulting yellow solution was stirred at room temperature for 5 minutes followed by addition of the diallyl ether (**107p**) (1.00 equiv., 0.1767 g, 0.68 mmol) *via* syringe. The reaction was heated at 90 ºC for 24 h using heating mantle. After cooling to room temperature, the solvent was evaporated under reduced pressure. The crude product was purified by column chromatography (Hexanes/Dichloromethane 8:2) on to afford (**109**) (70.8 mg, 40%) as a colorless oil.

R_f (Hexanes/Dichloromethane 8:2) = 0.24. ^{1}H-NMR (400 MHz, $CDCl_3$) δ 9.48 (1H, s), 7.39-7.28 (4H, m), 7.25-7.16 (1H, m), 6.32 (1H, d, *J* = 15.5 Hz), 6.09 (1H, dd, *J* = 15.5, 11.3 Hz), 2.05 (1H, d, *J* = 11.3 Hz), 1.20 (3H, s), 1.10 (3H, s), 0.07 (9H, s, ^{29}Si isotopomers *J* = 4.0 Hz). ^{13}C{1H}-NMR (100 MHz, $CDCl_3$) δ 206.1, 137.9, 131.2, 128.7, 127.6, 127.1, 126.1, 48.31, 41.5, 22.8, 21.3, -0.2. HRMS (ESI-TOF) *m/z*: $[M + H]^+$ Calcd. for $C_{16}H_{25}OSi$ 261.1669 found 261.1678.

Synthesis of Allyl Vinyl Ethers (**146**)

(*E*)-trimethyl(2-methylene-5-phenyl-3-(prop-1-en-1-yloxy)pentyl)silane (**146a**).

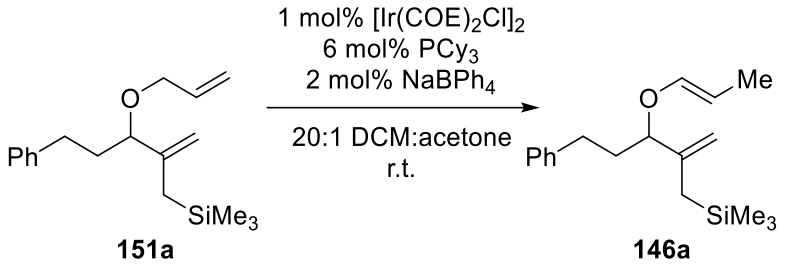

Scheme 99. Synthesis of (*E*)-trimethyl(2-methylene-5-phenyl-3-(prop-1-en-1-yloxy)pentyl)silane (**146a**).

The title compound was prepared by general procedure A from diallyl ether (**151a**)[45] (69.2 mg, 0.24 mmol), $[Ir(COE)_2Cl]_2$ (2.2 mg, 0.0024 mmol), PCy_3 (4.0 mg, 0.0144 mmol) and $NaBPh_4$ (1.6 mg, 0.0048 mmol) (Scheme 99). Isomerization was complete after 1.5 h. The crude product was purified *via* flash column chromatography (Hexanes/Dichloromethane 8:2) on based-washed silica to afford (**146a**) (51.5 mg, 74%) as an amber oil.

R_f (Hexanes/Dichloromethane 8:2) = 0.78. ^{1}H-NMR (500 MHz, $CDCl_3$) δ 7.33-7.25 (2H, m), 7.21-7.16 (3H, m), 6.01 (1H, dq, *J* = 12.2, 1.6 Hz), 4.91 (1H, dq, *J* = 12.0, 6.8 Hz), 4.89 (1H, br s), 4.78 (1H, br s), 3.85 (dd, *J* = 7.8, 4.9 Hz, 1H), 2.74 (1H, ddd, *J* = 14.7, 9.5, 5.6 Hz), 2.63 (1H, ddd, *J* = 13.9, 9.4, 7.0 Hz), 1.98 – 1.81 (m, 2H), 1.53 (3H, dd, *J* = 6.9, 1.5 Hz), 1.53 (1H, d, *J* = 14.5 Hz), 1.37 (1H, d, *J* = 14.5 Hz), 0.02 (s, 9H, ^{29}Si isotopomers *J* = 3.1 Hz). ^{13}C{1H}-NMR (125 MHz, $CDCl_3$) δ 146.2, 145.6, 142.1, 128.7, 128.5, 125.9, 110.5, 101.2, 83.5, 35.5, 31.9, 21.4, 12.6, -0.8. HRMS (ESI-TOF) *m/z*: $[M + H]^+$ Calcd. for $C_{18}H_{29}OSi$ 289.1982 found 289.1988.

(*E*)-trimethyl(2-methylene-4-phenyl-3-(prop-1-en-1-yloxy)butyl)silane (**146b**).

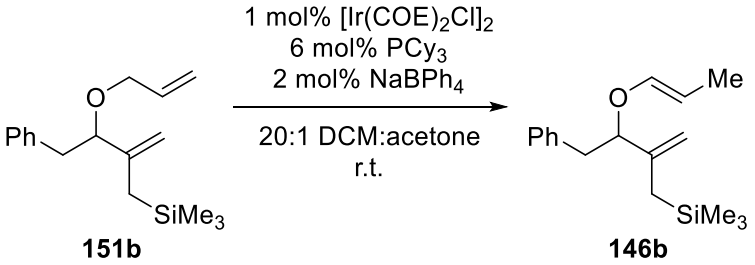

Scheme 100. Synthesis of (*E*)-trimethyl(2-methylene-4-phenyl-3-(prop-1-en-1-yloxy)butyl)silane (**146b**).

The title compound was prepared by general procedure A from diallyl ether (**151b**)[44,172] (98.6 mg, 0.36 mmol), $[Ir(COE)_2Cl]_2$ (3.2 mg, 0.0036 mmol), PCy_3 (6.1 mg, 0.0216 mmol) and $NaBPh_4$ (2.5 mg, 0.0072 mmol) (Scheme 100). Isomerization was complete after 1.5 h. The crude product was purified *via* flash column chromatography (Hexanes/Dichloromethane 9:1) on based-washed silica to afford (**146b**) (88.3 mg, 90%) as an amber oil.

R_f (Hexanes/Dichloromethane 9:1) = 0.56. ^{1}H-NMR (500 MHz, $CDCl_3$) δ 7.31-7.25 (2H, m), 7.25-7.17 (3H, m), 5.95 (1H, dq, *J* = 12.3, 1.6 Hz), 4.86 (1H, dq, *J* = 12.3, 6.8 Hz), 4.85 (1H, br s), 4.76-4.75 (1H, m), 4.07 (1H, dd, *J* = 7.6, 5.1 Hz), 2.89 (1H, ABX system, J_{AB} = -14.1 Hz, J_{AX} = 8.3 Hz), 2.86 (1H, ABX system, J_{AB} = -14.3 Hz, J_{BX} = 4.8 Hz), 1.60 (1H, dd, *J* = 14.5, 1.1 Hz), 1.48 (3H, dd, *J* = 6.8, 1.6 Hz), 1.42 (1H, dd, *J* = 14.5, 1.1 Hz), 0.06 (9H, s, ^{29}Si isotopomers *J* = 3.1 Hz). ^{13}C{1H}-NMR (125 MHz, $CDCl_3$) δ 145.9, 145.5, 138.8, 129.5, 128.3, 126.3, 110.7, 101.3, 85.4, 40.7, 21.6, 12.6, -0.7. HRMS (ESI-TOF) *m/z*: $[M + H]^+$ Calcd. for $C_{17}H_{27}OSi$ 275.1826 found 275.1838.

(*E*)-(2-(cyclohexyl(prop-1-en-1-yloxy)methyl)allyl)trimethylsilane (**146c**).

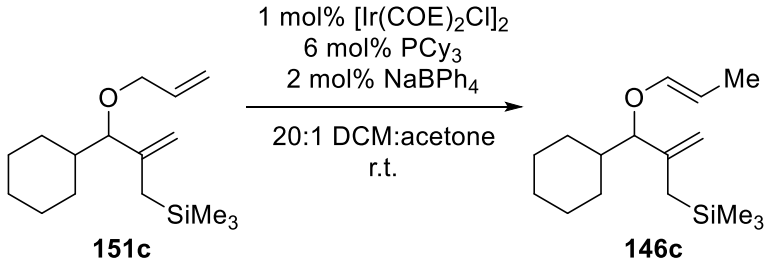

Scheme 101. Synthesis of (*E*)-(2-(cyclohexyl(prop-1-en-1-yloxy)methyl)allyl)trimethylsilane (**146c**).

The title compound was prepared by general procedure A from diallyl ether (**151c**)[44,172] (92.6 mg, 0.35 mmol), $[Ir(COE)_2Cl]_2$ (3.1 mg, 0.0035 mmol), PCy_3 (5.9 mg, 0.0210 mmol) and $NaBPh_4$ (2.4 mg, 0.0070 mmol) (Scheme 101). Isomerization was complete after 1.5 h. The crude product was purified *via* flash column chromatography (Hexanes/Dichloromethane 9:1) on based-washed silica to afford (**146c**) (83.3 mg, 90%) as an amber oil.

R_f (Hexanes/Dichloromethane 9:1) = 0.84. ^{1}H-NMR (500 MHz, $CDCl_3$) δ 6.02 (1H, dq, *J* = 12.3, 1.6 Hz), 4.87 (1H, dq, *J* = 12.3, 6.8 Hz), 4.83-4.82 (2H, m), 3.55 (1H, d, *J* = 7.1 Hz), 1.97-1.90 (1H, m), 1.80-1.71 (2H, m), 1.69-1.63 (1H, m), 1.57-1.46 (1H, m), 1.53 (3H, dd, *J* = 6.8, 1.6 Hz), 1.49 (1H, d, *J* = 14.9 Hz), 1.37 (1H, ddd, *J* = 14.7, 0.8, 0.8 Hz), 1.29-1.11 (3H, m), 1.06-0.93 (2H, m), 0.07 (s, 9H, ^{29}Si isotopomers *J* = 3.2 Hz). ^{13}C{1H}-NMR (125 MHz, $CDCl_3$) δ 146.4, 145.0, 111.9, 100.3, 90.2, 39.7, 30.0, 28.7, 26.7, 26.4, 26.2, 20.8, 12.6, -0.6. HRMS (ESI-TOF) *m/z*: $[M - H]^+$ Calcd. for $C_{16}H_{29}OSi$ 265.1982 found 265.1991.

(*E*)-trimethyl(2-(phenyl(prop-1-en-1-yloxy)methyl)allyl)silane (**146d**).

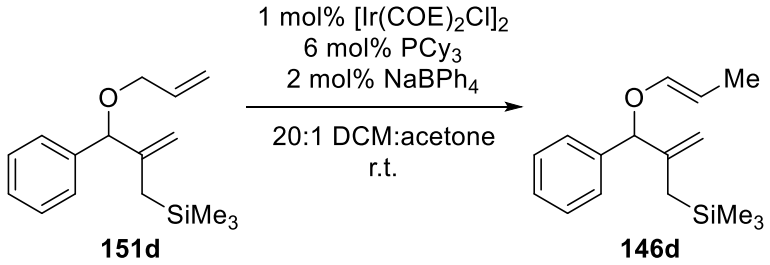

Scheme 102. Synthesis of (*E*)-trimethyl(2-(phenyl(prop-1-en-1-yloxy)methyl)allyl)silane (**146d**).

The title compound was prepared by general procedure A from diallyl ether (**151d**)[44,172] (393.6 mg, 1.60 mmol), $[Ir(COE)_2Cl]_2$ (14.3 mg, 0.0160 mmol), PCy_3 (26.9 mg, 0.0960 mmol) and $NaBPh_4$ (11.0 mg, 0.0320 mmol) (Scheme 102). Isomerization was complete after 1.5 h. The crude product was purified *via* flash column chromatography (Hexanes/Dichloromethane 9:1) on based-washed silica to afford (**146d**) (380.2 mg, 96%) as an amber oil.

R_f (Hexanes/Dichloromethane 9:1) = 0.67. ^{1}H-NMR (500 MHz, $CDCl_3$) δ 7.36-7.31 (4H, m), 7.30-7.27 (1H, m), 6.11 (1H, dq, *J* = 12.3, 1.6 Hz), 4.99 (1H, dd, *J* = 1.4, 1.4 Hz), 4.93 (1H, dq, *J* = 12.3, 6.8 Hz), 4.92 (1H, br s), 4.81-4.80 (1H, m), 1.52 (1H, dd, *J* = 14.2, 1.0 Hz), 1.50 (3H, dd, *J* = 6.8, 1.6 Hz), 1.32 (1H, dd, *J* = 14.2, 1.0 Hz), -0.01 (9H, s, ^{29}Si isotopomers *J* = 3.3 Hz). ^{13}C{1H}-NMR (125 MHz, $CDCl_3$) δ 146.4, 145.4, 140.0, 128.4, 127.8, 127.4, 110.6, 101.7, 85.8, 22.2, 12.7, -0.9. HRMS (ESI-TOF) *m/z*: $[M + H]^+$ Calcd. for $C_{16}H_{25}OSi$ 261.1669 found 261.1679.

(*E*)-(2-((2-fluorophenyl)(prop-1-en-1-yloxy)methyl)allyl)trimethylsilane (**146e**).

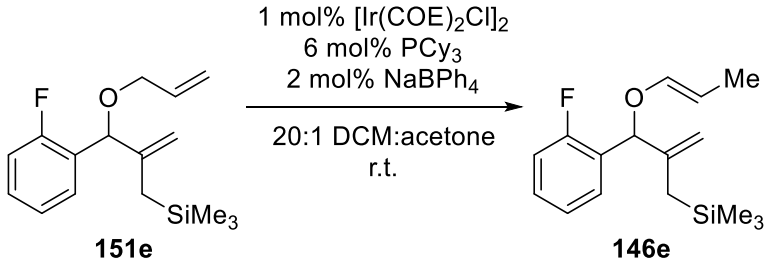

Scheme 103. Synthesis of (*E*)-(2-((2-fluorophenyl)(prop-1-en-1-yloxy)methyl)allyl)trimethylsilane (**146e**).

The title compound was prepared by general procedure A from diallyl ether (**151e**)[44,172] (275.6 mg, 0.99 mmol), $[Ir(COE)_2Cl]_2$ (8.9 mg, 0.0099 mmol), PCy_3 (16.7 mg, 0.0594 mmol) and $NaBPh_4$ (6.8 mg, 0.0198 mmol) (Scheme 103). Isomerization was complete after 1.5 h. The crude product was purified *via* flash column chromatography (Hexanes/Dichloromethane 8:2) on based-washed silica to afford (**146e**) (261.4 mg, 95%) as an amber oil.

R_f (Hexanes/Dichloromethane 8:2) = 0.83. ^{1}H-NMR (500 MHz, $CDCl_3$) δ 7.40 (1H, ddd, *J* = 7.5, 7.5, 1.8 Hz), 7.29-7.23 (1H, m), 7.14 (1H, ddd, *J* = 7.5, 1.0 Hz; $^4J_{HF}$ = 7.5 Hz), 7.03 (1H, ddd, *J* = 8.2, 1.1 Hz, $^3J_{HF}$ =9.5), 6.10 (1H, dq, *J* = 12.3, 1.6 Hz), 5.29 (1H, s), 4.94 (1H, br s), 4.91 (1H, dq *J* = 12.3, 6.8 Hz), 4.82-4.79 (1H, m), 1.60 (1H, dd, *J* = 14.1, 1.1 Hz), 1.49 (3H, dd, *J* = 6.8, 1.6 Hz), 1.35 (1H, d, *J* = 14.1 Hz), 0.02 (s, 9H, ^{29}Si isotopomers *J* = 3.3 Hz). ^{13}C{1H}-NMR (125 MHz, $CDCl_3$) δ 160.6 (d, $^1J_{CF}$ = 243.8 Hz), 145.3, 145.1, 129.4 (d, $^3J_{CF}$ = 7.5 Hz), 128.8 (d, $^3J_{CF}$ = 3.8 Hz), 127.2 (d, $^2J_{CF}$ = 13.8 Hz), 124.4 (d, $^4J_{CF}$ = 3.8 Hz), 115.3 (d, $^2J_{CF}$ = 22.5 Hz), 110.5, 101.8, 77.8 (d, $^3J_{CF}$ = 2.5 Hz), 22.7, 12.6, 1.1. ^{19}F-NMR (470.6 MHz, $CDCl_3$) δ -118.7 (m). HRMS (ESI-TOF) *m/z*: $[M + NH_4]^+$ Calcd. for $C_{16}H_{27}FNOSi$ 296.1840 found 296.1836.

Synthesis of Cyclopentenols (**110**) *via* Claisen-Sakurai Reaction

2-Benzyl-5-methylcyclopent-3-en-1-ol (**110a**).

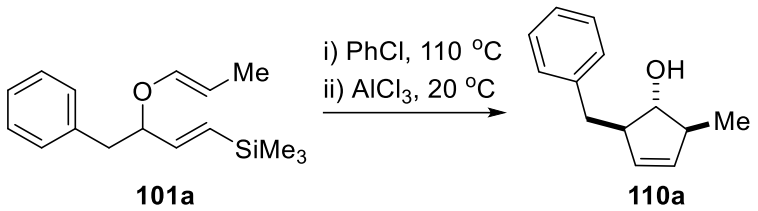

101a **110a**

Scheme 104. Synthesis of 2-benzyl-5-methylcyclopent-3-en-1-ol (**110a**).

The title compound was prepared by general procedure B from allyl vinyl ether (**101a**) (26.5 mg, 0.10 mmol) with initial heating at 110 °C for 20 hours followed by treatment with $AlCl_3$ (20.0 mg, 0.15 mmol) (Scheme 104). The crude product was purified *via* column chromatography (Hexanes/Ethyl acetate 95:5) to afford (**110a**) (10.9 mg, 58%) as a yellow oil.

R_f (Hexanes/Ethyl acetate 9:1) = 0.22. ^{1}H-NMR (500 MHz, $CDCl_3$) δ 7.32-7.29 (2H, m), 7.23-7.19 (3H, m), 5.56 (1H, ddd, *J* = 6.1, 1.8, 1.8 Hz), 5.54 (1H, ddd, *J* = 6.1, 1.8, 1.8 Hz), 3.64 (1H, dd, *J* = 5.4, 5.4 Hz), 2.82 (1H, dddddd, *J* = 8.7, 6.9, 5.3, 1.8, 1.8, 1.8 Hz), 2.76 (1H, ABX system, J_{AB} =13.2 Hz, J_{AX} =6.6 Hz), 2.74 (1H, ABX system, J_{AB} =13.3 Hz, J_{BX} =8.8 Hz), 2.58 (1H, qdddd, *J* = 7.0, 5.6, 1.8, 1.8, 1.8 Hz), 1.45 (1H, br s), 1.11 (3H, d, *J* = 7.0 Hz). ^{13}C{1H}-NMR (125 MHz, $CDCl_3$) δ 140.5, 134.5, 131.3, 129.0, 128.7, 126.3, 85.9, 56.0, 48.5, 40.6, 18.9. HRMS (ESI-TOF) *m/z*: $[M - H]^+$ Calcd. for $C_{13}H_{15}O$ 187.1117 found 187.1116.

2-Cyclohexyl-5-methylcyclopent-3-en-1-ol (**110b**).

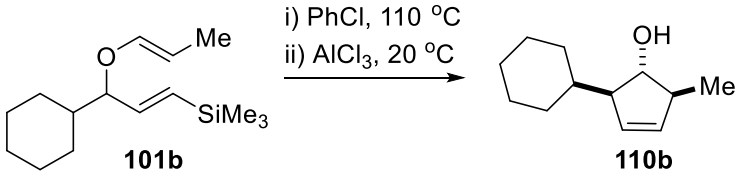

101b **110b**

Scheme 105. Synthesis of 2-cyclohexyl-5-methylcyclopent-3-en-1-ol (**110b**).

The title compound was prepared by general procedure B from allyl vinyl ether (**101b**) (25.2 mg, 0.10 mmol) with initial heating at 110 °C for 24 hours followed by treatment with $AlCl_3$ (20.0 mg, 0.15 mmol) (Scheme 105). The crude product was purified *via* column chromatography (Hexanes/Ethyl acetate 95:5) to afford (**110b**) (9.0 mg, 50%) as a light-yellow oil.

R_f (Hexanes/Ethyl acetate 9:1) = 0.23. ^{1}H-NMR (500 MHz, $CDCl_3$) δ 5.59 (1H, ddd, *J* = 6.1, 2.0, 2.0 Hz), 5.52 (1H, ddd, *J* = 6.0, 2.1, 2.1 Hz), 3.69 (1H, dd, *J* = 5.3, 5.3 Hz), 2.54 (1H, qdddd, *J* = 7.1, 5.3, 2.0, 2.0, 2.0 Hz), 2.31 (1H, ddddd, *J* = 7.3, 5.3, 2.0, 2.0, 2.0 Hz), 1.80-1.71 (4H, m), 1.69-1.65 (1H, m), 1.55 (1H, br s), 1.31-1.12 (4H, m), 1.10 (3H, d, *J* = 7.1 Hz), 1.07-0.92 (2H, m). ^{13}C{1H}-NMR (125 MHz, $CDCl_3$) δ 134.0, 130.3, 83.8, 60.8, 49.1, 41.1, 31.7, 31.0, 26.7, 26.6, 26.6, 19.1. HRMS (ESI-TOF) *m/z*: $[M - H]^+$ Calcd. for $C_{12}H_{19}O$ 179.1430 found 179.1430.

2-(2-(Benzyloxy)ethyl)-5-methylcyclopent-3-en-1-ol (**110c**).

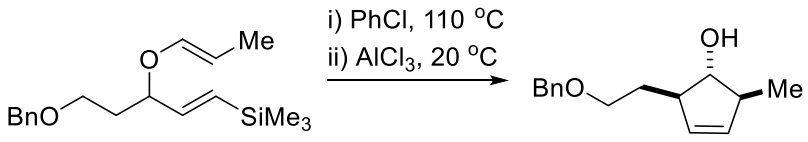

101c **110c**

Scheme 106. Synthesis of 2-(2-(benzyloxy)ethyl)-5-methylcyclopent-3-en-1-ol (**110c**).

The title compound was prepared by general procedure B from allyl vinyl ether (**101c**) (30.4 mg, 0.10 mmol) with initial heating at 110 °C for 24 hours followed by treatment with $AlCl_3$ (20.0 mg, 0.15 mmol) (Scheme 106). The crude product was purified *via* column chromatography (Hexanes/Ethyl acetate 9:1) to afford (**110c**) (10.0 mg, 43%) as a light-yellow oil.

R_f (Hexanes/Ethyl acetate 9:1) = 0.11. ^{1}H-NMR (500 MHz, $CDCl_3$) δ 7.38-7.28 (5H, m), 5.51 (1H, ddd, *J* = 6.0, 2.0, 2.0 Hz), 5.44 (1H, ddd, *J* = 6.0, 2.0, 2.0 Hz), 4.57-4.52 (2H, m), 3.66 (1H, ddd, *J* = 9.5, 4.8, 4.8 Hz), 3.61 (1H, ddd, *J* = 9.5, 9.5, 4.0 Hz), 3.53 (1H, dd, *J* = 6.8, 6.8 Hz), 2.63 (1H, qdddd, *J* = 6.9, 6.8, 2.3, 2.3, 2.3 Hz), 2.57 (1H, dddddd, *J* = 9.5, 6.8, 4.1, 2.3, 2.3, 2.3 Hz), 1.84 (1H, dddd, *J* = 14.4, 4.1, 4.1, 4.1 Hz), 1.69 (1H, dddd, *J* = 14.5, 9.5, 9.5, 4.9 Hz), 1.12 (3H, d, *J* = 6.9 Hz). ^{13}C{1H}-NMR (125 MHz, $CDCl_3$) δ 137.8, 134.7, 132.0, 128.7, 128.0, 128.0, 87.5, 73.5, 70.4, 53.2, 47.3, 34.5, 18.7. HRMS (ESI-TOF) *m/z*: $[M + H]^+$ Calcd. for $C_{15}H_{21}O_2$ 233.1536 found 233.1536.

2-Methyl-5-phenylcyclopent-3-en-1-ol (**110d**).

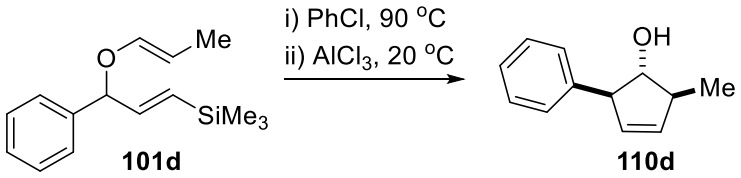

101d **110d**

Scheme 107. Synthesis of 2-methyl-5-phenylcyclopent-3-en-1-ol (**110d**).

The title compound was prepared by general procedure B from allyl vinyl ether (**101d**) (24.6 mg, 0.10 mmol) with initial heating at 90 °C for 16 hours followed by treatment with $AlCl_3$ (20.0 mg, 0.15 mmol) (Scheme 107). The crude product was purified *via* column chromatography (Hexanes/Ethyl acetate 95:5) to afford (**110d**) (11.8 mg, 68%) as a white solid.

Larger scale synthesis: the title compound was prepared by general procedure B from allyl vinyl ether **1d** (0.2464 g, 1.0 mmol) with initial heating at 90 °C for 16 hours followed by treatment with $AlCl_3$ (0.2 g, 1.5 mmol). The crude product was purified *via* column chromatography (Hexanes/Ethyl acetate 95:5) to afford (**2d**) (0.1219 g, 70%) as a white solid.

R_f (Hexanes/Ethyl acetate 9:1) = 0.22. ^{1}H-NMR (500 MHz, $CDCl_3$) δ 7.36-7.32 (2H, m), 7.27-7.24 (3H, m), 5.75 (1H, ddd, *J* = 5.9, 1.6, 1.6 Hz), 5.68 (1H, ddd, *J* = 5.9, 1.6, 1.6 Hz), 3.75-3.73 (2H, m), 2.72 (1H, qdddd, *J* = 7.0, 6.4, 2.1, 2.1, 2.1 Hz), 1.84 (1H, br s), 1.17 (3H, d, *J* = 7.0 Hz). ^{13}C{1H}-NMR (125 MHz, $CDCl_3$) δ 143.6, 135.7, 130.8, 128.7, 127.6, 126.8, 89.8, 59.9, 47.8, 18.4. HRMS (ESI-TOF) *m/z*: $[M - H]^+$ Calcd. for $C_{12}H_{13}O$ 173.0961 found 173.0958.

2-(4-Methoxyphenyl)-5-methylcyclopent-3-en-1-ol (**110e**).

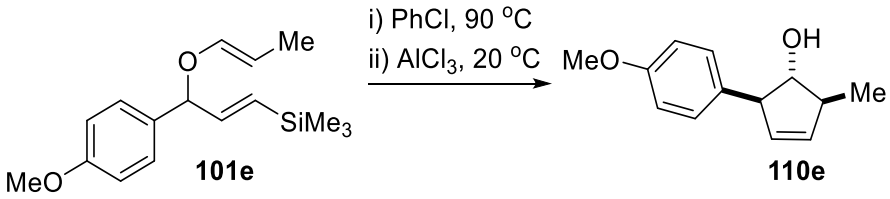

Scheme 108. Synthesis of 2-(4-methoxyphenyl)-5-methylcyclopent-3-en-1-ol (**110e**).

The title compound was prepared by general procedure B from allyl vinyl ether (**101e**) (27.6 mg, 0.10 mmol) with initial heating at 90 °C for 16 hours followed by treatment with $AlCl_3$ (20.0 mg, 0.15 mmol) (Scheme 108). The crude product was purified *via* column chromatography (Hexanes/Ethyl acetate 9:1) to afford (**110e**) (13.9 mg, 68%) as a yellow oil.

R_f (Hexanes/Ethyl acetate 9:1) = 0.12. ^{1}H-NMR (500 MHz, $CDCl_3$) δ 7.15 (2H, AA'XX' system, $J_{AA'}$ =2.5 Hz, J_{AX} =8.7 Hz, $J_{XX'}$ =2.5 Hz, $J_{AX'}$ =0.0 Hz), 6.87 (2H, AA'XX' system, $J_{AA'}$ =2.5 Hz, J_{AX} =8.7 Hz, $J_{XX'}$ =2.5 Hz, $J_{AX'}$ =0.0 Hz), 5.71 (1H, ddd, *J* = 5.9, 1.9, 1.9 Hz), 5.64 (1H, ddd, *J* = 5.9, 1.9, 1.9 Hz), 3.80 (3H, s), 3.70-3.68 (2H, m), 2.68 (1H, qdddd, *J* = 7.0, 5.7, 2.2,2.2, 2.2 Hz), 1.87 (1H, br s), 1.15 (3H, d, *J* = 7.0 Hz). ^{13}C{1H}-NMR (125 MHz, $CDCl_3$) δ 158.5, 135.7, 135.4, 131.1, 128.6, 114.1, 89.9, 59.0, 55.4, 47.7, 18.4. HRMS (ESI-TOF) *m/z*: $[M + H]^+$ Calcd. for $C_{13}H_{17}O_2$ 205.1223 found 205.1220.

2-(4-Fluoromethylphenyl)-5-methylcyclopent-3-en-1-ol (**110f**).

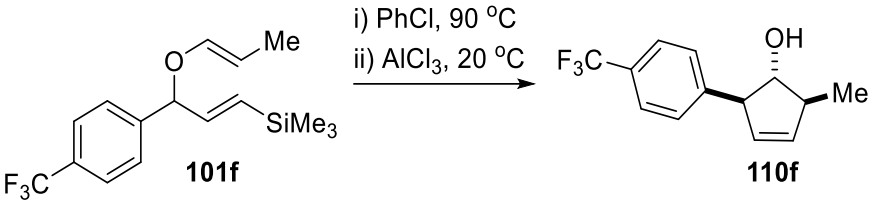

Scheme 109. Synthesis of 2-(4-fluoromethylphenyl)-5-methylcyclopent-3-en-1-ol (**110f**).

The title compound was prepared by general procedure B from allyl vinyl ether (**101f**) (31.4 mg, 0.10 mmol) with initial heating at 90 °C for 16 hours followed by treatment with $AlCl_3$ (20.0 mg, 0.15 mmol) (Scheme 109). The crude product was purified *via* column chromatography (Hexanes/Ethyl acetate 95:5) to afford (**110f**) (13.8 mg, 57%) as a beige solid.

R_f (Hexanes/Ethyl acetate 9:1) = 0.18. ^{1}H-NMR (500 MHz, $CDCl_3$) δ 7.58 (2H, d, *J* =8.1 Hz), 7.35 (2H, d, *J* =8.1 Hz), 5.79 (1H, ddd, *J* = 6.0, 2.1, 2.1 Hz), 5.65 (1H, ddd, *J* = 6.0, 2.1, 2.1 Hz), 3.80 (1H, dddd, *J* = 6.5, 2.1, 2.1, 2.1 Hz), 3.71 (1H, dd, *J* = 6.5, 6.5 Hz), 2.72 (1H, qdddd, *J* = 7.0, 7.0, 2.1, 2.1, 2.1 Hz), 1.83 (1H, br s), 1.16 (3H, d, *J* = 7.0 Hz). ^{13}C{1H}-NMR (125 MHz, $CDCl_3$) δ 147.7, 136.5, 129.9, 129.1 (q, $^2J_{CF}$ = 32.1 Hz), 127.9, 125.6 (q, $^3J_{CF}$ = 3.6 Hz), 124.5 (q, $^1J_{CF}$ = 271.8 Hz), 89.6, 59.5, 48.1, 18.3. ^{19}F-NMR (470.6 MHz, $CDCl_3$) δ -62.4 (s). HRMS (ESI-TOF) *m/z*: $[M - H]^+$ Calcd. for $C_{13}H_{12}F_3O$ 241.0835 found 241.0842.

2-Methyl-5-(4-(trifluoromethoxy)phenyl)cyclopent-3-en-1-ol (**110g**).

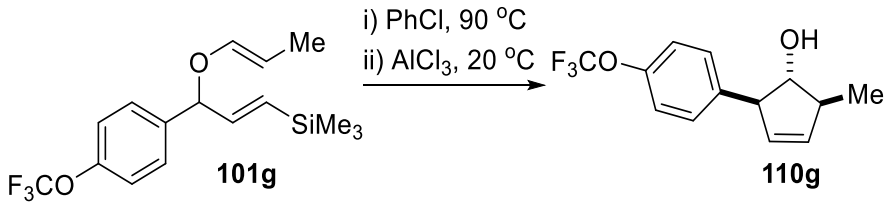

Scheme 110. Synthesis of 2-methyl-5-(4-(trifluoromethoxy)phenyl)cyclopent-3-en-1-ol (**110g**).

The title compound was prepared by general procedure B from allyl vinyl ether (**101g**) (33.0 mg, 0.10 mmol) with initial heating at 90 °C for 16 hours followed by treatment with $AlCl_3$ (20.0 mg, 0.15 mmol) (Scheme 110). The crude product was purified *via* column chromatography (Hexanes/Ethyl acetate 9:1) to afford (**110g**) (14.4 mg, 56%) as a yellow solid.

R_f (Hexanes/Ethyl acetate 9:1) = 0.16. ^{1}H-NMR (500 MHz, $CDCl_3$) δ 7.25 (2H, AA'BB' system, $J_{AA'}$ =2.3 Hz, J_{AB} =8.7 Hz, $J_{BB'}$ =2.3 Hz, $J_{AB'}$ =0.0 Hz), 7.17 (2H, AA'BB' system, $J_{AA'}$ =2.3 Hz, J_{AB} =8.7 Hz, $J_{BB'}$ =2.3 Hz, $J_{AB'}$ =0.0 Hz), 5.76 (1H, ddd, *J* = 6.0, 2.1, 2.1 Hz), 5.64 (1H, ddd, *J* = 6.0, 2.1, 2.1 Hz), 3.75 (1H, dddd, *J* = 6.7, 2.2, 2.2, 2.2 Hz), 3.70 (1H, dd, *J* = 6.5, 6.5 Hz), 2.70 (1H, qdddd, *J* = 7.0, 7.0, 2.2, 2.2, 2.2 Hz), 1.86 (1H, br s), 1.16 (3H, d, *J* = 7.0 Hz). ^{13}C{1H}-NMR (125 MHz, $CDCl_3$) δ 148.1, 142.4, 136.1, 130.3, 128.9, 121.3, 120.7 (q, $^1J_{CF}$ = 256.8 Hz), 89.8, 59.1, 47.9, 18.3. ^{19}F-NMR (470.6 MHz, $CDCl_3$) δ -57.9 (s). HRMS (ESI-TOF) *m/z*: $[M - H]^+$ Calcd. for $C_{13}H_{12}F_3O_2$ 257.0784 found 257.0783.

2-(4-Fluorophenyl)-5-methylcyclopent-3-en-1-ol (**110h**).

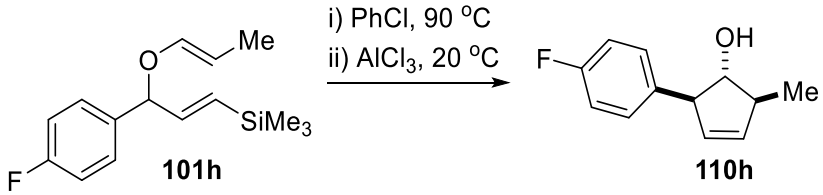

Scheme 111. Synthesis of 2-(4-fluorophenyl)-5-methylcyclopent-3-en-1-ol (**110h**).

The title compound was prepared by general procedure B from allyl vinyl ether (**101h**) (26.4 mg, 0.10 mmol) with initial heating at 90 °C for 16 hours followed by treatment with $AlCl_3$ (20.0 mg, 0.15 mmol) (Scheme 111). The crude product was purified *via* column chromatography (Hexanes/Ethyl acetate 95:5) to afford (**110h**) (12.8 mg, 67%) as a light-yellow oil.

R_f (Hexanes/Ethyl acetate 95:5) = 0.06. ^{1}H-NMR (500 MHz, $CDCl_3$) δ 7.19 (2H, AA'XX' system, $J_{AA'}$ = 2.5 Hz, J_{AX} = 9.0 Hz, $J_{XX'}$ = 2.5 Hz, $J_{AX'}$ = 0.0 Hz; $^4J_{HF}$ = 5.4 Hz), 7.01 (2H, AA'XX' system, $J_{AA'}$ = 2.5 Hz, J_{AX} = 9.0 Hz, $J_{XX'}$ = 2.5 Hz, $J_{AX'}$ = 0.0 Hz; $^3J_{HF}$ = 9.0 Hz), 5.74 (1H, ddd, *J* = 6.1, 2.1, 2.1 Hz), 5.63 (1H, ddd, *J* = 6.1, 2.1, 2.1 Hz), 3.71 (1H, dddd, *J* = 6.5, 2.1, 2.1, 2.1 Hz), 3.68 (1H, dd, *J* = 6.5, 6.5 Hz), 2.69 (1H, qdddd, *J* = 7.1, 7.1, 2.3, 2.3, 2.3 Hz), 1.84 (1H, br s), 1.15 (3H, d, *J* = 7.1 Hz). ^{13}C{1H}-NMR (125 MHz, $CDCl_3$) δ 161.9 (d, $^1J_{CF}$ = 244.3 Hz), 139.3 (d, $^4J_{CF}$ = 2.8 Hz), 135.8, 130.6, 129.0 (d, $^3J_{CF}$ = 8.1 Hz), 115.4 (d, $^2J_{CF}$ = 21.4 Hz), 89.8, 59.0, 47.9, 18.3. ^{19}F-NMR (470.6 MHz, $CDCl_3$) δ -116.7 (tt, $^3J_{HF}$ = 9.0 Hz, $^4J_{HF}$ = 5.4 Hz). HRMS (ESI-TOF) *m/z*: $[M + H]^+$ Calcd. for $C_{12}H_{14}FO$ 193.1023 found 193.1030.

2-(3-Fluorophenyl)-5-methylcyclopent-3-en-1-ol (**110i**).

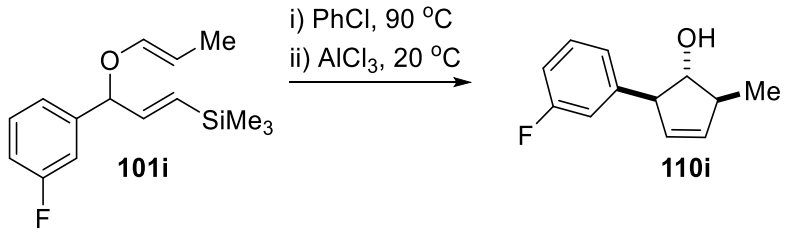

Scheme 112. Synthesis of 2-(3-fluorophenyl)-5-methylcyclopent-3-en-1-ol (**110i**).

The title compound was prepared by general procedure B from allyl vinyl ether (**101i**) (26.4 mg, 0.10 mmol) with initial heating at 90 °C for 17 hours followed by treatment with $AlCl_3$ (20.0 mg, 0.15 mmol) (Scheme 112). The crude product was purified *via* column chromatography (Hexanes/Ethyl acetate 95:5) to afford (**110i**) (12.2 mg, 64%) as a light-yellow oil.

R_f (Hexanes/Ethyl acetate 9:1) = 0.15. ^{1}H-NMR (500 MHz, $CDCl_3$) δ 7.30-7.27 (1H, m), 7.02 (1H, ddd, *J* = 7.6, 2.3, 2.3 Hz), 6.95-6.91 (2H, m), 5.76 (1H, ddd, *J* = 6.1, 2.0, 2.0 Hz), 5.64

(1H, ddd, *J* = 6.1, 2.1, 2.1 Hz), 3.74 (1H, dddd, *J* = 6.5, 2.1, 2.1, 2.1 Hz), 3.72 (1H, dd, *J* = 6.5, 6.5 Hz), 2.71 (1H, qdddd, *J* = 7.0, 7.0, 2.3, 2.3, 2.3 Hz), 1.83 (1H, br s), 1.16 (3H, d, *J* = 7.0 Hz). ^{13}C{1H}-NMR (125 MHz, $CDCl_3$) δ 163.2 (d, $^{1}J_{CF}$ = 245.5 Hz), 146.3 (d, $^{3}J_{CF}$ = 6.9 Hz), 136.2, 130.2, 130.1 (d, $^{3}J_{CF}$ = 8.4 Hz), 123.3 (d, $^{4}J_{CF}$ = 2.6 Hz), 114.4 (d, $^{2}J_{CF}$ = 21.5 Hz), 113.6 (d, $^{2}J_{CF}$ = 21.0 Hz), 89.6, 59.5, 48.0, 18.3. ^{19}F-NMR (470.6 MHz, $CDCl_3$) δ -113.2 (ddd, $^{3}J_{HF}$ = 8.6, 8.6 Hz, $^{4}J_{HF}$ = 5.3 Hz). HRMS (ESI-TOF) *m/z*: $[M - H]^+$ Calcd. for $C_{12}H_{12}FO$ 191.0867 found 191.0867.

2-(2-Fluorophenyl)-5-methylcyclopent-3-en-1-ol (**110j**).

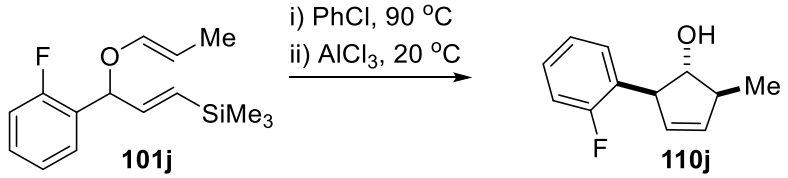

Scheme 113. Synthesis of 2-(2-fluorophenyl)-5-methylcyclopent-3-en-1-ol (**110j**).

The title compound was prepared by general procedure B from allyl vinyl ether (**101j**) (26.4 mg, 0.10 mmol) with initial heating at 90 °C for 16 hours followed by treatment with $AlCl_3$ (20.0 mg, 0.15 mmol) (Scheme 113). The crude product was purified *via* column chromatography (Hexanes/Ethyl acetate 95:5) to afford (**110j**) (10.1 mg, 53%) as a light-yellow oil.

R_f (Hexanes/Ethyl acetate 9:1) = 0.17. ^{1}H-NMR (500 MHz, $CDCl_3$) δ 7.24-7.20 (1H, m), 7.17 (1H, ddd, *J* = 7.5, 1.9 Hz; $^{4}J_{HF}$ = 7.5 Hz), 7.10 (1H, ddd, *J* = 7.5, 7.5, 1.3 Hz), 7.05 (1H, ddd, *J* =8.1, 1.1 Hz; $^{3}J_{HF}$ = 10.4 Hz), 5.80 (1H, ddd, *J* = 6.0, 2.1, 2.1 Hz), 5.64 (1H, ddd, *J* = 6.0, 2.1, 2.1 Hz), 4.08 (1H, dddd, *J* = 5.9, 2.0, 2.0, 2.0 Hz), 3.84 (1H, dd, *J* = 5.6, 5.6 Hz), 2.73 (1H, qdddd, *J* = 7.1, 5.6, 2.0, 2.0, 2.0 Hz), 1.89 (1H, br s), 1.13 (3H, d, *J* = 7.1 Hz). ^{13}C{1H}-NMR

(125 MHz, $CDCl_3$) δ 161.3 (d, $^1J_{CF}$ = 245.1 Hz), 136.3, 130.3 (d, $^2J_{CF}$ = 14.6 Hz), 129.4, 128.8 (d, $^3J_{CF}$ = 4.6 Hz), 128.2 (d, $^3J_{CF}$ = 8.2 Hz), 124.4 (d, $^4J_{CF}$ = 3.6 Hz), 115.4 (d, $^2J_{CF}$ = 22.6 Hz), 88.3, 53.2, 48.3, 18.6. ^{19}F-NMR (470.6 MHz, $CDCl_3$) δ -118.3 (m). HRMS (ESI-TOF) *m/z*: $[M - H]^+$ Calcd. for $C_{12}H_{12}FO$ 191.0867 found 191.0861.

2-Methyl-5-(naphthalen-2-yl)cyclopent-3-en-1-ol (**110k**).

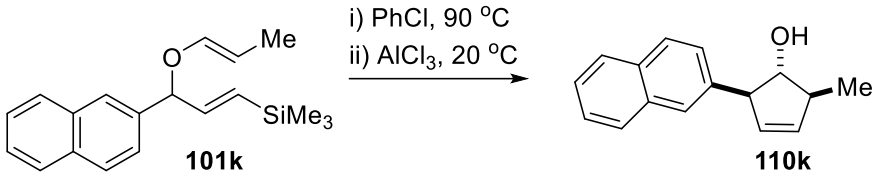

Scheme 114. Synthesis of 2-methyl-5-(naphthalen-2-yl)cyclopent-3-en-1-ol (**110k**).

The title compound was prepared by general procedure B from allyl vinyl ether (**101k**) (29.6 mg, 0.10 mmol) with initial heating at 90 °C for 17 hours followed by treatment with $AlCl_3$ (20.0 mg, 0.15 mmol) (Scheme 114). The crude product was purified *via* column chromatography (Hexanes/Ethyl acetate 95:5) to afford (**110k**) (15.8 mg, 71%) as a white solid.

R_f (Hexanes/Ethyl acetate 9:1) = 0.13. ^{1}H-NMR (500 MHz, $CDCl_3$) δ 7.83-7.79 (3H, m), 7.67 (1H, d, *J* = 1.7 Hz), 7.47 (1H, ddd, *J* = 6.9, 6.9, 1.5 Hz), 7.44 (1H, ddd, *J* = 6.9, 6.9, 1.5 Hz), 7.39 (1H, dd, *J* = 8.5, 1.7 Hz), 5.80 (1H, ddd, *J* = 6.0, 2.1, 2.1 Hz), 5.76 (1H, ddd, *J* = 6.0, 2.1, 2.1 Hz), 3.91 (1H, dddd, *J* = 6.5, 2.2, 2.2, 2.2 Hz), 3.85-3.82 (1H, m), 2.76 (1H, qdddd, *J* = 7.0, 7.0, 2.1, 2.1, 2.1 Hz), 1.89 (1H, d, *J* = 3.5 Hz), 1.19 (3H, d, *J* = 7.0 Hz). ^{13}C{1H}-NMR (125 MHz, $CDCl_3$) δ 141.0, 135.9, 133.7, 132.6, 130.8, 128.4, 127.8, 127.8, 126.2, 126.1, 126.0, 125.6, 89.6, 60.0, 48.0, 18.4. HRMS (ESI-TOF) *m/z*: $[M - H]^+$ Calcd. for $C_{16}H_{15}O$ 223.1117 found 223.1119.

2-(2-Fluoro-4-methoxyphenyl)-5-methylcyclopent-3-en-1-ol (**110l**).

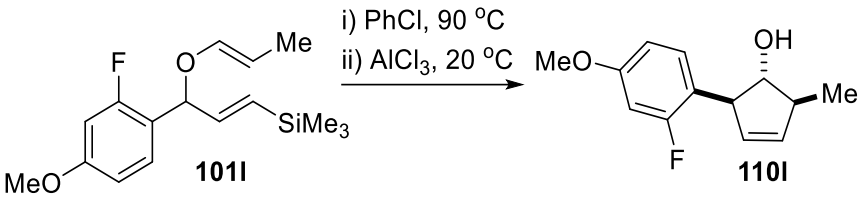

Scheme 115. Synthesis of 2-(2-fluoro-4-methoxyphenyl)-5-methylcyclopent-3-en-1-ol (**110l**).

The title compound was prepared by general procedure B from allyl vinyl ether (**101l**) (29.4 mg, 0.10 mmol) with initial heating at 90 °C for 16 hours followed by treatment with $AlCl_3$ (20.0 mg, 0.15 mmol) (Scheme 115). The crude product was purified *via* column chromatography (Hexanes/Ethyl acetate 9:1) to afford (**110l**) (15.5 mg, 70%) as a yellow oil.

R_f (Hexanes/Ethyl acetate 9:1) = 0.14. ^{1}H-NMR (500 MHz, $CDCl_3$) δ 7.05 (1H, dd, J = 8.6 Hz; $^4J_{HF}$ = 8.6 Hz), 6.66 (1H, dd, J = 8.6, 2.5 Hz), 6.62 (1H, dd, J = 2.5 Hz; $^3J_{HF}$ = 11.9 Hz), 5.77 (1H, ddd, J = 6.0, 2.2, 2.2 Hz), 5.61 (1H, ddd, J = 6.0, 2.2, 2.2 Hz), 3.99 (1H, dddd, J = 5.7, 1.9, 1.9, 1.9 Hz), 3.79 (1H, dd, J = 6.0, 6.0 Hz), 3.78 (3H, s), 2.69 (1H, qdddd, J = 7.1, 6.0, 2.0, 2.0, 2.0 Hz), 1.90 (1H, br s), 1.12 (3H, d, J = 7.1 Hz). ^{13}C{1H}-NMR (125 MHz, $CDCl_3$) δ 161.7 (d, $^1J_{CF}$ = 245.0 Hz), 159.6 (d, $^3J_{CF}$ = 11.0 Hz), 136.0, 129.7, 129.1 (d, $^3J_{CF}$ = 6.6 Hz), 122.1 (d, $^2J_{CF}$ = 15.4 Hz), 110.0 (d, $^4J_{CF}$ = 2.8 Hz), 101.7 (d, $^2J_{CF}$ = 26.0 Hz), 88.4, 55.7, 52.7, 48.2, 18.6. ^{19}F-NMR (470.6 MHz, $CDCl_3$) δ -116.2 (dd, $^3J_{HF}$ = 11.9, $^4J_{HF}$ = 8.6 Hz). HRMS (ESI-TOF) *m/z*: $[M + NH_4]^+$ Calcd. for $C_{13}H_{19}FNO_2$ 240.1394 found 240.1396.

2-(2,4-Difluorophenyl)-5-methylcyclopent-3-en-1-ol (**110m**).

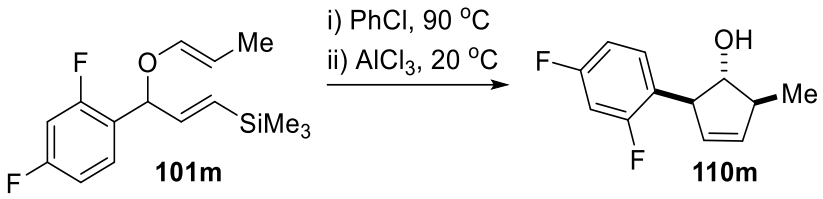

Scheme 116. Synthesis of 2-(2,4-difluorophenyl)-5-methylcyclopent-3-en-1-ol (**110m**).

The title compound was prepared by general procedure B from allyl vinyl ether (**101m**) (28.2 mg, 0.10 mmol) with initial heating at 90 °C for 16 hours followed by treatment with $AlCl_3$ (20.0 mg, 0.15 mmol) (Scheme 116). The crude product was purified *via* column chromatography (Hexanes/Ethyl acetate 95:5) to afford (**110m**) (12.0 mg, 57%) as a white solid.

R_f (Hexanes/Ethyl acetate 9:1) = 0.20. ^{1}H-NMR (500 MHz, $CDCl_3$) δ 7.13 (1H, ddd, J = 6.5 Hz; $^4J_{HF}$ = 8.6, 8.6 Hz), 6.85-6.79 (2H, m), 5.80 (1H, ddd, J = 6.0, 2.2, 2.2 Hz), 5.60 (1H, ddd, J = 6.0, 2.0, 2.0 Hz), 4.03-4.01 (1H, m), 3.80-3.77 (1H, m), 2.71 (1H, qdddd, J = 7.1, 5.3, 2.0, 2.0, 2.0 Hz), 1.91 (d, J = 3.8 Hz), 1.12 (d, J = 7.1 Hz). ^{13}C{1H}-NMR (125 MHz, $CDCl_3$) δ 161.8 (dd, $^1J_{CF}$ = 247.4 Hz, $^3J_{CF}$ = 12.2 Hz), 161.0 (dd, $^1J_{CF}$ = 247.5 Hz, $^3J_{CF}$ = 11.8 Hz), 136.6, 129.5 (dd, $^3J_{CF}$ = 9.2, 6.4 Hz), 129.2, 126.2 (dd, $^3J_{CF}$ = 15.2 Hz, $^4J_{CF}$ = 3.7 Hz), 111.4 (dd, $^3J_{CF}$ = 20.9 Hz, $^4J_{CF}$ = 3.7 Hz), 103.8 (dd, $^3J_{CF}$ = 25.8, 25.8 Hz), 88.3, 52.7, 48.3, 18.6. ^{19}F-NMR (470.6 MHz, $CDCl_3$) δ -112.9 (dddd, $^3J_{HF}$ = 11.9, 11.9 Hz, $^4J_{HF}$ = 8.6 Hz, $^4J_{FF}$ = 11.9 Hz), -114.2 (ddd, $^3J_{HF}$ = 11.9 Hz, $^4J_{HF}$ = 8.6 Hz, $^4J_{FF}$ = 11.9 Hz). HRMS (ESI-TOF) *m/z*: $[M + H]^+$ Calcd. for $C_{12}H_{13}F_2O$ 211.0929 found 211.0919.

2-(4-Chloro-2-fluorophenyl)-5-methylcyclopent-3-en-1-ol (**110n**).

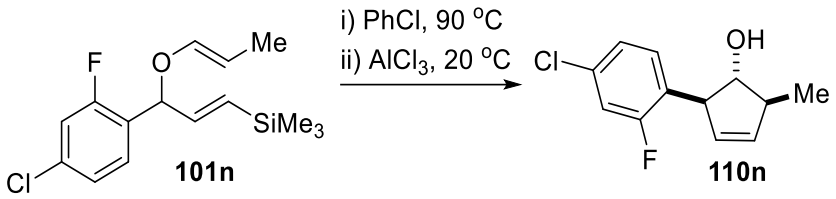

Scheme 117. Synthesis of 2-(4-chloro-2-fluorophenyl)-5-methylcyclopent-3-en-1-ol (**110n**).

The title compound was prepared by general procedure B from allyl vinyl ether (**101n**) (29.9 mg, 0.10 mmol) with initial heating at 90 °C for 16 hours followed by treatment with $AlCl_3$ (20.0 mg, 0.15 mmol) (Scheme 117). The crude product was purified *via* column chromatography (Hexanes/Ethyl acetate 95:5) to afford (**110n**) (10.2 mg, 45%) as a beige solid.

R_f (Hexanes/Ethyl acetate 9:1) = 0.20. ^{1}H-NMR (500 MHz, $CDCl_3$) δ 7.12-7.07 (3H, m), 5.81 (1H, ddd, *J* = 5.9, 2.0, 2.0 Hz), 5.60 (1H, ddd, *J* = 5.9, 2.0, 2.0 Hz), 4.03-4.02 (1H, m), 3.79 (1H, dd, *J* = 5.1, 5.1 Hz), 2.74-2.68 (1H, m), 1.91 (1H, br s), 1.12 (d, *J* = 7.1 Hz). ^{13}C{1H}-NMR (125 MHz, $CDCl_3$) δ 161.0 (d, $^1J_{CF}$ = 248.8 Hz), 136.8, 133.0 (d, $^3J_{CF}$ = 10.5 Hz), 129.6 (d, $^3J_{CF}$ = 5.6 Hz), 129.1 (d, $^2J_{CF}$ = 14.8 Hz), 128.9, 124.8 (d, $^4J_{CF}$ = 3.5 Hz), 116.2 (d, $^2J_{CF}$ = 25.9 Hz), 88.2, 52.9, 48.4, 18.6. ^{19}F-NMR (470.6 MHz, $CDCl_3$) δ -115.6 (m). HRMS (ESI-TOF) *m/z*: $[M - H]^+$ Calcd. for $C_{12}H_{12}{}^{35}ClFO$ 225.0477 found 225.0484.

2-Methyl-5-(1-tosyl-1H-indol-3-yl)cyclopent-3-en-1-ol (**110o**).

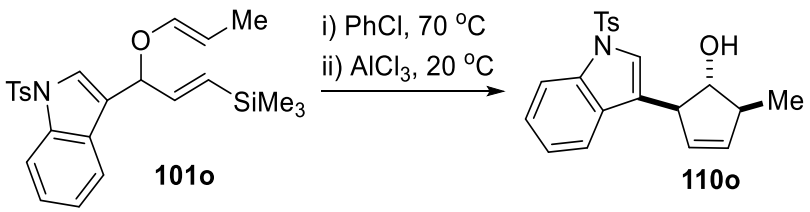

Scheme 118. Synthesis of 2-methyl-5-(1-tosyl-1H-indol-3-yl)cyclopent-3-en-1-ol (**110o**).

The title compound was prepared by general procedure B from allyl vinyl ether (**101o**) (52.6 mg, 0.11 mmol) with initial heating at 70 °C for 16 hours followed by treatment with $AlCl_3$ (22.0 mg, 0.165 mmol) (Scheme 118). The crude product was purified *via* column chromatography (Hexanes/Ethyl acetate 9:1) to afford (**110o**) (22.0 mg, 54%) as a light green solid.

R_f (Hexanes/Ethyl acetate 9:1) = 0.05. ^{1}H-NMR (500 MHz, $CDCl_3$) δ 7.98 (1H, ddd, *J* = 8.3, 0.8, 0.8 Hz), 7.75 (2H, AA'XX' system, $J_{AA'}$ = 1.9 Hz, J_{AX} = 8.4 Hz, $J_{XX'}$ = 1.9 Hz, $J_{AX'}$ = 0.0 Hz), 7.65 (1H, ddd, *J* = 7.6, 1.0, 1.0 Hz), 7.33 (1H, d, *J* = 0.5 Hz), 7.32 (1H, ddd, *J* = 8.3, 7.3, 1.0 Hz), 7.23 (1H, ddd, *J* = 8.0, 7.3, 1.0 Hz), 7.20 (2H, AA'XX' system, $J_{AA'}$ = 1.9 Hz, J_{AX} = 8.4 Hz, $J_{XX'}$ = 1.9 Hz, $J_{AX'}$ = 0.0 Hz), 5.80 (1H, ddd, *J* = 6.0, 2.0, 2.0 Hz), 5.76 (1H, ddd, *J* = 6.0, 1.9, 1.9 Hz), 3.92-3.90 (1H, m), 3.89 (1H, dd, *J* = 5.4, 5.4 Hz), 2.72 (1H, qdddd, *J* = 7.1, 5.4, 2.0, 2.0, 2.0 Hz), 2.33 (3H, s), 1.91 (1H, br s), 1.11 (3H, d, *J* = 7.1 Hz). ^{13}C{1H}-NMR (125 MHz, $CDCl_3$) δ 145.0, 136.1, 135.7, 135.4, 130.5, 130.0, 129.5, 126.9, 124.9, 124.8, 123.2, 122.6, 120.3, 113.9, 86.7, 51.1, 48.7, 21.7, 18.8. HRMS (ESI-TOF) *m/z*: $[M + H]^+$ Calcd. for $C_{21}H_{22}NO_3S$ 368.1315 found 368.1325.

2,2-Dimethyl-5-phenylcyclopent-3-en-1-ol **(110p**).

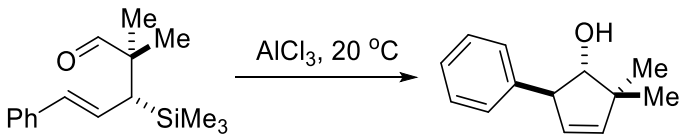

109 **110p**

Scheme 119. Synthesis of 2,2-dimethyl-5-phenylcyclopent-3-en-1-ol **(110p**).

To an oven dried round bottom flask equipped with magnetic stirrer bar and purged with nitrogen was added (**109**) (126.0 mg, 0.10 mmol). Dry chlorobenzene was added (0.05 M, 2 mL)

and aluminum trichloride (20.0 mg, 0.15 mmol) was added in a single portion (Scheme 119). The reaction was allowed to stir for 30 minutes at 20 ºC. The reaction mixture was diluted with ether and cooled to 0 ºC. Water (0.006 mL) was added and stirred for 5 minutes, followed by the sequential addition of NaOH ($15\%_{(aq)}$, 0.006 mL) and water (0.015 mL). The mixture was warmed to room temperature, stirred for 45 min, the white precipitate was filtered, and the filtrate concentrated *in vacuo*. The crude product was purified by column chromatography (Hexanes/Ethyl acetate 95:5) to afford (**110p**) (8.9 mg, 47%) as a white solid.

R_f (Hexanes/Ethyl acetate 9:1) = 0.25. ^{1}H-NMR (400 MHz, $CDCl_3$) δ 7.38-7.29 (2H, m), 7.29-7.20 (3H, m), 5.74 (1H, dd, *J* = 6.1, 2.1 Hz), 5.59 (1H, dd, *J* = 6.1, 1.4 Hz), 3.80 – 3.68 (2H, m), 1.7 (1H, br s), 1.14 (3H, s), 1.08 (3H, s). ^{13}C{1H}-NMR (100 MHz, $CDCl_3$) δ 143.4, 141.5, 129.1, 128.7, 127.7, 126.8, 89.5, 57.3, 46.8, 26.9, 20.4. HRMS (ESI-TOF) *m/z*: $[M + NH_4]^+$ Calcd. for $C_{13}H_{20}NO$ 206.1539 found 206.1543.

Synthesis of Cyclopentanol Derivatives

2-Methyl-4-phenyl-6-oxabicyclo[3.1.0]hexan-3-ol (**111**).

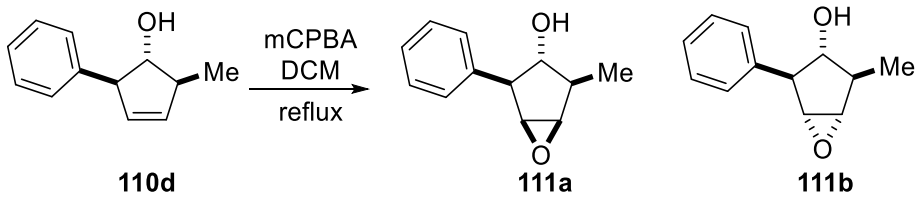

110d **111a** **111b**

Scheme 120. Synthesis of 2-methyl-4-phenyl-6-oxabicyclo[3.1.0]hexan-3-ol (**111**).

Epoxidation was conducted according to the procedure described previously (Scheme 120).[152] To an oven dried 3 mL reaction vial, equipped with a magnetic stirrer bar, was added 2-methyl-5-phenylcyclopent-3-en-1-ol (**110d**) (27.6 mg, 0.16 mmol) and dichloromethane (0.12 M,

1.3 mL) under a nitrogen atmosphere (Scheme 120). To a stirring solution, *meta*-chloroperoxybenzoic acid (40.0 mg, 0.176 mmol) was added in one portion and the reaction mixture was heated at 40 ºC for 2 h using heating mantle. The reaction mixture was cooled to room temperature, quenched with Na_2CO_3 ($5\%_{(aq)}$, 1.5 mL), extracted with dichloromethane (3 × 4 mL). Combined organic layers were dried over Na_2SO_4, filtered and the filtrate concentrated *in vacuo*. The crude product was purified by column chromatography (Hexanes/Ethyl acetate 95:5 to 8:1) to afford (**111**) (12.6 mg, 40%, (**111a**)/(**111b**)=6:1 d.r.) as a white solid.

Diastereomer 1 (**111a**): R_f (Hexanes/Ethyl acetate 8:1) = 0.24. ^{1}H-NMR (400 MHz, $CDCl_3$) δ 7.48 – 7.42 (2H, m), 7.38 – 7.31 (2H, m), 7.31 – 7.27 (1H, m), 3.65 (1H, dd, *J* = 3.0, 1.3 Hz), 3.42 – 3.40 (1H, m), 3.39 (1H, dd, *J* = 8.0, 8.0 Hz), 2.07 (1H, qdd, *J* = 7.0, 7.0, 1.2 Hz), 1.29 (3H, d, *J* = 6.9 Hz). ^{13}C{1H}-NMR (100 MHz, $CDCl_3$) δ 140.3, 128.8, 128.0, 127.3, 81.7, 58.2, 57.4, 54.1, 42.8, 13.7. Diastereomer 2 (**111b**): R_f (Hexanes/Ethyl acetate 8:1) = 0.24. ^{1}H-NMR (400 MHz, $CDCl_3$) δ 7.48 – 7.42 (2H, m), 7.38 – 7.31 (2H, m), 7.31 – 7.27 (1H, m), 4.01 – 3.97 (1H, m), 3.79 (1H, br s), 3.69 (1H, br s), 3.50 (1H, br s), 2.34 (1H, q, *J* = 7.7 Hz), 0.85 (3H, d, *J* = 7.7 Hz). ^{13}C{1H}-NMR (100 MHz, $CDCl_3$) δ 139.6, 128.8, 127.7, 127.0, 85.0, 63.3, 60.6, 54.4, 44.7, 14.8. HRMS (ESI-TOF) *m/z*: $[M + H]^+$ Calcd. for $C_{12}H_{15}O_2$ 191.1067 found 191.1070.

2-Methyl-5-phenylcyclopent-3-en-1-yl sulfamate **(112)**.

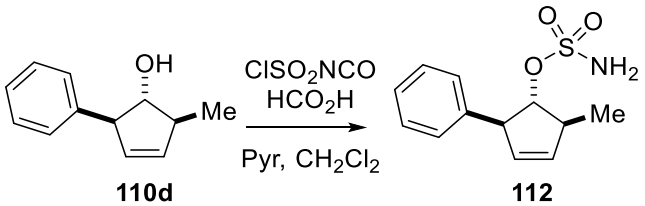

110d **112**

Scheme 121. Synthesis of 2-methyl-5-phenylcyclopent-3-en-1-yl sulfamate **(112)**.

Sulfamate ester was synthesized according to the procedure described previously (Scheme 121).[154] To an oven dried round bottom flask equipped with magnetic stirrer bar and purged with nitrogen was added neat chlorosulfonyl isocyanate (0.075 mL, 0.86 mmol) and cooled to 0 ºC. Formic acid (0.032 mL, 0.86 mmol) was added dropwise and the mixture stirred for 5 minutes until the mixture solidified. Following that, dichloromethane (3.4 mL) was added, and the reaction was stirred for 1 hour at 0 ºC and for 12 hours at room temperature. A solution of 2-methyl-5-phenylcyclopent-3-en-1-ol (**110d**) (99.1 mg, 0.57 mmol) and pyridine (0.062 mL, 0.86 mmol) in dichloromethane (0.8 mL) was added to the reaction at 0 ºC and the reaction was stirred for 8 hours at room temperature. The reaction was quenched by the addition of ethyl acetate and water and the aqueous layer extracted with ethyl acetate (3 × 15 mL). The combined organic layers were washed with brine, dried over Na_2SO_4, filtered and the filtrate concentrated *in vacuo*. The crude product was purified by column chromatography (Hexanes/Ethyl acetate 9:1 to 8:2) to afford (**112**) (61.6 mg, 40%) as amorphous beige solid.

R_f (Hexanes/Ethyl acetate 8:2) = 0.26. ^{1}H-NMR (400 MHz, $CDCl_3$) δ 7.39-7.30 (2H, m), 7.30-7.22 (3H, m), 5.81 (1H, ddd, *J* = 6.0, 2.2, 2.2 Hz), 5.68 (1H, ddd, *J* = 6.0, 2.1, 2.1 Hz), 4.60 (1H, dd, *J* = 4.6, 4.6 Hz), 4.12 – 4.10 (m, 1H), 3.04 (1H, qdddd, *J* = 7.2, 7.2, 2.6, 2.6, 2.6 Hz), 1.20 (3H, d, J = 7.2 Hz). ^{13}C{1H}-NMR (100 MHz, $CDCl_3$) δ 141.9, 135.3, 130.2, 129.0, 127.9, 127.5, 96.4, 57.6, 46.6, 18.5. HRMS (ESI-TOF) *m/z*: $[M + K]^+$ Calcd. for $C_{12}H_{15}KNO_3S$ 292.0405 found 292.0419.

Methyl-phenyl-3,3a,6,6a-tetrahydrocyclopenta[d][1,2,3]oxathiazole 2,2-dioxide (**113**).

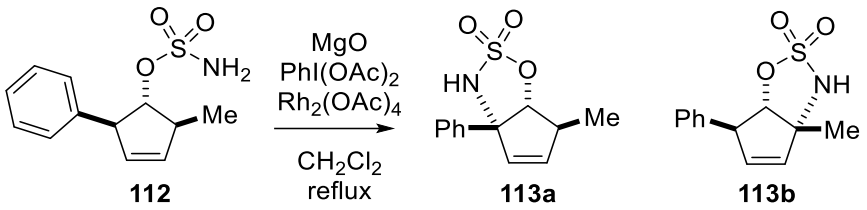

Scheme 122. Synthesis of methyl-phenyl-3,3a,6,6a-tetrahydrocyclopenta[d][1,2,3]oxathiazole 2,2-dioxide (**113**).

Sulfamate ester was synthesized according to the procedure described previously (Scheme 122).[154] To an oven dried 3 mL reaction vial, equipped with a magnetic stirrer bar, was added sulfamate ester (**112**) (48.6 mg, 0.18 mmol) followed by dichloromethane (0.14 M, 1.3 mL) under a nitrogen atmosphere. To a stirring solution, were sequentially added MgO (22.0 mg, 0.55 mmol), $PhI(OAc)_2$ (0.1414 g, 0.44 mmol) and $Rh_2(OAc)_4$ (8.8 mg, 0.020 mmol). The suspension was stirred vigorously and heated at 40 ºC for 24 h using heating mantle. After that, reaction mixture was filtered through celite with dichloromethane and the filtrate concentrated *in vacuo*. The crude product was purified by column chromatography (Hexanes/Ethyl acetate 9:1 to 1:1) to afford a mixture of (**113a**) and (**113b**) (22.0 mg, 46%, (**113a**)/(**113b**)=3/1) as light-yellow oil.

Regioisomer 1 (**113a**): R_f (Hexanes/Ethyl acetate 8:2) = 0.29. ^{1}H-NMR (400 MHz, $CDCl_3$) δ 7.56-7.49 (2H, m), 7.44-7.38 (2H, m), 7.38-7.34 (1H, m), 6.15 (1H, ddd, *J* = 5.8, 2.6, 0.9 Hz), 5.86 (1H, dd, *J* = 5.7, 1.4 Hz), 4.84 (1H, br s), 4.71 (1H, s), 3.18 (1H, qddd, J = 7.6, 2.8, 1.4, 1.4 Hz), 1.12 (3H, d, *J* = 7.5 Hz). ^{13}C{1H}-NMR (100 MHz, $CDCl_3$) δ 140.4, 139.4, 130.3, 129.2, 128.8, 126.1, 95.9, 78.9, 46.0, 18.0. Regioisomer 2 (**113b**): R_f (Hexanes/Ethyl acetate 8:2) = 0.29. ^{1}H-NMR (400 MHz, $CDCl_3$) δ 7.38-7.27 (3H, m), 7.19-7.14 (2H, m), 6.03 (1H, dd, *J* =

5.7, 2.2 Hz), 5.94 (1H, dd, *J* = 5.8, 2.1 Hz), 4.64 (1H, s), 4.56 (1H, br s), 4.31 (1H, dd, J = 2.1, 2.1 Hz), 1.60 (3H, s). ^{13}C{1H}-NMR (100 MHz, $CDCl_3$) δ 139.5, 134.7, 134.2, 129.3, 127.9, 127.5, 95.4, 74.1, 57.2, 25.9. HRMS (ESI-TOF) *m/z*: $[M+H]^+$ Calcd. for $C_{12}H_{14}NO_3S$ 252.0689 found 252.0698.

2-Methyl-5-phenylcyclopenta-1-ol (**115**).

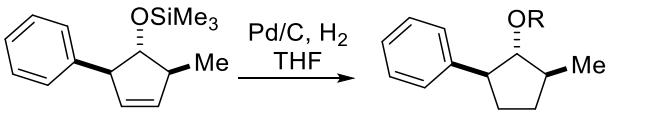

114 **115a** R=$SiMe_3$, **115b** R=H

Scheme 123. Synthesis of 2-methyl-5-phenylcyclopenta-1-ol (**115**).

Title compound was synthesized according to the procedure described previously (Scheme 123).[155] To an oven dried round bottom flask equipped with magnetic stirrer bar was added palladium on carbon (3.5 mg). Flask was purged nitrogen and dry tetrahydrofuran (0.07 M, 1.7 mL) was added followed by trimethyl((2-methyl-5-phenylcyclopent-3-en-1-yl)oxy)silane (**114**) (29.1 mg, 0.12 mmol). The resulting suspension was purged with H_2 for 5-10 minutes and then allowed to stir vigorously under a hydrogen atmosphere for 2 hours. After that, reaction mixture was filtered through celite with dichloromethane and the filtrate concentrated *in vacuo*. The crude product was purified by column chromatography (Hexanes/Dichloromethane 9:1) to afford OTMS (**115a**) (14.1 mg, 48%) as light-yellow oil and OH (**115b**) as light-yellow solid (6.8 mg, 33%).

Trimethyl((2-methyl-5-phenylcyclopentyl)oxy)silane (**115a**): R_f (Hexanes/ Dichloromethane 9:1) = 0.20. ^{1}H-NMR (400 MHz, $CDCl_3$) δ 7.32-7.26 (2H, m), 7.25-7.16 (3H, m), 3.50 (1H, dd, *J* = 8.6, 8.6 Hz), 2.89 (1H, ddd, *J* = 9.4, 9.4, 9.4 Hz), 2.16-2.04 (1H, m), 2.03-

1.86 (2H, m), 1.82-1.70 (1H, m), 1.45-1.35 (1H, m), 1.05 (3H, d, *J* = 6.3 Hz), -0.23 (9H, s, ^{29}Si isotopomers *J* = 4.0 Hz). ^{13}C{1H}-NMR (100 MHz, $CDCl_3$) δ 143.6, 127.4, 127.1, 125.3, 87.3, 52.9, 40.9, 28.8, 28.5, 17.2, -0.7. HRMS (ESI-TOF) *m/z*: $[M - H]^+$ Calcd. for $C_{15}H_{23}OSi$ 247.1512 found 247.1502.

2-Methyl-5-phenylcyclopentan-1-ol (**115b**): R_f (Hexanes/Ethyl acetate 8:2) = 0.47. ^{1}H-NMR (400 MHz, $CDCl_3$) δ 7.33-7.27 (2H, m), 7.27-7.23 (2H, m), 7.23-7.17 (1H, m), 3.55 (1H, dd, *J* = 8.9, 8.9 Hz), 2.88 (1H, ddd, *J* = 9.4, 9.4, 9.4 Hz), 2.11 (1H, dddd, *J* = 12.9, 9.0, 9.0, 5.4 Hz), 2.04 – 1.86 (m, 2H), 1.74 (1H, dddd, *J* = 13.0, 10.1, 10.1 5.1 Hz), 1.66 (1H, br s), 1.44 – 1.33 (1H, m, 1H), 1.11 (3H, d, *J* = 6.3 Hz). ^{13}C{1H}-NMR (100 MHz, $CDCl_3$) δ 143.7, 128.7, 127.6, 126.6, 86.5, 53.7, 41.3, 29.7, 29.6, 18.3. HRMS (ESI-TOF) *m/z*: $[M + NH_4]^+$ Calcd. for $C_{12}H_{20}NO$ 194.1539 found 194.1546.

Synthesis of Methylene Cyclopentanols (**148**) *via* Claisen-Sakurai Reaction

5-Methyl-3-methylene-2-phenethylcyclopentan-1-ol (**148a**).

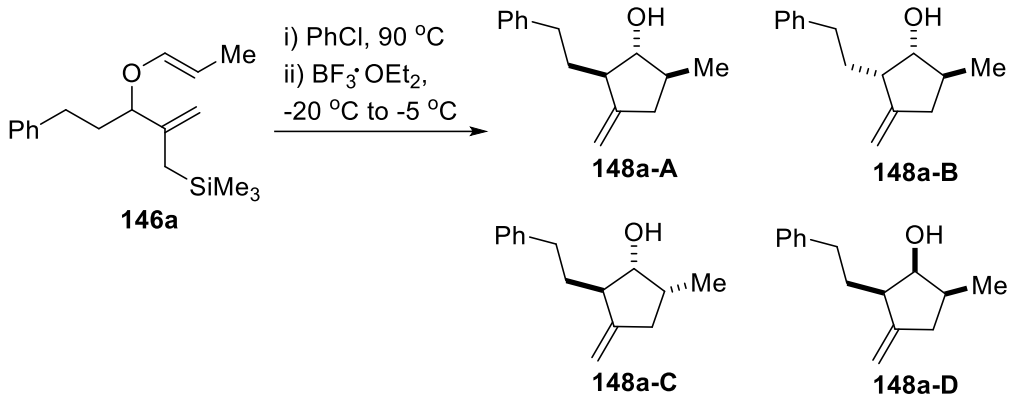

Scheme 124. Stepwise synthesis of 5-methyl-3-methylene-2-phenethylcyclopentan-1-ol (**148a**).

The title compound was prepared by general procedure C from allyl vinyl ether (**146a**) (22.7 mg, 0.0788 mmol) with initial heating at 110 °C for 16 hours followed by treatment with BF_3•OEt_2 (0.015 mL, 0.118 mmol, 1.130 g/mL, min. 46.5% BF_3) (Scheme 124). The crude product was purified *via* column chromatography (Hexanes/Ethyl acetate 95:5) to afford (**148a-A**)/(**148a-B**)/(**148a-C**)/(**148a-D**)=13.7:4.3:2.0:1.0 (8.8 mg, 52%) as a colorless oil.

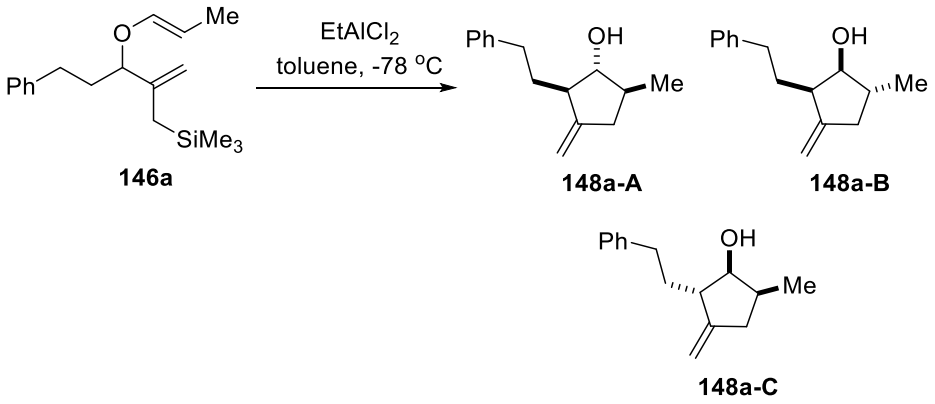

146a **148a-A** **148a-B** **148a-C**

Scheme 125. Cascade synthesis of 5-methyl-3-methylene-2-phenethylcyclopentan-1-ol (**148a**).

The title compound was prepared by general procedure D from allyl vinyl ether (**146a**) (20.0 mg, 0.0694 mmol) treated with $EtAlCl_2$ (0.058 mL, 0.104 mmol, 1.8 M solution in toluene) (Scheme 125). The crude product was purified *via* column chromatography (Hexanes/Ethyl acetate 95:5) to afford (**148a-A**)/(**148a-B**)/(**148a-C**)=5.0:10.0:1.0 (10.2 mg, 68%) as a colorless oil.

Diastereomer A: R_f (Hexanes/Ethyl acetate 9:1) = 0.18. ^{1}H-NMR (500 MHz, $CDCl_3$) δ 7.32-7.27 (2H, m), 7.25-7.16 (3H, m), 4.92-4.89 (1H, m), 4.87-4.84 (1H, m), 3.39 (1H, dd, *J* = 8.7, 8.7 Hz), 2.86-2.67 (2H, m), 2.58 (1H, dddd, *J* = 16.3, 7.8, 1.8, 1.8 Hz), 2.37-2.30 (1H, m), 2.06-1.98 (1H, m), 1.94 (1H, ddddd, *J* = 16.4, 11.2, 2.9, 2.9, 2.9 Hz), 1.88-1.75 (2H, m), 1.54 (1H, br s), 1.09 (3H, d, *J* = 6.4 Hz). ^{13}C{1H}-NMR (125 MHz, $CDCl_3$) δ 151.2, 142.9, 128.5,

128.5, 125.9, 106.4, 84.3, 51.3, 41.0, 38.8, 34.0, 33.1, 17.4. Diastereomer B: R_f (Hexanes/Ethyl acetate 9:1) = 0.29. ^{1}H-NMR (500 MHz, $CDCl_3$) δ 7.32-7.27 (2H, m), 7.25-7.16 (3H, m), 4.96-4.94 (1H, m), 4.89-4.87 (1H, m), 3.86 (1H, br s), 2.85-2.68 (3H, m), 2.53-2.46 (1H, m), 2.11-2.02 (1H, m), 2.02-1.95 (1H, m), 1.90-1.76 (3H, m), 1.54 (1H, br s), 0.98 (3H, d, *J* = 7.1 Hz). ^{13}C{1H}-NMR (125 MHz, $CDCl_3$) δ 152.6, 142.7, 128.5, 128.5, 126.0, 107.2, 79.8, 46.9, 39.5, 37.7, 34.2, 28.9, 19.1. Diastereomer C: R_f (Hexanes/Ethyl acetate 9:1) = 0.18. ^{1}H-NMR (500 MHz, $CDCl_3$) δ 7.32-7.27 (2H, m), 7.25-7.16 (3H, m), 4.94-4.92 (1H, m), 4.84-4.82 (1H, m), 4.07-4.02 (1H, m), 2.85-2.68 (2H, m), 2.53-2.46 (1H, m), 2.11-2.02 (1H, m), 2.02-1.95 (1H, m), 1.90-1.76 (3H, m), 1.54 (1H, br s), 1.07 (3H, d, *J* = 6.7 Hz). ^{13}C{1H}-NMR (125 MHz, $CDCl_3$) δ 153.8, 142.7, 125.9, 128.5, 126.0, 106.1, 76.1, 50.1, 37.5, 34.2, 34.0, 29.8, 14.3. Diastereomer D: R_f (Hexanes/Ethyl acetate 9:1) = 0.18. ^{1}H-NMR (500 MHz, $CDCl_3$) δ 7.32-7.27 (2H, m), 7.25-7.16 (3H, m), 4.98-4.96 (1H, m), 4.91-4.89 (1H, m), 3.93-3.90 (1H, m), 2.85-2.68 (2H, m), 2.53-2.46 (1H, m), 2.11-2.02 (1H, m), 2.02-1.95 (1H, m), 1.90-1.76 (3H, m), 1.54 (1H, br s), 1.04 (3H, d, *J* = 6.7 Hz). ^{13}C{1H}-NMR (125 MHz, $CDCl_3$) δ 153.5, 142.5, 125.9, 128.5, 126.0, 107.7, 80.2, 52.2, 37.7, 36.6, 35.4, 33.9, 13.7. HRMS (ESI-TOF) *m/z*: $[M + H]^+$ Calcd. for $C_{15}H_{21}N$ 217.1587 found 217.1589.

2-Benzyl-5-methyl-3-methylenecyclopentan-1-ol (**148b**).

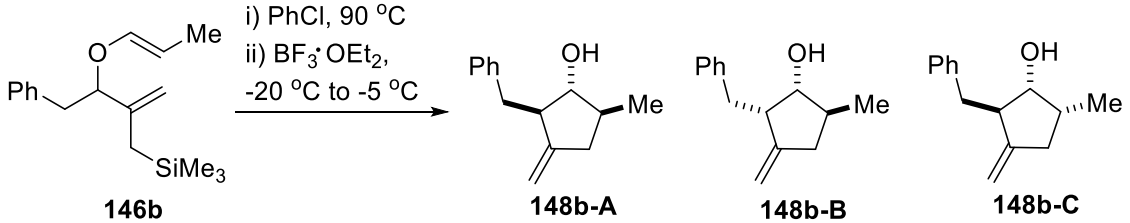

146b **148b-A** **148b-B** **148b-C**

Scheme 126. Stepwise synthesis of 2-benzyl-5-methyl-3-methylenecyclopentan-1-ol (**148b**).

The title compound was prepared by general procedure C from allyl vinyl ether (**146b**) (20.0 mg, 0.0730 mmol) with initial heating at 110 °C for 16 hours followed by treatment with BF_3•OEt_2 (0.014 mL, 0.109 mmol, 1.130 g/mL, min. 46.5% BF_3) (Scheme 126). The crude product was purified *via* column chromatography (Hexanes/Ethyl acetate 95:5) to afford (**148b-A**)/(**148b-B**)/(**148b-C**)=7.2:3.4:1.0 (7.6 mg, 52%) as a light yellow oil.

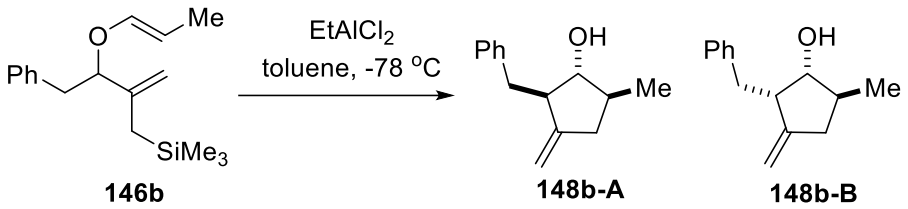

146b **148b-A** **148b-B**

Scheme 127. Cascade synthesis of 2-benzyl-5-methyl-3-methylenecyclopentan-1-ol (**148b**).

The title compound was prepared by general procedure D from allyl vinyl ether (**146b**) (20.0 mg, 0.0730 mmol) treated with $EtAlCl_2$ (0.061 mL, 0.109 mmol, 1.8 M solution in toluene) (Scheme 127). The crude product was purified *via* column chromatography (Hexanes/Ethyl acetate 98:2) to afford (**148b-A**)/(**148b-B**)=1.0:3.0 (10.0 mg, 68%) as a light yellow oil.

Diastereomer A: R_f (Hexanes/Dichloromethane 1:1) = 0.14. ^{1}H-NMR (500 MHz, $CDCl_3$) δ 7.30-7.26 (4H, m), 7.24-7.18 (1H, m), 4.92-4.90 (1H, m), 4.86-4.84 (1H, m), 3.36 (1H, dd, *J* = 8.7, 8.7 Hz), 3.10 (1H, dd, *J* = 13.4, 5.6 Hz), 2.69 (1H, dd, *J* = 13.5, 8.7 Hz), 2.62 (1H, dddd, *J* = 11.6, 5.8, 2.6, 2.6 Hz), 2.56 (1H, dddd, *J* = 16.2, 7.7, 1.9, 1.9 Hz), 1.91 (1H, ddddd, J = 16.4, 11.3, 2.6, 2.6, 2.6 Hz), 1.86-1.77 (1H, m), 1.26 (1H, s), 1.04 (3H, d, *J* = 6.4 Hz). ^{13}C{1H}-NMR (125 MHz, $CDCl_3$) δ 151.3, 140.2, 129.1, 128.9, 126.5, 106.8, 84.1, 52.9, 39.9, 39.0, 38.3, 17.4. Diastereomer B: R_f (Hexanes/Dichloromethane 1:1) = 0.14. ^{1}H-NMR (500 MHz, $CDCl_3$) δ 7.30-7.26 (4H, m), 7.24-7.18 (1H, m), 4.98-4.95 (1H, m), 4.83-4.81 (1H, m), 3.68 (1H, dd, *J* = 3.6, 3.6 Hz), 2.87 – 2.80 (3H, m), 2.77 (1H, ddddd, *J* = 17.6, 9.0, 2.1, 2.1, 2.1 Hz), 2.09 – 2.00 (2H, m),

1.26 (1H, s), 0.94 (3H, d, *J* = 7.0 Hz). ^{13}C{1H}-NMR (125 MHz, $CDCl_3$) δ 152.2, 141.1, 129.1, 128.5, 126.0, 107.3, 79.5, 48.8, 39.4, 38.0, 33.5, 19.1. Diastereomer C: R_f (Hexanes/Dichloromethane 1:1) = 0.14. ^{1}H-NMR (400 MHz, $CDCl_3$) δ 7.30-7.26 (4H, m), 7.24-7.18 (1H, m), 5.03-5.00 (1H, m), 4.98-4.95 (1H, m), 3.86 (1H, dd, *J* = 4.1, 4.8 Hz), 3.72 (1H, dd, *J* = 3.4, 3.4 Hz), 2.97 (1H, dd, *J* = 15.1, 4.0 Hz), 2.51-2.43 (1H, m), 2.23-2.13 (3H, m), 1.26 (1H, s), 1.00 (3H, d, *J* = 6.3 Hz). ^{13}C{1H}-NMR (100 MHz, $CDCl_3$) δ 153.4, 140.3, 129.0, 128.5, 126.3, 106.3, 75.8, 52.5, 37.8, 37.2, 33.4, 24.3. HRMS (ESI-TOF) *m/z*: $[M + NH_4]^+$ Calcd. for $C_{14}H_{22}NO$ 220.1696 found 220.1699.

2-Cyclohexyl-5-methyl-3-methylenecyclopentan-1-ol (**148c**).

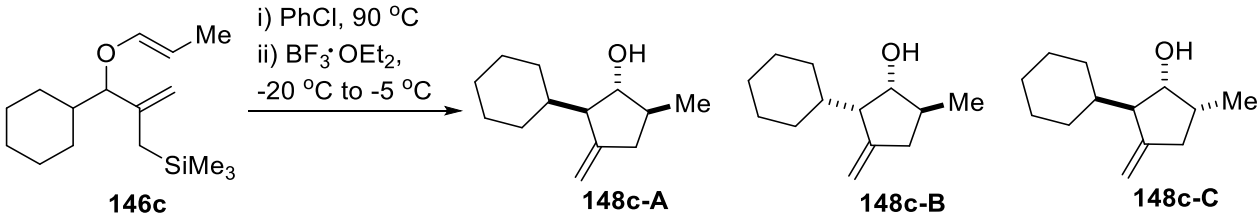

146c **148c-A** **148c-B** **148c-C**

Scheme 128. Stepwise synthesis of 2-cyclohexyl-5-methyl-3-methylenecyclopentan-1-ol (**148c**).

The title compound was prepared by general procedure C from allyl vinyl ether (**146c**) (20.0 mg, 0.0752 mmol) with initial heating at 110 °C for 16 hours followed by treatment with BF_3•OEt_2 (0.015 mL, 0.113 mmol, 1.130 g/mL, min. 46.5% BF_3) (Scheme 128). The crude product was purified *via* column chromatography (Hexanes/Dichloromethane 1:1) to afford afford (**148c-A**)/(**148c-B**)/(**148c-C**)=15.0:2.7:1.0 (6.9 mg, 47%) as a white solid.

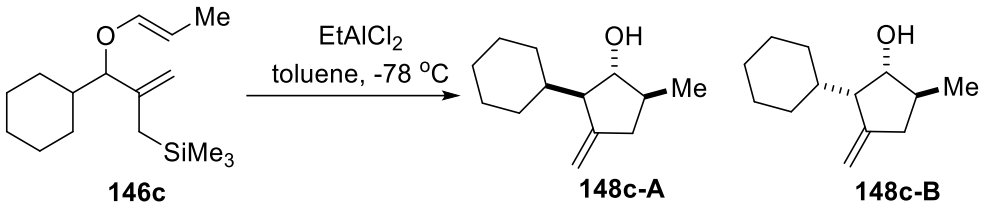

146c **148c-A** **148c-B**

Scheme 129. Cascade synthesis of 2-cyclohexyl-5-methyl-3-methylenecyclopentan-1-ol (**148c**).

The title compound was prepared by general procedure D from allyl vinyl ether (**146c**) (20.0 mg, 0.0752 mmol) treated with $EtAlCl_2$ (0.063 mL, 0.113 mmol, 1.8 M solution in toluene) (Scheme 129). The crude product was purified *via* column chromatography (Hexanes/Dichloromethane 1:1) to afford (**148c-A**)/(**148c-B**)=9.5:1.0 (8.1 mg, 56%) as a white solid.

Diastereomer A: R_f (Hexanes/Dichloromethane 1:1) = 0.23. ^{1}H-NMR (500 MHz, $CDCl_3$) δ 4.90 (1H, dddd, *J* = 2.4, 2.4, 1,2, 1.2 Hz), 4.74 (1H, dddd, *J* = 2.3, 2.3, 1.2, 1.2 Hz), 3.53 (1H, dd, *J* = 8.1, 8.1 Hz), 2.42 (1H, dd, *J* = 14.8, 6.5 Hz), 2.20 (1H, ddddd, *J* = 7.2, 4.8, 2.5, 2.5, 2.5 Hz), 1.81 (1H, ddddd, *J* = 14.9, 12.4, 2.7, 2.7, 2.7 Hz), 1.77-1.64 (6H, m), 1.62-1.54 (1H, m), 1.49 (1H, br s), 1.31-1.09 (3H, m), 1.19 – 1.09 (m, 2H), 1.07 (3H, d, *J* = 6.3 Hz). ^{13}C{1H}-NMR (125 MHz, $CDCl_3$) δ 150.7, 106.5, 81.5, 57.6, 41.8, 40.7, 40.6, 31.4, 29.3, 27.2, 27.0, 26.8, 17.3. Diastereomer B: R_f (Hexanes/Dichloromethane 1:1) = 0.23. ^{1}H-NMR (500 MHz, $CDCl_3$) δ 4.98-4.96 (1H, m), 4.85-4.82 (1H, m), 4.03 (1H, dd, *J* = 4.5, 3.1 Hz), 2.13-2.03 (2H, m), 1.85-1.62 (7H, m), 1.62-1.54 (1H, m), 1.49 (1H, br s), 1.31-1.09 (3H, m), 1.19 – 1.09 (m, 2H), 1.00 (3H, d, *J* = 7.0 Hz). ^{13}C{1H}-NMR (125 MHz, $CDCl_3$) δ 152.1, 108.1, 77.5, 58.7, 40.0, 38.5, 37.0, 31.7, 30.3, 29.9, 26.9, 26.7, 13.7. Diastereomer C: R_f (Hexanes/Dichloromethane 1:1) = 0.23. ^{1}H-NMR (500 MHz, $CDCl_3$) δ 4.94-4.91 (1H, m), 4.78-4.75 (1H, m), 3.82 (1H, dd, *J* = 4.9, 3.5 Hz),), 2.13-2.03 (2H, m), 1.85-1.62 (7H, m), 1.62-1.54 (1H, m), 1.49 (1H, br s), 1.31-1.09 (3H,

m), 1.19 – 1.09 (m, 2H), 0.90 (3H, d, J = 6.4 Hz). ^{13}C{1H}-NMR (100 MHz, $CDCl_3$) δ) δ 150.6, 107.0, 76.4, 56.4, 40.4, 38.3, 37.12, 36.76, 30.9, 26.8, 26.7, 14.3. HRMS (ESI-TOF) *m/z*: [M - OH]$^+$ Calcd. for $C_{13}H_{21}N$ 177.1638 found 177.1643.

5-Methyl-3-methylene-2-phenylcyclopentan-1-ol (**148d**).

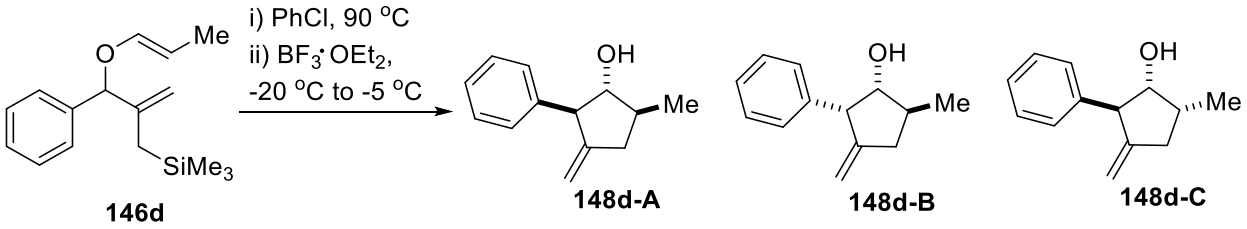

146d **148d-A** **148d-B** **148d-C**

Scheme 130. Stepwise synthesis of 5-methyl-3-methylene-2-phenylcyclopentan-1-ol (**148d**).

The title compound was prepared by general procedure C from allyl vinyl ether (**146d**) (20.0 mg, 0.0768 mmol) with initial heating at 90 °C for 16 hours followed by treatment with BF_3•OEt_2 (0.015 mL, 0.115 mmol, 1.130 g/mL, min. 46.5% BF_3) (Scheme 130). The crude product was purified *via* column chromatography (Hexanes/Ethyl acetate 95:5) to afford afford (**148d-A**)/(**148d-B**)/(**148d-C**)=5.5:2.0:1.0 (7.8 mg, 54%) as a light-yellow solid.

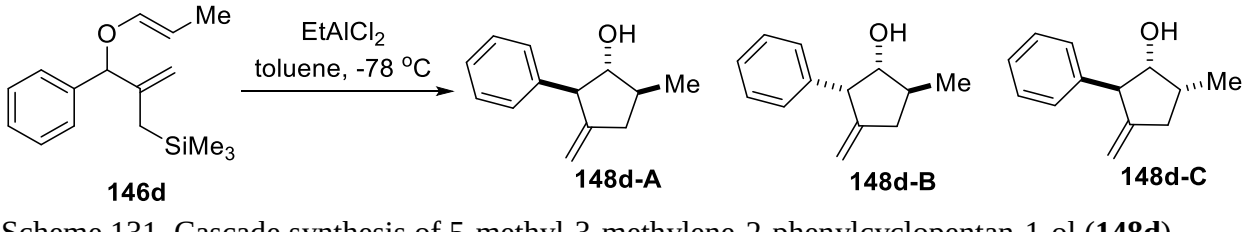

146d **148d-A** **148d-B** **148d-C**

Scheme 131. Cascade synthesis of 5-methyl-3-methylene-2-phenylcyclopentan-1-ol (**148d**).

The title compound was prepared by general procedure D from allyl vinyl ether (**146d**) (20.0 mg, 0.0768 mmol) treated with $EtAlCl_2$ (0.064 mL, 0.115 mmol, 1.8 M solution in toluene) (Scheme 131). The crude product was purified *via* column chromatography (Hexanes/Ethyl

acetate 95:5) to afford (**148d-A**)/(**148d-B**)/(**148d-C**)=1.9:6.4:1.0 (7.1 mg, 49%) as a light yellow oil.

Diastereomer A: R_f (Hexanes/Ethyl acetate 95:5) = 0.07. ^{1}H-NMR (500 MHz, $CDCl_3$) δ 7.36-7.30 (2H, m), 7.27-7.20 (3H, m), 4.96-4.93 (1H, m), 4.59-4.52 (1H, m), 3.62 (1H, dd, *J* = 9.5, 9.5 Hz), 3.43 (1H, dddd, *J* = 9.3, 2.9, 2.9, 2.9 Hz), 2.77 (1H, dddd, *J* = 16.8, 8.2, 2.1, 2.1 Hz), 2.14 (1H, ddddd, *J* = 16.6, 11.2, 2.7, 2.7, 2,7 Hz), 2.06-1.96 (1H, m), 1.64 (1H, br s), 1.15 (3H, d, *J* = 6.5 Hz). ^{13}C{1H}-NMR (125 MHz, $CDCl_3$) δ 151.2, 141.8, 129.0, 128.7, 126.9, 109.1, 85.8, 60.2, 39.7, 38.5, 17.4. Diastereomer C: R_f (Hexanes/Ethyl acetate 95:5) = 0.27. ^{1}H-NMR (500 MHz, $CDCl_3$) δ 7.36-7.30 (2H, m), 7.27-7.20 (3H, m), 5.10-5.05 (1H, m), 4.73 (1H, dddd, *J* = 2.4, 2.4, 2.4 0.9 Hz), 4.11 (1H, dd, *J* = 6.4, 5.1 Hz), 2.68 (1H, ddddd, *J* = 18.2, 9.2, 2.4, 2.4, 2.4 Hz), 2.35-2.27 (2H, m), 1.64 (1H, br s), 1.06 (3H, d, *J* = 6.7 Hz). ^{13}C{1H}-NMR (125 MHz, $CDCl_3$) δ 152.0, 142.6, 128.7, 128.6, 126.6, 110.3, 82.4, 57.7, 35.9, 29.9, 13.7. HRMS (ESI-TOF) *m/z*: $[M + NH_4]^+$ Calcd. for $C_{13}H_{20}NO$ 206.1539 found 206.1532.

Diastereomer B: R_f (Hexanes/Ethyl acetate 95:5) = 0.16. ^{1}H-NMR (500 MHz, $CDCl_3$) δ 7.38-7.31 (2H, m), 7.29-7.24 (3H, m), 5.14-5.11 (1H, m), 4.82 (1H, dddd, *J* = 2.3, 2.3, 2.3, 0.9 Hz), 3.95 (1H, dddd, *J* = 4.9, 2.4, 2.4, 2.4 Hz), 3.84 (1H, dd, *J* = 5.8, 4.1 Hz), 2.89 (1H, ddddd, *J* = 17.6, 8.8, 2.0, 2.0, 2.0 Hz), 2.2-2.1 (2H, m), 1.53 (1H, br s), 1.06 (3H, d, *J* = 6.8 Hz). ^{13}C{1H}-NMR (125 MHz, $CDCl_3$) δ 151.8, 139.2, 130.3, 128.7, 127.1, 110.1, 81.5, 54.7, 39.3, 38.6, 18.2. HRMS (ESI-TOF) *m/z*: $[M + NH_4]^+$ Calcd. for $C_{13}H_{20}NO$ 206.1539 found 206.1546.

2-(2-Fluorophenyl)-5-methyl-3-methylenecyclopentan-1-ol (**148e**).

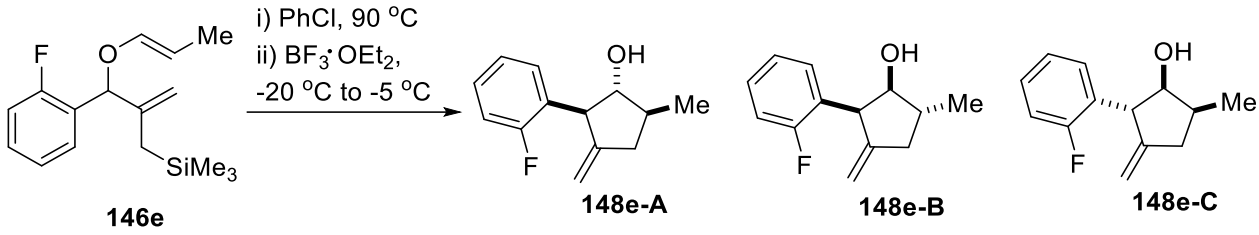

Scheme 132. Stepwise synthesis of 2-(2-fluorophenyl)-5-methyl-3-methylenecyclopentan-1-ol (**148e**).

The title compound was prepared by general procedure C from allyl vinyl ether (**146e**) (27.8 mg, 0.10 mmol) with initial heating at 90 °C for 16 hours followed by treatment with BF_3•OEt_2 (0.019 mL, 0.15 mmol, 1.130 g/mL, min. 46.5% BF_3) (Scheme 132). The crude product was purified *via* column chromatography (Hexanes/Ethyl acetate 95:5) to afford afford (**148e-A**)/(**148e-B**)/(**148e-C**)=15.0:1.0:1.0 (10.6 mg, 51%) as a clear oil.

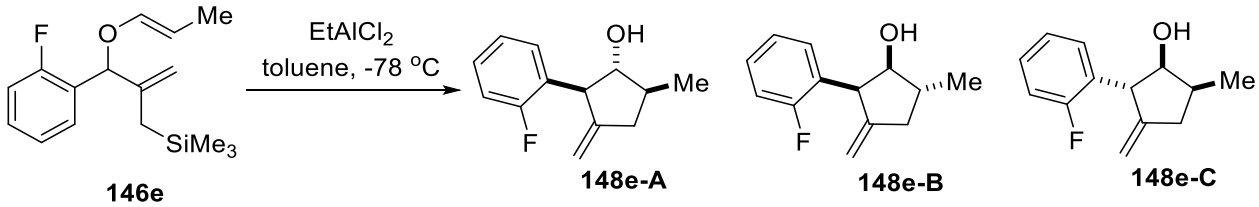

Scheme 133. Cascade synthesis of 2-(2-fluorophenyl)-5-methyl-3-methylenecyclopentan-1-ol (**148e**).

The title compound was prepared by general procedure D from allyl vinyl ether (**146e**) (27.8 mg, 0.10 mmol) treated with $EtAlCl_2$ (0.083 mL, 0.15 mmol, 1.8 M solution in toluene) (Scheme 133). The crude product was purified *via* column chromatography (Hexanes/Ethyl acetate 95:5) to afford (**148e-A**)/(**148e-B**)/(**148e-C**)=4.8:6.4:1.0 (12.8 mg, 62%) as a clear oil.

Diastereomer A: R_f (Hexanes/Ethyl acetate 9:1) = 0.20. ^{1}H-NMR (500 MHz, $CDCl_3$) δ 7.25-7.20 (2H, m), 7.13-7.09 (1H, m), 7.08-7.02 (1H, m), 4.93-4.90 (1H, m), 4.52 (1H, ddd, *J* =

2.5, 2.5, 2.5 Hz), 3.80-3.71 (2H, m), 2.75 (1H, dddd, *J* = 16.8, 8.1, 2.0, 2.0 Hz), 2.17 (1H, ddddd, *J* = 16.8, 11.5, 2.7, 2.7, 2.7 Hz), 2.06-1.96 (1H, m), 1.78 (1H, br s), 1.16 (3H, d, *J* = 6.4 Hz). ^{13}C{1H}-NMR (125 MHz, $CDCl_3$) δ 161.8 (d, $^{1}J_{CF}$ = 245.0 Hz), 150.1, 130.6 (d, $^{3}J_{CF}$ = 5.0 Hz), 128.9 (d, $^{2}J_{CF}$ = 13.8 Hz), 128.4 (d, $^{3}J_{CF}$ = 8.2 Hz), 124.4 (d, $^{4}J_{CF}$ = 3.8 Hz), 115.8 (d, $^{2}J_{CF}$ = 22.5 Hz), 108.2, 84.6 (d, $^{4}J_{CF}$ = 2.5 Hz), 53.9, 40.4, 38.4, 17.3. ^{19}F-NMR (470.6 MHz, $CDCl_3$) δ -117.1 (m). HRMS (ESI-TOF) *m/z*: $[M + NH_4]^+$ Calcd. for $C_{13}H_{19}FNO$ 224.1445 found 224.1445.

Diastereomer B: R_f (Hexanes/Ethyl acetate 9:1) = 0.23. ^{1}H-NMR (500 MHz, $CDCl_3$) δ 7.31 (1H, ddd, *J* = 7.5, 7.5 1.9 Hz), 7.25-7.20 (1H, m), 7.13-7.09 (1H, m), 7.08-7.02 (1H, m), 5.16-5.12 (1H, m), 4.82-4.78 (1H, m), 4.30 (1H, dddd, J = 5.1, 2.5, 2.5, 2.5 Hz), 3.98-3.94 (1H, m), 2.89 (1H, ddddd, *J* = 11.3, 9.0, 6.7, 2.2, 2.2 Hz), 2.22-2.11 (2H, m), 1.79 (1H, d, *J* = 4.3 Hz), 1.06 (3H, d, *J* = 6.9 Hz). ^{13}C{1H}-NMR (125 MHz, $CDCl_3$) δ 161.8 (d, $^{1}J_{CF}$ = 245.0 Hz), 150.9, 131.7 (d, $^{4}J_{CF}$ = 3.8 Hz), 128.4 (d, $^{3}J_{CF}$ = 7.5 Hz), 126.4 (d, $^{2}J_{CF}$ = 13.8 Hz), 124.0 (d, $^{4}J_{CF}$ = 3.8 Hz), 115.2 (d, $^{2}J_{CF}$ = 22.5 Hz), 110.0, 80.5, 40.7 (d, $^{4}J_{CF}$ = 1.3 Hz), 39.5, 38.5, 18.1. ^{19}F-NMR (470.6 MHz, $CDCl_3$) δ -117.0 (m). Diastereomer C: R_f (Hexanes/Ethyl acetate 9:1) = 0.37. ^{1}H-NMR (500 MHz, $CDCl_3$) δ 7.25-7.20 (2H, m), 7.13-7.09 (1H, m), 7.08-7.02 (1H, m), 5.08-5.06 (1H, m), 4.74-4.72 (1H, m), 4.18 (1H, ddd, *J* = 5.1, 5.1, 5.1 Hz), 3.89 (1H, dddd, J = 4.8, 2.3, 2.3, 2.3 Hz), 2.69 (1H, ddddd, J = 14.0, 7.4, 2.3, 2.3, 2.3 Hz), 2.37-2.25 (2H, m), 1.67 (1H, d, J = 4.7 Hz), 1.07 (3H, d, *J* = 7.0 Hz). ^{13}C{1H}-NMR (125 MHz, $CDCl_3$) δ 161.4 (d, $^{1}J_{CF}$ = 250.0 Hz), 151.0, 130.2 (d, $^{3}J_{CF}$ = 5.0 Hz), 129.6 (d, $^{2}J_{CF}$ = 13.8 Hz), 128.2 (d, $^{3}J_{CF}$ = 7.5 Hz), 124.2 (d, $^{4}J_{CF}$ = 3.8 Hz), 115.5 (d, $^{2}J_{CF}$ = 21.3 Hz), 109.9, 81.1 (d, $^{4}J_{CF}$ = 1.1 Hz), 51.8, 38.3, 36.2, 13.5. ^{19}F-NMR (470.6 MHz, $CDCl_3$) δ -116.7 (m). HRMS (ESI-TOF) *m/z*: $[M + NH_4]^+$ Calcd. for $C_{13}H_{19}FNO$ 224.1445 found 224.1441.

Computational Details

General Comments

The calculations were performed with the Gaussian 16.0 software.[174] The optimized structures were visualized using CYLview 1.0b.[175] The molecular orbitals were generated and rendered in GaussView 6.0.16.[176] The potential energy surfaces were generated using GoodVibes.[177]

Geometries were optimized using B3LYP functional [178,179] and 6-31G+(d) basis set. B3LYP has been extensively used for DFT studies of Claisen rearrangement providing reliable results.[180–183] Solvation by chlorobenzene or dichloromethane was accounted by using conductor-like polarizable continuum model (C-PCM).[184,185] The nature of stationary points in each case was confirmed by harmonic frequency calculations. The nature of located transition states was confirmed by unique imaginary vibrational mode and intrinsic reaction coordinate (IRC) calculations. Transition states for Claisen rearrangement were additionally calculated at UB3LYP and evaluated for wave function stability.

To get refined energies, single point (SP) energy calculations were performed using dual-range local meta functional M11L,[186] long-range corrected hybrid functional with empirical atom–atom dispersion corrections ωB97XD[187] or hybrid meta exchange-correlation functional M06-2X[188] and 6-311++G(2d,2p) basis set. The single point solvation by chlorobenzene was accounted by using conductor-like polarizable continuum model (C-PCM).[184,185] The single point energies were corrected using thermal correction to Gibbs free energy calculated at CPCM-B3LYP/6-31G+(d).

The obtained Gibbs Free energies were further corrected to 1 mol/L standard state and temperature (unless otherwise indicated). The Grimme's quasi-rigid-rotor harmonic oscillator (quasi-RRHO) approximation was used to account for entropic contributions of low frequency modes below 100 cm^{-1}.[189,190] All corrections were obtained using the GoodVibes 3.0.1 program by Prof. Robert Paton.[177]

Lowest energy conformations of allyl vinyl ethers, corresponding aldehydes and Lewis acid-bound aldehydes were found in CREST[191] using default iMTD-GC algorithm at the GFN2-xTB level.[192] Reactive conformations of allyl vinyl ethers and corresponding aldehydes were found using results of IRC calculations. For Claisen rearrangement two possible arrangements in transition state (chair and boat conformation) were considered (unless otherwise indicated).

For $AlCl_3$-mediated Sakurai allylation four transition states representing different relative disposition between the aldehyde group and trans-alkene and the direction of electrophilic attack were calculated for Sakurai carbocyclization: AP *anti* S_E'(AP1), AP *syn* S_E' (AP2), SC *syn* S_E' (SC1), and SC *anti* S_E' (SC2). Alternative conformations of $AlCl_3$-carbonyl binding in transition state were also considered. Four diastereomeric products and their ring-flipped forms were calculated. In each case alternative conformations of $AlCl_3$-carbonyl binding and TMS binding were considered.[52]

For BF_3- and $EtAlCl_2$-mediated Sakurai allylation four transition states representing *AP anti-S_E'* and *SC anti-S_E'* reactivity mode for *(Z)*- and *(E)*-alkenes were calculated.

Conformational studies for (**110j**) series were done in CREST.[191] Each experiment was repeated twice to ensure reproducibility, the typical run was as follows. The conformational search was performed using default iMTD-GC algorithm at the GFN2-xTB level.[192] The lowest

energy structures were reoptimized at C-PCM (chloroform)-M11L/6-311++G(2d,2p)//C-PCM (chloroform)-B3LYP/6-31+G(d).[52]

Stereospecific Claisen-Sakurai Approach to Densely Functionalized Cyclopentenols

Energies and lowest frequencies of minimum energy structures for Claisen rearrangement of allyl vinyl ethers (**101**) obtained by DFT are shown in Table 12 and 13.

Structure	E[a], Ha	E_SPC[b], Ha	G(T)_SPC[c]	qh-G(T)_SPC[d]	Lowest freq.[e]
101a-VE_{CC}	-988.903741	-988.932409	-988.650628	-988.641925 [f]	15.89
101a-VE_{CB}	-988.900763	-988.930170	-988.647914	-988.639553 [f]	14.31
101a-TS_{CC}	-988.860425	-988.892611	-988.608801	-988.602222 [f]	-275.00
101a-TS_{CB}	-988.855707	-988.888463	-988.605791	-988.598872 [f]	-193.94
101a-ALD_{CC}	-988.917842	-988.957239	-988.671798	-988.664749 [f]	16.77
101a-ALD_{CB}	-988.920866	-988.956372	-988.673925	-988.665062 [f]	10.73
101d-VE_{CC}	-949.586195	-949.611417	-949.349389	-949.342400 [g]	14.16
101d-VE_{CB}	-949.583725	-949.609931	-949.347468	-949.340777 [g]	15.60
101d-TS_{CC}	-949.550514	-949.580319	-949.315786	-949.311243 [g]	-200.65
101d-TS_{CB}	-949.547123	-949.577779	-949.314078	-949.309363 [g]	-114.44
101d-ALD_{CC}	-949.608230	-949.644630	-949.378662	-949.373403 [g]	16.06
101d-ALD_{CB}	-949.611663	-949.644507	-949.380185	-949.374076 [g]	18.87
101q-VE_{CC}	-757.844769	-757.864428	-757.651537	-757.646747 [f]	19.86
101q-VE_{CB}	-757.842144	-757.862532	-757.648937	-757.644485 [f]	19.67
101q-TS_{CC}	-757.801284	-757.825466	-757.611128	-757.608401 [f]	-289.46
101q-TS_{CB}	-757.796584	-757.821417	-757.607569	-757.604835 [f]	-204.52
101q-ALD_{CC}	-757.857971	-757.889002	-757.672607	-757.669670 [f]	40.42
101q-ALD_{CB}	-757.861270	-757.887991	-757.673905	-757.669504 [f]	26.42
PhCl	-691.857745	-691.864912	-691.805362	-691.805358 [g]	187.47
PhCl	-691.857745	-691.864912	-691.807553	-691.807546 [f]	187.47

Table 12. Energies and lowest frequencies of minimum energy structures for thermal Claisen rearrangement of allyl vinyl ethers (**101**). [a] Electronic energies calculated at C-PCM (chlorobenzene)-B3LYP/6-31+G(d); [b] Single point energies calculated at C-PCM (chlorobenzene)-M11L/6-311++G(2d,2p); [c] Harmonic solvent and temperature corrected Gibbs free energies; [d] Quasi-harmonic solvent and temperature corrected Gibbs free energies at 1 mol/L

standard state; [e] Unscaled; calculated at C-PCM (chlorobenzene)-B3LYP/6-31+G(d); [f] Correction calculated at 383.15 K; [g] Correction calculated at 363.15 K.

Structure	E_{elec} [a], Ha	G_{corr} [b], Ha	G [c], Ha	Lowest freq.
101d-VE_{CC}	-949.586195	0.275324	-949.310871	14.16
101d-TS_{CC}	-949.550514	0.276947	-949.273567	-200.65
101e-VE_{CC}	-1064.114483	0.304086	-1063.810398	8.92
101e-TS_{CC}	-1064.080354	0.305573	-1063.774781	-166.73
101f-VE_{CC}	-1286.647595	0.272046	-1286.375549	7.95
101f-TS_{CC}	-1286.611379	0.274524	-1286.336856	-220.83
101h-VE_{CC}	-1048.828669	0.265989	-1048.562680	20.84
101h-TS_{CC}	-1048.793014	0.267114	-1048.525900	-201.73
101r-VE_{CC}	-988.904681	0.299690	-988.604991	21.28
101r-TS_{CC}	-988.869535	0.300491	-988.569043	-188.77
101s-VE_{CC}	-1409.182339	0.263831	-1408.918509	18.17
101s-TS_{CC}	-1409.146563	0.264973	-1408.881590	-205.79

Table 13. Energies and Lowest Frequencies of Minimum Energy Structures for thermal Claisen Rearrangement of allyl vinyl ethers (**101**) used for Hammett plot.[a] Electronic energies calculated at C-PCM (chlorobenzene)-B3LYP/6-31+G(d); [b] Thermal Corrections to Free Energy calculated at C-PCM (chlorobenzene)-B3LYP/6-31+G(d); [c] Gibbs free energies calculated at C-PCM (chlorobenzene)-B3LYP/6-31+G(d).

Scheme 134 provides a graphical guide to numbered compounds for thermal Claisen rearrangement of allyl vinyl ethers (**101**).

Claisen Rearrangement

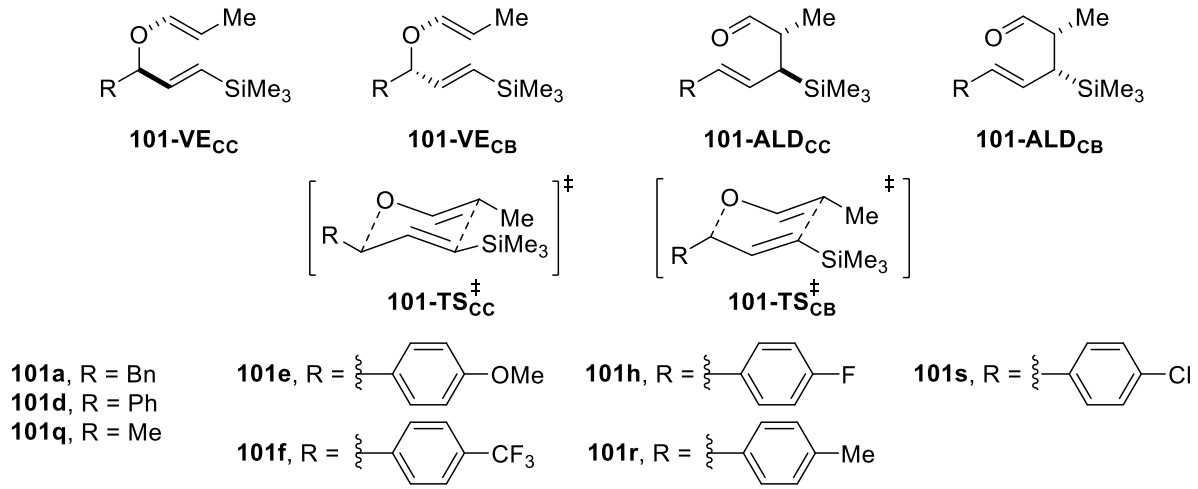

Scheme 134. Graphical guide to numbered compounds for thermal Claisen rearrangement of allyl vinyl ethers (**101**).

Energies and lowest frequencies of minimum energy structures including conformers for $AlCl_3$-mediated Sakurai allylation obtained by DFT are shown in Table 14 and 15.

Structure	E[a], Ha	E_SPC[b], Ha	G(T)_SPC[c]	qh-G(T)_SPC[d]	Lowest freq.[e]
ALD_{AP1}-$AlCl_3$	-2572.901206	-2572.947810	-2572.669662	-2572.662914	11.05
ALD_{AP2}-$AlCl_3$	-2572.903939	-2572.949090	-2572.671749	-2572.664453	9.61
ALD_{SC1}-$AlCl_3$	-2572.897673	-2572.948019	-2572.671635	-2572.664240	6.33
ALD_{SC2}-$AlCl_3$	-2572.901823	-2572.947550	-2572.670083	-2572.662836	7.78
TS_{AP1}-a	-2572.869762	-2572.921731	-2572.641298	-2572.635499	-420.22
TS_{AP1}-b	-2572.874167	-2572.924198	-2572.644185	-2572.638094	-420.78
TS_{AP2}-a	-2572.881193	-2572.933125	-2572.652659	-2572.646665	-349.20
TS_{AP2}-b	-2572.882691	-2572.931767	-2572.651673	-2572.645499	-345.94
TS_{SC1}	-2572.871526	-2572.922227	-2572.641975	-2572.636000	-412.78
TS_{SC2}-a	-2572.878825	-2572.928482	-2572.649571	-2572.643058	-349.68
TS_{SC2}-b	-2572.875364	-2572.927319	-2572.646477	-2572.640792	-344.49
P_{AP1}-$AlCl_3$-a	-2572.884752	-2572.940168	-2572.655387	-2572.650539	23.77
P_{AP1}-$AlCl_3$-b	-2572.889318	-2572.941331	-2572.658599	-2572.652793	9.78
P_{AP1}-$AlCl_3$-c	-2572.883411	-2572.935473	-2572.654048	-2572.647390	9.40
P_{AP2}-$AlCl_3$-a	-2572.891378	-2572.945086	-2572.663229	-2572.656848	11.45
P_{AP2}-$AlCl_3$-b	-2572.892336	-2572.942219	-2572.661463	-2572.654430	8.48

P_{AP2}-$AlCl_3$-c	-2572.895370	-2572.949248	-2572.667312	-2572.660819	7.70
P_{SC1}-$AlCl_3$-a	-2572.890500	-2572.946287	-2572.663199	-2572.657258	10.82
P_{SC1}-$AlCl_3$-b	-2572.881047	-2572.935017	-2572.654906	-2572.647498	1.02
P_{SC2}-$AlCl_3$-a	-2572.889064	-2572.943717	-2572.662344	-2572.656149	7.87
P_{SC2}-$AlCl_3$-b	-2572.884008	-2572.941225	-2572.658708	-2572.653099	19.89
P_{SC2}-$AlCl_3$-c	-2572.888955	-2572.941161	-2572.658570	-2572.652215	6.52
R_{AP1}-a	-949.649627	-949.688429	-949.401605	-949.398072	23.55
R_{AP1}-b	-949.647718	-949.690483	-949.404136	-949.400365	20.20
R_{AP2}-a	-949.647420	-949.688375	-949.400779	-949.397576	27.63
R_{AP2}-b	-949.650704	-949.692230	-949.405511	-949.402017	18.45
R_{AP2}-c	-949.644498	-949.685094	-949.397533	-949.394016	17.18
R_{SC1}-a	-949.647531	-949.688276	-949.402076	-949.398274	15.35
R_{SC1}-b	-949.647948	-949.689424	-949.402839	-949.399158	16.38
R_{SC2}-a	-949.646062	-949.690561	-949.403364	-949.400073	15.42
R_{SC2}-b	-949.635739	-949.681648	-949.393877	-949.390968	20.37
R_{SC2}-c	-949.645186	-949.686315	-949.399608	-949.395917	17.38
$AlCl_3$	-1623.242152	-1623.250966	-1623.274016	-1623.273961	138.51
PhCl	-691.857745	-691.864912	-691.798048	-691.798053	187.47

Table 14. Energies and lowest frequencies of minimum energy structures including conformers for $AlCl_3$-mediated Sakurai allylation.[a] Electronic energies calculated at C-PCM (chlorobenzene)-B3LYP/6-31+G(d); [b] Single point energies calculated at C-PCM (chlorobenzene)-M11L/6-311++G(2d,2p); [c] Harmonic solvent and temperature (293.15 K) corrected Gibbs free energies; [d] Quasi-harmonic solvent and temperature (293.15 K) corrected Gibbs free energies at 1 mol/L standard state; [e] Unscaled; calculated at C-PCM (chlorobenzene)-B3LYP/6-31+G(d).

Structure	E[a], Ha	E_SPC[b], Ha	G(T)_SPC[c]	qh-G(T)_SPC[d]	Lowest freq.[e]
110j-a	-640.174287	-640.193046	-640.006603	-640.005093	35.77
110j-b	-640.172140	-640.191116	-640.004899	-640.003140	21.65
110j-c	-640.172217	-640.191210	-640.004614	-640.002984	35.65
110j-d	-640.171538	-640.191180	-640.004472	-640.002892	25.87
110j-e	-640.171563	-640.191692	-640.004959	-640.003486	34.95
110j-f	-640.169918	-640.190165	-640.002657	-640.001399	43.38
110j-g	-640.172077	-640.191176	-640.004531	-640.002991	41.64
110j-h	-640.172687	-640.192186	-640.005286	-640.003819	40.37
Chloroform	-1419.286898	-1419.288045	-1419.291576	-1419.291583	259.36

Table 15. Energies and lowest frequencies of minimum energy structures for (**110j**).[a] Electronic energies calculated at C-PCM (chloroform)-B3LYP/6-31+G(d); [b] Single point energies

calculated at C-PCM (chloroform)-M11L/6-311++G(2d,2p); [c] Harmonic solvent and temperature (293.15 K) corrected Gibbs free energies; [d] Quasi-harmonic solvent and temperature (293.15 K) corrected Gibbs free energies at 1 mol/L standard state; [e] Unscaled; calculated at C-PCM (chloroform)-B3LYP/6-31+G(d).

Schemes 135 and 136 provide graphical guides to numbered compounds for $AlCl_3$-mediated Sakurai allylation and (**110j**) conformational studies.

Sakurai Allylation

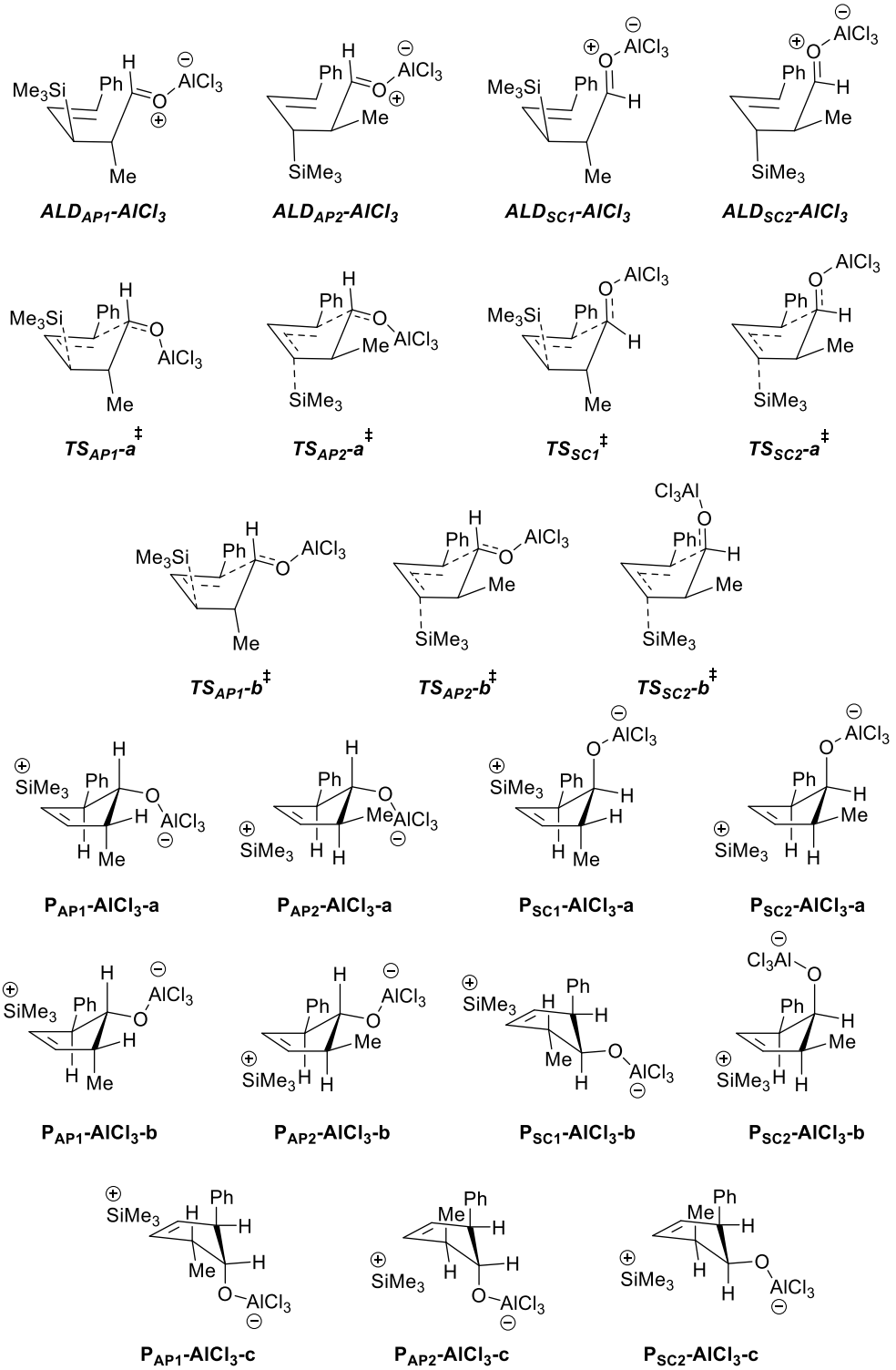

Scheme 135. Graphical guide to numbered compounds to numbered compounds for $AlCl_3$-mediated Sakurai allylation.

Sakurai Allylation

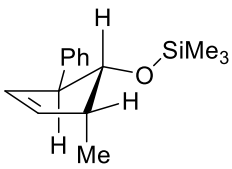

P_{AP1}-a

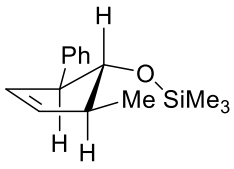

P_{AP2}-a

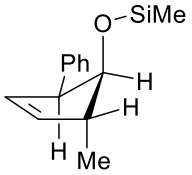

P_{SC1}-a

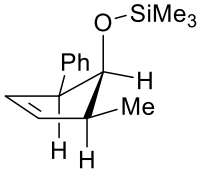

P_{SC2}-a

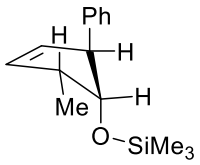

P_{AP1}-b

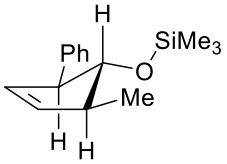

P_{AP2}-b

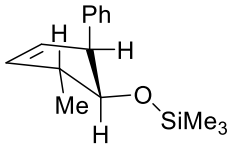

P_{SC1}-b

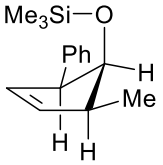

P_{SC2}-b

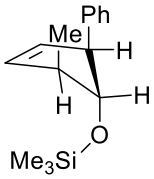

P_{AP2}-c

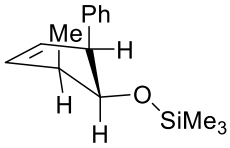

P_{SC2}-c

Structures for NOE

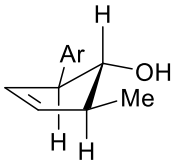

110j-a
AP2

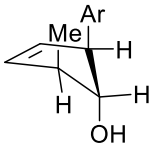

110j-b
AP2

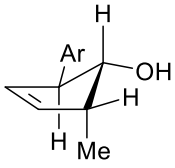

110j-c
AP1

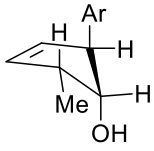

110j-d
AP1

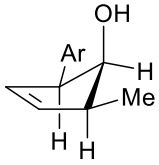

110j-e
SC2

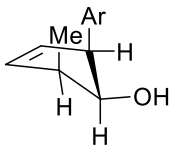

110j-f
SC2

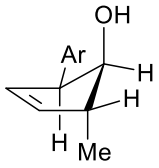

110j-g
SC1

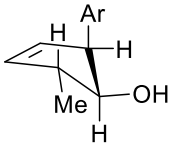

110j-h
SC1

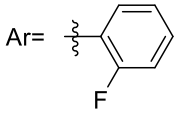

Scheme 136. Graphical guide to numbered compounds to numbered compounds for $AlCl_3$-mediated Sakurai allylation and (**110j**) conformational studies.

Energies and lowest frequencies of minimum energy structures including conformers for Et_2AlCl-mediated Claisen-Sakurai cascade reaction and obtained by DFT are shown in Table 16 and 17.

Structure	E_{elec} [a], Ha	G_{corr} [b], Ha	G [c], Ha	Lowest freq.
101q-$SiMe_2Ph$	-949.585508	0.276769	-949.308739	13.52
116-TS_{LA}	-1810.759724	0.386191	-1810.373533	-10.78
117	-1810.776054	0.393455	-1810.382599	7.43
118-TS_{BOAT}	-1810.751468	0.393488	-1810.357980	-78.72
119-TS_{ION}	-1810.755726	0.391943	-1810.363783	-72.45
120-TS_{CHAIR}	-1810.759032	0.391913	-1810.367119	-80.48
121	-1810.805886	0.395495	-1810.410391	11.84
Et_2AlCl	-861.174574	0.092895	-861.081679	21.39

Table 16. Energies and Lowest Frequencies of Minimum Energy Structures for the Claisen rearrangement catalyzed by Et_2AlCl and other competing pathways. [a] Electronic energies calculated at C-PCM (dichloromethane)-B3LYP/6-31+G(d); [b] Thermal Corrections to Free Energy calculated at C-PCM (dichloromethane)-B3LYP/6-31+G(d); [c] Gibbs free energies calculated at C-PCM (dichloromethane)-B3LYP/6-31+G(d).

Structure	E_{elec} [a], Ha	G_{corr} [b], Ha	G [c], Ha	Lowest freq.
121	-1810.805886	0.395495	-1810.410391	11.84
124-TS_{Alk}	-1810.768490	0.399152	-1810.369338	-322.60
125-TS_{SC1}	-1810.767468	0.395967	-1810.371501	-451.10
126-TS_{AP1}	-1810.771179	0.395199	-1810.375980	-443.11
127-TS_{SC2}	-1810.774983	0.395684	-1810.379299	-379.96
128-TS_{AP2}	-1810.779063	0.397615	-1810.381448	-344.99
129	-1810.785488	0.400170	-1810.385318	16.11
130	-949.643849	0.284104	-949.359745	14.42
Et_2AlCl	-861.174574	0.092895	-861.081679	21.39

Table 17. Energies and Lowest Frequencies of Minimum Energy Structures for Sakurai intramolecular allylation catalyzed by Et_2AlCl and other competing pathways. [a] Electronic energies calculated at C-PCM (dichloromethane)-B3LYP/6-31+G(d); [b] Thermal Corrections to

Free Energy calculated at C-PCM (dichloromethane)-B3LYP/6-31+G(d); [c] Gibbs free energies calculated at C-PCM (dichloromethane)-B3LYP/6-31+G(d).

Scheme 137 provides a graphical guide to numbered compounds for Et_2AlCl-mediated Claisen-Sakurai cascade reaction.

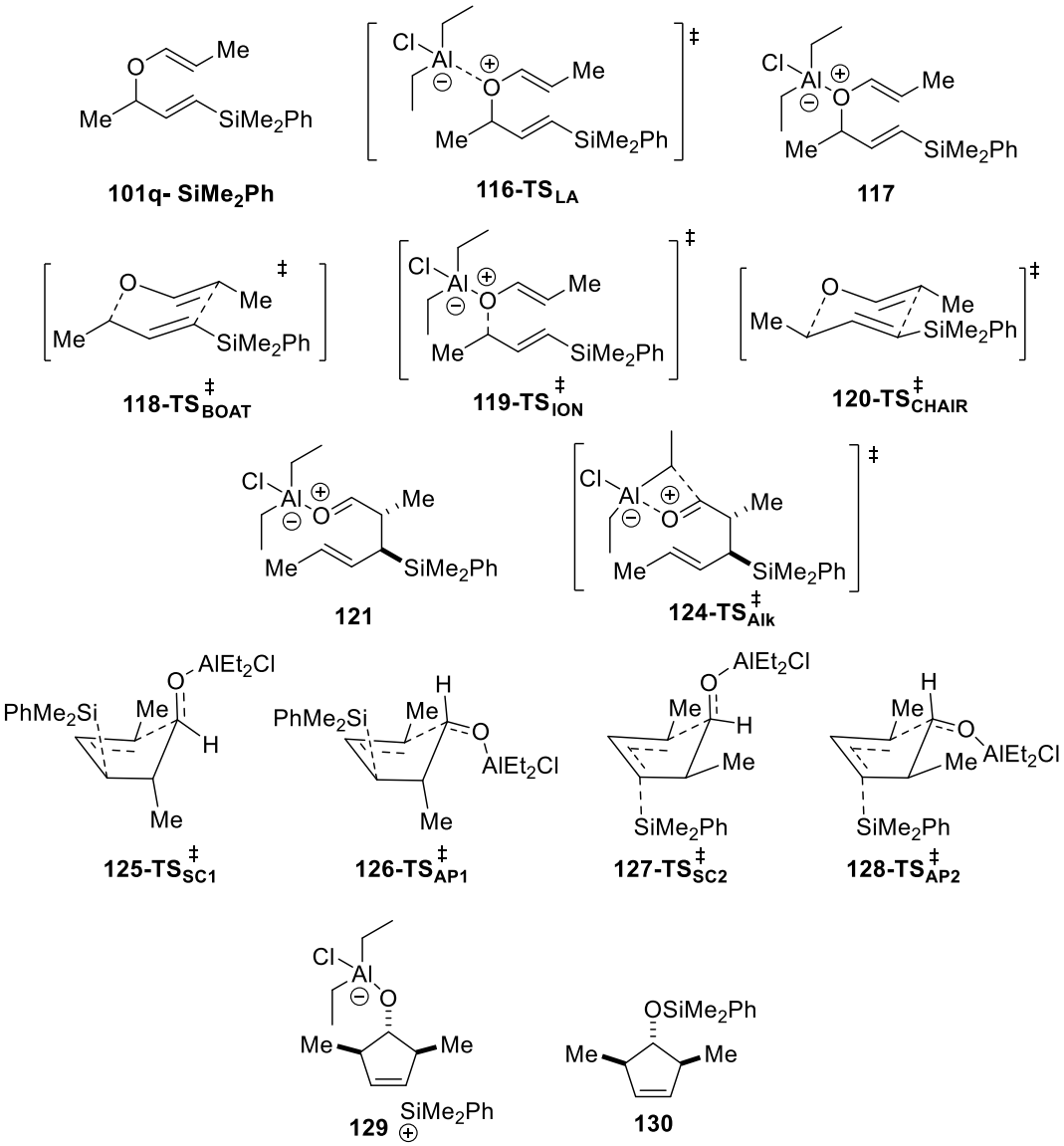

Scheme 137. Graphical guide to numbered compounds to numbered compounds for Et_2AlCl-mediated Claisen-Sakurai cascade reaction.

Energies and lowest frequencies of minimum energy structures for complexes of allyl vinyl ether (**101q- $SiMe_2Ph$)** with $AlMe_3$, Et_2AlCl, $EtAlCl_2$, $AlCl_3$ optimized by DFT are shown in Table 18.

Structure	E_{elec} [a], Ha	G_{corr} [b], Ha	G [c], Ha	Lowest freq.
101q-$SiMe_2Ph$-$AlMe_3$	-1311.796520	0.372887	-1311.423633	9.00
101q-$SiMe_2Ph$-Et_2AlCl	-1810.776054	0.393455	-1810.382599	7.43
101q-$SiMe_2Ph$-$EtAlCl_2$	-2191.827534	0.331260	-2191.496274	4.62
101q-$SiMe_2Ph$-$AlCl_3$	-2572.867923	0.272099	-2572.595825	10.13

Table 18. Energies and lowest frequencies of minimum energy structures for complexes of allyl vinyl ether (**101q- $SiMe_2Ph$)** with $AlMe_3$, Et_2AlCl, $EtAlCl_2$, $AlCl_3$ optimized by DFT.[a] Electronic energies calculated at C-PCM (dichloromethane)-B3LYP/6-31+G(d); [b] Thermal Corrections to Free Energy calculated at C-PCM (dichloromethane)-B3LYP/6-31+G(d); [c] Gibbs free energies calculated at C-PCM (dichloromethane)-B3LYP/6-31+G(d).

Scheme 138 provides a graphical guide to numbered compounds for complexes of allyl vinyl ether (**101q- $SiMe_2Ph$)** with $AlMe_3$, Et_2AlCl, $EtAlCl_2$, $AlCl_3$ optimized by DFT**.**

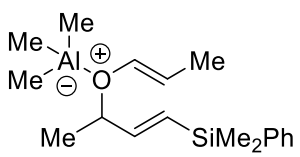

101q- $SiMe_2Ph$-$AlMe_3$

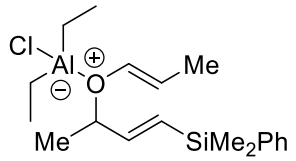

101q- $SiMe_2Ph$-Et_2AlCl

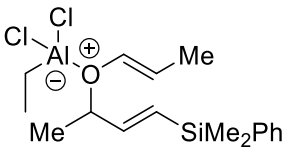

101q- $SiMe_2Ph$-$EtAlCl_2$

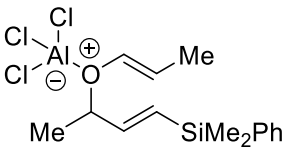

101q- $SiMe_2Ph$-$AlCl_3$

Scheme 138. Graphical guide to numbered compounds for complexes of allyl vinyl ether (**101q- $SiMe_2Ph$)** with $AlMe_3$, Et_2AlCl, $EtAlCl_2$, $AlCl_3$ optimized by DFT**.**

Stereodivergent Approach to Methylene Cyclopentanols

Energies and lowest frequencies of minimum energy structures for thermal Claisen rearrangement of allyl vinyl ethers (**146**) are presented in Table 19.

Structure	E[a], Ha	E_SPC[b], Ha	G(T)_SPC[c]	qh-G(T)_SPC[d]	Lowest freq.[e]
146d-VE_C	-988.895288	-988.863971	-988.576303	-988.568842	15.75
146d-VE_B	-988.895826	-988.866928	-988.578015	-988.570993	15.45
146d-TS_{CZ}	-988.860167	-988.821109	-988.531293	-988.525814	-315.23
146d-TS_{CE}	-988.859782	-988.819706	-988.531129	-988.525139	-286.81
146d-TS_{BZ}	-988.855605	-988.814749	-988.525926	-988.520073	-247.20
146d-TS_{BE}	-988.856052	-988.813714	-988.525398	-988.519505	-210.83
147d-ALD_{CZ}	-988.929294	-988.901965	-988.612136	-988.604867	14.72
147d-ALD_{CE}	-988.929020	-988.901179	-988.611375	-988.604204	15.78
147d-ALD_{BZ}	-988.927925	-988.900381	-988.609714	-988.602895	21.19
147d-ALD_{BE}	-988.927427	-988.899603	-988.610101	-988.602732	14.99
146a-TS_{CZ}	-1067.491393	-1067.452655	-1067.118391	-1067.110111[f]	-344.34
146a-TS_{CE}	-1067.489309	-1067.450662	-1067.117362	-1067.108660[f]	-353.10
146b-TS_{CZ}	-1028.175030	-1028.136813	-1027.827696	-1027.820407[f]	-354.93
146b-TS_{CE}	-1028.172578	-1028.134854	-1027.826206	-1027.818651[f]	-357.11
146c-TS_{CZ}	-992.481028	-992.470470	-992.116716	-992.111202[f]	-325.97
146c-TS_{CE}	-992.481784	-992.471343	-992.118926	-992.112806[f]	-329.04
146e-TS_{CZ}	-1088.101938	-1088.065705	-1087.785438	-1087.779792[g]	-327.90
146e-TS_{CE}	-1088.100579	-1088.062188	-1087.782538	-1087.776695[g]	-290.93
PhCl	-691.857745	-691.841989	-691.782439	-691.782435 [g]	187.47
PhCl	-691.857745	-691.841989	-691.784630	-691.784623[f]	187.47

Table 19. Energies and lowest frequencies of minimum energy structures for thermal Claisen rearrangement of allyl vinyl ethers (**146**).[a] Electronic energies calculated at C-PCM (chlorobenzene)-B3LYP/6-31+G(d); [b] Single point energies calculated at C-PCM (chlorobenzene)- ωB97XD/6-311++G(2d,2p); [c] Harmonic solvent and temperature corrected Gibbs free energies; [d] Quasi-harmonic solvent and temperature corrected Gibbs free energies at 1 mol/L standard state; [e] Unscaled; calculated at C-PCM (chlorobenzene)-B3LYP/6-31+G(d); [f] Correction calculated at 383.15 K; [g] Correction calculated at 363.15 K.

Scheme 139 provides a graphical guide to numbered compounds for thermal Claisen rearrangement of allyl vinyl ethers (**146**).

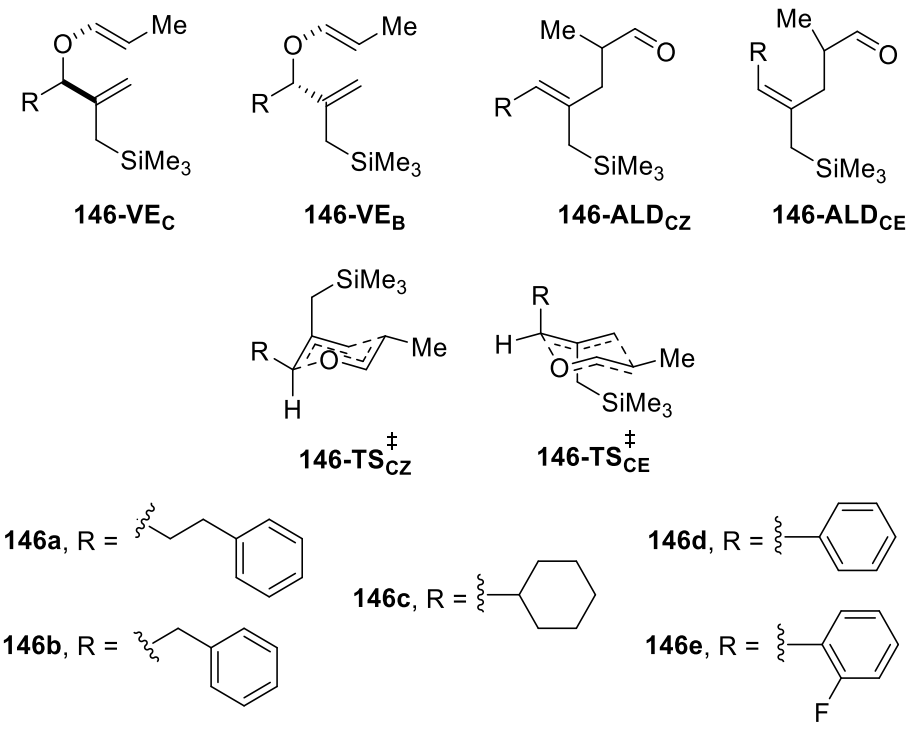

Scheme 139. Graphical guide to numbered compounds for thermal Claisen rearrangement of allyl vinyl ethers (**146**).

Energies and lowest frequencies of minimum energy structures for competing chair transition states in $EtAlCl_2$-catalyzed Claisen rearrangement of allyl vinyl ethers (**146**) are presented in Table 20.

Structure	E[a], Ha	E_SPC[b], Ha	G(T)_SPC[c]	qh-G(T)_SPC[d]	Lowest freq.[e]
146a-TS_{CZ}-Al	-2309.748664	-2309.747120	-2309.301054	-2309.296933	-148.90
146a-TS_{CE}-Al	-2309.752692	-2309.750175	-2309.305883	-2309.301292	-139.71
146b-TS_{CZ}-Al	-2270.431609	-2270.429879	-2270.012353	-2270.008220	-153.51
146b-TS_{CE}-Al	-2270.434801	-2270.433671	-2270.016814	-2270.012534	-143.60
146c-TS_{CZ}-Al	-2234.739745	-2234.767220	-2234.305799	-2234.302698	-126.35
146c-TS_{CE}-Al	-2234.746710	-2234.772435	-2234.312342	-2234.308785	-115.60
146d-TS_{CZ}-Al	-2231.117003	-2231.117912	-2230.726333	-2230.723052	-191.12
146d-TS_{CE}-Al	-2231.124764	-2231.122319	-2230.731311	-2230.727845	-151.48
146e-TS_{CZ}-Al	-2330.357653	-2330.361098	-2329.978510	-2329.974980	-190.11
146e-TS_{CE}-Al	-2330.362178	-2330.361666	-2329.979628	-2329.976003	-133.91

Toluene -271.578917 -271.548497 -271.435813 -271.435436 33.34

Table 20. Energies and lowest frequencies of minimum energy structures for competing chair transition states in $EtAlCl_2$-catalyzed Claisen rearrangement of allyl vinyl ethers (**146**). [a] Electronic energies calculated at C-PCM (toluene)-B3LYP/6-31+G(d); [b] Single point energies calculated at C-PCM (toluene)- ωB97XD /6-311++G(2d,2p); [c] Harmonic solvent and temperature corrected Gibbs free energies; [d] Quasi-harmonic solvent and temperature corrected Gibbs free energies at 195.15K and 1 mol/L standard state; [e] Unscaled; calculated at C-PCM (toluene)-B3LYP/6-31+G(d).

Scheme 140 provides a graphical guide to numbered compounds for $EtAlCl_2$-catalyzed Claisen rearrangement of allyl vinyl ethers (**146**).

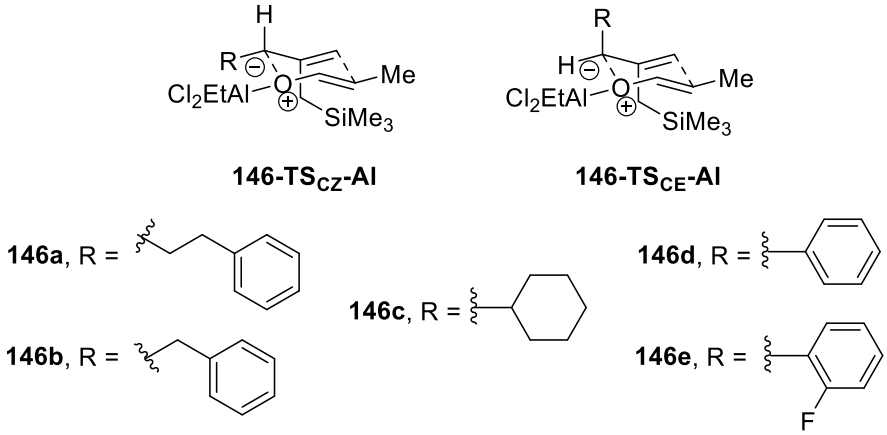

Scheme 140. Graphical guide to numbered compounds for $EtAlCl_2$-catalyzed Claisen rearrangement of allyl vinyl ethers (**146**).

Energies and lowest frequencies of minimum energy structures for BF_3-mediated Sakurai allylation are presented in Table 21, 22 and 23.

Structure	E[a], Ha	E_SPC[b], Ha	G(T)_SPC[c]	qh-G(T)_SPC[d]	Lowest freq.[e]
147d-BF_3-ALD_{APZ}	-1313.529181	-1313.508146	-1313.180157	-1313.175431	17.66
147d-BF_3-ALD_{SCZ}	-1313.531599	-1313.509361	-1313.182713	-1313.177432	13.31
147d-BF_3-ALD_{APE}	-1313.532468	-1313.509041	-1313.184438	-1313.178197	3.49
147d-BF_3-ALD_{SCE}	-1313.533797	-1313.510153	-1313.184726	-1313.178797	8.04
147d-BF_3-TS_{APZ}	-1313.518940	-1313.496679	-1313.166885	-1313.162772	-266.86
147d-BF_3-TS_{SCZ}	-1313.515975	-1313.494398	-1313.164667	-1313.160588	-264.87

147d-BF_3-TS_{APE}	-1313.514167	-1313.494093	-1313.163572	-1313.159664	-275.83
147d-BF_3-TS_{SCE}	-1313.512430	-1313.492979	-1313.163118	-1313.158857	-262.59
147d-BF_3-P_{APZ}	-1313.529689	-1313.516098	-1313.184579	-1313.180672	14.21
147d-BF_3-P_{SCZ}	-1313.528908	-1313.514606	-1313.184056	-1313.180019	19.36
147d-BF_3-P_{APE}	-1313.521167	-1313.506689	-1313.174850	-1313.171124	21.20
147d-BF_3-P_{SCE}	-1313.523793	-1313.509580	-1313.177681	-1313.173925	18.13
Chlorobenzene	-691.857745	-691.841989	-691.771193	-691.771201	187.47

Table 21. Energies and lowest frequencies of minimum energy structures for BF_3-mediated Sakurai allylation of Ph-substituted variant. [a] Electronic energies calculated at C-PCM (chlorobenzene)-B3LYP/6-31+G(d); [b] Single point energies calculated at C-PCM (chlorobenzene)- ωB97XD /6-311++G(2d,2p); [c] Harmonic solvent and temperature corrected Gibbs free energies; [d] Quasi-harmonic solvent and temperature corrected Gibbs free energies at 253.15K and 1 mol/L standard state; [e] Unscaled; calculated at C-PCM (chlorobenzene)-B3LYP/6-31+G(d).

Structure	E[a], Ha	E_SPC[b], Ha	G(T)_SPC[c]	qh-G(T)_SPC[d]	Lowest freq.[e]
147c-BF_3-ALD_{APZ}	-1317.155252	-1317.160218	-1316.764635	-1316.759182	14.29
147c-BF_3-ALD_{SCZ}	-1317.153890	-1317.159175	-1316.763928	-1316.758321	11.96
147c-BF_3-ALD_{APE}	-1317.155394	-1317.158800	-1316.763569	-1316.758025	14.26
147c-BF_3-ALD_{SCE}	-1317.155455	-1317.159593	-1316.764188	-1316.758721	14.01
147c-BF_3-TS_{APZ}	-1317.136096	-1317.145653	-1316.745741	-1316.741952	-263.22
147c-BF_3-TS_{SCZ}	-1317.136675	-1317.146105	-1316.746119	-1316.742321	-223.14
147c-BF_3-TS_{APE}	-1317.134338	-1317.142758	-1316.742910	-1316.738921	-257.29
147c-BF_3-TS_{SCE}	-1317.134298	-1317.143978	-1316.744179	-1316.740089	-221.63
147c-BF_3-P_{APZ}	-1317.151398	-1317.164953	-1316.763909	-1316.760172	19.67
147c-BF_3-P_{SCZ}	-1317.145600	-1317.161064	-1316.761146	-1316.756925	14.55
147c-BF_3-P_{APE}	-1317.139647	-1317.151218	-1316.751138	-1316.746831	21.15
147c-BF_3-P_{SCE}	-1317.142279	-1317.154513	-1316.753776	-1316.749649	17.79
Chlorobenzene	-691.857745	-691.841989	-691.771193	-691.771201	187.47

Table 22. Energies and lowest frequencies of minimum energy structures for BF_3-mediated Sakurai allylation of Cy-substituted variant. [a] Electronic energies calculated at C-PCM (chlorobenzene)-B3LYP/6-31+G(d); [b] Single point energies calculated at C-PCM (chlorobenzene)- ωB97XD /6-311++G(2d,2p); [c] Harmonic solvent and temperature corrected Gibbs free energies; [d] Quasi-harmonic solvent and temperature corrected Gibbs free energies at 253.15K and 1 mol/L standard state; [e] Unscaled; calculated at C-PCM (chlorobenzene)-B3LYP/6-31+G(d).

Structure	E[a], Ha	E_SPC[b], Ha	G(T)_SPC[c]	qh-G(T)_SPC[d]	Lowest freq.[e]
147a-BF_3-TS_{APZ}	-1392.148176	-1392.126317	-1391.742907	-1391.737385	-230.12
147a-BF_3-TS_{SCZ}	-1392.146250	-1392.126058	-1391.743196	-1391.737567	-248.53
147a-BF_3-TS_{APE}	-1392.145766	-1392.123887	-1391.740483	-1391.734951	-251.14
147a-BF_3-TS_{SCE}	-1392.142815	-1392.122474	-1391.738911	-1391.733433	-221.60
147b-BF_3-TS_{APZ}	-1352.832285	-1352.812701	-1352.456400	-1352.451424	-226.43
147b-BF_3-TS_{SCZ}	-1352.829140	-1352.810979	-1352.453845	-1352.449244	-215.89
147b-BF_3-TS_{APE}	-1352.830056	-1352.810339	-1352.454158	-1352.449053	-261.67
147b-BF_3-TS_{SCE}	-1352.826796	-1352.808616	-1352.452288	-1352.447117	-228.63
147e-BF_3-TS_{APZ}	-1412.760839	-1412.741409	-1412.420842	-1412.416504	-272.35
147e-BF_3-TS_{SCZ}	-1412.758221	-1412.739167	-1412.418442	-1412.414152	-271.13
147e-BF_3-TS_{APE}	-1412.755464	-1412.737889	-1412.416243	-1412.412289	-273.72
147e-BF_3-TS_{SCE}	-1412.753524	-1412.736356	-1412.415151	-1412.410927	-256.46
Chlorobenzene	-691.857745	-691.841989	-691.771193	-691.771201	187.47

Table 23. Energies and lowest frequencies of minimum energy structures for BF_3-mediated Sakurai allylation. [a] Electronic energies calculated at C-PCM (chlorobenzene)-B3LYP/6-31+G(d); [b] Single point energies calculated at C-PCM (chlorobenzene)- ωB97XD /6-311++G(2d,2p); [c] Harmonic solvent and temperature corrected Gibbs free energies; [d] Quasi-harmonic solvent and temperature corrected Gibbs free energies at 253.15K and 1 mol/L standard state; [e] Unscaled; calculated at C-PCM (chlorobenzene)-B3LYP/6-31+G(d).

Scheme 141 provides a graphical guide to numbered compounds for BF_3-mediated Sakurai allylation.

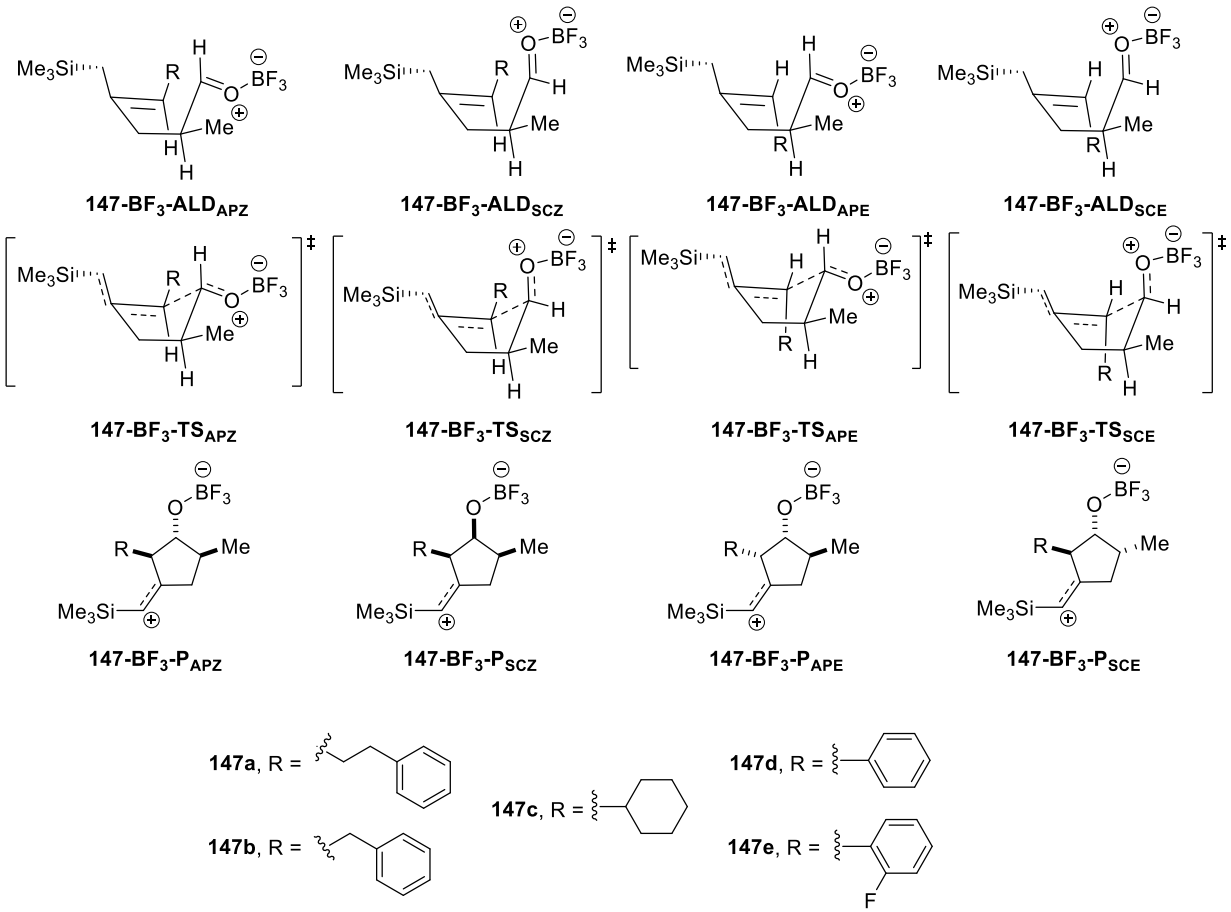

Scheme 141. Graphical guide to numbered compounds for BF_3-mediated Sakurai allylation.

Energies and lowest frequencies of minimum energy structures for $EtAlCl_2$-mediated Sakurai allylation are presented in Table 24 and 25.

Structure	E[a], Ha	E_SPC[b], Ha	G(T)_SPC[c]	qh-G(T)_SPC[d]	Lowest freq.[e]
147d-EtAlCl$_2$-ALD$_{APZ}$	-2231.173118	-2231.227949	-2230.835035	-2230.830873	11.06
147d-EtAlCl$_2$-ALD$_{SCZ}$	-2231.172389	-2231.225099	-2230.832724	-2230.828432	9.72
147d-EtAlCl$_2$-ALD$_{APE}$	-2231.176512	-2231.227217	-2230.835154	-2230.830645	7.02
147d-EtAlCl$_2$-ALD$_{SCE}$	-2231.177078	-2231.228566	-2230.836580	-2230.831971	8.26
147d-EtAlCl$_2$-TS$_{APZ}$	-2231.157902	-2231.218492	-2230.823502	-2230.820285	-244.55
147d-EtAlCl$_2$-TS$_{SCZ}$	-2231.153669	-2231.212618	-2230.818208	-2230.814791	-261.42
147d-EtAlCl$_2$-TS$_{APE}$	-2231.152333	-2231.211520	-2230.815996	-2230.812773	-233.36
147d-EtAlCl$_2$-TS$_{SCE}$	-2231.152461	-2231.211269	-2230.815693	-2230.812481	-252.68
147d-EtAlCl$_2$-P$_{APZ}$	-2231.165849	-2231.232255	-2230.836056	-2230.833022	16.33

147d-EtAlCl$_2$-P$_{SCZ}$	-2231.160875	-2231.226129	-2230.830381	-2230.827181	13.83
147d-EtAlCl$_2$-P$_{APE}$	-2231.154801	-2231.218593	-2230.822769	-2230.819381	13.04
147d-EtAlCl$_2$-P$_{SCE}$	-2231.159056	-2231.223882	-2230.828270	-2230.824835	10.07
Toluene	-271.578917	-271.589311	-271.476627	-271.476250	33.34

Table 24. Energies and lowest frequencies of minimum energy structures for intramolecular $EtAlCl_2$-mediated Sakurai allylation of phenyl variant. [a] Electronic energies calculated at C-PCM (toluene)-B3LYP/6-31+G(d); [b] Single point energies calculated at C-PCM (toluene)- M11L/6-311++G(2d,2p); [c] Harmonic solvent and temperature corrected Gibbs free energies; [d] Quasi-harmonic solvent and temperature corrected Gibbs free energies at 195.15K and 1 mol/L standard state; [e] Unscaled; calculated at C-PCM (toluene)-B3LYP/6-31+G(d).

Structure	E[a], Ha	E_SPC[b], Ha	G(T)_SPC[c]	qh-G(T)_SPC[d]	Lowest freq.[e]
147a- EtAlCl$_2$-TS$_{APZ}$	-2309.786281	-2309.850261	-2309.401121	-2309.396675	-195.58
147a- EtAlCl$_2$-TS$_{SCZ}$	-2309.785745	-2309.851878	-2309.402877	-2309.398440	-251.26
147a- EtAlCl$_2$-TS$_{APE}$	-2309.784754	-2309.847674	-2309.398273	-2309.393720	-220.90
147a- EtAlCl$_2$-TS$_{SCE}$	-2309.782607	-2309.844776	-2309.395430	-2309.390929	-223.07
147b- EtAlCl$_2$-TS$_{APZ}$	-2270.470854	-2270.536504	-2270.113498	-2270.109996	-205.68
147b- EtAlCl$_2$-TS$_{SCZ}$	-2270.467519	-2270.529356	-2270.107744	-2270.103738	-252.82
147b- EtAlCl$_2$-TS$_{APE}$	-2270.469697	-2270.531234	-2270.109245	-2270.105157	-247.69
147b- EtAlCl$_2$-TS$_{SCE}$	-2270.466972	-2270.527902	-2270.105253	-2270.101357	-231.09
147c- EtAlCl$_2$-TS$_{APZ}$	-2234.774377	-2234.849232	-2234.384125	-2234.381032	-217.54
147c- EtAlCl$_2$-TS$_{SCZ}$	-2234.773908	-2234.846228	-2234.381793	-2234.378384	-218.55
147c- EtAlCl$_2$-TS$_{APE}$	-2234.772103	-2234.842543	-2234.377827	-2234.374276	-243.91
147c- EtAlCl$_2$-TS$_{SCE}$	-2234.774713	-2234.845036	-2234.380132	-2234.376708	-223.17
147e- EtAlCl$_2$-TS$_{APZ}$	-2330.397943	-2330.449528	-2330.063516	-2330.060046	-239.38
147e- EtAlCl$_2$-TS$_{SCZ}$	-2330.396116	-2330.446355	-2330.060943	-2330.057305	-265.58
147e- EtAlCl$_2$-TS$_{APE}$	-2330.394434	-2330.444734	-2330.057984	-2330.054700	-243.11
147e- EtAlCl$_2$-TS$_{SCE}$	-2330.394359	-2330.444609	-2330.057783	-2330.054474	-252.36
Toluene	-271.578917	-271.589311	-271.476627	-271.476250	33.34

Table 25. Energies and lowest frequencies of minimum energy structures for intramolecular $EtAlCl_2$-mediated Sakurai allylation. [a] Electronic energies calculated at C-PCM (toluene)-B3LYP/6-31+G(d); [b] Single point energies calculated at C-PCM (toluene)- M11L/6-311++G(2d,2p); [c] Harmonic solvent and temperature corrected Gibbs free energies; [d] Quasi-harmonic solvent and temperature corrected Gibbs free energies at 195.15K and 1 mol/L standard state; [e] Unscaled; calculated at C-PCM (toluene)-B3LYP/6-31+G(d).

Scheme 142 provides a graphical guide to numbered compounds for $EtAlCl_2$-mediated Sakurai allylation.

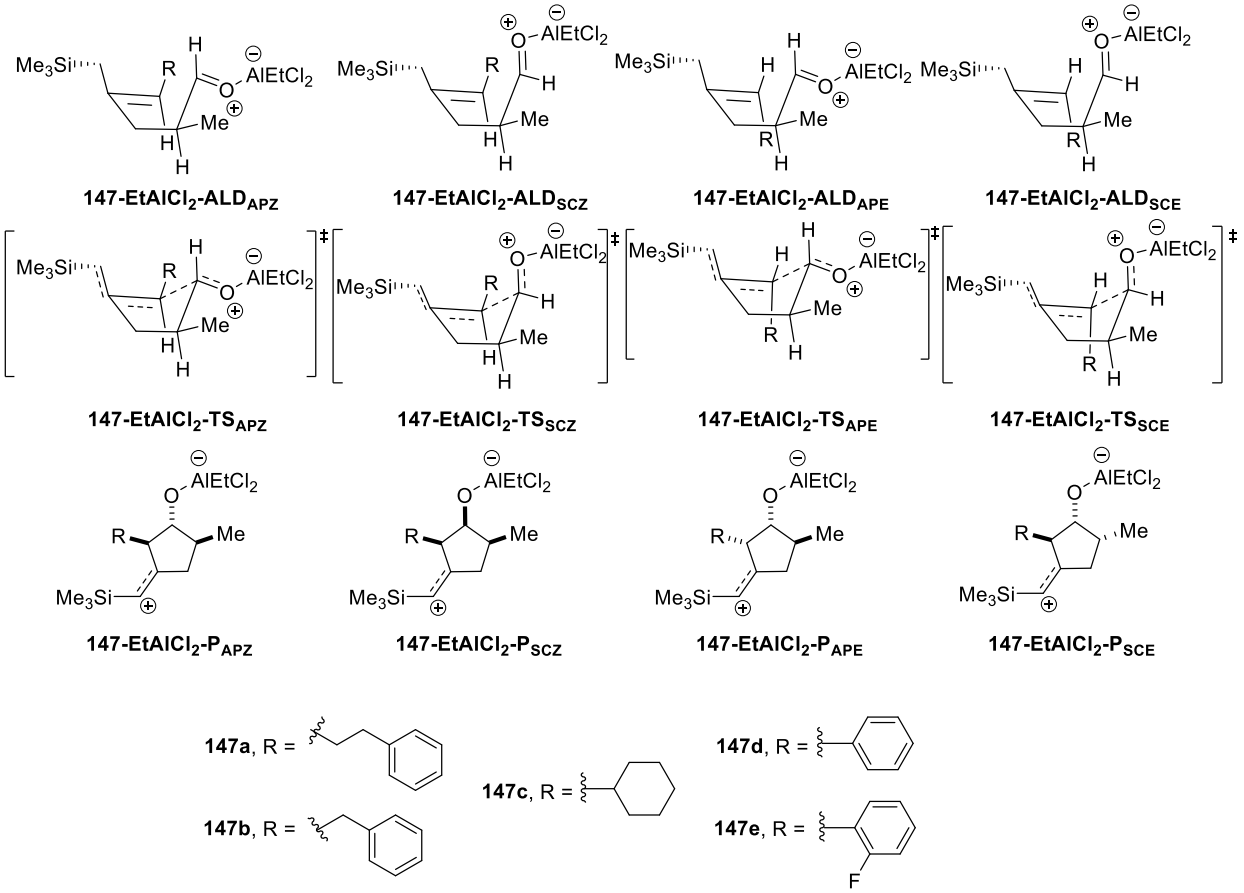

Scheme 142. Graphical guide to numbered compounds for $EtAlCl_2$-mediated Sakurai allylation.

Experimental Section (pages 100-116, 123-135), Computational Details (pages 151-159) and Appendix A (pages 300-333, 336-373) are

CHAPTER TWO

PALLADIUM-CATALYZED REARRANGEMENT OF *N*-ALLOC-*N*-ALLYL YNAMIDES TO COMPLEX NITRILES: MECHANISTIC STUDIES

Introduction

Nitriles are versatile moieties which can undergo a myriad of transformations.[193] Indeed, they can act as electrophiles, nucleophiles, and dienophiles, alongside other reactivity modes and are key intermediates in the syntheses of amines, carboxylic acids and heterocycles. Aside from their synthetic utility, nitriles are important functional groups in many pharmaceutical products due to their metabolic stability (Figure 16).[194] Due to the paucity of nitrile containing natural products,[195] there are few nitrile processing enzymes, leading to long half-lives *in vivo*. Despite their importance, the synthesis of complex nitriles continues to be a synthetic challenge, especially when a fully substituted α-carbon is present.

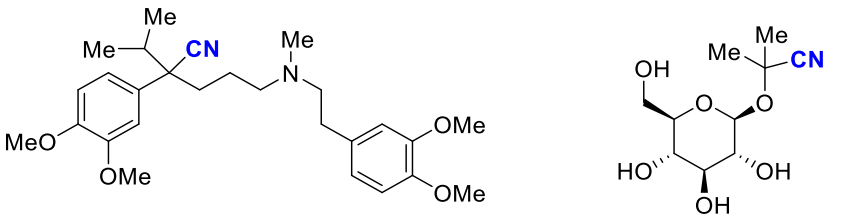

Figure 16. Example of pharmaceuticals and natural products containing nitrile moiety.

The Cook group has previously investigated both the synthesis of complex nitriles and allylic rearrangement of conjugated carbamates. These two areas have been merged into a single transformation whereby *N*-alloc-*N*-allyl ynamides (**165**, **167, 170**) can undergo a double allylic

rearrangement to form highly substituted and sterically congested nitrile products (**166**, **169, 172**) (Scheme 144).[196–198] This reaction was built upon the previous reports of decarboxylative allylic rearrangements of *N*-alloc indoles and ynamides (Scheme 143). These rearrangements provide ready and access to C-3 quaternary indolenines[199] (**160**-**161**) and ketenimines[200] (**163**), respectively.

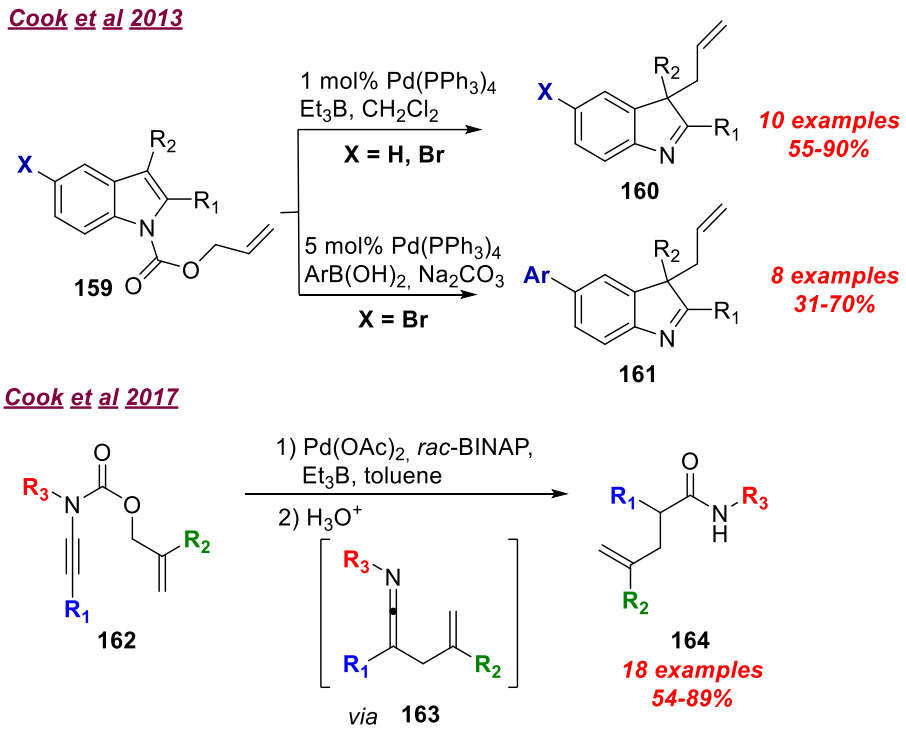

Scheme 143. The palladium catalyzed decarboxylative allylic rearrangements of *N*-alloc indoles and ynamides.

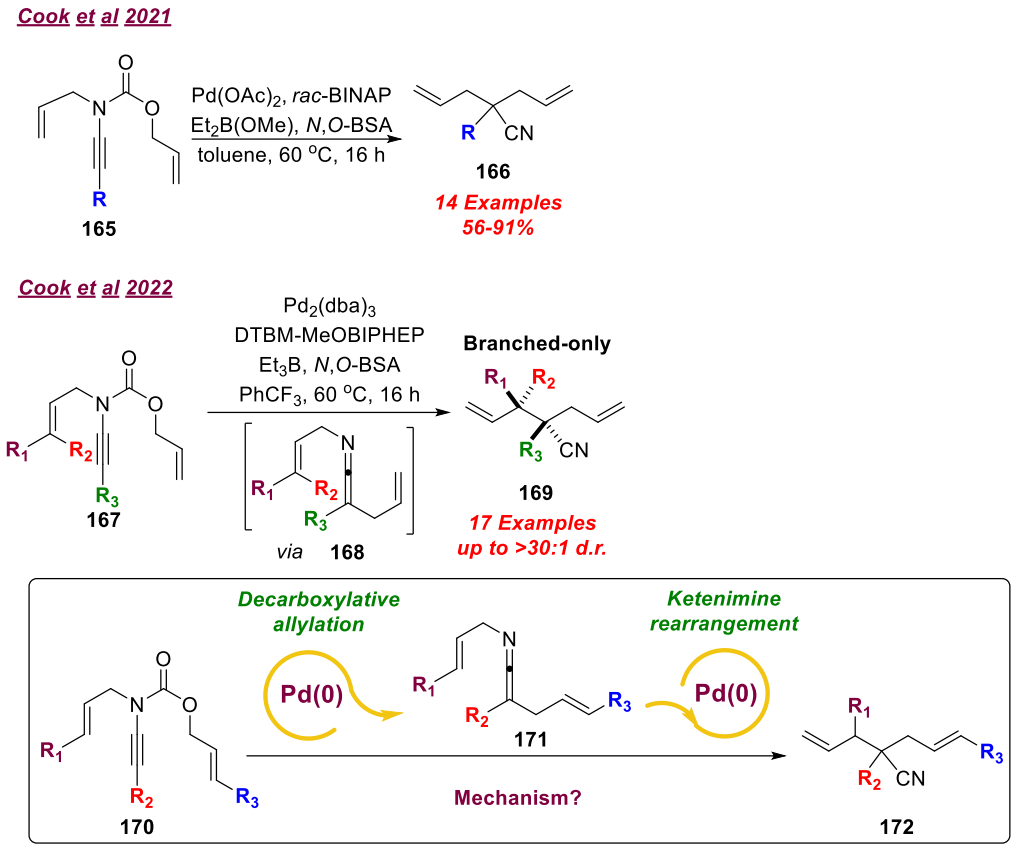

Scheme 144. The palladium catalyzed rearrangement of *N*-alloc-*N*-allyl ynamides to quaternary diallyl nitriles.

In this chapter, our mechanistic studies into the palladium-catalyzed rearrangement of *N*-alloc-*N*-allyl ynamides are described.[196-198] First, a background in this area will be discussed including mechanism of palladium catalyzed allylic alkylation reactions, alongside decarboxylative allylation and ketenimine rearrangements. The computational methods most commonly used for similar studies will be also reviewed.

Tsuji−Trost Reaction

The synthetic uses of π-allyl palladium complexes, first introduced by Tsuji in 1960's,[201] have enabled access to one of the most complex and sought-after transformations pursued by organic chemists – a stereoselective formation of C-C bond at a quaternary carbon. Being

constantly developed over the subsequent six-decades, metal-catalyzed allylic alkylation reactions currently allow for the construction of diverse bond types, including C-C, C-O and C-N, in a stereocontrolled manner, making it a powerful methodology for the synthesis of biologically active compounds.[202,203]

Allylic alkylation chemistry can be achieved using a variety of transition metals such as nickel,[204] molybdenum,[205] ruthenium,[206] iridium,[207,208] and rhodium.[209,210] However, allylic alkylations catalyzed by palladium complexes were historically the first and still remain the most abundant reaction type.[203] The general catalytic cycle of this reaction is shown in Scheme 145.[202,203] It involves an alkene complexation with Pd(0) catalyst followed by oxidative addition (ionization) *via* an S_N2-type mechanism to form a π-allyl-Pd intermediate. This intermediate is further attacked by a nucleophile either inside, *via* nucleophile complexation and reductive elimination, or outside of the coordination sphere of the metal, *via* an S_N2-type mechanism. The former is referred as an inner-sphere, while the latter as an outer-sphere mechanistic pathway. The following decomplexation of an alkene furnishes the desired product. The regioselectivity of the reaction depends on the metal, ligand and reagents used, however, the general trend is that the attack at the less-substituted terminus is preferred with palladium to give the linear product.[203]

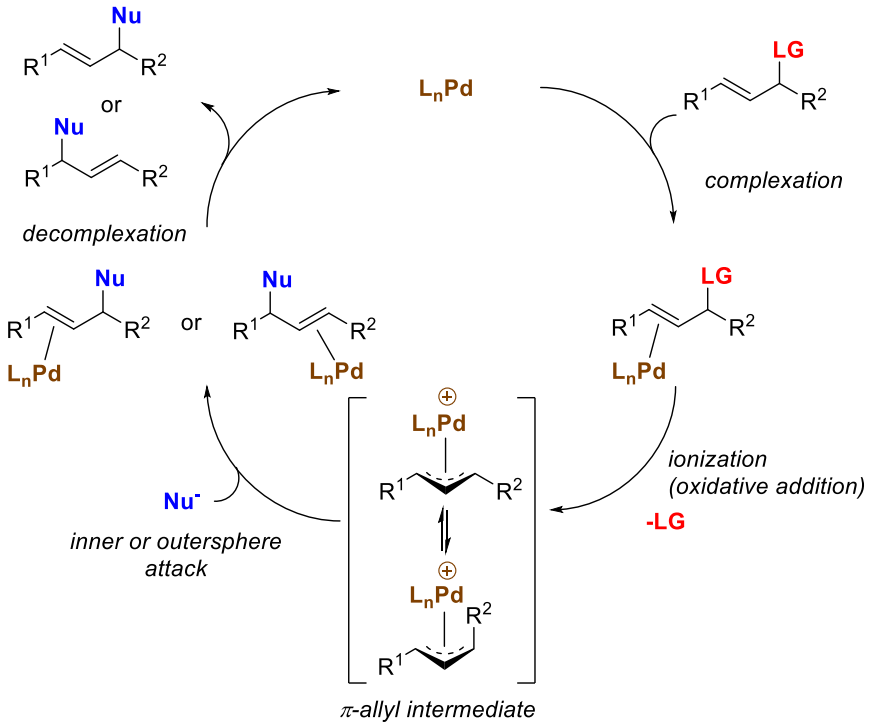

Scheme 145. Catalytic cycle of Tsuji-Trost reaction.

Although many π-allyl reactions appear similar, there are significant differences in their mechanisms and new catalytic reactions cannot be assumed to proceed through identical routes to previously reported reactions. Indeed, much is known about the influence of Pd complex structure and reagent identities on enantio- and regio- selectivity in the classic Tsuji-Trost reaction,[202,203] however applying these studies to new reactivity modes can lead to misleading results. An experimental study aimed at in-depth elucidation of the mechanism of such catalytic reactions often requires significant amount of time and resources and, yet not always gives a conclusive answer.[211] Furthermore, these studies can only provide limited information as standard kinetic studies cannot provide information following the first irreversible step. On the contrary, computational methods allow to explore multiple possible mechanistic pathways in quite accurate and much less resource-consuming way. Additionally, short-living reactive

species and transition states that are challenging to detect and study experimentally can be located.[55,211] We will further explore both experimental and computational studies done in the area of Pd(0)-catalyzed decarboxylative allylation and ketenimine generation and rearrangements.

Decarboxylative Allylation

Since the mechanism of palladium-catalyzed decarboxylative allylation of *N*-alloc-*N*-allyl ynamides has not been described in the literature, we will explore examples of mechanistic studies performed for related systems.

The palladium-catalyzed decarboxylative allylation was first independently published by Tsuji (Scheme 146)[212] and Saegusa[213] (Scheme 147). The reactions utilized *in situ* generated enolates and this variant had been extensively developed.[214]

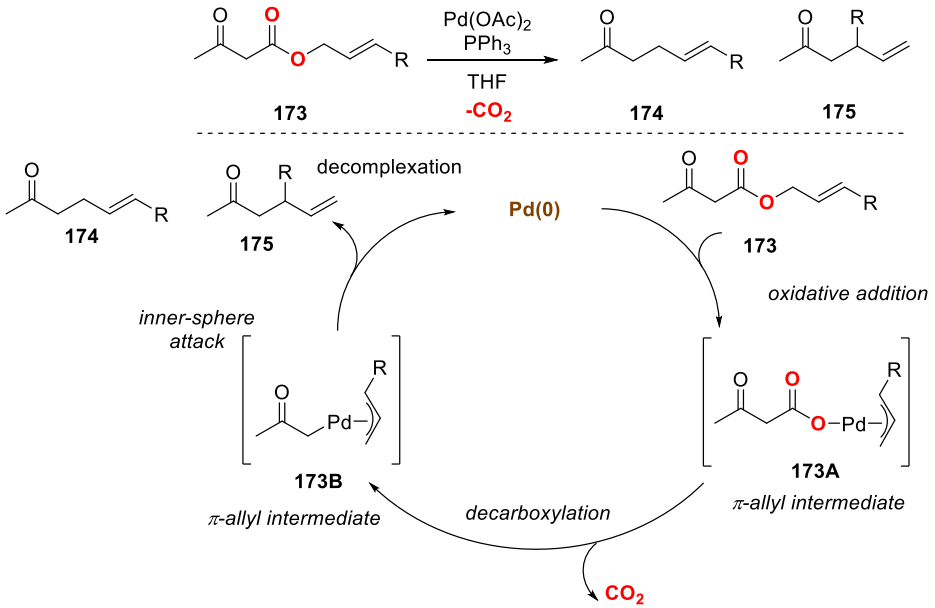

Scheme 146. Palladium-catalyzed decarboxylative allylation of enolates by Tsuji.

Both Tsuji[212] and Saegusa[213] proposed that the mechanism of this transformation involves oxidative addition of the substrate to Pd(0) catalyst resulting in the formation of palladium π-allyl complex, where carboxylate is coordinated to Pd ((**173A**) in Scheme 146 and (**178**) in Scheme 147). However, Tsuji suggested that upon decarboxylation complex (**173A**) produces π-allyl intermediate (**173B**) containing C-bound enolate that then undergoes inner-sphere nucleophilic attack to provide the product (Scheme 146).[212] On the contrary, Saegusa proposed that after decarboxylation, complex (**178**) results in π-allyl intermediate (**179**) with O-bound enolate that dissociates to form ion pair (**180**) which undergoes an outer-sphere nucleophilic attack furnishing product (**177**) (Scheme 147).[213]

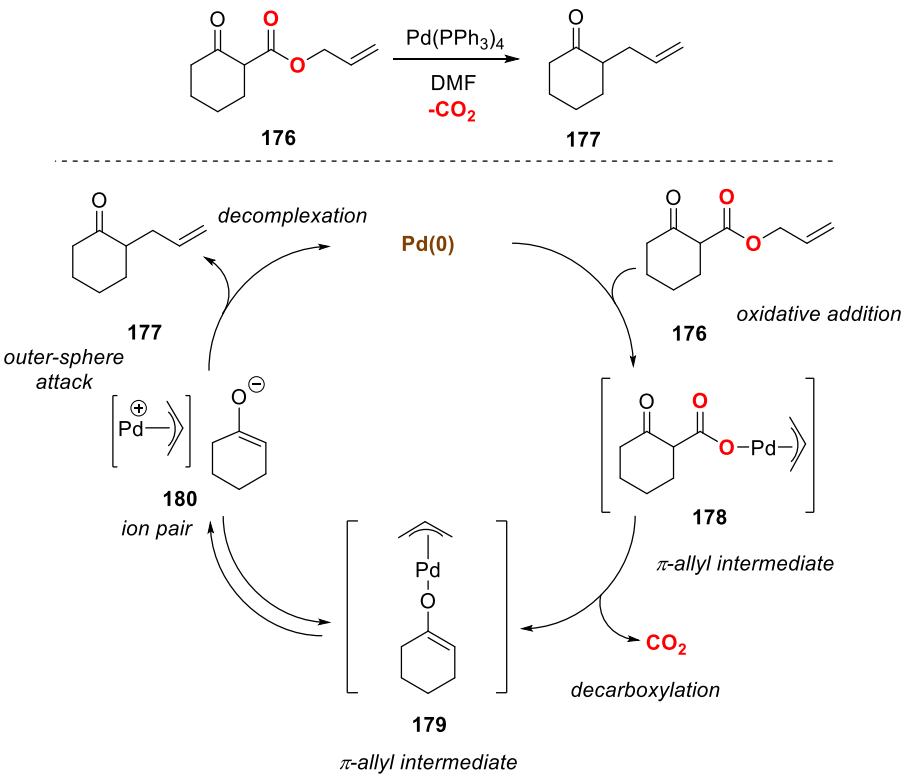

Scheme 147. Decarboxylative allylation of enolates and catalytic cycle proposed by Saegusa.

Further mechanistic studies of palladium-catalyzed decarboxylative allylation reactions involving formation of enolates proposed various reactivity modes including both outer- and inner-sphere processes.[214–218]

For example, when the mechanism of the enantioselective decarboxylative allylation of enol carbonate (**181**) was studied by Stoltz and Goddard using DFT (Scheme 148),[216] it was shown that inner-sphere nucleophilic attack occurs through a seven-membered transition state that is energetically more preferable than the outer-sphere variant and significantly lower in energy than a three-centered C−C reductive elimination transition state (Scheme 149).

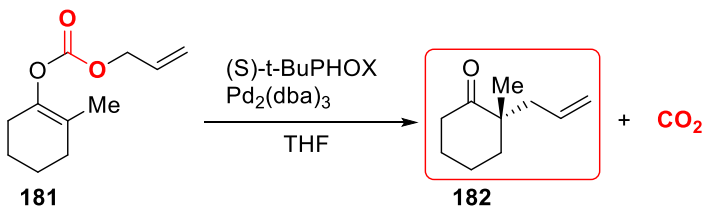

Scheme 148. Enantioselective decarboxylative allylation of enol carbonate (**182**).

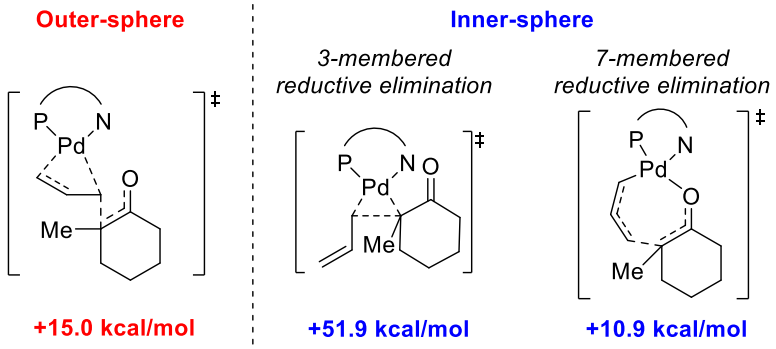

Scheme 149. Transition states considered for inner- and outer-sphere nucleophilic attack.

Recently, a comprehensive DFT mechanistic study of decarboxylative allylation of allyl β-ketoester (**183**) has been reported by Stoltz and Goddard (Scheme 150).[217] This report will be covered in detail as it describes various reactivity modes and pathways that were considered for each step of the catalytic cycle (oxidative addition, decarboxylation, and reductive elimination).

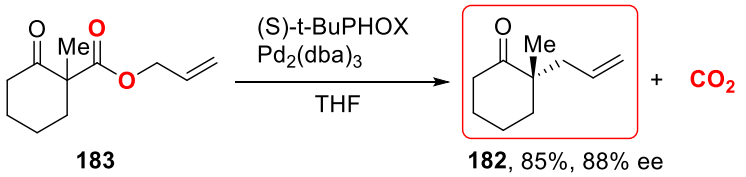

Scheme 150. Enantioselective decarboxylative allylation of enol carbonate (**182**).

For oxidative addition step, authors considered 3- and 7-membered ring transition states alongside transition states representing *syn*- and *anti*-displacement-type mechanisms (Scheme 151). It was found that comparing to other variants, *anti*-S_N2-type transition states are lower in energy with the lowest energy isomer containing allyl group in *exo*- orientation and C-O bond positioned *trans* with respect to nitrogen in PHOX ligand (Scheme 151, in the box). Oxidative addition was predicted to afford an ion pair that is further transformed into η^1-bound allyl palladium complex, which can produce a variety of intermediates for the next step.[217]

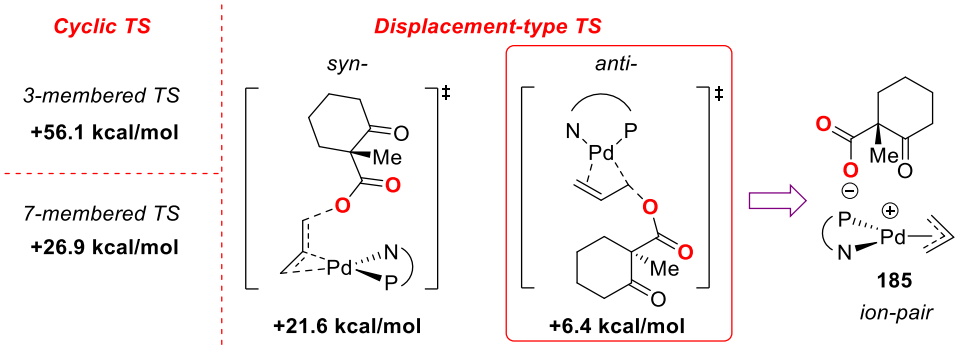

Scheme 151. Transition states considered for oxidative addition step. $\Delta G^{\neq}$ energies calculated at C-PCM (THF)-M06/def2-TZVP//BP86-D3/LANL2TZ(f)−6-31G(d).

For decarboxylation step, authors examined cyclic (pathway 1), acyclic (pathway 2) and ion-pair (pathway 3) configurations of transition states signifying different mechanistic pathways (Scheme 152). It was discovered that the energetic preference towards each mechanism depended on solvent polarity, in particular, pathway 2 was the lowest energy one in toluene, Et_2O and THF, while pathway 3 was the most favored in more polar DMF. The observed effect

was rationalized based on a large dipole moment of transition state on the pathway 3 comparing to pathway 1 and 2. Importantly, in all three cases decarboxylation was found to be a rate-determining step. It is highlighted in the study that the decarboxylation pathway has a substantial effect on the mechanism of the following reductive elimination, in particular, it dictates whether nucleophile would attack in inner- or outer-sphere fashion. Thus, decarboxylation *via* pathway 1 and 2 directs reactivity towards an inner-sphere nucleophilic attack, whereas decarboxylation *via* pathway 3 would likely lead to an outer-sphere process (Scheme 152).[217]

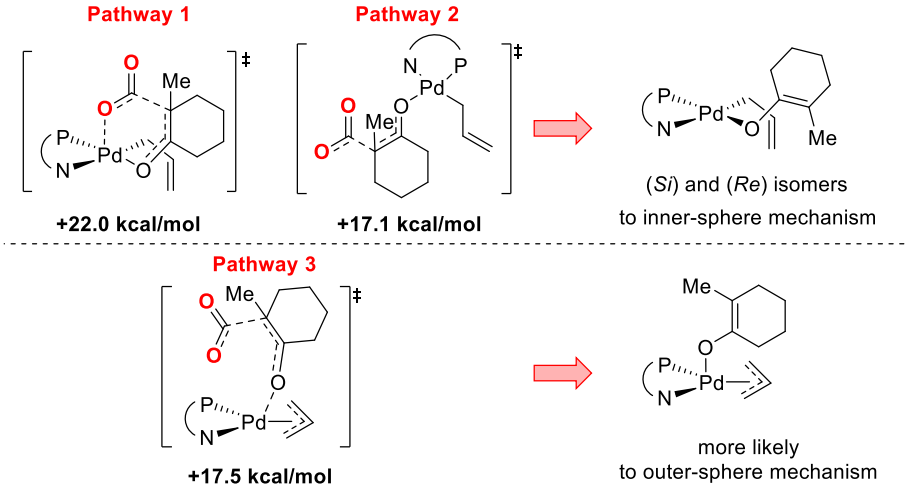

Scheme 152. Decarboxylation transition states. $\Delta G^{\neq}$ energies calculated at C-PCM (THF)-M06/def2-TZVP//BP86-D3/LANL2TZ(f)−6-31G(d).

A variety of transition states have been considered for reductive elimination step in this report. Inner-sphere mechanism *via* *C*-bound and *O*-bound Pd enolate was examined. For *C*-bound Pd enolate, 3- and 5-membered ring transition states were calculated, while for *O*-bound Pd enolate, 5- and 7-membered ring transition states were considered. It was found that the overall lowest energy transition state is *Si* diastereomer of 7-membered chair-type cyclic transition state derived from *O*-bound Pd enolate (Scheme 153). The energetic difference

between this transition state and the next lowest-energy *Re*-diastereomer correlated well with the enantioselectivity observed experimentally, and this step was proposed to be enantiodetermining.[217]

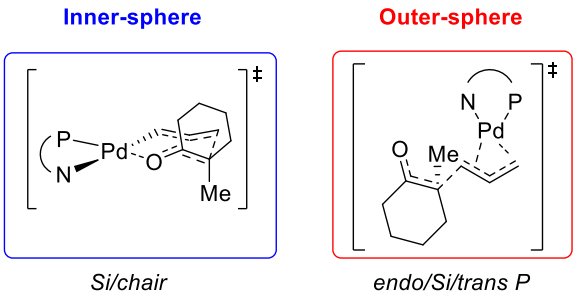

Scheme 153. Lowest energy transition states for inner and outer-sphere mechanism of reductive elimination transition states.

For the outer-sphere mechanism, authors accounted for various directions of nucleophilic attack which provided eight possible transition states, six of which were located. It was found that in this case stereoselectivity originates from two lowest-energy competing transition states – *endo*/*Si*/*trans* to phosphorus and *exo*/*Re*/*trans* to nitrogen (Scheme 153). However, this pathway predicted lower selectivity comparing to an inner-sphere route.[217]

Solvation was shown to have a significant effect on the energies of transition states corresponding to C−C bond formation. It was shown that the inner-sphere mechanism is favored in solvents with lower polarity due to destabilization of the ionic intermediates of the outer-sphere mechanism. The following catalytic cycle was proposed by the authors (Scheme 154).[217]

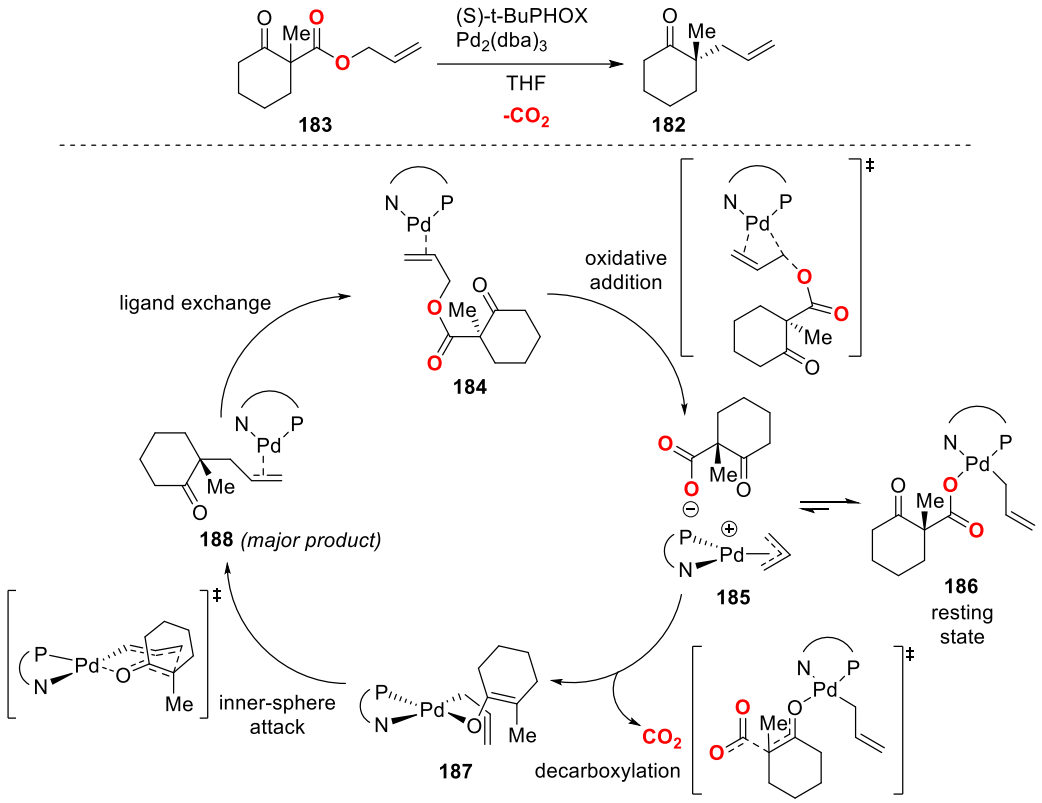

Scheme 154. Catalytic cycle proposed by Stoltz and Goddard.

Tunge *et al*. developed Pd-catalyzed decarboxylative allylation of nitriles and studied the mechanism of this reaction.[219] This approach avoids the use of strong bases necessary to form α-deprotonated nitriles, which have been utilized in other catalytic methods.[220–222] To elucidate the mechanism of this transformation, they incorporated an internal mechanistic probe to investigate whether a free anionic intermediate was formed (Scheme 155).[219]

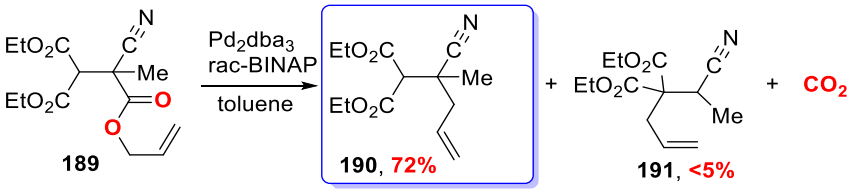

Scheme 155. Internal mechanistic probe utilized by Tunge.

In this case, they installed a malonate group with a lower pK_a than the conjugate acid of the decarboxylated nitrile. If a free anionic intermediate was present, a rapid proton transfer should occur to form the anion with the lower pK_a (roughly 10 pK_a units lower). They observed minimal amounts of the malonate allylated product (**191**), suggesting that the decarboxylation occurs after *N*-allylation or any nitrile anion is metal bound.[219]

Based on this evidence, they proposed two different mechanistic pathways, both of which start with the formation of π-allyl palladium complex (**193**). This complex could undergo decarboxylation forming another π-allyl intermediate (**194**) that upon *C*-allylation provides the product (**197**). Alternatively, π-allyl palladium complex (**193**) can be transformed into *N*-allylation product (**195**) that upon decarboxylation furnishes *N*-allyl ketenimine (**196**). The latter undergoes uncatalyzed [3,3]-sigmatropic rearrangement providing the product (**197**). Notably, *N*-allyl ketenimine (**196**) can be formed as a result of *N*-allylation from (**194**) as well.[219]

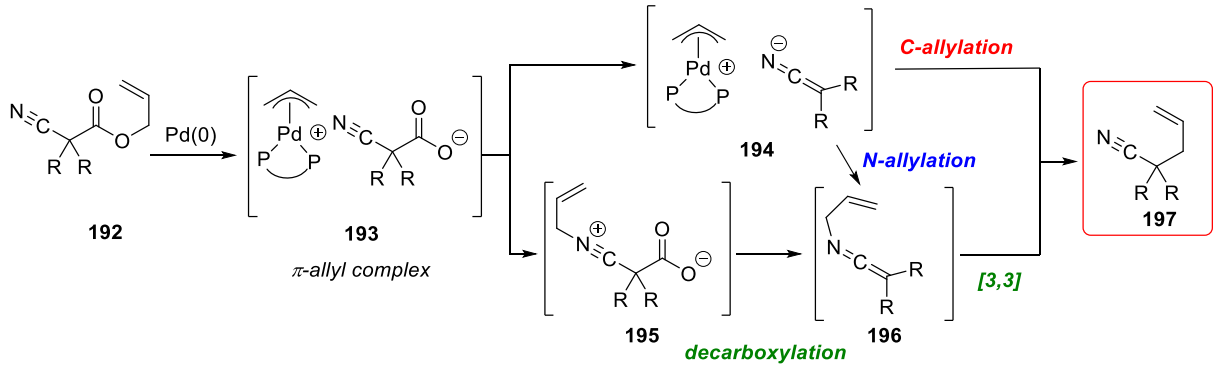

Scheme 156. C-allylation and *N*-allylation mechanisms proposed by Tunge.

An experimental attempt to distinguish between *C*- and *N*-allylation pathways relied on utilizing substituted allyl group that would result in formation of either linear (**199**) or branched (**200**) product (Scheme 157, selected example shown). It was hypothesized that if linear product is formed than *C*-allylation mechanism is in operation, while if branched isomer is obtained than

N-allylation pathway is preffered. A mixture of products was observed with (**198**) providing slight excess of linear product (Scheme 157), which led to the conclusion that *C*-allylation and *N*-allylation mechanisms are competing. However, the authors point out that both branched and linear isomers could be formed as a result of reductive elimination from η^1-allyl Pd complexes (Scheme 157).[219]

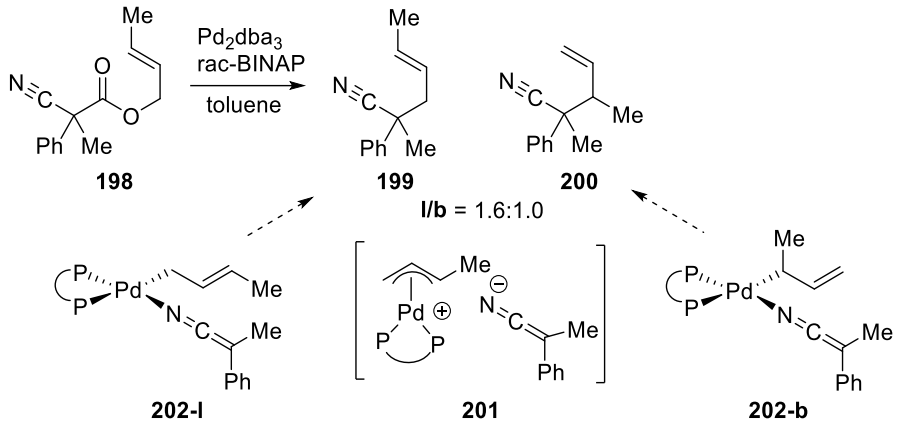

Scheme 157. Studies of *C*-allylation and *N*-allylation mechanisms and preference towards linear or branched product.

Fu *et al.* studied the mechanism of decarboxylative allylation of σ-imino esters catalyzed by Pd(0) (**203**) using DFT (Scheme 158).[223] They examined mono- (PPh_3) and bidentate (dppb) phosphine ligands for this transformation and found that in both cases decarboxylation step proceeds *via* a transition state where the loss of CO_2 occurs from carboxylate anion in a solvent-separated ion pair (Scheme 158, TS shown for PPh_3 ligand). An outer-sphere mechanism was proposed for C-C bond formation with the 2-aza-allyl anion acting is a nucleophile. This step was found to be regiodetermining with calculations predicting the same major product as the one observed experimentally.[223]

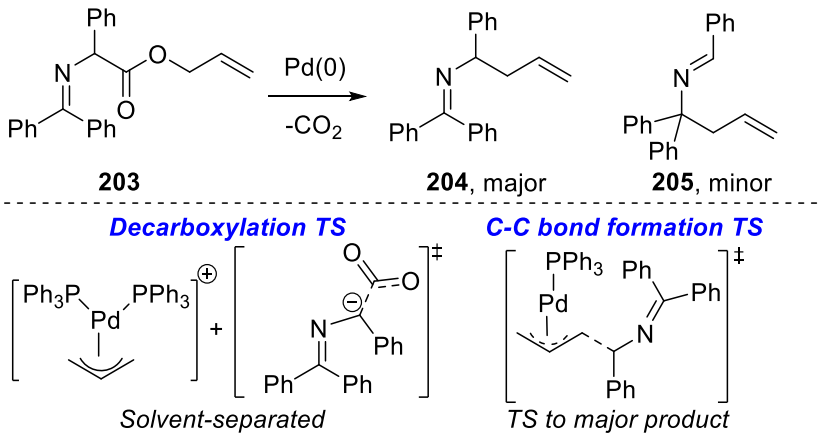

Scheme 158. Mechanism of Pd-catalyzed decarboxylative allylation of σ-imino esters.

Overall, mechanistic and experimental studies of Pd-catalyzed decarboxylative allylation suggest the following key steps of the reaction catalytic cycle: coordination of Pd(0) to allylic fragment, oxidative addition, decarboxylation, reductive elimination and product decomplexation. The nature of transition state in each step is highly dependent on the substrate class (especially, basicity), ligand, substitution pattern as well as additives and solvent. In cases, where different stereochemical outcomes are possible, both decarboxylation and reductive elimination have to be carefully investigated.

N-Allyl Ketenimine Generation and Rearrangement

Early reports demonstrated that *N*-allyl ketenimines can be generated *in situ* from *N*-allylamides (**206**) and undergo concomitant aza-Cope reaction to furnish corresponding nitriles (**207**) (Scheme 159).[224] Although, the latter occurred at very mild temperatures, the formation of *N*-allyl ketenimines required strong dehydrating conditions, which limited the synthetic utility of this transformation. Additionally, the reaction was only efficient if aromatic substituents on the amide was present.[224]

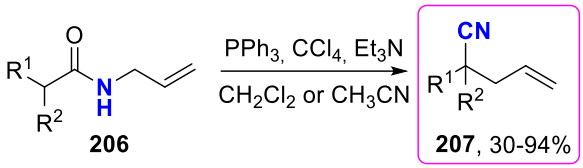

Scheme 159. Aza-Cope rearrangement of *N*-allyl ketenimines.

Mechanistic studies by Walters *et al.* demonstrated that *N*-allyl ketenimines (**212**) undergo uncatalyzed [3,3]-sigmatropic rearrangement *via* early half-chair transition state with predicted energetic barrier of 18 kcal/mol. These studies explained experimentally observed facile nature of this transformation comparing to other aza-Claisen variants (**208**) and (**210**) (Scheme 160).[225,226]

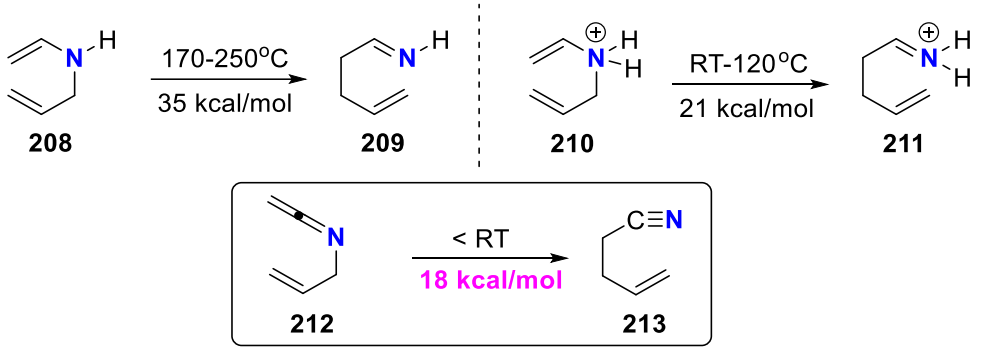

Scheme 160. Aza-Claisen rearrangement of *N*-allyl ketenimines. Energies calculated at MP4(SDTQ)/6-31G*//MP2/6-31G* level of theory.

The formation of ketenimine intermediates during Pd(0)-catalyzed rearrangement *N*-allyl ynamides has been reported by Hsung *et al.*[227,228] They were able to isolate stable silyl ketenimine (**215**) when ynamide (**214**) was subjected to the reaction conditions (Scheme 161). In the absence of the TIPS group an uncatalyzed N-C migration of the tosyl group was observed to provide the corresponding nitrile. This migration could only be prevented by moving to a phosphoramidate activating group, further limiting the synthetic utility of this reaction.[228]

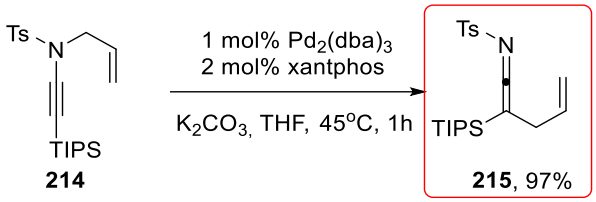

Scheme 161. Pd-catalyzed rearrangement *N*-allyl ynamides.

It was proposed that *N*-allyl ynamides (**216**) undergo oxidative addition with Pd(0), to form a π-allyl complex, followed by either inner or outer-sphere nucleophilic attack furnishing the ketenimine product (Scheme 162).[227] Based on the results of cross-over experiments performed on *N*-allyl and *N*-crotyl ynamides, the authors concluded that it is more likely that an inner-sphere process is in operation.[227]

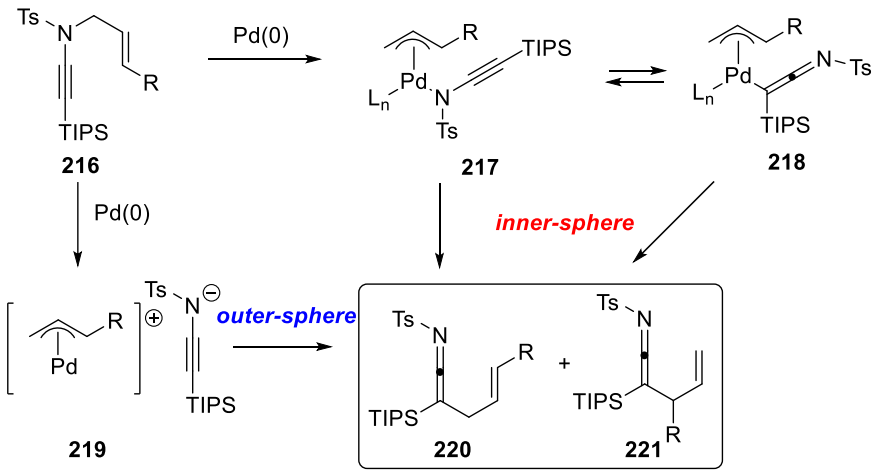

Scheme 162. Mechanism of ketenimine formation.

Interestingly, they proposed that the Pd π-allyl ynamide complex (**216**) can tautomerize to Pd π-allyl ketenimine complex (**217**) *via* 1,3 metallotropic shift. This intermediate could either undergo reductive elimination to provide ketenimine or enter a Pd-catalyzed aza-Claisen rearrangement to form (**223**) followed by aza-Rautenstrauch-type cyclization to furnish cyclopentenimine (**226**) *via* the mechanism shown in Scheme 163.[227]

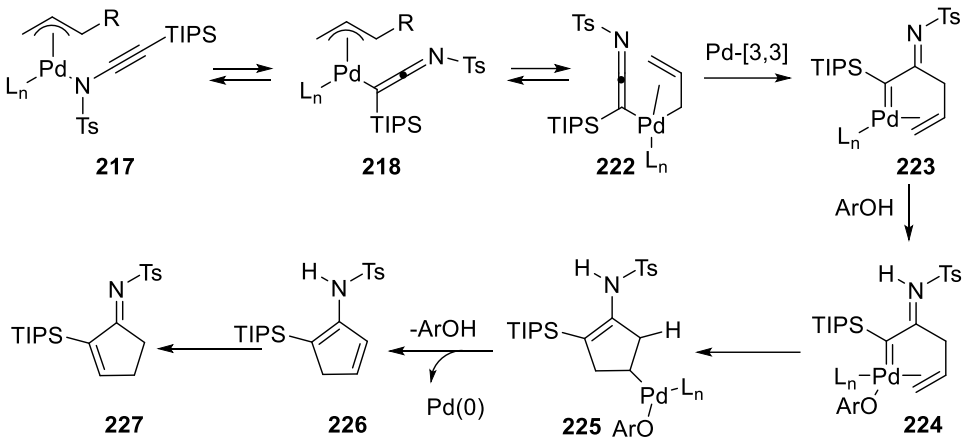

Scheme 163. Mechanism of cyclopentenimine formation.

Cook *et al.* reported Pd-catalyzed formation of ketenimines from *N*-alloc ynamides *via* a decarboxylative allylation utilizing borane as an additive (Scheme 164).[200] They hypothesized that the borane stabilizes the forming ynamide anion in a borate complex. Since ketenimines are unstable, the products of their hydrolysis were isolated. Interestingly, while (**229**) was the major product under optimized conditions, almost equal amounts of (**229**) and *N*-allylated product (**230**) were isolated without BEt_3 (Scheme 164).[200]

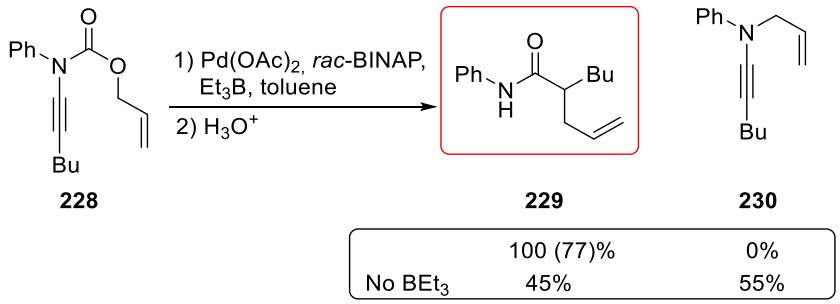

Scheme 164. Pd-catalyzed formation of ketenimines from *N*-alloc ynamides.

The catalytic cycle suggested for this transformation includes oxidative addition of *N*-alloc ynamide to Pd(0) to form solvent-separated ion pair (**232**) which further undergoes decarboxylation to produce another ion pair (**233**) (Scheme 165). In this complex, the Pd π-allyl

species is attacked by a nucleophile *via* an outer-sphere mechanism to furnish Pd-bound ketenimine (**234**). The outer-sphere pathway was proposed by the authors based on isotopic labeling and the cross-over studies. Thus, in cross-over experiment a statistical mixture of products was observed suggesting that catalytic cycle involves the formation of solvent-separated ion pair.[200]

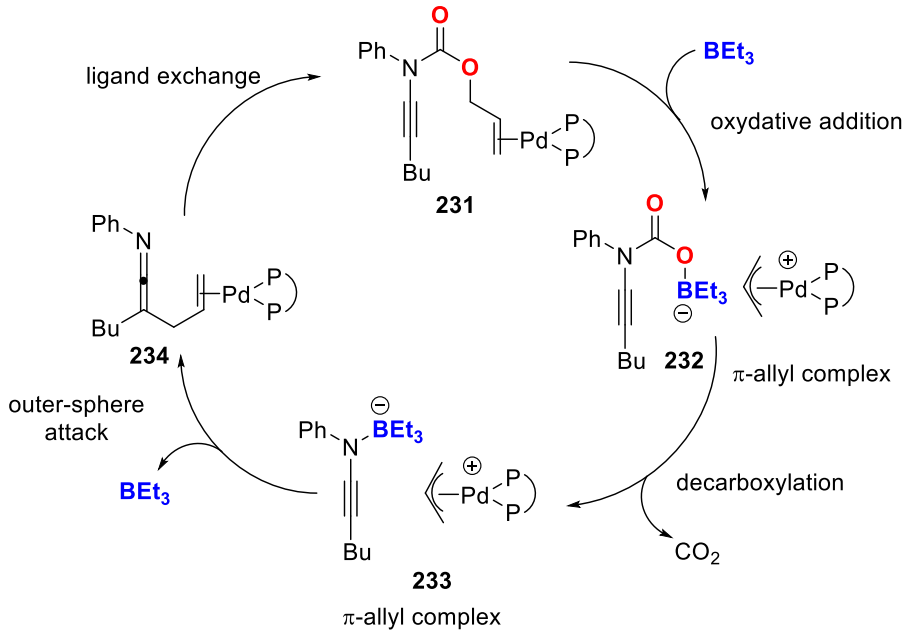

Scheme 165. Catalytic cycle proposed for the Pd-catalyzed formation of ketenimines from *N*-alloc ynamides.

To summarize, *N*-allyl ketenimines can be converted to corresponding nitriles *via* both uncatalyzed [3,3]-sigmatropic rearrangement and Pd-catalyzed process, therefore during mechanistic studies both possibilities must be considered. *N*-allyl ketenimines can be formed *via* Pd(0)-catalyzed rearrangement *N*-allyl or *N*-alloc ynamides. In the first case, catalytic cycle consists of complexation, oxidative addition, reductive elimination and decomplexation, whereas in the second case it involves complexation, oxidative addition, decarboxylation, reductive elimination and decomplexation. As in Pd-catalyzed decarboxylative allylation, the nature of

transition state in each step is dependent on the substrate, ligand, substitution pattern, additives and the solvent used.

Computational Methods

Since we envisioned mechanistic studies of *N*-alloc-*N*-allyl ynamide using computations, the methods and approaches utilized for the computational investigation of palladium π-allyl chemistry will be reviewed. This minireview highlights some the major challenges that computational chemist can face in this area based on the review by Schoenebeck *et al*.[211] These include identifying the right computational approach for conducting geometry optimization and energy calculations, performing conformational analysis as well as accounting for solvation effects on charged species.[211]

Level of Theory Computational studies in the area of palladium π-allyl chemistry employed various levels of theory and methods depending on the aim of the study and the size of the system.

For example, the palladium π-allyl complexes have been studied using post-Hartree–Fock methods.[229–231] In these studies, the geometries optimization of the complexes was performed by using second-order Møller-Plesset (MP2) perturbation theory, while subsequent single point calculations have been performed using MP3,[230] MP4(SDQ),[230,231]configuration interaction (SD-CI)[231] and coupled-cluster with double substitution (CCD) methods.[231] Such studies are rather expensive and, as examples provided above show, are performed on relatively small palladium complexes as it would be challenging to study conformationally flexible palladium π-allyl complexes with large ligands at such a high level of theory.[211] However, the approximations

developed for post-Hartree–Fock methods, such as domain based local pair natural orbital coupled cluster method DLPNO-CCSD(T),[232] made these computations feasible for large systems.[233] Thus, Goddard and Stolz utilized DLPNO-CCSD(T) alongside with DFT to perform single point energy calculations for structures optimized by DFT in their study of Pd-catalyzed asymmetric allylation (see Schemes 151-154).[217]

Palladium π-allyl complexes have been also studied with specially parametrized molecular mechanics (MM) methods, which are MM2[234] and MM3*[235] force fields, and in both cases the predicted structures were in good agreement with experimental ones.

A combination of MM and other methods such as DFT was employed for these systems.[236,237] For instance, Monte Carlo/Low Mode (MC/LMOD) method together with OPLS3 force field were utilized by Garcia *et al*. to generate sets of conformers of palladium π-allyl complex with TADDOL-based phosphoramidite *P*, *N*-ligand (**235**) (Figure 17, shown in blue), whereas further refinement of the results of the conformational search was done using DFT methods.[236]

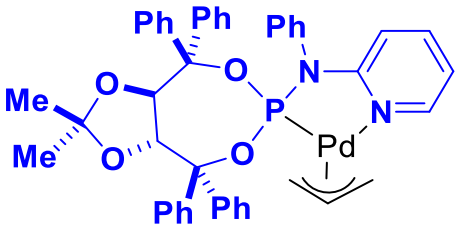

235

Figure 17. TADDOL-based phosphoramidite P, N ligand in palladium π-allyl complex.

Another interesting approach is pairing MM with QSAR methodology as was done by Norrby *et al.* in the study aimed to predict the selectivity of Pd-catalyzed allylic alkylation based on steric parameters originating from palladium π-allyl complexes and their interaction with the

nucleophile.[238] In this case, MM was used to calculate an array of palladium π-allyl complexes having symmetrical, unsymmetrical and cyclic allyl groups and substituted phenanthroline ligands as well as energy excess originating from steric interaction of the complex with model nucleophile. The descriptors based on the structural parameters of these computed complexes alongside energies mentioned above were used to build a number of QSAR models. It was shown that model utilizing four key descriptors is sufficient and predicts selectivities that correlate well with experimental data.[238]

Currently, the method of choice for the computational studies of palladium π-allyl complexes is density functional theory (DFT).[211] Early studies by Sasaki *et al.* aimed at evaluating the binding energies of Pd complexes to conjugated alkenes, showed that, comparing to post-Hartree–Fock methods, DFT provides substantially lower binding energy values, with the difference increasing as alkene becomes larger.[239,240] Later studies of these systems by Truhlar *et al.*, however, proved that modern DFT methods allow to keep this difference relatively small.[240] The computational cost of DFT depends on particular method and basis set used, although, the computational time remains feasible only for relatively small Pd complexes, whereas dealing with larger systems becomes challenging.[241] This problem is frequently addressed by replacing large complex with small model system which do not accurately reflect the electronics of the reaction and could not account for steric interactions of large bulky ligands.[241]

Another approach utilized for calculations of palladium π-allyl complexes is ONIOM.[223,241–244] It allows to circumvent limitations associated with the size of the system by splitting large complex into several layers and applying to each layer different level of theory. In this case, the key part, such as a reactive metal center (often reffered to as “high layer”), can be

optimized using post-Hartree–Fock or DFT methods, whereas the rest of the molecule can be calculated with Hartree–Fock, semi-empirical or MM methods.[245,246]

As the last two methods have been more commonly used for the computational studies of palladium π-allyl complexes, the following sections will focus on comparing them in terms of geometry optimizations and energy calculations.

Optimization of π-allyl Complex Geometry A correct and precise prediction of the geometrical parameters of palladium π-allyl complexes is very important as these geometries are used for further analysis, e.g. effect of structure on reactivity, as well as energy calculations.[211]

Literature analysis shows that the most common DFT functional used for geometry optimization of palladium π-allyl complexes is B3LYP. [211,216,218,247–255] B3LYP is a hybrid functional [178,179] that has been extensively used by computational chemists, however, as highlighted by Truhlar, B3LYP has certain problems and limitations when applied for calculations of barrier heights of the reactions, evaluation of noncovalent interations and transition metal complexes.[256] The examples of other functionals with reference to corresponding studies of palladium π-allyl complexes are M06,[217,247,254,257–259] M05,[237] B3PW91,[260] MPW1K,[261] BP86,[262] and mPW1PW91.[263]

It is not surprising that ONIOM models of palladium π-allyl complexes, that utilized DFT method for optimization of the electronically important parts, employed similar functionals to those described above.[223,241–243] Thus, mechanistic studies of decarboxylative allylation of σ-imino esters by Fu *et al.*, described earlier (Scheme 158), utilized ONIOM model with B3LYP being used for geometry optimization of the higher layer.[223] When Wu *et al*. studied the influence of substitution on the phoshines in silyl pincer ligand on the mechanism of CO_2

insertion into Pd-C bond in palladium η^1-allyl complexes, they conducted geometry optimizations using ONIOM model where the higher layer was calculated with DFT employing M06/6-31G(d)/LANL2DZ(Pd) and lower - with HF/LANL2MB. It is worth noting that the reliability of geometry optimization at the chosen level of theory was tested by comparing calculated and experimental structure of the analogous (η^3-allyl)-nickel complex.[242]

Guo and Liu conducted a systematic study aimed to evaluate the accuracy of ONIOM methods in the structure optimization of Pd and Ni complexes.[241] In this report, 10 palladium complexes, including palladium π-allyl complex with *N*-heterocyclic carbene (**236**), were considered. For the geometry optimization of the reacting site (examples of complexes are shown in Figure 18, reactive site is shown in red) authors tested 7 different functionals, including B3LYP, and 6 basis sets, with the results being evaluated by comparing the structures of the complexes optimized computationally with the corresponding crystal structures. First, the errors produced by the basis sets were evaluated (B3LYP used as a functional) and LANL2DZ+p was found to perform best. Then, a set of seven functionals paired with LANL2DZ+p basis set was tested. It was shown that with this basis set for Pd complexes B3P86 produces the most accurate bond lengths, B3PW91 provides the best bond angles, and PBEP86 is most efficient for the dihedral bond angle calculations with B3P86 being considered the overall best method.[241]

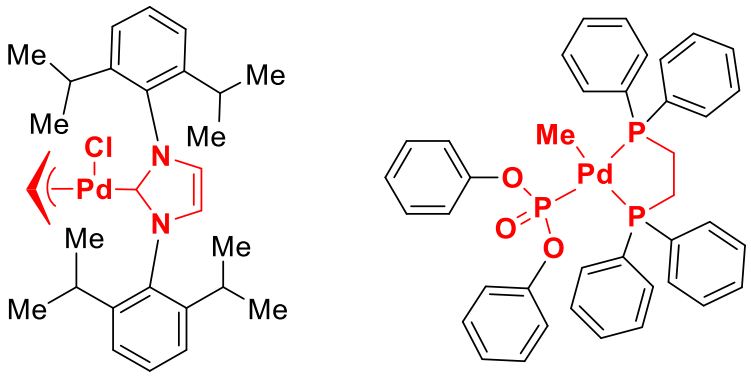

236 **237**

Figure 18. Examples of two-layered ONIOM model application for Pd complexes. Reacting site treated with DFT is shown in red; the second layer treated with HF is shown in black.

Calculating Energy of Palladium π-allyl Complexes Accurate energy calculations are as important as precise geometry prediction as calculated energies are used to construct reaction potential energy surface and derive conclusions regarding the reaction mechanism.[211] For the energy calculations of palladium π-allyl complexes various methods were employed.

B3LYP is a common functional used to predict energetic barriers for transformations involving palladium π-allyl complexes (see examples [237,248–250,255,264]). Guiry *et al.* employed B3LYP in their study of asymmetric allylic alkylation catalyzed by palladium complexes containing Quinazolinap ligands.[237] To rationalize the enantioselectivities observed experimentally with ligands bearing different substituients, authors calculated the ratios between the diastereomeric palladium π-allyl species with allyl group in *endo*- and *exo*- orientations (for example, see (**238**) in Figure 19). Energies calculated with B3LYP were compared to energies obtained after single point energy calculations with M05 using B3LYP geometries as well as experimental NMR data. M05 is a functional that accounts for dispersion and was suggested for energy calculations in transition metal catalysis[265] and, therefore it was chosen by the authors for

the additional calculations. Overall, results obtained by both functionals were in agreement with experimental data (aside few cases), although M05 gave more accurate predictions.[237]

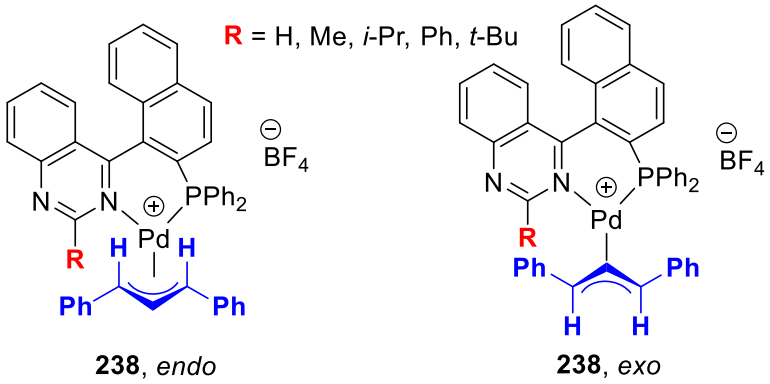

Figure 19. Structures of *endo*- and *exo*- [1,3-diphenyl- η^3-allyl]palladium complexes with Quinazolinap ligands.

The other commonly used functional that is employed for both geometry optimization and single point energy calculations is M06 (see examples [217,247,254,257,258]). M06 takes in account non-covalent interactions, alongside dispersion, and has shown to perform well in organometallic chemistry applications where it provides reliable thermochemistry.[188]

For example, in the study of asymmetric Pd-catalyzed allylation of aldehydes by Jindal and Sunoj, the geometry optimization was performed using B3LYP, whereas single point energies, solvation energies as well as geometry optimizations for main transition states were done with M06.[247] In this cooperative multicatalytic transformation benzylaldehyde first reacts with benzhydryl amine to form enamine that then acts as a nucleophile attacking palladium π-allyl specie. In this case the enantioselectivity is guided by the chiral BINOL-phosphate counterion that forms a hydrogen bond with enamine in corresponding transition state (Figure 20, TS structure was visualized in CYLview 1.0b.[175] using coordinates provided in supporting information).[247]

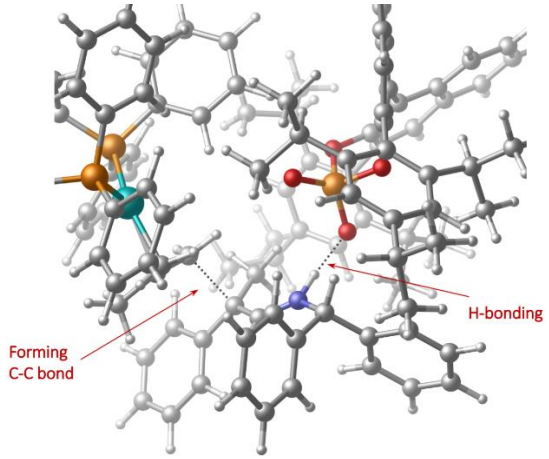

Figure 20. Transition state proposed by Jindal and Sunoj.

Goddard and Stolz also utilized M06 along with DLPNO-CCSD(T) for single point calculations in their study of Pd-catalyzed asymmetric allylation.[217]

When Huang *et al.* studied Pd-catalyzed amination mechanism involving the formation of palladium π-allyl species, they included Grimme's empirical dispersion corrections (DFT-D3) in both single point energy calculations at PCM (THF)-BP86/def2-TZVP and geometry optimization.[262] This is another approach that can be utilized if one needs to account for dispersion during energy calculations of palladium-π-allyl species.

Fewer examples are available regarding accuracy in evaluation of energies when ONIOM model is applied. For instance, conformational studies conducted by Helmchen *et al.* for palladium π-allyl complexes containing 1,3-dimethylallyl group and *i*-Pr or *t*-Bu-phosphinooxazoline (PHOX) ligands utilized QM/MM ONIOM model for both geometry optimizations and energy calculations.[244] These computations accurately predicted the most abundant isomer of the allyl group among possible variants in each complex, which was established by comparing calculated relative energies with NMR data.

The study of the mechanism of CO_2 insertion into Pd-C bond in palladium η^1-allyl complexes by Wu *et al*., mentioned ealier, used ONIOM for both geometry optimization and single point energy calculations as well, although for energy calculations all ONIOM layers were treated with DFT.[242]

Conformational Analysis of Palladium π-allyl Complexes One of the major challenges associated with computational studies of palladium π-allyl complexes is their conformational flexibility, with both the ability of allyl group to bind in *endo* or *exo* mode and conformational flexibility of the ligands[211] proving challenging.

For instance, in a study of asymmetric Tsuji allylation catalyzed by palladium (*S*)-*t*-Bu-phosphinooxazoline (PHOX) complex by Goddard and Stolz, the two conformations of π-allyl intermediate (**239**), i.e. *exo* and *endo*, were evaluated (Figure 21).[263] Such a selection was based on the fact that the crystal structure of the corresponding π-allyl specie contained isomers with both *exo* and *endo* allyl groups. Calculations predicted *endo* conformer to be 0.2 kcal/mol lower in energy than *exo*, which is overall consistent with the experimental observation of *endo* to *exo* ratio of 49% to 51%.[263]

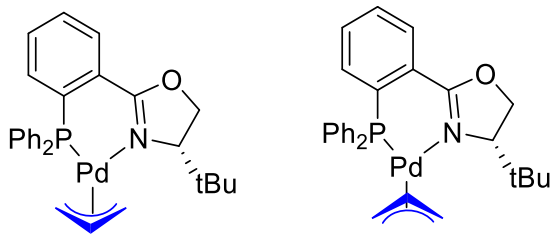

239, *exo* **239**, *endo*

Figure 21. Structures of *exo*- and *endo*- (*S*)-*t*-Bu-phosphinooxazoline palladium π-allyl complexes.

Another example that has been already mentioned earlier is a conformational search done for palladium π-allyl complex with TADDOL-based phosphoramidite *P, N*-ligand conducted by Garcia *et al*. (Figure 17).[236] As indicated in this report, TADDOL-based phosphoramidite ligands has been extensively used in asymmetric catalysis, however, little is known about the structure of Pd(II) complexes containing these ligands. Using Monte Carlo/Low Mode (MC/LMOD) methods, authors found 53 unique conformers of this complex within 5 kcal/mol energy window. Further optimization by DFT at SMD (CH_3CN) M06/SDD(d,f)-6-31G(d,p) resulted in identifying 13 different conformers with relative energies within 9.2 kcal/mol, among which 7 had *exo*- configuration of the allyl group and 6 had *endo*- configuration. Importantly, the lowest energy conformers had *exo* and *endo* allyl group orientations with *exo* variant being a global minimum and thermodynamically preferred over *endo* by 0.2 kcal/mol.[236]

In summary, even with a variety of methods available, the conformational lability of π-allyl complexes remains challenging for computations. Although, the energy differences between conformers appear to be small, the geometry of the complexes can affect the prediction of reaction selectivity as various possible nucleophile attack modes on different conformers are possible as shown in several studies.[217,218,236–238,262]

Solvation Effects on Palladium π-allyl Mechanisms The interaction between the π-allyl complex and the solvent can have a substantial effect on the palladium-catalyzed allylic alkylation mechanism as will be demonstrated in this section. It is therefore important to use methods that accurately estimate the solvation effects.[211]

The solvation models that were found to be the most commonly used in the studies of palladium-π-allyl reactions are polarizable continuum model (PCM)[266] (see examples [218,243,248-250,253-254,262]) and solvation model based on density (SMD)[267] (see examples [247,257,259]).

Thus, Norrby *et al.* studied the effect of solvation on the transition states in the reaction of a cationic palladium π-allyl complexes (**240**) with NH_3, F^- and CN^- nucleophiles using the two different solvation models – PCM/DIR (water and dichloromethane) and SM2 (water) and B3LYP as a functional (Figure 22).[264]

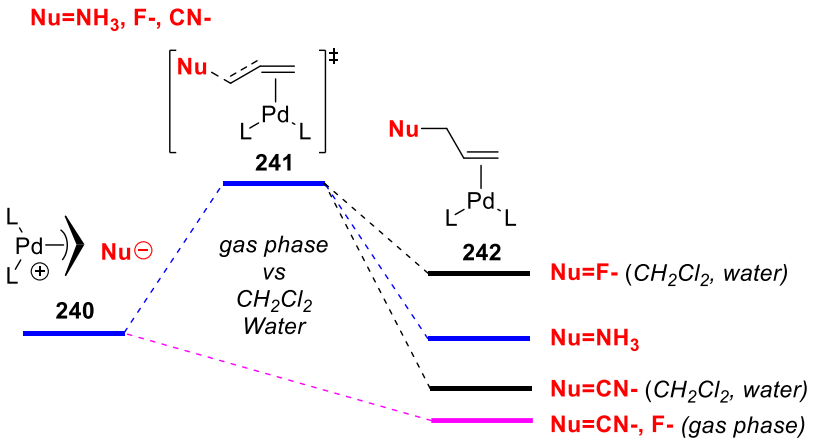

Figure 22. Solvation effect on the reaction of palladium π-allyl complex with nucleophiles.

It was found that in case of ammonia, the energy of transition state in both water and dichloromethane was approximately 8 kcal/mol higher than that in a gas phase. While transition states were not be located for the addition of anionic nucleophiles (F^- and CN^-) to cationic palladium π-allyl complexes in the gas phase, they were found when solvation was taken into account. Interestingly, a complete change of the reaction profile was observed for fluoride anion with the reaction being very exothermic in gas phase and endothermic when solvation was included. These differences were attributed to the better solvation of free ions, e.g. F^- and

cationic palladium π-allyl complexes. This study exemplifies importance of including solvation in computational studies of palladium π-allyl complexes.[264]

Doyle *et al.* studied palladium-catalyzed allylic fluorination with AgF in toluene using PCM at M06/cc-pVTZ (P, C, H)/aug-cc-pVTZ(F, Cl)/SDD(ECP Ag, Pd)//B3LYP/6-31G(d) (P, C, H)/6-31+G(d)(F, Cl)/LANL2DZ(ECP Ag, Pd).[254] They considered several possible electrophiles and nucleophiles including those generated from π-allyl complexes and proposed a homobimetallic mechanism for the C−F bond formation. In this mechanism a neutral allylpalladium fluoride serves as a nucleophile that attacks a cationic allylpalladium specie (Figure 23). This finding explained observed regioselectivity and has been supported by experimental mechanistic studies. In this study authors accounted for solvation during both geometry optimization and single point energy calculations and utilized dispersion-aware functional for single point energy calculations.[254]

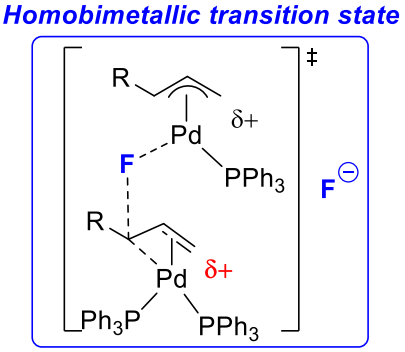

Figure 23. The transition state proposed by Doyle for the C−F bond formation.

The effect of solvation on the stereochemistry of asymmetric 3-butene-2-ol amination catalyzed by palladium with a chiral ligand has been demonstrated by Huang *et al.* using PCM (THF).[262] They considered two possible directions of nucleophilic attack on π-allyl intermediate leading to the *R* and *S* products, respectively. It was shown that while the energy gap between

these transition states in gas phase was negligible (*R* being lower than *S* by 0.3 kcal/mol), when solvation in THF was considered, the $\Delta\Delta G^{\ddagger}$ increased to 5.3 kcal/mol which was in agreement with experimental data.[262]

Goddard and Stolz also discovered a significant effect of solvation on both decarboxylation and reductive elimination mechanisms in the catalytic cycle of decarboxylative allylation of allyl β-ketoesters.[217] Thus, it was shown that in reductive elimination step solvents with lower polarity (low dielectric constant in C-PCM model) favor inner-sphere mechanism, *via* neutral Pd-species, over the cationic outer-sphere mechanism.

In conclusion, adding solvation allows for the more accurate description of transition states lying between π-allyl intermediate and the product of nucleophilic attack by DFT. Therefore, including solvation during geometry optimization as well as single point calculations for palladium π-allyl complexes is essential for accurate mechanism description. This is especially important in π-allyl chemistry where both neutral and cationic mechanisms are possible, alongside hapticity changes (see examples [217,254,264]).

To summarize, the computational studies of palladium π-allyl complexes provided many insights into their structural features as well as mechanistic details of the reactions involving these species as intermediates. Although, in many cases these computations must deal with complex large systems, there are methods and approaches available to address this challenge, however these are a subject for a carefull consideration.[211]

Decarboxylative Allylation

Mechanism of Decarboxylative Allylation

Initially, we focused on elucidating the mechanism of decarboxylative allylation, using compound (**247**) as a model substrate. Computational study utilized ONIOM model [241,246,268] for geometry optimization of palladium complexes due to the large size of the system. In this model reactive site was calculated at M06L/6-31+G(d) (C, H, P, B, O)/LANL2DZ (ECP Pd)[188] and the rest of the system was treated with PM6. We further applied C-PCM (toluene) M06L/6-311++G(2d,2p) (C, H, P, B, O)/ LANL2DZ (ECP Pd) to calculate single point energies for optimized structures.[184,185] Further detailes regarding calculation methods are provided in section describing Computational Details.[196]

Based on the previous research in the area of Pd-catalyzed decarboxylative allylation,[200,212–219,223] our initial hypothesis included the following catalytic cycle: coordination of Pd(0) to allylic fragment of the alloc group forming (**243**), oxidative addition with the formation of (**244**), decarboxylation, nucleophilic attack/reductive elimination and product (**246**) decomplexation (Scheme 166). We also considered coordination to the borane at each of the catalytic cycle.

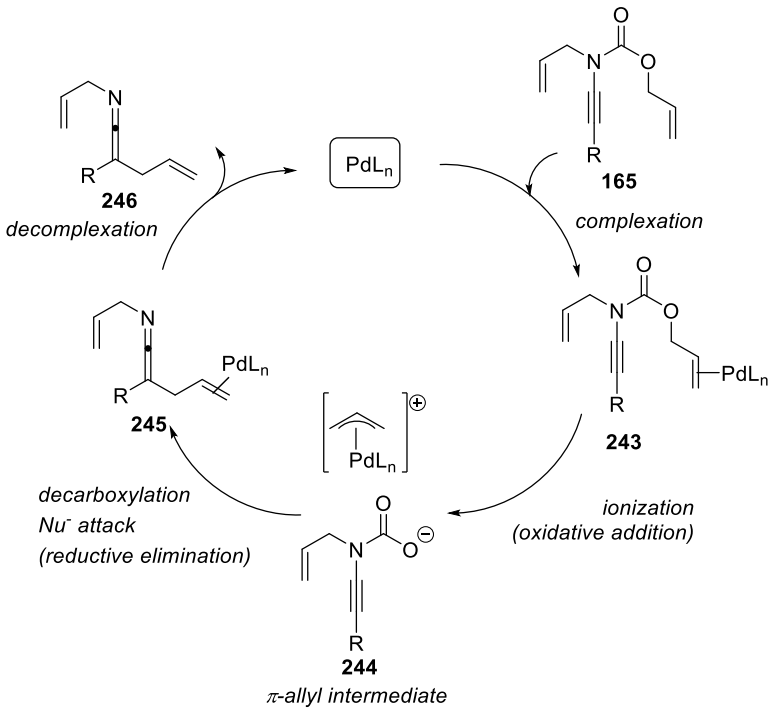

Scheme 166. Initial hypothesis for decarboxylative allylation of *N*-alloc-*N*-allyl ynamides.

It was found that the coordination of (**247**) with Pd(0) catalyst resulting in complex (**247A**) is exergonic (-7.6 kcal/mol). The following oxidative addition step proceeds *via* an *anti*-displacement type mechanism[217] ((**247A TS**), 9.6 kcal/mol from (**247A**)) providing the tight ion pair (**247B**), where carboxylate anion is coordinated to Pd in Pd(η^3-allyl) complex (Pd-O distance is 2.52 Å). The η^3- η^1 interconversion of the allyl group in (**247B**) results in less thermodynamically favorable neutral complex (**247C**) and represents a non-productive pathway. Complex (**247C**) is analogous to (**248**) that was isolated and characterized as the catalyst resting state in Pd-catalyzed decarboxylative allylation of allyl β-ketoester by Stoltz *et al.* (Scheme 167).[217,269]

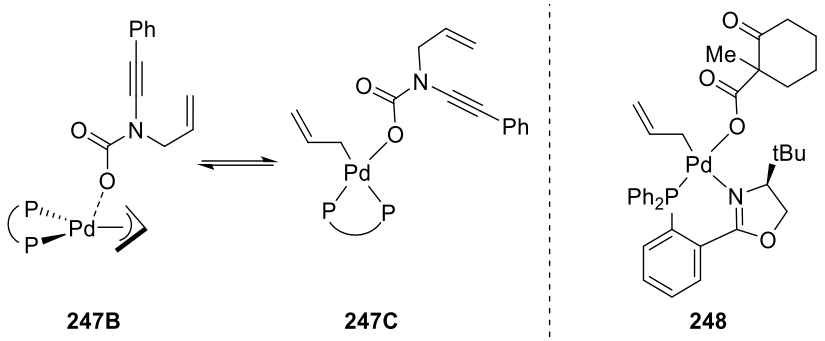

Scheme 167. Calculated neutral carboxylate complex (**247C**).

After the formation of π-allyl complex (**247B**), the mechanism diverges into two possible pathways (Figure 24). One represents a previously unreported (**247Bs TS**) (18.8 kcal/mol from `(**247B**)) leading directly to the product (**247G**). This is an S_N2-like transition state, where C-C bond formation and concomitant decarboxylation occur. The other pathway includes CO_2 release *via* (**247B TS**) (8.3 kcal/mol from (**247B**)) with the formation of ion pair (**247D**). In this scenario, there is another branching point as (**247D**) can react *via* either an outer- (Figure 24) or inner-sphere (Figure 25) mechanism.

The outer-sphere route starts from an ion pair conformational change to (**247D'**) and is followed by C-C bond formation *via* (**247D' TS**) resulting in **(247G**) (1.0 kcal/mol from **247D'**). In the inner-sphere pathway, (**247D**) interconverts to (**247En**) and undergoes C-C bond formation *via* (**247En TS**‡) (9.8 kcal/mol from **247En**). Interestingly, the ynamide can change binding mode from (**247En**)/(**247En'**) to ketenimine (**247Ec**)/(**247Ec'**) *via* (**247En'**)/(**247En'' TS**) (16.6/27.0 kcal/mol from (**247En**)/(**247En'**)). This allows for one more route that includes allylic amination *via* (**247Ec' TS**) (14.4 kcal/mol from (**247Ec'**)) followed [3,3]-rearrangement of diallyl ynamide (**247F**) *via* (**247F TS**) (24.4 kcal/mol from (**247F**)) to the product. This interconversion between Pd-π-allyl ynamide and ketenimine complexes was shown to be

involved in the mechanism of Pd-catalyzed or thermal aza-Claisen–carbocyclization sequence using *N*-allyl ynamides by Hsung *et al*.[227,228] The final step includes the decomplexation of ketenimine (**254**) from (**247G**), which is endergonic by 5.0 kcal/mol (not shown).

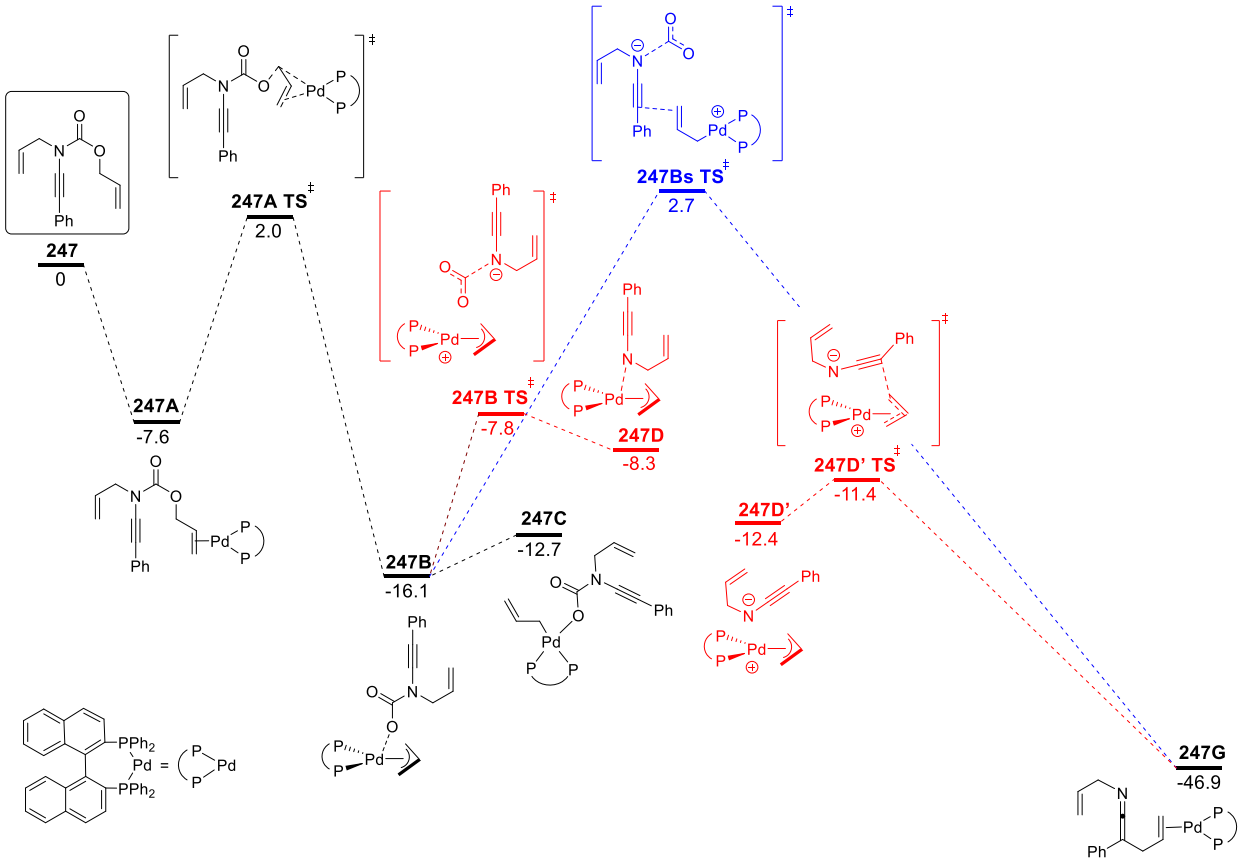

Figure 24. Potential energy surface demonstrating possible competitive pathways of decarboxylative allylation of (**247**) including outer-sphere attack.

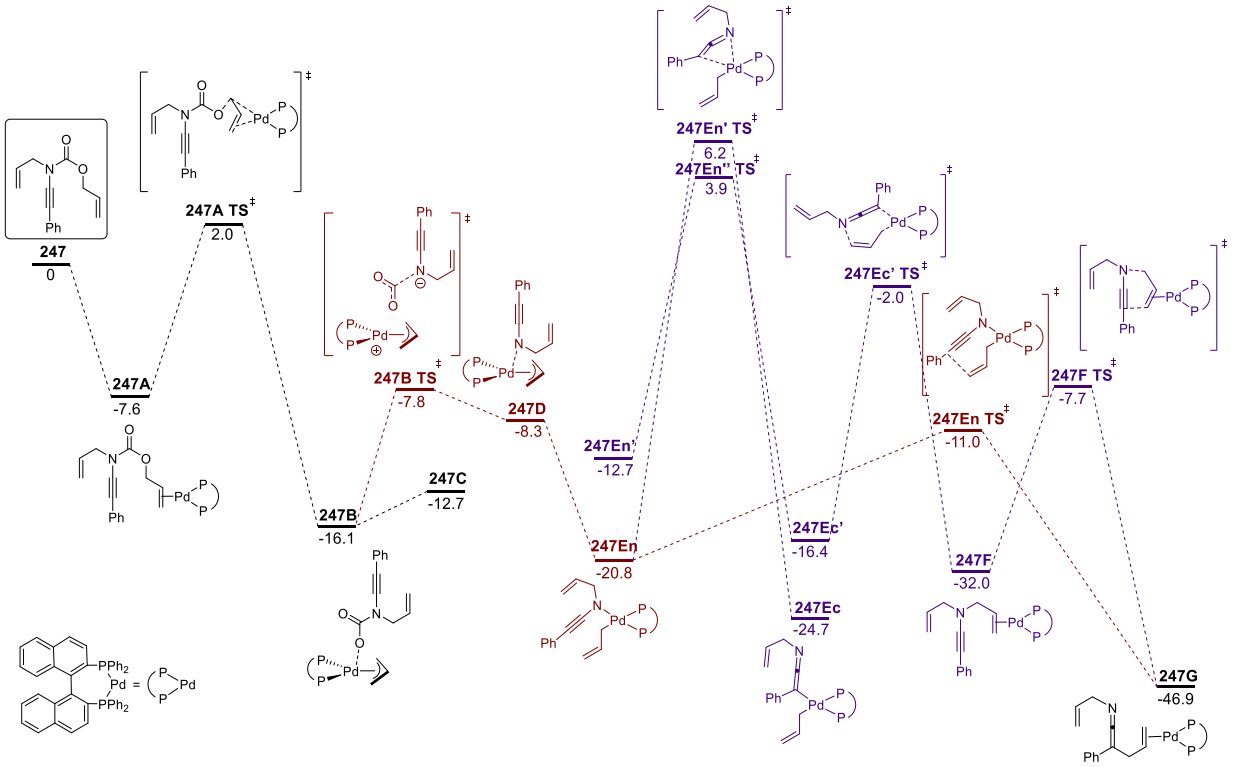

Figure 25. Potential energy surface demonstrating possible competitive pathways of decarboxylative allylation of (**247**) including inner-sphere attack.

The Lewis acid-base adduct of (**247**) with the borane additive was also considered (Figure 26). It was found that addition of borane to *N*-allyl-*N*-alloc ynamide (**247**) is not thermodynamically favored (+4.8 kcal/mol). One might expect that the borane adduct of carbamate anion (**250**) would be favored, however calculations predicted otherwise (Scheme 168). In this complex (**251**), the C-N bond is shorter (1.46 Å) comparing to (**250**) (1.58 Å). All transition states involving boron association to carbamate oxygen ((**249A TS**), (**249B-O TS**), (**249Bs TS**)) were significantly higher in energy than the corresponding boron-unbound variants ((**247A TS**), (**247B TS**), (**247Bs TS**)) suggesting that BEt_2OMe does not participate in oxidative addition or decarboxylation steps. When binding of boron to nitrogen was considered in (**249B-N TS**) instead, the energy difference between (**249B TS**) and (**249B-N TS**) reduced to 0.8

kcal/mol, respectively. Indeed, among all substrate-derived intermediates, allyl ynamide anion (**252**) is the only species that favors binding to BEt_2OMe ($\Delta G° = -5.9$ kcal/mol). It was found that boron bound ion pairs (**249D**) and (**249D'**) are lower in energy comparing to boron unbound variants (**247D**) and (**247D'**) by 1.3 and 4.6 kcal/mol, respectively. Additionally, binding to BEt_2OMe lowers the energy of transition state corresponding to outer-sphere attack (**249D' TS**) by 2.1 kcal/mol (Figure 26). Therefore, we believe that one of the roles that BEt_2OMe plays in this reaction is stabilization of forming allyl ynamide anion (**252**) that might have proven to be problematic otherwise.[270]

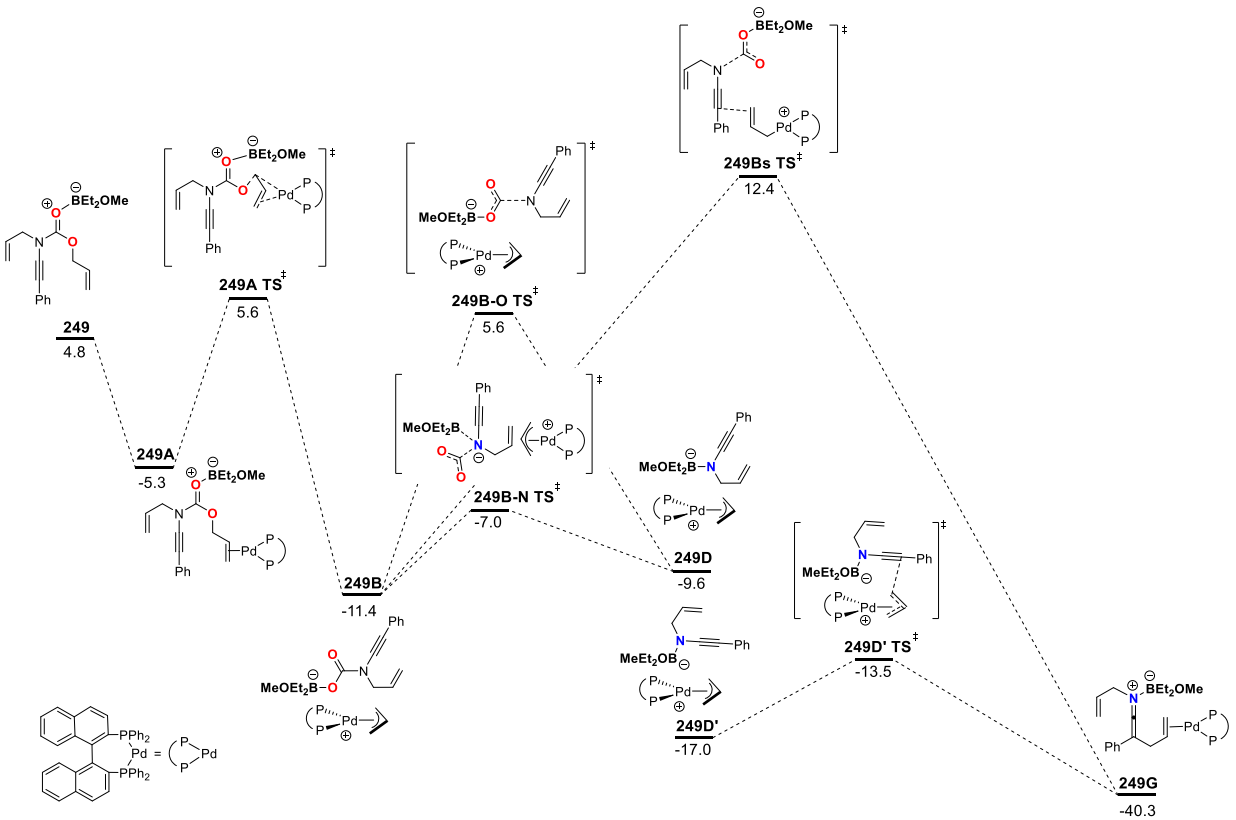

Figure 26. Potential energy surface demonstrating possible competitive pathways of decarboxylative allylation of (**249**).

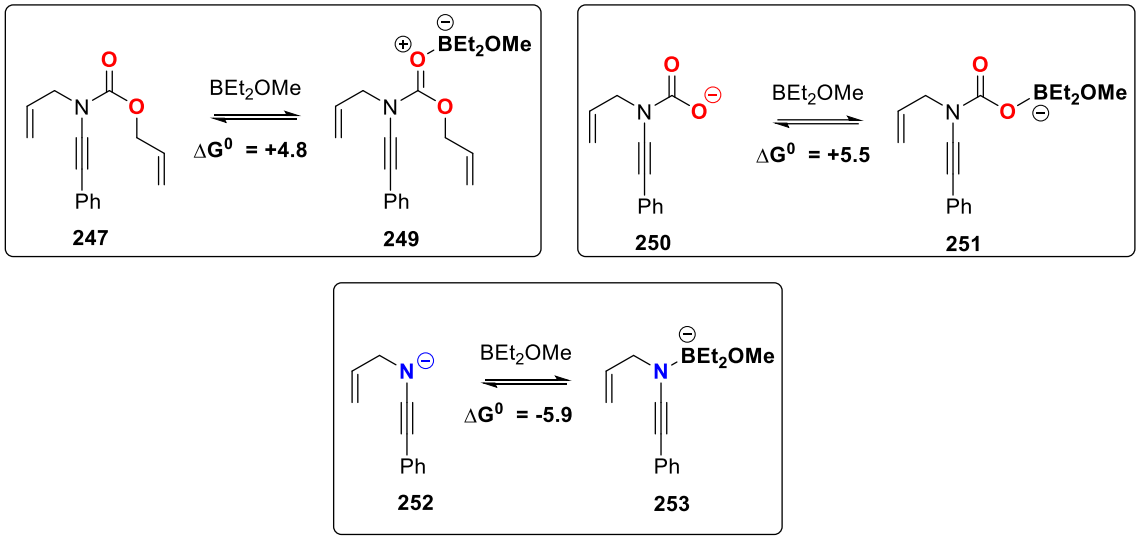

Scheme 168. Thermodynamics of binding of boron to starting ynamide and ynamide-derived intermediates.

We have also discovered an uncatalyzed rearrangement of *N*-allyl-*N*-alloc ynamide (**247**) directly to the product though an 8-membered transition state (**247 TS**) where C-O and C-N bond breaking occurs simultaneously with C-C bond formation (Figure 27). However, this transition state is significantly higher than any catalyzed pathway (+35.3 kcal/mol). We were not able to locate analogous Pd(0)-catalyzed transition state.

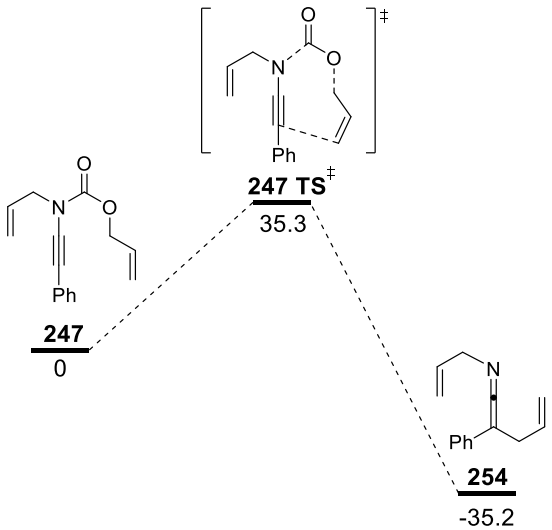

Figure 27. Uncatalyzed rearrangement of *N*-allyl-*N*-alloc ynamide.

For (**247**) among all the possible pathways, decarboxylation *via* (**247A TS**) followed by outer-sphere nucleophilic attack through boron-bound (**249B-N TS**) has the lowest kinetic barrier. We found that the preference towards either decarboxylation or simultaneous decarboxylation/outer-sphere nucleophilic attack is highly dependent on the substrate electronics, in particular the stabilization of anionic groups. We therefore calculated the energetic barriers required for non-stabilizing butyl group substituent (**255**) (Figure 28). We found that the catalyst binding and ionization steps were similar to that of the phenyl analog (**247**), however the lack of anionic stabilization disfavors the two-step decarboxylation-allylation process and instead promotes concerted decarboxylative C-C bond formation. Indeed, the transition state energy for dissociative pathway (**255B TS**) is 2.8 kcal/mol higher in energy than the concerted variant (**255Bs TS**).

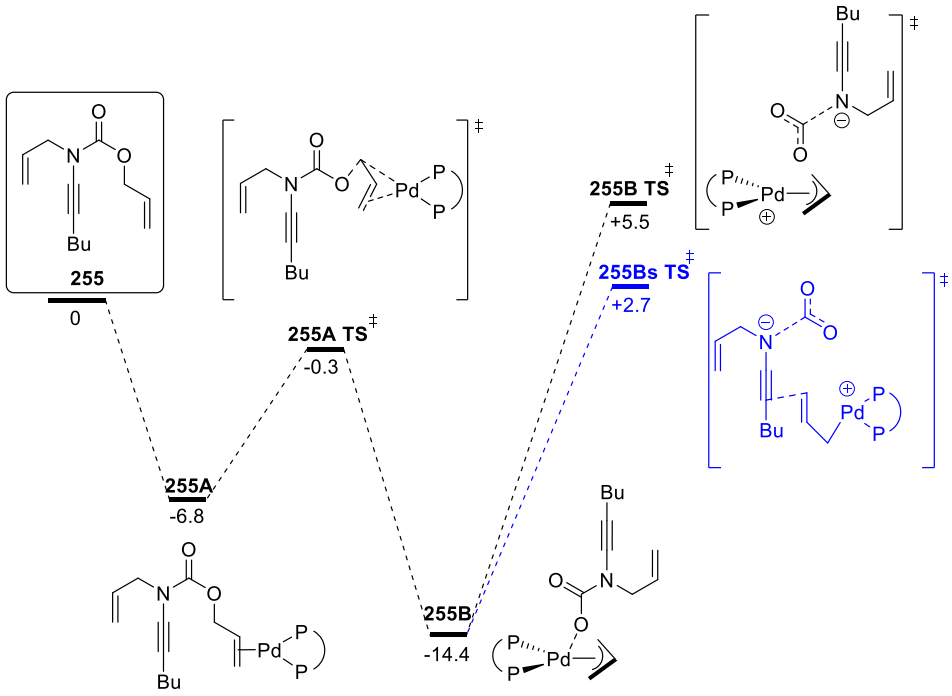

Figure 28. Potential energy surface demonstrating possible competitive pathways of decarboxylative allylation of (**255**).

Regioselectivity of Decarboxylative Rearrangement

The reactions described in Figures 24, 25 and 28 utilized unsubstituted allyl groups, however these transformations can also be used when substitution is present. When the alloc group is replaced with a cinnamyl moiety (**256**), the reaction is now complicated by the possibility to form both linear (**257**) and branched (**258**) regioisomers. It was discovered in the Cook group (Shchepetkina V.I., Benedict R.J.) that the regioselectivity of this reaction was ligand controlled (Scheme 169). Indeed, the $Pd(OAc)_2$/BINAP conditions produced a moderate 4.1:1 mixture of linear to branched isomers experimentally, whereas narrower bite-angle ligands gave lower selectivity and larger bite-angle ligand higher selectivity. Interestingly, experimentally optimized ligand for these substrates is xantphos (11.5:1 selectivity), however when one replaces the phenyl groups with cyclohexyl variants, a 1:1 mixture is obtained (Scheme 169).

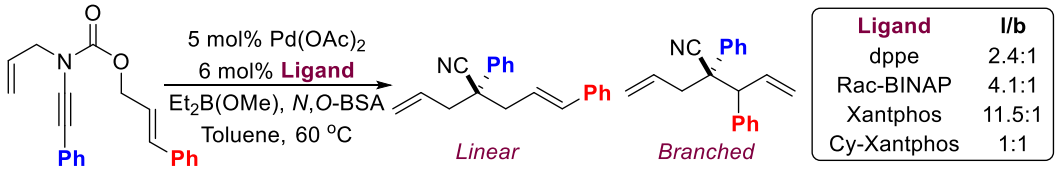

256 **257** **258**

Scheme 169. Effect of ligand on the rearrangement of (**256**) found in the Cook group.

These ligand effects suggest that the regioselectivity is determined by the binding mode of the allylic group (Scheme 170). It was shown that when allyl group has a substituent at one terminus, the symmetry of η^3-Pd π-allyl complex is distorted towards η^1- η^2 type structure.[271] In this case, one would expect that linear selectivity would originate from an outer-sphere pathway with the nucleophile reacting at the least hindered terminus and would be favored sterically,

while branched isomer would be derived from the outer-sphere attack occurring at the most electrophilic terminus and would be favored electronically.[271]

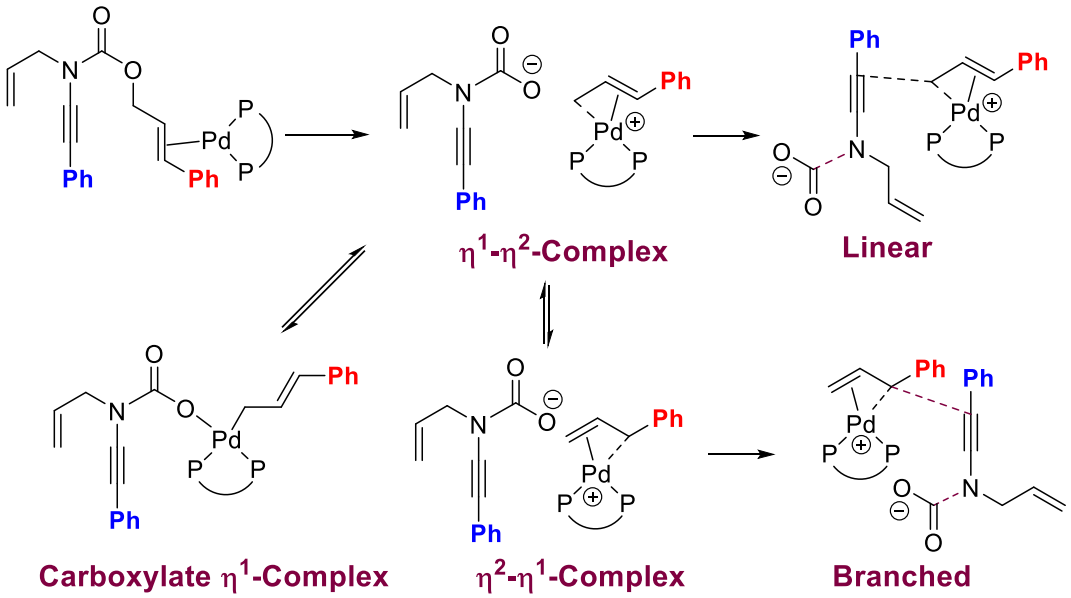

Scheme 170. Possible binding modes of the carboxylate and allylic group.

To investigate this hypothesis computationally, we examined the $Pd(OAc)_2$/BINAP conditions outlined above (Figure 29). We found that the initial Pd-alkene complexation is a more exergonic process, however this can still ionize to the corresponding π-allylic ion pair (**256B**). In this case, the concerted process is again more favored over the stepwise with (**256Bs TS**) being lower in energy than (**256B TS**). Since in this case an allyl group is unsymmetrical, two distinctive conformers can be formed - (**256B**) and (**256B'**) which correspond to the relative position of carbamate anion with respect to the allyl group. These conformers are prerequisites to corresponding transition states leading to either branched (**256Bsb TS**) or linear product (**256Bsl TS**). This is a classic Curtin-Hammett scenario; therefore, the reaction is expected to proceed *via* TS with the lower energy, which in this case is (**256Bsl TS**). The $\Delta\Delta G^{\ddagger}$ between (**256Bsl TS**)

and (**256Bsb TS**) is 0.2 kcal/mol, which at 60 °C would provide relative rates of 1.3:1, showing slight preference towards linear product. This overall correlates with experimental results as the experimentally observed d.r. is 4.1:1.

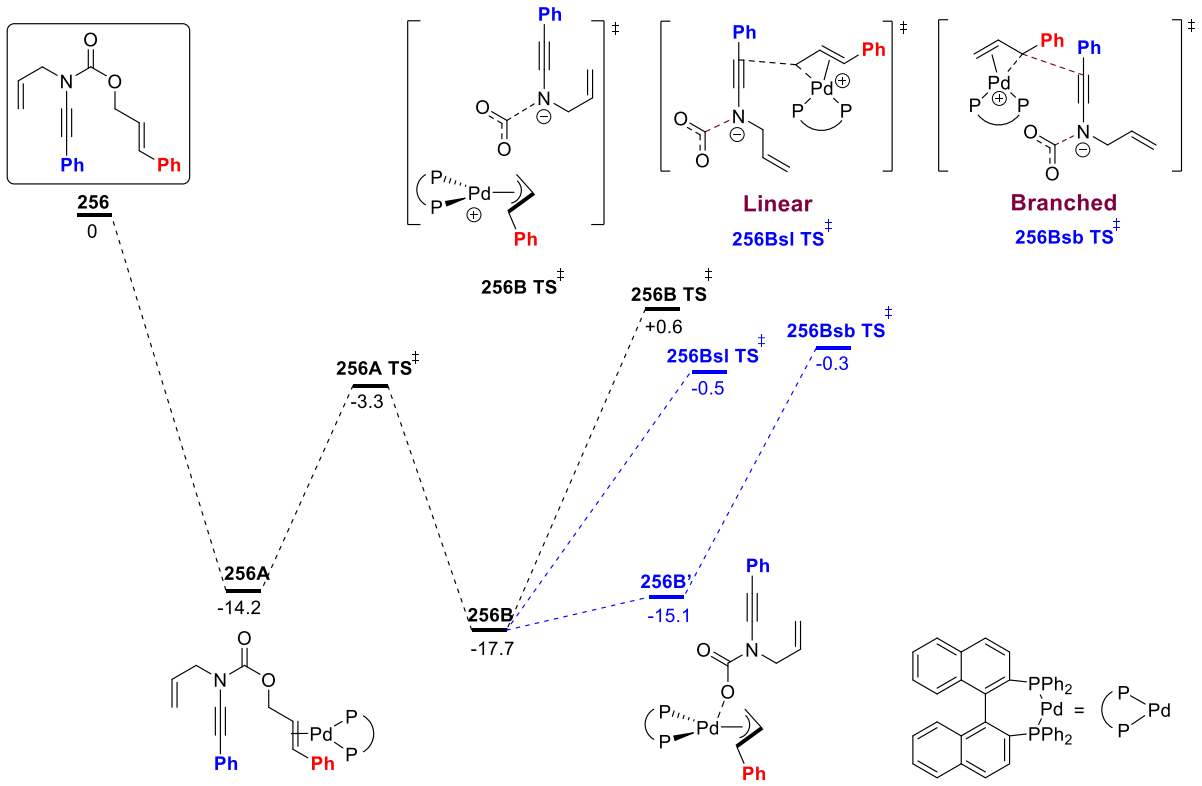

Figure 29. Potential energy surface demonstrating possible competitive pathways of decarboxylative allylation of (**256**). BINAP used as a ligand.

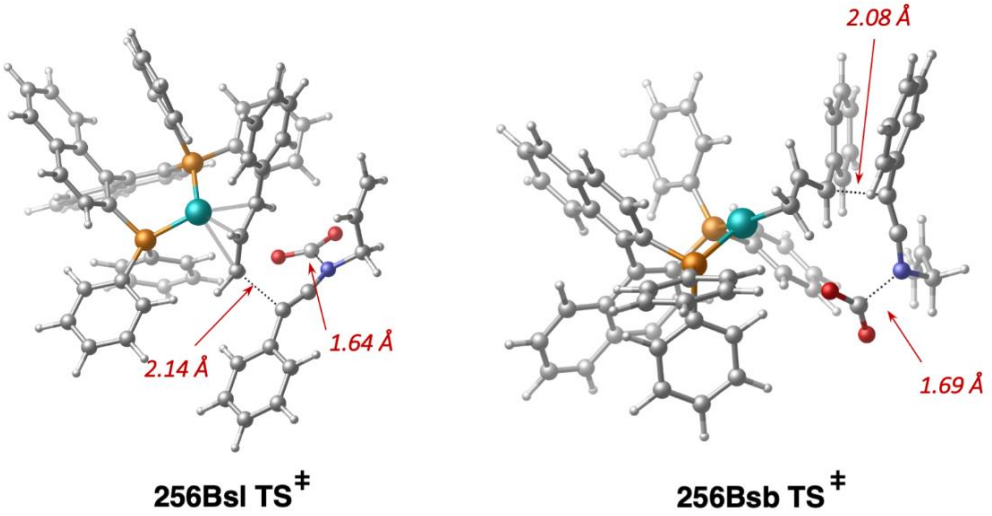

Figure 30. Transition state structures representing formation of linear and branched product.

When one examines the geometry of (**256Bsl TS**) and (**256Bsb TS**), it can be noted that oxygen is only weekly coordinated to Pd (Figure 30). In particular, Pd-O distance in both cases is around 3.5 Å, whereas in their prerequisite conformers this distance is shorter - 2.62 Å in linear and 2.66 Å in branched variant. Small energy difference observed for these transition states can be rationalized based on electrophilicity of linear and branched terminus of the allyl group in transition state. Previous studies in palladium π-allyl chemistry have shown that the allylic carbon, that is the furthest from Pd, is preferred for nucleophilic attack.[271] In (**256Bsl TS**) leading to linear product the distance between Pd and allylic carbon at linear terminus is 2.81 Å, while in (**256Bsb TS**) leading to branched product the distance between Pd and allylic carbon at branched terminus it is 2.92 Å. Therefore, based on electronic effects one would expect slight preference towards the branched product. However, (**256Bsb TS**) is more hindered with allylic group rotated with out of P-Pd-P plane to minimize steric interaction of phenyl substituent with phenyl groups on the BINAP. In this case, steric factor overweighs electronic considerations resulting in slight preference towards linear product.

Deuterium Scrambling Studies: Evidence towards Proposed Mechanism

The computational data is supported by deuterium scrambling experiments performed in the Cook group by Shchepetkina V.I. (Scheme 171).[196] Thus, when deuteration was installed at the allylic position of the *N*-alloc group of (**247**) and (**255**), isotopic scrambling was observed in both cases, indicating a dissociative π-allylic mechanism. Butyl analog (**255a**) provided a slight excess of the allylic CD_2 compound (**260b**), whereas phenyl analog (**247a**) provided equimolar quantities of (**259a**) and (**260a**). This suggests that for the phenyl analog (**247a**) C-O bond ionization is the rate limiting step in the reaction and is, therefore, irreversible, while for butyl analog (**255a**) C-O bond ionization is reversible and antecedes the rate limiting step. These results agree with DFT calculations that predicted (**247**) to react *via* the pathway including C-O bond ionization *via* (**247A TS**) (2.0 kcal/mol) and C-C bond formation *via* outer-sphere nucleophilic attack (-13.5 kcal/mol) and (**255**) to react *via* the pathway including C-O bond ionization *via* (**255A TS**) (-0.3 kcal/mol) and C-C bond formation *via* simultaneous decarboxylation/outer-sphere nucleophilic attack *via* (**255Bs TS**) (2.7 kcal/mol).[196]

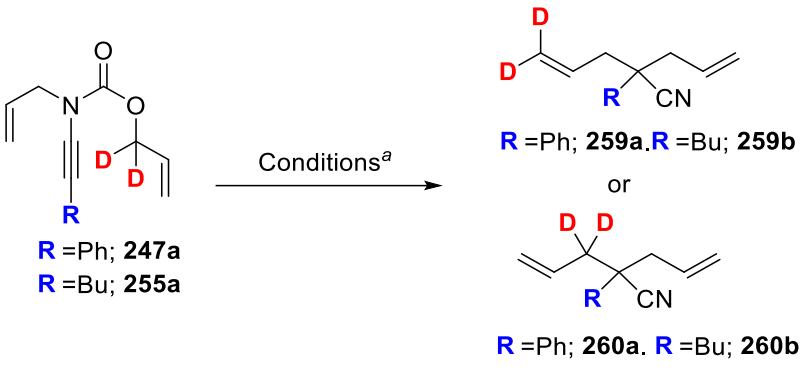

Entry	Substrate	Product	8:9[b]
1	**247a**	**259a/260a**	1:1
2	**255a**	**259b/260b**	0.83:1

Scheme 171. Deuterium scrambling studies. [a] Conditions: 5 mol% $Pd(OAc)_2$, 6 mol% *rac*-BINAP, $Et_2B(OMe)$ (1 eq.), *N*,*O*-BSA (1 eq.), toluene, 60 °C, 16 h; [b] Ratios by ^1H NMR of unpurified reaction mixture.

Effect of the Ligand on Reaction Mechanism

With these results in hand, we continued our studies by investigating the effect of the ligand on the reaction mechanism. We started with investigating potential energy surface of the reaction when xantphos used as a ligand as it was shown to be optimal for these substrates providing the best selectivity.

In this case, for the initial binding step two conformations can be adopted (complexes (**256A-X1**) and (**256A-X2**)) that differ in orientation of the allylic groups with the respect to xantphos were considered (Figure 31). It was found that complexation of (**256**) leading to complex (**256A-X2**) is 5.5 kcal/mol more exergonic comparing to (**256A-X1**) (Figure 33, 34). Both complexes ionize to the corresponding π-allylic ion pair (**256B-X1/2**) with (**256A-X1 TS**) being 3.0 kcal/mol lower in energy. However, in case of (**256A-X1**) ionization is reversible and all subsequent decarboxylation transitions states (**256A-X1 TS**)**,** (**256Asl-X1 TS**) and (**256Asb-X1 TS**) are significantly higher in energy comparing to (**256B-X2 TS**)**,** (**256Bsl-X2 TS**) and

(**256Bsb-X2 TS**). Therefore, under thermodynamic conditions reaction would proceed *via* the pathway involving formation of complex (**256A-X2**)**.**

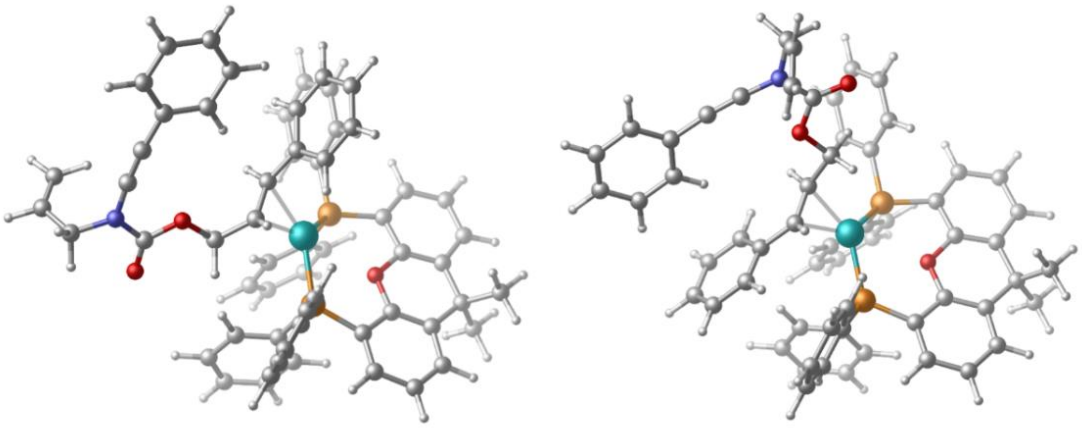

Figure 31. Complexes (**256A-X1**) and (**256A-X2**).

The preference towards complex (**256A-X2**) can be rationalized by examining the topology of catalytic pocket[272] of xantphos (Figure 32). The SW and SE quadrants of the catalytic pocket are more occupied due to the phenyl groups on the ligand, proving this area to be more sterically hindered. Consequently, this would affect geometry and coordination to Pd in tight ion pairs and transition states.

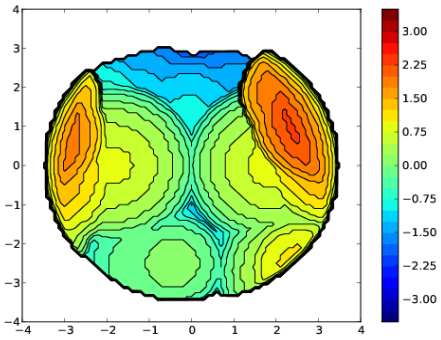

Figure 32. Topology of xantphos catalytic pocket.

Further analysis of the reaction mechanism showed reaction is under Curtin-Hammett control. Between competing transition states representing both stepwise and concerted processes, concerted transition state (**256Bsl-X2 TS**) leading to linear product is the lowest energy one. The $\Delta\Delta G^{\ddagger}$ between (**256Bsl-X2 TS**) and the next lowest energy transition state (**256B-X2 TS**) is 4.4 kcal/mol, showing strong preference towards linear product.

Comparison between Pd-C distances in (**256Bsl-X2 TS**) and (**256Bsb-X2 TS**) analogous to one performed for BINAP shows that in (**256Bsl-X2 TS**) leading to linear product the distance between Pd and allylic carbon at linear terminus is 2.70 Å, while in (**256Bsb-X2 TS**) leading to branched product the distance between Pd and allylic carbon at branched terminus it is 2.48 Å. Therefore, in this case both electronic and steric effects favor the formation of linear product,[271] which leads to the improved selectivity.

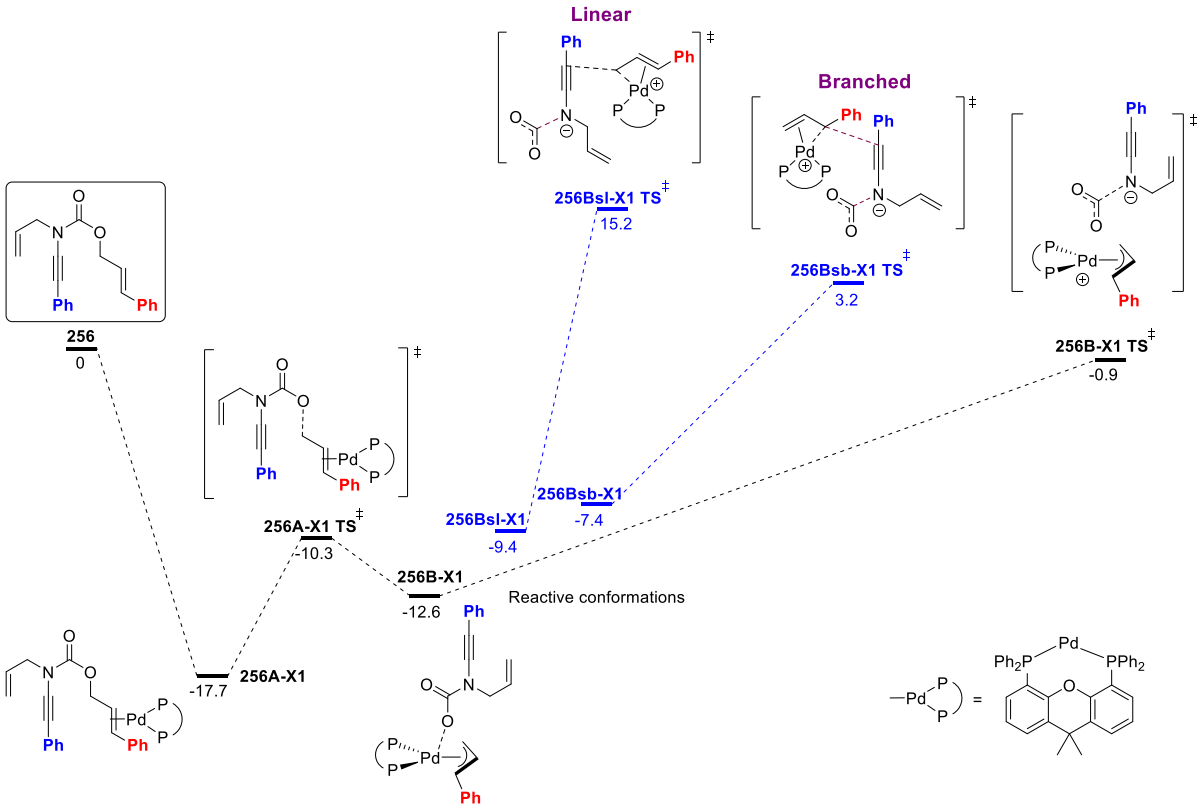

Figure 33. Potential energy surface demonstrating possible competitive pathways of decarboxylative allylation of (**256**) *via* formation of (**256-X1**). Xantphos used as a ligand.

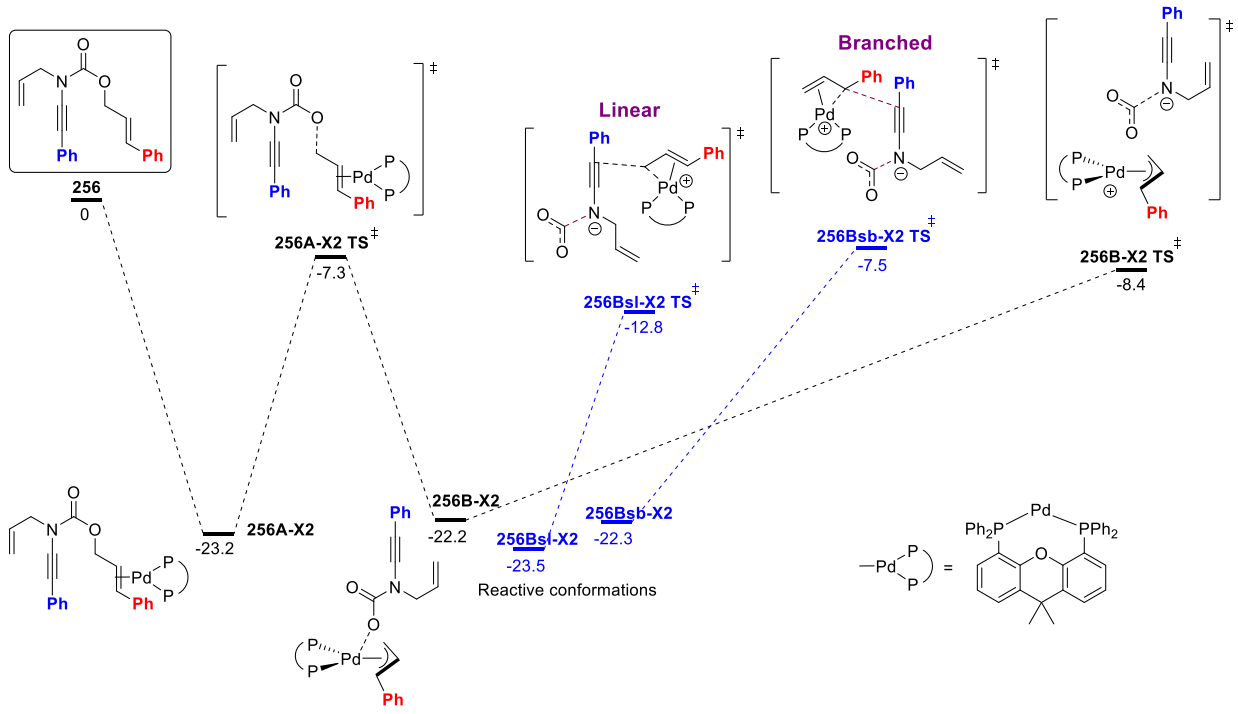

Figure 34. Potential energy surface demonstrating possible competitive pathways of decarboxylative allylation of (**256**) *via* formation of (**256-X2**). Xantphos used as a ligand.

When dppe was examined as a ligand, it was found that decarboxylation *via* (**256B-D TS**) is lower in energy than concerted decarboxylative C-C bond formation (Figure 35). This change in mechanism leads to an alternative C-C bond forming step determining the linear to branched ratio compared to BINAP or xantphos. For transformation utilizing *cy*-xantphos we were not able to locate transition states representing concerted decarboxylative C-C bond formation, suggesting the change in mechanism as well.

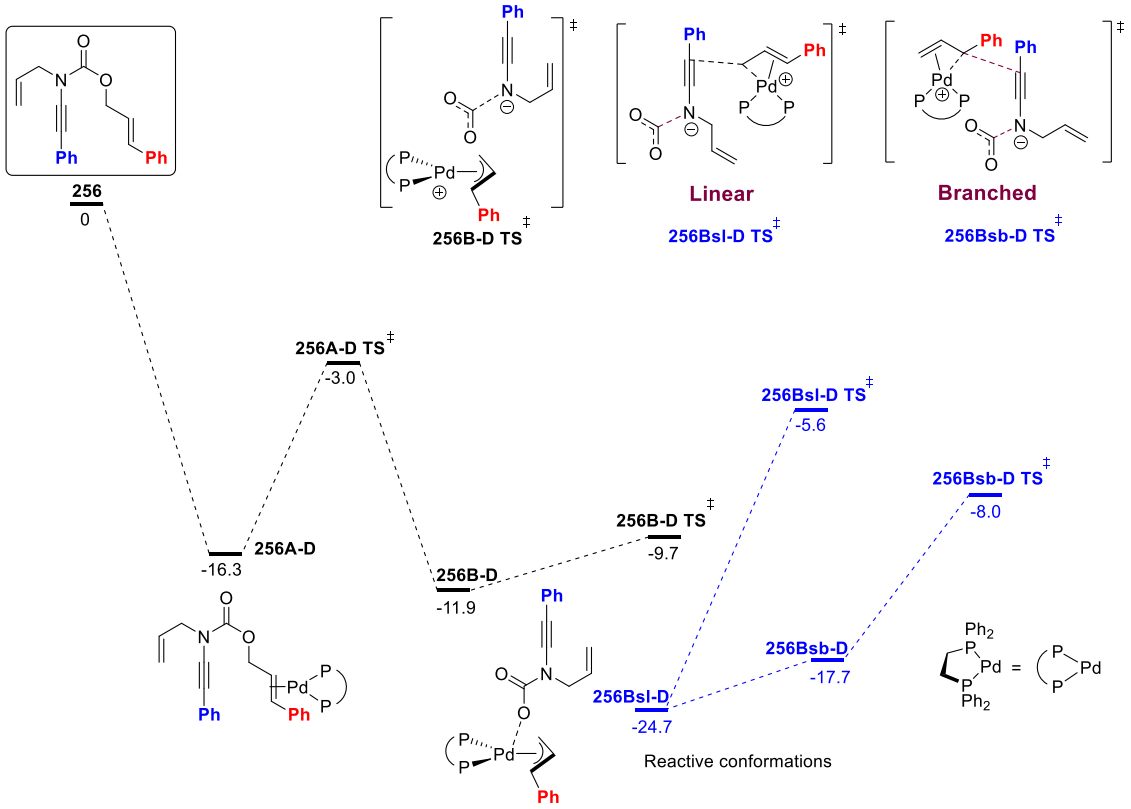

Figure 35. Potential energy surface demonstrating possible competitive pathways of decarboxylative allylation of (**256**). Dppe used as a ligand.

The divergence in the mechanism observed for these ligands can be rationalized by steric properties of the ligand. For instance, from dppe, to BINAP, xantphos to *cy*-xantphos, the buried volume[272] of the ligand as well as bite angle are increasing (Table 26). It has been shown that phosphine ligands with large bite angles lead to decreased backdonation from Pd to the allylic group resulting in higher reactivity of the latter.[271] It can be noticed that with an increase of the ligand buried volume and bite angle, energetic preference towards concerted process increases until the ligand becomes too crowded resulting in further change in the mechanism (Table 26).

Further analysis shows that narrow bite angle ligands give poor linear/branched selectivity, yet this ratio improves (and becomes more linear selective) with increased bite-angles, with xantphos providing almost complete linear selectivity (Table 26). However, *cy*-

xantphos results in no selectivity and is an outlier, although this ligand has vastly different steric and electronic properties. A good correlation (R^2=0.7805) is observed between the bite angle of the ligand and linear to branched ratio when *cy*-xantphos is excluded from the dataset (Figure 36).

Ligand	Bite angle lit.	%V_{bur}	l/b	$\Delta\Delta G^{\ddagger}$ (kcal/mol) Concerted vs. stepwise
Dppbenz	83	46.8	2.6:1.0	-
Dppe	85	50.0	2.4:1.0	-1.7
Dppp	91	52.8	4.6:1.0	-
rac-BINAP	92	56.6	4.1:1.0	+1.1
DPEPhos	103	n/a	4.6:1.0	-
Xantphos	111	56.5	11.5:1.0	+4.3
Cy-xantphos	113[a]	59.5	1.0:1.0	-

Table 26. Ligand parameters and observed selectivity. [a] Calculated in PdL-ynamide complex.

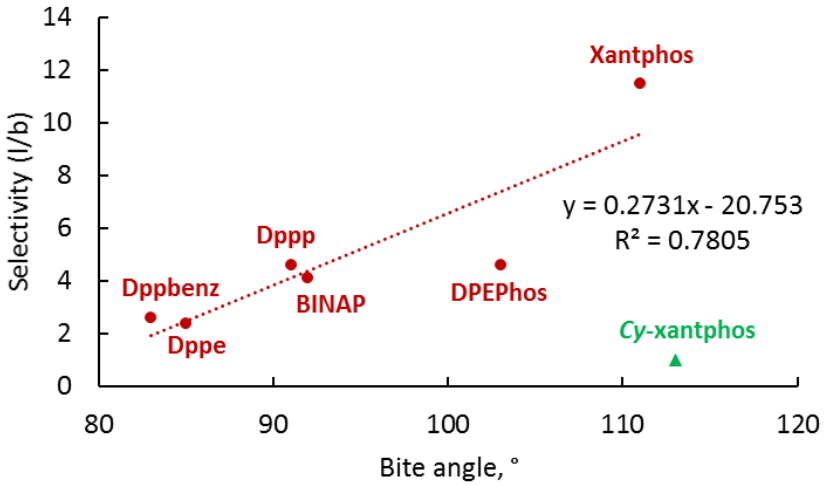

Figure 36. Plot of linear to branched selectivity versus bite angle.

Interestingly, the opposite trend between linear to branched selectivity and ligand bite angle was observed by van Leeuwen *et al.* in Pd-catalyzed allylic alkylation of 3-Me-but-2-enyl acetate (**261**) by sodium diethyl 2-methylmalonate (**262**) (Scheme 172).[271] They found that a

preference towards branched product (**263**) increases with an increase in the bite angle. The difference in trends observed by van Leeuwen *et al.* and us can be explained by a difference in both steric and electronic properties of phenyl and dimethyl substituted allylic group in forming π-allyl complexes.

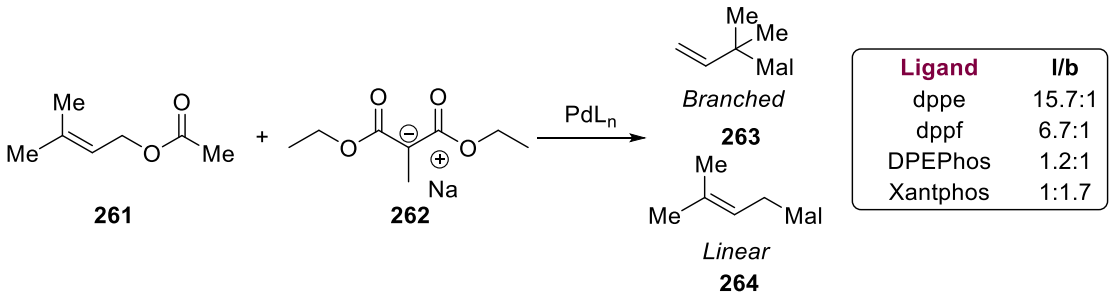

Scheme 172. Regioselectivity in catalytic allylic alkylation observed by van Leeuwen *et al.*

Conclusions

The mechanism of Pd-catalyzed decarboxylative allylation of *N*-alloc-*N*-Allyl ynamides was elucidated. Proposed catalytic cycle includes oxidative addition of alloc group to Pd(0) *via* S_N2-like transition state followed by either stepwise decarboxylation/C-C formation *via* outer-sphere nucleophile attack or previously unknown concomitant decarboxylation/C-C bond formation (Scheme 173). The preference towards stepwise or concerted process is highly dependent on electronics of the substrate. Alkyl substituted *N*-alloc-*N*-allyl ynamides favor concerted process due to the lack of anionic stabilization. These computational findings are supported by the results of deuterium scrambling studies.[196]

When coordination to the boron additive at each step of the mechanism was examined, it was found that while BEt_2OMe does not participate in oxidative addition or decarboxylation steps, it lowers the energy of the tight ion pair and transition state corresponding to outer-sphere attack (**249B-N TS**) by coordinating to nitrogen in allyl ynamide anion. Therefore, we believe

that one of the roles that BEt_2OMe plays in this reaction is stabilization of forming allyl ynamide anion (**252**) and preventing decomposition or off-cycle reactivity.

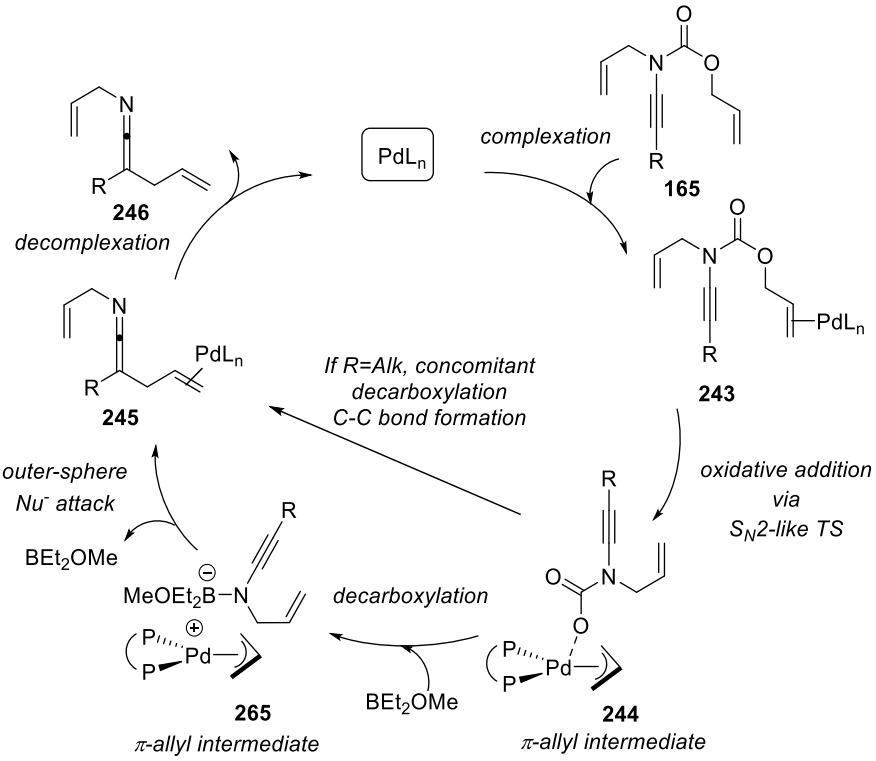

Scheme 173. Catalytic cycle for decarboxylative allylation of *N*-alloc-*N*-Allyl ynamides.

We have also discovered the uncatalyzed rearrangement of *N*-allyl-*N*-alloc ynamides directly to the product *via* 8-membered transition state (**247 TS**) where C-O and C-N bond breaking occurs simultaneously with C-C bond formation.

Regioselectivity of this reaction was examined by studying the mechanism of decarboxylative allylation for cinnamyl substituted substrate. When BINAP and xantphos are used as ligands in this transformation, the linear to branched ratio is determined by two competing transition states representing concomitant decarboxylation/C-C bond formation and leading to branched or linear product. It was found that while for BINAP the preference towards

linear product is determined by sterics, in case of xantphos both steric and electronic factors favor linear product, leading to improved selectivity. We discovered that ligand steric parameters affect the mechanism of overall transformation resulting in alternative regioselectivity determining step. In particular, dppe favors stepwise decarboxylation/C-C formation over concerted process. Despite this, we were able to identify bite angle as parameter that provided good correlation with experimentally observed selectivity across available ligand dataset (R^2=0.7805).

Based on these results, further research in this area can include examining series of xantphos ligands and other ligands with wide bite angle[273] to achieve on higher reaction regioselectivity.

Ketenimine Rearrangement

Mechanism of Ketenimine Rearrangement

Reprinted (adapted) with permission from Alexander, J. R.; Shchepetkina, V. I.; Stankevich, K. S.; Benedict, R. J.; Bernhard, S. P.; Dreiling, R. J.; Cook, M. J. Pd-Catalyzed Rearrangement of *N*-Alloc-*N*-allyl Ynamides via Auto-Tandem Catalysis: Evidence for Reversible C–N Activation and Pd(0)-Accelerated Ketenimine Aza-Claisen Rearrangement. *Org. Lett.* **2021**, *23* (2), 559–564. DOI: 10.1021/acs.orglett.0c04078. Copyright 2021 American Chemical Society. http://pubs.acs.org/articlesonrequest/AOR-SQUVAMWDKP8QMJBDVJCZ

We continued studying the mechanism of this transformation using phenyl ketenimine (**254**), formed as a result of decarboxylative allylation of (**247**) as an initial model. Because of the large ligand, we applied the two-layer quantum-mechanical (QM)/semiempirical (SE) ONIOM model to the palladium complexes.[241,246,268] The QM layer was treated with M06L/6-

31+G(d) (C, H, P, B, O)/LANL2DZ (ECP Pd)[188] and the SE layer with PM6. Single point (SP) energies of these optimized structures were calculated utilizing M06L/6-311++G(2d,2p) (C, H, P, B, O)/ LANL2DZ (ECP Pd). The solvation by toluene was accounted for using C-PCM.[184,185] Transition states (TS) were located using either relaxed scan of potential energy surface or NEB method implemented in ORCA 4.2.1[274,275] at the M06L level with def2-SV(P) basis set followed by the ONIOM/SP process described above. Conformational flexibility was addressed through the mixed torsional/low mode method and relaxed torsion scans. Further description of methods can be found in Computational Details.[196]

The initial hypothesis for the catalytic cycle based on the previous research in the area[200,219,223,227,228] included complexation of ketenimine (**246**) with Pd(0) catalyst; oxidative addition with the formation of π-allyl complex (**267**); reductive elimination; and decomplexation of nitrile (**166**) (Scheme 174).

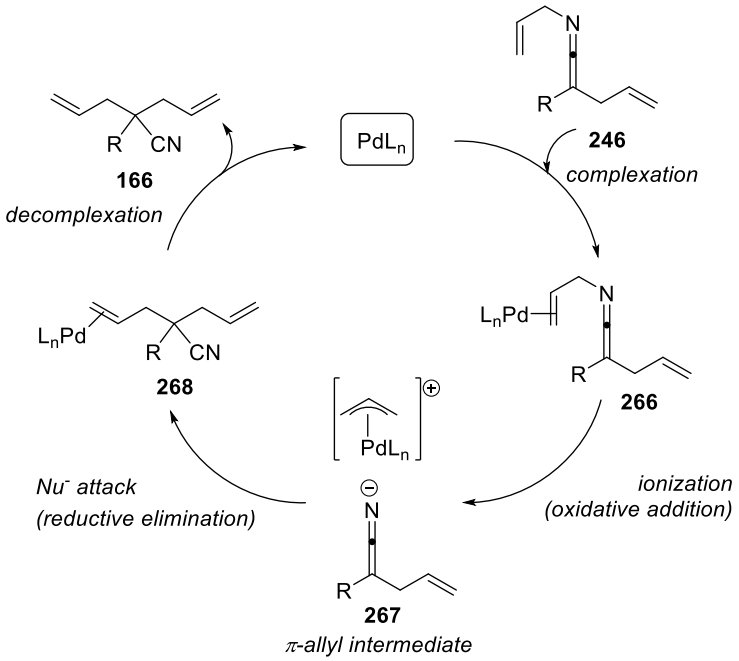

Scheme 174. Initial hypothesis for the rearrangement of *N*-allyl ketenimines.

We explored both catalytic and uncatalyzed pathways for the sigmatropic rearrangement and discovered a complex potential energy surface. The uncatalyzed ketenimine aza-Claisen rearrangement of (**254**) proceeded through an early transition state analogous to those described by Walters.[225,226] This rearrangement is significantly faster with the free ketenimine, rather than *via* a Lewis acid-base adduct with the borane additive (Figure 37, 38). In palladium-catalyzed routes (Figure 37),[218,263] coordination of ketenimine (**254**) with the Pd(0) catalyst to form (**254A**), is exergonic by 11.7 kcal/mol. π-Allylic ionization mechanisms were examined with and without the borane additive bound. Direct ionization of (**254A**) to form π-allyl species (**254B**) (*via* (**254 TS-ION**) was readily accessible with a TS energy of just 11.4 kcal/mol (from (**254A**)).

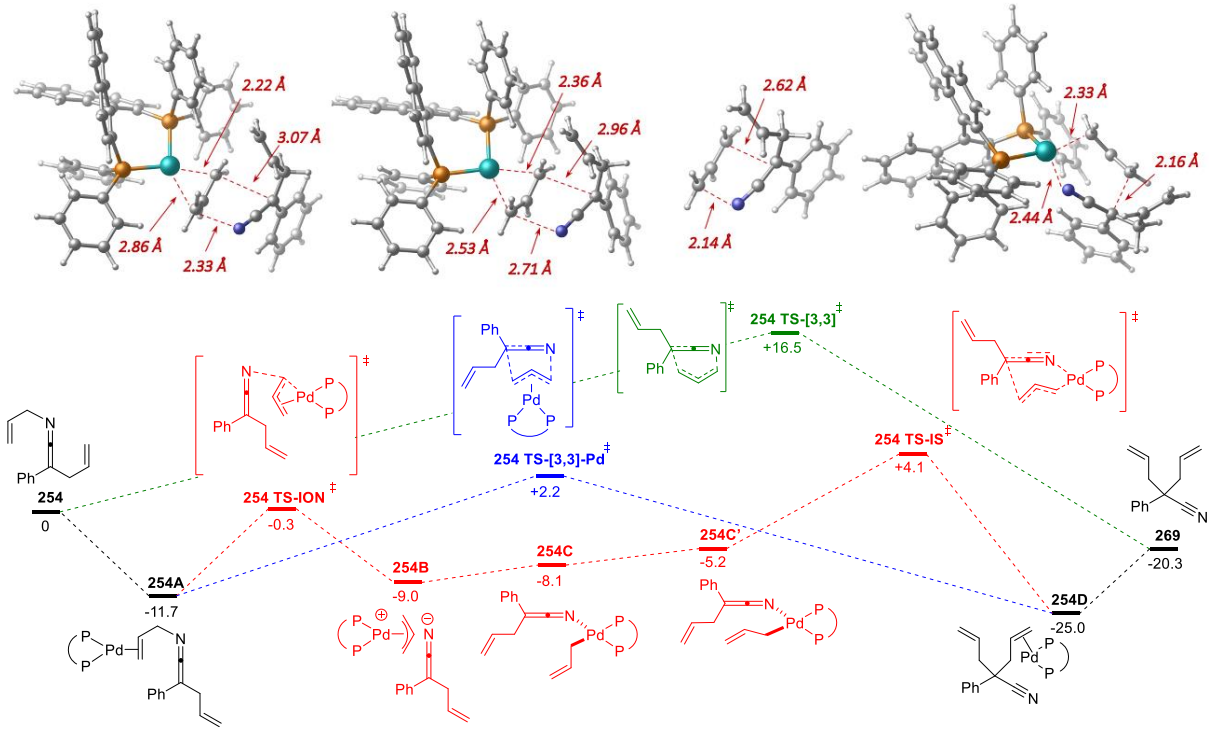

Figure 37. Potential energy surface demonstrating possible pathways for the rearrangement of ketenimine (**254**) without borane additive.

The structure of (**254B**), is a heavily distorted η^3-π-allyl tight ion pair, which can easily isomerize between the η^3 and η^1-haptomers ((**254B**) and (**254C**)). Bond rotation is required to form the reactive conformer (**254C'**) which can rearrange *via* an inner-sphere C-C bond forming mechanism ((**254 TS-IS**). The palladium bound rearranged nitrile (**254D**) is formed with an overall TS energy of 15.8 kcal/mol from (**254A**).

When the borane additive was included into the mechanism, we were able to locate additional transition state (**270 TS-OS-B**) representing outer-sphere C-C bond formation, which was 8.5 kcal/mol lower in energy comparing to inner-sphere pathway (**270 TS-IS-B**). However, the borane-adduct route was overall significantly higher in energy than the direct ionization of (**254A**) (Figure 38), therefore we do not believe the borane additive is participating in the rearrangement of (**254**).

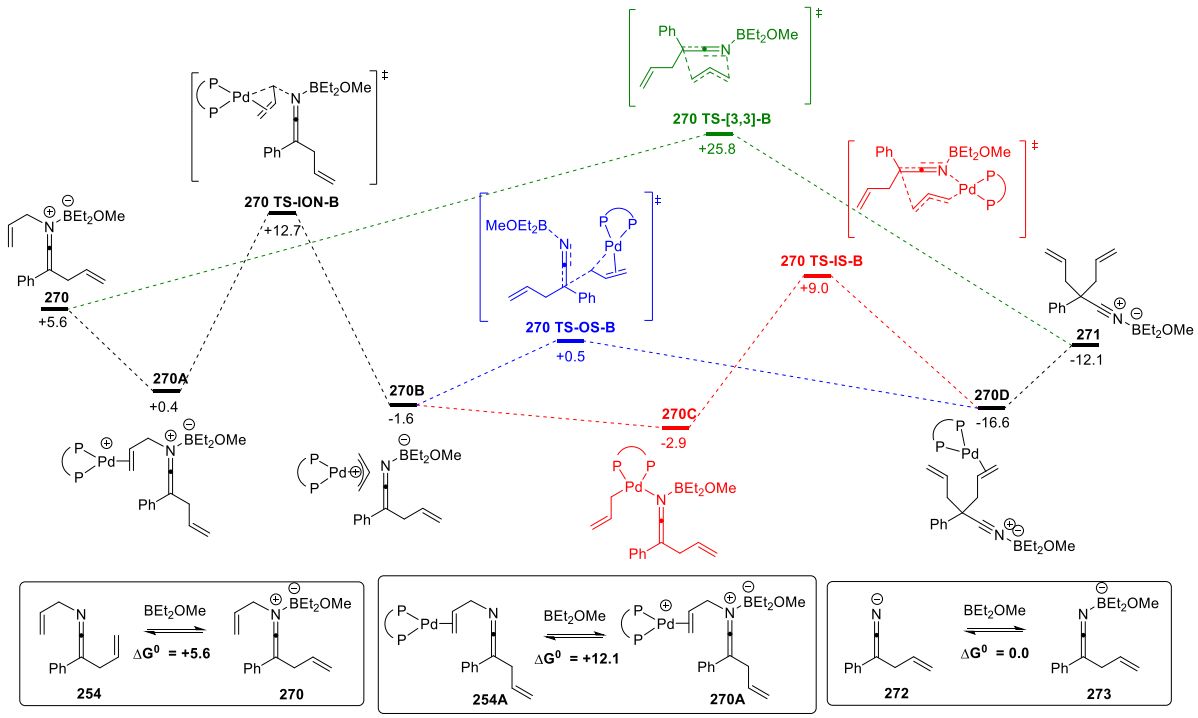

Figure 38. Potential energy surface demonstrating possible pathways for the rearrangement of ketenimine (**254**) without borane additive. Energies are shown relative to free ketenimiane (**254**).

A concerted Pd(0)-catalyzed pericyclic process was also investigated. This mechanism proceeds through highly ordered (**254 TS-[3,3]-Pd**) and is 1.9 kcal/mol lower in energy than the (**254 TS-IS**) route. The structure of (**254 TS-[3,3]-Pd**) is a hybrid between π-allylic and sigmatropic processes where the reaction is aided by donation of electron density from the Pd(0) center into the C-N σ*-orbital leading to a later TS than the uncatalyzed variant (**254 TS-[3,3]**). When one examines the migrating allylic portion, all three carbon atoms are almost trigonal planar and the terminal C-Pd bond lengths (2.36 & 2.53 Å) indicate substantial interactions between the Pd-catalyst and both termini. This effect can be seen more clearly when the HOMO and LUMO coefficients are examined (Figure 39). There is significant overlap from the d-orbitals of the Pd(0) atom (in the HOMO) with the σ*-orbital of the C-N bond (in the LUMO). Additionally, both the forming C-C and breaking C-N σ-bonds are significant contributors to the HOMO, indicative of a sigmatropic process. Furthermore, the HOMO and LUMO contain 2 and 4-nodes, respectively indicating an aromatic TS. The HOMO/LUMO gap is just -0.87 eV demonstrating facile transfer of electron density between these two molecular orbitals. The described reactivity mode is different comparing to other aza-Claisen rearrangements catalyzed by Pd that occur *via* an electrophilic Pd(II) pathway with the metal acting as a π-Lewis acid.[276–279,197] As the $\Delta\Delta G^{\ddagger}$ between the (**254 TS-[3,3]-Pd**) and (**254 TS-IS**) routes is 1.9 kcal/mol, representing a 18:1 difference in relative rates at 60 °C, we believe that both Pd(0)-assisted [3,3]- and inner-sphere mechanisms are occurring, with the former being the much faster pathway.

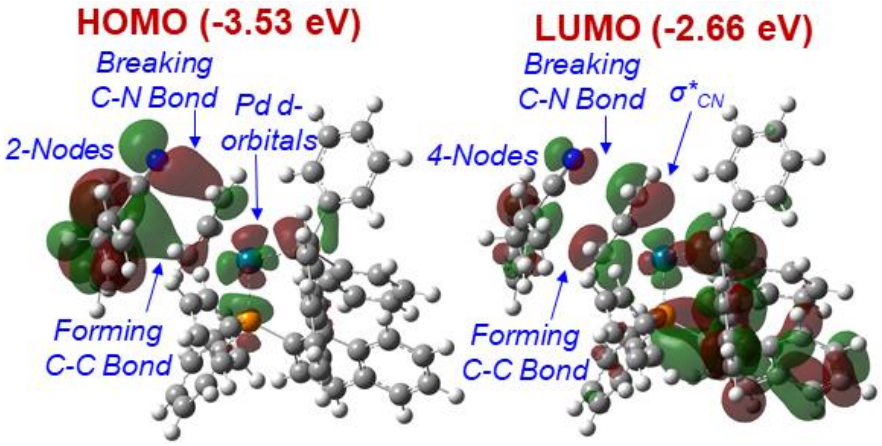

Figure 39. Calculated Molecular Orbitals for (**254 TS-[3,3]-Pd**).

Analogous computational studies performed on butyl ketenimine (**274**) indicate the reaction proceeds through a similar Pd(0)-catalyzed [3,3]- rearrangement, but the ionization pathway is much higher energy because of the lower stability of the ketenimine anion formed in ionized intermediate (**274B**). Once again the concerted uncatalyzed rearrangement was significantly higher in energy than the catalyzed process indicating the Pd(0)-catalyzed [3,3]-rearrangement is the only productive pathway.[196]

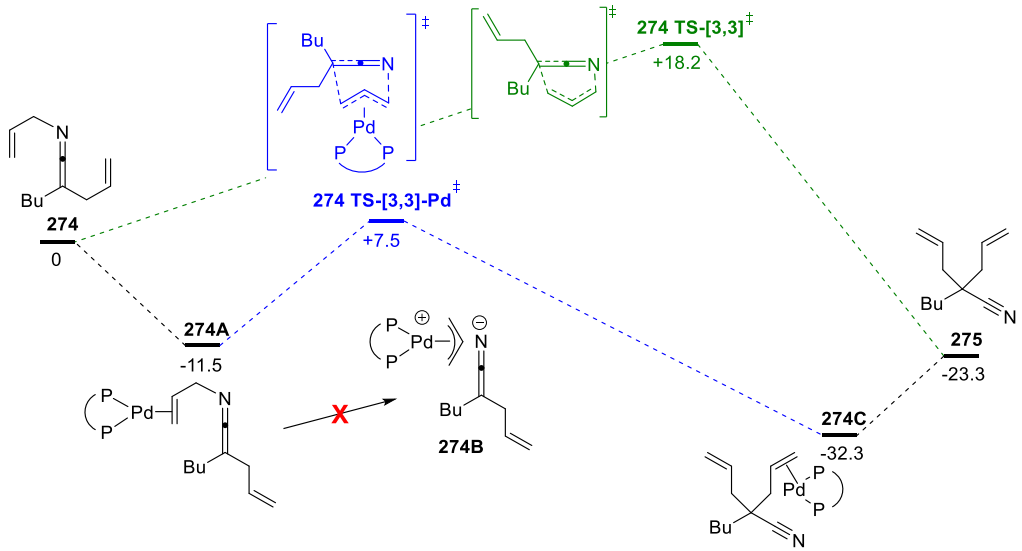

Figure 40. Potential energy surface demonstrating possible pathways for the rearrangement of ketenimine (**274**).

Deuterium Scrambling and Crossover Experiments

Computational results are supported by deuterium scrambling and crossover experiments performed in the Cook group by Shchepetkina V.I.[196] Deuterium labeled analogs of phenyl and butyl substrates were prepared where CH_2 had been replaced with a CD_2 group at the *N*-allyl position (Scheme 175). Two reactivity patterns were observed. The butyl substrate (**255b**) provided a single regioisomer (**260b**) with the deuterium exclusively at the terminal vinylic position. With phenyl analog (**247b**), deuterium scrambling was observed in a (**259a**):(**260a**) ratio of 1.2:1. These results clearly demonstrate a divergence in mechanisms between the two substrates ((**247b**) and (**255b**)) and indicate that a dissociative allylic pathway is occurring for (**247b**) which is not accessible to (**255b**). This supports DFT results indicating a concerted Pd(0)-catalyzed [3,3]- rearrangement as the only viable route for rearrangement of (**274**). In case of phenyl analog of note is the slight excess for the terminal vinylic deuterium isomer (**259a**). The origin of the selectivity in (**247b**) could be produced by either two competing (concerted and dissociative) mechanisms or a secondary kinetic isotope effect in a rapidly isomerizing Curtin-Hammett system. In the latter case, it would suggest a facile formation to a π-allyl intermediate followed by a higher energy C-C bond forming step with rehybridization from sp^3 to sp^2 being

selectivity determining. These observations are consistent with the mechanistic hypothesis presented for the rearrangement of (**254**) based on DFT studies.

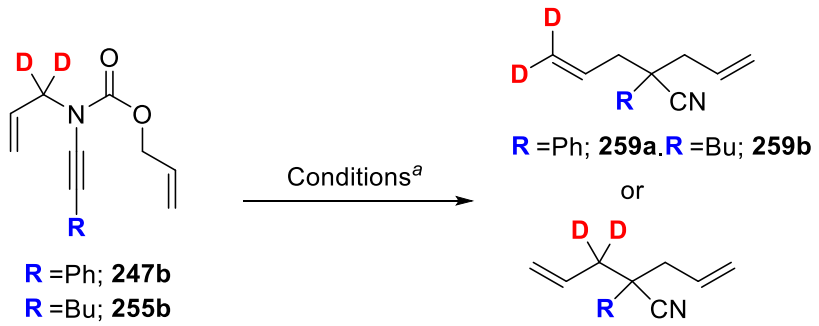

Entry	Substrate	Product	15:16[b]
1	**247b**	**259a/260a**	1.2:1
2	**255b**	**259b/260b**	>20:1

Scheme 175. Deuterium scrambling studies. [a] Conditions: 5 mol% $Pd(OAc)_2$, 6 mol% *rac*-BINAP, $Et_2B(OMe)$ (1 eq.), *N*,*O*-BSA (1 eq.), toluene, 60 °C, 16 h; [b] Ratios by ^1H NMR of unpurified reaction mixture.

Crossover studies were performed, with 0.5 equivalents each of (**247b**) and (**255b**) and a structurally similar unlabeled compound (**276**) and (**278**), to probe whether any solvent separated dissociation or π-allyl ligand exchange was occurring (Scheme 176). The competition reaction of butyl (**255b**) and with hexyl (**278**) ynamides provided no evidence of dissociation with complete retention of the deuterium label in the butyl substrate. Phenyl (**247b**) and 4-F-phenyl (**276**) ynamides gave trace amounts of deuterium crossover. This suggests that the dissociative pathway for (**247b**), that leads to deuterium scrambling, is short-lived and/or solvent separation not favored.[196]

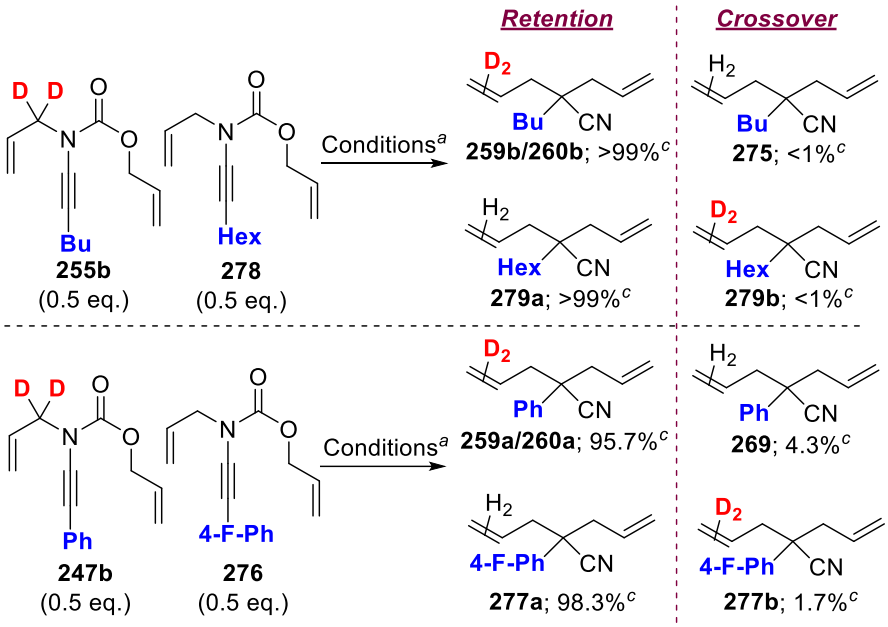

Scheme 176. Crossover studies. [a] Conditions: 5 mol% $Pd(OAc)_2$, 6 mol% *rac*-BINAP, $Et_2B(OMe)$ (1 eq.), *N*,*O*-BSA (1 eq.), toluene, 60 °C, 16 h; [b] Ratios by ^1H NMR of unpurified reaction mixture.

Conclusions

Our studies revealed a variety of competing mechanistic pathways in a complex potential energy surface. The key findings were that although energetically accessible, the uncatalyzed ketenimine aza-Claisen rearrangement has a significantly higher activation barrier than the catalytic variants. In both the catalyzed and uncatalyzed processes, borane complexation (or participation) is not energetically favored and increases both ground and transition state energies. The palladium catalyst allows for two mechanistically interesting pathways to occur, the first is a reversible oxidative ionization of the C-N bond, and the subsequent an inner-sphere mechanism (Scheme 177). This pathway is only accessible when anion stabilizing groups are present. The second route is the Pd(0) catalyzed [3,3]-rearrangement, which has not been previously reported and is of great significance.[196]

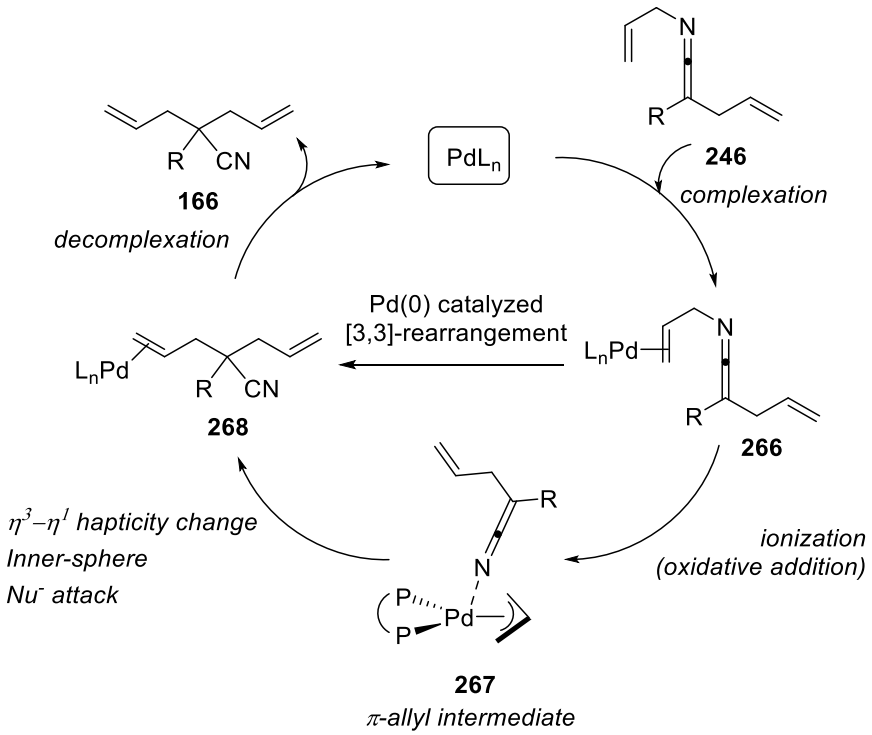

Scheme 177. Catalytic cycle for Pd-catalyzed rearrangement of *N*-allyl ketenimines.

Further studies in this area can be aimed at examining the ligand influence on the reaction mechanism and attempting to build predictive models.

Diastereo- and Branched-Selective Rearrangement

Reproduced/Adapted from Ref. 197 with permission from The Royal Society of Chemistry. https://doi.org/10.1039/D2CC03399B

To further develop this synthetic methodology, Cook *et al.* suggested that utilizing substrates containing γ-substituted *N*-allyl groups, would provide branched products with two contiguous stereogenic centers, including at least one all-carbon substituted quaternary center. Moreover, if substrates contain γ,γ-disubstitution, contiguous all-carbon quaternary stereocenters could be formed. An auto-tandem catalytic, branched selective rearrangement of substituted *N*-

alloc-*N*-allyl ynamides was developed (Scheme 178). This reaction provides ready access to complex quaternary nitrile products with vinylogous stereocenters in excellent diastereoselectivity, including the formation of contiguous all-carbon quaternary centers.

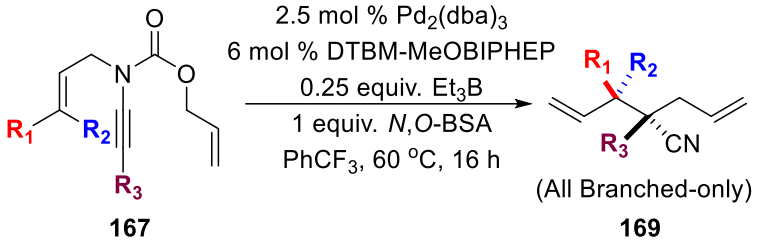

Scheme 178. Diastereo- and branched-selective palladium catalyzed rearrangement of γ,γ-disubstitution *N*-alloc-*N*-allyl ynamides to quaternary diallyl nitriles.

Herein, we present the computational study that aims to elucidate the origin of the high diastereoselectivity observed experimentally in the Cook group by Jackson O.D. using DTBM-MeOBIPHEP ligand (**L1**) (Scheme 178).[197,198] The study utilizes ketenimine (**280**) as a model substrate (Scheme 179). The calculations were performed at C-PCM(trifluorotoluene) M06L/BSII// ONIOM(M06L/BSI:PM6) level of theory, where BSI = 6-31+G(d) (C, H, P, O)/LANL2DZ (ECP Pd) and BSII = 6-311++G(2d,2p) (C, H, P, O)/LANL2DZ (ECP Pd).[184,185,188,241,246,268] Quasi-harmonic solvent and temperature (333.15 K) corrected Gibbs free energies at 1 mol/L standard state are reported.[177,189,190] More details regarding the computational methods used can be found in section providing Computational Details.[197]

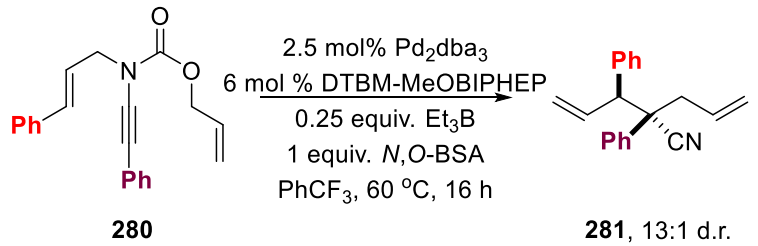

Scheme 179. Model substrate utilized for mechanistic study.

It was found that the bulky palladium bound ligand (**L1**) forms a deep cleft in which reactivity occurs. This conformational restriction results in a dissociative formal process rather than a concerted [3,3]-rearrangement.[196] Although ketenimines are stereogenic, they are highly epimerizable and exist as a dynamic mixture of isomers.[280] Allyl ketenimine (**280**) coordinates deep within the binding pocket, forming diastereomeric complexes (**282**)/(**288**) in a highly exergonic process (-20.0 and -17.0 kcal/mol, respectively) (Figure 41). These interconvertible complexes (**282**)/(**288**) can ionize though transition states (**TS-283**)/(**TS-289**), which is the stereodetermining step, to form ion pairs (**284**)/(**290**). The $\Delta\Delta G^{\ddagger}$ between (**TS-283**) and (**TS-289**) is 1.7 kcal/mol, which at 60 °C, equates to relative rates of 13:1, closely mirroring our experiment observations.

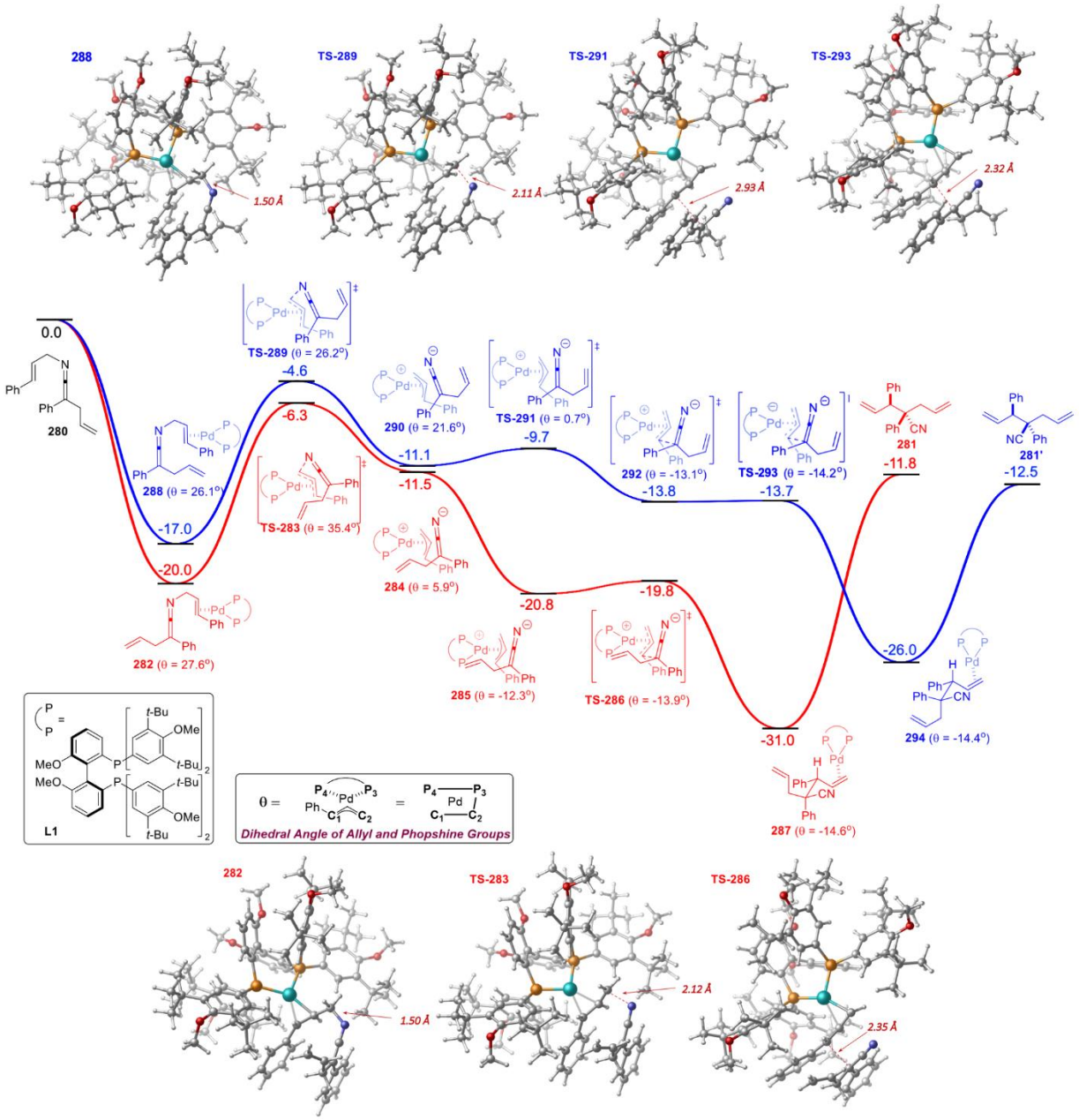

Figure 41. Potential energy surface of the rearrangement of (**280**) and structures of the key transition states and intermediates.

A possible explanation for this selectivity is the coplanarity of the phenyl groups leading to an offset π-stacking interaction (3.5 Å) in (**TS-283**) that is not present in **TS-24**.[281,282] To evaluate noncovalent interactions between phenyl groups in these transition states, we utilized

independent gradient model approach (IGM-δg).[283] Three-dimensional (3D) IGM isosurfaces representing non-covalent interactions were constructed (Figure 42, A, B). These isosurfaces are color-coded with green and blue demonstrating van der Waals and strong attraction, respectively and yellow and red – weak and strong repulsion, respectively. IGM 3D plot revealed green isosurface between coplanar phenyl rings in (**TS-283**) confirming the presence of stabilizing non-covalent interaction. Similar green isosurface was found in (**TS-289**) albeit with smaller area. We also analyzed IGM 2D-signature plots produced for each transition state (Figure 42, C, D). Both plots contained two spikes in Van der Waals region at positive and negative λ_2 values. In this method, positive λ_2 region represents repulsive interactions, whereas negative -attractive ones.[283] Analysis of each plot showed that the peak in the negative region is more pronounced, however larger attractive part was calculated for (**TS-283**).

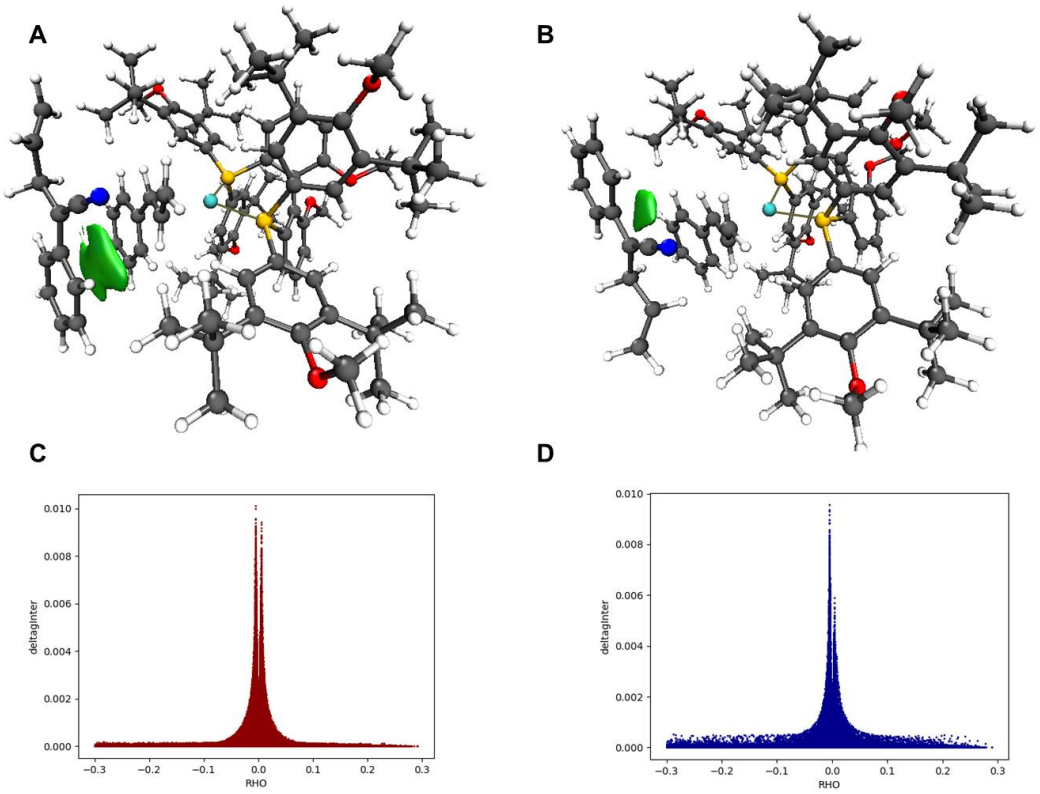

Figure 42. IGM isosurfaces (IGM- δg^{inter}, isovalue 0.004): A - (**TS-283**); B - (**TS-289**) and IGM 2D-signature plots: C - (**TS-283**) (attractive part 1.0107^{-2} a.u.); D - (**TS-289**) (attractive part 9.5506^{-3} a.u.).

The possibility of competing concerted [3,3]-process was considered; however, (**282**)/(**288**) do not have the necessary orbital overlap and no [3,3]-transition state could be located. The dissociative nature of the transformation is exemplified by HOMO and LUMO coefficients in (**TS-283**) (Figure 43). There is a significant backdonation from Pd atom (in HOMO) into π*-orbital of the bound alkene (in LUMO), while the major contribution to the σ*-orbital of the C-N bond (in LUMO) comes from the alkyne (in HOMO). At the same time, LUMO coefficients show the formation of the cationic π-allyl complex as LUMO of the Pd-bound alkene contains one node. Therefore, this is a mechanistically distinct mode of reactivity compared to the [3,3]-process observed with BINAP.[196]

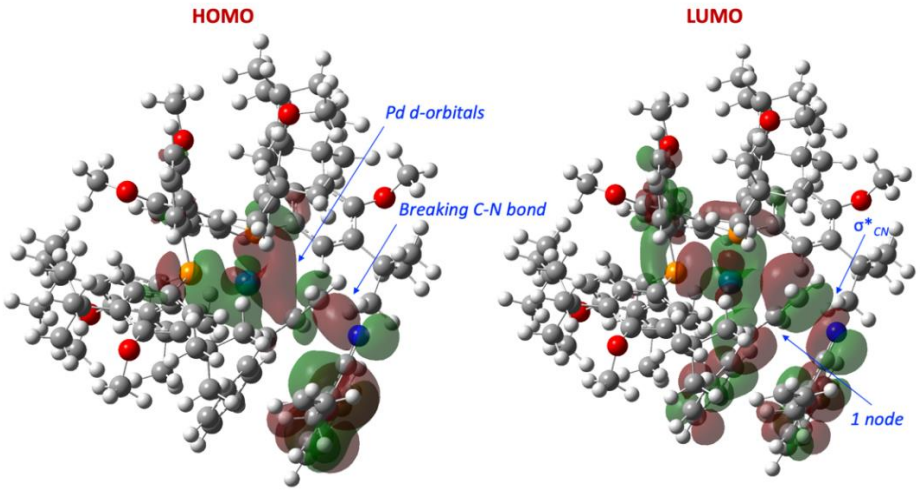

Figure 43. Calculated molecular orbitals for (**TS-283**).

The dihedral angle between the allylic termini and the phosphines can be used to highlight the conformational changes required between C-N bond breaking and C-C bond formation (Figure 41). Following ionization, the two reaction pathways diverge for C-C bond formation. In the major pathway, ion-pair (**284**) (5.9°) undergoes a reorganisation of the ligand, rotating the π-allyl group within the cleft. Initially, intermediate (**285**) (-12.3°) is formed, which is in the reactive conformation for C-C bond formation *via* (**TS-286**) (-13.9°; +1.0 kcal/mol from (**285**)), to afford (**287**). In contrast, ion pair (**290**) (21.6°) is much further from the reactive conformation for C–C bond formation, requiring rotation through (**TS-291**) (0.7°; +1.4 kcal/mol from (**290**)). This produces shallow intermediate (**292**) (-13.1°) before proceeding directly into a C-C bond formation *via* (**TS-293**) (-14.2°; +0.1 kcal/mol from (**292**)). Despite the dipolar pathway, the ion pair does not fully dissociate or solvent separate, with the energetics suggesting a very rapid C–C bond formation following ionisation. Following (**TS-293**), the palladium bound rearranged nitrile (**294**) is formed. Finally, decomplexation of (**287**)/(**294**) and ligand exchange with (**280**) provides the requisite nitriles (**281**)/(**281**)**'**. These computations agree with the

experimental data and the diastereoselectivity is determined by the relative magnitudes (**TS-283**) of (**TS-289**). This model also explains the mesomeric effects observed experimentally with π-accepting groups lowering (**TS-283**)/(**TS-289**) allowing for higher levels of stereodiscrimination.

In conclusion, this study highlights the effect of sterically hindered DTBM-MeOBIPHEP ligand on the mechanism of ketenimine rearrangement. Unlike the concerted [3,3]-rearrangement described above, this reaction proceeds *via* a dipolar formal [3,3]-process which occurs entirely in a deep cleft within the catalyst. Ionization of C-N bond was found to be diastereodetermining step. Stereodiscrimination was attributed to an offset π-stacking interaction within lower energy transition state.[197,198]

Since (R)-DTBM-MeOBIPHEP and other ligands in this family are commercially available as single enantiomers and the reaction was shown to provide small enantiomeric excess (16% ee),[197] further studies can be aimed at elucidating the origin of enantioselectivity. In this case, computational data can be used for rational optimization of enantioselective conditions, while experimental determination of the absolute stereochemistry of the product would allow us to further refine computational model.

Conclusions and Future Work

We have developed computational models for the rearrangement of *N*-alloc-*N*-allyl ynamides to quaternary nitriles in highly complex auto-tandem catalytic systems, consisting of two previously unstudied reactions (Scheme 180). First catalytic cycle includes decarboxylative allylation of *N*-alloc-*N*-allyl ynamide to ketenimine with the key step proceeding through either stepwise decarboxylation/C-C formation *via* outer sphere nucleophile attack or previously unknown concomitant decarboxylation/C-C bond formation (Scheme 180). The second catalytic

cycle involves rearrangement of ketenimine to quaternary nitrile and can proceed through reversible oxidative ionization of the C-N bond with the subsequent inner-sphere mechanism or the Pd(0) catalyzed [3,3]-rearrangement.[196] Concerted transition states found in both cycles have not been previously reported and is of great significance. These models closely mirror the experimental data, provide valuable insight into these reactions, and have rationalized the reactivity observed. A major factor in these reaction pathways is the very dynamical nature of the catalyst systems with large degrees of conformational flexibility and a flat potential energy surface. In both catalytic cycles the mechanism is highly dependent on substrate electronics and ligand properties, which makes studying these processes even more challenging.

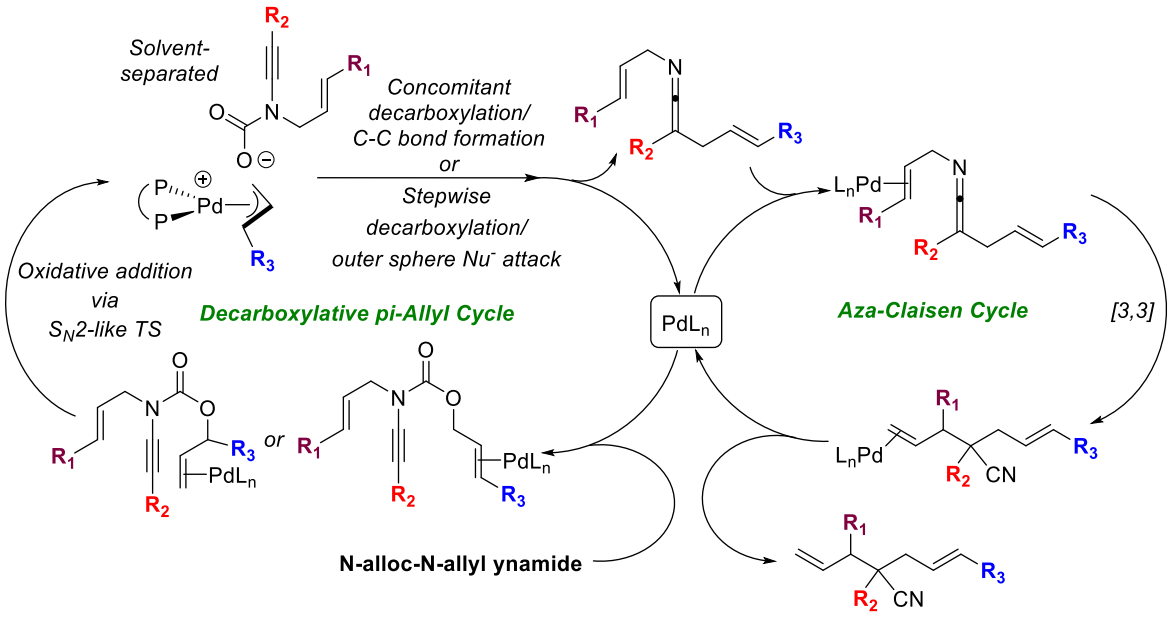

Scheme 180. Proposed auto-tandem catalytic cycle.

Computations suggest that both decarboxylative allylation and ketenimine rearrangement can occur without a catalyst and proceed *via* concerted transition states. This finding opens an

interesting avenue that can be explored experimentally as this uncatalyzed transformation should provide high regioselectivity in both reactions.

A remaining challenge in these studies is understanding the role of borane Lewis additive in this transformation. Computationally, we have found that borane coordinates to nitrogen in allyl ynamide anion, stabilizing the latter, and lowers the energy of transition state corresponding to outer-sphere nucleophile attack. On the one hand, this explains experimental results by Cook *et al.* showing that in the absence of borane substantial amounts of *N*-diallyl ynamide are formed.[200] On the other hand, this is not in agreement with the rate law established during kinetic studies in the Cook group (Shchepetkina V.I.) that demonstrated the reverse order in borane. This paradox can be rationalized when one considers the effect of borane coordination prior to the rate-determining step. Our results suggest that the borane is required to stabilize an ionic intermediate following the RDS, therefore would not be seen in the rate law, however it plays a crucial role in preventing decomposition and off-cycle pathways. Since calculations do not predict a strong binding to any other ynamide-derived species, further experimental studies are needed to address this problem. For example, to gain an insight into the connectivity between the phosphine ligand and intermediates in the catalytic cycle along the reaction coordinate, one could conduct 3D-NMR experiment to obtain correlations between ^{1}H, ^{31}P and ^{13}C, ^{15}N or ^{11}B. Additionally, it could be possible to synthesize, isolate and study the reactivity of proposed Pd-intermediates defining thermodynamic and kinetic parameters.

The further efforts in this area can be directed at building predictive models using correlation between ligand parameters and reaction yield and selectivity. The major challenge in this case is collecting large experimental datasets due to multistep starting material synthesis. A

robust method for rapid and quantitative evaluation of reaction outcome needs to be developed as well. Change in the mechanism and reaction outcome with the change in substrate is another challenge as it might be impossible to extrapolate the results across the reaction scope.

Computational Details

Decarboxylative allylation and Ketenimine Rearrangement

To explore the possible mechanistic pathways, we applied the two-layered QM/SE ONIOM method to palladium complexes.[241,246,268] In this model, the substrate and the Lewis acid as well as palladium and phosphorous atoms of the catalyst were included in the high layer, whereas BINAP was placed in the low layer. The high level was treated with DFT using local meta-generalized gradient approximation functional M06L highly recommended for transition-metal chemistry calculations.[188] The 6-31G+(d) basis set was used for C, H, P, B, and O atoms in conjunction with the LANL2DZ relativistic pseudopotential for Pd (BSI). The low level was handled with semi-empirical method PM6. Given the bulky nature of the ligand, this two-layered ONIOM model allowed us to perform geometry optimization of palladium complexes within the reasonable timescale. In non-catalyzed pathways, the structures of organic compounds were fully optimized using DFT at M06L/BSI level. The nature of stationary points in each case was confirmed by harmonic frequency calculations.

To get refined energies, we further performed single point (SP) energy calculations using the ONIOM geometries. The palladium complexes were fully treated by DFT. The larger basis set 6-311++G(2d,2p) for C, H, P, B, and O atoms and LANL2DZ ECP for Pd (BSII) and M06L functional were employed. The single point solvation by toluene was accounted by using

conductor-like polarizable continuum model (C-PCM).[184,185] The calculations were performed with the Gaussian 16.0 software.[174] The corrected single point energy was calculated as follows:

$$G_{SP\ Corrected}=E_{elec}[(C\text{-}PCM)|M06L|BSII]+G_{Corr\ ONIOM}[ONIOM(M06L|BSI{:}PM6)],$$

where $G_{corr\ ONIOM}$ is the thermal correction to Gibbs free energy obtained in the gas phase at ONIOM(M06L|BSI:PM6) or M06L|BSI.

To locate the transition states we performed numerous relaxed scans of potential energy surface or utilized nudged elastic band method implemented in ORCA 4.2.1 software.[274,275] In second case, calculations were done at M06L level with def2-SV(P) basis set. The TS structures of palladium complexes were further reoptimized with ONIOM model in Gaussian 16.0 as described above. The nature of located TSs was confirmed by unique imaginary vibrational mode and IRC calculations.

The optimized structures were visualized using CYLview 1.0b.[175] The molecular orbitals were generated and rendered in GaussView 6.0.16.[176] Topographic map was generated in SambVca 2.1.[272]

To account for conformational flexibility of the studied substrates, the PES for (**254**) and (**274**) was explored by mixed torsional/low mode method (MTLMOD) in OPLS_2005 force field implemented in MacroModel.[284] The generated large conformer set was reduced to 25 unique lowest energy structures that were further optimized by PM6 method in Gaussian 16.0. Redundant conformers were eliminated, and 10 lowest energy structures were optimized using DFT at M06L/BSI level. The lowest energy structure was taken and additional scan of allyl group position relative to allene system was performed to account for energy change while adopting reactive conformation. Both *endo*- and *exo*- final arrangements were considered. Based

on the major conformers of (**254**) and (**274**) found during the scan, further calculations (geometries, vibrations and single-point energies) were performed on the analogous conformations of Pd-complexes (**254A**) and (**274A**). In the case of (**254C**), the C-C-Pd-P dihedral angle was rotated, and individual conformers of the allyl group calculated in the same manner as above.[196]

Energies and lowest frequencies of minimum energy structures for decarboxylative allylation of (**247**) are shown in Table 27.

Structure	$E_{elec\ ONIOM}$, Ha	$G_{corr\ ONIOM}$, Ha	$G_{SP\ corrected}$ [b], Ha	Lowest freq.	# of imaginary freq.
		Uncatalyzed pathway			
247	-785.633286	0.214176	-785.633583	21.31	0
247 TS	-785.57073	0.210445	-785.787791	-365.66	1
		Catalyzed pathway			
247A	-1598.479434	0.744503	-3290.900741	4.27	0
247A TS	-1598.451157	0.745019	-3290.885476	-87.81	1
247B	-1598.480690	0.745942	-3290.914177	3.88	0
247B TS	-1598.449872	0.740891	-3290.901031	-56.88	1
247C	-1598.479317	0.745740	-3290.908759	7.03	0
247Bs TS	-1598.453896	0.746485	-3290.884224	-360.34	1
247D	-1409.871949	0.735634	-3102.257275	6.63	0
247D'	-1409.864200	0.732873	-3102.263727	9.24	0
247D' TS	-1409.862100	0.733901	-3102.258899	-41.45	1
247En	-1409.877708	0.734131	-3102.277147	7.25	0
247En'	-1409.876658	0.736902	-3102.264309	3.93	0
247En TS	-1409.873115	0.736060	-3102.261582	-246.55	1
247En' TS	-1409.856972	0.738359	-3102.234177	-114.78	1
247En'' TS	-1409.852794	0.737657	-3102.237840	-139.59	1
247Ec	-1409.895133	0.737046	-3102.283383	6.59	0
247Ec'	-1409.894133	0.737262	-3102.270109	13.85	0
247Ec' TS	-1409.862903	0.737123	-3102.247214	-464.07	1
247F	-1409.913234	0.734474	-3102.295068	6.37	0
247F TS	-1409.863245	0.731680	-3102.256255	-70.77	1
247G	-1409.946965	0.736536	-3102.318803	7.77	0
254	-597.097631	0.204479	-597.055871	29.17	0
BINAP-Pd	-812.724642	0.506333	-2505.255011	7.24	1
CO_2	-188.581590	-0.008881	-188.644576	664.19	0

Table 27. Energies and lowest frequencies of minimum energy structures for decarboxylative allylation of (**247**). [a] Energy values calculated at C-PCM(Toluene)-M06L/BSII//[ONIOM(M06L/BSI:PM6)], where BSI = 6-31+G(d) (C, H, P, B, O)/LANL2DZ (ECP Pd) and BSII = 6-311++G(2d,2p) (C, H, P, B, O)/LANL2DZ (ECP Pd). Thermal corrections at 298.15 K. [b] Solvent-corrected free energy given by $G_{\text{SP corrected}}$ [(C-PCM)/M06L/BSII] = E_{elec}[(C-PCM)/M06L/BSII] + $G_{\text{corr ONIOM}}$ [ONIOM(M06L/BSI:PM6)], where $G_{\text{corr ONIOM}}$ is the thermal correction to Gibbs free energy obtained in the gas phase at ONIOM(M06L/BSI:PM6) or M06L/BSI.

Scheme 181 provides a graphical guide to numbered compounds for decarboxylative allylation of (**247**).

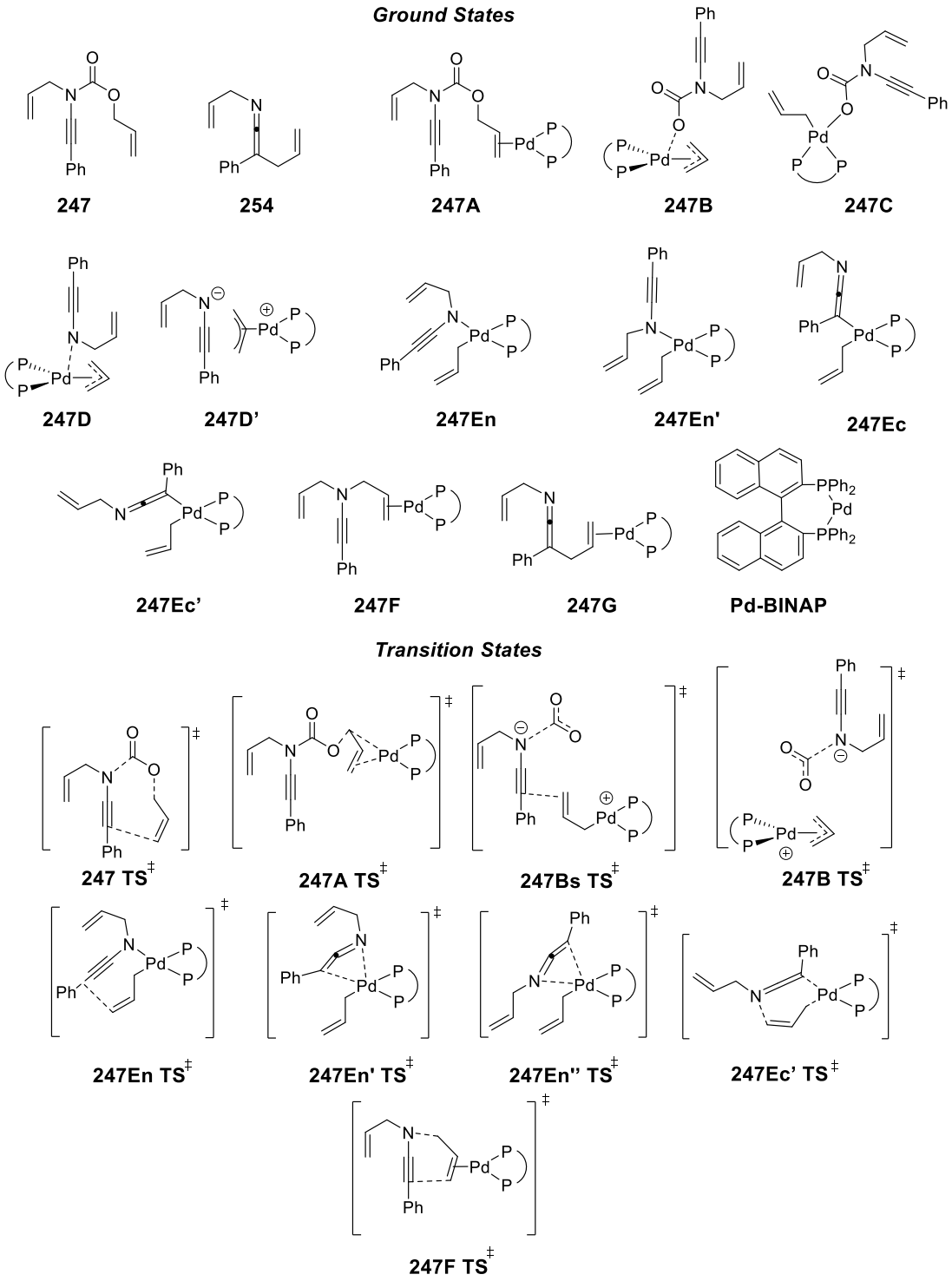

Scheme 181. Graphical guide to numbered compounds for decarboxylative allylation of (**247**).

Energies and lowest frequencies of minimum energy structures for decarboxylative allylation of (**249**) are shown in Table 28.

Structure	$E_{elec\ ONIOM}$, Ha	$G_{corr\ ONIOM}$, Ha	$G_{SP\ corrected}$ [b], Ha	Lowest freq.	# of imaginary freq.
249	-1084.082498	0.376275	-1084.020291	7.39	0
249A	-1896.932989	0.912117	-3589.291412	3.25	0
249A TS	-1896.907098	0.911641	-3589.273956	-118.55	1
249B	-1896.928211	0.918485	-3589.301069	7.51	0
249B-O TS	-1896.891700	0.908798	-3589.275349	-122.61 -8.83	2
249B-N TS	-1896.908447	0.910283	-3589.294064	-126.22	1
249Bs TS	-1896.898277	0.915510	-3589.263049	-407.18	1
249D	-1708.332976	0.907238	-3400.653555	12.06	0
249D'	-1708.336977	0.904899	-3400.665477	6.53	0
249D' TS	-1708.334075	0.904294	-3400.659794	-239.05	1
249G	-1708.391319	0.902736	-3400.702529	5.57	0
250	-668.428415	0.144481	-668.504042	28.58	0
251	-966.888078	0.312247	-966.889559	12.46	0
252	-479.825049	0.133653	-479.859899	24.99	0
253	-778.305713	0.301860	-778.263591	17.99	0
BEt_2OMe	-298.437332	0.144383	-298.394294	57.67	0

Table 28. Energies and lowest frequencies of minimum energy structures for decarboxylative allylation of (**249**) and other borane adducts. [a] Energy values calculated at C-PCM(Toluene)-M06L/BSII//[ONIOM(M06L/BSI:PM6)], where BSI = 6-31+G(d) (C, H, P, B, O)/LANL2DZ (ECP Pd) and BSII = 6-311++G(2d,2p) (C, H, P, B, O)/LANL2DZ (ECP Pd). Thermal corrections at 298.15 K. [b] Solvent-corrected free energy given by $G_{SP\ corrected}$ [(C-PCM)/M06L/BSII] = E_{elec}[(C-PCM)/M06L/BSII] + $G_{corr\ ONIOM}$ [ONIOM(M06L/BSI:PM6)], where $G_{corr\ ONIOM}$ is the thermal correction to Gibbs free energy obtained in the gas phase at ONIOM(M06L/BSI:PM6) or M06L/BSI.

Scheme 182 provides a graphical guide to numbered compounds for decarboxylative allylation of (**249**) and other borane adducts.

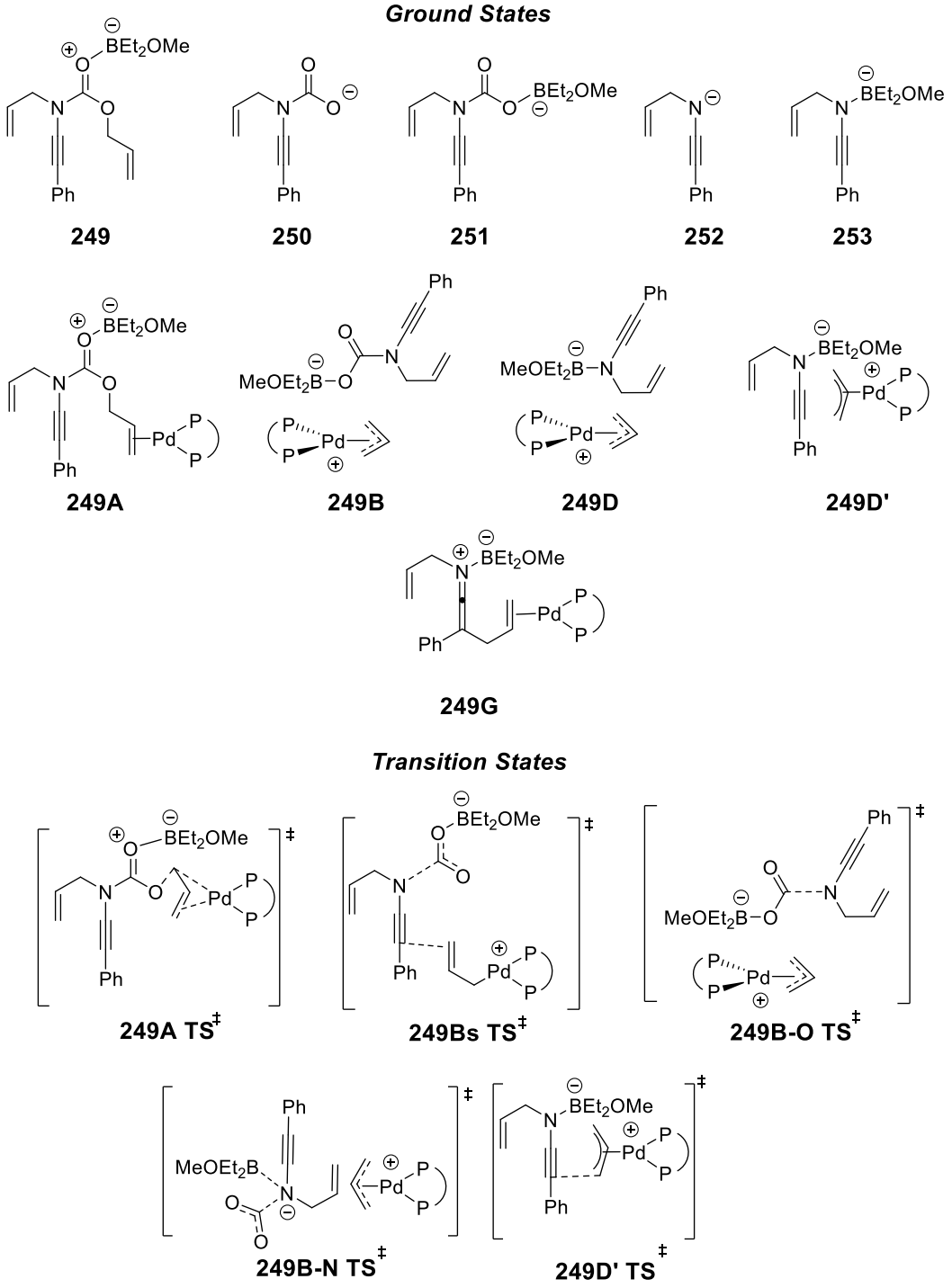

Scheme 182. Graphical guide to numbered compounds for decarboxylative allylation of (**249**) and other borane adducts.

Energies and lowest frequencies of minimum energy structures for decarboxylative allylation of (**255**) are shown in Table 29.

Structure	$E_{elec\ ONIOM}$, Ha	$G_{corr\ ONIOM}$, Ha	$G_{SP\ corrected}$ [b], Ha	Lowest freq.	# of imaginary freq.
255	-711.829822	0.245186	-711.794070	12.06	0
255A	-1524.675611	0.776136	-3217.059883	3.71	0
255A TS	-1524.640910	0.773521	-3217.049568	-26.33	1
255B	-1524.671860	0.777728	-3217.072031	8.57	0
255B TS	-1524.633394	0.771492	-3217.040339	-16.96	1
255Bs TS	-1524.651514	0.777518	-3217.044713	-337.06	1

Table 29. Energies and lowest frequencies of minimum energy structures for decarboxylative allylation of (**255**). [a] Energy values calculated at C-PCM(Toluene)-M06L/BSII//[ONIOM(M06L/BSI:PM6)], where BSI = 6-31+G(d) (C, H, P, B, O)/LANL2DZ (ECP Pd) and BSII = 6-311++G(2d,2p) (C, H, P, B, O)/LANL2DZ (ECP Pd). Thermal corrections at 298.15 K. [b] Solvent-corrected free energy given by $G_{SP\ corrected}$ [(C-PCM)/M06L/BSII] = E_{elec}[(C-PCM)/M06L/BSII] + $G_{corr\ ONIOM}$ [ONIOM(M06L/BSI:PM6)], where $G_{corr\ ONIOM}$ is the thermal correction to Gibbs free energy obtained in the gas phase at ONIOM(M06L/BSI:PM6) or M06L/BSI.

Scheme 183 provides a graphical guide to numbered compounds for decarboxylative allylation of (**255**).

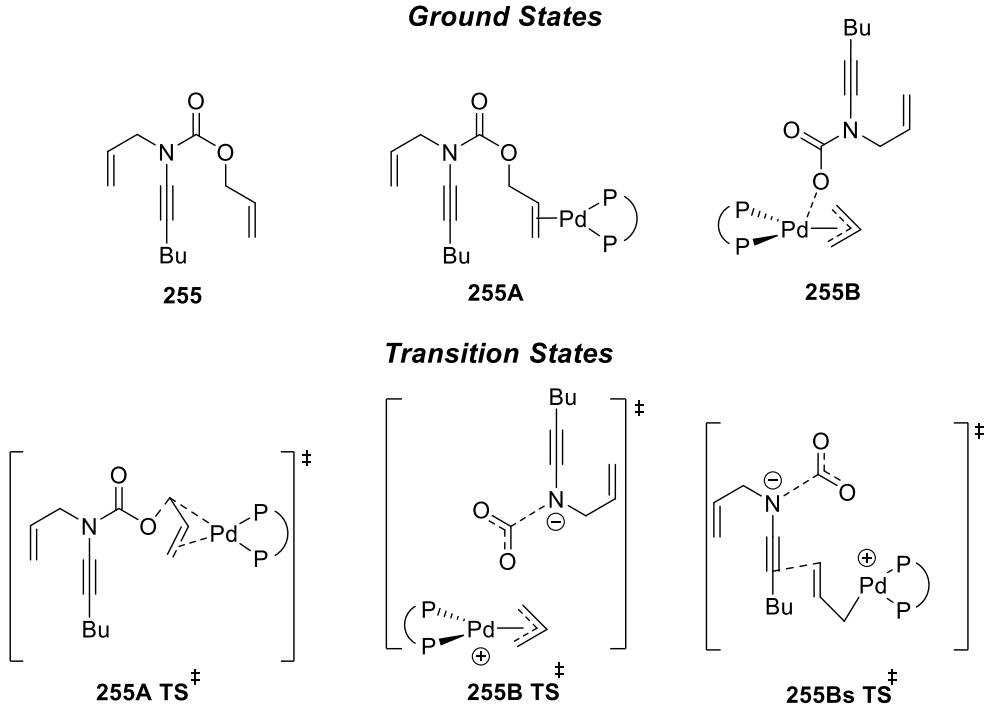

Scheme 183. Graphical guide to numbered compounds for decarboxylative allylation of (**255**).

Energies and lowest frequencies of minimum energy structures for decarboxylative allylation of (**256**) with BINAP as ligand are shown in Table 30.

Structure	E $_{elec\ ONIOM}$, Ha	G $_{corr\ ONIOM}$, Ha	G $_{SP\ corrected}$ [b], Ha	Lowest freq.	# of imaginary freq.
256	-1016.668052	0.287407	-1016.649939	13.12	0
256A	-1829.512576	0.818085	-3521.927606	3.95	0
256A TS	-1829.489841	0.820724	-3521.910136	-186.89	1
256B	-1829.517884	0.823640	-3521.933231	10.77	0
256B'	-1829.518319	0.822134	-3521.928973	8.40	0
256B TS	-1829.489767	0.816091	-3521.903941	-66.02	1
256Bsl TS	-1829.494835	0.823376	-3521.905727	-394.43	1
256Bsb TS	-1829.492384	0.821949	-3521.905452	-473.54	1

Table 30. Energies and lowest frequencies of minimum energy structures for decarboxylative allylation of (**256**) with BINAP as ligand. [a] Energy values calculated at C-PCM(Toluene)-M06L/BSII//[ONIOM(M06L/BSI:PM6)], where BSI = 6-31+G(d) (C, H, P, B, O)/LANL2DZ (ECP Pd) and BSII = 6-311++G(2d,2p) (C, H, P, B, O)/LANL2DZ (ECP Pd). Thermal corrections at 298.15 K. [b] Solvent-corrected free energy given by G $_{SP\ corrected}$ [(C-PCM)/M06L/BSII] = E_{elec}[(C-PCM)/M06L/BSII] + G $_{corr\ ONIOM}$ [ONIOM(M06L/BSI:PM6)],

where $G_{corr\ ONIOM}$ is the thermal correction to Gibbs free energy obtained in the gas phase at ONIOM(M06L/BSI:PM6) or M06L/BSI.

Energies and lowest frequencies of minimum energy structures for decarboxylative allylation of (**256**) with xantphos as ligand are shown in Table 31.

Structure	$E_{elec\ ONIOM}$, Ha	$G_{corr\ ONIOM}$, Ha	$G_{SP\ corrected}$ [b], Ha	Lowest freq.	# of imaginary freq.
256	-1016.668052	0.287407	-1016.649939	13.12	0
256A-X1	-1829.648998	0.792733	-3406.601841	5.35	0
256A TS-X1	-1829.622929	0.791753	-3406.589921	-58.62	1
256B-X1	-1829.647320	0.796373	-3406.593708	5.28	0
256Bsl-X1	-1829.652205	0.797346	-3406.588569	8.41	0
256Bsb-X1	-1829.653853	0.797891	-3406.585331	3.61	0
256B TS-X1	-1829.624283	0.793670	-3406.575056	-94.81	1
256Bsl TS-X1	-1829.615444	0.798290	-3406.549364	-422.74	1
256Bsb TS-X1	-1829.623950	0.795176	-3406.568512	-456.35	1
256A-X2	-1829.651059	0.792709	-3406.610591	6.96	0
256A TS-X2	-1829.618274	0.793443	-3406.585114	-68.90	1
256B-X2	-1829.643687	0.798451	-3406.608990	8.97	0
256Bsl-X2	-1829.648151	0.795330	-3406.610945	9.49	0
256Bsb-X2	-1829.643687	0.798422	-3406.609026	9.01	0
256B TS-X2	-1829.619846	0.786508	-3406.586951	-193.94	1
256Bsl TS-X2	-1829,625129	0.790334	-3406.593882	-256.96	1
256Bsb TS-X2	-1829.628665	0.796978	-3406.585516	-424.34	1
Xantphos-Pd	-812.960597	0.478660	-2389.923617	7.15	0

Table 31. Energies and lowest frequencies of minimum energy structures for decarboxylative allylation of (**256**) with xantphos as ligand.[a] Energy values calculated at C-PCM(Toluene)-M06L/BSII//[ONIOM(M06L/BSI:PM6)], where BSI = 6-31+G(d) (C, H, P, B, O)/LANL2DZ (ECP Pd) and BSII = 6-311++G(2d,2p) (C, H, P, B, O)/LANL2DZ (ECP Pd). Thermal corrections at 298.15 K. [b] Solvent-corrected free energy given by $G_{SP\ corrected}$ [(C-PCM)/M06L/BSII] = E_{elec}[(C-PCM)/M06L/BSII] + $G_{corr\ ONIOM}$ [ONIOM(M06L/BSI:PM6)], where $G_{corr\ ONIOM}$ is the thermal correction to Gibbs free energy obtained in the gas phase at ONIOM(M06L/BSI:PM6) or M06L/BSI.

Energies and lowest frequencies of minimum energy structures for decarboxylative allylation of (**256**) with dppe as ligand are shown in Table 32.

Structure	$E_{elec\ ONIOM}$, Ha	$G_{corr\ ONIOM}$, Ha	$G_{SP\ corrected}$ [b], Ha	Lowest freq.	# of imaginary freq.
256	-1016.668052	0.287407	-1016.649939	13.12	0
256A-D	-1829.670579	0.642393	-2831.245652	5.65	0
256A TS-D	-1829.647127	0.647609	-2831.224477	-144.66	1
256B-D	-1829.676797	0.648916	-2831.238759	11.36	0
256Bsl-D	-1829.682389	0.647203	-2831.259166	6.96	0
256Bsb-D	-1829,67892	0,64621	-2831,248002	7.64	0
256B TS-D	-1829.651254	0.641050	-2831.235151	-82.67	1
256Bsl TS-D	-1829.650302	0.645191	-2831.228627	-419.07	1
256Bsb TS-D	-1829.655278	0.646390	-2831.232527	-455.50	1
Dppe-Pd	-812.973626	0.333402	-1814.569814	9.10	0

Table 32. Energies and lowest frequencies of minimum energy structures for decarboxylative allylation of (**256**) with dppe as ligand. [a] Energy values calculated at C-PCM(Toluene)-M06L/BSII//[ONIOM(M06L/BSI:PM6)], where BSI = 6-31+G(d) (C, H, P, B, O)/LANL2DZ (ECP Pd) and BSII = 6-311++G(2d,2p) (C, H, P, B, O)/LANL2DZ (ECP Pd). Thermal corrections at 298.15 K. [b] Solvent-corrected free energy given by $G_{SP\ corrected}$ [(C-PCM)/M06L/BSII] = E_{elec}[(C-PCM)/M06L/BSII] + $G_{corr\ ONIOM}$ [ONIOM(M06L/BSI:PM6)], where $G_{corr\ ONIOM}$ is the thermal correction to Gibbs free energy obtained in the gas phase at ONIOM(M06L/BSI:PM6) or M06L/BSI.

Scheme 184 provides a graphical guide to numbered compounds for decarboxylative allylation of (**256**) with BINAP, dppe and xantphos as ligands.

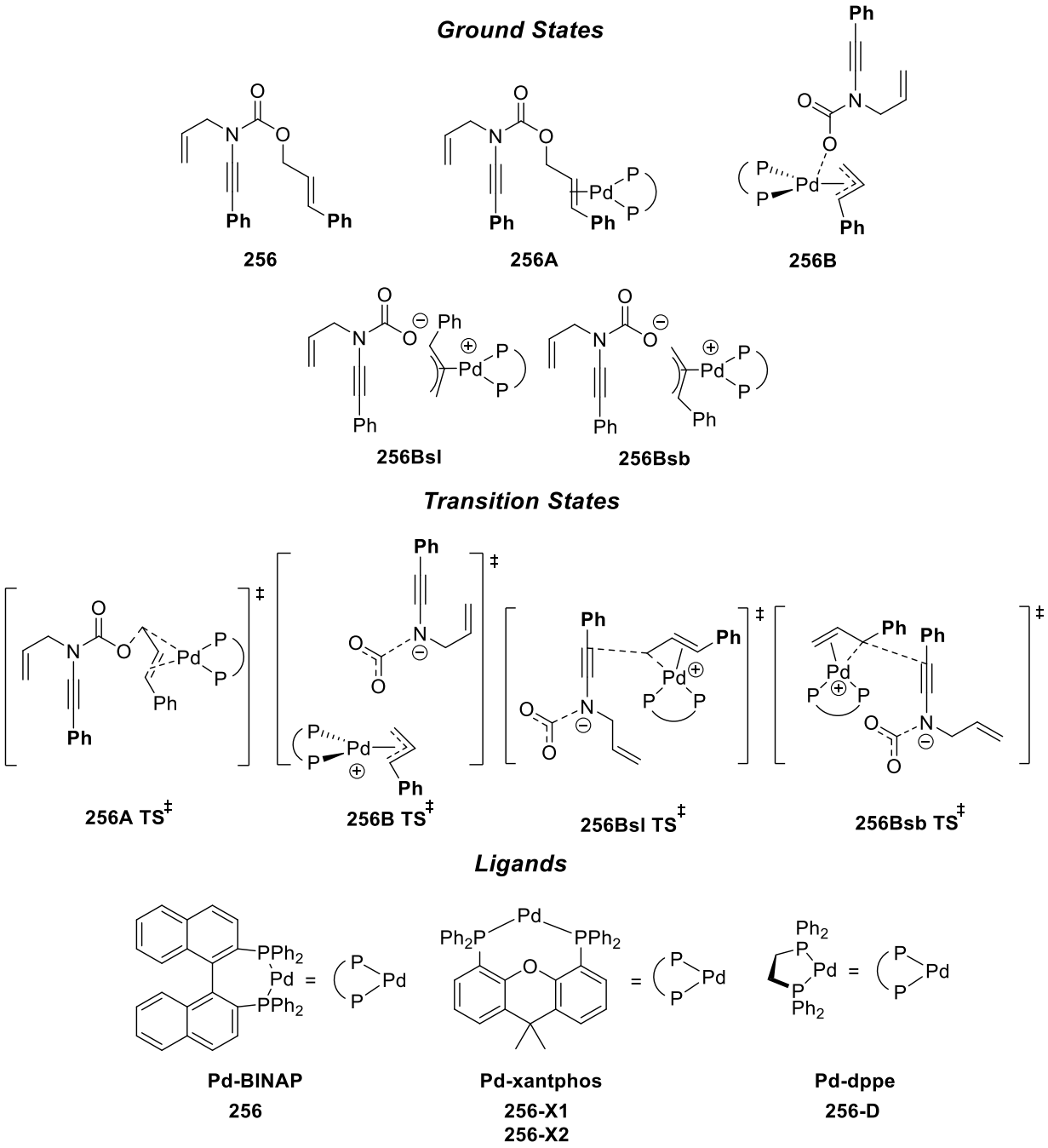

Scheme 184. Graphical guide to numbered compounds for decarboxylative allylation of (**256**) with BINAP, dppe and xantphos as ligands.

Energies and lowest frequencies of minimum energy structures for ketenimine (**254**) rearrangement are shown in Table 33.

Structure	$E_{elec\ ONIOM}$, Ha	$G_{corr\ ONIOM}$, Ha	$G_{SP\ corrected}$ [b], Ha	Lowest freq.	# of imaginary freq.
		Uncatalyzed Pathway			
269	-597.131559	0.206632	-597.088263	32.39	0
254-1	-597.097631	0.204479	-597.055871	29.17	0
254-2	-597.098277	0.204460	-597.056708	28.81	0
254-3	-597.098911	0.204120	-597.057488	23.96	0
254-4	-597.098025	0.203889	-597.056431	20.25	0
254-5	-597.099121	0.204802	-597.056929	28.17	0
254-6	-597.099166	0.204657	-597.056973	29.73	0
254 TS-[3,3]-endo	-597.070457	0.205292	-597.028229	-280.60	1
254 TS-[3,3]-exo	-597.068843	0.204487	-597.028177	-262.18	1
		Catalyzed Pathway			
254A-a	-1409.944866	0.735400	-3102.321464	6.14	0
254A-b	-1409.946731	0.735471	-3102.322940	6.18	0
254A-c	-1409.946833	0.734862	-3102.329274	7.02	0
254A-d	-1409.945806	0.736429	-3102.321001	7.36	0
254A-e	-1409.947730	0.735388	-3102.323220	6.14	0
254A-f	-1409.723396	0.737561	-3102.329518	7.29	0
254B	-1409.929229	0.735097	-3102.325274	11.10	0
254C-a	-1409.931390	0.734273	-3102.323829	5.27	0
254C-b	-1409.929545	0.737813	-3102.316965	7.05	0
254C'	-1409.929498	0.737523	-3102.319931	3.73	0
254C-d	-1409.928457	0.734138	-3102.317060	5.94	0
254C-e	-1409.927355	0.737296	-3102.314795	6.76	0
254C-f	-1409.929140	0.738485	-3102.320269	6.50	0
254D	-1409.975412	0.738592	-3102.353239	9.02	0
254 TS-[3,3]-Pd-endo	-1409.908367	0.730950	-3103.038294	-101.56	1
254 TS-ION-endo	-1409.916177	0.732929	-3102.311387	-118.92	1
254 TS-ION-exo	-1409.915342	0.733694	-3102.305103	-189.60	1
254 TS-IS-endo	-1409.920071	0.736669	-3102.304373	-455.55	1
254 TS-IS-exo	-1409.919520	0.736951	-3102.299609	-429.76	1
254 TS-10	-1409.915574	0.732746	-3102.311253	-50.68	1
254 TS-20	-1409.914074	0.732911	-3102.310705	-30.57	1
254 TS-30	-1409.911617	0.732591	-3102.309297	-70.54	1
254 TS-50	-1409.904740	0.730751	-3102.303631	-99.36	1
254 TS-75	-1409.896916	0.733174	-3102.291702	-131.55	2

254 TS-90	-1409.897388	0.733867	-3102.291273	-62.63 -132.05 -47.09	2

Table 33. Energies and lowest frequencies of minimum energy structures for ketenimine (**254**) rearrangement. [a] Energy values calculated at C-PCM(Toluene)-M06L/BSII//[ONIOM(M06L/BSI:PM6)], where BSI = 6-31+G(d) (C, H, P, B, O)/LANL2DZ (ECP Pd) and BSII = 6-311++G(2d,2p) (C, H, P, B, O)/LANL2DZ (ECP Pd). Thermal corrections at 298.15 K. [b] Solvent-corrected free energy given by $G_{\text{SP corrected}}$ [(C-PCM)/M06L/BSII] = E_{elec}[(C-PCM)/M06L/BSII] + $G_{\text{corr ONIOM}}$ [ONIOM(M06L/BSI:PM6)], where $G_{\text{corr ONIOM}}$ is the thermal correction to Gibbs free energy obtained in the gas phase at ONIOM(M06L/BSI:PM6) or M06L/BSI.

Scheme 185 show graphical guide to numbered compounds for ketenimine (**254**) rearrangement. Schemes 186 and 187 show conformational analysis for ketenimine (**254**), complexes (**254A**) and (**254C**) and transition states.

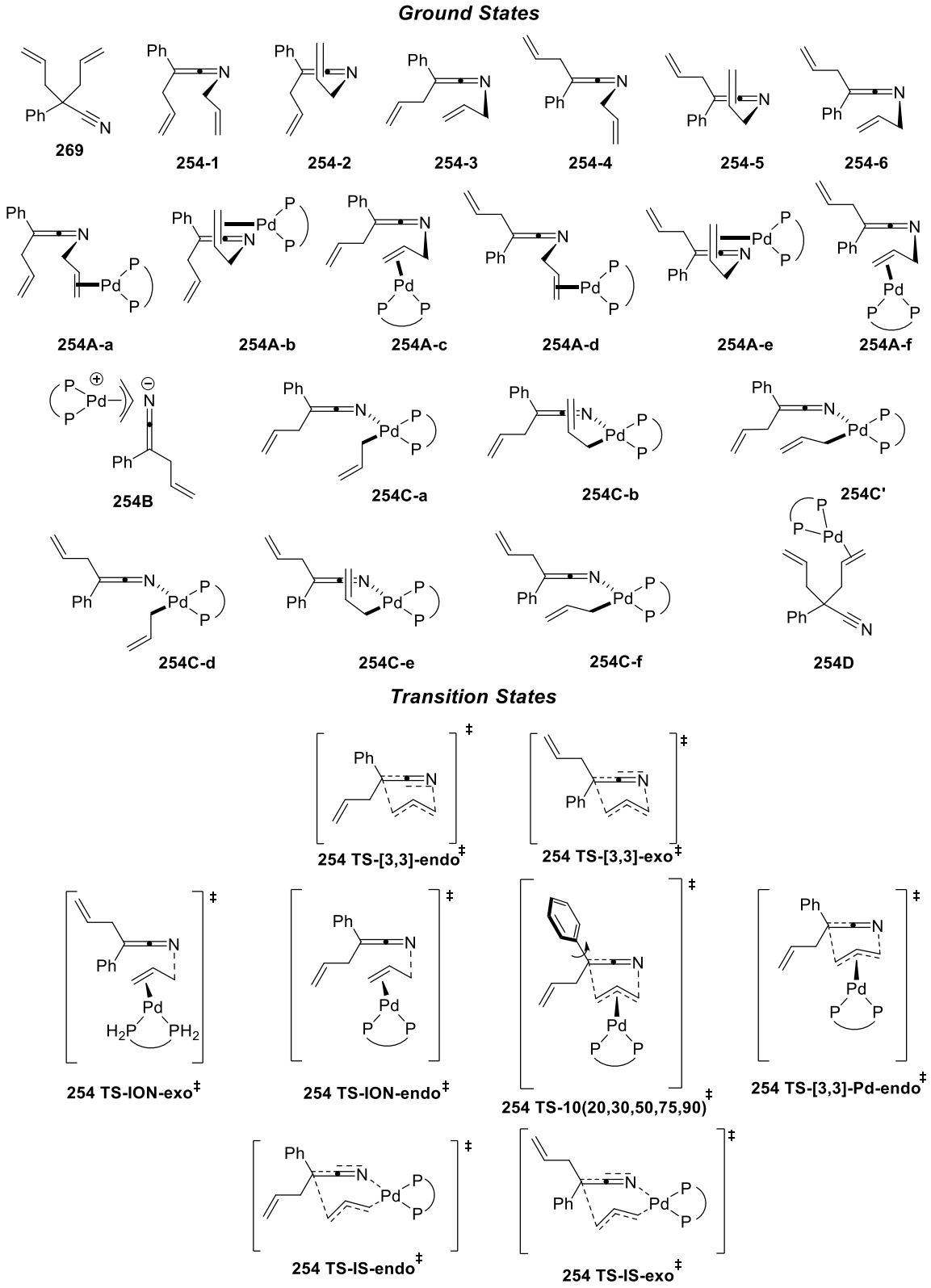

Scheme 185. Graphical guide to numbered compounds for ketenimine (**254**) rearrangement.

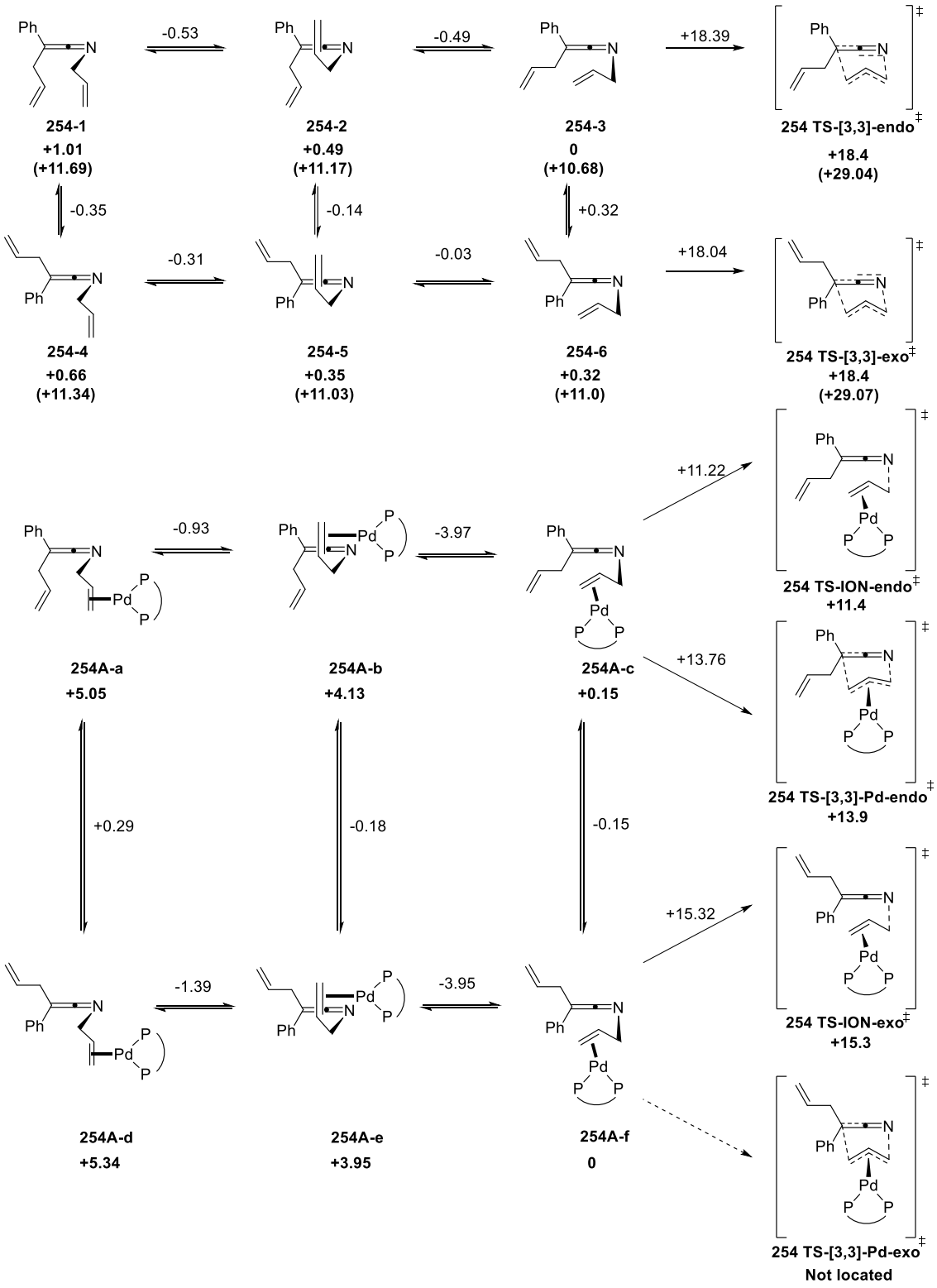

Scheme 186. Conformational analysis for ketenimine (**254**), complex (**254A**) and transition states.

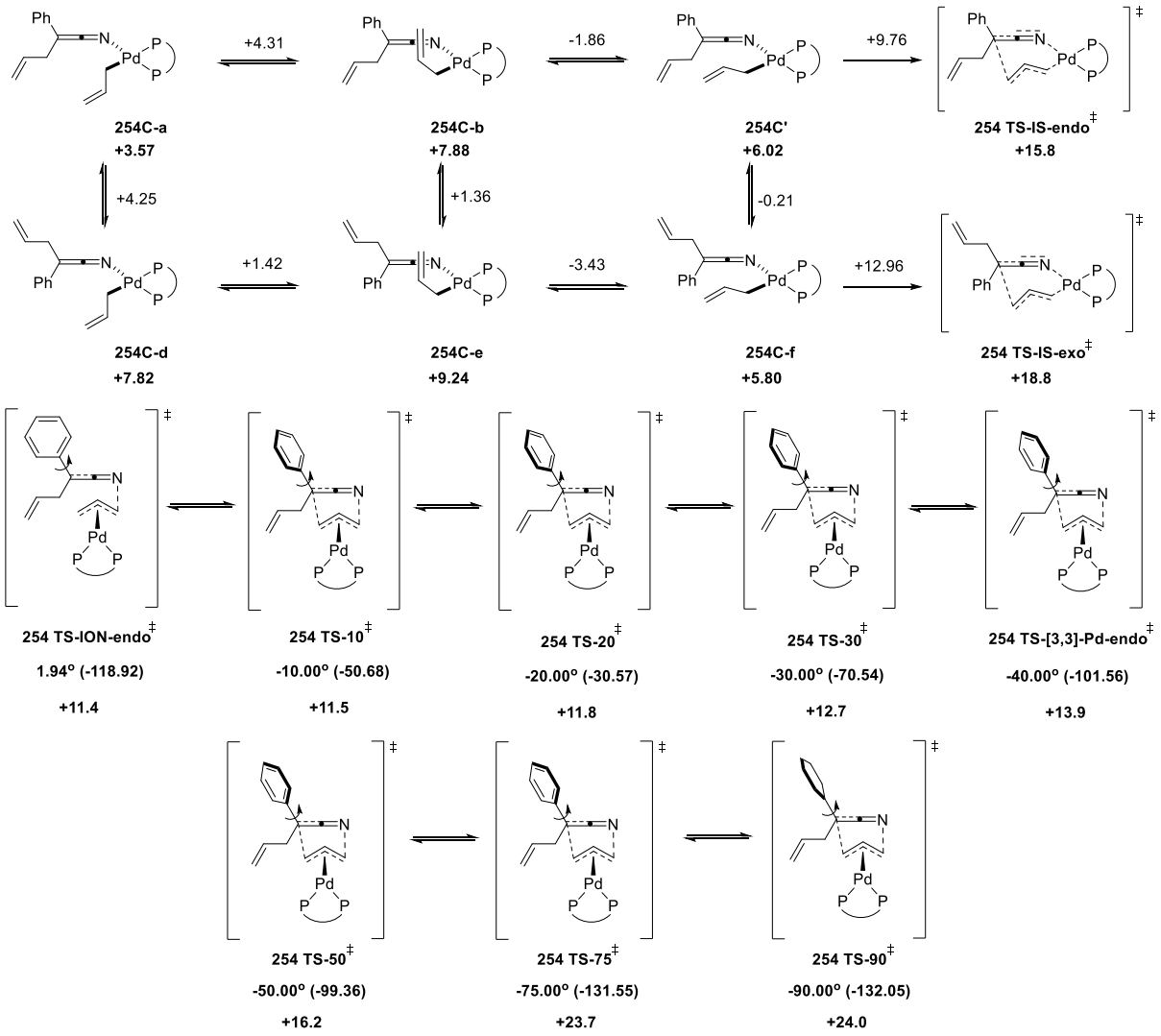

Scheme 187. Conformational analysis for complex (**254C**) and (**254 TS-[3,3]-Pd-endo**).

Energies and lowest frequencies of minimum energy structures for borane-bound ketenimine (**270**) rearrangement are shown in Table 34.

Structure	$E_{elec\ ONIOM}$, Ha	$G_{corr\ ONIOM}$, Ha	$G_{SP\ corrected}$ [b], Ha	Lowest freq.	# of imaginary freq.
		Uncatalyzed Pathway			
270	-895.550382	0.367538	-895.444859	7.54	0
271	-895.581625	0.370351	-895.473067	17.47	0
270 TS-[3,3]-B-endo	-895.518741	0.368895	-895.41262	-257.54	1
272	-479.881263	0.136139	-479.913279	38.55	0
273	-778.350649	0.302616	-778.307533	16.62	
		Catalyzed Pathway			
270A	-1708.105368	0.906577	-3400.708097	5.67	0
270B	-1708.372789	0.902837	-3400.711364	6.82	0
270C	-1708.385670	0.903148	-3400.713429	10.78	0
270D	-1708.419465	0.899790	-3400.735201	3.20	0
270 TS-ION-B	-1708.364045	0.903695	-3400.688532	-229.95	1
270 TS-OS	-1708.372682	0.903529	-3400.707966	-94.60	1
270 TS-IS-B-endo	-1708.371192	0.905459	-3400.694542	-464.09	1

Table 34. Energies and lowest frequencies of minimum energy structures for borane-bound ketenimine (**270**) rearrangement. [a] Energy values calculated at C-PCM(Toluene)-M06L/BSII//[ONIOM(M06L/BSI:PM6)], where BSI = 6-31+G(d) (C, H, P, B, O)/LANL2DZ (ECP Pd) and BSII = 6-311++G(2d,2p) (C, H, P, B, O)/LANL2DZ (ECP Pd). Thermal corrections at 298.15 K. [b] Solvent-corrected free energy given by $G_{SP\ corrected}$ [(C-PCM)/M06L/BSII] = E_{elec}[(C-PCM)/M06L/BSII] + $G_{corr\ ONIOM}$ [ONIOM(M06L/BSI:PM6)], where $G_{corr\ ONIOM}$ is the thermal correction to Gibbs free energy obtained in the gas phase at ONIOM(M06L/BSI:PM6) or M06L/BSI.

Scheme 188 shows graphical guide to numbered compounds for borane-bound ketenimine (**270**) rearrangement.

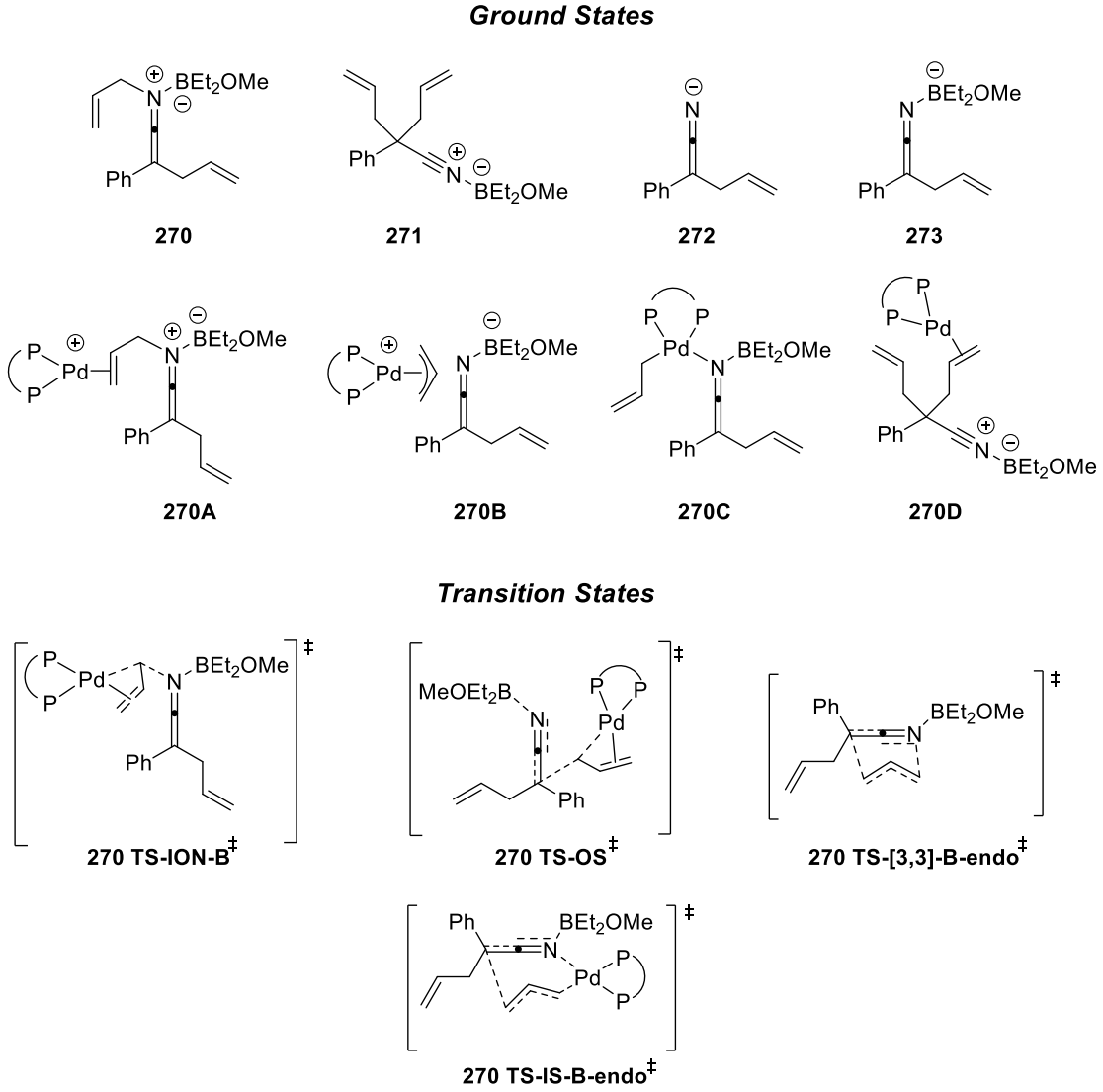

Scheme 188. Graphical guide to numbered compounds for borane-bound ketenimine (**270**) rearrangement.

Energies and lowest frequencies of minimum energy structures for ketenimine (**274**) rearrangement are shown in Table 35.

Structure	$E_{elec\ ONIOM}$, Ha	$G_{corr\ ONIOM}$, Ha	$G_{SP\ corrected}$ [b], Ha	Lowest freq.	# of imaginary freq.
		Uncatalyzed Pathway			
275	-523.335101	0.240073	-523.252012	44.16	0
274-1	-523.293171	0.235826	-523.214184	29.29	0
274-2	-523.293323	0.234765	-523.215431	17.19	0
274-3	-523.293780	0.235704	-523.214846	30.83	0
274-4	-523.292702	0.234762	-523.214554	22.83	0
274-5	-523.293394	0.234331	-523.216057	17.88	0
274-6	-523.293900	0.234019	-523.216486	11.31	0
274 TS-[3,3]-exo	-523.265051	0.236548	-523.185798	-400.45	1
274 TS-[3,3]-endo	-523.263196	0.236389	-523.184884	-367.71	1
		Catalyzed Pathway			
274A-a	-1336.140119	0.765647	-3028.479243	4.10	0
274A-b	-1336.141412	0.765621	-3028.480463	6.30	0
274A-c	-1336.141355	0.765679	-3028.485591	6.18	0
274A-d	-1336.141715	0.766519	-3028.479771	5.45	0
274A-e	-1336.141852	0.766210	-3028.479815	5.57	0
274A-f	-1336.143183	0.765116	-3028.488136	6.46	0
274C	-1336.180272	0.769660	-3028.521363	6.66	0
274 TS-[3,3]-Pd-exo	-1336.100309	0.761778	-3028.457853	-209.49	1
274 TS-[3,3]-Pd-endo	-1336.100908	0.762700	-3028.449875	-255.05	1

Table 35. Energies and lowest frequencies of minimum energy structures for ketenimine (**274**) rearrangement. [a] Energy values calculated at C-PCM(Toluene)-M06L/BSII//[ONIOM(M06L/BSI:PM6)], where BSI = 6-31+G(d) (C, H, P, B, O)/LANL2DZ (ECP Pd) and BSII = 6-311++G(2d,2p) (C, H, P, B, O)/LANL2DZ (ECP Pd). Thermal corrections at 298.15 K. [b] Solvent-corrected free energy given by $G_{SP\ corrected}$ [(C-PCM)/M06L/BSII] = E_{elec}[(C-PCM)/M06L/BSII] + $G_{corr\ ONIOM}$ [ONIOM(M06L/BSI:PM6)], where $G_{corr\ ONIOM}$ is the thermal correction to Gibbs free energy obtained in the gas phase at ONIOM(M06L/BSI:PM6) or M06L/BSI.

Schemes 189 shows graphical guide to numbered compounds for ketenimine (**274**) rearrangement.

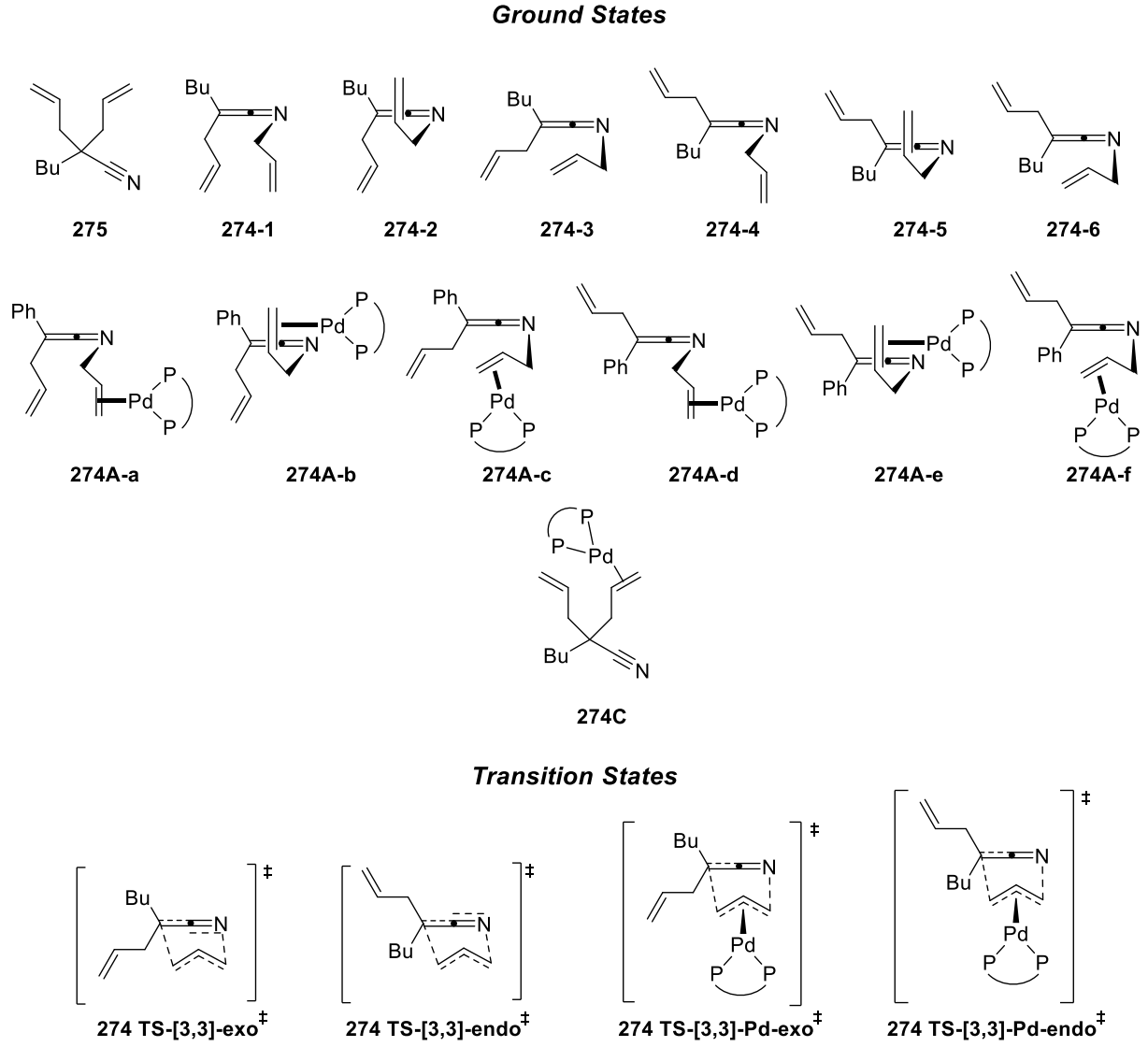

Scheme 189. Graphical guide to numbered compounds for ketenimine (**274**) rearrangement.

Scheme 190 shows conformational analysis for ketenimine (**274**), complex (**274A**) and transition states.

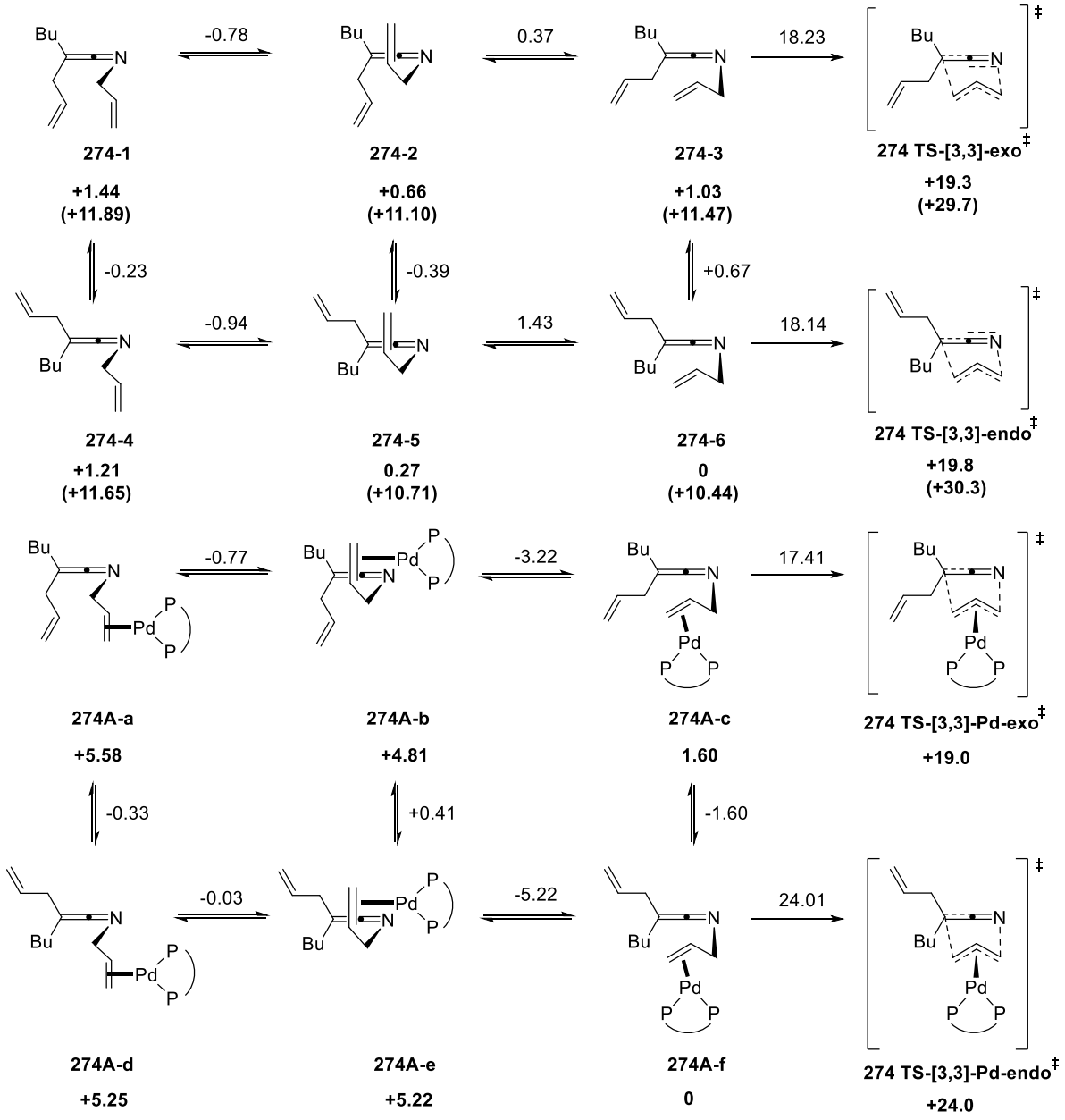

Scheme 190. Conformational analysis for ketenimine (**274**), complex (**274A**) and transition states.

Section Decarboxylative allylation and Ketenimine Rearrangement (pages 244-246, 256-265) is

Reprinted (adapted) with permission from Alexander, J. R.; Shchepetkina, V. I.; Stankevich, K. S.; Benedict, R. J.; Bernhard, S. P.; Dreiling, R. J.; Cook, M. J. Pd-Catalyzed Rearrangement of *N*-Alloc-*N*-allyl Ynamides via Auto-Tandem Catalysis: Evidence for Reversible C–N Activation and Pd(0)-Accelerated Ketenimine Aza-Claisen Rearrangement. *Org. Lett.* **2021**, *23* (2), 559–564. DOI: 10.1021/acs.orglett.0c04078. Copyright 2021 American Chemical Society. http://pubs.acs.org/articlesonrequest/AOR-SQUVAMWDKP8QMJBDVJCZ

Material is Reprinted (adapted) from Supporting Information.

Diastereo- and Branched-Selective Rearrangement

Reproduced/Adapted from Ref. 197 with permission from The Royal Society of Chemistry. https://doi.org/10.1039/D2CC03399B

To explore the possible mechanistic pathways, we applied the two-layered QM/SE ONIOM method to palladium complexes.[241,246,268] In this model, the substrate as well as palladium and phosphorous atoms of the catalyst were included in the high layer, whereas the rest was placed in the low layer. The high level was treated with DFT using local meta-generalized gradient approximation functional M06L recommended for transition-metal chemistry calculations.[188] The 6-31G+(d) basis set was used for C, H, P, and O atoms in conjunction with the LANL2DZ relativistic pseudopotential for Pd (BSI). The low level was handled with semi-empirical method PM6. Given the bulky nature of the ligand, this two-layered ONIOM model allowed us to perform geometry optimization of palladium complexes within the reasonable timescale. The nature of stationary points in each case was confirmed by harmonic

frequency calculations. The nature of located TSs was confirmed by unique imaginary vibrational mode and IRC calculations.

To get refined energies, we further performed single point (SP) energy calculations using the ONIOM geometries. The palladium complexes were fully treated by DFT. The larger basis set 6-311++G(2d,2p) for C, H, P and O atoms and LANL2DZ ECP for Pd (BSII) and M06L functional were employed. The single point solvation by trifluorotoluene was accounted by using conductor-like polarizable continuum model (C-PCM)[184,185] specifying the following parameters: static dielectric constant $\varepsilon = 9.4$, dynamic dielectric constant $n^2 = 1.414$. The calculations were performed with the Gaussian 16.0 software.[174] The corrected single point energy was calculated as follows:

$$G_{\text{SP Corrected}} = E_{\text{elec}}[\text{C} - \text{PCM}(\text{PhCF}_3)\text{M06L/BSII}] + G_{\text{Corr ONIOM}}[\text{ONIOM(M06L/BSI:PM6)}],$$

where $G_{\text{corr ONIOM}}$ is the thermal correction to Gibbs free energy obtained in the gas phase at ONIOM(M06L/BSI:PM6) or M06L/BSI.

The obtained Gibbs Free energies were temperature-corrected and reported at 333.15 K. At the same temperature all energies were corrected to 1 mol/L standard state. The Grimme's quasi-rigid-rotor harmonic oscillator (quasi-RRHO) approximation was used to account for entropic contributions of low frequency modes below 100 cm^{-1}.[189,190] All corrections were obtained using the GoodVibes program by Prof. Robert Paton.[177] Trifluorotoluene parameters (molecular weight and density) were manually added to media.py.

The optimized structures were visualized using CYLview 1.0b.[175] The molecular orbitals were generated and rendered in GaussView 6.0.16.[176] The potential energy surfaces were generated using GoodVibes.[177]

Conformational studies were done in CREST.[191] Each experiment was repeated twice to ensure reproducibility, the typical run was as follows. The conformational search for **6** was performed using default iMTD-GC algorithm at the GFN2-xTB level,[192] which resulted in 781 conformers within an energy window of 4.2 kcal/mol. The generated conformational ensemble was reduced to 25 lowest energy structures that were optimized using DFT at M06L/BSI level. The redundant conformers were eliminated. The structures in reactive conformation were considered for further analysis. The conformational search for (**280**) bound to (**Pd-L1**) was performed using special NCI mode for non-covalently bound complexes at GFN-FF level.[285] The allyl group and allene system atoms were constrained in reactive conformation during meta-dynamic simulations. The search resulted in 1784 conformers within an energy window of 5.8 kcal/mol. From generated conformational ensemble 3 conformers reflecting *exo*- and 3 conformers reflecting *endo*- binding mode of (**280**) to (**Pd-L1**) were selected and reoptimized using ONIOM(M06L|BSI:PM6). The conformational changes occurring between C-N bond cleavage and C-C bond formation were found during potential energy surface scans.
To evaluate noncovalent interactions between phenyl groups in transition states (**TS-283**) and (**TS-289**), we utilized independent gradient model approach (IGM-δg) implemented in IGMplot (http://igmplot.univ-reims.fr).[283] Three-dimensional (3D) IGM isosurfaces representing non-covalent interactions were visualized in VMD.[286] These isosurfaces were color-coded with green and blue demonstrating van der Waals and strong attraction, respectively and yellow and red – weak and strong repulsion, respectively.[197]

Energies and lowest frequencies of minimum energy structures for ketenimine (**280**) rearrangement are shown in Table 36.

Structure	E[a], Ha	E_SPC[b], Ha	G(T)_SPC[c]	qh-G(T)_SPC[d]	Lowest freq.[e]
Pd-L1	-813.501332	-4143.787235	-4142.463347	-4142.439363	7.63
281	-828.153777	-828.374439	-828.095958	-828.092312	29.89
281'	-828.154072	-828.374968	-828.097850	-828.093492	33.42
280	-828.133083	-828.352815	-828.080602	-828.073598	3.01
282	-1641.674213	-4972.203260	-4970.576857	-4970.544879	7.31
284	-1641.660257	-4972.184384	-4970.563143	-4970.531380	5.93
285	-1641.663736	-4972.201144	-4970.576452	-4970.546098	10.87
287	-1641.686505	-4972.222121	-4970.591749	-4970.562400	10.42
288	-1641.674562	-4972.196636	-4970.572826	-4970.540080	6.18
290	-1641.659140	-4972.181976	-4970.563541	-4970.530636	8.04
292	-1641.662663	-4972.189895	-4970.565076	-4970.535013	9.22
294	-1641.680854	-4972.212984	-4970.585144	-4970.554390	3.23
$PhCF_3$	-569.237725	-569.391876	-569.319973	-569.318936	30.35
TS-283	-1641.650520	-4972.178215	-4970.553822	-4970.523034	-311.03
TS-286	-1641.661300	-4972.201236	-4970.573806	-4970.544546	-296.81
TS-289	-1641.652256	-4972.174166	-4970.552030	-4970.520387	-311.12
TS-291	-1641.661361	-4972.184066	-4970.557784	-4970.528542	-11.10
TS-293	-1641.658554	-4972.191876	-4970.563820	-4970.534853	-321.39

Table 36. Energies and lowest frequencies of minimum energy structures for ketenimine (**280**) rearrangement. [a] Electronic energies calculated at ONIOM(M06L/BSI:PM6), where BSI = 6-31+G(d) (C, H, P, O)/LANL2DZ (ECP Pd); [b] Single point energies calculated at at C-PCM (Trifluorotoluene) M06L/BSII//[ONIOM(M06L/BSI:PM6)], where BSI = 6-31+G(d) (C, H, P, O)/LANL2DZ (ECP Pd) and BSII = 6-311++G(2d,2p) (C, H, P, O) /LANL2DZ (ECP Pd); [c] Harmonic solvent and temperature (333.15 K) corrected Gibbs free energies; [d] Quasi-harmonic solvent and temperature (333.15 K) corrected Gibbs free energies at 1 mol/L standard state; [e] Unscaled; calculated at ONIOM(M06L/BSI:PM6), where BSI = 6-31+G(d) (C, H, P, O)/LANL2DZ (ECP Pd).

Scheme 191 provides a graphical guide to numbered compounds for ketenimine (**280**) rearrangement.

Ground States

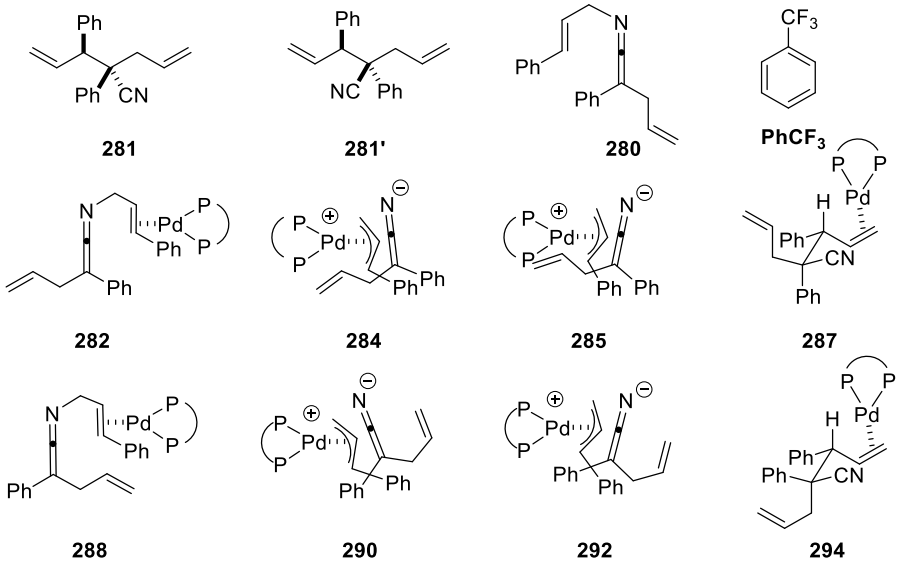

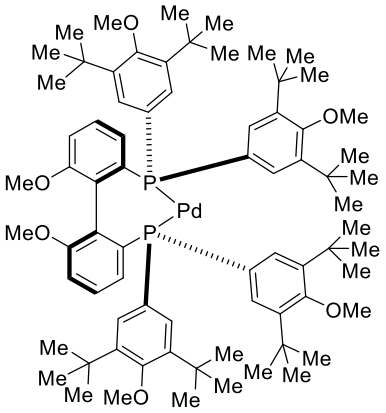

Transition States

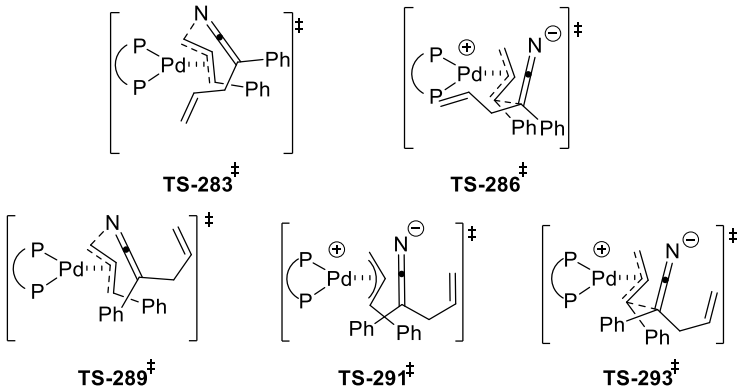

Scheme 191. Graphical guide to numbered compounds for ketenimine (**280**) rearrangement.

REFERENCES CITED

(1) Heasley, B. Stereocontrolled Preparation of Fully Substituted Cyclopentanes: Relevance to Total Synthesis. *European J. Org. Chem.* **2009**, *2009* (10), 1477–1489. https://doi.org/10.1002/ejoc.200801229.

(2) Heasley, B. Recent Developments in the Stereocontrolled Synthesis of Highly Substituted Cyclopentane Core Structures: From Drug Discovery Research to Natural Product Synthesis. *Curr. Org. Chem.* **2014**, *18* (6), 641–686. https://doi.org/10.2174/1385272813176660150.

(3) Lovering, F.; Bikker, J.; Humblet, C. Escape from Flatland: Increasing Saturation as an Approach to Improving Clinical Success. *J. Med. Chem.* **2009**, *52* (21), 6752–6756. https://doi.org/10.1021/jm901241e.

(4) Lovering, F. Escape from Flatland 2: Complexity and Promiscuity. *Medchemcomm* **2013**, *4* (3), 515. https://doi.org/10.1039/c2md20347b.

(5) Zheng, Y.; Tice, C. M.; Singh, S. B. The Use of Spirocyclic Scaffolds in Drug Discovery. *Bioorg. Med. Chem. Lett.* **2014**, *24* (16), 3673–3682. https://doi.org/10.1016/j.bmcl.2014.06.081.

(6) Ojeda-Porras, A. C.; Roy, V.; Agrofoglio, L. A. Chemical Approaches to Carbocyclic Nucleosides. *Chem. Rec.* **2022**, *22* (5). https://doi.org/10.1002/tcr.202100307.

(7) Babu, Y. S.; Chand, P.; Bantia, S.; Kotian, P.; Dehghani, A.; El-Kattan, Y.; Lin, T.-H.; Hutchison, T. L.; Elliott, A. J.; Parker, C. D.; Ananth, S. L.; Horn, L. L.; Laver, G. W.; Montgomery, J. A. BCX-1812 (RWJ-270201): Discovery of a Novel, Highly Potent, Orally Active, and Selective Influenza Neuraminidase Inhibitor through Structure-Based Drug Design. *J. Med. Chem.* **2000**, *43* (19), 3482–3486. https://doi.org/10.1021/jm0002679.

(8) Minami, A.; Ozaki, T.; Liu, C.; Oikawa, H. Cyclopentane-Forming Di/Sesterterpene Synthases: Widely Distributed Enzymes in Bacteria, Fungi, and Plants. *Nat. Prod. Rep.* **2018**, *35* (12), 1330–1346. https://doi.org/10.1039/C8NP00026C.

(9) Olano, C. Hutchinson's Legacy: Keeping on Polyketide Biosynthesis. *J. Antibiot. (Tokyo).* **2011**, *64* (1), 51–57. https://doi.org/10.1038/ja.2010.126.

(10) Jin, Z. Muscarine, Imidazole, Oxazole and Thiazole Alkaloids. *Nat. Prod. Rep.* **2016**, *33* (11), 1268–1317. https://doi.org/10.1039/C6NP00067C.

(11) Buchanan, M. S.; Carroll, A. R.; Quinn, R. J. Revised Structure of Palau'amine. *Tetrahedron Lett.* **2007**, *48* (26), 4573–4574. https://doi.org/10.1016/j.tetlet.2007.04.128.

(12) Simeonov, S. P.; Nunes, J. P. M.; Guerra, K.; Kurteva, V. B.; Afonso, C. A. M. Synthesis of Chiral Cyclopentenones. *Chem. Rev.* **2016**, *116* (10), 5744–5893. https://doi.org/10.1021/cr500504w.

(13) Das, S.; Chandrasekhar, S.; Yadav, J. S.; Grée, R. Recent Developments in the Synthesis of Prostaglandins and Analogues. *Chem. Rev.* **2007**, *107* (7), 3286–3337. https://doi.org/10.1021/cr068365a.

(14) Peng, H.; Chen, F.-E. Recent Advances in Asymmetric Total Synthesis of Prostaglandins. *Org. Biomol. Chem.* **2017**, *15* (30), 6281–6301. https://doi.org/10.1039/C7OB01341H.

(15) Collins, P. W.; Djuric, S. W. Synthesis of Therapeutically Useful Prostaglandin and Prostacyclin Analogs. *Chem. Rev.* **1993**, *93* (4), 1533–1564. https://doi.org/10.1021/cr00020a007.

(16) Boutureira, O.; Matheu, M. I.; Díaz, Y.; Castillón, S. Advances in the Enantioselective Synthesis of Carbocyclic Nucleosides. *Chem. Soc. Rev.* **2013**, *42* (12), 5056. https://doi.org/10.1039/c3cs00003f.

(17) Manna, M. S.; Mukherjee, S. Catalytic Asymmetric Desymmetrization Approaches to Enantioenriched Cyclopentanes. *Org. Biomol. Chem.* **2015**, *13* (1), 18–24. https://doi.org/10.1039/C4OB01649A.

(18) Fleck, M.; Yang, C.; Wada, T.; Inoue, Y.; Bach, T. Regioselective [2 + 2]-Photocycloaddition Reactions of Chiral Tetronates—Influence of Temperature, Pressure, and Reaction Medium. *Chem. Commun.* **2007**, No. 8, 822–824. https://doi.org/10.1039/B613985J.

(19) Jiang, M. X.-W.; Warshakoon, N. C.; Miller, M. J. Chemoenzymatic Asymmetric Total Synthesis of Phosphodiesterase Inhibitors: Preparation of a Polycyclic Pyrazolo[3,4-d]pyrimidine from an Acylnitroso Diels−Alder Cycloadduct-Derived Aminocyclopentenol. *J. Org. Chem.* **2005**, *70* (7), 2824–2827. https://doi.org/10.1021/jo0484070.

(20) Lee, S.; Paek, S.-M.; Yun, H.; Kim, N.-J.; Suh, Y.-G. Enantioselective Total Synthesis of a Natural Iridoid. *Org. Lett.* **2011**, *13* (13), 3344–3347. https://doi.org/10.1021/ol201089f.

(21) Parthasarathy, G.; Eggert, U.; Kalesse, M. Synthesis of (+)-Omphadiol and (+)-Pyxidatol C. *Org. Lett.* **2016**, *18* (9), 2320–2322. https://doi.org/10.1021/acs.orglett.6b00814.

(22) Tanaka, M.; Norimine, Y.; Fujita, T.; Suemune, H.; Sakai, K. Chemoenzymatic Synthesis of Antiviral Carbocyclic Nucleosides: Asymmetric Hydrolysis of Meso-3,5-Bis(Acetoxymethyl)Cyclopentenes using Rhizopus Delemar Lipase. *J. Org. Chem.* **1996**, *61* (20), 6952–6957. https://doi.org/10.1021/jo9608230.

(23) Chun, B. K.; Song, G. Y.; Chu, C. K. Stereocontrolled Syntheses of Carbocyclic C-Nucleosides and Related Compounds. *J. Org. Chem.* **2001**, *66* (14), 4852–4858. https://doi.org/10.1021/jo010224f.

(24) Jung, Y. H.; Kim, S. I.; Hong, Y. J.; Park, S. J.; Kang, K. T.; Kim, S. Y.; Kim, I. S. Total Synthesis of Carbocyclic Nucleoside (+)-Neplanocin A. *Tetrahedron* **2015**, *71* (7), 1068–1073. https://doi.org/10.1016/j.tet.2014.12.093.

(25) Craig, R. A.; Roizen, J. L.; Smith, R. C.; Jones, A. C.; Stoltz, B. M. Enantioselective Synthesis of a Hydroxymethyl-cis-1,3-cyclopentenediol Building Block. *Org. Lett.* **2012**, *14* (22), 5716–5719. https://doi.org/10.1021/ol3027297.

(26) Xiong, Y.; Lin, H.; Zhu, C.-L.; Chen, Y.-H.; Ye, R.; Hu, G.-W.; Xie, J.-H.; Zhou, Q.-L. Asymmetric Hydrogenation of Racemic α-Aryl-β-Ethoxycarbonyl Cyclopentanones via Dynamic Kinetic Resolution and Its Application to the Synthesis of (+)-Burmaniol A. *Org. Lett.* **2021**, *23* (22), 8883–8887. https://doi.org/10.1021/acs.orglett.1c03384.

(27) Aikawa, K.; Okamoto, T.; Mikami, K. Copper(I)-Catalyzed Asymmetric Desymmetrization: Synthesis of Five-Membered-Ring Compounds Containing All-Carbon Quaternary Stereocenters. *J. Am. Chem. Soc.* **2012**, *134* (25), 10329–10332. https://doi.org/10.1021/ja3032345.

(28) Jarugumilli, G. K.; Cook, S. P. A Simple, Nontoxic Iron System for the Allylation of Zinc Enolates. *Org. Lett.* **2011**, *13* (8), 1904–1907. https://doi.org/10.1021/ol200059u.

(29) Siewert, J.; Textor, A.; Grond, S.; von Zezschwitz, P. Spirodionic Acid, a Novel Metabolite FromStreptomyces Sp., Part 2: Total Synthesis through a Twofold Michael Addition as a Selective Spiroannelation Strategy. *Chem. - A Eur. J.* **2007**, *13* (26), 7424–7431. https://doi.org/10.1002/chem.200601688.

(30) Lee, K. M.; Choi, W. J.; Lee, Y.; Lee, H. J.; Zhao, L. X.; Lee, H. W.; Park, J. G.; Kim, H. O.; Hwang, K. Y.; Heo, Y.-S.; Choi, S.; Jeong, L. S. X-Ray Crystal Structure and Binding Mode Analysis of Human S -Adenosylhomocysteine Hydrolase Complexed with Novel Mechanism-Based Inhibitors, Haloneplanocin A Analogues. *J. Med. Chem.* **2011**, *54* (4), 930–938. https://doi.org/10.1021/jm1010836.

(31) Trost, B. M.; Crawley, M. L. Asymmetric Transition-Metal-Catalyzed Allylic Alkylations: Applications in Total Synthesis. *Chem. Rev.* **2003**, *103* (8), 2921–2944. https://doi.org/10.1021/cr020027w.

(32) Wenz, D. R.; Read de Alaniz, J. The Nazarov Cyclization: A Valuable Method to Synthesize Fully Substituted Carbon Stereocenters. *European J. Org. Chem.* **2015**, *2015* (1), 23–37. https://doi.org/10.1002/ejoc.201402825.

(33) Matsumoto, N.; Nakazaki, A.; Nishikawa, T. Concise Synthesis of a Cyclopentane Intermediate Possessing All Nitrogen Functionalities for Pactamycin. *Synlett* **2017**, *28* (17), 2303–2306. https://doi.org/10.1055/s-0036-1588495.

(34) Parr, B. T.; Davies, H. M. L. Highly Stereoselective Synthesis of Cyclopentanes Bearing Four Stereocentres by a Rhodium Carbene-Initiated Domino Sequence. *Nat. Commun.* **2014**, *5* (1), 4455. https://doi.org/10.1038/ncomms5455.

(35) Trost, B. M.; Morris, P. J.; Sprague, S. J. Palladium-Catalyzed Diastereo- and Enantioselective Formal [3 + 2]-Cycloadditions of Substituted Vinylcyclopropanes. *J. Am. Chem. Soc.* **2012**, *134* (42), 17823–17831. https://doi.org/10.1021/ja309003x.

(36) Trost, B. M.; Silverman, S. M.; Stambuli, J. P. Development of an Asymmetric Trimethylenemethane Cycloaddition Reaction: Application in the Enantioselective Synthesis of Highly Substituted Carbocycles. *J. Am. Chem. Soc.* **2011**, *133* (48), 19483–19497. https://doi.org/10.1021/ja207550t.

(37) Wilson, J. E.; Fu, G. C. Synthesis of Functionalized Cyclopentenes through Catalytic Asymmetric [3+2] Cycloadditions of Allenes with Enones. *Angew. Chemie Int. Ed.* **2006**, *45* (9), 1426–1429. https://doi.org/10.1002/anie.200503312.

(38) Chandra, G.; Majik, M. S.; Lee, J. Y.; Jeong, L. S. Stereoselective Synthesis of Fluoro-Homoneplanocin A as a Potential Antiviral Agent. *Org. Lett.* **2012**, *14* (8), 2134–2137. https://doi.org/10.1021/ol300667q.

(39) Mulamoottil, V. A.; Nayak, A.; Jeong, L. S. Recent Advances in the Synthesis of Carbocyclic Nucleosides via Ring-Closing Metathesis. *Asian J. Org. Chem.* **2014**, *3* (7), 748–761. https://doi.org/10.1002/ajoc.201402032.

(40) Ye, W.; He, M.; Schneller, S. W. Synthesis of the 6′-iso Analogues of Neplanocin A and 5′-homoneplanocin A. *Tetrahedron Lett.* **2009**, *50* (51), 7156–7158. https://doi.org/10.1016/j.tetlet.2009.10.016.

(41) McAdam, C. A. Claisen-Sakurai Approaches to Cyclopentane Scaffolds, Queen's University Belfast, 2015.

(42) Martín Castro, A. M. Claisen Rearrangement over the Past Nine Decades. *Chem. Rev.* **2004**, *104* (6), 2939–3002. https://doi.org/10.1021/cr020703u.

(43) Nonoshita, K.; Banno, H.; Maruoka, K.; Yamamoto, H. Organoaluminum-Promoted Claisen Rearrangement of Allyl Vinyl Ethers. *J. Am. Chem. Soc.* **1990**, *112* (1), 316–322. https://doi.org/10.1021/ja00157a049.

(44) Nelson, S. G.; Bungard, C. J.; Wang, K. Catalyzed Olefin Isomerization Leading to Highly Stereoselective Claisen Rearrangements of Aliphatic Allyl Vinyl Ethers. *J. Am. Chem. Soc.* **2003**, *125* (43), 13000–13001. https://doi.org/10.1021/ja037655v.

(45) McLaughlin, M. G.; Cook, M. J. Domino Alkene-Isomerization–Claisen Rearrangement Strategy to Substituted Allylsilanes. *J. Org. Chem.* **2012**, *77* (4), 2058–2063. https://doi.org/10.1021/jo202560g.

(46) Mikami, K.; Maeda, T.; Kishi, N.; Nakai, T. Asymmetric Allylsilane-Mediated Carbocyclization: A Highly Enantiospecific Synthesis of (1S, 2S)-(+)-2-Methyl-3-Cyclopenten-1-ol. *Tetrahedron Lett.* **1984**, *25* (45), 5151–5154. https://doi.org/10.1016/S0040-4039(01)81549-5.

(47) Borrelly, S.; Paquette, L. A. An Intramolecular Cyclization Approach to Optically Active Cyclopentenyl Bromides. *J. Org. Chem.* **1993**, *58* (10), 2714–2717. https://doi.org/10.1021/jo00062a011.

(48) Paquette, L. A.; Ladouceur, G. Synthetic Studies Targeted at the Cytotoxic 8,9-seco-ent-Kaurene Diterpenes. Concise Complementary Stereocontrolled Construction of the Bridgehead Olefin Core. *J. Org. Chem.* **1989**, *54* (18), 4278–4279. https://doi.org/10.1021/jo00279a010.

(49) Masse, C. E.; Dakin, L. A.; Knight, B. S.; Panek, J. S. Lewis Acid-Mediated Carbocyclization Reactions of Chiral (E)-Crotylsilanes. *J. Org. Chem.* **1997**, *62* (26), 9335–9338. https://doi.org/10.1021/jo970832o.

(50) McLaughlin, M. G.; Cook, M. J. $PtCl_2$/XPhos: A Highly Efficient and Readily Available Catalyst for the Hydrosilylation of Propargylic Alcohols. *Chem. Commun.* **2011**, *47* (39), 11104. https://doi.org/10.1039/c1cc14433b.

(51) McAdam, C. A.; McLaughlin, M. G.; Johnston, A. J. S.; Chen, J.; Walter, M. W.; Cook, M. J. Platinum Catalysed Hydrosilylation of Propargylic Alcohols. *Org. Biomol. Chem.* **2013**, *11* (27), 4488. https://doi.org/10.1039/c3ob40496j.

(52) Stankevich, K. S.; Cook, M. J. A Highly Stereospecific Claisen–Sakurai Approach to Densely Functionalized Cyclopentenols. *J. Org. Chem.* **2022**, *87* (18), 12250–12256. https://doi.org/10.1021/acs.joc.2c01397.

(53) Stankevich, K. S.; Cook, M. J. A Highly Stereoselective Claisen–Sakurai Approach to Densely Functionalized Cyclopentenols. *ChemRxiv* **2022**. https://doi.org/10.26434/chemrxiv-2022-t2lkm.

(54) Claisen, L. Über Umlagerung von Phenol-allyläthern in C-Allyl-phenole. *Berichte der Dtsch. Chem. Gesellschaft* **1912**, *45* (3), 3157–3166. https://doi.org/10.1002/cber.19120450348.

(55) Rehbein, J.; Hiersemann, M. Claisen Rearrangement of Aliphatic Allyl Vinyl Ethers from 1912 to 2012: 100 Years of Electrophilic Catalysis. *Synthesis (Stuttg).* **2013**, *45* (09), 1121–1159. https://doi.org/10.1055/s-0032-1316869.

(56) Hiersemann, M.; Abraham, L. Catalysis of the Claisen Rearrangement of Aliphatic Allyl Vinyl Ethers. *European J. Org. Chem.* **2002**, *2002* (9), 1461–1471. https://doi.org/10.1002/1099-0690(200205)2002:9<1461::AID-EJOC1461>3.0.CO;2-1.

(57) Vance, R. L.; Rondan, N. G.; Houk, K. N.; Jensen, F.; Borden, W. T.; Komornicki, A.; Wimmer, E. Transition Structures for the Claisen Rearrangement. *J. Am. Chem. Soc.* **1988**, *110* (7), 2314–2315. https://doi.org/10.1021/ja00215a059.

(58) Dewar, M. J. S.; Jie, C. Mechanism of the Claisen Rearrangement of Allyl Vinyl Ethers. *J. Am. Chem. Soc.* **1989**, *111* (2), 511–519. https://doi.org/10.1021/ja00184a018.

(59) Kupczyk-Subotkowska, L.; Saunders, W. H.; Shine, H. J.; Subotkowski, W. Thermal Rearrangement of Allyl Vinyl Ether: Heavy-Atom Kinetic Isotope Effects and the Transition Structure. *J. Am. Chem. Soc.* **1993**, *115* (14), 5957–5961. https://doi.org/10.1021/ja00067a009.

(60) Meyer, M. P.; DelMonte, A. J.; Singleton, D. A. Reinvestigation of the Isotope Effects for the Claisen and Aromatic Claisen Rearrangements: The Nature of the Claisen Transition States. *J. Am. Chem. Soc.* **1999**, *121* (47), 10865–10874. https://doi.org/10.1021/ja992372h.

(61) Xu, Y.; Wong, K.-Y.; Wang, M.; Liu, D.; Zhao, W.; Zou, D.; Li, X. Theoretical Simulations of Heavy-Atom Kinetic Isotope Effects in Aliphatic Claisen Rearrangement. *J. Phys. Chem. A* **2020**, *124* (51), 10678–10686. https://doi.org/10.1021/acs.jpca.0c07784.

(62) Chen, H.; Li, Z.; Shao, P.; Yuan, H.; Chen, S.-C.; Luo, T. Total Synthesis of (+)-Mutilin: a Transannular [2+2] Cycloaddition/Fragmentation Approach. *J. Am. Chem. Soc.* **2022**, *144* (34), 15462–15467. https://doi.org/10.1021/jacs.2c06934.

(63) Geherty, M. E.; Dura, R. D.; Nelson, S. G. Catalytic Asymmetric Claisen Rearrangement of Unactivated Allyl Vinyl Ethers. *J. Am. Chem. Soc.* **2010**, *132* (34), 11875–11877. https://doi.org/10.1021/ja1039314.

(64) Wang, K.; Bungard, C. J.; Nelson, S. G. Stereoselective Olefin Isomerization Leading to Asymmetric Quaternary Carbon Construction. *Org. Lett.* **2007**, *9* (12), 2325–2328. https://doi.org/10.1021/ol0706511.

(65) Calas, R.; Dunogues, J.; Deleris, G.; Pisciotti, F. Addition d'hydrocarbures Silicies Possedant Une Liaison Si-C Activee a Des Composes Carbonyles α-Chlores. *J. Organomet. Chem.* **1974**, *69* (2), C15–C17. https://doi.org/10.1016/S0022-328X(00)90228-6.

(66) Deleris, G.; Dunogues, J.; Calas, R. Addition d'hydrocarbures Silicies Possedant Une Liaison Si-C Activee a Des Composes Carbonyles. *J. Organomet. Chem.* **1975**, *93* (1), 43–50. https://doi.org/10.1016/S0022-328X(00)94143-3.

(67) Abel, E. W.; Rowley, R. J. The Reaction of Perhalogenoketones with Allylic Derivatives of Silicon and Tin. *J. Organomet. Chem.* **1975**, *84* (2), 199–229. https://doi.org/10.1016/S0022-328X(00)90032-9.

(68) Hosomi, A.; Sakurai, H. Syntheses of γ,δ-Unsaturated Alcohols from Allylsilanes and Carbonyl Compounds in the Presence of Titanium Tetrachloride. *Tetrahedron Lett.* **1976**, *17* (16), 1295–1298. https://doi.org/10.1016/s0040-4039(00)78044-0.

(69) Fleming, I. Tilden Lecture. Some Uses of Silicon Compounds in Organic Synthesis. *Chem. Soc. Rev.* **1981**, *10* (1), 83–111. https://doi.org/10.1039/cs9811000083.

(70) Fleming, I.; Pearce, A.; Snowden, R. L. Controlling the Outcome of a Carbonium Ion Reaction: The Use of a Trimethylsilyl Group to Dictate the Formation of a Specific Olefin. *J. Chem. Soc. Chem. Commun.* **1976**, No. 5, 182–183. https://doi.org/10.1039/c39760000182.

(71) Mayr, H.; Kempf, B.; Ofial, A. R. π-Nucleophilicity in Carbon−Carbon Bond-Forming Reactions. *Acc. Chem. Res.* **2003**, *36* (1), 66–77. https://doi.org/10.1021/ar020094c.

(72) Mayr, H.; Bug, T.; Gotta, M. F.; Hering, N.; Irrgang, B.; Janker, B.; Kempf, B.; Loos, R.; Ofial, A. R.; Remennikov, G.; Schimmel, H. Reference Scales for the Characterization of Cationic Electrophiles and Neutral Nucleophiles. *J. Am. Chem. Soc.* **2001**, *123* (39), 9500–9512. https://doi.org/10.1021/ja010890y.

(73) Corral-Bautista, F.; Klier, L.; Knochel, P.; Mayr, H. From Carbanions to Organometallic Compounds: Quantification of Metal Ion Effects on Nucleophilic Reactivities. *Angew. Chemie Int. Ed.* **2015**, *54* (42), 12497–12500. https://doi.org/10.1002/anie.201501385.

(74) Magnus, P. D.; Sarkar, T.; Djuric, S. Organosilicon Compounds in Organic Synthesis. In *Comprehensive Organometallic Chemistry*; Stone, F. G. A., Abel, E. W., Eds.; Pergamon: Oxford, 1982; pp 515–659. https://doi.org/10.1016/b978-008046518-0.00104-5.

(75) Hosomi, A.; Sakurai, H. Conjugate Addition of Allylsilanes to α,β-Enones. A New Method of Stereoselective Introduction of the Angular Allyl Group in Fused Cyclic α,β-Enones. *J. Am. Chem. Soc.* **1977**, *99* (5), 1673–1675. https://doi.org/10.1021/ja00447a080.

(76) Hosomi, A.; Kobayashi, H.; Sakurai, H. Latent Acetonylation of α,β-Enones with allyltrimethylsilane or 2-methyl-2-propenyltrimethylsilane:Synthesis of 1,5-diketones and Annelation to Fused Cyclohexenones. *Tetrahedron Lett.* **1980**, *21* (10), 955–958. https://doi.org/10.1016/S0040-4039(00)77749-5.

(77) Ojima, I.; Kumagai, M.; Miyazawa, Y. 3-TMS-Cyclopentene-1 a New Reagent for the Synthesis of Cyclopentene Derivatives. *Tetrahedron Lett.* **1977**, *18* (16), 1385–1388. https://doi.org/10.1016/s0040-4039(01)93050-3.

(78) Ochiai, M.; Arimoto, M.; Fujita, E. Reaction of Allylsilane with α-Nitro Olefin and Its Development to Synthesis of Cyclopentenone. *Tetrahedron Lett.* **1981**, *22* (12), 1115–1118. https://doi.org/10.1016/s0040-4039(01)90251-5.

(79) Fleming, I.; Paterson, I. Allylsilanes in Organic Synthesis: A Method for the Introduction of Two Carbon Substituents in Place of Carbonyl Oxygen. *Synthesis (Stuttg).* **1979**, *1979* (06), 446–448. https://doi.org/10.1055/s-1979-28713.

(80) Hosomi, A.; Endo, M.; Sakurai, H. Allylsilanes as Synthetic Intermediates. II. Syntheses of Homoallyl Ethers from Allylsilanes and Acetals Promoted by Titanium Tetrachloride. *Chem. Lett.* **1976**, *5* (9), 941–942. https://doi.org/10.1246/cl.1976.941.

(81) Yamasaki, S.; Fujii, K.; Wada, R.; Kanai, M.; Shibasaki, M. A General Catalytic Allylation Using Allyltrimethoxysilane. *J. Am. Chem. Soc.* **2002**, *124* (23), 6536–6537. https://doi.org/10.1021/ja0262582.

(82) Cao, Z.-Y.; Zhang, Y.; Ji, C.-B.; Zhou, J. A $Hg(ClO_4)_2 \cdot 3H_2O$ Catalyzed Sakurai–Hosomi Allylation of Isatins and Isatin Ketoimines Using Allyltrimethylsilane. *Org. Lett.* **2011**, *13* (24), 6398–6401. https://doi.org/10.1021/ol202705g.

(83) Schinzer, D. Intramolecular Addition-Reactions of Allylic and Propargylic Silanes. *Synthesis-Stuttgart* **1988**, *1988* (4), 263–273. https://doi.org/10.1055/s-1988-27540.

(84) Yamamoto, Y.; Asao, N. Selective Reactions Using Allylic Metals. *Chem. Rev.* **1993**, *93* (6), 2207–2293. https://doi.org/10.1021/cr00022a010.

(85) Bols, M.; Skrydstrup, T. Silicon-Tethered Reactions. *Chem. Rev.* **1995**, *95* (5), 1253–1277. https://doi.org/10.1021/cr00037a006.

(86) Langkopf, E.; Schinzer, D. Uses of Silicon-Containing Compounds in the Synthesis of Natural-Products. *Chem. Rev.* **1995**, *95* (5), 1375–1408. https://doi.org/10.1021/cr00037a011.

(87) Fleming, I.; Barbero, A.; Walter, D. Stereochemical Control in Organic Synthesis Using Silicon-Containing Compounds. *Chem. Rev.* **1997**, *97* (6), 2063–2192. https://doi.org/10.1021/cr941074u.

(88) Denmark, S. E.; Fu, J. Catalytic Enantioselective Addition of Allylic Organometallic Reagents to Aldehydes and Ketones. *Chem. Rev.* **2003**, *103* (8), 2763–2794. https://doi.org/10.1021/cr020050h.

(89) Dilman, A. D.; Ioffe, S. L. Carbon−Carbon Bond Forming Reactions Mediated by Silicon Lewis Acids. *Chem. Rev.* **2003**, *103* (3), 733–772. https://doi.org/10.1021/cr020003p.

(90) Fleming, I.; Dunoguès, J.; Smithers, R. The Electrophilic Substitution of Allylsilanes and Vinylsilanes. In *Organic Reactions*; John Wiley & Sons, Inc., 2004; pp 57–575. https://doi.org/10.1002/0471264180.or037.02.

(91) Masse, C. E.; Panek, J. S. Diastereoselective Reactions of Chiral Allyl and Allenyl Silanes with Activated C=X π -Bonds. *Chem. Rev.* **1995**, *95* (5), 1293–1316. https://doi.org/10.1021/cr00037a008.

(92) Sarkar, T. K.; Andersen, N. H. Allylsilanes in Organic Synthesis: A Facile Intramolecular Allyl Transfer, Evidence for a Non-Concerted Process. *Tetrahedron Lett.* **1978**, *19* (38), 3513–3516. https://doi.org/10.1016/S0040-4039(01)94979-2.

(93) Andersen, N. H.; McCrae, D. A.; Grotjahn, D. B.; Gabhe, S. Y.; Theodore, L. J.; Ippolito, R. M.; Sarkar, T. K. The Use of Metalloids (-$SiMe_3$,-SnR_3) as Protected Carbanions. *Tetrahedron* **1981**, *37* (23), 4069–4079. https://doi.org/10.1016/S0040-4020(01)93282-X.

(94) Itoh, A.; Oshima, K.; Nozaki, H. Stereospecific 2-Vinylcyclohexanol Formation via Internal Attack of an Allylsilane Moiety on an Aldehyde Group. *Tetrahedron Lett.* **1979**, *20* (20), 1783–1786. https://doi.org/10.1016/S0040-4039(01)86217-1.

(95) Trost, B. M.; Coppola, B. P. 2-Bromo-3-trimethylsilylpropene. An Annulating Agent for Five-Membered Carbo- and Heterocycles. *J. Am. Chem. Soc.* **1982**, *104* (24), 6879–6881. https://doi.org/10.1021/ja00388a112.

(96) Cernijenko, A.; Risgaard, R.; Baran, P. S. 11-Step Total Synthesis of (−)-Maoecrystal V. *J. Am. Chem. Soc.* **2016**, *138* (30), 9425–9428. https://doi.org/10.1021/jacs.6b06623.

(97) Denmark, S. E.; Almstead, N. G. Stereochemical Studies on the Addition of Allylsilanes to Aldehydes. The S_E' Component. *J. Org. Chem.* **1994**, *59* (18), 5130–5132. https://doi.org/10.1021/jo00097a008.

(98) Denmark, S. E.; Hosoi, S. Stereochemical Studies on the Addition of Allylstannanes to Aldehydes. The S_E' Component. *J. Org. Chem.* **1994**, *59* (18), 5133–5135. https://doi.org/10.1021/jo00097a009.

(99) Denmark, S. E.; Weber, E. J. On the Stereochemistry of Allylmetal-Aldehyde Condensations. Preliminary Communication. *Helv. Chim. Acta* **1983**, *66* (6), 1655–1660. https://doi.org/10.1002/hlca.19830660604.

(100) Denmark, S. E.; Weber, E. J.; Wilson, T. M.; Willson, T. M. Stereochemical and Spectroscopic Studies on the Reaction of Allylstannanes with Aldehydes. *Tetrahedron* **1989**, *45* (4), 1053–1065. https://doi.org/10.1016/0040-4020(89)80016-X.

(101) Beresis, R. T.; Salomon, J. S.; Yang, M. G.; Jain, N. F.; Panek, J. S. Synthesis of Chiral (E)-Crotylsilanes: [3R- and 3S-]-(4E)-Methyl 3-(Dimethylphenylsilyl)-4-Hexenoate. *Org. Synth.* **1998**, *75*, 78. https://doi.org/10.15227/orgsyn.075.0078.

(102) Fleming, I.; Hill, J. H. M.; Parker, D.; Waterson, D. Diastereoselectivity in the Alkylation and Protonation of Some β-Silyl Enolates. *J. Chem. Soc., Chem. Commun.* **1985**, No. 6, 318–321. https://doi.org/10.1039/C39850000318.

(103) Murphy, P. J.; Russell, A. T.; Procter, G. Allylsilanes in Organic Synthesis; Stereoselective Preparation and Reactions of Functionalised β,γ-Epoxysilanes. *Tetrahedron Lett.* **1990**, *31* (7), 1055–1058. https://doi.org/10.1016/s0040-4039(00)94429-0.

(104) Panek, J. S.; Beresis, R.; Xu, F.; Yang, M. Diastereoselective Electrophilic Addition-Reactions to Chiral β-Dimethylphenylsilyl Ester Enolates. Synthesis of 2,3-Anti-α-substituted-β-silyl-(E)-hex-4-enoates. *J. Org. Chem.* **1991**, *56* (26), 7341–7344. https://doi.org/10.1021/jo00026a030.

(105) Procter, G.; Russell, A. T.; Murphy, P. J.; Tan, T. S.; Mather, A. N. Epoxy-Silanes in Organic-Synthesis. *Tetrahedron* **1988**, *44* (13), 3953–3973. https://doi.org/10.1016/S0040-4020(01)86648-5.

(106) Wu, J.; Pu, Y.; Panek, J. S. Divergent Synthesis of Functionalized Carbocycles through Organosilane-Directed Asymmetric Alkyne–Alkene Reductive Coupling and Annulation Sequence. *J. Am. Chem. Soc.* **2012**, *134* (44), 18440–18446. https://doi.org/10.1021/ja3083945.

(107) Kuwajima, I.; Tanaka, T.; Atsumi, K. Preparation and Reactions of 2-Substituted 3-Trimethylsilyl-4-en-1-one System. *Chem. Lett.* **1979**, *8* (7), 779–782. https://doi.org/10.1246/cl.1979.779.

(108) Ladouceur, G.; Paquette, L. A. Application of the Anionic Oxy-Cope Rearrangement to Stereocontrolled Synthesis of the A/B Subunit of Cytoxic 8,9-Seco-Ent-Kaurenes. *Synthesis (Stuttg).* **1992**, *1992* (1/2), 185–191. https://doi.org/10.1055/s-1992-34185.

(109) Tsuna, K.; Noguchi, N.; Nakada, M. Enantioselective Total Synthesis of (+)-Ophiobolin A. *Chem. - A Eur. J.* **2013**, *19* (17), 5476–5486. https://doi.org/10.1002/chem.201204119.

(110) Kong, L.; Su, F.; Yu, H.; Jiang, Z.; Lu, Y.; Luo, T. Total Synthesis of (-)-Oridonin: An Interrupted Nazarov Approach. *J. Am. Chem. Soc.* **2019**, *141* (51), 20048–20052. https://doi.org/10.1021/jacs.9b12034.

(111) Hofstra, J. L.; Cherney, A. H.; Ordner, C. M.; Reisman, S. E. Synthesis of Enantioenriched Allylic Silanes via Nickel-Catalyzed Reductive Cross-Coupling. *J. Am. Chem. Soc.* **2018**, *140* (1), 139–142. https://doi.org/10.1021/jacs.7b11707.

(112) Majetich, G.; Hull, K.; Defauw, J.; Shawe, T. Geometrical Limitations in the Intramolecular Addition of Unsymmetrical Allylsilanes to Enones. *Tetrahedron Lett.* **1985**, *26* (23), 2755–2758. https://doi.org/10.1016/S0040-4039(00)94903-7.

(113) Majetich, G.; Behnke, M.; Hull, K. A Stereoselective Synthesis of (±)-Nootkatone and (±)-Valencene via an Intramolecular Sakurai Reaction. *J. Org. Chem.* **2002**, *50* (19), 3615–3618. https://doi.org/10.1021/jo00219a034.

(114) Lee, P. H.; Lee, K.; Sung, S.; Chang, S. The Catalytic Sakurai Reaction. *J. Org. Chem.* **2001**, *66* (25), 8646–8649. https://doi.org/10.1021/jo0105641.

(115) Tokoroyama, T.; Tsukamoto, M.; Asada, T.; Iio, H. One-Pot Stereospecific Construction of cis-Clerodane Skeleton by Means of Doubly Stereocontrolled Cyclization: Total Synthesis of Linaridial. *Tetrahedron Lett.* **1987**, *28* (52), 6645–6648. https://doi.org/10.1016/S0040-4039(00)96935-1.

(116) Anderson, J. C.; Pearson, D. J. A Strategy for the Synthesis of Popolohuanone E: Formal Total Synthesis of (±)-Arenarol. *J. Chem. Soc. Perkin Trans. 1* **1998**, No. 13, 2023–2030. https://doi.org/10.1039/a802413h.

(117) Munday, R. H.; Denton, R. M.; Anderson, J. C. Asymmetric Synthesis of 6′-Hydroxyarenarol: The Proposed Biosynthetic Precursor to Popolohuanone E. *J. Org. Chem.* **2008**, *73* (20), 8033–8038. https://doi.org/10.1021/jo801404u.

(118) Rodgen, S. A.; Schaus, S. E. Efficient Construction of the Clerodane Decalin Core by an Asymmetric Morita–Baylis–Hillman Reaction/Lewis Acid Promoted Annulation Strategy. *Angew. Chemie Int. Ed.* **2006**, *45* (30), 4929–4932. https://doi.org/10.1002/anie.200601076.

(119) Tietze, L. F.; Rischer, M. The Tandem Sakurai Carbonyl Ene Reaction: a New and Highly Stereoselective Sequential Transformation and Its Use for the Synthesis of Steroid Derivatives. *Angew. Chemie-International Ed. English* **1992**, *31* (9), 1221–1222. https://doi.org/10.1002/anie.199212211.

(120) Stevens, B. D.; Nelson, S. G. Tandem Sakurai-Aldol Addition Reactions as a Route to Structurally Complex Carbocycles. *J. Org. Chem.* **2005**, *70* (11), 4375–4379. https://doi.org/10.1021/jo050225y.

(121) Gimazetdinov, A. M.; Al'mukhametov, A. Z.; Spirikhin, L. V; Miftakhov, M. S. Fluoride Anion-Induced Intramolecular Cyclopropanation of Allylsilanes. *Tetrahedron Lett.* **2017**, *58* (33), 3242–3245. https://doi.org/10.1016/j.tetlet.2017.07.023.

(122) Overman, L. E.; Bell, K. L.; Ito, F. Enantioselective Total Syntheses of Pumiliotoxin B and Pumiliotoxin 251D. A General Entry to the Pumiliotoxin A Alkaloids via Stereospecific Iminium Ion Vinylsilane Cyclizations. *J. Am. Chem. Soc.* **1984**, *106* (15), 4192–4201. https://doi.org/10.1021/ja00327a022.

(123) Overman, L. E.; Malone, T. C.; Meier, G. P. Iminium Ion and Acyl Iminium Ion Initiated Cyclizations of Vinylsilanes. Regiocontrolled Construction of Unsaturated Azacyclics. *J. Am. Chem. Soc.* **2002**, *105* (23), 6993–6994. https://doi.org/10.1021/ja00361a058.

(124) Overman, L. E.; Goldstein, S. W. Enantioselective Total Synthesis of Allopumiliotoxin A Alkaloids 267A and 339B. *J. Am. Chem. Soc.* **2002**, *106* (18), 5360–5361. https://doi.org/10.1021/ja00330a059.

(125) Anderson, B. K.; Livinghouse, T. Divergent Stereocontrolled Synthesis of the Enantiopure Tetracyclic Cores of Asparagamine A and Stemofoline via an Intramolecular 2-Propylidine-1,3-(bis)silane Bicyclization. *J. Org. Chem.* **2015**, *80* (20), 9847–9855. https://doi.org/10.1021/acs.joc.5b01625.

(126) Park, Y.; Schindler, C. S.; Jacobsen, E. N. Enantioselective Aza-Sakurai Cyclizations: Dual Role of Thiourea as H-Bond Donor and Lewis Base. *J. Am. Chem. Soc.* **2016**, *138* (45), 14848–14851. https://doi.org/10.1021/jacs.6b09736.

(127) Yang, D.; Micalizio, G. C. Synthesis of Alkaloid (−)-205B via Stereoselective Reductive Cross-Coupling and Intramolecular [3+2] Cycloaddition. *J. Am. Chem. Soc.* **2012**, *134* (37), 15237–15240. https://doi.org/10.1021/ja306362m.

(128) Wang, Y.; Zhu, L.; Zhang, Y.; Hong, R. Bioinspired and Concise Synthesis of (±)-Stemoamide. *Angew. Chemie Int. Ed.* **2011**, *50* (12), 2787–2790. https://doi.org/10.1002/anie.201005833.

(129) Liu, H.; Yu, J.; Li, X.; Yan, R.; Xiao, J.-C.; Hong, R. Stereoselectivity in N-Iminium Ion Cyclization: Development of an Efficient Synthesis of (±)-Cephalotaxine. *Org. Lett.* **2015**, *17* (18), 4444–4447. https://doi.org/10.1021/acs.orglett.5b02106.

(130) Chen, Y.; Song, X.; Gao, L.; Song, Z. Intramolecular Sakurai Allylation of Geminal Bis(silyl) Enamide with Indolenine. A Diastereoselective Cyclization To Form Functionalized Hexahydropyrido[3,4-*b*]Indole. *Org. Lett.* **2021**, *23* (1), 124–128. https://doi.org/10.1021/acs.orglett.0c03806.

(131) Lepovitz, L. T.; Martin, S. F. Diversity-Oriented Synthesis of Bioactive Azaspirocycles. *Tetrahedron* **2019**, *75* (47), 130637. https://doi.org/10.1016/j.tet.2019.130637.

(132) Goodnough, A. M.; Sahn, J. J.; Martin, S. F. Facile Entry to Substituted 2-Arylpiperidines via an Aza-Sakurai Reaction. *Tetrahedron Lett.* **2020**, *61* (18), 151777. https://doi.org/10.1016/j.tetlet.2020.151777.

(133) Sun, P.; Sun, C.; Weinreb, S. M. A New Total Synthesis of the Marine Tunicate Alkaloid Lepadiformine. *Org. Lett.* **2001**, *3* (22), 3507–3510. https://doi.org/10.1021/ol010179y.

(134) Nocket, A. J.; Weinreb, S. M. Total Synthesis of the Tetracyclic Antimalarial Alkaloid (±)-Myrioneurinol. *Angew. Chemie Int. Ed.* **2014**, *53* (51), 14162–14165. https://doi.org/10.1002/anie.201407810.

(135) Yanagita, Y.; Suto, T.; Matsuo, N.; Kurosu, Y.; Sato, T.; Chida, N. Synthesis of Diazatricyclic Common Structure of Madangamine Alkaloids. *Org. Lett.* **2015**, *17* (8), 1946–1949. https://doi.org/10.1021/acs.orglett.5b00661.

(136) Fernández-Rivas, C.; Méndez, M.; Echavarren, A. M. Metal-Catalyzed Carbocyclization by Intramolecular Reaction of Allylsilanes and Allylstannanes with Alkynes. *J. Am. Chem. Soc.* **2000**, *122* (6), 1221–1222. https://doi.org/10.1021/ja993524b.

(137) Zhang, J.; Hazra, C. K.; Park, S.; Chang, S. Metal-Free Carbocyclization of Homoallylic Silyl Ethers Leading to Cyclopropanes and Cyclobutanes. *Asian J. Org. Chem.* **2019**, *8* (9), 1637–1640. https://doi.org/10.1002/ajoc.201900270.

(138) Reid, J. P.; McAdam, C. A.; Johnston, A. J. S.; Grayson, M. N.; Goodman, J. M.; Cook, M. J. Base-Mediated Cascade Rearrangements of Aryl-Substituted Diallyl Ethers. *J. Org. Chem.* **2015**, *80* (3), 1472–1498. https://doi.org/10.1021/jo502403n.

(139) Cheng, L.-J.; Cordier, C. J. Catalytic Nucleophilic Fluorination of Secondary and Tertiary Propargylic Electrophiles with a Copper-N-Heterocyclic Carbene Complex. *Angew. Chemie Int. Ed.* **2015**, *54* (46), 13734–13738. https://doi.org/10.1002/anie.201506882.

(140) Aspinall, H. C.; Greeves, N.; Lee, W.-M.; McIver, E. G.; Smith, P. M. An Improved Williamson Etherification of Hindered Alcohols Promoted by 15-Crown-5 and Sodium Hydride. *Tetrahedron Lett.* **1997**, *38* (26), 4679–4682. https://doi.org/10.1016/S0040-4039(97)00965-9.

(141) Xie, P.; Wo, X.; Yang, X.; Cai, X.; Li, S.; Gao, C.; Fu, W.; Sun, Z.; Loh, T.-P. Calcium-Catalyzed Regioselective Dehydrative Cross-Coupling of Propargylic Alcohols with 1,3-Dicarbonyl Compounds. *Green Chem.* **2019**, *21* (19), 5207–5211. https://doi.org/10.1039/C9GC02635E.

(142) Mizuno, A.; Kusama, H.; Iwasawa, N. Rhodium(I)-Catalyzed [4+1] Cycloaddition Reactions of α,β-Unsaturated Imines with Terminal Alkynes for the Preparation of Pyrrole Derivatives. *Angew. Chemie Int. Ed.* **2009**, *48* (44), 8318–8320. https://doi.org/10.1002/anie.200904402.

(143) Lumbroso, A.; Cooke, M. L.; Breit, B. Catalytic Asymmetric Synthesis of Allylic Alcohols and Derivatives and Their Applications in Organic Synthesis. *Angew. Chemie Int. Ed.* **2013**, *52* (7), 1890–1932. https://doi.org/10.1002/anie.201204579.

(144) Wisniewska, H. M.; Jarvo, E. R. Enantioselective Propargylation and Allenylation Reactions of Ketones and Imines. *J. Org. Chem.* **2013**, *78* (23), 11629–11636. https://doi.org/10.1021/jo4019107.

(145) Sasaki, M.; Ikemoto, H.; Kawahata, M.; Yamaguchi, K.; Takeda, K. [2,3]-Wittig Rearrangement of Enantiomerically Enriched 3-Substituted 1-Propenyloxy-1-phenyl-2-propen-1-yl Carbanions: Effect of Heteroatoms and Conjugating Groups on Planarization of an α-Oxy-Benzylcarbanion through a Double Bond. *Chem. - A Eur. J.* **2009**, *15* (18), 4663–4666. https://doi.org/10.1002/chem.200802322.

(146) Hansch, C.; Leo, A.; Taft, R. W. A Survey of Hammett Substituent Constants and Resonance and Field Parameters. *Chem. Rev.* **1991**, *91* (2), 165–195. https://doi.org/10.1021/cr00002a004.

(147) Wolf, L. M.; Denmark, S. E. A Theoretical Investigation on the Mechanism and Stereochemical Course of the Addition of (E)-2-Butenyltrimethylsilane to Acetaldehyde by Electrophilic and Nucleophilic Activation. *J. Am. Chem. Soc.* **2013**, *135* (12), 4743–4756. https://doi.org/10.1021/ja311889v.

(148) Denmark, S. E.; Weber, E. J.; Almstead, N. G.; Wolf, L. M. On the Stereochemical Course of the Addition of Allylsilanes to Aldehydes. *Tetrahedron* **2012**, *68* (37), 7701–7718. https://doi.org/10.1016/j.tet.2012.05.084.

(149) Kahn, S. D.; Pau, C. F.; Chamberlin, A. R.; Hehre, W. J. Modeling Chemical Reactivity. 4. Regiochemistry and Stereochemistry of Electrophilic Additions to Allylic Double Bonds. *J. Am. Chem. Soc.* **1987**, *109* (3), 650–663. https://doi.org/10.1021/ja00237a003.

(150) Lambert, J. B.; Emblidge, R. W.; Malany, S. The Question of Vertical or Nonvertical Participation of Silicon β to a Cation in the Antiperiplanar Stereochemistry. *J. Am. Chem. Soc.* **1993**, *115* (4), 1317–1320. https://doi.org/10.1021/ja00057a014.

(151) Butts, C. P.; Jones, C. R.; Towers, E. C.; Flynn, J. L.; Appleby, L.; Barron, N. J. Interproton Distance Determinations by NOE – Surprising Accuracy and Precision in a Rigid Organic Molecule. *Org. Biomol. Chem.* **2011**, *9* (1), 177–184. https://doi.org/10.1039/C0OB00479K.

(152) Guan, Y.; Bissantz, C.; Bergstrom, D. E.; Link, A. 1,2,4-Trisubstituted Cyclopentanes as Platforms for Diversity. *Arch. Pharm. (Weinheim).* **2012**, *345* (9), 677–686. https://doi.org/10.1002/ardp.201200101.

(153) Barrett, S.; O'Brien, P.; Steffens, H. C.; Towers, T. D.; Voith, M. New Route to 4-Aminocyclopent-2-en-1-ols: Synthesis and Enantioselective Rearrangement of 4-Amino-substituted Cyclopentene Oxides. *Tetrahedron* **2000**, *56* (49), 9633–9640. https://doi.org/10.1016/S0040-4020(00)00911-X.

(154) Ranatunga, S.; Valle, J. R. Del. Synthesis of Boc-Protected Bicycloproline. *Tetrahedron Lett.* **2009**, *50* (21), 2464–2466. https://doi.org/10.1016/j.tetlet.2009.03.092.

(155) Ovaska, T. V.; Reisman, S. E.; Flynn, M. A. Facile Entry to the Tetracyclic 5-7-6-3 Tigliane Ring System. *Org. Lett.* **2001**, *3* (1), 115–117. https://doi.org/10.1021/ol006823a.

(156) Casey, A. Organocatalytic Approaches to Claisen Rearrangements of Acid Sensitive Substrates, Montana State University, 2021.

(157) Takai, K.; Mori, I.; Oshima, K.; Nozaki, H. Aliphatic Claisen Rearrangement Promoted by Organoaluminium Compounds. *Tetrahedron Lett.* **1981**, *22* (40), 3985–3988. https://doi.org/10.1016/S0040-4039(01)82044-X.

(158) Takai, K.; Mori, I.; Oshima, K.; Nozaki, H. Aliphatic Claisen Rearrangement Promoted by Organoaluminium Reagents. *Bull. Chem. Soc. Jpn.* **1984**, *57* (2), 446–451. https://doi.org/10.1246/bcsj.57.446.

(159) Burt, J.; Levason, W.; Light, M. E.; Reid, G. Phosphine Complexes of Aluminium(III) Halides – Preparation and Structural and Spectroscopic Systematics. *Dalt. Trans.* **2014**, *43* (39), 14600–14611. https://doi.org/10.1039/C4DT02051K.

(160) Okazoe, T.; Takai, K.; Oshima, K.; Utimoto, K. Alkylidenation of Ester Carbonyl Groups by Means of a Reagent Derived from $RCHBr_2$, Zn, $TiCl_4$, and TMEDA. Stereoselective Preparation of (Z)-Alkenyl Ethers. *J. Org. Chem.* **1987**, *52* (19), 4410–4412. https://doi.org/10.1021/jo00228a055.

(161) Feng, Z.-G.; Bai, W.-J.; Pettus, T. R. R. Unified Total Syntheses of (−)-Medicarpin, (−)-Sophoracarpan A, and (±)-Kushecarpin A with Some Structural Revisions. *Angew. Chemie Int. Ed.* **2015**, *54* (6), 1864–1867. https://doi.org/10.1002/anie.201408910.

(162) Li, C.; Li, X.; Hong, R. Synthetic Study on Tetrapetalones: Stereoselective Cyclization of N-Acyliminium Ion To Construct Substituted 1-Benzazepines. *Org. Lett.* **2009**, *11* (18), 4036–4039. https://doi.org/10.1021/ol901349b.

(163) Trost, B. M.; Matelich, M. C. Synthesis and Palladium-Catalyzed Cycloaddition of the Bifunctional Conjunctive Reagent Methyl (Z)-1-Methyl-2-trimethylsilylmethyl-2-butenyl Carbonate. *Synthesis (Stuttg).* **1992**, *1992* (1/2), 151–156. https://doi.org/10.1055/s-1992-34152.

(164) Zirimwabagabo, J.-O.; Harrity, J. P. A. Pd-Catalyzed Kinetic Resolution of Cyclic Enol Ethers. An Enantioselective Route to Functionalised Pyrans. *Chem. Commun.* **2014**, *50* (21), 2735–2737. https://doi.org/10.1039/C4CC00109E.

(165) Hashmi, A. S. K.; Häffner, T.; Rudolph, M.; Rominger, F. Gold Catalysis: Domino Reaction of En-Diynes to Highly Substituted Phenols. *Chem. - A Eur. J.* **2011**, *17* (29), 8195–8201. https://doi.org/10.1002/chem.201100305.

(166) Riaz, M. T.; Pohorilets, I.; Hernandez, J. J.; Rios, J.; Totah, N. I. Preparation of 2-(trimethylsilyl)methyl-2-propen-1-ol Derivatives by Cobalt Catalyzed sp2-sp3 Coupling. *Tetrahedron Lett.* **2018**, *59* (29), 2809–2812. https://doi.org/10.1016/j.tetlet.2018.06.018.

(167) Trost, B. M.; Chan, D. M. T.; Nanninga, T. N. Silylation of 2-Methyl-2-propen-1-ol Dianion: 2-(Hydroxymethyl)Allyltrimethylsilane. In *Organic Syntheses*; John Wiley & Sons, Inc.: Hoboken, NJ, USA, 2003; pp 58–58. https://doi.org/10.1002/0471264180.os062.08.

(168) Trost, B. M.; Buch, M.; Miller, M. L. Convenient Alternative Approach to 2-(Acetoxymethyl)-3-(trimethylsilyl)propene. *J. Org. Chem.* **1988**, *53* (20), 4887–4888. https://doi.org/10.1021/jo00255a048.

(169) Smith, J. G.; Drozda, S. E.; Petraglia, S. P.; Quinn, N. R.; Rice, E. M.; Taylor, B. S.; Viswanathan, M. Regioselective Synthesis of Allyltrimethylsilanes from Allylic Halides and Allylic Sulfonates. Application to the Synthesis of 2,3-Bis(trimethylsilyl)alk-1-enes. *J. Org. Chem.* **1984**, *49* (22), 4112–4120. https://doi.org/10.1021/jo00196a002.

(170) Trost, B. M.; Grese, T. A.; Chan, D. M. T. Intramolecular Palladium-Catalyzed Trimethylenemethane Cycloadditions: Initial Studies. *J. Am. Chem. Soc.* **1991**, *113* (19), 7350–7362. https://doi.org/10.1021/ja00019a036.

(171) Smith III, A. B.; Duffey, M. O. Bifunctional Molecular Linchpins: A Three-Component Coupling Protocol Employing 2-Bromoallyltrimethylsilane. *Synlett* **2004**, No. 8, 1363–1366. https://doi.org/10.1055/s-2004-825621.

(172) Kim, H.; Lee, C. A Mild and Efficient Method for the Stereoselective Formation of C−O Bonds: Palladium-Catalyzed Allylic Etherification Using Zinc(II) Alkoxides. *Org. Lett.* **2002**, *4* (24), 4369–4371. https://doi.org/10.1021/ol027104u.

(173) Mayr, H.; Bug, T.; Gotta, M. F.; Hering, N.; Irrgang, B.; Janker, B.; Kempf, B.; Loos, R.; Ofial, A. R.; Remennikov, G.; Schimmel, H. Reference Scales for the Characterization of Cationic Electrophiles and Neutral Nucleophiles. *J. Am. Chem. Soc.* **2001**, *123* (39), 9500–9512. https://doi.org/10.1021/ja010890y.

(174) Frisch, M. J.; Trucks, G. W.; Schlegel, H. B.; Scuseria, G. E.; Robb, M. A.; Cheeseman, J. R.; Scalmani, G.; Barone, V.; Petersson, G. A.; Nakatsuji, H.; Li, X.; Caricato, M.; Marenich, A. V.; Bloino, J.; Janesko, B. G.; Gomperts, R.; Mennucci, B.; Hratchian, H. P.; Ortiz, J. V.; Izmaylov, A. F.; Sonnenberg, J. L.; Williams-Young, D.; Ding, F.; Lipparini, F.; Egidi, F.; Goings, J.; Peng, B.; Petrone, A.; Henderson, T.; Ranasinghe, D.; Zakrzewski, V. G.; Gao, J.; Rega, N.; Zheng, G.; Liang, W.; Hada, M.; Ehara, M.; Toyota, K.; Fukuda, R.; Hasegawa, J.; Ishida, M.; Nakajima, T.; Honda, Y.; Kitao, O.; Nakai, H.; Vreven, T.; Throssell, K.; Montgomery, J. A., J.; Peralta, J. E.; Ogliaro, F.; Bearpark, M. J.; Heyd, J. J.; Brothers, E. N.; Kudin, K. N.; Staroverov, V. N.; Keith, T. A.; Kobayashi, R.; Normand, J.; Raghavachari, K.; Rendell, A. P.; Burant, J. C.; Iyengar, S. S.; Tomasi, J.; Cossi, M.; Millam, J. M.; Klene, M.; Adamo, C.; Cammi, R.; Ochterski, J. W.; Martin, R. L.; Morokuma, K.; Farkas, O.; Foresman, J. B.; Fox, D. J. Gaussian 16, Revision A.03. Gaussian, Inc., Wallingford CT 2016.

(175) Legault, C. Y. CYLview, 1.0b. Université de Sherbrooke 2009.

(176) Dennington, R.; Keith, T. A.; Millam, J. M. GaussView, Version 6.1. Semichem Inc., Shawnee Mission, KS 2016.

(177) Luchini, G.; Alegre-Requena, J.; IFunes; Rodríguez-Guerra, J.; Chen, J.; Paton, R. GoodVibes v3.0.0. 2019. https://doi.org/10.5281/zenodo.3346166.

(178) Becke, A. D. Density-Functional Exchange-Energy Approximation with Correct Asymptotic Behavior. *Phys. Rev. A* **1988**, *38* (6), 3098–3100. https://doi.org/10.1103/PhysRevA.38.3098.

(179) Lee, C.; Yang, W.; Parr, R. G. Development of the Colle-Salvetti Correlation-Energy Formula into a Functional of the Electron Density. *Phys. Rev. B* **1988**, *37* (2), 785–789. https://doi.org/10.1103/PhysRevB.37.785.

(180) Gozzo, F. C.; Fernandes, S. A.; Rodrigues, D. C.; Eberlin, M. N.; Marsaioli, A. J. Regioselectivity in Aromatic Claisen Rearrangements. *J. Org. Chem.* **2003**, *68* (14), 5493–5499. https://doi.org/10.1021/jo026385g.

(181) Lee, C. W.; Taylor, B. L. H.; Petrova, G. P.; Patel, A.; Morokuma, K.; Houk, K. N.; Stoltz, B. M. An Unexpected Ireland–Claisen Rearrangement Cascade During the Synthesis of the Tricyclic Core of Curcusone C: Mechanistic Elucidation by Trial-and-Error and Automatic Artificial Force-Induced Reaction (AFIR) Computations. *J. Am. Chem. Soc.* **2019**, *141* (17), 6995–7004. https://doi.org/10.1021/jacs.9b01146.

(182) Aviyente, V.; Houk, K. N. Cyano, Amino, and Trifluoromethyl Substituent Effects on the Claisen Rearrangement. *J. Phys. Chem. A* **2001**, *105* (2), 383–391. https://doi.org/10.1021/jp003574z.

(183) Khaledy, M. M.; Kalani, M. Y. S.; Khuong, K. S.; Houk, K. N.; Aviyente, V.; Neier, R.; Soldermann, N.; Velker, J. Origins of Boat or Chair Preferences in the Ireland−Claisen Rearrangements of Cyclohexenyl Esters: A Theoretical Study. *J. Org. Chem.* **2003**, *68* (2), 572–577. https://doi.org/10.1021/jo020595b.

(184) Barone, V.; Cossi, M. Quantum Calculation of Molecular Energies and Energy Gradients in Solution by a Conductor Solvent Model. *J. Phys. Chem. A* **1998**, *102* (11), 1995–2001. https://doi.org/10.1021/jp9716997.

(185) Klamt, A.; Schüürmann, G. COSMO: A New Approach to Dielectric Screening in Solvents with Explicit Expressions for the Screening Energy and Its Gradient. *J. Chem. Soc., Perkin Trans. 2* **1993**, No. 5, 799–805. https://doi.org/10.1039/P29930000799.

(186) Peverati, R.; Truhlar, D. G. M11-L: A Local Density Functional That Provides Improved Accuracy for Electronic Structure Calculations in Chemistry and Physics. *J. Phys. Chem. Lett.* **2012**, *3* (1), 117–124. https://doi.org/10.1021/jz201525m.

(187) Chai, J.-D.; Head-Gordon, M. Long-Range Corrected Hybrid Density Functionals with Damped Atom–Atom Dispersion Corrections. *Phys. Chem. Chem. Phys.* **2008**, *10* (44), 6615. https://doi.org/10.1039/b810189b.

(188) Zhao, Y.; Truhlar, D. G. The M06 Suite of Density Functionals for Main Group Thermochemistry, Thermochemical Kinetics, Noncovalent Interactions, Excited States, and Transition Elements: Two New Functionals and Systematic Testing of Four M06-Class Functionals and 12 Other Functionals. *Theor. Chem. Acc.* **2008**, *120* (1–3), 215–241. https://doi.org/10.1007/s00214-007-0310-x.

(189) Grimme, S. Supramolecular Binding Thermodynamics by Dispersion-Corrected Density Functional Theory. *Chem. - A Eur. J.* **2012**, *18* (32), 9955–9964. https://doi.org/10.1002/chem.201200497.

(190) Li, Y.-P.; Gomes, J.; Mallikarjun Sharada, S.; Bell, A. T.; Head-Gordon, M. Improved Force-Field Parameters for QM/MM Simulations of the Energies of Adsorption for Molecules in Zeolites and a Free Rotor Correction to the Rigid Rotor Harmonic Oscillator Model for Adsorption Enthalpies. *J. Phys. Chem. C* **2015**, *119* (4), 1840–1850. https://doi.org/10.1021/jp509921r.

(191) Pracht, P.; Bohle, F.; Grimme, S. Automated Exploration of the Low-Energy Chemical Space with Fast Quantum Chemical Methods. *Phys. Chem. Chem. Phys.* **2020**, *22* (14), 7169–7192. https://doi.org/10.1039/C9CP06869D.

(192) Bannwarth, C.; Ehlert, S.; Grimme, S. GFN2-XTB—An Accurate and Broadly Parametrized Self-Consistent Tight-Binding Quantum Chemical Method with Multipole Electrostatics and Density-Dependent Dispersion Contributions. *J. Chem. Theory Comput.* **2019**, *15* (3), 1652–1671. https://doi.org/10.1021/acs.jctc.8b01176.

(193) Larock, R. C. *Comprehensive Organic Transformations*, 3rd Editio.; Wiley, 2018. https://doi.org/10.1002/9781118662083.

(194) Fleming, F. F.; Yao, L.; Ravikumar, P. C.; Funk, L.; Shook, B. C. Nitrile-Containing Pharmaceuticals: Efficacious Roles of the Nitrile Pharmacophore. *J. Med. Chem.* **2010**, *53* (22), 7902–7917. https://doi.org/10.1021/jm100762r.

(195) Fleming, F. F.; Fleming, F. F. Nitrile-Containing Natural Products. *Nat. Prod. Rep.* **1999**, *16* (5), 597–606. https://doi.org/10.1039/a804370a.

(196) Alexander, J. R.; Shchepetkina, V. I.; Stankevich, K. S.; Benedict, R. J.; Bernhard, S. P.; Dreiling, R. J.; Cook, M. J. Pd-Catalyzed Rearrangement of *N*-Alloc-*N*-allyl Ynamides via Auto-Tandem Catalysis: Evidence for Reversible C–N Activation and Pd(0)-Accelerated Ketenimine Aza-Claisen Rearrangement. *Org. Lett.* **2021**, *23* (2), 559–564. https://doi.org/10.1021/acs.orglett.0c04078.

(197) Jackson, O. D.; Stankevich, K. S.; Cook, M. J. Highly Diastereo- and Branched-Selective Rearrangement of Substituted *N*-Alloc-*N*-Allyl Ynamides. *Chem. Commun.* **2022**, *58* (84), 11855–11858. https://doi.org/10.1039/D2CC03399B.

(198) Jackson, O. D.; Stankevich, K. S.; Cook, M. J. Highly Diastereo- and Branched-Selective Rearrangement of Substituted *N*-Alloc-*N*-Allyl Ynamides via Pd-Auto-Tandem Catalysis. *ChemRxiv* **2022**. https://doi.org/10.26434/chemrxiv-2022-wxqb2.

(199) Chen, J.; Cook, M. J. Palladium Catalyzed Decarboxylative Rearrangement of *N*-Alloc Indoles. *Org. Lett.* **2013**, *15* (5), 1088–1091. https://doi.org/10.1021/ol400110c.

(200) Alexander, J. R.; Cook, M. J. Formation of Ketenimines via the Palladium-Catalyzed Decarboxylative π-Allylic Rearrangement of *N*-Alloc Ynamides. *Org. Lett.* **2017**, *19* (21), 5822–5825. https://doi.org/10.1021/acs.orglett.7b02780.

(201) Tsuji, J.; Takahashi, H. Organic Syntheses by Means of Noble Metal Compounds. XII.[1] Reaction of the Cyclooctadiene-Palladium Chloride Complex with Ethyl Malonate. *J. Am. Chem. Soc.* **1965**, *87* (14), 3275–3276. https://doi.org/10.1021/ja01092a067.

(202) Trost, B. M.; Crawley, M. L. Asymmetric Transition-Metal-Catalyzed Allylic Alkylations: Applications in Total Synthesis. *Chem. Rev.* **2003**, *103* (8), 2921–2944. https://doi.org/10.1021/cr020027w.

(203) Hartwig, J. F. *Organotransition Metal Chemistry: From Bonding to Catalysis*; University Science Books, 2010.

(204) Kita, Y.; Kavthe, R. D.; Oda, H.; Mashima, K. Asymmetric Allylic Alkylation of β-Ketoesters with Allylic Alcohols by a Nickel/Diphosphine Catalyst. *Angew. Chemie Int. Ed.* **2016**, *55* (3), 1098–1101. https://doi.org/10.1002/anie.201508757.

(205) Belda, O.; Moberg, C. Molybdenum-Catalyzed Asymmetric Allylic Alkylations. *Acc. Chem. Res.* **2004**, *37* (3), 159–167. https://doi.org/10.1021/ar030239v.

(206) Bruneau, C.; Achard, M. Allylic Ruthenium(IV) Complexes in Catalysis. *Coord. Chem. Rev.* **2012**, *256* (5–8), 525–536. https://doi.org/10.1016/j.ccr.2011.10.018.

(207) Hethcox, J. C.; Shockley, S. E.; Stoltz, B. M. Enantioselective Synthesis of Vicinal All-Carbon Quaternary Centers via Iridium-Catalyzed Allylic Alkylation. *Angew. Chemie Int. Ed.* **2018**, *57* (28), 8664–8667. https://doi.org/10.1002/anie.201804820.

(208) Tosatti, P.; Nelson, A.; Marsden, S. P. Recent Advances and Applications of Iridium-Catalysed Asymmetric Allylic Substitution. *Org. Biomol. Chem.* **2012**, *10* (16), 3147. https://doi.org/10.1039/c2ob07086c.

(209) Evans, P. A.; Kennedy, L. J. Enantiospecific and Regioselective Rhodium-Catalyzed Allylic Alkylation: Diastereoselective Approach to Quaternary Carbon Stereogenic Centers. *Org. Lett.* **2000**, *2* (15), 2213–2215. https://doi.org/10.1021/ol005953g.

(210) Tang, S.-B.; Zhang, X.; Tu, H.-F.; You, S.-L. Regio- and Enantioselective Rhodium-Catalyzed Allylic Alkylation of Racemic Allylic Alcohols with 1,3-Diketones. *J. Am. Chem. Soc.* **2018**, *140* (24), 7737–7742. https://doi.org/10.1021/jacs.8b05126.

(211) Sperger, T.; Fisher, H. C.; Schoenebeck, F. Computationally Deciphering Palladium-Catalyzed Reaction Mechanisms. *Wiley Interdiscip. Rev. Comput. Mol. Sci.* **2016**, *6* (3), 226–242. https://doi.org/10.1002/wcms.1244.

(212) Shimizu, I.; Yamada, T.; Tsuji, J. Palladium-Catalyzed Rearrangement of Allylic Esters of Acetoacetic Acid to Give γ,δ-Unsaturated Methyl Ketones. *Tetrahedron Lett.* **1980**, *21* (33), 3199–3202. https://doi.org/10.1016/S0040-4039(00)77444-2.

(213) Tsuda, T.; Chujo, Y.; Nishi, S.; Tawara, K.; Saegusa, T. Facile Generation of a Reactive Palladium(II) Enolate Intermediate by the Decarboxylation of Palladium(II) β-Ketocarboxylate and Its Utilization in Allylic Acylation. *J. Am. Chem. Soc.* **1980**, *102* (20), 6381–6384. https://doi.org/10.1021/ja00540a053.

(214) Tunge, J. A. The Evolution of Decarboxylative Allylation: Overcoming pKa Limitations. *Isr. J. Chem.* **2020**, *60* (3–4), 351–359. https://doi.org/10.1002/ijch.201900177.

(215) Trost, B. M.; Xu, J.; Schmidt, T. Palladium-Catalyzed Decarboxylative Asymmetric Allylic Alkylation of Enol Carbonates. *J. Am. Chem. Soc.* **2009**, *131* (51), 18343–18357. https://doi.org/10.1021/ja9053948.

(216) Keith, J. A.; Behenna, D. C.; Mohr, J. T.; Ma, S.; Marinescu, S. C.; Oxgaard, J.; Stoltz, B. M.; Goddard, W. A. The Inner-Sphere Process in the Enantioselective Tsuji Allylation Reaction with (S)-t-Bu-Phosphinooxazoline Ligands. *J. Am. Chem. Soc.* **2007**, *129* (39), 11876–11877. https://doi.org/10.1021/ja070516j.

(217) Cusumano, A. Q.; Stoltz, B. M.; Goddard, W. A. Reaction Mechanism, Origins of Enantioselectivity, and Reactivity Trends in Asymmetric Allylic Alkylation: A Comprehensive Quantum Mechanics Investigation of a $C(sp^3)$–$C(sp^3)$ Cross-Coupling. *J. Am. Chem. Soc.* **2020**, *142* (32), 13917–13933. https://doi.org/10.1021/jacs.0c06243.

(218) McPherson, K. E.; Croatt, M. P.; Morehead, A. T.; Sargent, A. L. DFT Mechanistic Investigation of an Enantioselective Tsuji–Trost Allylation Reaction. *Organometallics* **2018**, *37* (21), 3791–3802. https://doi.org/10.1021/acs.organomet.8b00507.

(219) Recio, A.; Tunge, J. A. Regiospecific Decarboxylative Allylation of Nitriles. *Org. Lett.* **2009**, *11* (24), 5630–5633. https://doi.org/10.1021/ol902065p.

(220) Beare, N. A.; Hartwig, J. F. Palladium-Catalyzed Arylation of Malonates and Cyanoesters Using Sterically Hindered Trialkyl- and Ferrocenyldialkylphosphine Ligands. *J. Org. Chem.* **2002**, *67* (2), 541–555. https://doi.org/10.1021/jo016226h.

(221) Culkin, D. A.; Hartwig, J. F. Synthesis, Characterization, and Reactivity of Arylpalladium Cyanoalkyl Complexes: Selection of Catalysts for the α-Arylation of Nitriles. *J. Am. Chem. Soc.* **2002**, *124* (32), 9330–9331. https://doi.org/10.1021/ja026584h.

(222) Wright, B. A.; Ardolino, M. J. Surprising Reactivity in NiXantphos/Palladium-Catalyzed α-Arylation of Substituted Cyclopropyl Nitriles. *J. Org. Chem.* **2019**, *84* (8), 4670–4679. https://doi.org/10.1021/acs.joc.8b02238.

(223) Li, Z.; Jiang, Y.-Y.; Yeagley, A. A.; Bour, J. P.; Liu, L.; Chruma, J. J.; Fu, Y. Mechanism of the Pd-Catalyzed Decarboxylative Allylation of α-Imino Esters: Decarboxylation via Free Carboxylate Ion. *Chem. - A Eur. J.* **2012**, *18* (45), 14527–14538. https://doi.org/10.1002/chem.201201425.

(224) Walters, M. A.; Hoem, A. B.; McDonough, C. S. Rearrangements of Substituted 3-Aza-1,2,5-Hexatrienes. 3. The Scope and Versatility of an Extremely Mild 3-Aza-Cope Reaction. *J. Org. Chem.* **1996**, *61* (1), 55–62. https://doi.org/10.1021/jo951587g.

(225) Walters, M. A. Ab Initio Investigation of the 3-Aza-Cope Reaction. *J. Org. Chem.* **1996**, *61* (3), 978–983. https://doi.org/10.1021/jo951131z.

(226) Walters, M. A. Ab Initio Investigation of Three 3-Aza-Claisen Variations. *J. Am. Chem. Soc.* **1994**, *116* (25), 11618–11619. https://doi.org/10.1021/ja00104a072.

(227) DeKorver, K. A.; Hsung, R. P.; Lohse, A. G.; Zhang, Y. A Divergent Mechanistic Course of Pd(0)-Catalyzed Aza-Claisen Rearrangement and Aza-Rautenstrauch-Type Cyclization of N-Allyl Ynamides. *Org. Lett.* **2010**, *12* (8), 1840–1843. https://doi.org/10.1021/ol100446p.

(228) Wang, X.-N.; Winston-McPherson, G. N.; Walton, M. C.; Zhang, Y.; Hsung, R. P.; DeKorver, K. A. Synthesis of Cyclopentenimines from N-Allyl Ynamides via a Tandem Aza-Claisen Rearrangement–Carbocyclization Sequence. *J. Org. Chem.* **2013**, *78* (12), 6233–6244. https://doi.org/10.1021/jo400960e.

(229) Suzuki, T.; Fujimoto, H. Mechanisms of the Nucleophilic Substitution of the Allyl Carbons of (π-Allyl)Platinum and (π-Allyl)Palladium Complexes. *Inorg. Chem.* **1999**, *38* (2), 370–382. https://doi.org/10.1021/ic9805877.

(230) Szabó, K. J. Effects of the Ancillary Ligands on Palladium−Carbon Bonding in (η^3-Allyl)Palladium Complexes. Implications for Nucleophilic Attack at the Allylic Carbons. *Organometallics* **1996**, *15* (4), 1128–1133. https://doi.org/10.1021/om950715o.

(231) Sakaki, S.; Satoh, H.; Shono, H.; Ujino, Y. Ab Initio MO Study of the Geometry, $\eta^3 \rightleftarrows \eta^1$ Conversion, and Reductive Elimination of a Palladium(II) η^3-Allyl Hydride Complex and Its Platinum(II) Analogue. *Organometallics* **1996**, *15* (6), 1713–1720. https://doi.org/10.1021/om9600046.

(232) Riplinger, C.; Neese, F. An Efficient and near Linear Scaling Pair Natural Orbital Based Local Coupled Cluster Method. *J. Chem. Phys.* **2013**, *138* (3), 034106. https://doi.org/10.1063/1.4773581.

(233) Sandler, I.; Chen, J.; Taylor, M.; Sharma, S.; Ho, J. Accuracy of DLPNO-CCSD(T): Effect of Basis Set and System Size. *J. Phys. Chem. A* **2021**, *125* (7), 1553–1563. https://doi.org/10.1021/acs.jpca.0c11270.

(234) Norrby, P. O.; Aakermark, B.; Haeffner, F.; Hansson, S.; Blomberg, M. Molecular Mechanics (MM2) Parameters for the (η^3-Allyl)Palladium Moiety. *J. Am. Chem. Soc.* **1993**, *115* (11), 4859–4867. https://doi.org/10.1021/ja00064a054.

(235) Hagelin, H.; Åkermark, B.; Norrby, P.-O. New Molecular Mechanics (MM3*) Force Field Parameters for Calculations on (η^3 -Allyl)Palladium Complexes with Nitrogen and Phosphorus Ligands. *Organometallics* **1999**, *18* (15), 2884–2895. https://doi.org/10.1021/om990153z.

(236) Ateşin, T. A.; Atesin, A. C.; Rodriguez, O.; Rivera, D.; Garcia, L. Y. Conformational Analysis of a TADDOL-Based Phosphoramidite P,N Ligand in a Palladium(II) η^3-π-Allyl Complex. *Comput. Theor. Chem.* **2018**, *1139*, 70–76. https://doi.org/10.1016/j.comptc.2018.07.007.

(237) Carroll, A.-M.; McCarthy, M.; Lacey, P. M.; Saunders, C. P.; Connolly, D. J.; Farrell, A.; Rokade, B. V.; Goddard, R.; Fristrup, P.; Norrby, P.-O.; Guiry, P. J. Synthetic and Mechanistic Studies in Enantioselective Allylic Substitutions Catalysed by Palladium Complexes of a Modular Class of Axially Chiral Quinazoline-Containing Ligands. *Tetrahedron* **2020**, *76* (1), 130780. https://doi.org/10.1016/j.tet.2019.130780.

(238) Oslob, J. D.; Åkermark, B.; Helquist, P.; Norrby, P.-O. Steric Influences on the Selectivity in Palladium-Catalyzed Allylation. *Organometallics* **1997**, *16* (13), 3015–3021. https://doi.org/10.1021/om9700371.

(239) Ikeda, A.; Nakao, Y.; Sato, H.; Sakaki, S. Binding Energy of Transition-Metal Complexes with Large π-Conjugate Systems. Density Functional Theory vs Post-Hartree−Fock Methods. *J. Phys. Chem. A* **2007**, *111* (30), 7124–7132. https://doi.org/10.1021/jp0708648.

(240) Averkiev, B. B.; Zhao, Y.; Truhlar, D. G. Binding Energy of d^{10} Transition Metals to Alkenes by Wave Function Theory and Density Functional Theory. *J. Mol. Catal. A Chem.* **2010**, *324* (1–2), 80–88. https://doi.org/10.1016/j.molcata.2010.03.016.

(241) Li, Z.; Liu, L.; Fu, Y.; Guo, Q.-X. Assessing Performance of Diverse ONIOM Methods in Calculation of Structures of Organonickel and Organopalladium Compounds. *J. Mol. Struct. THEOCHEM* **2005**, *757* (1–3), 69–76. https://doi.org/10.1016/j.theochem.2005.07.014.

(242) Wang, Q.; Guo, C.-H.; Ren, Y.; Wu, H.-S. A Computational Study on the Insertion of CO_2 into (PSiP)Palladium Allyl σ-Bond. *J. Mol. Model.* **2015**, *21* (5), 122. https://doi.org/10.1007/s00894-015-2678-1.

(243) Yamamoto, Y. The First General and Selective Palladium(II)-Catalyzed Alkoxycarbonylation of Arylboronates: Interplay among Benzoquinone-Ligated Palladium(0) Complex, Organoboron, and Alcohol Solvent. *Adv. Synth. Catal.* **2010**, *352* (2–3), 478–492. https://doi.org/10.1002/adsc.200900836.

(244) Vázquez, J.; Goldfuss, B.; Helmchen, G. Isomerism of (π-1,3-Dimethylallyl)(Phosphinooxazoline)Pd Complexes: A Comparison between Experiment and Theory. *J. Organomet. Chem.* **2002**, *641* (1–2), 67–70. https://doi.org/10.1016/S0022-328X(01)01308-0.

(245) Chung, L. W.; Sameera, W. M. C.; Ramozzi, R.; Page, A. J.; Hatanaka, M.; Petrova, G. P.; Harris, T. V.; Li, X.; Ke, Z.; Liu, F.; Li, H.-B.; Ding, L.; Morokuma, K. The ONIOM Method and Its Applications. *Chem. Rev.* **2015**, *115* (12), 5678–5796. https://doi.org/10.1021/cr5004419.

(246) Ananikov, V. P.; Musaev, D. G.; Morokuma, K. Real Size of Ligands, Reactants and Catalysts: Studies of Structure, Reactivity and Selectivity by ONIOM and Other Hybrid Computational Approaches. *J. Mol. Catal. A Chem.* **2010**, *324* (1–2), 104–119. https://doi.org/10.1016/j.molcata.2010.03.015.

(247) Jindal, G.; Sunoj, R. B. Mechanistic Insights on Cooperative Asymmetric Multicatalysis Using Chiral Counterions. *J. Org. Chem.* **2014**, *79* (16), 7600–7606. https://doi.org/10.1021/jo501322v.

(248) Ardolino, M. J.; Eno, M. S.; Morken, J. P. Stereocontrol in Palladium-Catalyzed Propargylic Substitutions: Kinetic Resolution to Give Enantioenriched 1,5-Enynes and Propargyl Acetates. *Adv. Synth. Catal.* **2013**, *355* (17), 3413–3419. https://doi.org/10.1002/adsc.201300720.

(249) Ardolino, M. J.; Morken, J. P. Branched/Linear Selectivity in Palladium-Catalyzed Allyl-Allyl Cross-Couplings: The Role of Ligands. *Tetrahedron* **2015**, *71* (37), 6409–6413. https://doi.org/10.1016/j.tet.2015.05.015.

(250) Ardolino, M. J.; Morken, J. P. Congested C–C Bonds by Pd-Catalyzed Enantioselective Allyl–Allyl Cross-Coupling, a Mechanism-Guided Solution. *J. Am. Chem. Soc.* **2014**, *136* (19), 7092–7100. https://doi.org/10.1021/ja502280w.

(251) Tomé, M.; Grabulosa, A.; Rocamora, M.; Aullón, G.; Font-Bardía, M.; Calvet, T.; López, C. Synthesis, Characterization, Solution Behavior and Theoretical Studies of Pd(II) Allyl Complexes with 2-Phenyl-3H-Indoles as Ligands. *Catalysts* **2019**, *9* (10), 811. https://doi.org/10.3390/catal9100811.

(252) Tsutsumi, H.; Sunada, Y.; Shiota, Y.; Yoshizawa, K.; Nagashima, H. Nickel(II), Palladium(II), and Platinum(II) η^3-Allyl Complexes Bearing a Bidentate Titanium(IV) Phosphinoamide Ligand: A Ti←M_2 Dative Bond Enhances the Electrophilicity of the π-Allyl Moiety. *Organometallics* **2009**, *28* (7), 1988–1991. https://doi.org/10.1021/om8011085.

(253) Margalef, J.; Coll, M.; Norrby, P.-O.; Pàmies, O.; Diéguez, M. Asymmetric Catalyzed Allylic Substitution Using a Pd/P–S Catalyst Library with Exceptional High Substrate and Nucleophile Versatility: DFT and Pd-π-Allyl Key Intermediates Studies. *Organometallics* **2016**, *35* (19), 3323–3335. https://doi.org/10.1021/acs.organomet.6b00547.

(254) Katcher, M. H.; Norrby, P.-O.; Doyle, A. G. Mechanistic Investigations of Palladium-Catalyzed Allylic Fluorination. *Organometallics* **2014**, *33* (9), 2121–2133. https://doi.org/10.1021/om401240p.

(255) Tang, D.; Luo, X.; Shen, W.; Li, M. The Mechanism of Enantioselective Palladium(0)-Catalyzed Allylic Alkylation with Chiral Oxazolinylpyridines: A DFT Study. *J. Mol. Struct. THEOCHEM* **2005**, *716* (1–3), 79–87. https://doi.org/10.1016/j.theochem.2004.10.087.

(256) Zhao, Y.; Truhlar, D. G. Density Functionals with Broad Applicability in Chemistry. *Acc. Chem. Res.* **2008**, *41* (2), 157–167. https://doi.org/10.1021/ar700111a.

(257) Ateşin, T. A.; Martinez, G. M.; Flores, D. It Is Not Just Up to the Substrate: Palladium(0) Cyclizes Nazarov Substrates through Intramolecular Allylic Alkylation. *Organometallics* **2017**, *36* (18), 3589–3596. https://doi.org/10.1021/acs.organomet.7b00494.

(258) Amadio, E.; Scrivanti, A.; Bortoluzzi, M.; Bertoldini, M.; Beghetto, V.; Matteoli, U.; Chessa, G. A New Palladium(II)–Allyl Complex Containing a Thioether-Triazole Ligand as Active Catalyst in Suzuki–Miyaura Reaction. Use of Tetraalkylammonium Salts as Promoters: Influence of the Salt Anion and Cation on the Catalytic Activity. *Inorganica Chim. Acta* **2013**, *405*, 188–195. https://doi.org/10.1016/j.ica.2013.05.028.

(259) Xu, L.; Zhang, X.; McCammant, M. S.; Sigman, M. S.; Wu, Y.-D.; Wiest, O. Mechanism and Selectivity in the Pd-Catalyzed Difunctionalization of Isoprene. *J. Org. Chem.* **2016**, *81* (17), 7604–7611. https://doi.org/10.1021/acs.joc.6b01317.

(260) Szabó, K. J. Nature of the Interaction between β-Substituents and the Allyl Moiety in (η^3-allyl)Palladium Complexes. *Chem. Soc. Rev.* **2001**, *30* (2), 136–143. https://doi.org/10.1039/a908934i.

(261) Iuliis, M. Z. De; Watson, I. D.; Yudin, A. K.; Morris, R. H. A DFT Investigation into the Origin of Regioselectivity in Palladium-Catalyzed Allylic Amination. *Can. J. Chem.* **2009**, *87* (1), 54–62. https://doi.org/10.1139/v08-078.

(262) Lyu, L.; Feng, W.; Yang, S.; Liu, H.; Huang, X. Exploring the Mechanism of the Palladium-Catalyzed 3-Butene-2-ol Amination Reaction: A DFT Study. *Front. Chem.* **2020**, *8*. https://doi.org/10.3389/fchem.2020.00048.

(263) Keith, J. A.; Behenna, D. C.; Sherden, N.; Mohr, J. T.; Ma, S.; Marinescu, S. C.; Nielsen, R. J.; Oxgaard, J.; Stoltz, B. M.; Goddard, W. A. The Reaction Mechanism of the Enantioselective Tsuji Allylation: Inner-Sphere and Outer-Sphere Pathways, Internal Rearrangements, and Asymmetric C–C Bond Formation. *J. Am. Chem. Soc.* **2012**, *134* (46), 19050–19060. https://doi.org/10.1021/ja306860n.

(264) Hagelin, H.; Åkermark, B.; Norrby, P.-O. A Solvated Transition State for the Nucleophilic Attack on Cationic η^3-Allylpalladium Complexes. *Chem. - A Eur. J.* **1999**, *5* (3), 902–909. https://doi.org/10.1002/(SICI)1521-3765(19990301)5:3<902::AID-CHEM902>3.0.CO;2-W.

(265) Zhao, Y.; Truhlar, D. G. Comparative Assessment of Density Functional Methods for 3d Transition-Metal Chemistry. *J. Chem. Phys.* **2006**, *124* (22), 224105. https://doi.org/10.1063/1.2202732.

(266) Miertuš, S.; Scrocco, E.; Tomasi, J. Electrostatic Interaction of a Solute with a Continuum. A Direct Utilizaion of Ab Initio Molecular Potentials for the Prevision of Solvent Effects. *Chem. Phys.* **1981**, *55* (1), 117–129. https://doi.org/10.1016/0301-0104(81)85090-2.

(267) Marenich, A. V.; Cramer, C. J.; Truhlar, D. G. Universal Solvation Model Based on Solute Electron Density and on a Continuum Model of the Solvent Defined by the Bulk Dielectric Constant and Atomic Surface Tensions. *J. Phys. Chem. B* **2009**, *113* (18), 6378–6396. https://doi.org/10.1021/jp810292n.

(268) Karami, K.; Abedanzadeh, S.; Farrokhpour, H.; Lipkowski, J. Synthesis and Characterization of the P,C-Palladacycles with Bridging and Chelating Dinitrogen Ligands and ONIOM Calculations on the Pyrazine-Bridged Organometallic Polymers (n = 1 to n = 10). *J. Organomet. Chem.* **2016**, *805*, 68–76. https://doi.org/10.1016/j.jorganchem.2016.01.013.

(269) Sherden, N. H.; Behenna, D. C.; Virgil, S. C.; Stoltz, B. M. Unusual Allylpalladium Carboxylate Complexes: Identification of the Resting State of Catalytic Enantioselective Decarboxylative Allylic Alkylation Reactions of Ketones. *Angew. Chemie Int. Ed.* **2009**, *48* (37), 6840–6843. https://doi.org/10.1002/anie.200902575.

(270) Evano, G.; Michelet, B.; Zhang, C. The Anionic Chemistry of Ynamides: A Review. *Comptes Rendus Chim.* **2017**, *20* (6), 648–664. https://doi.org/10.1016/j.crci.2016.12.002.

(271) van Haaren, R. J.; Goubitz, K.; Fraanje, J.; van Strijdonck, G. P. F.; Oevering, H.; Coussens, B.; Reek, J. N. H.; Kamer, P. C. J.; van Leeuwen, P. W. N. M. An X-Ray Study of the Effect of the Bite Angle of Chelating Ligands on the Geometry of Palladium(Allyl) Complexes: Implications for the Regioselectivity in the Allylic Alkylation. *Inorg. Chem.* **2001**, *40* (14), 3363–3372. https://doi.org/10.1021/ic0009167.

(272) Falivene, L.; Cao, Z.; Petta, A.; Serra, L.; Poater, A.; Oliva, R.; Scarano, V.; Cavallo, L. Towards the Online Computer-Aided Design of Catalytic Pockets. *Nat. Chem.* **2019**, *11* (10), 872–879. https://doi.org/10.1038/s41557-019-0319-5.

(273) van Leeuwen, P. W. N. M.; Kamer, P. C. J.; Reek, J. N. H.; Dierkes, P. Ligand Bite Angle Effects in Metal-Catalyzed C−C Bond Formation. *Chem. Rev.* **2000**, *100* (8), 2741–2770. https://doi.org/10.1021/cr9902704.

(274) Neese, F. Software Update: The ORCA Program System, Version 4.0. *WIREs Comput. Mol. Sci.* **2018**, *8* (1). https://doi.org/10.1002/wcms.1327.

(275) Neese, F. The ORCA Program System. *WIREs Comput. Mol. Sci.* **2012**, *2* (1), 73–78. https://doi.org/10.1002/wcms.81.

(276) Bao, H.; Tambar, U. K. Catalytic Enantioselective Allylic Amination of Unactivated Terminal Olefins via an Ene Reaction/[2,3]-Rearrangement. *J. Am. Chem. Soc.* **2012**, *134* (45), 18495–18498. https://doi.org/10.1021/ja307851b.

(277) Cannon, J. S.; Overman, L. E. Palladium(II)-Catalyzed Enantioselective Reactions Using COP Catalysts. *Acc. Chem. Res.* **2016**, *49* (10), 2220–2231. https://doi.org/10.1021/acs.accounts.6b00398.

(278) Gutierrez, O.; Hendrick, C. E.; Kozlowski, M. C. Divergent Reactivity in Pd-Catalyzed [3,3]-Sigmatropic Rearrangement of Allyloxy- and Propargyloxyindoles Revealed by Computation and Experiment. *Org. Lett.* **2018**, *20* (20), 6539–6543. https://doi.org/10.1021/acs.orglett.8b02864.

(279) Siebert, M. R.; Tantillo, D. J. Transition-State Complexation in Palladium-Promoted [3,3] Sigmatropic Shifts. *J. Am. Chem. Soc.* **2007**, *129* (28), 8686–8687. https://doi.org/10.1021/ja072159i.

(280) Jochims, J. C.; Anet, F. A. L. Ketenimines. Geometry and Barriers to Racemization. *J. Am. Chem. Soc.* **1970**, *92* (18), 5524–5525. https://doi.org/10.1021/ja00721a044.

(281) Zheng, C.; Zhuo, C.-X.; You, S.-L. Mechanistic Insights into the Pd-Catalyzed Intermolecular Asymmetric Allylic Dearomatization of Multisubstituted Pyrroles: Understanding the Remarkable Regio- and Enantioselectivity. *J. Am. Chem. Soc.* **2014**, *136* (46), 16251–16259. https://doi.org/10.1021/ja5080135.

(282) Rossi-Ashton, J. A.; Clarke, A. K.; Donald, J. R.; Zheng, C.; Taylor, R. J. K.; Unsworth, W. P.; You, S. Iridium-Catalyzed Enantioselective Intermolecular Indole C2-Allylation. *Angew. Chemie Int. Ed.* **2020**, *59* (19), 7598–7604. https://doi.org/10.1002/anie.202001956.

(283) Lefebvre, C.; Khartabil, H.; Boisson, J.-C.; Contreras-García, J.; Piquemal, J.-P.; Hénon, E. The Independent Gradient Model: A New Approach for Probing Strong and Weak Interactions in Molecules from Wave Function Calculations. *ChemPhysChem* **2018**, *19* (6), 724–735. https://doi.org/10.1002/cphc.201701325.

(284) Schrödinger Release 2018-4: MacroModel. Schrödinger, LLC, New York, NY 2018.

(285) Spicher, S.; Grimme, S. Robust Atomistic Modeling of Materials, Organometallic, and Biochemical Systems. *Angew. Chemie* **2020**, *132* (36), 15795–15803. https://doi.org/10.1002/ange.202004239.

(286) Humphrey, W.; Dalke, A.; Schulten, K. VMD: Visual Molecular Dynamics. *J. Mol. Graph.* **1996**, *14* (1), 33–38. https://doi.org/10.1016/0263-7855(96)00018-5.

APPENDIX A

NMR SPECTRA

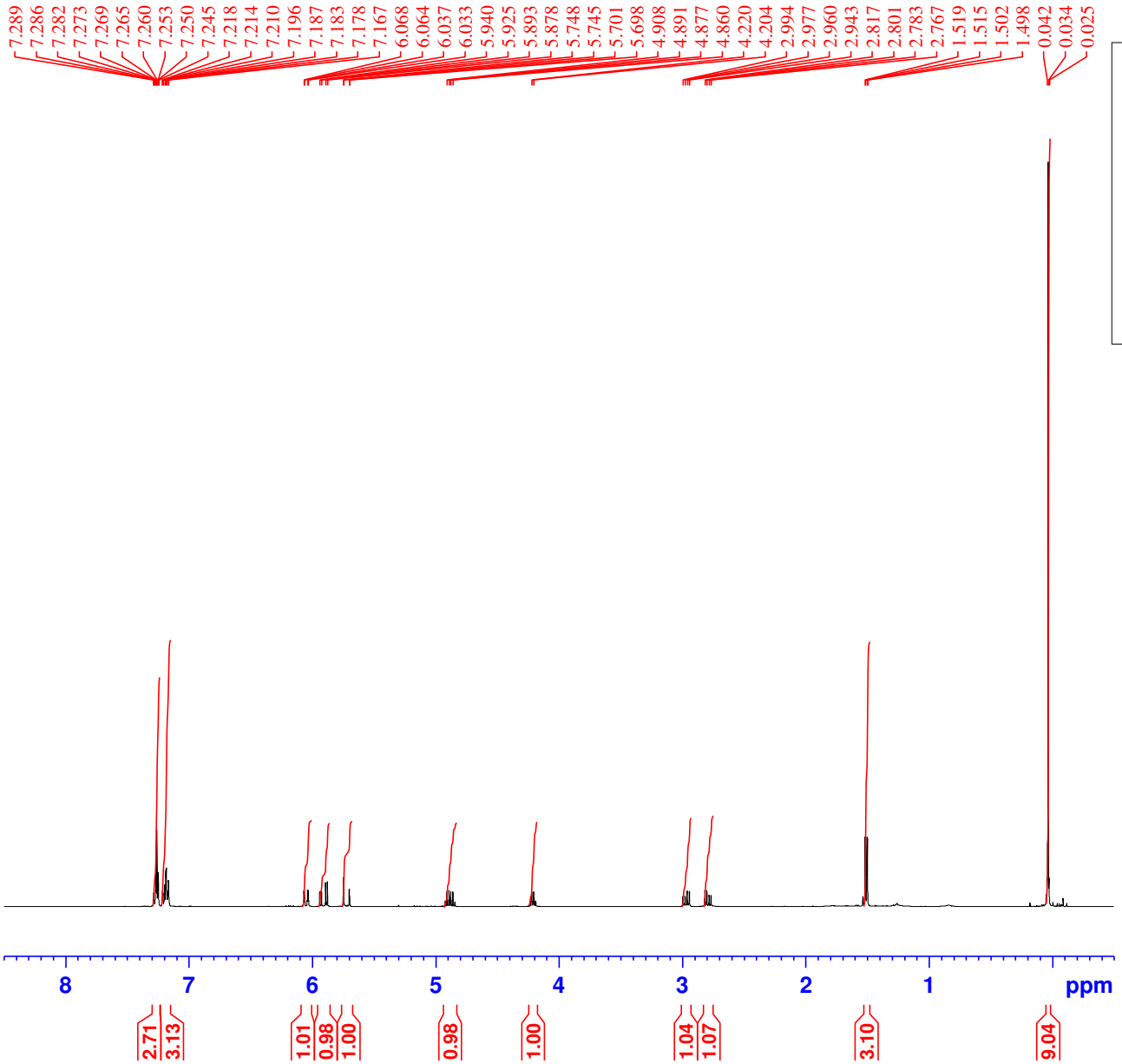

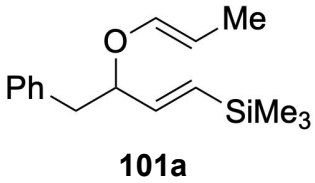

101a

```
Current Data Parameters
NAME      KS-02-93
EXPNO               10
PROCNO               1

F2 - Acquisition Parameters
Date_          20220214
Time              15.57 h
INSTRUM       Avance Neo
PROBHD    Z152088_0031 (
PULPROG             zg30
TD                 65536
SOLVENT            CDCl3
NS                    16
DS                     2
SWH             8196.722 Hz
FIDRES          0.250144 Hz
AQ              3.9976959 sec
RG                   101
DW                61.000 usec
DE                13.89 usec
TE                298.0 K
D1            1.00000000 sec
TD0                    1
SFO1         400.1324708 MHz
NUC1                 1H
P0                 2.67 usec
P1                 8.00 usec
PLW1         24.03499985 W

F2 - Processing parameters
SI                 65536
SF           400.1300096 MHz
WDW                   EM
SSB                    0
LB                  0.30 Hz
GB                     0
PC                  1.00
```

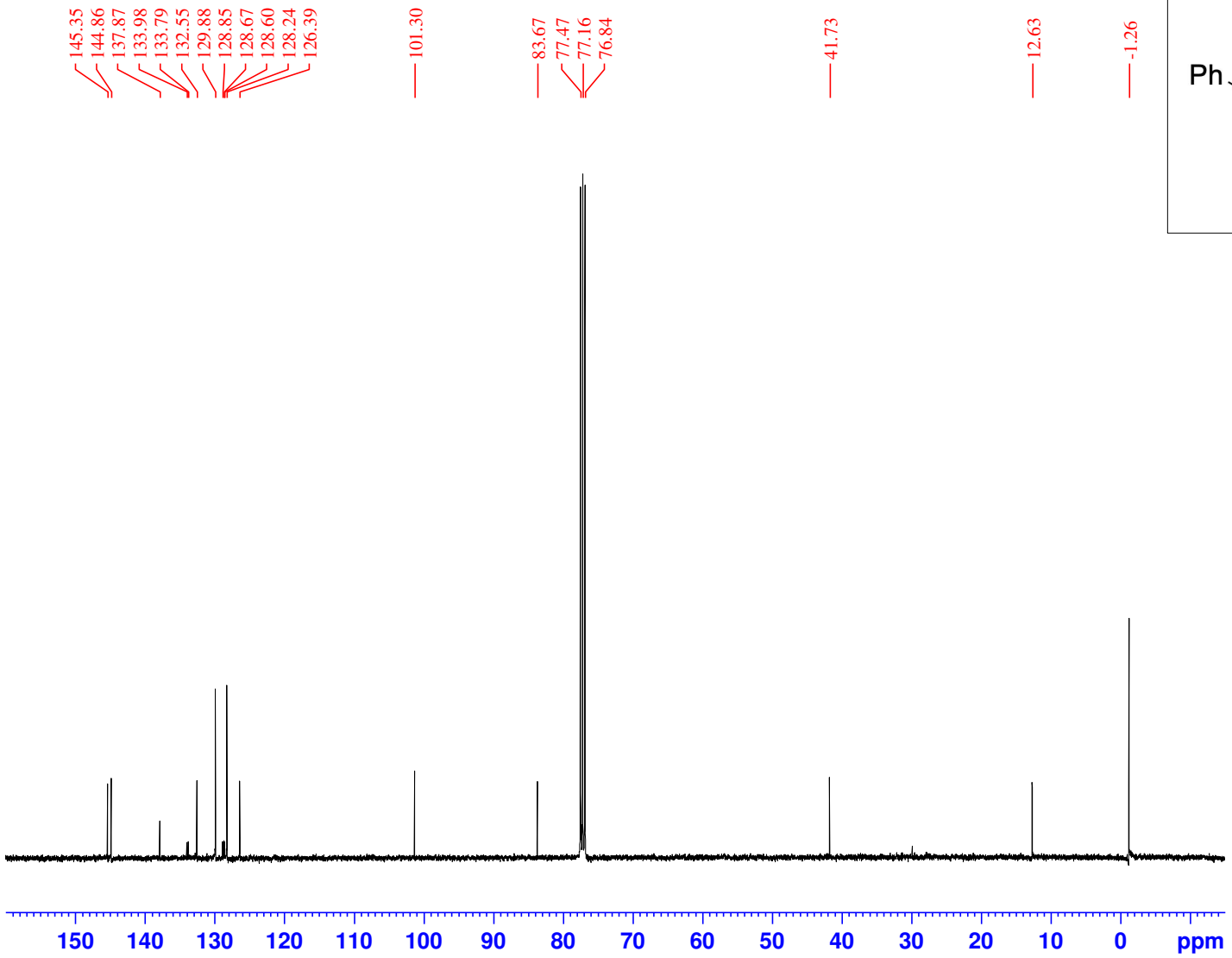

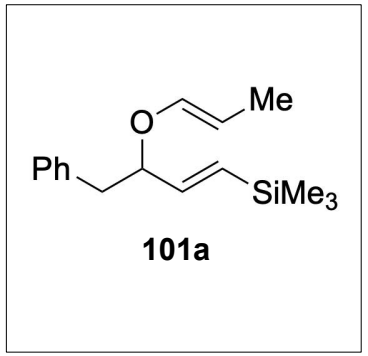

101a

```
Current Data Parameters
NAME      KS-02-93
EXPNO               11
PROCNO               1

F2 - Acquisition Parameters
Date_          20210830
Time              20.01 h
INSTRUM       Avance Neo
PROBHD   Z152088_0031 (
PULPROG          zgpg30
TD                65536
SOLVENT           CDCl3
NS                 1024
DS                    4
SWH           23809.523 Hz
FIDRES         0.726609 Hz
AQ             1.3762560 sec
RG                8.125
DW               21.000 usec
DE                6.50 usec
TE               298.1 K
D1            2.00000000 sec
D11           0.03000000 sec
TD0                   1
SFO1         100.6228298 MHz
NUC1                13C
P0                2.67 usec
P1                8.00 usec
PLW1         86.55400085 W
SFO2         400.1316005 MHz
NUC2                1H
CPDPRG[2         waltz65
PCPD2             90.00 usec
PLW2         24.03499985 W
PLW12         0.18990999 W
PLW13         0.09552100 W

F2 - Processing parameters
SI                32768
SF           100.6127544 MHz
WDW                  EM
SSB                   0
LB                 1.00 Hz
GB                    0
PC                 1.40
```

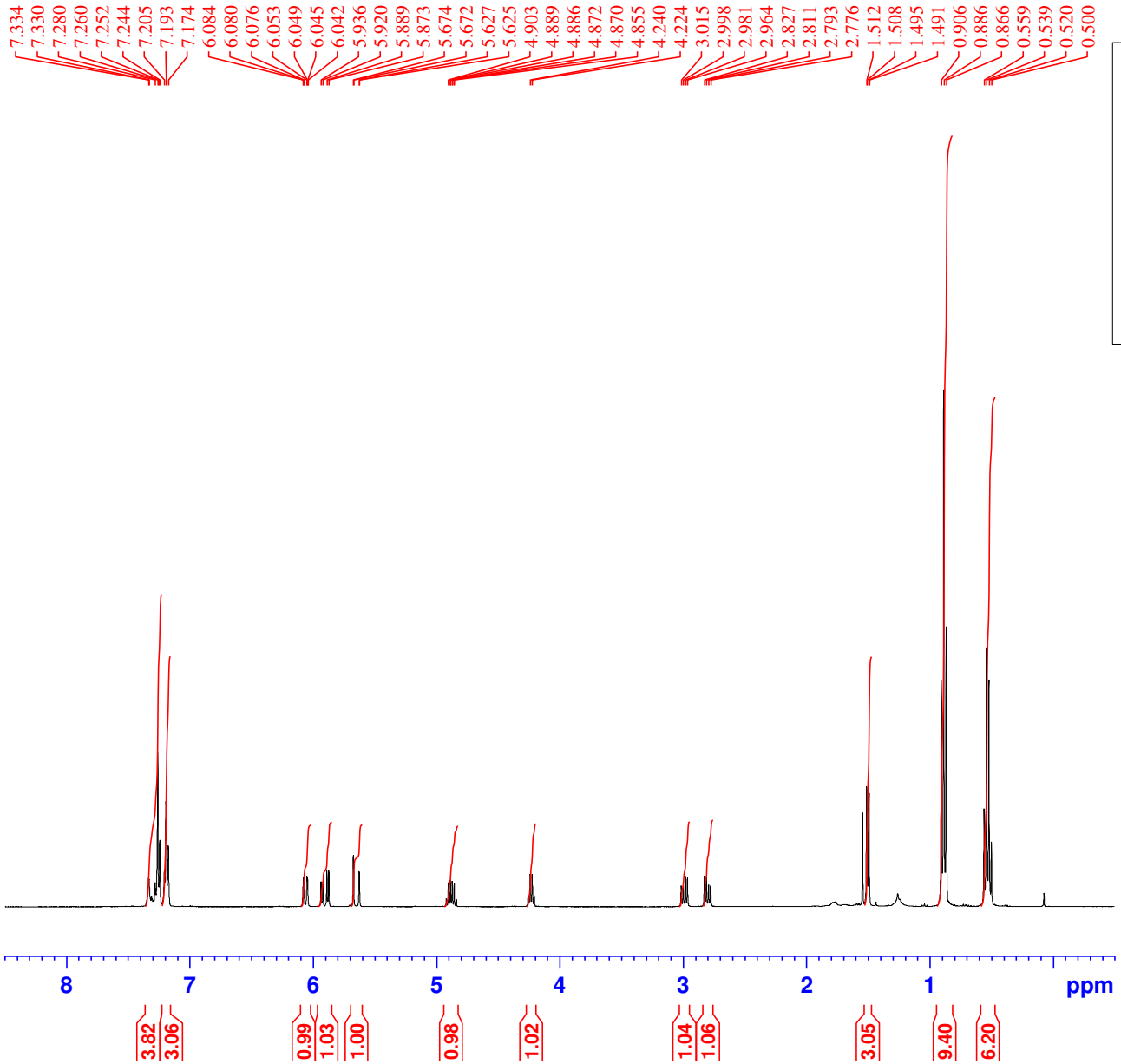

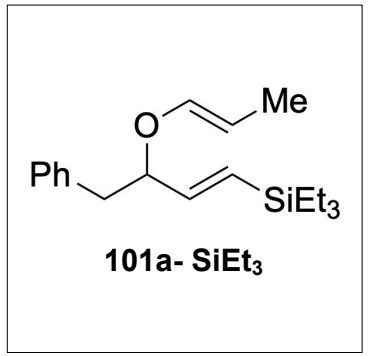

101a- $SiEt_3$

```
Current Data Parameters
NAME      KS-02-97
EXPNO                10
PROCNO                1

F2 - Acquisition Parameters
Date_          20210901
Time               16.20 h
INSTRUM       Avance Neo
PROBHD    Z152088_0031 (
PULPROG             zg30
TD                 65536
SOLVENT            CDCl3
NS                    16
DS                     2
SWH             8196.722 Hz
FIDRES          0.250144 Hz
AQ              3.9976959 sec
RG                   101
DW                61.000 usec
DE                13.89 usec
TE                298.2 K
D1             1.00000000 sec
TD0                    1
SFO1         400.1324708 MHz
NUC1                 1H
P0                 2.67 usec
P1                 8.00 usec
PLW1         24.03499985 W

F2 - Processing parameters
SI                 65536
SF           400.1300095 MHz
WDW                   EM
SSB                    0
LB                  0.30 Hz
GB                     0
PC                  1.00
```

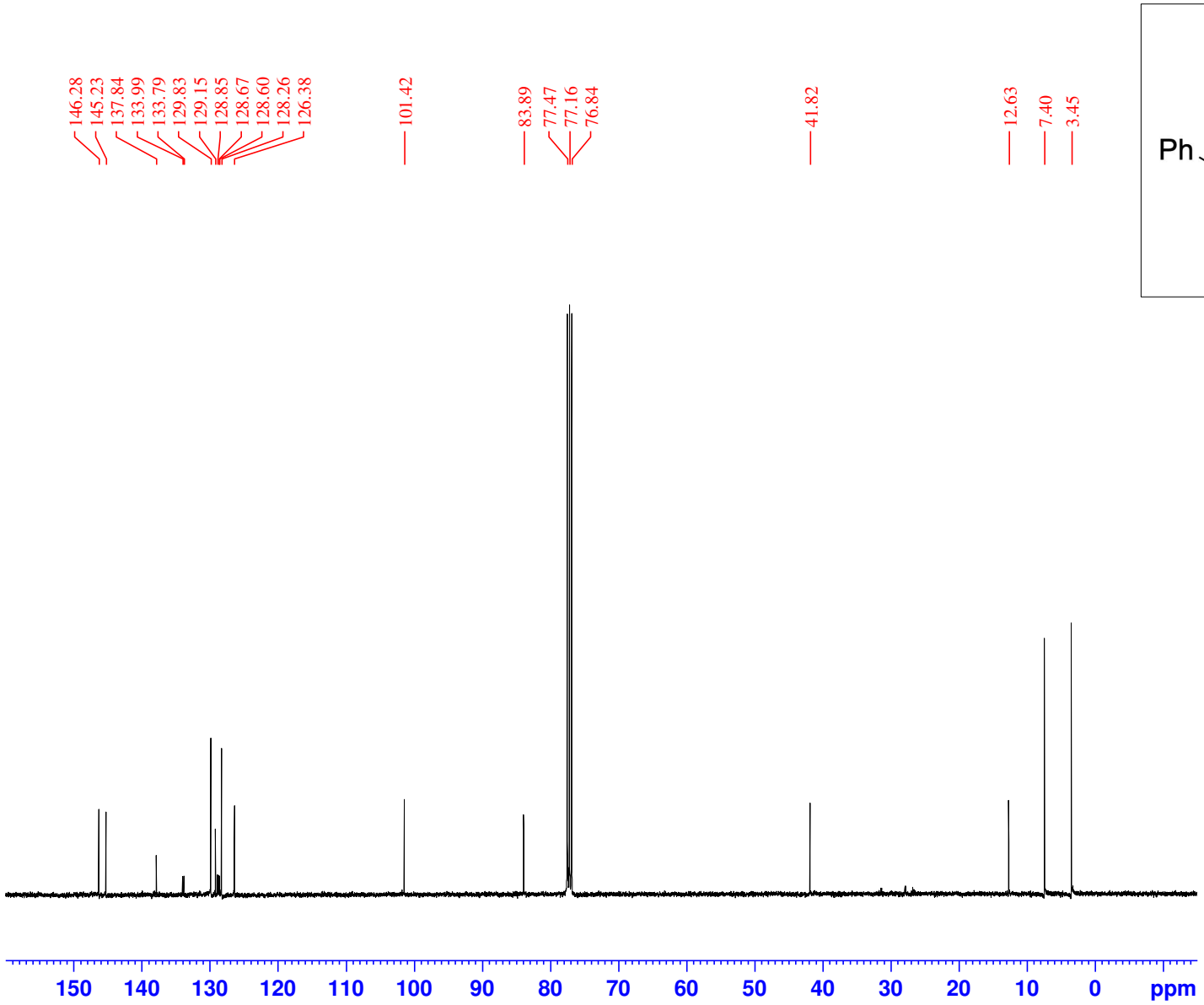

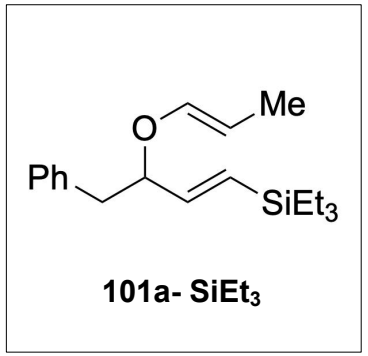

101a- $SiEt_3$

```
Current Data Parameters
NAME      KS-02-97
EXPNO               11
PROCNO               1

F2 - Acquisition Parameters
Date_          20210901
Time             21.06 h
INSTRUM      Avance Neo
PROBHD   Z152088_0031 (
PULPROG          zgpg30
TD                65536
SOLVENT           CDCl3
NS                 1024
DS                    4
SWH           23809.523 Hz
FIDRES         0.726609 Hz
AQ             1.3762560 sec
RG                8.125
DW               21.000 usec
DE                6.50 usec
TE               298.1 K
D1            2.00000000 sec
D11           0.03000000 sec
TD0                   1
SFO1         100.6228298 MHz
NUC1                13C
P0                 2.67 usec
P1                 8.00 usec
PLW1         86.55400085 W
SFO2         400.1316005 MHz
NUC2                1H
CPDPRG[2         waltz65
PCPD2             90.00 usec
PLW2         24.03499985 W
PLW12         0.18990999 W
PLW13         0.09552100 W

F2 - Processing parameters
SI                32768
SF           100.6127544 MHz
WDW                  EM
SSB                   0
LB                 1.00 Hz
GB                    0
PC                 1.40
```

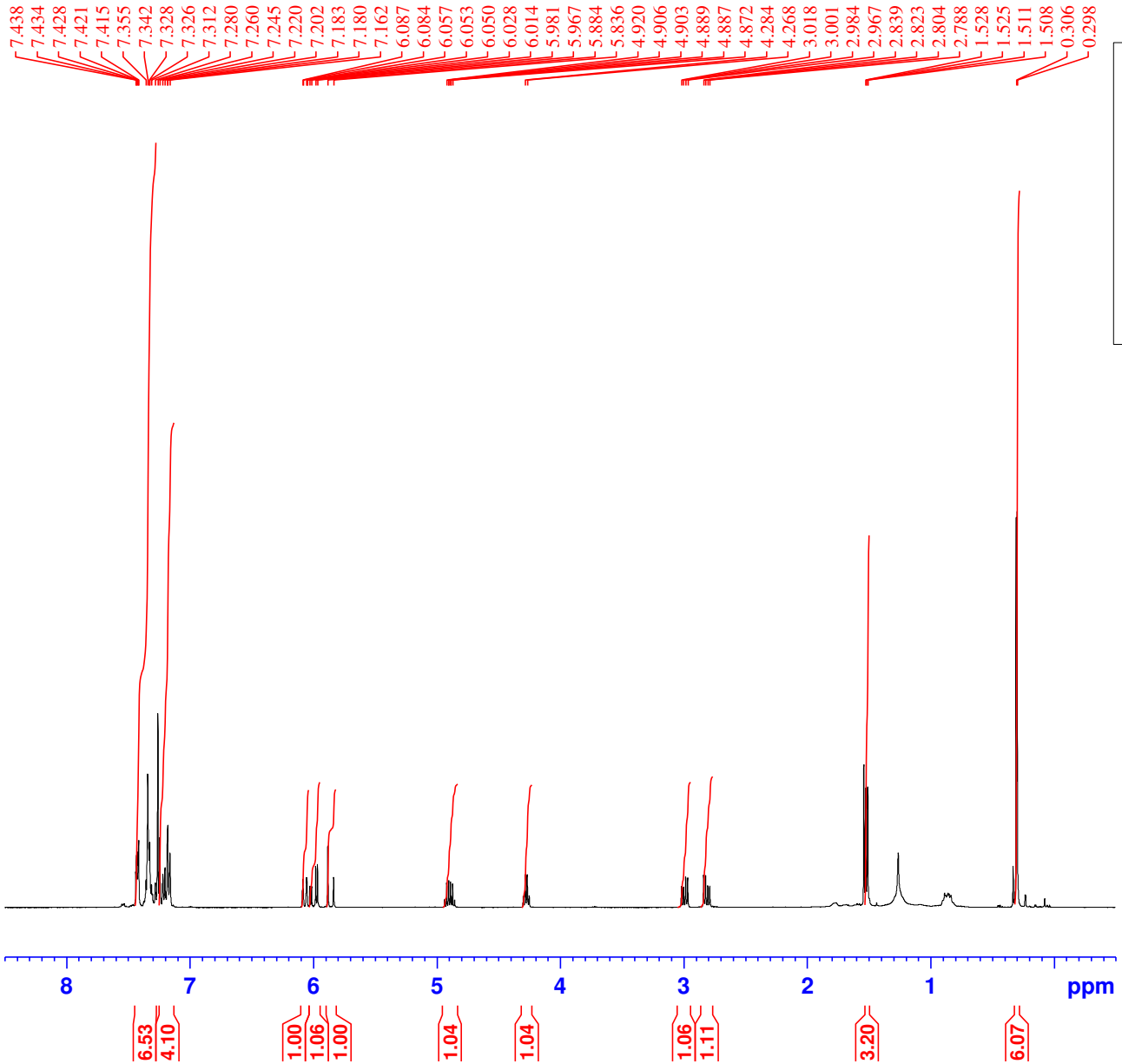

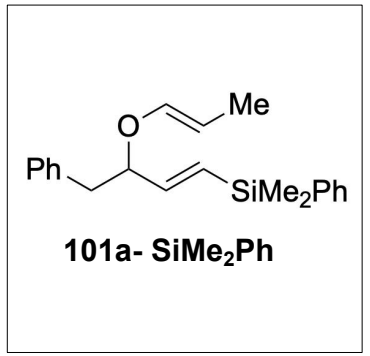

101a- $SiMe_2Ph$

```
Current Data Parameters
NAME      KS-02-96
EXPNO               10
PROCNO               1

F2 - Acquisition Parameters
Date_          20210901
Time             16.14 h
INSTRUM      Avance Neo
PROBHD   Z152088_0031 (
PULPROG            zg30
TD                65536
SOLVENT           CDCl3
NS                   16
DS                    2
SWH            8196.722 Hz
FIDRES         0.250144 Hz
AQ             3.9976959 sec
RG                  101
DW                61.000 usec
DE                13.89 usec
TE                298.2 K
D1           1.00000000 sec
TD0                   1
SFO1        400.1324708 MHz
NUC1                1H
P0                2.67 usec
P1                8.00 usec
PLW1        24.03499985 W

F2 - Processing parameters
SI                65536
SF          400.1300097 MHz
WDW                  EM
SSB                   0
LB                 0.30 Hz
GB                    0
PC                 1.00
```

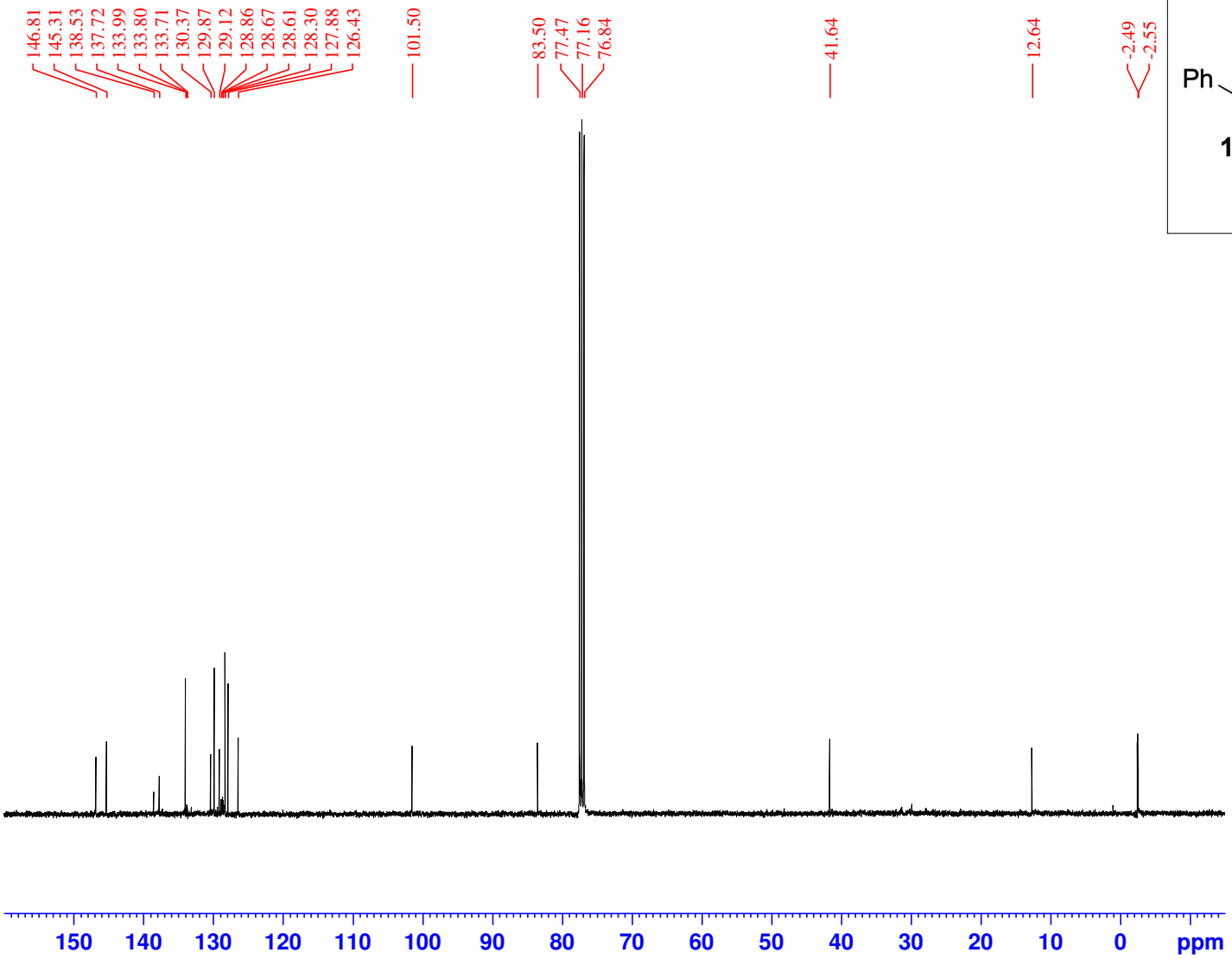

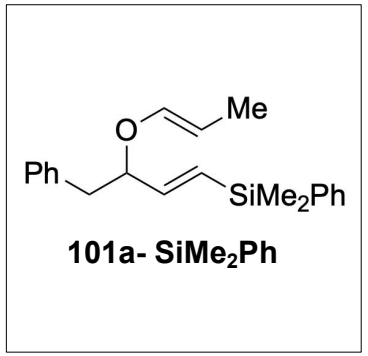

101a- $SiMe_2Ph$

```
Current Data Parameters
NAME      KS-02-96
EXPNO               11
PROCNO               1

F2 - Acquisition Parameters
Date_         20210901
Time             20.03 h
INSTRUM      Avance Neo
PROBHD   Z152088_0031 (
PULPROG         zgpg30
TD               65536
SOLVENT          CDCl3
NS                1024
DS                   4
SWH          23809.523 Hz
FIDRES        0.726609 Hz
AQ            1.3762560 sec
RG                8.125
DW               21.000 usec
DE                6.50 usec
TE                298.2 K
D1           2.00000000 sec
D11          0.03000000 sec
TD0                  1
SFO1        100.6228298 MHz
NUC1               13C
P0                2.67 usec
P1                8.00 usec
PLW1        86.55400085 W
SFO2        400.1316005 MHz
NUC2               1H
CPDPRG[2        waltz65
PCPD2             90.00 usec
PLW2        24.03499985 W
PLW12        0.18990999 W
PLW13        0.09552100 W

F2 - Processing parameters
SI                32768
SF          100.6127546 MHz
WDW                EM
SSB                 0
LB                1.00 Hz
GB                  0
PC                1.40
```

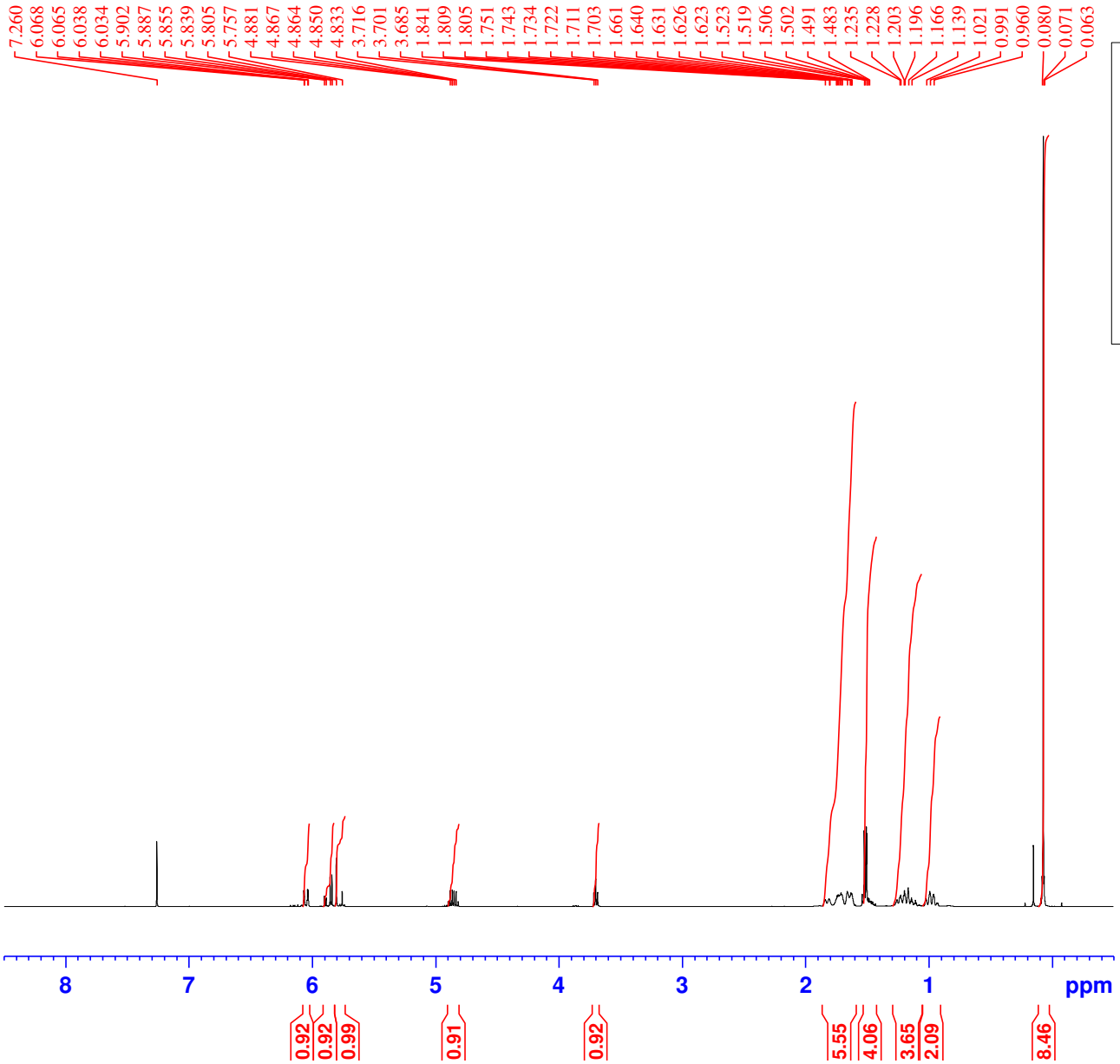

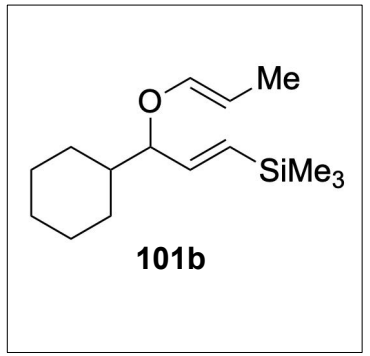

101b

```
Current Data Parameters
NAME        KS-02-259
EXPNO              10
PROCNO              1

F2 - Acquisition Parameters
Date_          20220218
Time             14.13 h
INSTRUM       Avance Neo
PROBHD    Z152088_0031 (
PULPROG            zg30
TD                65536
SOLVENT           CDCl3
NS                   16
DS                    2
SWH           8196.722 Hz
FIDRES        0.250144 Hz
AQ            3.9976959 sec
RG                  101
DW               61.000 usec
DE               13.89 usec
TE               298.0 K
D1            1.00000000 sec
TD0                   1
SFO1        400.1324708 MHz
NUC1                1H
P0                2.67 usec
P1                8.00 usec
PLW1        24.03499985 W

F2 - Processing parameters
SI                65536
SF          400.1300096 MHz
WDW                  EM
SSB                   0
LB                 0.30 Hz
GB                    0
PC                 1.00
```

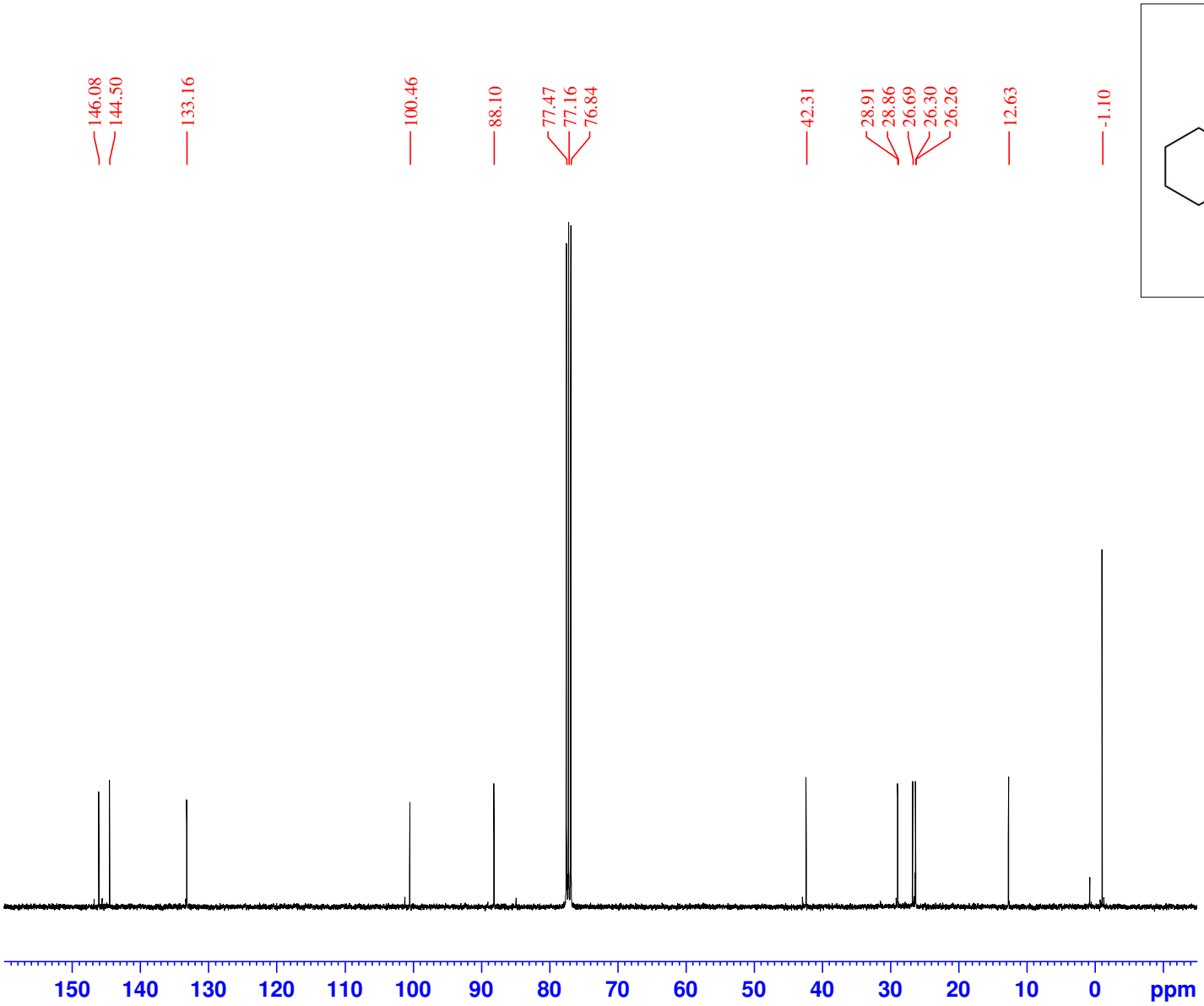

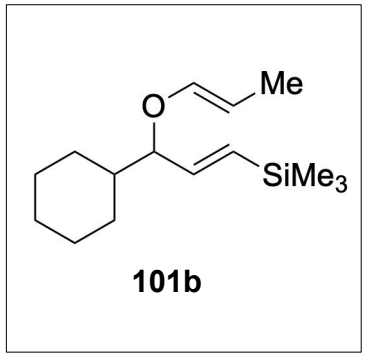

101b

```
Current Data Parameters
NAME       KS-02-259
EXPNO             11
PROCNO             1

F2 - Acquisition Parameters
Date_        20220218
Time             20.09 h
INSTRUM      Avance Neo
PROBHD   Z152088_0031 (
PULPROG        zgpg30
TD              65536
SOLVENT         CDCl3
NS               1024
DS                  4
SWH         23809.523 Hz
FIDRES       0.726609 Hz
AQ           1.3762560 sec
RG               8.125
DW              21.000 usec
DE               6.50 usec
TE              298.0 K
D1           2.00000000 sec
D11          0.03000000 sec
TD0                 1
SFO1       100.6228298 MHz
NUC1              13C
P0                2.67 usec
P1                8.00 usec
PLW1       86.55400085 W
SFO2       400.1316005 MHz
NUC2              1H
CPDPRG[2       waltz65
PCPD2            90.00 usec
PLW2       24.03499985 W
PLW12       0.18990999 W
PLW13       0.09552100 W

F2 - Processing parameters
SI               32768
SF         100.6127541 MHz
WDW                EM
SSB                 0
LB               1.00 Hz
GB                  0
PC               1.40
```

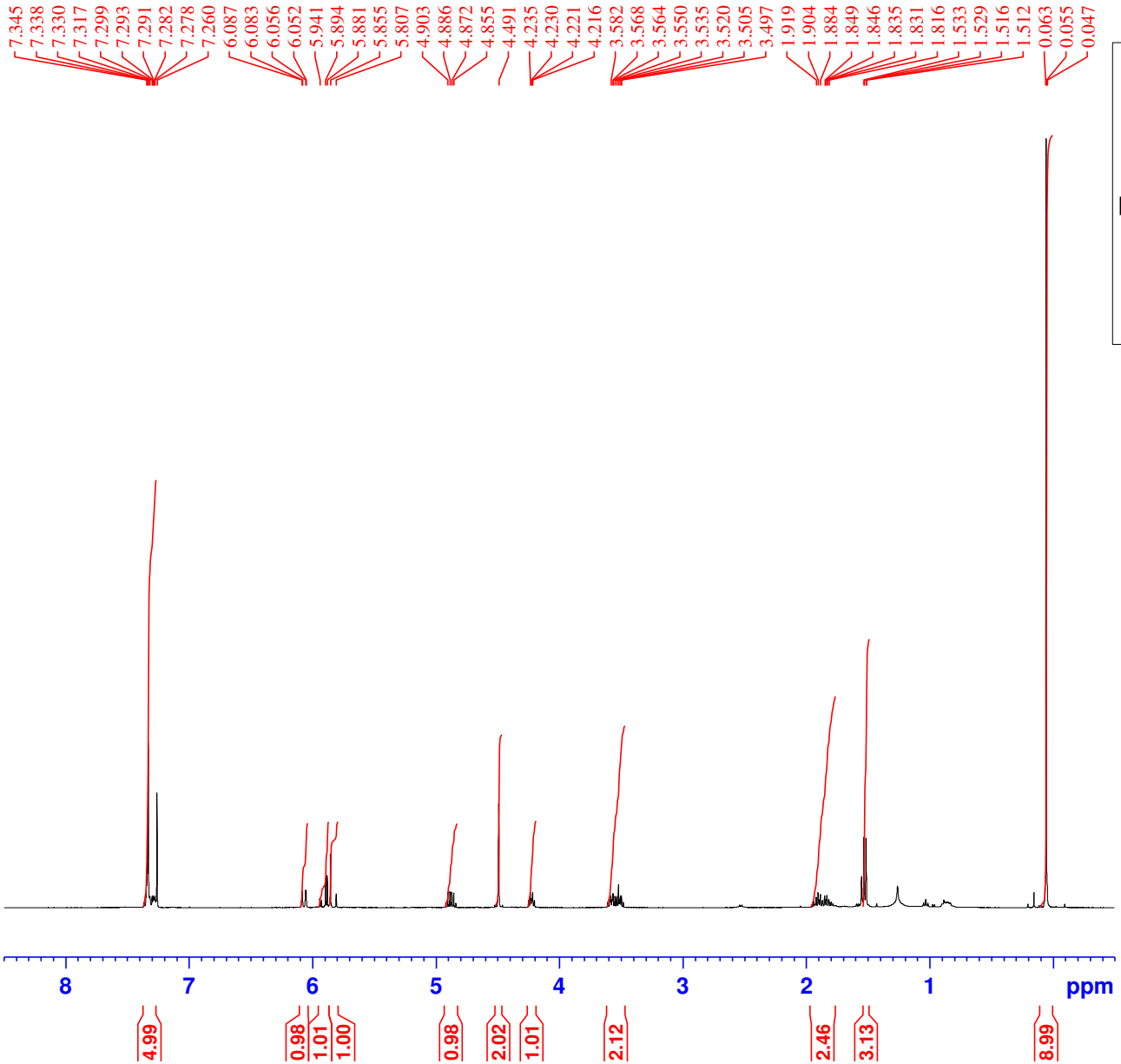

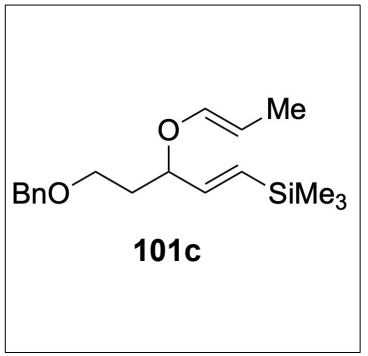

101c

```
Current Data Parameters
NAME      KS-02-106
EXPNO                10
PROCNO                1

F2 - Acquisition Parameters
Date_          20210629
Time              17.09 h
INSTRUM       Avance Neo
PROBHD    Z152088_0031 (
PULPROG             zg30
TD                 65536
SOLVENT            CDCl3
NS                    16
DS                     2
SWH             8196.722 Hz
FIDRES          0.250144 Hz
AQ              3.9976959 sec
RG                   101
DW                61.000 usec
DE                13.89 usec
TE                298.0 K
D1           1.00000000 sec
TD0                    1
SFO1         400.1324708 MHz
NUC1                  1H
P0                 2.67 usec
P1                 8.00 usec
PLW1         24.03499985 W

F2 - Processing parameters
SI                 65536
SF           400.1300096 MHz
WDW                   EM
SSB                    0
LB                 0.30 Hz
GB                     0
PC                 1.00
```

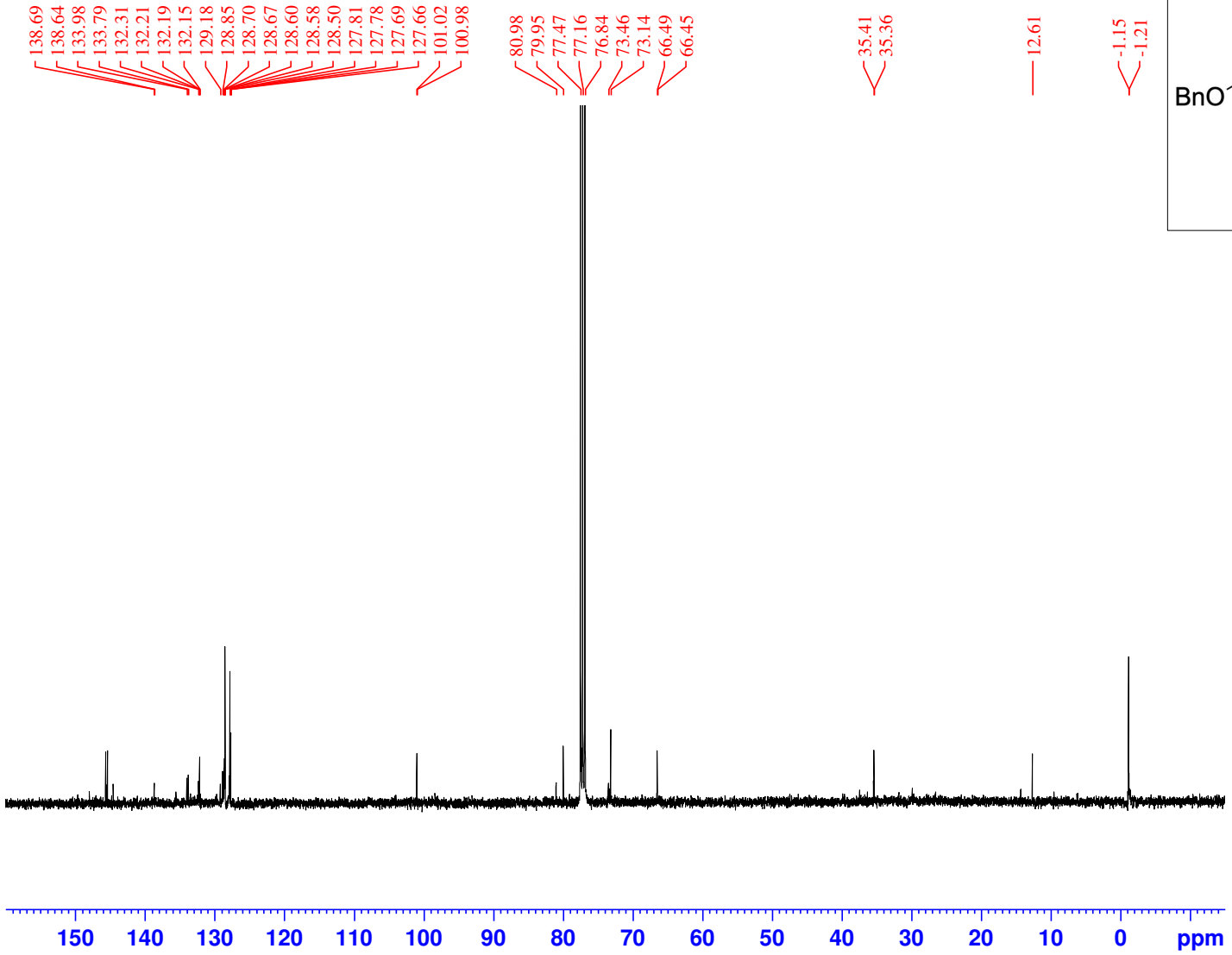

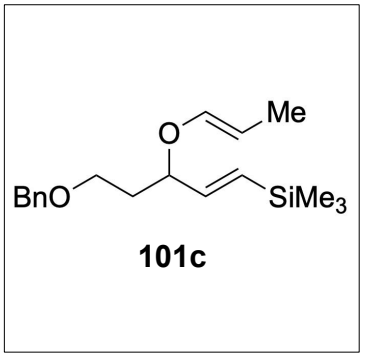

101c

```
Current Data Parameters
NAME      KS-02-106
EXPNO                11
PROCNO                1

F2 - Acquisition Parameters
Date_          20210915
Time               20.05 h
INSTRUM       Avance Neo
PROBHD   Z152088_0031 (
PULPROG          zgpg30
TD                65536
SOLVENT           CDCl3
NS                 1024
DS                    4
SWH           23809.523 Hz
FIDRES         0.726609 Hz
AQ             1.3762560 sec
RG                 8.125
DW                21.000 usec
DE                 6.50 usec
TE                298.0 K
D1            2.00000000 sec
D11           0.03000000 sec
TD0                   1
SFO1        100.6228298 MHz
NUC1                13C
P0                 2.67 usec
P1                 8.00 usec
PLW1         86.55400085 W
SFO2        400.1316005 MHz
NUC2                1H
CPDPRG[2         waltz65
PCPD2              90.00 usec
PLW2         24.03499985 W
PLW12         0.18990999 W
PLW13         0.09552100 W

F2 - Processing parameters
SI                32768
SF          100.6127545 MHz
WDW                  EM
SSB                   0
LB                 1.00 Hz
GB                    0
PC                 1.40
```

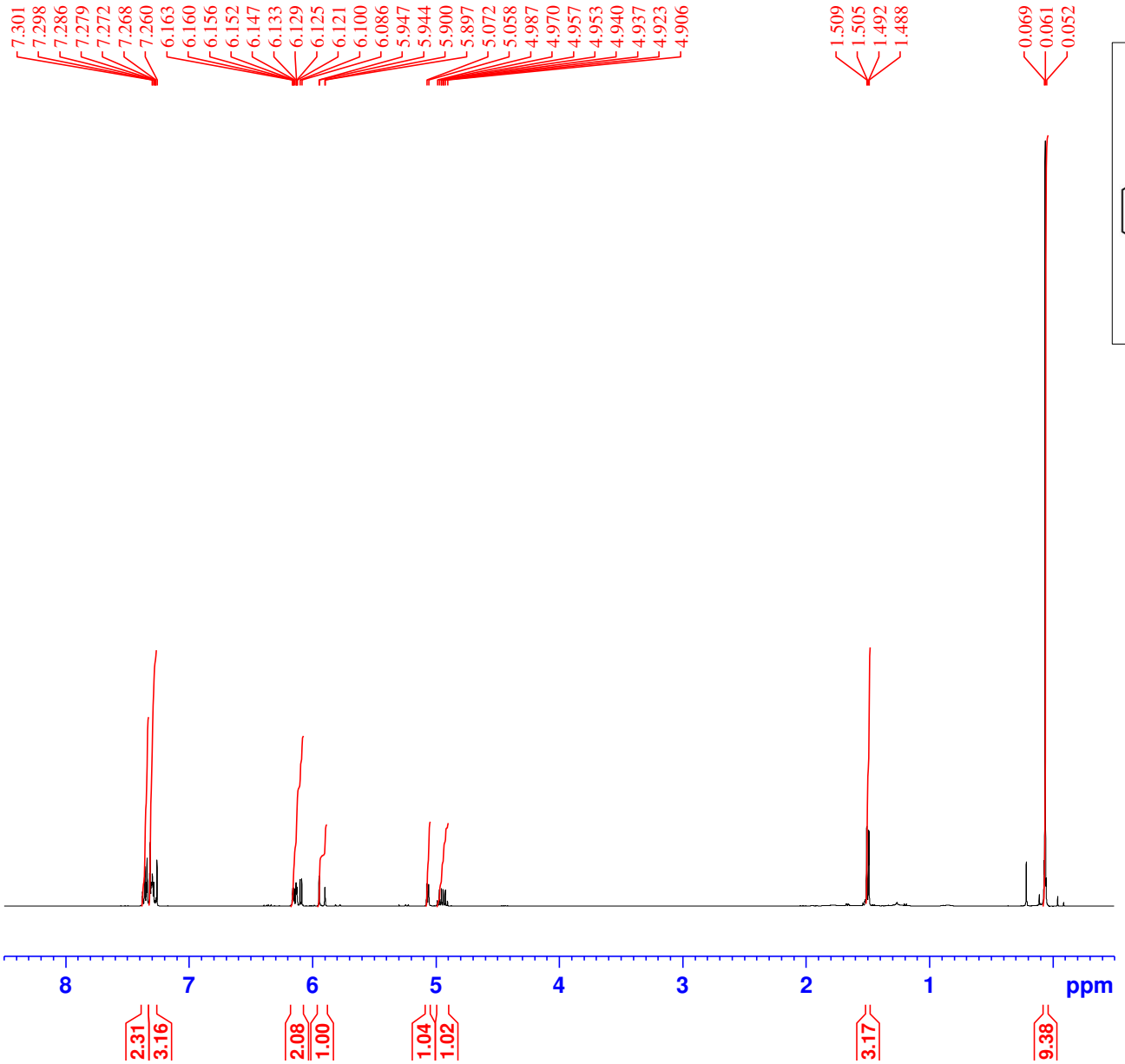

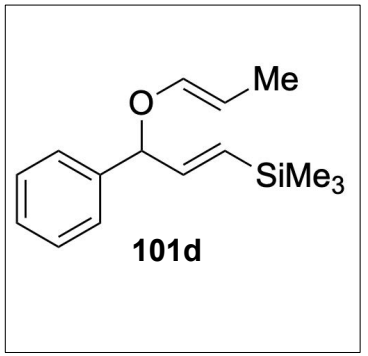


```
Current Data Parameters
NAME        KS-02-138
EXPNO              10
PROCNO              1

F2 - Acquisition Parameters
Date_           20220405
Time              14.10 h
INSTRUM       Avance Neo
PROBHD    Z152088_0031 (
PULPROG            zg30
TD                65536
SOLVENT           CDCl3
NS                   16
DS                    2
SWH            8196.722 Hz
FIDRES         0.250144 Hz
AQ             3.9976959 sec
RG                  101
DW                61.000 usec
DE                13.89 usec
TE                298.0 K
D1           1.00000000 sec
TD0                   1
SFO1         400.1324708 MHz
NUC1                1H
P0                2.67 usec
P1                8.00 usec
PLW1         24.03499985 W

F2 - Processing parameters
SI                65536
SF           400.1300096 MHz
WDW                  EM
SSB                   0
LB                 0.30 Hz
GB                    0
PC                 1.00
```

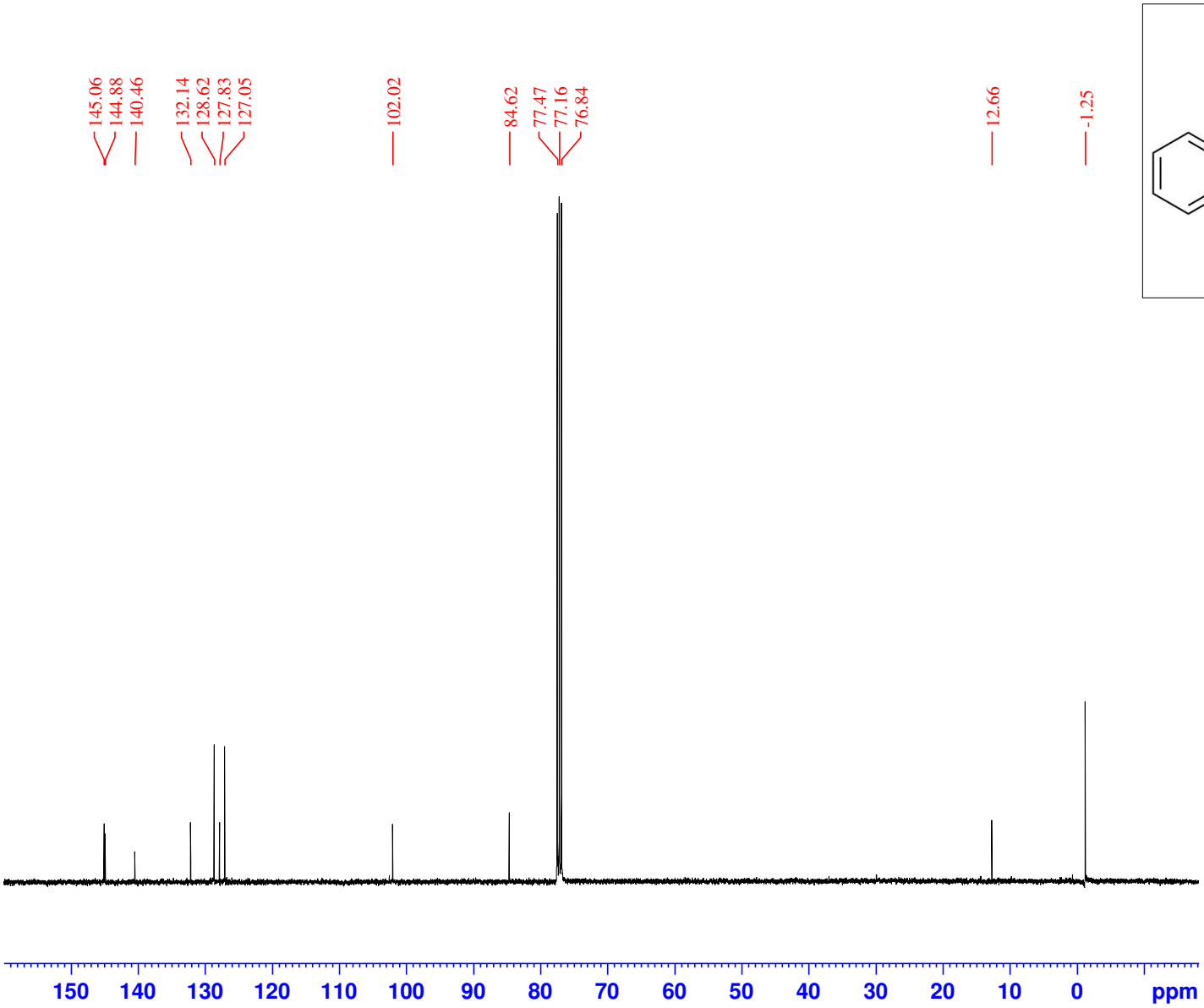

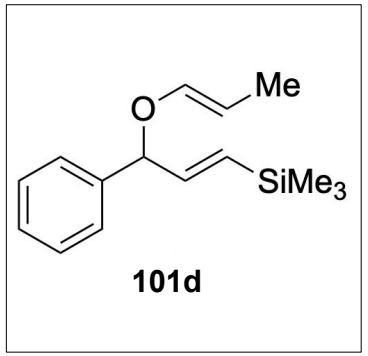

101d

```
Current Data Parameters
NAME       KS-02-138
EXPNO             11
PROCNO             1

F2 - Acquisition Parameters
Date_        20211013
Time             23.04 h
INSTRUM      Avance Neo
PROBHD   Z152088_0031 (
PULPROG          zgpg30
TD              65536
SOLVENT          CDCl3
NS               1024
DS                  4
SWH         23809.523 Hz
FIDRES       0.726609 Hz
AQ           1.3762560 sec
RG               8.125
DW              21.000 usec
DE               6.50 usec
TE              298.0 K
D1           2.00000000 sec
D11          0.03000000 sec
TD0                 1
SFO1       100.6228298 MHz
NUC1              13C
P0               2.67 usec
P1               8.00 usec
PLW1       86.55400085 W
SFO2       400.1316005 MHz
NUC2              1H
CPDPRG[2       waltz65
PCPD2            90.00 usec
PLW2       24.03499985 W
PLW12       0.18990999 W
PLW13       0.09552100 W

F2 - Processing parameters
SI               32768
SF         100.6127544 MHz
WDW                 EM
SSB                 0
LB               1.00 Hz
GB                  0
PC               1.40
```

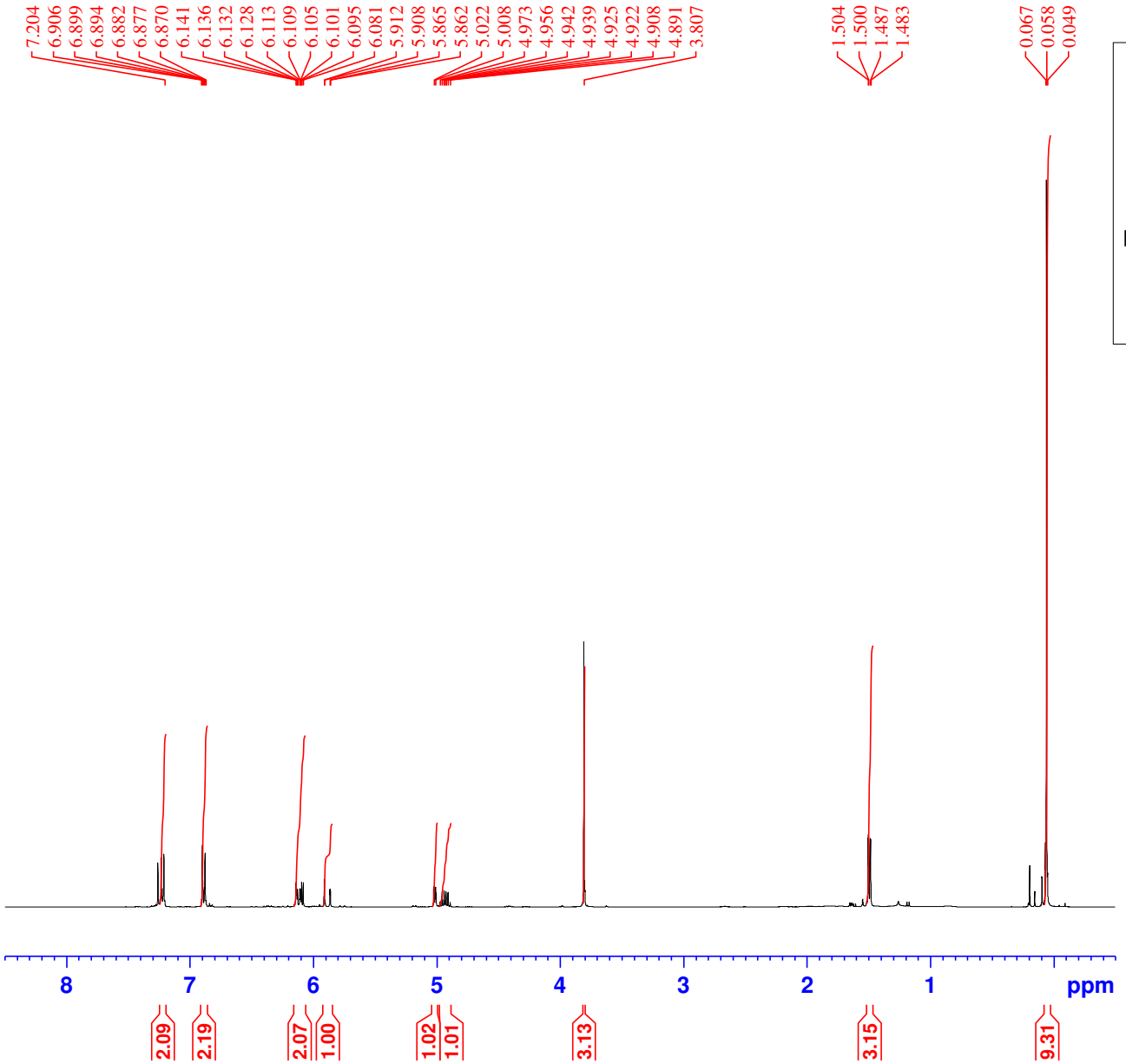

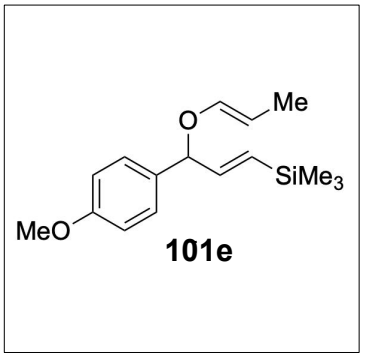

Current Data Parameters
NAME KS-02-150
EXPNO 10
PROCNO 1

F2 - Acquisition Parameters
Date_ 20211021
Time 16.23 h
INSTRUM Avance Neo
PROBHD Z152088_0031 (
PULPROG zg30
TD 65536
SOLVENT CDCl3
NS 16
DS 2
SWH 8196.722 Hz
FIDRES 0.250144 Hz
AQ 3.9976959 sec
RG 101
DW 61.000 usec
DE 13.89 usec
TE 298.0 K
D1 1.00000000 sec
TD0 1
SFO1 400.1324708 MHz
NUC1 1H
P0 2.67 usec
P1 8.00 usec
PLW1 24.03499985 W

F2 - Processing parameters
SI 65536
SF 400.1300097 MHz
WDW EM
SSB 0
LB 0.60 Hz
GB 0
PC 1.00

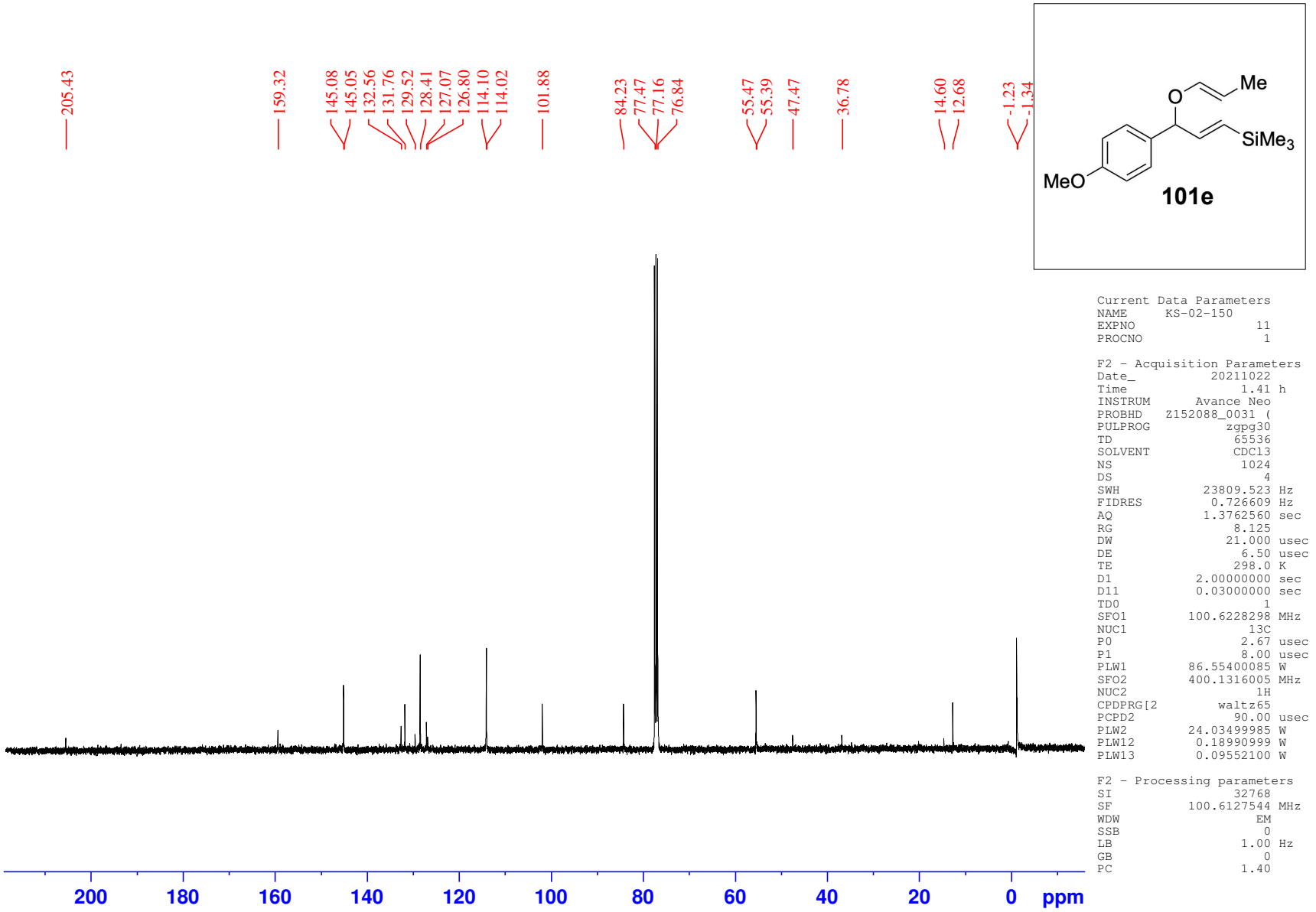
205.43
159.32
145.08
145.05
132.56
131.76
129.52
128.41
127.07
126.80
114.10
114.02
101.88
84.23
77.47
77.16
76.84
55.47
55.39
47.47
36.78
14.60
12.68
-1.23
-1.34
Me
O
SiMe3
MeO
101e
200
180
160
140
120
100
80
60
40
20
0
ppm
Current Data Parameters
NAME KS-02-150
EXPNO 11
PROCNO 1
F2 - Acquisition Parameters
Date_ 20211022
Time 1.41 h
INSTRUM Avance Neo
PROBHD Z152088_0031 (
PULPROG zgpg30
TD 65536
SOLVENT CDCl3
NS 1024
DS 4
SWH 23809.523 Hz
FIDRES 0.726609 Hz
AQ 1.3762560 sec
RG 8.125
DW 21.000 usec
DE 6.50 usec
TE 298.0 K
D1 2.00000000 sec
D11 0.03000000 sec
TD0 1
SFO1 100.6228298 MHz
NUC1 13C
P0 2.67 usec
P1 8.00 usec
PLW1 86.55400085 W
SFO2 400.1316005 MHz
NUC2 1H
CPDPRG[2 waltz65
PCPD2 90.00 usec
PLW2 24.03499985 W
PLW12 0.18990999 W
PLW13 0.09552100 W
F2 - Processing parameters
SI 32768
SF 100.6127544 MHz
WDW EM
SSB 0
LB 1.00 Hz
GB 0
PC 1.40

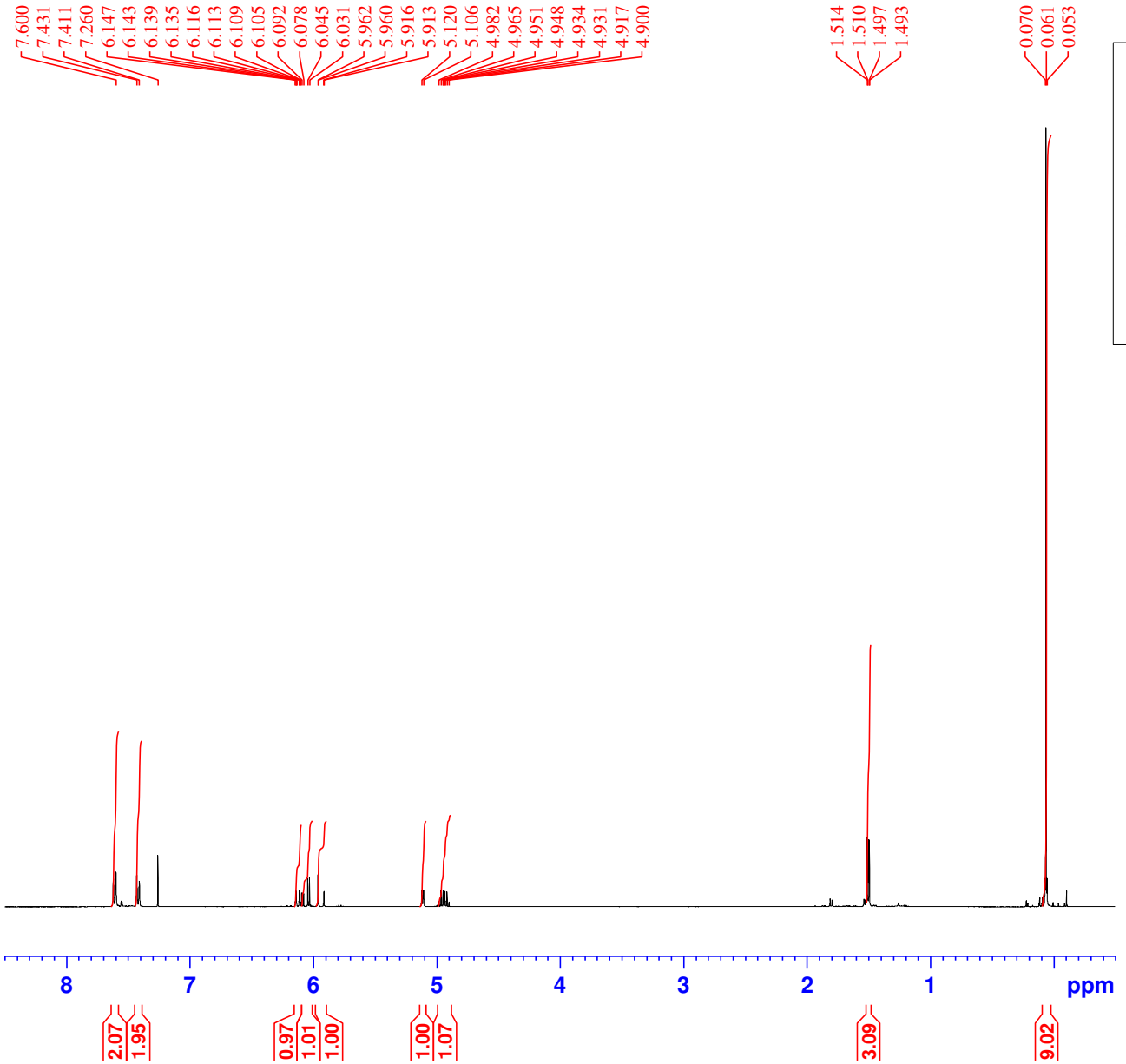

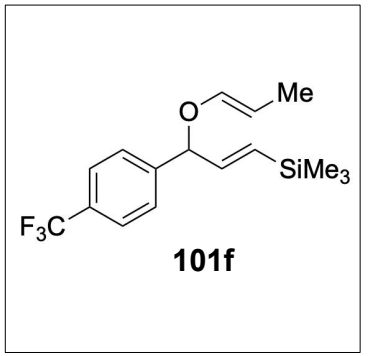

101f

```
Current Data Parameters
NAME      KS-02-151
EXPNO                10
PROCNO                1

F2 - Acquisition Parameters
Date_          20211021
Time              16.29 h
INSTRUM       Avance Neo
PROBHD    Z152088_0031 (
PULPROG             zg30
TD                 65536
SOLVENT            CDCl3
NS                    16
DS                     2
SWH             8196.722 Hz
FIDRES          0.250144 Hz
AQ              3.9976959 sec
RG                   101
DW                61.000 usec
DE                13.89 usec
TE                298.0 K
D1            1.00000000 sec
TD0                    1
SFO1         400.1324708 MHz
NUC1                 1H
P0                 2.67 usec
P1                 8.00 usec
PLW1         24.03499985 W

F2 - Processing parameters
SI                 65536
SF           400.1300097 MHz
WDW                   EM
SSB                    0
LB                  0.30 Hz
GB                     0
PC                  1.00
```

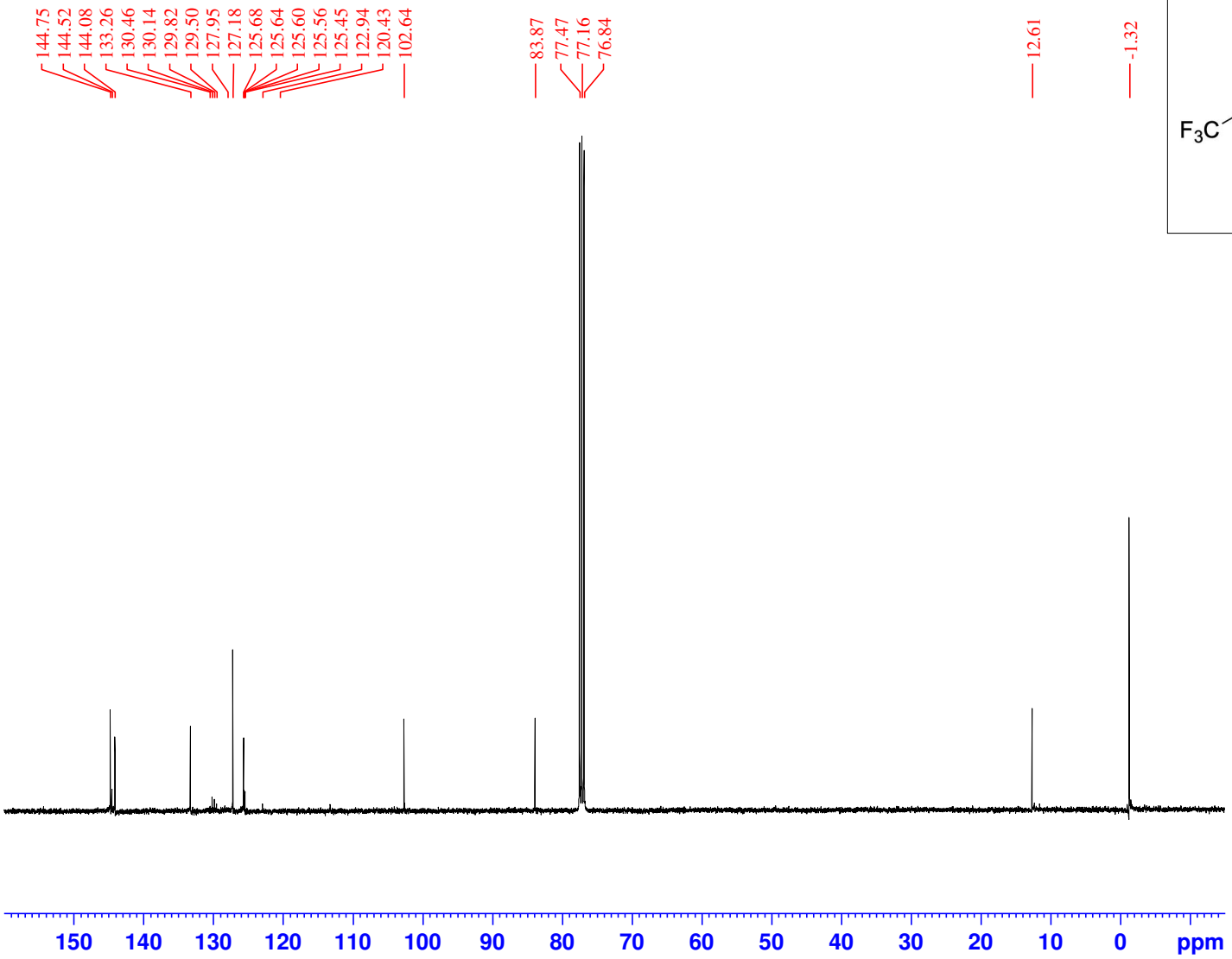

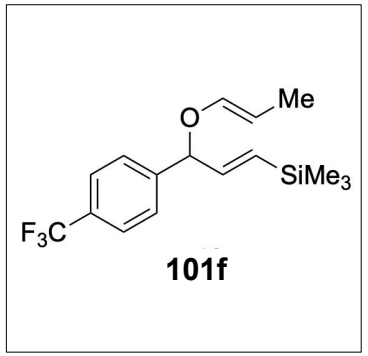

101f

```
Current Data Parameters
NAME      KS-02-151
EXPNO                11
PROCNO                1

F2 - Acquisition Parameters
Date_          20211021
Time               17.41 h
INSTRUM       Avance Neo
PROBHD    Z152088_0031 (
PULPROG          zgpg30
TD                65536
SOLVENT           CDCl3
NS                 1024
DS                    4
SWH           23809.523 Hz
FIDRES         0.726609 Hz
AQ             1.3762560 sec
RG                8.125
DW               21.000 usec
DE                6.50 usec
TE               298.0 K
D1            2.00000000 sec
D11           0.03000000 sec
TD0                   1
SFO1         100.6228298 MHz
NUC1                13C
P0                 2.67 usec
P1                 8.00 usec
PLW1         86.55400085 W
SFO2         400.1316005 MHz
NUC2                1H
CPDPRG[2         waltz65
PCPD2             90.00 usec
PLW2         24.03499985 W
PLW12         0.18990999 W
PLW13         0.09552100 W

F2 - Processing parameters
SI                32768
SF           100.6127538 MHz
WDW                  EM
SSB                   0
LB                 1.00 Hz
GB                    0
PC                 1.40
```

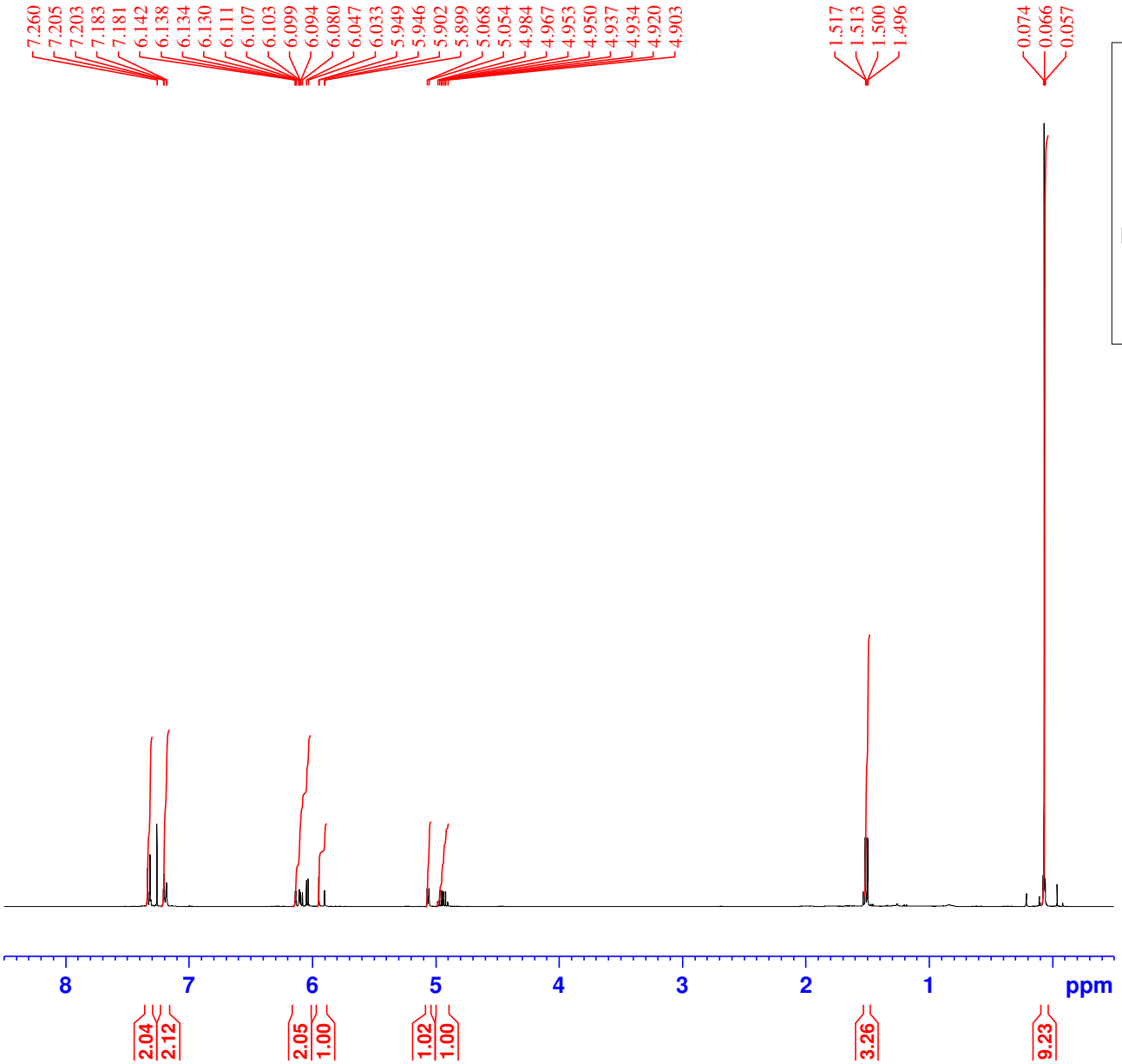

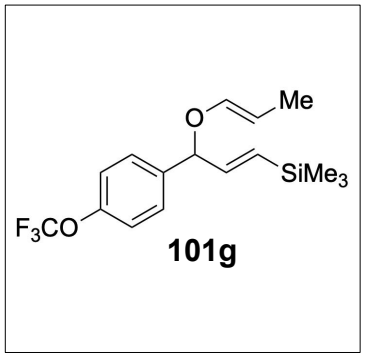

101g

```
Current Data Parameters
NAME      KS-02-203
EXPNO                10
PROCNO                1

F2 - Acquisition Parameters
Date_          20211208
Time              16.55 h
INSTRUM       Avance Neo
PROBHD    Z152088_0031 (
PULPROG             zg30
TD                 65536
SOLVENT            CDCl3
NS                    16
DS                     2
SWH             8196.722 Hz
FIDRES          0.250144 Hz
AQ              3.9976959 sec
RG                   101
DW                61.000 usec
DE                13.89 usec
TE                298.0 K
D1             1.00000000 sec
TD0                    1
SFO1         400.1324708 MHz
NUC1                 1H
P0                 2.67 usec
P1                 8.00 usec
PLW1         24.03499985 W

F2 - Processing parameters
SI                 65536
SF           400.1300098 MHz
WDW                   EM
SSB                    0
LB                  0.30 Hz
GB                     0
PC                  1.00
```

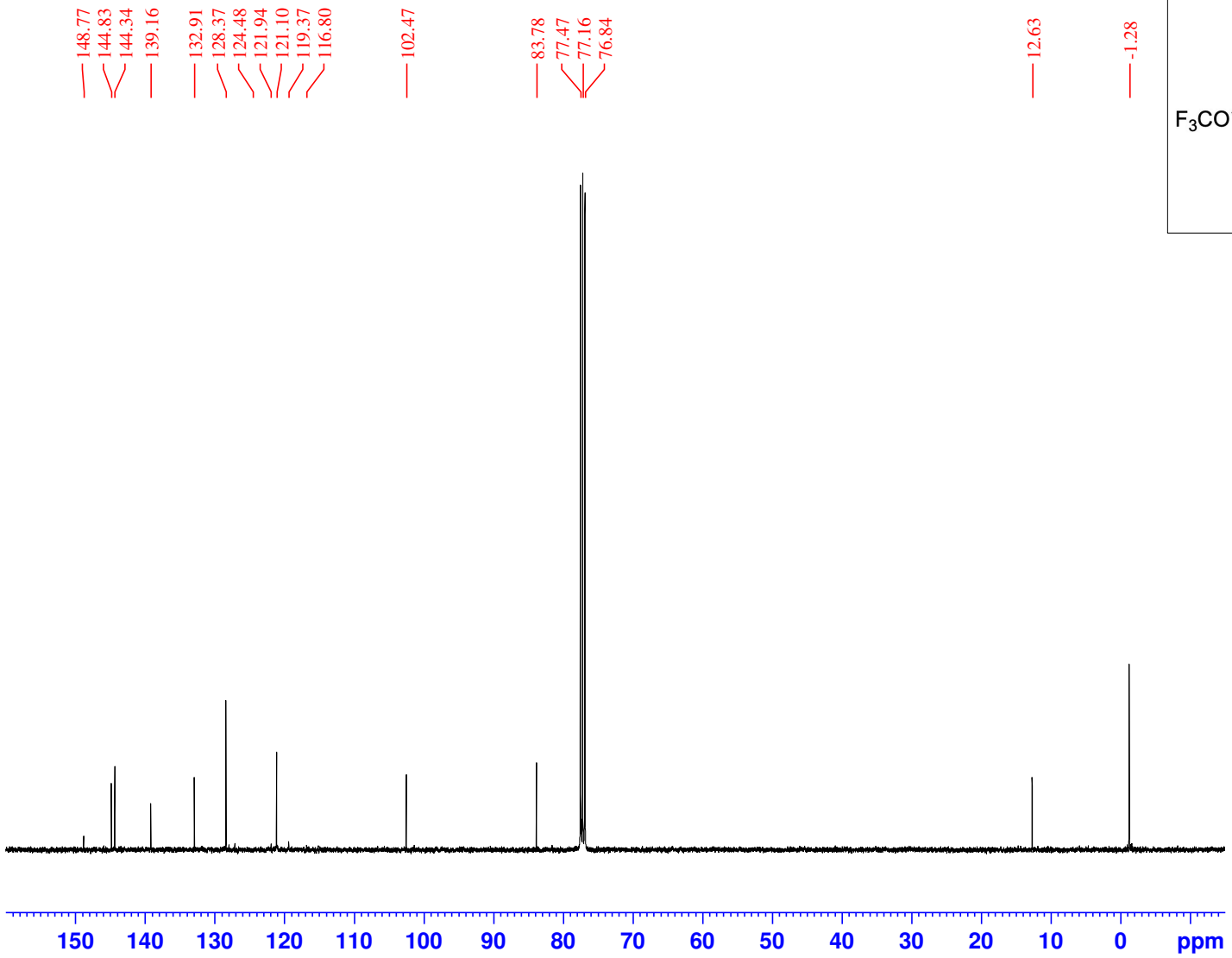

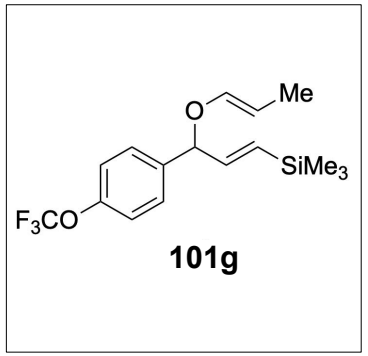

101g

```
Current Data Parameters
NAME      KS-02-203
EXPNO                11
PROCNO                1

F2 - Acquisition Parameters
Date_          20211208
Time               20.07 h
INSTRUM       Avance Neo
PROBHD    Z152088_0031 (
PULPROG          zgpg30
TD                65536
SOLVENT           CDCl3
NS                 1024
DS                    4
SWH           23809.523 Hz
FIDRES         0.726609 Hz
AQ             1.3762560 sec
RG                8.125
DW               21.000 usec
DE                6.50 usec
TE               298.0 K
D1            2.00000000 sec
D11           0.03000000 sec
TD0                   1
SFO1         100.6228298 MHz
NUC1                13C
P0                 2.67 usec
P1                 8.00 usec
PLW1         86.55400085 W
SFO2         400.1316005 MHz
NUC2                1H
CPDPRG[2         waltz65
PCPD2             90.00 usec
PLW2         24.03499985 W
PLW12         0.18990999 W
PLW13         0.09552100 W

F2 - Processing parameters
SI                32768
SF           100.6127539 MHz
WDW                  EM
SSB                   0
LB                 1.00 Hz
GB                    0
PC                 1.40
```

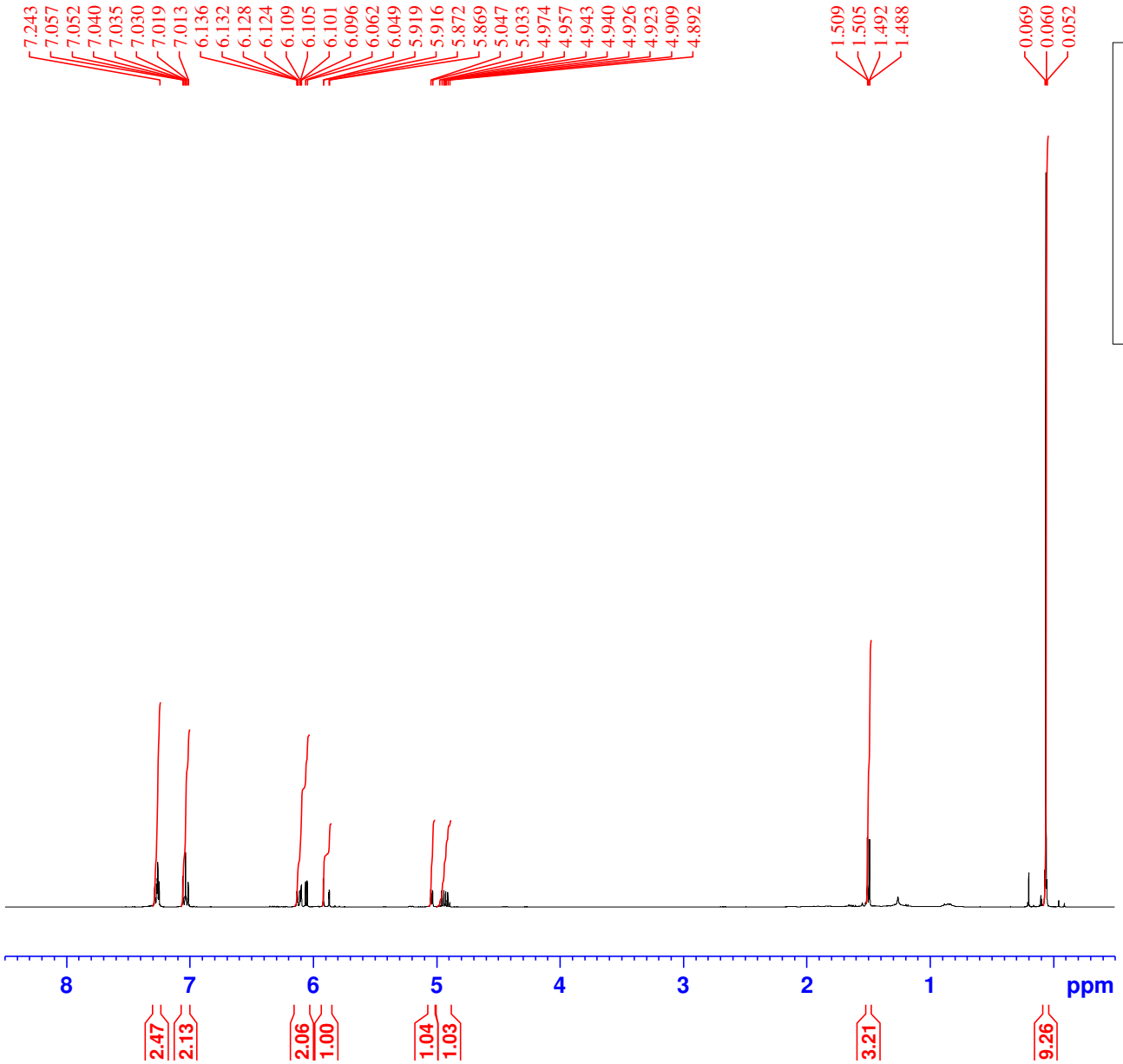

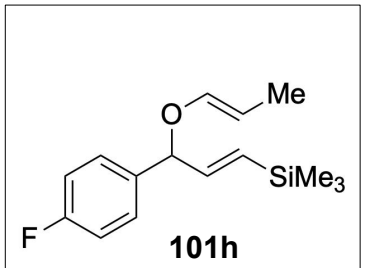

101h

```
Current Data Parameters
NAME      KS-02-139
EXPNO                10
PROCNO                1

F2 - Acquisition Parameters
Date_          20211013
Time              18.29 h
INSTRUM       Avance Neo
PROBHD    Z152088_0031 (
PULPROG             zg30
TD                 65536
SOLVENT            CDCl3
NS                    16
DS                     2
SWH             8196.722 Hz
FIDRES          0.250144 Hz
AQ              3.9976959 sec
RG                   101
DW                61.000 usec
DE                13.89 usec
TE                298.0 K
D1            1.00000000 sec
TD0                    1
SFO1         400.1324708 MHz
NUC1                 1H
P0                 2.67 usec
P1                 8.00 usec
PLW1         24.03499985 W

F2 - Processing parameters
SI                 65536
SF           400.1300097 MHz
WDW                   EM
SSB                    0
LB                  0.30 Hz
GB                     0
PC                  1.00
```

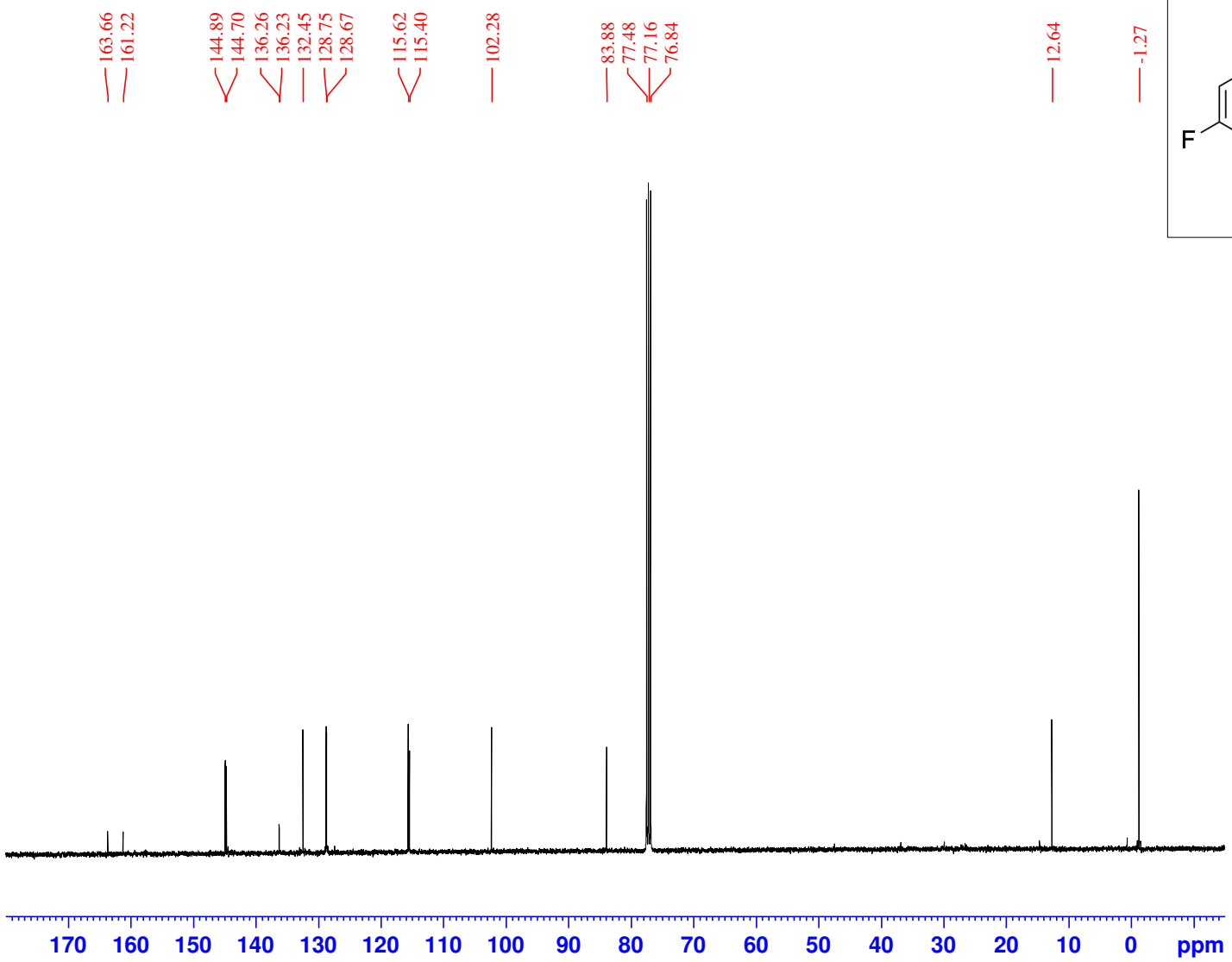

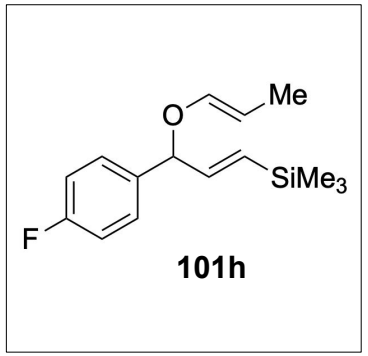


```
Current Data Parameters
NAME      KS-02-139
EXPNO                11
PROCNO                1

F2 - Acquisition Parameters
Date_          20211014
Time                0.18 h
INSTRUM       Avance Neo
PROBHD    Z152088_0031 (
PULPROG          zgpg30
TD                65536
SOLVENT           CDCl3
NS                 1024
DS                    4
SWH           23809.523 Hz
FIDRES         0.726609 Hz
AQ             1.3762560 sec
RG                 8.125
DW                21.000 usec
DE                 6.50 usec
TE                298.0 K
D1             2.00000000 sec
D11            0.03000000 sec
TD0                   1
SFO1         100.6228298 MHz
NUC1                13C
P0                 2.67 usec
P1                 8.00 usec
PLW1         86.55400085 W
SFO2         400.1316005 MHz
NUC2                1H
CPDPRG[2         waltz65
PCPD2             90.00 usec
PLW2         24.03499985 W
PLW12         0.18990999 W
PLW13         0.09552100 W

F2 - Processing parameters
SI                32768
SF           100.6127541 MHz
WDW                  EM
SSB                   0
LB                 1.00 Hz
GB                    0
PC                 1.40
```

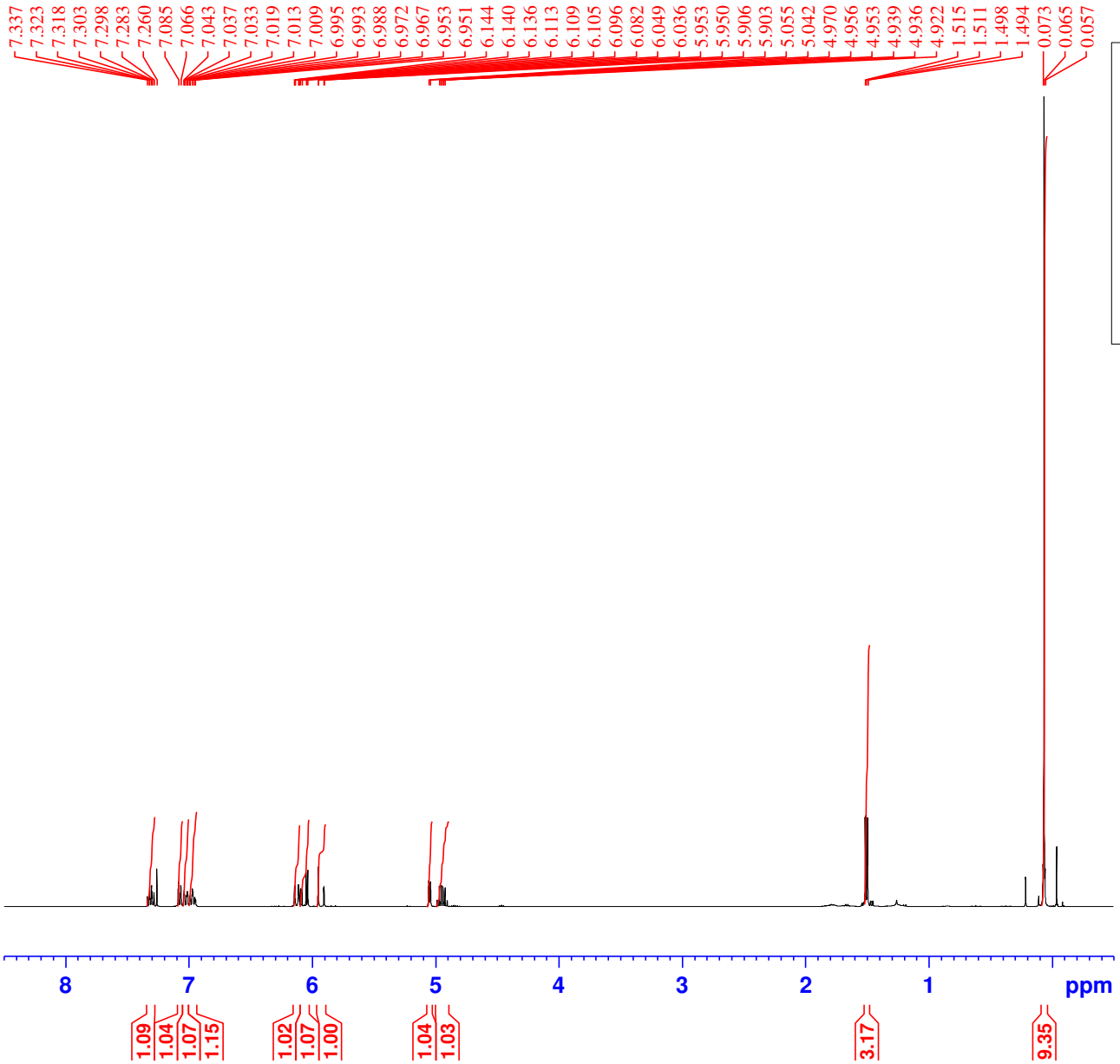

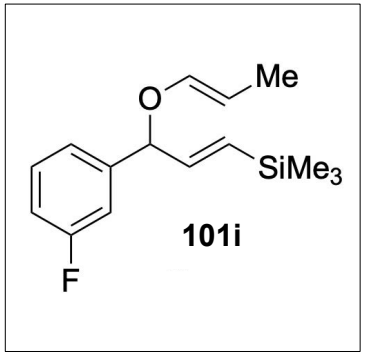


```
Current Data Parameters
NAME      KS-02-297
EXPNO                10
PROCNO                1

F2 - Acquisition Parameters
Date_           20220426
Time               14.16 h
INSTRUM       Avance Neo
PROBHD    Z152088_0031 (
PULPROG             zg30
TD                 65536
SOLVENT            CDCl3
NS                    16
DS                     2
SWH             8196.722 Hz
FIDRES          0.250144 Hz
AQ              3.9976959 sec
RG                   101
DW                61.000 usec
DE                13.89 usec
TE                298.0 K
D1            1.00000000 sec
TD0                    1
SFO1         400.1324708 MHz
NUC1                 1H
P0                 2.67 usec
P1                 8.00 usec
PLW1         24.03499985 W

F2 - Processing parameters
SI                 65536
SF           400.1300096 MHz
WDW                   EM
SSB                    0
LB                  0.30 Hz
GB                     0
PC                  1.00
```

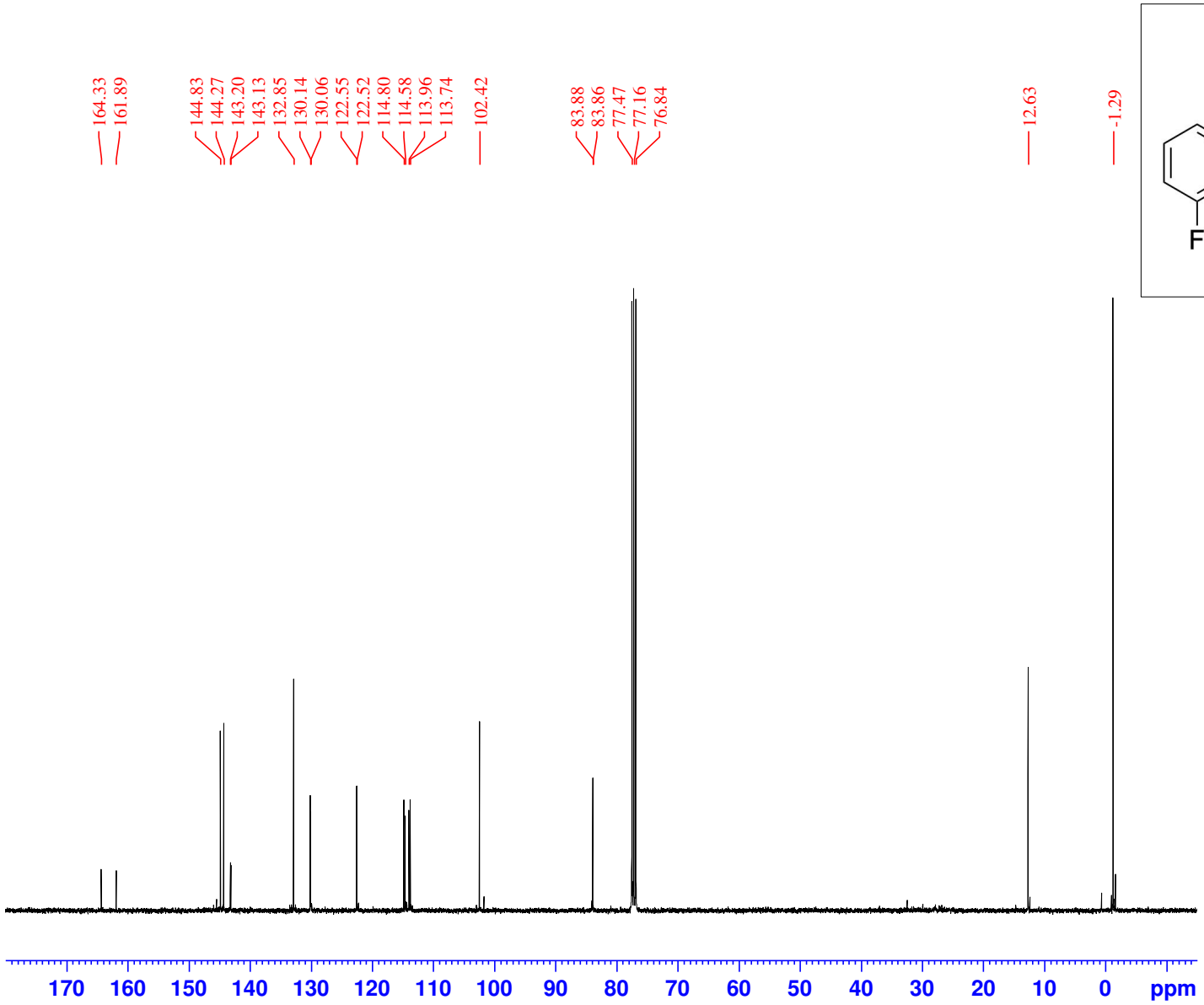

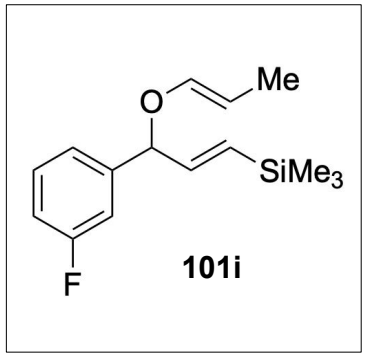


```
Current Data Parameters
NAME      KS-02-297
EXPNO                11
PROCNO                1

F2 - Acquisition Parameters
Date_          20220426
Time               15.28 h
INSTRUM       Avance Neo
PROBHD    Z152088_0031 (
PULPROG          zgpg30
TD                65536
SOLVENT           CDCl3
NS                 1024
DS                    4
SWH           23809.523 Hz
FIDRES         0.726609 Hz
AQ             1.3762560 sec
RG                8.125
DW               21.000 usec
DE                6.50 usec
TE               298.0 K
D1             2.00000000 sec
D11            0.03000000 sec
TD0                   1
SFO1         100.6228298 MHz
NUC1                13C
P0                 2.67 usec
P1                 8.00 usec
PLW1         86.55400085 W
SFO2         400.1316005 MHz
NUC2                1H
CPDPRG[2         waltz65
PCPD2             90.00 usec
PLW2         24.03499985 W
PLW12         0.18990999 W
PLW13         0.09552100 W

F2 - Processing parameters
SI                32768
SF           100.6127545 MHz
WDW                  EM
SSB                   0
LB                 1.00 Hz
GB                    0
PC                 1.40
```

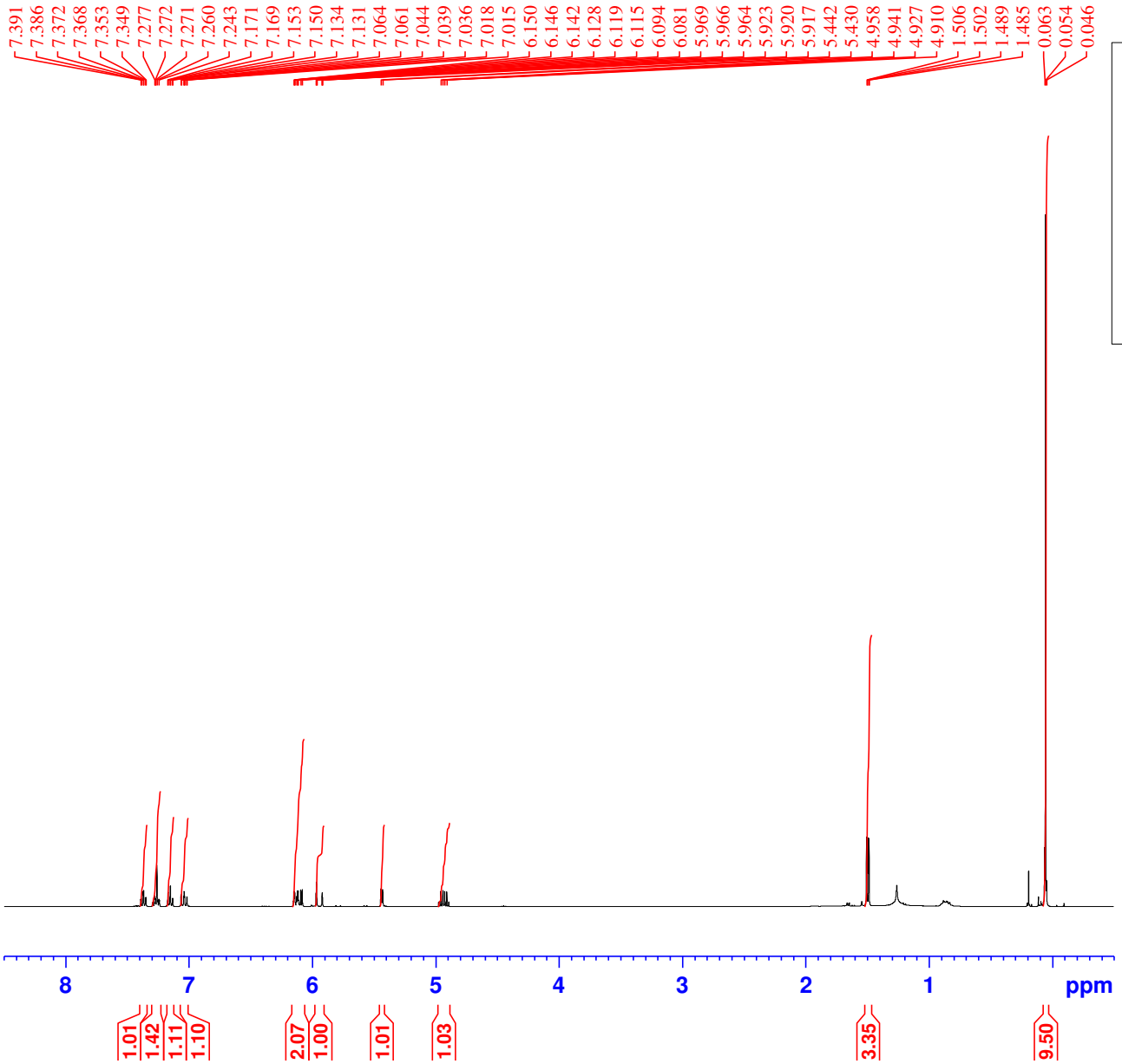

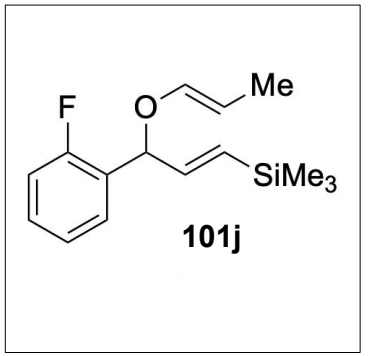


```
Current Data Parameters
NAME      KS-02-160
EXPNO                10
PROCNO                1

F2 - Acquisition Parameters
Date_          20211028
Time              15.58 h
INSTRUM       Avance Neo
PROBHD    Z152088_0031 (
PULPROG             zg30
TD                 65536
SOLVENT            CDCl3
NS                    16
DS                     2
SWH             8196.722 Hz
FIDRES          0.250144 Hz
AQ              3.9976959 sec
RG                   101
DW                61.000 usec
DE                13.89 usec
TE                298.0 K
D1             1.00000000 sec
TD0                    1
SFO1         400.1324708 MHz
NUC1                 1H
P0                 2.67 usec
P1                 8.00 usec
PLW1         24.03499985 W

F2 - Processing parameters
SI                 65536
SF           400.1300097 MHz
WDW                   EM
SSB                    0
LB                  0.30 Hz
GB                     0
PC                  1.00
```

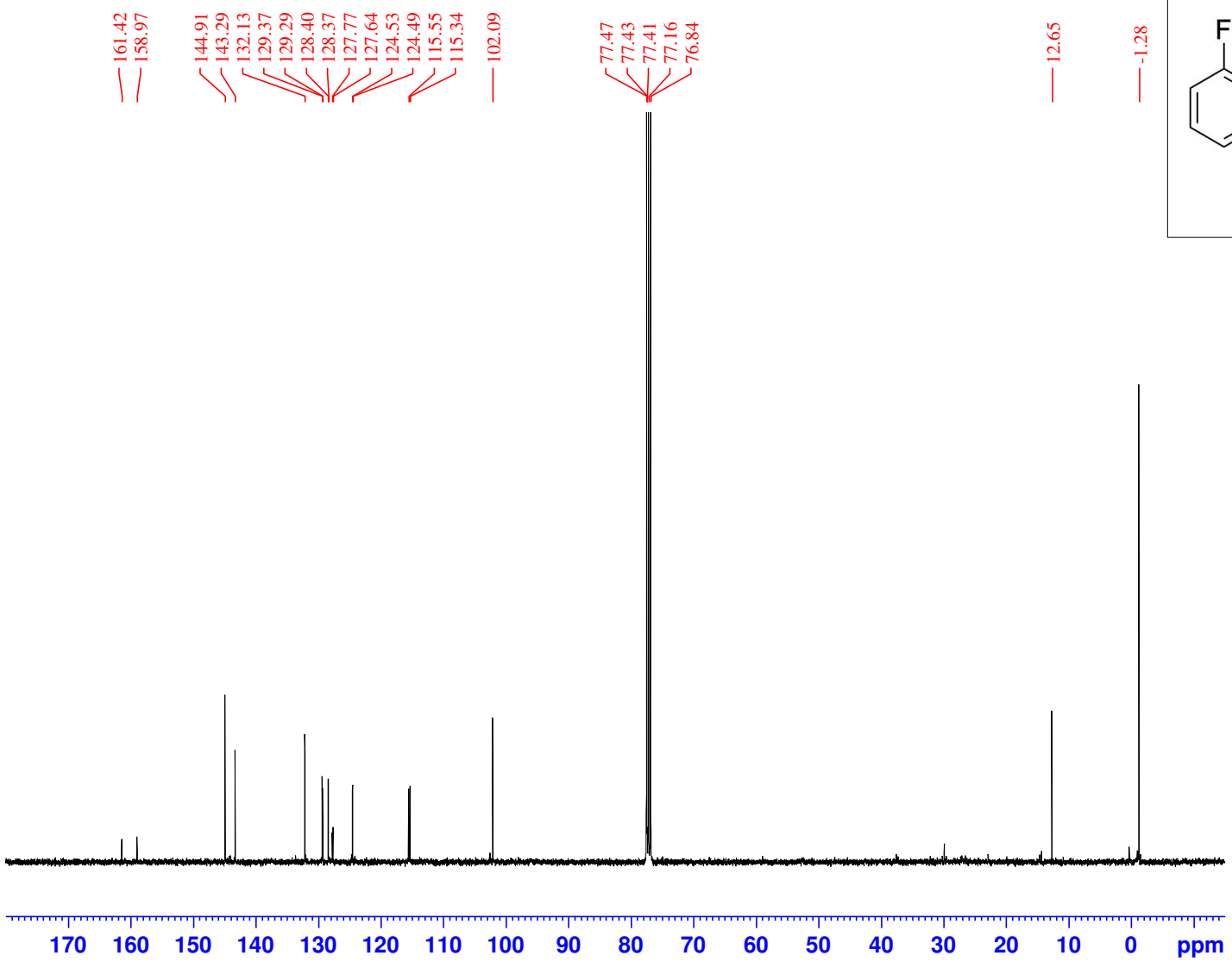

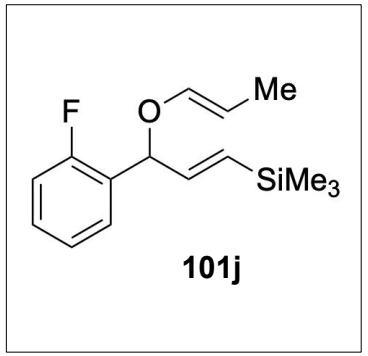


```
Current Data Parameters
NAME      KS-02-160
EXPNO                11
PROCNO                1

F2 - Acquisition Parameters
Date_          20211028
Time               20.11 h
INSTRUM       Avance Neo
PROBHD    Z152088_0031 (
PULPROG          zgpg30
TD                65536
SOLVENT           CDCl3
NS                 1024
DS                    4
SWH           23809.523 Hz
FIDRES         0.726609 Hz
AQ             1.3762560 sec
RG                8.125
DW               21.000 usec
DE                6.50 usec
TE               298.0 K
D1            2.00000000 sec
D11           0.03000000 sec
TD0                   1
SFO1         100.6228298 MHz
NUC1                13C
P0                 2.67 usec
P1                 8.00 usec
PLW1         86.55400085 W
SFO2         400.1316005 MHz
NUC2                1H
CPDPRG[2         waltz65
PCPD2             90.00 usec
PLW2         24.03499985 W
PLW12         0.18990999 W
PLW13         0.09552100 W

F2 - Processing parameters
SI                32768
SF           100.6127544 MHz
WDW                  EM
SSB                   0
LB                 1.00 Hz
GB                    0
PC                 1.40
```

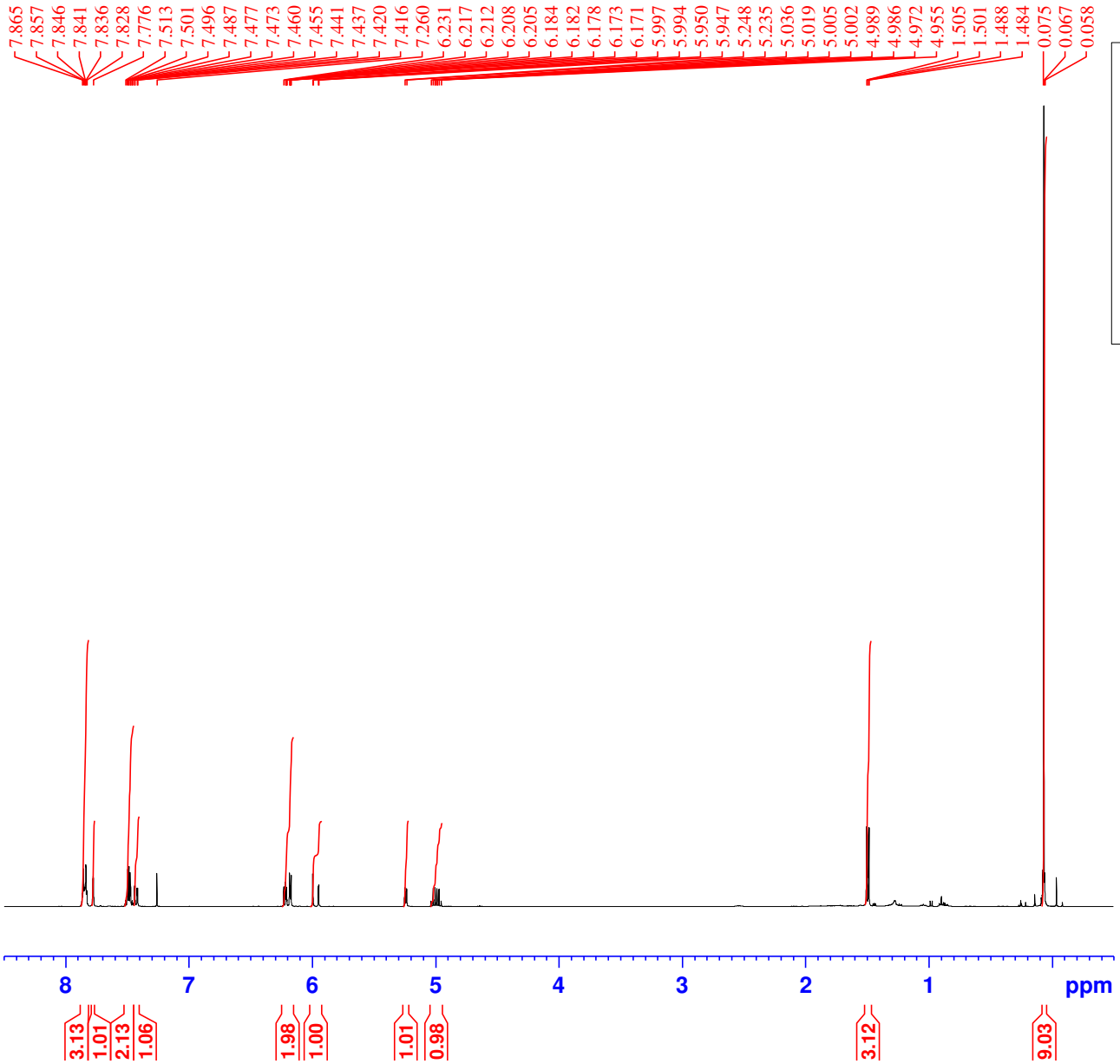

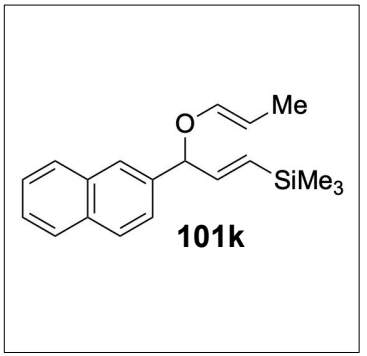


```
Current Data Parameters
NAME       KS-02-206
EXPNO                10
PROCNO                1

F2 - Acquisition Parameters
Date_          20211214
Time               13.33 h
INSTRUM       Avance Neo
PROBHD    Z152088_0031 (
PULPROG             zg30
TD                 65536
SOLVENT            CDCl3
NS                    16
DS                     2
SWH             8196.722 Hz
FIDRES          0.250144 Hz
AQ              3.9976959 sec
RG                   101
DW                61.000 usec
DE                13.89 usec
TE                298.0 K
D1             1.00000000 sec
TD0                    1
SFO1         400.1324708 MHz
NUC1                 1H
P0                 2.67 usec
P1                 8.00 usec
PLW1         24.03499985 W

F2 - Processing parameters
SI                 65536
SF           400.1300096 MHz
WDW                   EM
SSB                    0
LB                  0.30 Hz
GB                     0
PC                  1.00
```

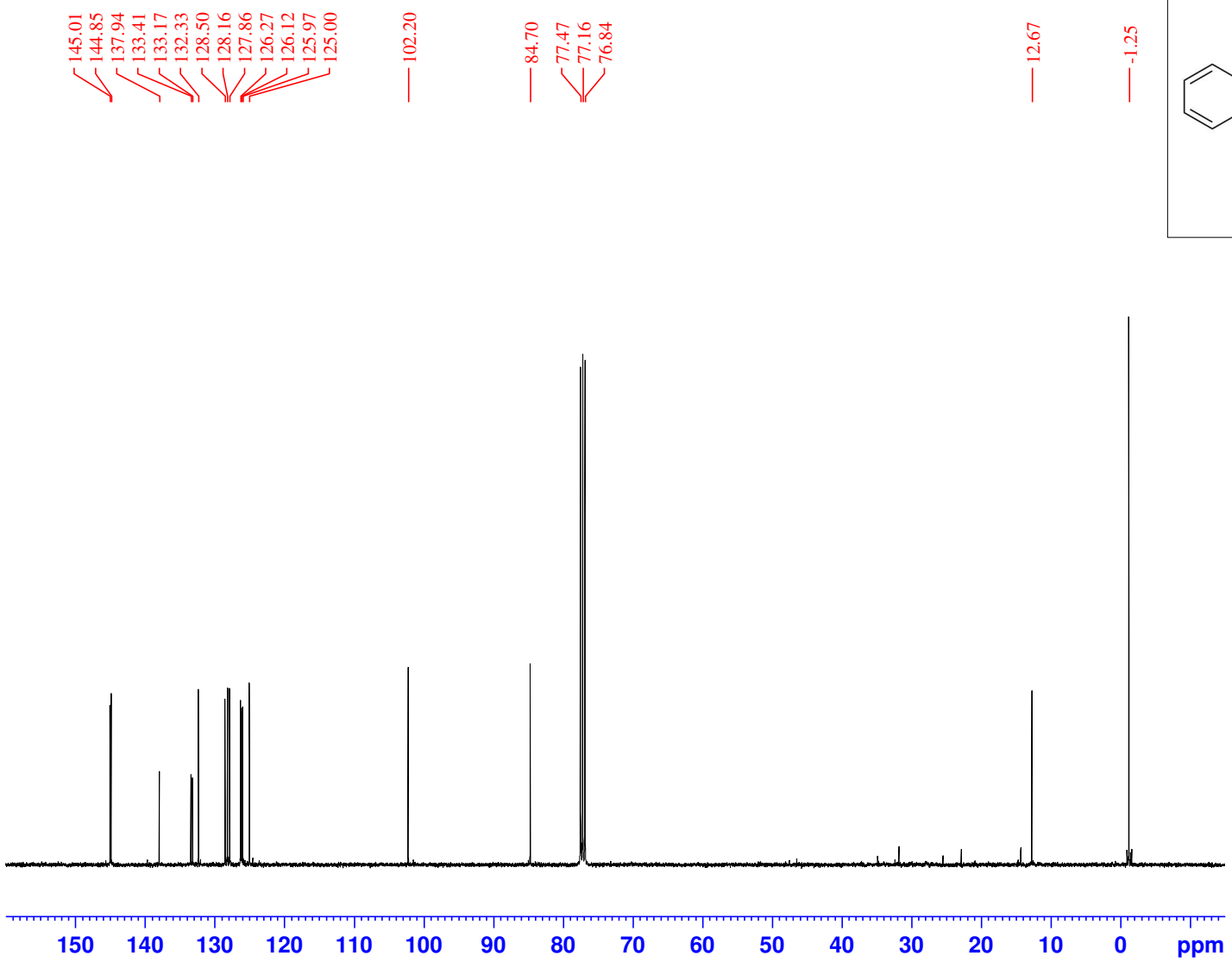

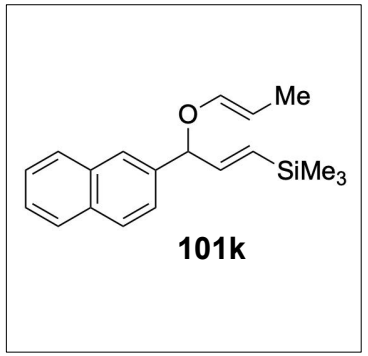


```
Current Data Parameters
NAME      KS-02-206
EXPNO                11
PROCNO                1

F2 - Acquisition Parameters
Date_          20211214
Time               14.48 h
INSTRUM      Avance Neo
PROBHD   Z152088_0031 (
PULPROG          zgpg30
TD                65536
SOLVENT           CDCl3
NS                 1024
DS                    4
SWH           23809.523 Hz
FIDRES         0.726609 Hz
AQ             1.3762560 sec
RG                 8.125
DW                21.000 usec
DE                 6.50 usec
TE                298.0 K
D1             2.00000000 sec
D11            0.03000000 sec
TD0                   1
SFO1         100.6228298 MHz
NUC1                13C
P0                 2.67 usec
P1                 8.00 usec
PLW1         86.55400085 W
SFO2         400.1316005 MHz
NUC2                1H
CPDPRG[2         waltz65
PCPD2             90.00 usec
PLW2         24.03499985 W
PLW12         0.18990999 W
PLW13         0.09552100 W

F2 - Processing parameters
SI                32768
SF           100.6127558 MHz
WDW                  EM
SSB                   0
LB                 1.00 Hz
GB                    0
PC                 1.40
```

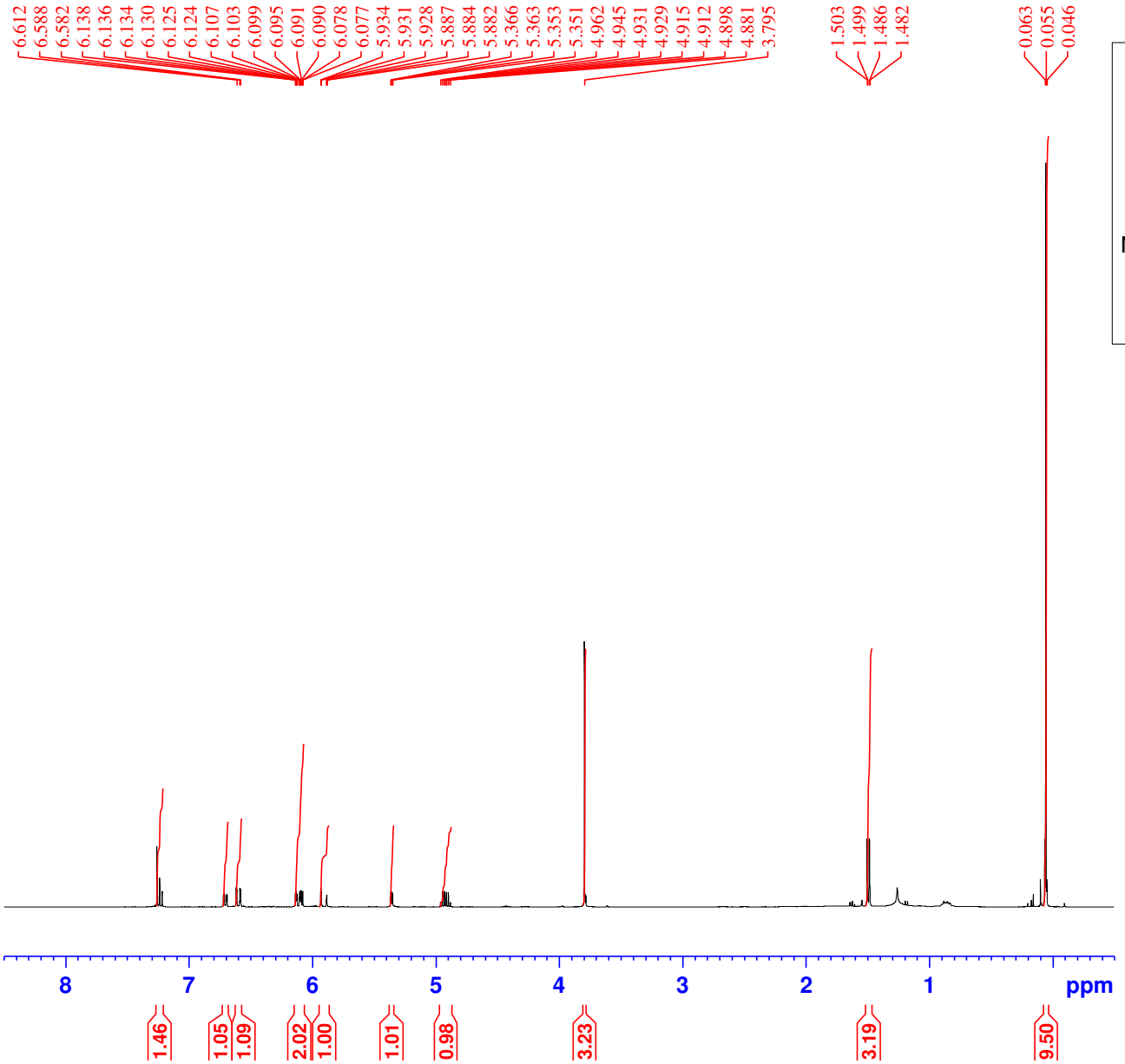

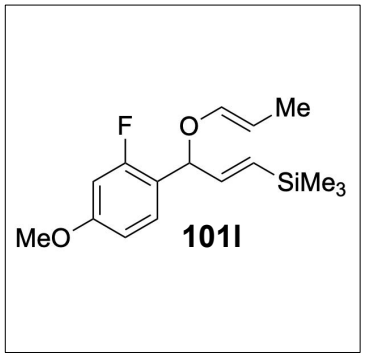


```
Current Data Parameters
NAME      KS-02-161
EXPNO                10
PROCNO                1

F2 - Acquisition Parameters
Date_          20211028
Time              16.04 h
INSTRUM       Avance Neo
PROBHD    Z152088_0031 (
PULPROG           zg30
TD               65536
SOLVENT          CDCl3
NS                  16
DS                   2
SWH            8196.722 Hz
FIDRES         0.250144 Hz
AQ             3.9976959 sec
RG                 101
DW                61.000 usec
DE                13.89 usec
TE                298.0 K
D1           1.00000000 sec
TD0                  1
SFO1         400.1324708 MHz
NUC1                1H
P0                2.67 usec
P1                8.00 usec
PLW1         24.03499985 W

F2 - Processing parameters
SI               65536
SF           400.1300097 MHz
WDW                 EM
SSB                  0
LB                0.30 Hz
GB                   0
PC                1.00
```

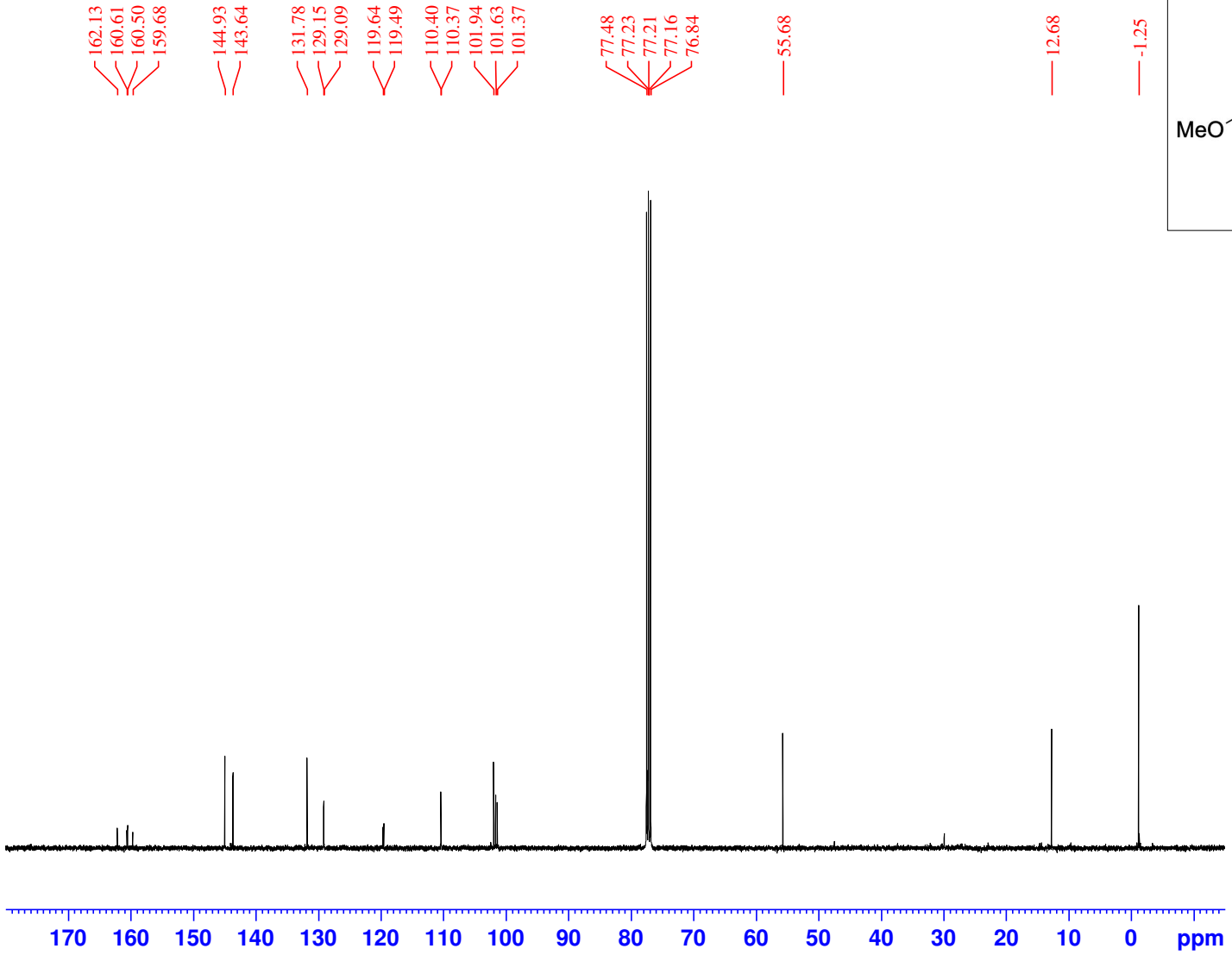

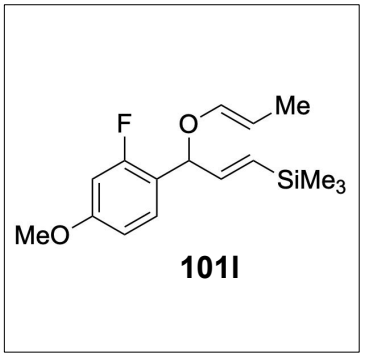

101l

```
Current Data Parameters
NAME      KS-02-161
EXPNO                11
PROCNO                1

F2 - Acquisition Parameters
Date_          20211028
Time               17.09 h
INSTRUM       Avance Neo
PROBHD   Z152088_0031 (
PULPROG          zgpg30
TD                65536
SOLVENT           CDCl3
NS                 1024
DS                    4
SWH           23809.523 Hz
FIDRES         0.726609 Hz
AQ             1.3762560 sec
RG                8.125
DW               21.000 usec
DE                6.50 usec
TE                298.0 K
D1            2.00000000 sec
D11           0.03000000 sec
TD0                   1
SFO1        100.6228298 MHz
NUC1                13C
P0                 2.67 usec
P1                 8.00 usec
PLW1         86.55400085 W
SFO2        400.1316005 MHz
NUC2                1H
CPDPRG[2         waltz65
PCPD2              90.00 usec
PLW2         24.03499985 W
PLW12         0.18990999 W
PLW13         0.09552100 W

F2 - Processing parameters
SI                 32768
SF          100.6127540 MHz
WDW                   EM
SSB                    0
LB                 1.00 Hz
GB                     0
PC                 1.40
```

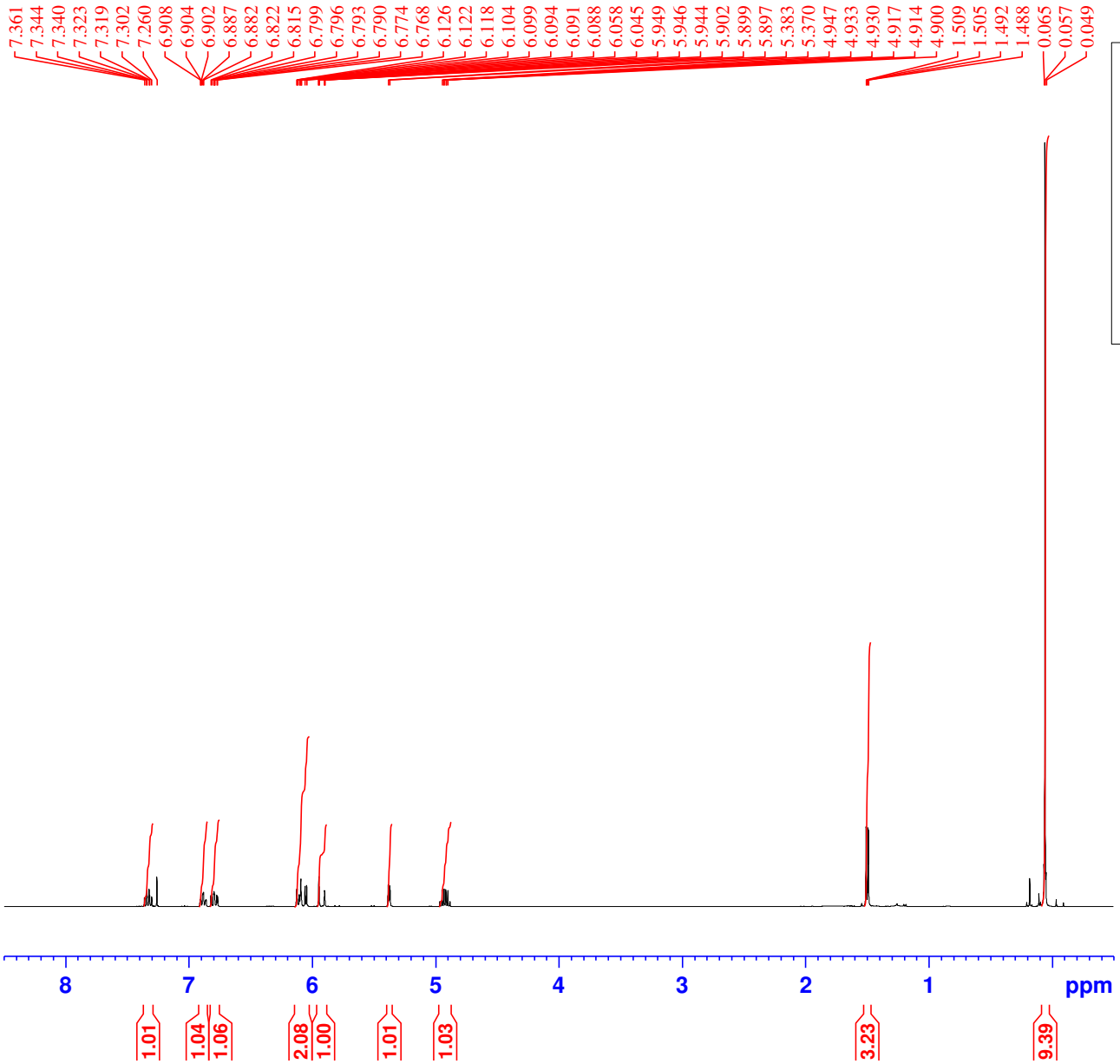

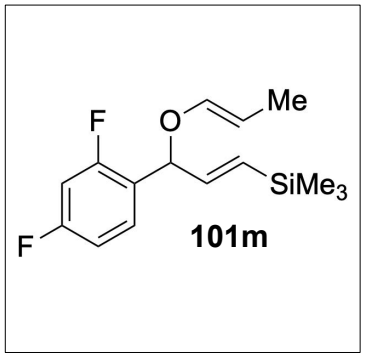


```
Current Data Parameters
NAME      KS-02-276
EXPNO                10
PROCNO                1

F2 - Acquisition Parameters
Date_           20220309
Time              18.14 h
INSTRUM       Avance Neo
PROBHD    Z152088_0031 (
PULPROG             zg30
TD                 65536
SOLVENT            CDCl3
NS                    16
DS                     2
SWH             8196.722 Hz
FIDRES          0.250144 Hz
AQ              3.9976959 sec
RG                   101
DW                61.000 usec
DE                13.89 usec
TE                298.0 K
D1            1.00000000 sec
TD0                    1
SFO1         400.1324708 MHz
NUC1                 1H
P0                 2.67 usec
P1                 8.00 usec
PLW1         24.03499985 W

F2 - Processing parameters
SI                 65536
SF           400.1300096 MHz
WDW                   EM
SSB                    0
LB                  0.30 Hz
GB                     0
PC                  1.00
```

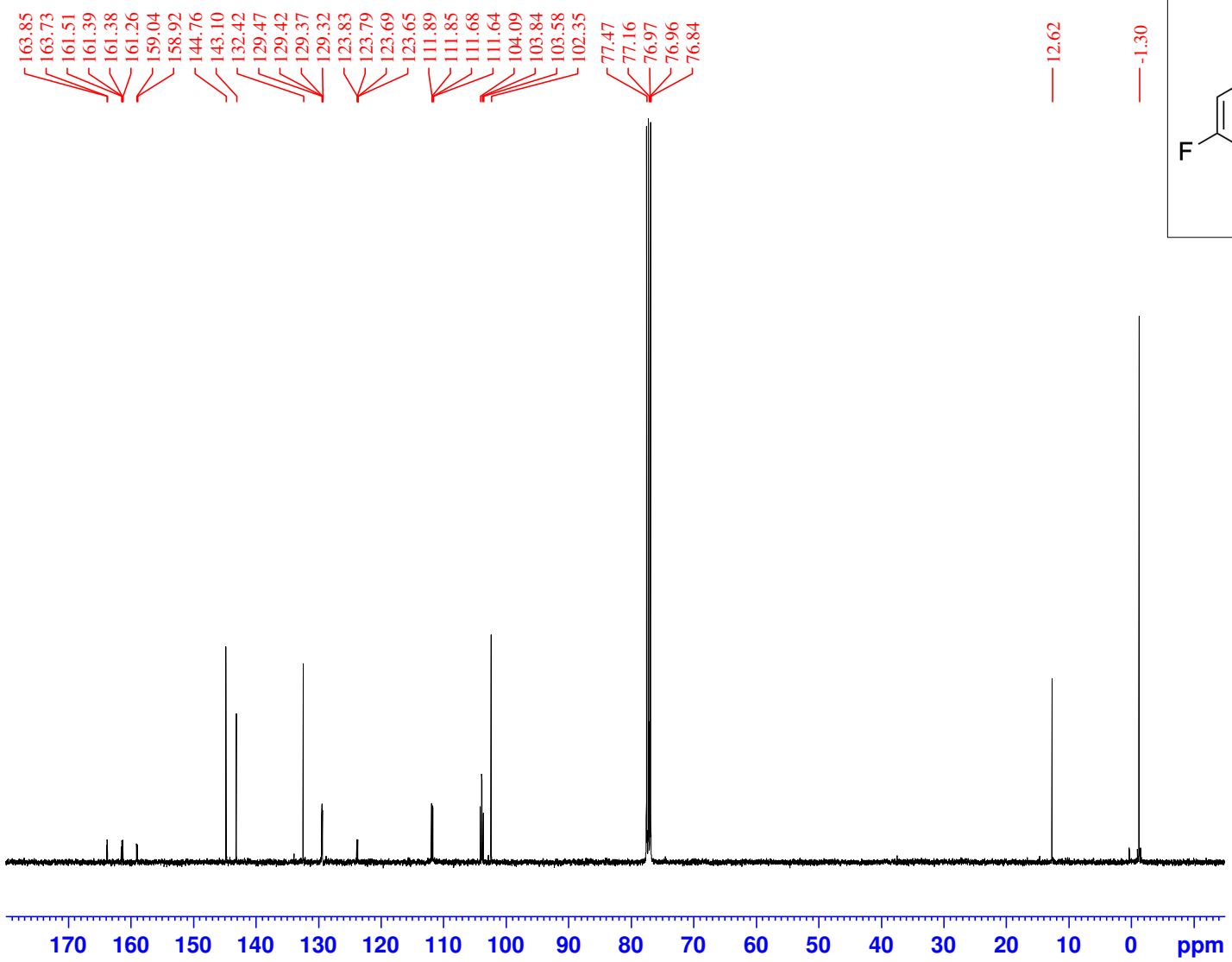

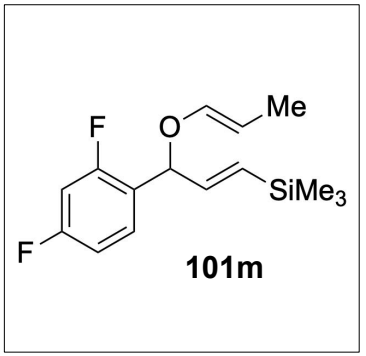


```
Current Data Parameters
NAME      KS-02-276
EXPNO                12
PROCNO                1

F2 - Acquisition Parameters
Date_          20220309
Time               20.06 h
INSTRUM       Avance Neo
PROBHD    Z152088_0031 (
PULPROG          zgpg30
TD                65536
SOLVENT           CDCl3
NS                 1024
DS                    4
SWH           23809.523 Hz
FIDRES         0.726609 Hz
AQ             1.3762560 sec
RG                8.125
DW               21.000 usec
DE                6.50 usec
TE               298.0 K
D1            2.00000000 sec
D11           0.03000000 sec
TD0                   1
SFO1         100.6228298 MHz
NUC1                13C
P0                 2.67 usec
P1                 8.00 usec
PLW1         86.55400085 W
SFO2         400.1316005 MHz
NUC2                1H
CPDPRG[2         waltz65
PCPD2             90.00 usec
PLW2         24.03499985 W
PLW12         0.18990999 W
PLW13         0.09552100 W

F2 - Processing parameters
SI                32768
SF           100.6127540 MHz
WDW                  EM
SSB                   0
LB                 1.00 Hz
GB                    0
PC                 1.40
```

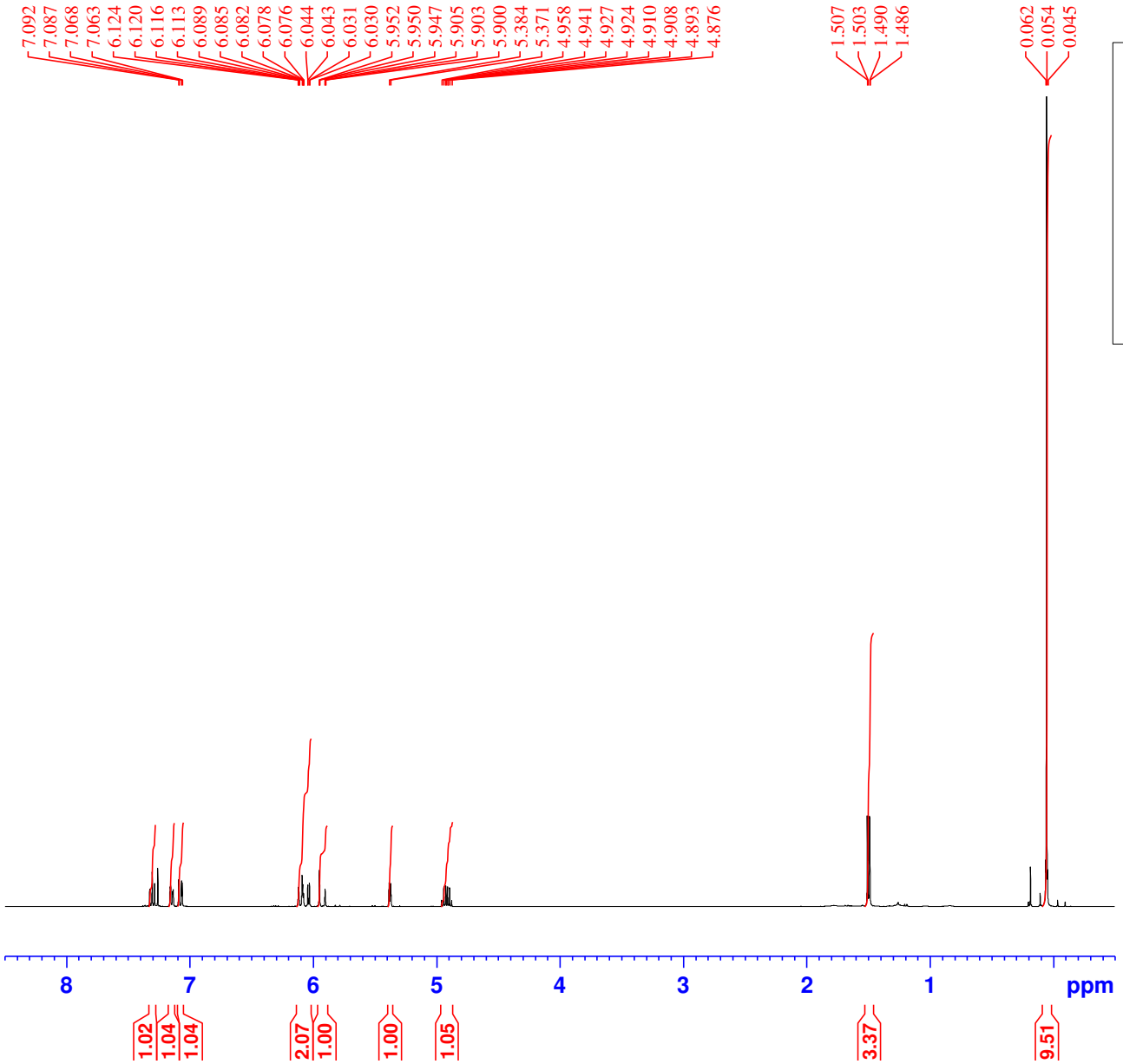

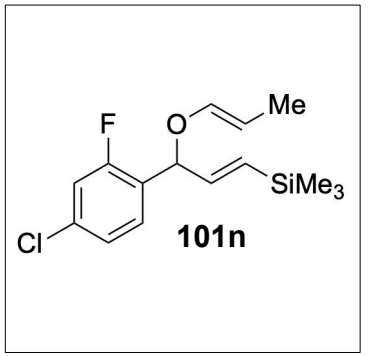

Current Data Parameters
NAME KS-02-284
EXPNO 10
PROCNO 1

F2 - Acquisition Parameters
Date_ 20220316
Time 15.49 h
INSTRUM Avance Neo
PROBHD Z152088_0031 (
PULPROG zg30
TD 65536
SOLVENT CDCl3
NS 16
DS 2
SWH 8196.722 Hz
FIDRES 0.250144 Hz
AQ 3.9976959 sec
RG 101
DW 61.000 usec
DE 13.89 usec
TE 298.0 K
D1 1.00000000 sec
TD0 1
SFO1 400.1324708 MHz
NUC1 1H
P0 2.67 usec
P1 8.00 usec
PLW1 24.03499985 W

F2 - Processing parameters
SI 65536
SF 400.1300096 MHz
WDW EM
SSB 0
LB 0.30 Hz
GB 0
PC 1.00

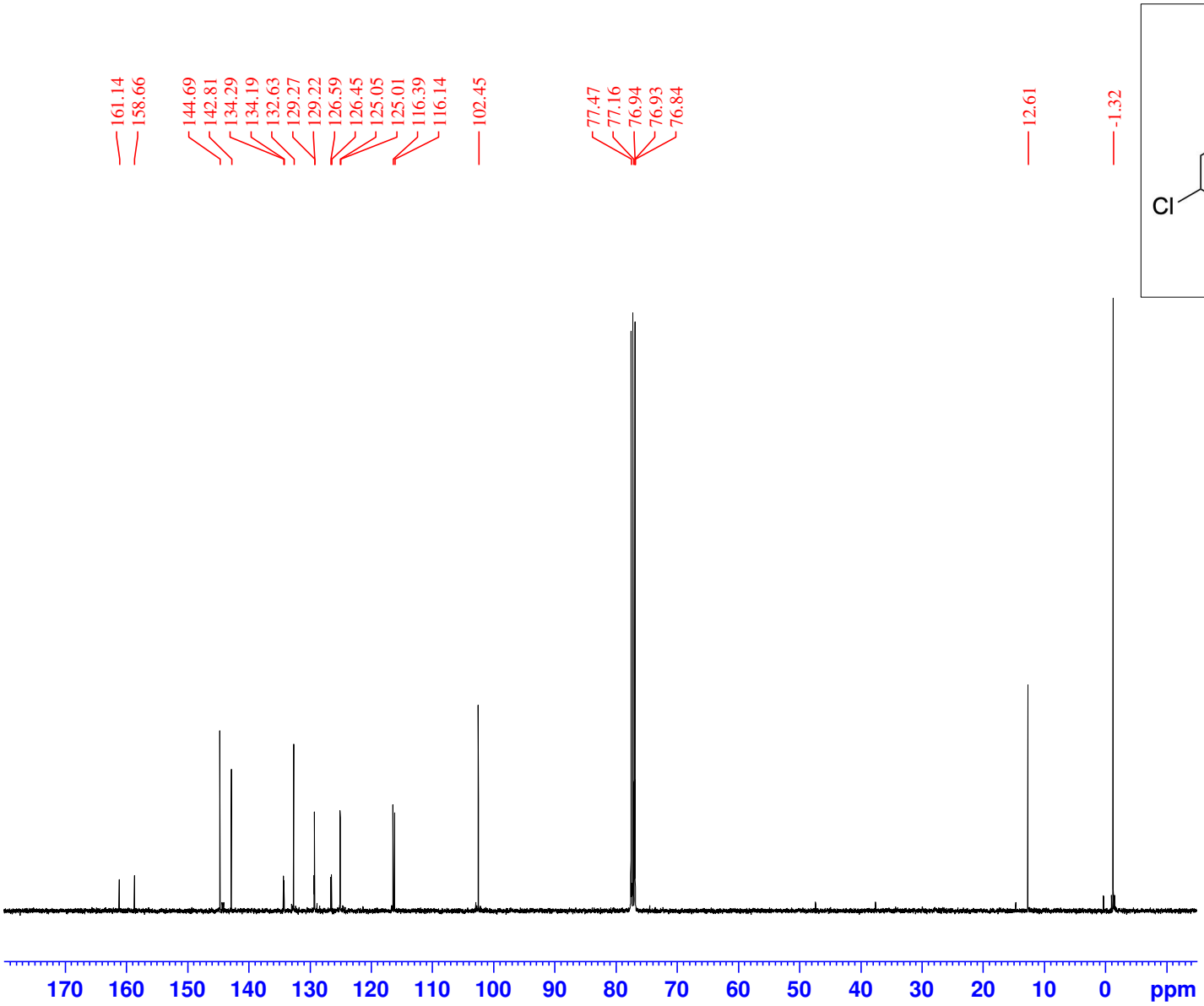


```
Current Data Parameters
NAME      KS-02-284
EXPNO                12
PROCNO                1

F2 - Acquisition Parameters
Date_          20220316
Time                21.06 h
INSTRUM       Avance Neo
PROBHD   Z152088_0031 (
PULPROG           zgpg30
TD                65536
SOLVENT           CDCl3
NS                 1024
DS                    4
SWH           23809.523 Hz
FIDRES         0.726609 Hz
AQ            1.3762560 sec
RG                8.125
DW               21.000 usec
DE                6.50 usec
TE                298.0 K
D1           2.00000000 sec
D11          0.03000000 sec
TD0                   1
SFO1        100.6228298 MHz
NUC1                13C
P0                 2.67 usec
P1                 8.00 usec
PLW1        86.55400085 W
SFO2        400.1316005 MHz
NUC2                1H
CPDPRG[2         waltz65
PCPD2             90.00 usec
PLW2        24.03499985 W
PLW12        0.18990999 W
PLW13        0.09552100 W

F2 - Processing parameters
SI                32768
SF          100.6127544 MHz
WDW                EM
SSB                   0
LB                 1.00 Hz
GB                    0
PC                 1.40
```

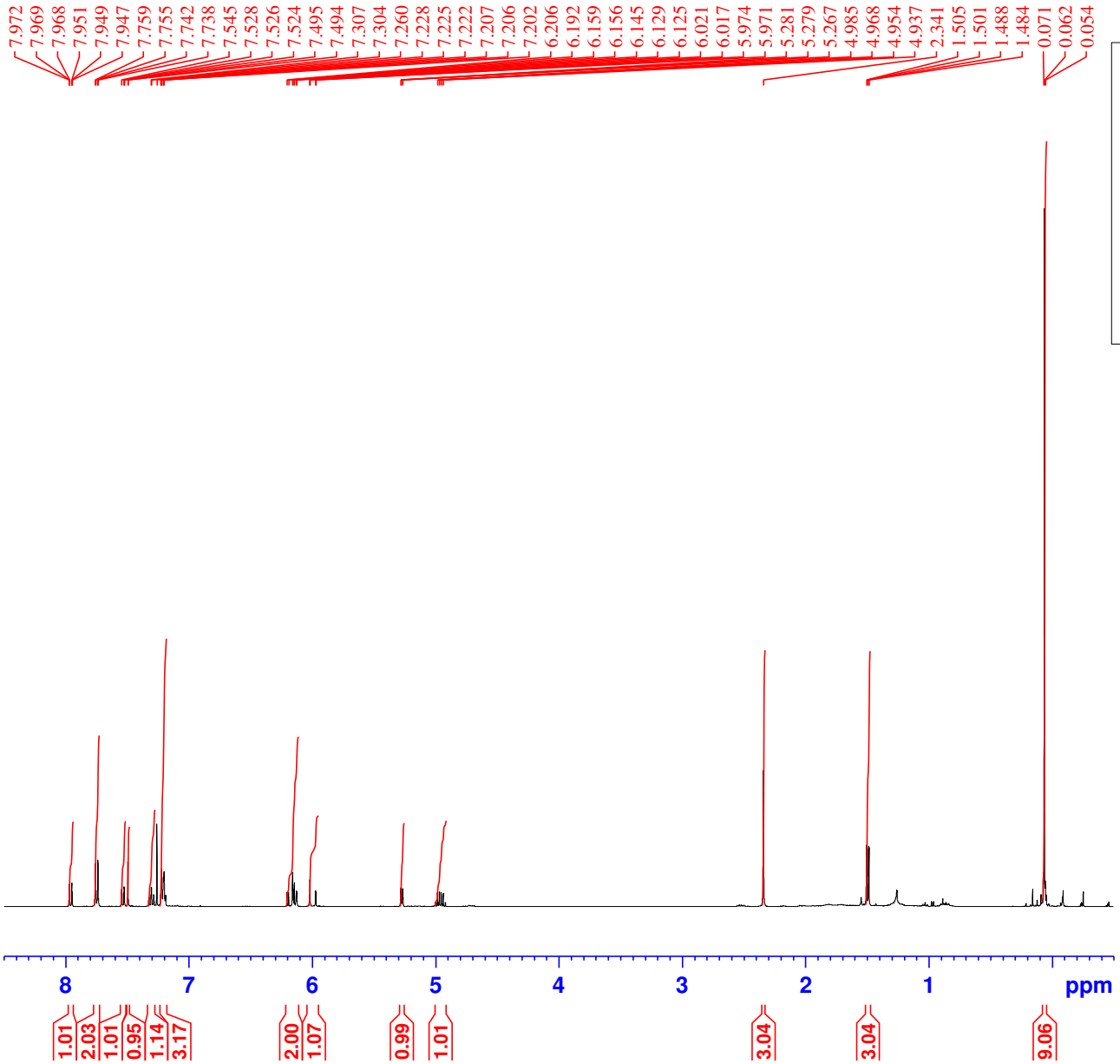

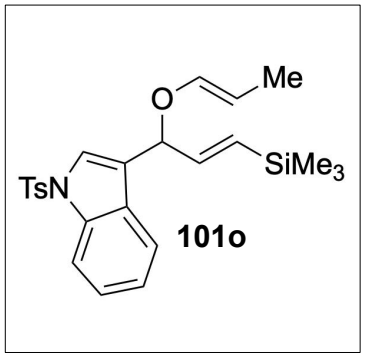


```
Current Data Parameters
NAME      KS-02-233
EXPNO               10
PROCNO               1

F2 - Acquisition Parameters
Date_          20220124
Time              18.15 h
INSTRUM       Avance Neo
PROBHD    Z152088_0031 (
PULPROG             zg30
TD                 65536
SOLVENT            CDCl3
NS                    16
DS                     2
SWH             8196.722 Hz
FIDRES          0.250144 Hz
AQ              3.9976959 sec
RG                   101
DW                61.000 usec
DE                13.89 usec
TE                298.0 K
D1             1.00000000 sec
TD0                    1
SFO1         400.1324708 MHz
NUC1                 1H
P0                 2.67 usec
P1                 8.00 usec
PLW1         24.03499985 W

F2 - Processing parameters
SI                 65536
SF           400.1300096 MHz
WDW                   EM
SSB                    0
LB                  0.30 Hz
GB                     0
PC                  1.00
```

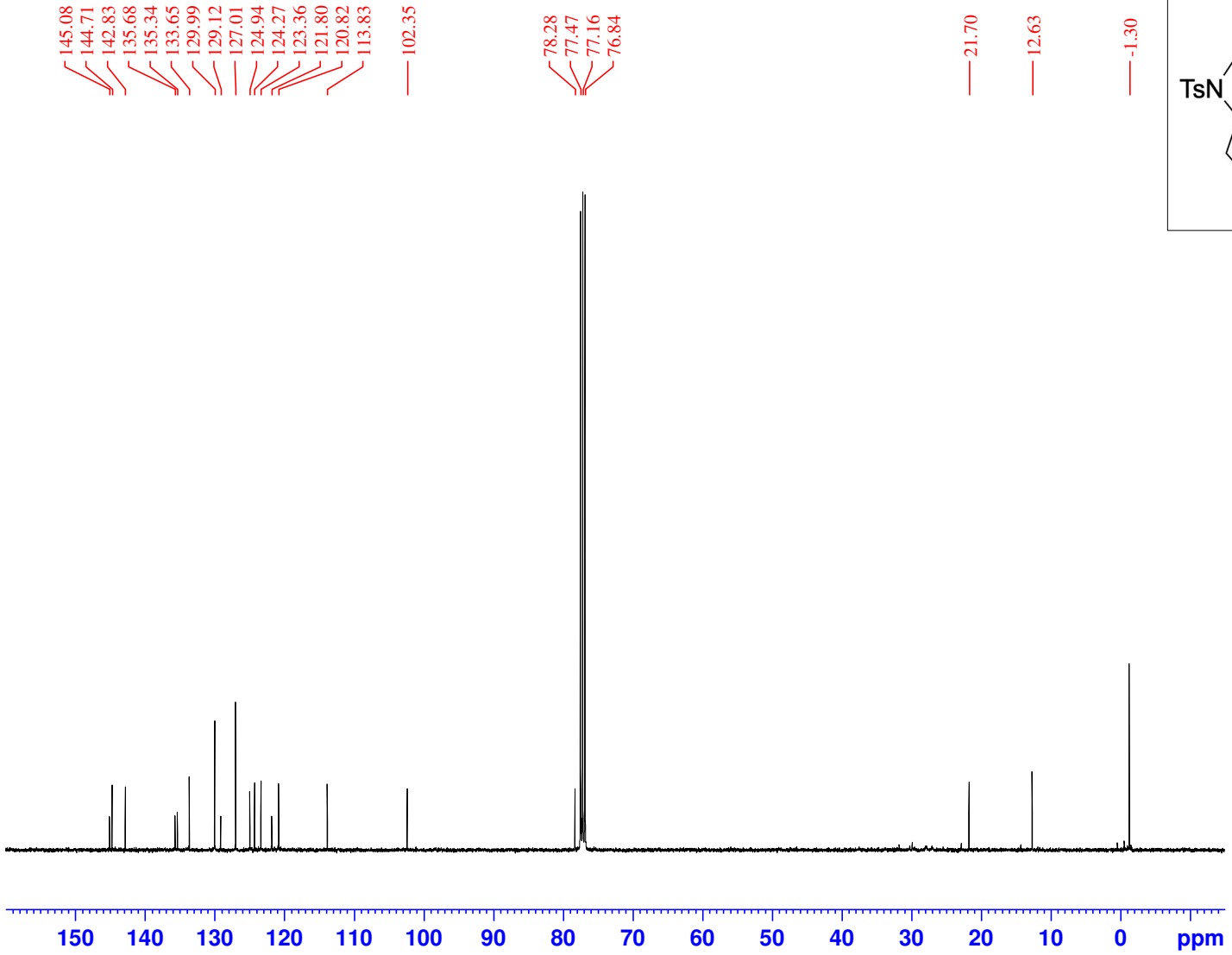

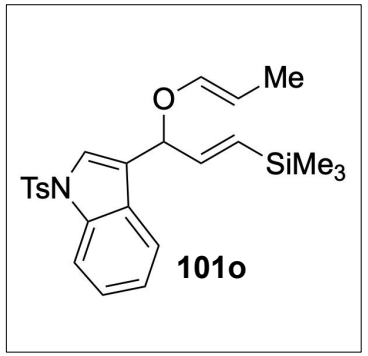


```
Current Data Parameters
NAME      KS-02-233
EXPNO                11
PROCNO                1

F2 - Acquisition Parameters
Date_          20220124
Time               21.08 h
INSTRUM       Avance Neo
PROBHD    Z152088_0031 (
PULPROG          zgpg30
TD                65536
SOLVENT           CDCl3
NS                 2048
DS                    4
SWH           23809.523 Hz
FIDRES         0.726609 Hz
AQ             1.3762560 sec
RG                8.125
DW               21.000 usec
DE                6.50 usec
TE               298.0 K
D1            2.00000000 sec
D11           0.03000000 sec
TD0                   1
SFO1         100.6228298 MHz
NUC1                13C
P0                 2.67 usec
P1                 8.00 usec
PLW1         86.55400085 W
SFO2         400.1316005 MHz
NUC2                1H
CPDPRG[2         waltz65
PCPD2             90.00 usec
PLW2         24.03499985 W
PLW12         0.18990999 W
PLW13         0.09552100 W

F2 - Processing parameters
SI                32768
SF           100.6127549 MHz
WDW                  EM
SSB                   0
LB                 1.00 Hz
GB                    0
PC                 1.40
```

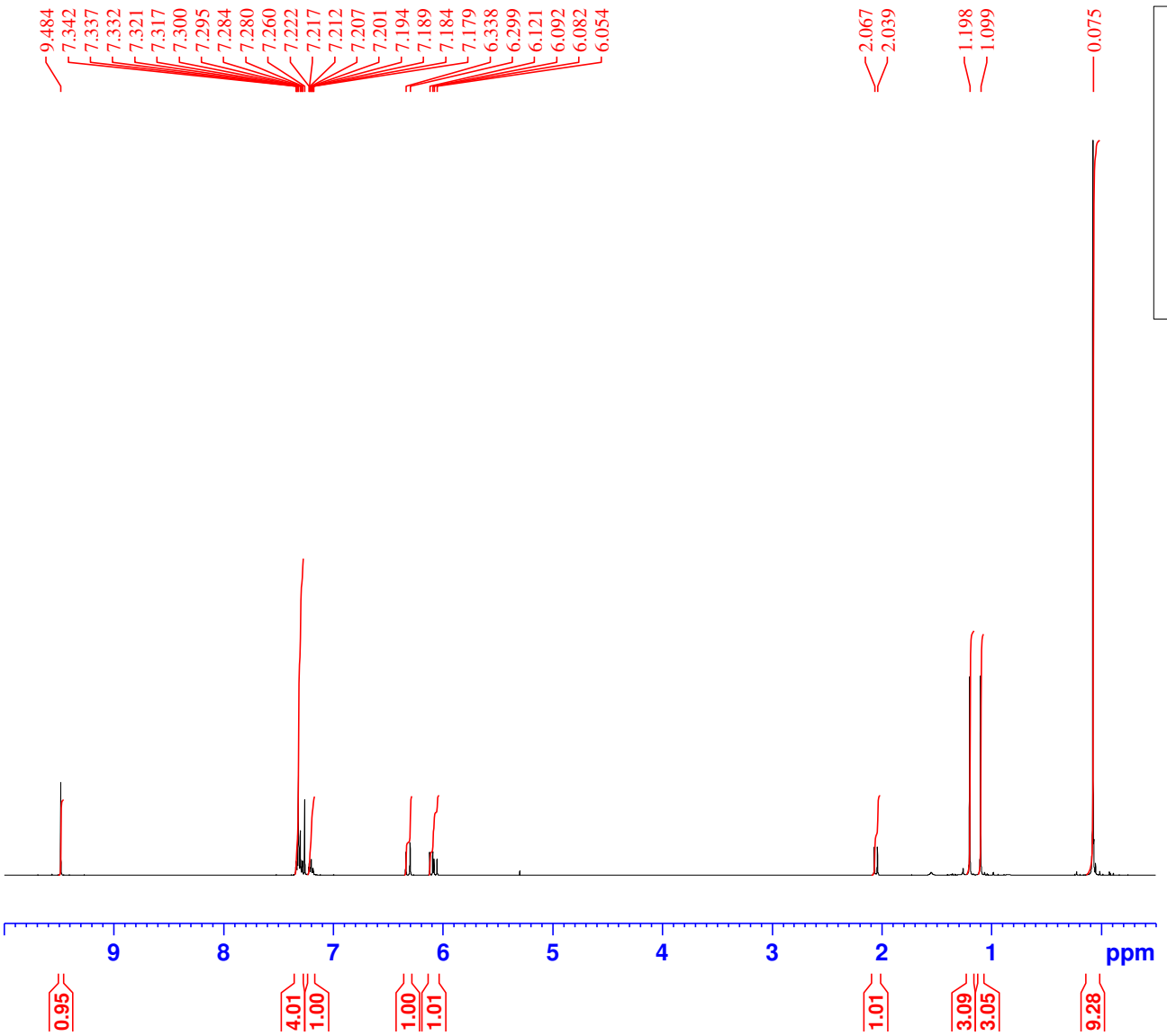

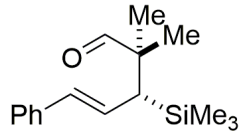

109

```
Current Data Parameters
NAME         KS-03-95
EXPNO              10
PROCNO              1

F2 - Acquisition Parameters
Date_          20220810
Time             16.02 h
INSTRUM       Avance Neo
PROBHD   Z152088_0031 (
PULPROG            zg30
TD                65536
SOLVENT           CDCl3
NS                   16
DS                    2
SWH            8196.722 Hz
FIDRES         0.250144 Hz
AQ             3.9976959 sec
RG                  101
DW               61.000 usec
DE               13.89 usec
TE               298.0 K
D1            1.00000000 sec
TD0                   1
SFO1         400.1324708 MHz
NUC1                 1H
P0                2.67 usec
P1                8.00 usec
PLW1         24.03499985 W

F2 - Processing parameters
SI                65536
SF           400.1300097 MHz
WDW                  EM
SSB       0
LB                0.30 Hz
GB        0
PC                1.00
```

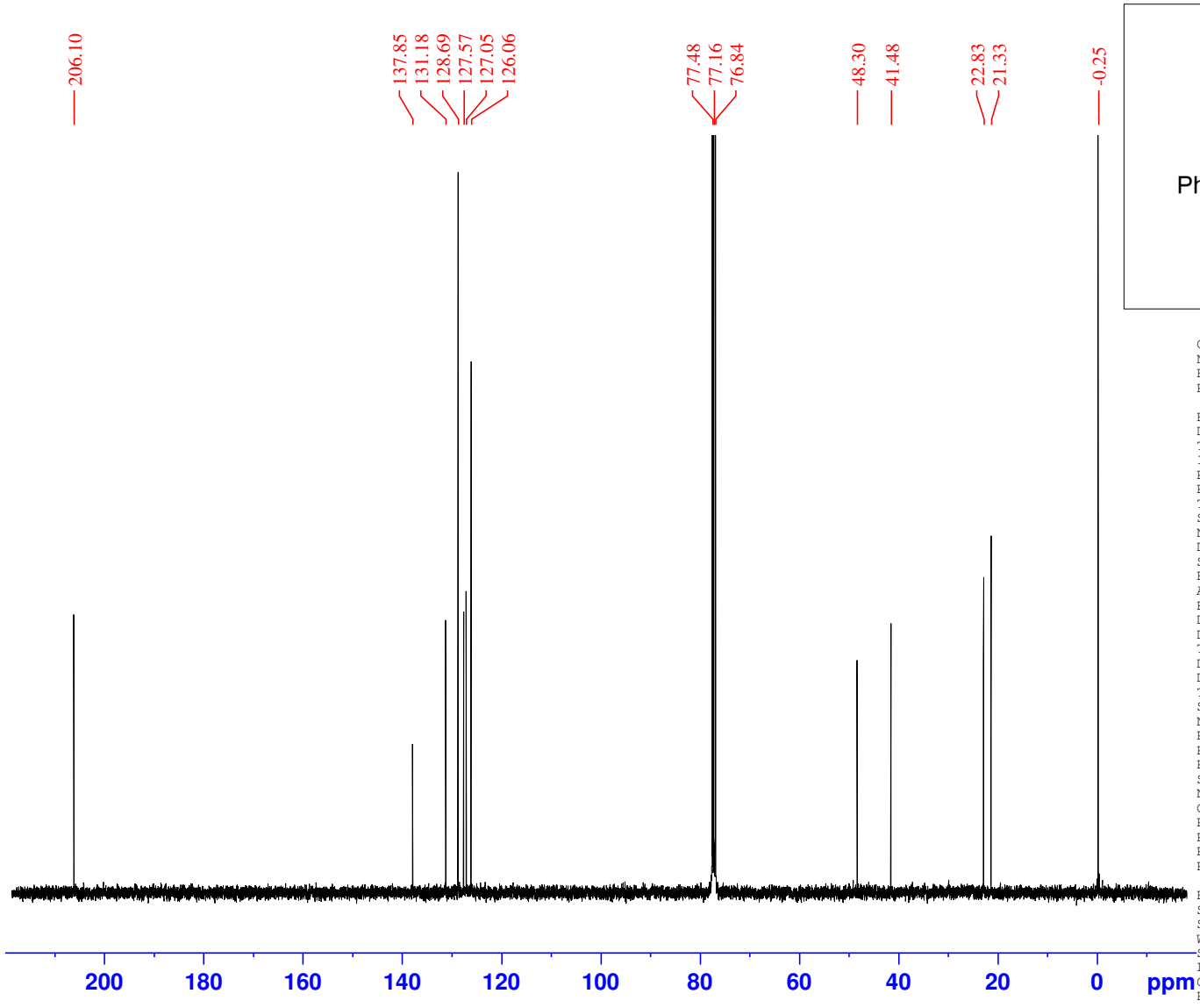

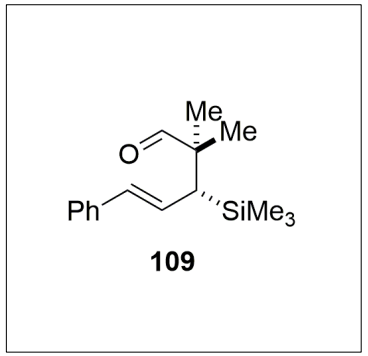

109

```
Current Data Parameters
NAME         KS-03-95
EXPNO              11
PROCNO              1

F2 - Acquisition Parameters
Date_          20220810
Time              20.46 h
INSTRUM       Avance Neo
PROBHD    Z152088_0031 (
PULPROG         zgpg30
TD              65536
SOLVENT          CDCl3
NS                1024
DS                   4
SWH          23809.523 Hz
FIDRES        0.726609 Hz
AQ            1.3762560 sec
RG                8.125
DW               21.000 usec
DE                6.50 usec
TE               298.0 K
D1            2.00000000 sec
D11           0.03000000 sec
TD0                  1
SFO1        100.6228298 MHz
NUC1               13C
P0                2.67 usec
P1                8.00 usec
PLW1         86.55400085 W
SFO2        400.1316005 MHz
NUC2               1H
CPDPRG[2        waltz65
PCPD2            90.00 usec
PLW2         24.03499985 W
PLW12         0.18990999 W
PLW13         0.09552100 W

F2 - Processing parameters
SI                32768
SF          100.6127545 MHz
WDW                EM
SSB       0
LB                1.00 Hz
GB        0
PC                1.40
```

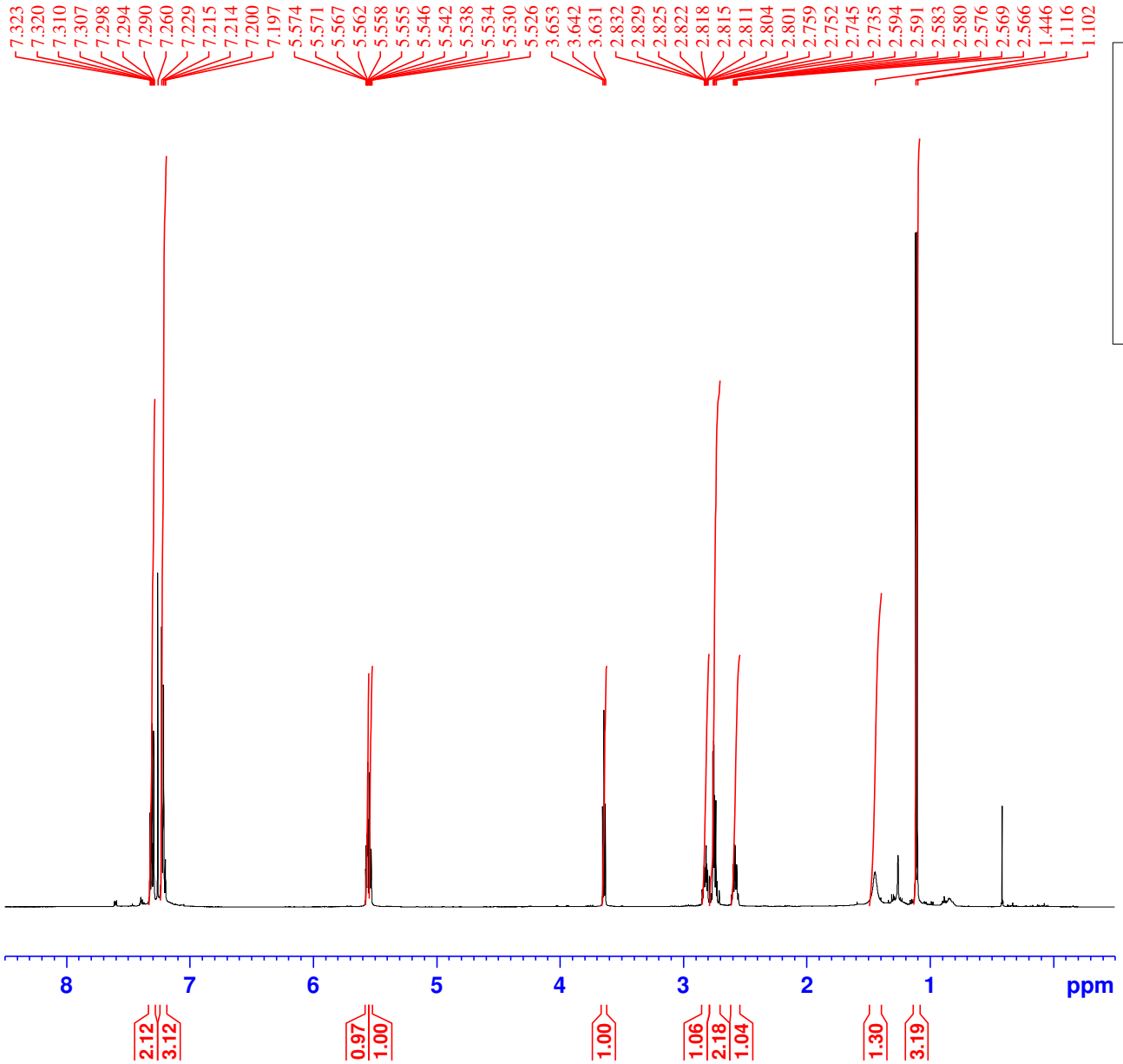

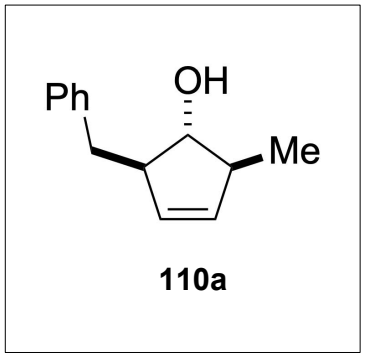

110a

```
Current Data Parameters
NAME      KS-02-094
EXPNO                10
PROCNO                1

F2 - Acquisition Parameters
Date_          20210909
Time              17.28 h
INSTRUM             spect
PROBHD   Z125869_0055 (
PULPROG             zg30
TD                 65536
SOLVENT            CDCl3
NS                    32
DS                     2
SWH           10000.000 Hz
FIDRES            0.305176 Hz
AQ             3.2767999 sec
RG                151.18
DW                50.000 usec
DE                16.00 usec
TE                300.0 K
D1            2.00000000 sec
TD0                    1
SFO1         500.2330889 MHz
NUC1                  1H
P0                 4.00 usec
P1                12.00 usec
PLW1         11.44699955 W

F2 - Processing parameters
SI                 65536
SF           500.2300119 MHz
WDW                   EM
SSB                    0
LB                 0.30 Hz
GB                     0
PC                 1.00
```

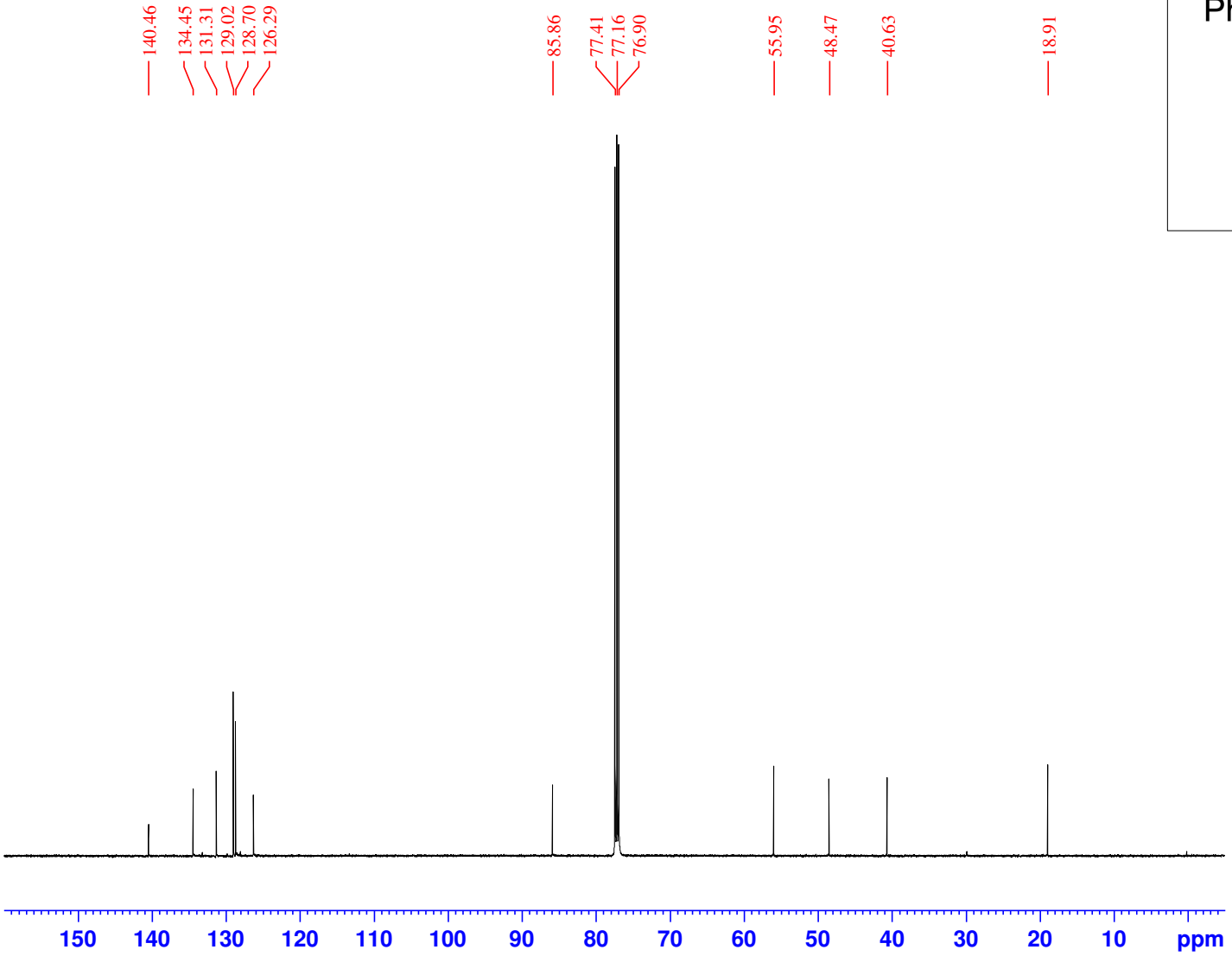

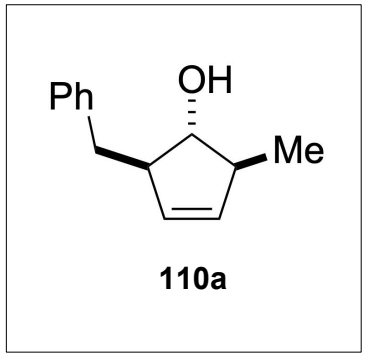

110a

```
Current Data Parameters
NAME      KS-02-094
EXPNO                10
PROCNO                1

F2 - Acquisition Parameters
Date_          20210911
Time               13.36 h
INSTRUM            spect
PROBHD    Z125869_0055 (
PULPROG          zgpg30
TD                65536
SOLVENT           CDCl3
NS                 1024
DS                    4
SWH           29761.904 Hz
FIDRES         0.908261 Hz
AQ             1.1010048 sec
RG                190.44
DW                16.800 usec
DE                18.00 usec
TE                298.0 K
D1             2.00000000 sec
D11            0.03000000 sec
TD0                   1
SFO1         125.7955118 MHz
NUC1                 13C
P0                 3.33 usec
P1                10.00 usec
PLW1         56.90299988 W
SFO2         500.2320009 MHz
NUC2                 1H
CPDPRG[2         waltz16
PCPD2             80.00 usec
PLW2         11.44699955 W
PLW12         0.25756001 W
PLW13         0.12955000 W

F2 - Processing parameters
SI                32768
SF           125.7829164 MHz
WDW                  EM
SSB                   0
LB                 1.00 Hz
GB                    0
PC                 1.40
```

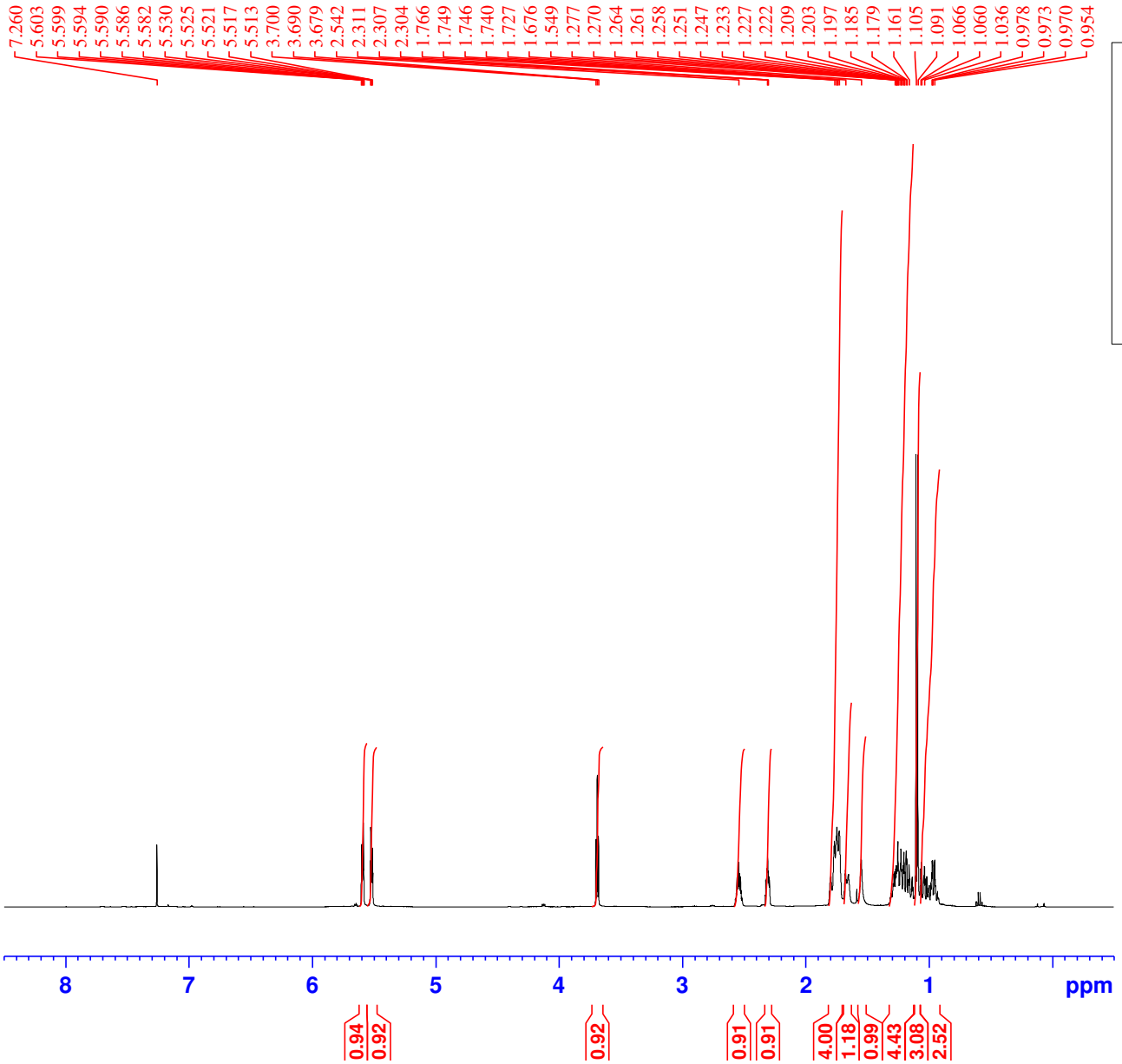

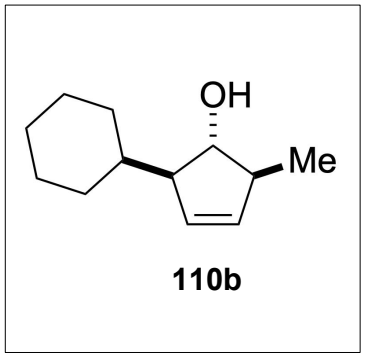

110b

```
Current Data Parameters
NAME      KS-02-107
EXPNO                10
PROCNO                1

F2 - Acquisition Parameters
Date_          20210918
Time              17.13 h
INSTRUM            spect
PROBHD   Z125869_0055 (
PULPROG            zg30
TD                65536
SOLVENT           CDCl3
NS                   64
DS                    2
SWH           10000.000 Hz
FIDRES            0.305176 Hz
AQ             3.2767999 sec
RG                37.93
DW               50.000 usec
DE               16.00 usec
TE               298.0 K
D1            2.00000000 sec
TD0                   1
SFO1         500.2330889 MHz
NUC1                 1H
P0                4.00 usec
P1               12.00 usec
PLW1         11.44699955 W

F2 - Processing parameters
SI                65536
SF           500.2300119 MHz
WDW                  EM
SSB                   0
LB                0.30 Hz
GB                    0
PC                1.00
```

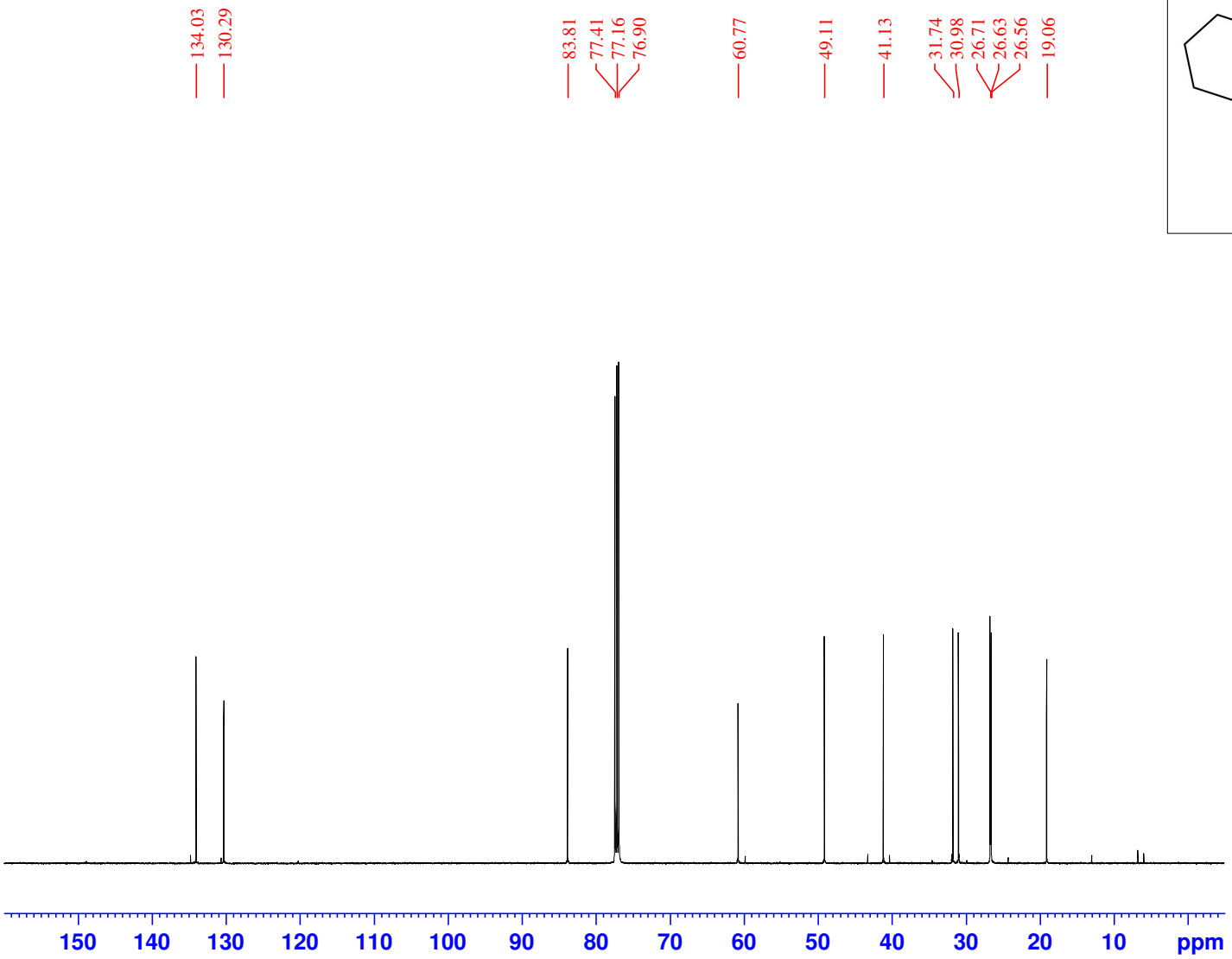

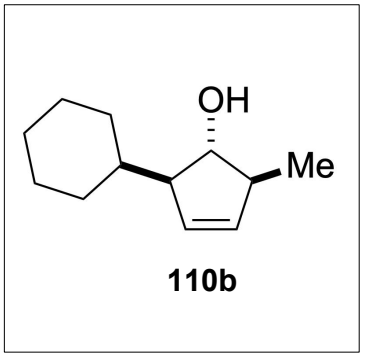

110b

```
Current Data Parameters
NAME      KS-02-107
EXPNO                11
PROCNO                1

F2 - Acquisition Parameters
Date_          20210918
Time               18.09 h
INSTRUM            spect
PROBHD   Z125869_0055 (
PULPROG          zgpg30
TD                65536
SOLVENT           CDCl3
NS                 1024
DS                    4
SWH           29761.904 Hz
FIDRES         0.908261 Hz
AQ             1.1010048 sec
RG                190.44
DW                16.800 usec
DE                18.00 usec
TE                298.0 K
D1            2.00000000 sec
D11           0.03000000 sec
TD0                   1
SFO1         125.7955118 MHz
NUC1                 13C
P0                 3.33 usec
P1                10.00 usec
PLW1         56.90299988 W
SFO2         500.2320009 MHz
NUC2                 1H
CPDPRG[2         waltz16
PCPD2             80.00 usec
PLW2         11.44699955 W
PLW12         0.25756001 W
PLW13         0.12955000 W

F2 - Processing parameters
SI                32768
SF           125.7829164 MHz
WDW                  EM
SSB                   0
LB                 1.00 Hz
GB                    0
PC                 1.40
```

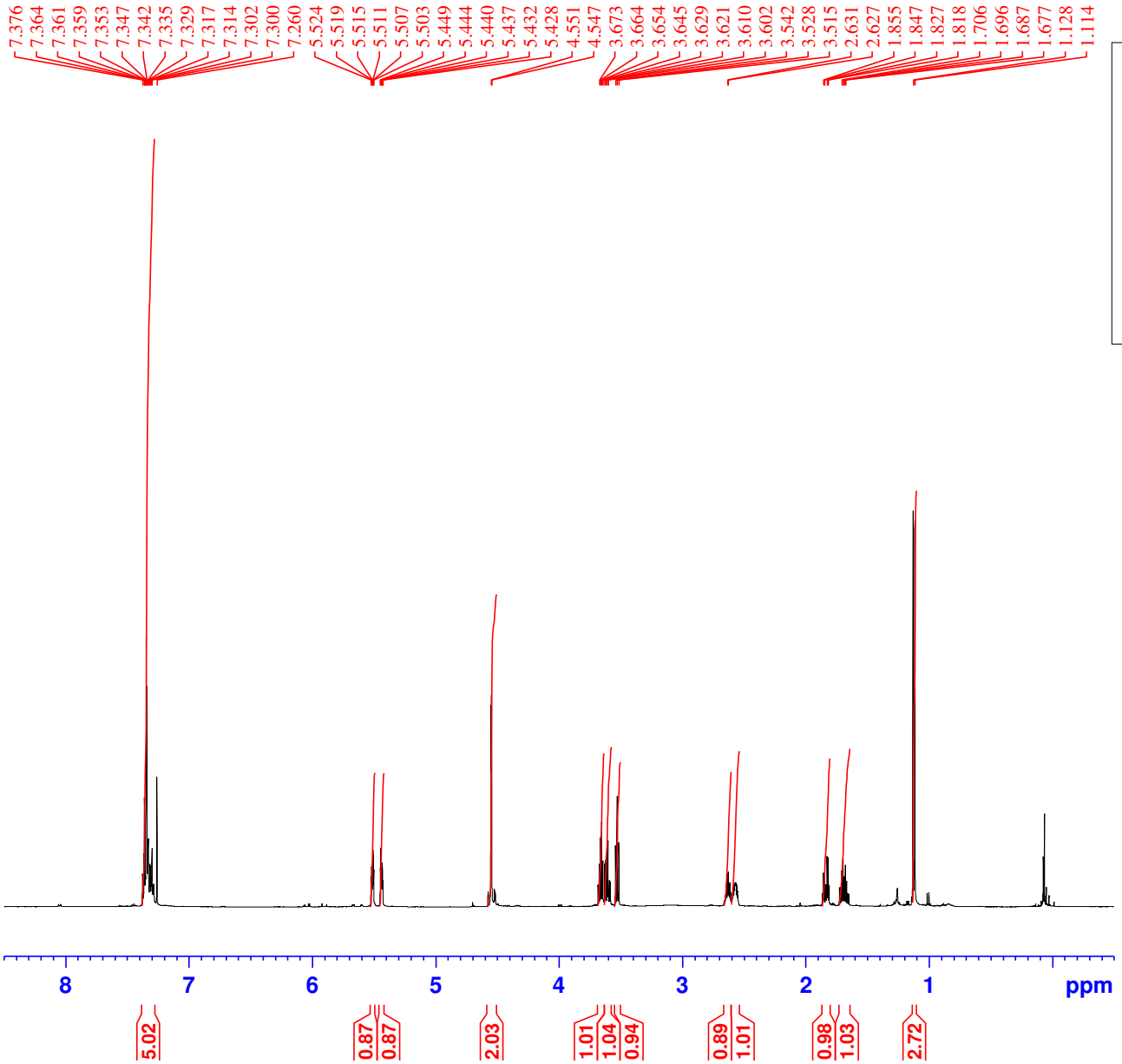

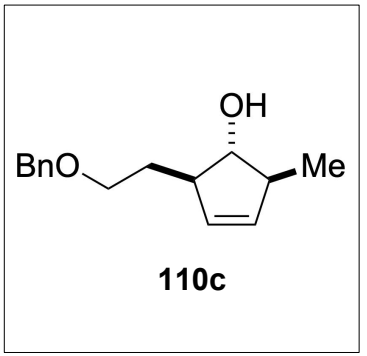


```
Current Data Parameters
NAME      KS-02-110
EXPNO              10
PROCNO              1

F2 - Acquisition Parameters
Date_        20210918
Time             18.19 h
INSTRUM            spect
PROBHD   Z125869_0055 (
PULPROG            zg30
TD                65536
SOLVENT           CDC13
NS                   64
DS                    2
SWH          10000.000 Hz
FIDRES           0.305176 Hz
AQ           3.2767999 sec
RG                94.51
DW               50.000 usec
DE               16.00 usec
TE               298.0 K
D1           2.00000000 sec
TD0                   1
SFO1        500.2330889 MHz
NUC1                 1H
P0                4.00 usec
P1               12.00 usec
PLW1        11.44699955 W

F2 - Processing parameters
SI                65536
SF          500.2300119 MHz
WDW                  EM
SSB                   0
LB                0.30 Hz
GB                    0
PC                1.00
```

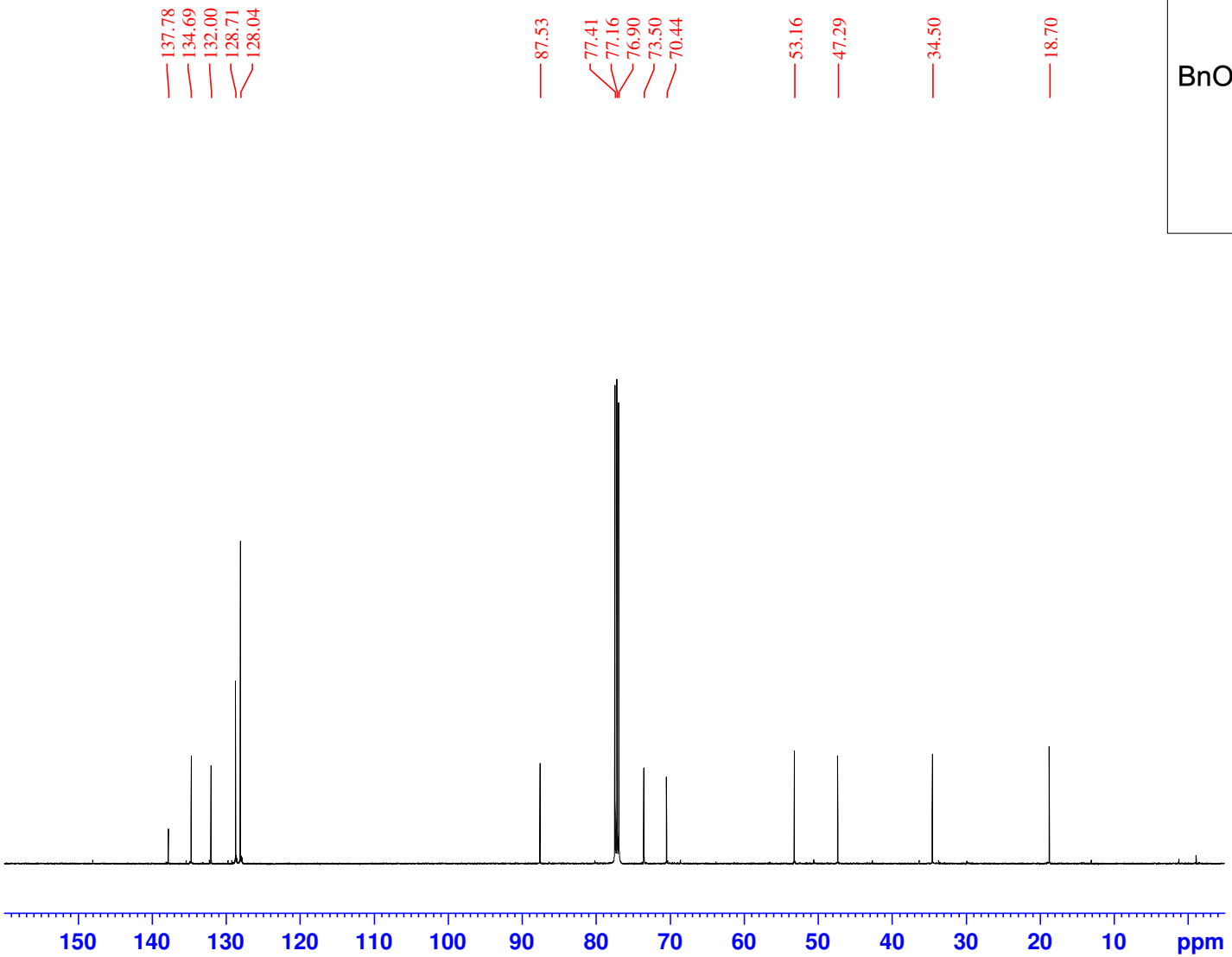

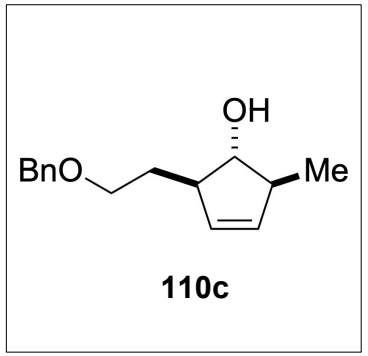


```
Current Data Parameters
NAME      KS-02-110
EXPNO              11
PROCNO              1

F2 - Acquisition Parameters
Date_        20210918
Time             19.14 h
INSTRUM          spect
PROBHD   Z125869_0055 (
PULPROG         zgpg30
TD               65536
SOLVENT          CDCl3
NS                1024
DS                   4
SWH          29761.904 Hz
FIDRES         0.908261 Hz
AQ           1.1010048 sec
RG              190.44
DW               16.800 usec
DE               18.00 usec
TE               298.0 K
D1           2.00000000 sec
D11          0.03000000 sec
TD0                  1
SFO1       125.7955118 MHz
NUC1              13C
P0                3.33 usec
P1               10.00 usec
PLW1       56.90299988 W
SFO2       500.2320009 MHz
NUC2              1H
CPDPRG[2        waltz16
PCPD2            80.00 usec
PLW2       11.44699955 W
PLW12       0.25756001 W
PLW13       0.12955000 W

F2 - Processing parameters
SI               32768
SF         125.7829172 MHz
WDW                 EM
SSB                  0
LB                1.00 Hz
GB                   0
PC                1.40
```

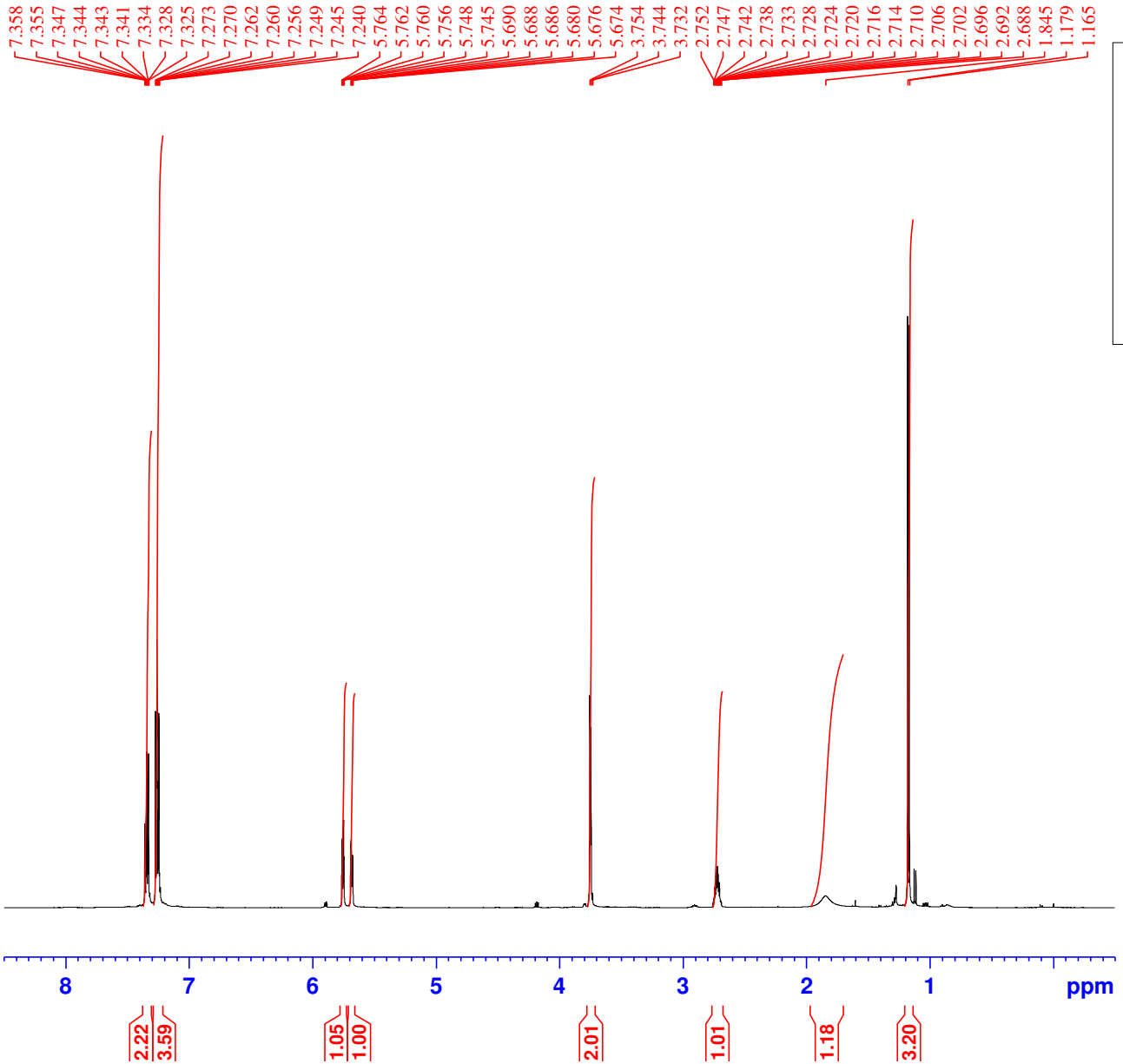

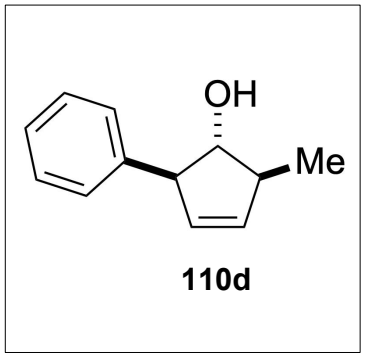

110d

```
Current Data Parameters
NAME      KS-02-140
EXPNO                10
PROCNO                1

F2 - Acquisition Parameters
Date_           20211015
Time              16.04 h
INSTRUM             spect
PROBHD    Z125869_0055 (
PULPROG             zg30
TD                 65536
SOLVENT            CDCl3
NS                    64
DS                     2
SWH           10000.000 Hz
FIDRES            0.305176 Hz
AQ                3.2767999 sec
RG                  107.7
DW                 50.000 usec
DE                 16.00 usec
TE                 298.0 K
D1              2.00000000 sec
TD0                    1
SFO1          500.2330889 MHz
NUC1                  1H
P0                  4.00 usec
P1                 12.00 usec
PLW1          11.44699955 W

F2 - Processing parameters
SI                 65536
SF            500.2300054 MHz
WDW                   EM
SSB                    0
LB                  0.30 Hz
GB                     0
PC                  1.00
```

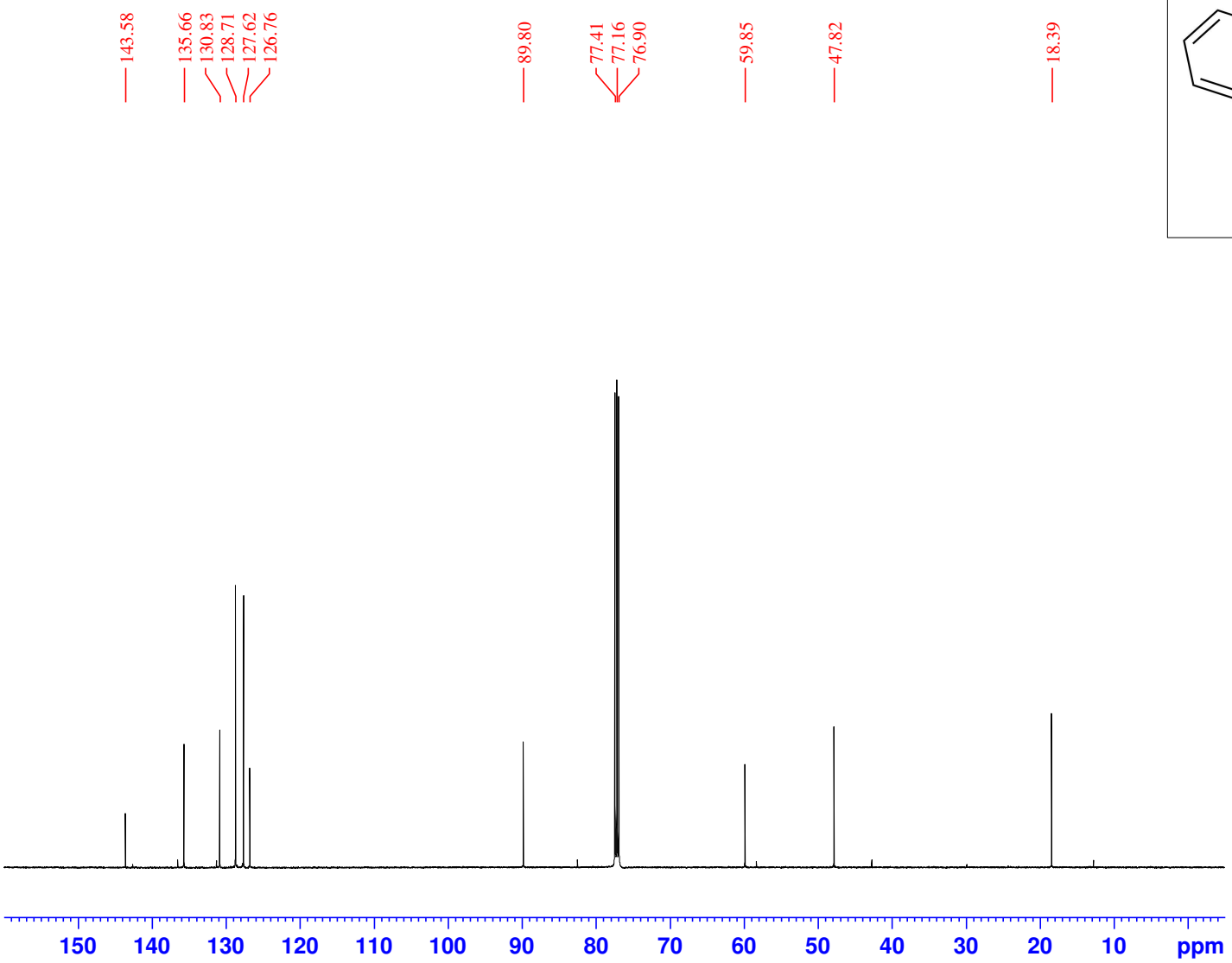

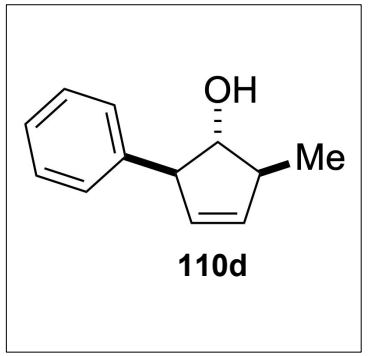

110d

```
Current Data Parameters
NAME      KS-02-140
EXPNO                11
PROCNO                1

F2 - Acquisition Parameters
Date_          20211015
Time              18.39 h
INSTRUM           spect
PROBHD    Z125869_0055 (
PULPROG          zgpg30
TD                65536
SOLVENT           CDCl3
NS                 1024
DS                    4
SWH           29761.904 Hz
FIDRES         0.908261 Hz
AQ            1.1010048 sec
RG               190.44
DW               16.800 usec
DE               18.00 usec
TE               298.0 K
D1            2.00000000 sec
D11           0.03000000 sec
TD0                   1
SFO1         125.7955118 MHz
NUC1                 13C
P0                3.33 usec
P1               10.00 usec
PLW1         56.90299988 W
SFO2         500.2320009 MHz
NUC2                 1H
CPDPRG[2         waltz16
PCPD2            80.00 usec
PLW2         11.44699955 W
PLW12         0.25756001 W
PLW13         0.12955000 W

F2 - Processing parameters
SI                32768
SF           125.7829172 MHz
WDW                  EM
SSB                   0
LB                 1.00 Hz
GB                    0
PC                 1.40
```

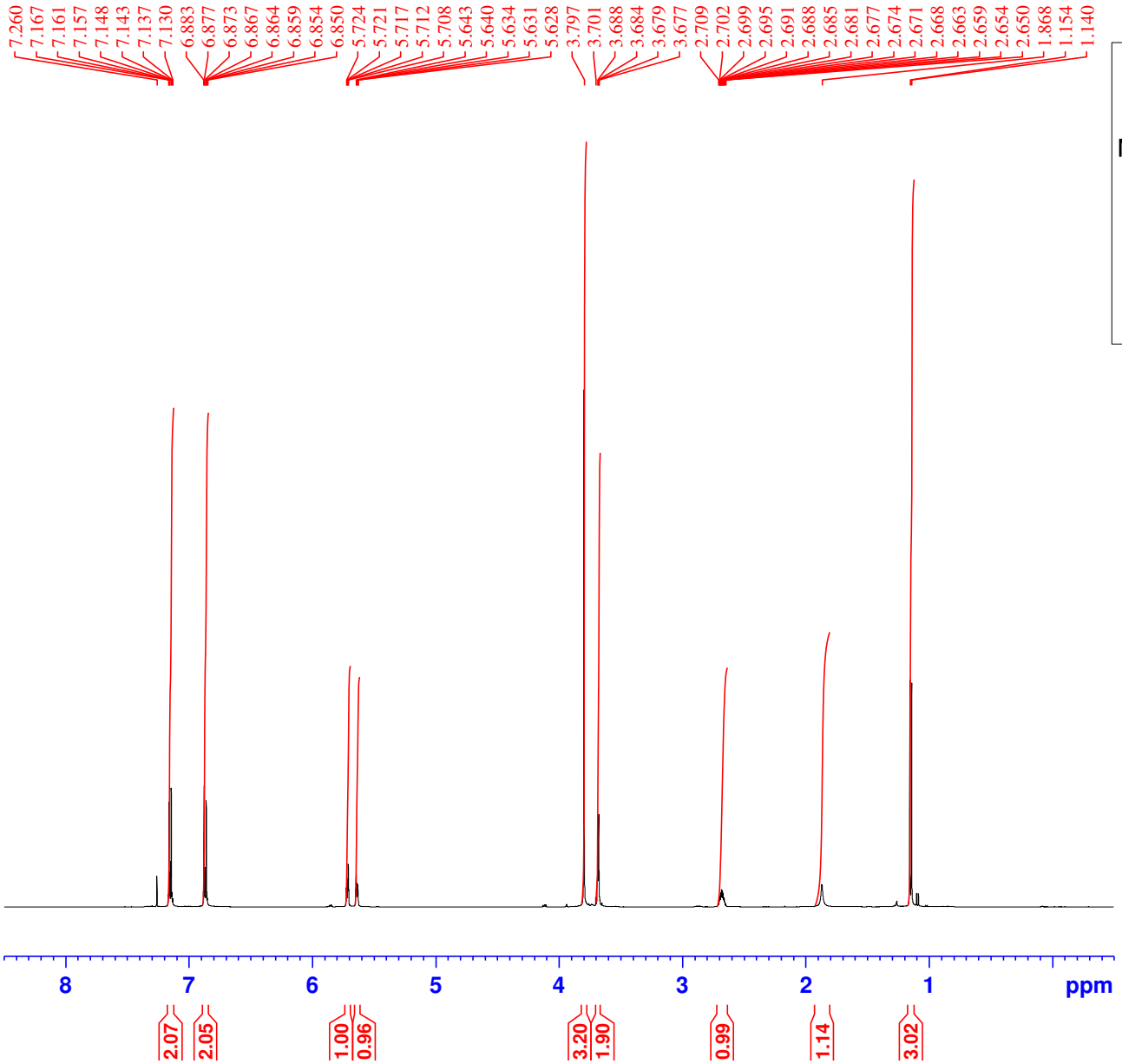

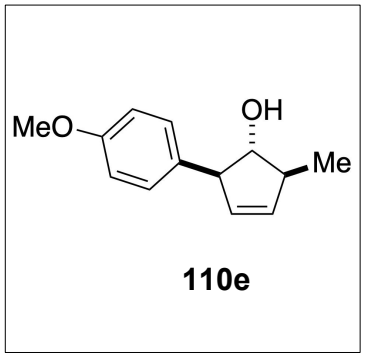

110e

```
Current Data Parameters
NAME      KS-02-152
EXPNO                10
PROCNO                1

F2 - Acquisition Parameters
Date_          20211022
Time              16.17 h
INSTRUM            spect
PROBHD   Z125869_0055 (
PULPROG            zg30
TD                65536
SOLVENT           CDCl3
NS                   64
DS                    2
SWH           10000.000 Hz
FIDRES            0.305176 Hz
AQ             3.2767999 sec
RG                43.72
DW                50.000 usec
DE                16.00 usec
TE                298.0 K
D1            2.00000000 sec
TD0                   1
SFO1          500.2330889 MHz
NUC1                 1H
P0                 4.00 usec
P1                12.00 usec
PLW1         11.44699955 W

F2 - Processing parameters
SI                65536
SF            500.2300120 MHz
WDW                  EM
SSB                   0
LB                 0.30 Hz
GB                    0
PC                 1.00
```

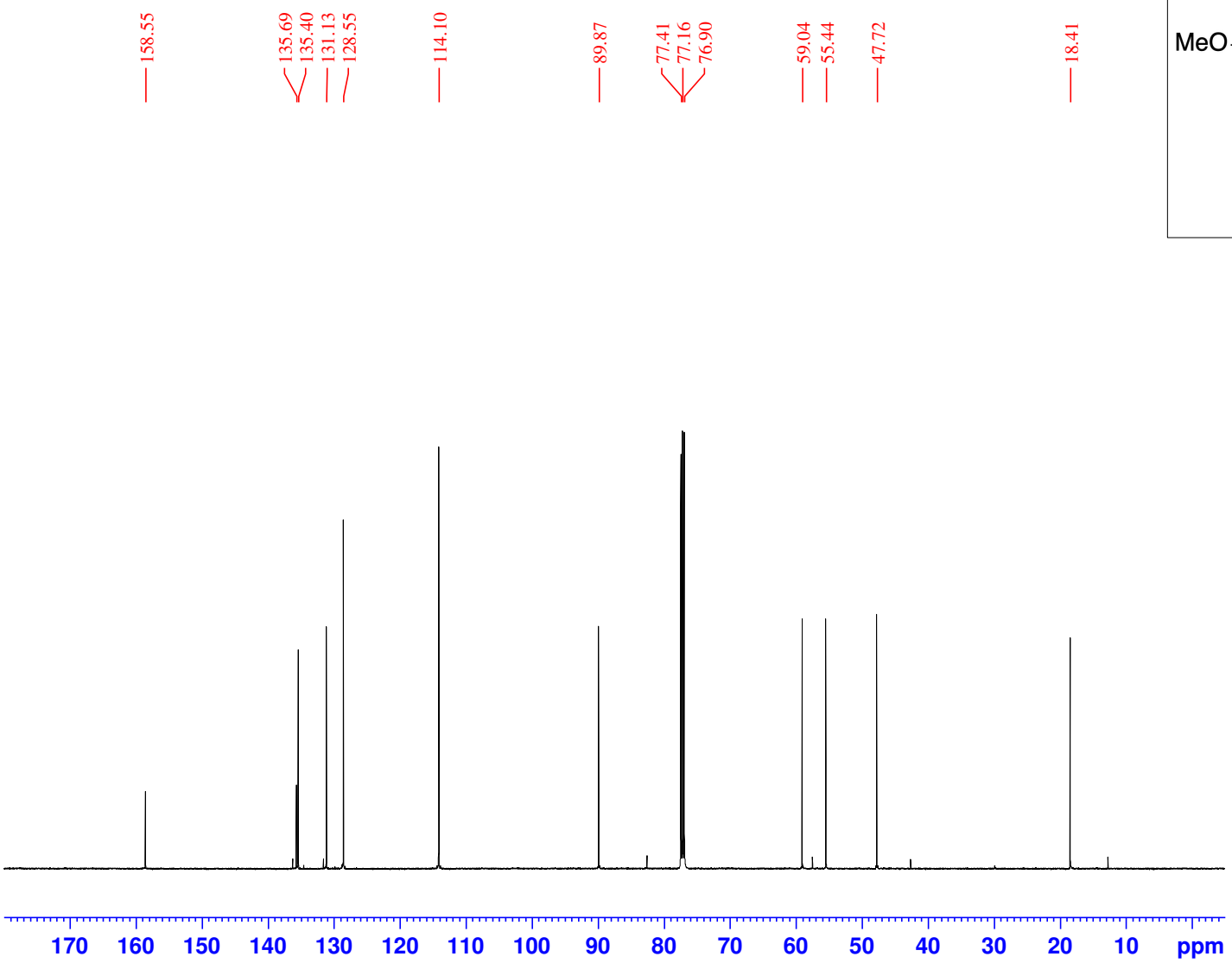

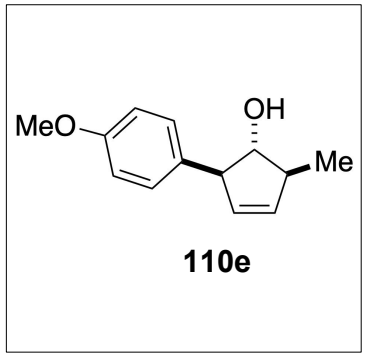

110e

```
Current Data Parameters
NAME      KS-02-152
EXPNO                11
PROCNO                1

F2 - Acquisition Parameters
Date_          20211022
Time               18.23 h
INSTRUM            spect
PROBHD   Z125869_0055 (
PULPROG          zgpg30
TD                65536
SOLVENT           CDCl3
NS                 1024
DS                    4
SWH           29761.904 Hz
FIDRES         0.908261 Hz
AQ            1.1010048 sec
RG               190.44
DW               16.800 usec
DE               18.00 usec
TE               298.0 K
D1           2.00000000 sec
D11          0.03000000 sec
TD0                   1
SFO1        125.7955118 MHz
NUC1               13C
P0                3.33 usec
P1               10.00 usec
PLW1        56.90299988 W
SFO2        500.2320009 MHz
NUC2               1H
CPDPRG[2        waltz16
PCPD2             80.00 usec
PLW2        11.44699955 W
PLW12        0.25756001 W
PLW13        0.12955000 W

F2 - Processing parameters
SI                32768
SF          125.7829181 MHz
WDW                EM
SSB                   0
LB                 1.00 Hz
GB                    0
PC                 1.40
```

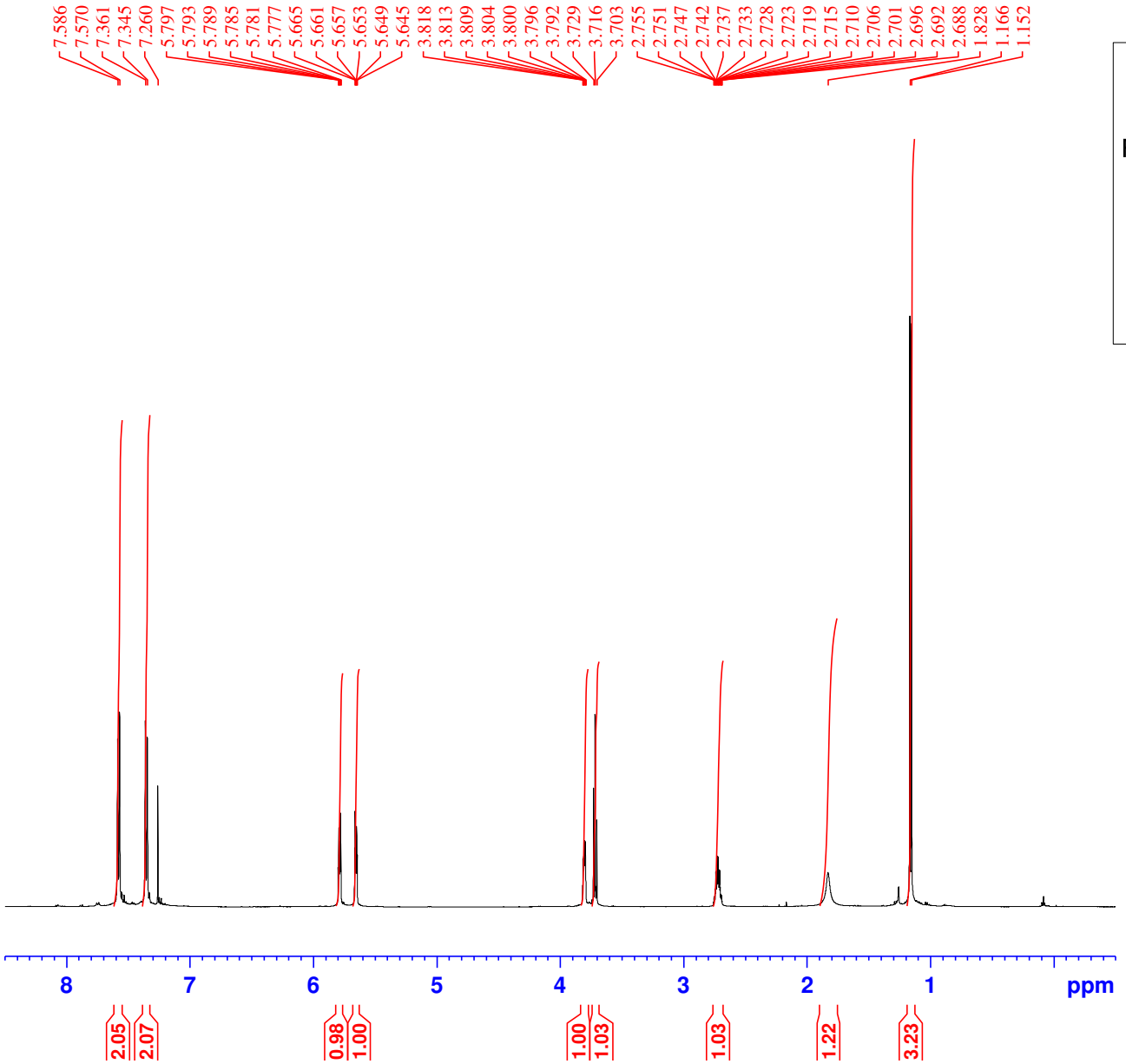

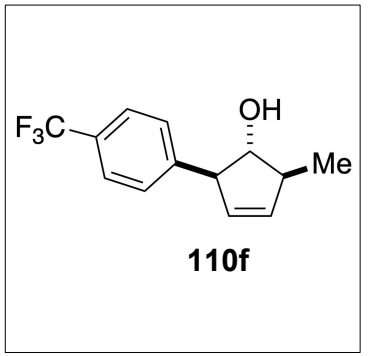

110f

```
Current Data Parameters
NAME      KS-02-153
EXPNO                10
PROCNO                1

F2 - Acquisition Parameters
Date_          20211022
Time              16.26 h
INSTRUM            spect
PROBHD   Z125869_0055 (
PULPROG            zg30
TD                65536
SOLVENT           CDCl3
NS                   64
DS                    2
SWH           10000.000 Hz
FIDRES            0.305176 Hz
AQ             3.2767999 sec
RG                94.51
DW               50.000 usec
DE               16.00 usec
TE               298.0 K
D1            2.00000000 sec
TD0                   1
SFO1         500.2330889 MHz
NUC1                 1H
P0                4.00 usec
P1               12.00 usec
PLW1         11.44699955 W

F2 - Processing parameters
SI                65536
SF           500.2300122 MHz
WDW                  EM
SSB                   0
LB                0.30 Hz
GB                    0
PC                1.00
```

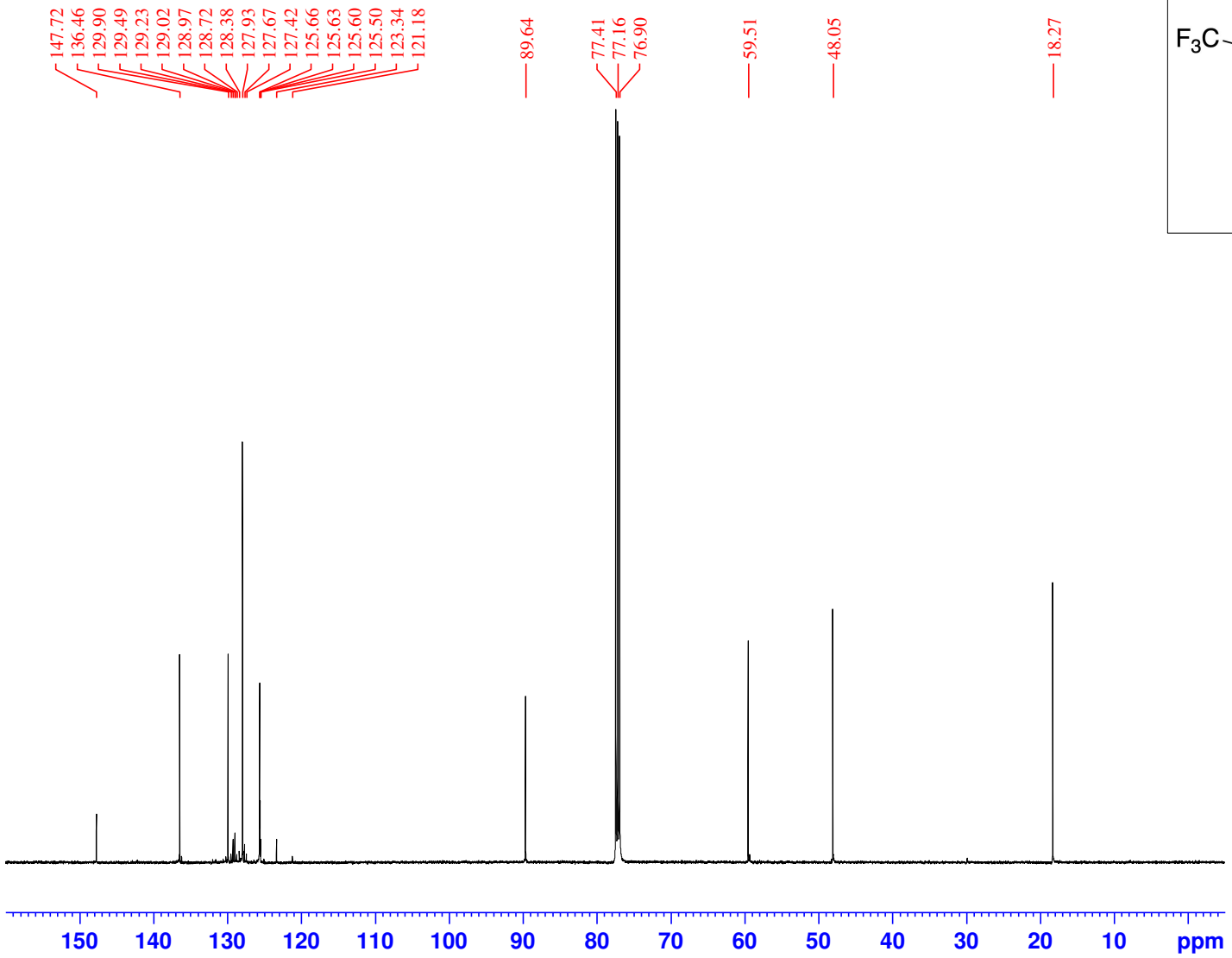

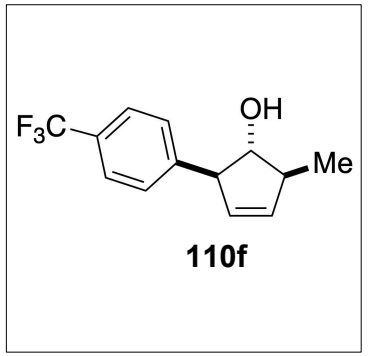

110f

```
Current Data Parameters
NAME      KS-02-153
EXPNO                12
PROCNO                1

F2 - Acquisition Parameters
Date_          20211022
Time               17.25 h
INSTRUM            spect
PROBHD   Z125869_0055 (
PULPROG          zgpg30
TD                65536
SOLVENT           CDCl3
NS                 1024
DS                    4
SWH           29761.904 Hz
FIDRES         0.908261 Hz
AQ            1.1010048 sec
RG               190.44
DW               16.800 usec
DE               18.00 usec
TE               298.0 K
D1           2.00000000 sec
D11          0.03000000 sec
TD0                   1
SFO1        125.7955118 MHz
NUC1               13C
P0                3.33 usec
P1               10.00 usec
PLW1        56.90299988 W
SFO2        500.2320009 MHz
NUC2               1H
CPDPRG[2        waltz16
PCPD2             80.00 usec
PLW2        11.44699955 W
PLW12        0.25756001 W
PLW13        0.12955000 W

F2 - Processing parameters
SI                32768
SF          125.7829162 MHz
WDW                EM
SSB                   0
LB                 1.00 Hz
GB                    0
PC                 1.40
```

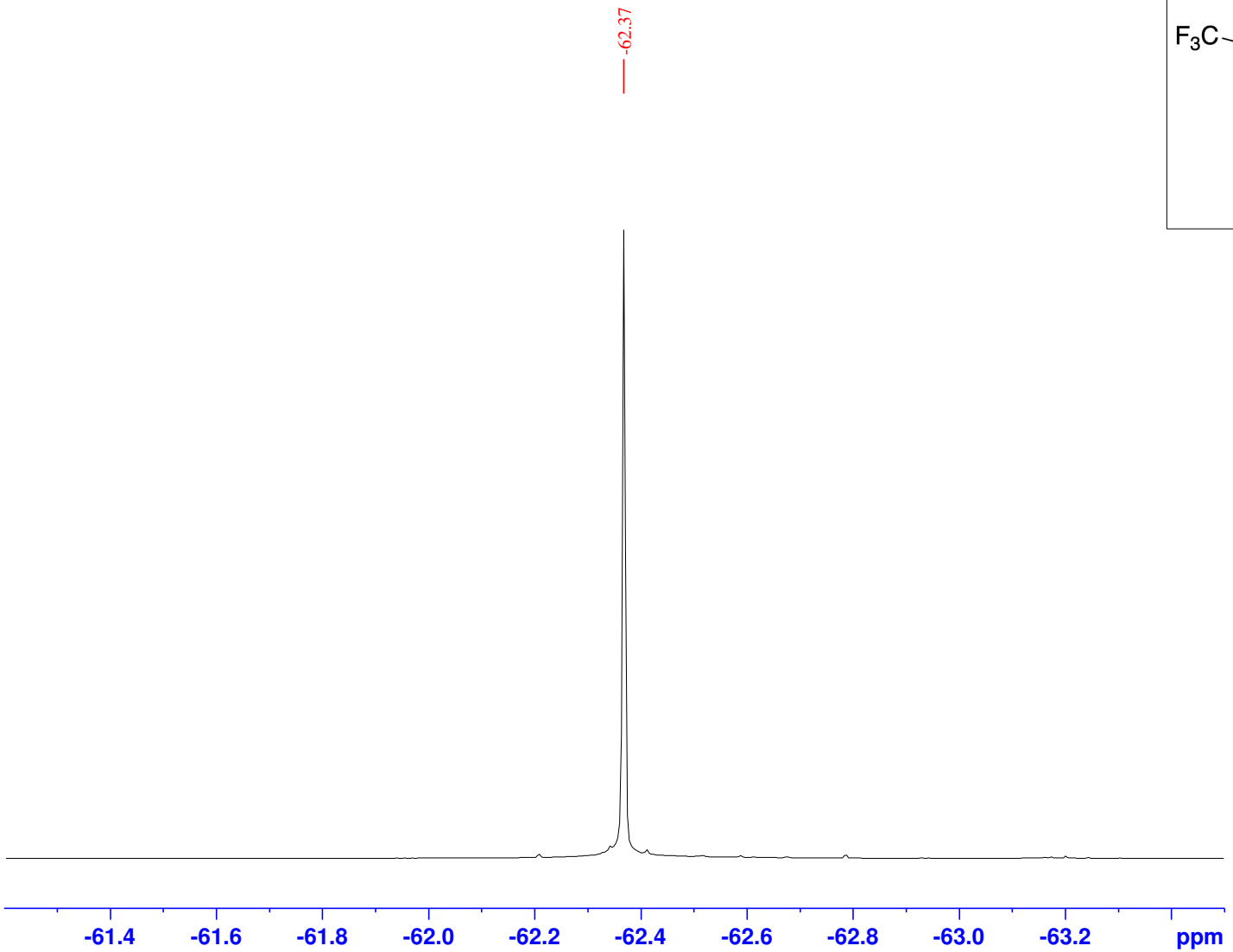

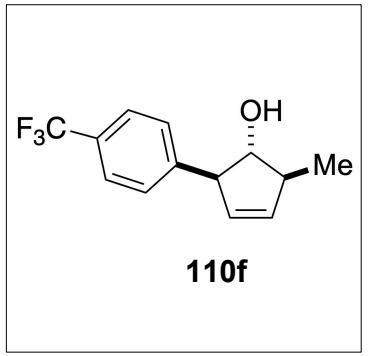

110f

```
Current Data Parameters
NAME      KS-02-153
EXPNO                11
PROCNO                1

F2 - Acquisition Parameters
Date_          20211022
Time               16.29 h
INSTRUM            spect
PROBHD   Z125869_0055 (
PULPROG          zgflqn
TD               131072
SOLVENT             CDCl3
NS                     16
DS                      4
SWH           113636.367 Hz
FIDRES          1.733953 Hz
AQ             0.5767168 sec
RG                 15.61
DW                 4.400 usec
DE                18.00 usec
TE                298.0 K
D1            1.00000000 sec
TD0                    1
SFO1         470.6394024 MHz
NUC1                 19F
P1                 15.00 usec
PLW1         11.70800018 W

F2 - Processing parameters
SI                 65536
SF           470.6864710 MHz
WDW                   EM
SSB                    0
LB                  0.30 Hz
GB                     0
PC                  1.00
```

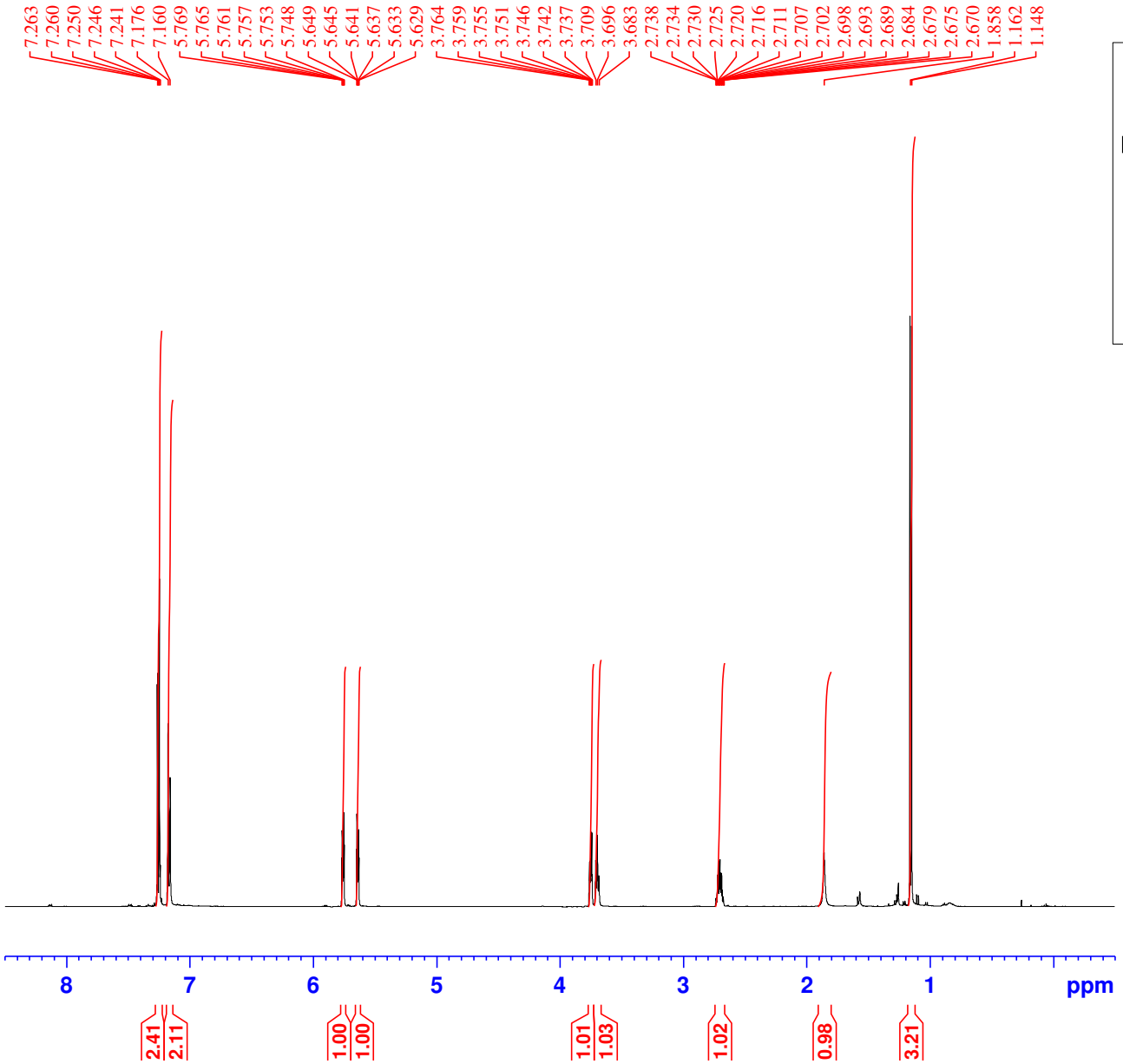

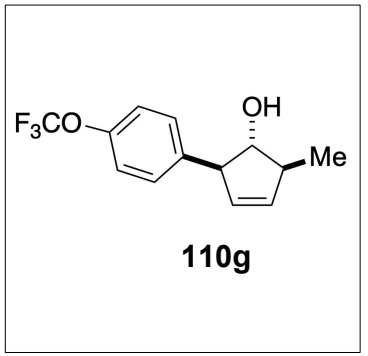


```
Current Data Parameters
NAME      KS-02-205
EXPNO                10
PROCNO                1

F2 - Acquisition Parameters
Date_          20211210
Time                4.50 h
INSTRUM            spect
PROBHD   Z125869_0055 (
PULPROG            zg30
TD                65536
SOLVENT           CDCl3
NS                   64
DS                    2
SWH           10000.000 Hz
FIDRES            0.305176 Hz
AQ             3.2767999 sec
RG                94.51
DW                50.000 usec
DE                16.00 usec
TE                298.0 K
D1             2.00000000 sec
TD0                   1
SFO1         500.2330889 MHz
NUC1                  1H
P0                 4.00 usec
P1                12.00 usec
PLW1         11.44699955 W

F2 - Processing parameters
SI                65536
SF           500.2300120 MHz
WDW                  EM
SSB                   0
LB                 0.30 Hz
GB                    0
PC                 1.00
```

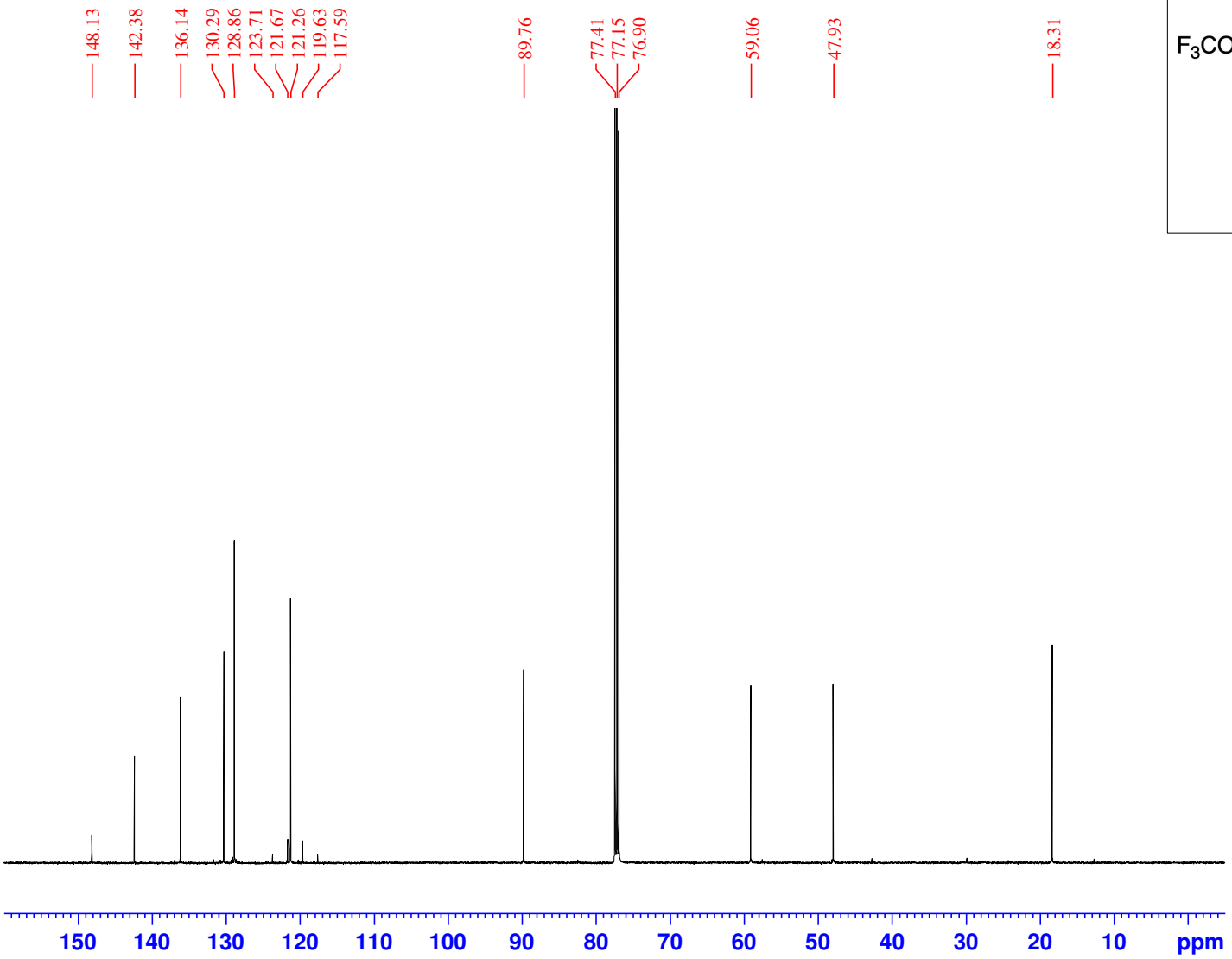

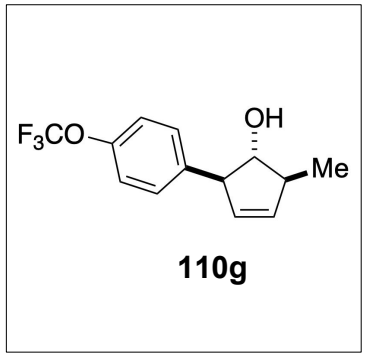


```
Current Data Parameters
NAME      KS-02-205
EXPNO                12
PROCNO                1

F2 - Acquisition Parameters
Date_          20211210
Time               4.40 h
INSTRUM           spect
PROBHD   Z125869_0055 (
PULPROG         zgpg30
TD                65536
SOLVENT           CDCl3
NS                 1024
DS                    4
SWH           29761.904 Hz
FIDRES         0.908261 Hz
AQ             1.1010048 sec
RG                190.44
DW                16.800 usec
DE                18.00 usec
TE                298.0 K
D1            2.00000000 sec
D11           0.03000000 sec
TD0                   1
SFO1         125.7955118 MHz
NUC1                 13C
P0                 3.33 usec
P1                10.00 usec
PLW1         56.90299988 W
SFO2         500.2320009 MHz
NUC2                 1H
CPDPRG[2         waltz16
PCPD2             80.00 usec
PLW2         11.44699955 W
PLW12         0.25756001 W
PLW13         0.12955000 W

F2 - Processing parameters
SI                32768
SF           125.7829164 MHz
WDW                  EM
SSB                   0
LB                 1.00 Hz
GB                    0
PC                 1.40
```

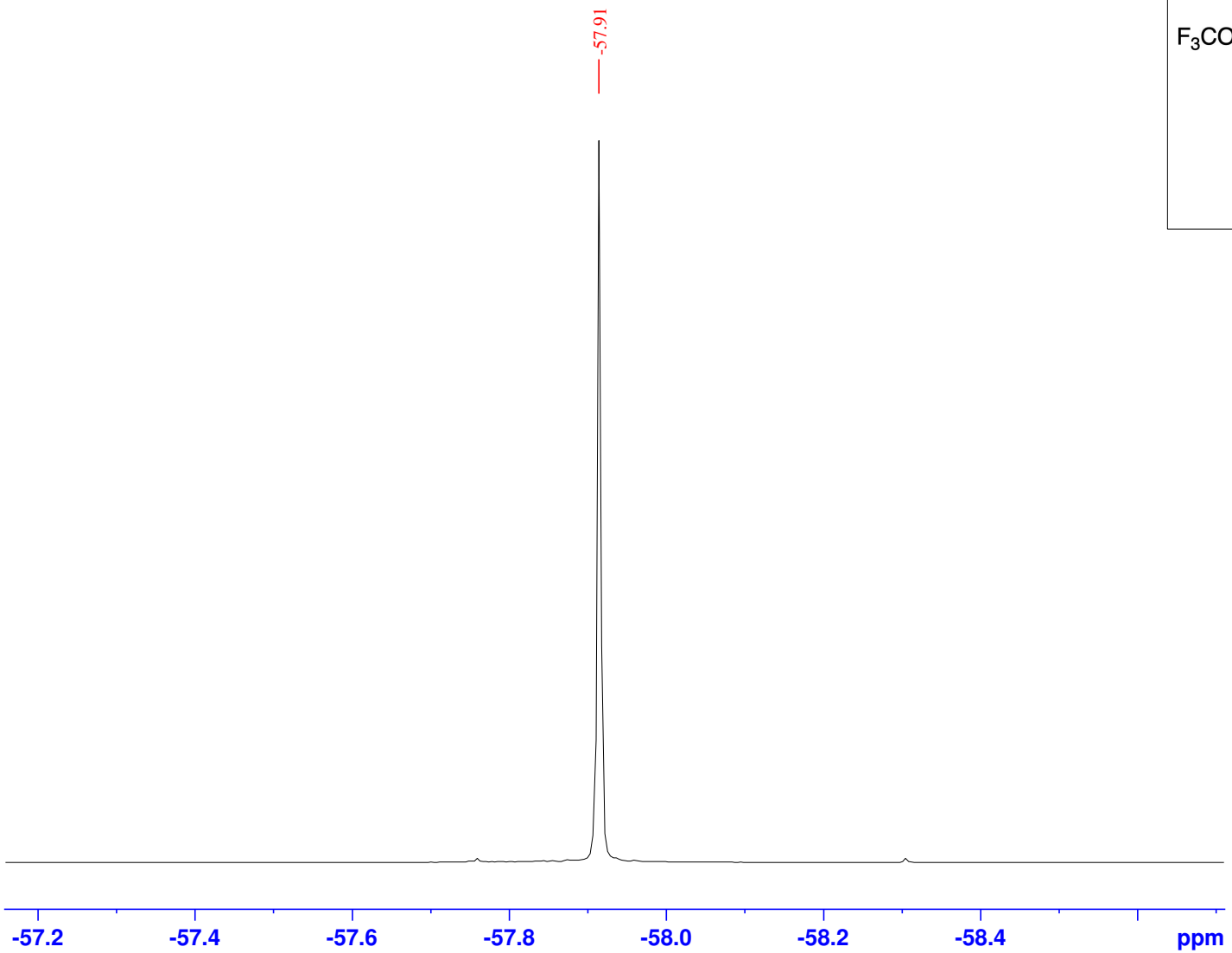

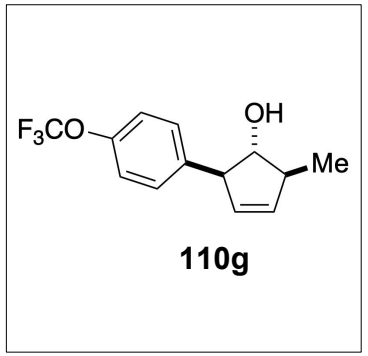

110g

```
Current Data Parameters
NAME      KS-02-205
EXPNO                11
PROCNO                1

F2 - Acquisition Parameters
Date_          20211210
Time               4.43 h
INSTRUM            spect
PROBHD   Z125869_0055 (
PULPROG          zgflqn
TD               131072
SOLVENT            CDCl3
NS                    16
DS                     4
SWH           113636.367 Hz
FIDRES          1.733953 Hz
AQ              0.5767168 sec
RG                 14.14
DW                 4.400 usec
DE                 18.00 usec
TE                 298.0 K
D1            1.00000000 sec
TD0                    1
SFO1         470.6394024 MHz
NUC1                19F
P1                 15.00 usec
PLW1        11.70800018 W

F2 - Processing parameters
SI                 65536
SF           470.6864712 MHz
WDW                   EM
SSB                    0
LB                  0.30 Hz
GB                     0
PC                  1.00
```

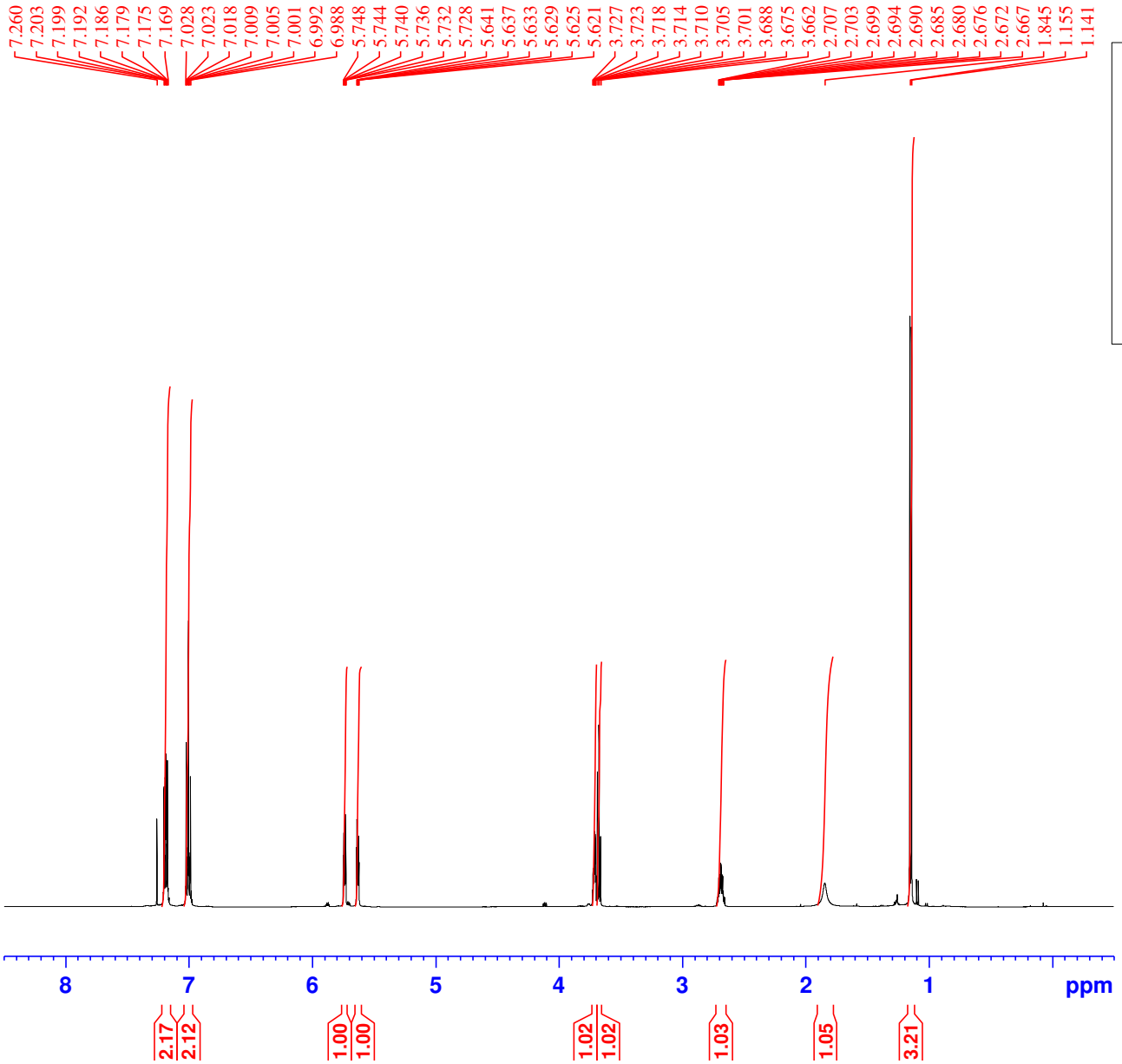

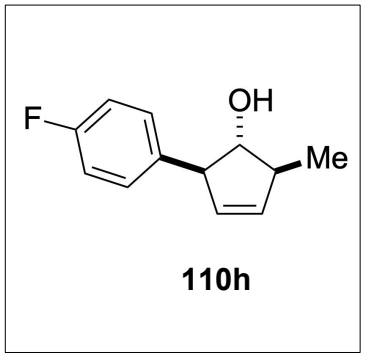

110h

```
Current Data Parameters
NAME      KS-02-141
EXPNO                10
PROCNO                1

F2 - Acquisition Parameters
Date_          20211015
Time              13.20 h
INSTRUM           spect
PROBHD   Z125869_0055 (
PULPROG           zg30
TD               65536
SOLVENT          CDCl3
NS                  64
DS                   2
SWH           10000.000 Hz
FIDRES            0.305176 Hz
AQ             3.2767999 sec
RG                53.13
DW              50.000 usec
DE              16.00 usec
TE              298.0 K
D1           2.00000000 sec
TD0                  1
SFO1        500.2330889 MHz
NUC1               1H
P0               4.00 usec
P1              12.00 usec
PLW1        11.44699955 W

F2 - Processing parameters
SI               65536
SF          500.2300120 MHz
WDW                EM
SSB                 0
LB               0.30 Hz
GB                  0
PC               1.00
```

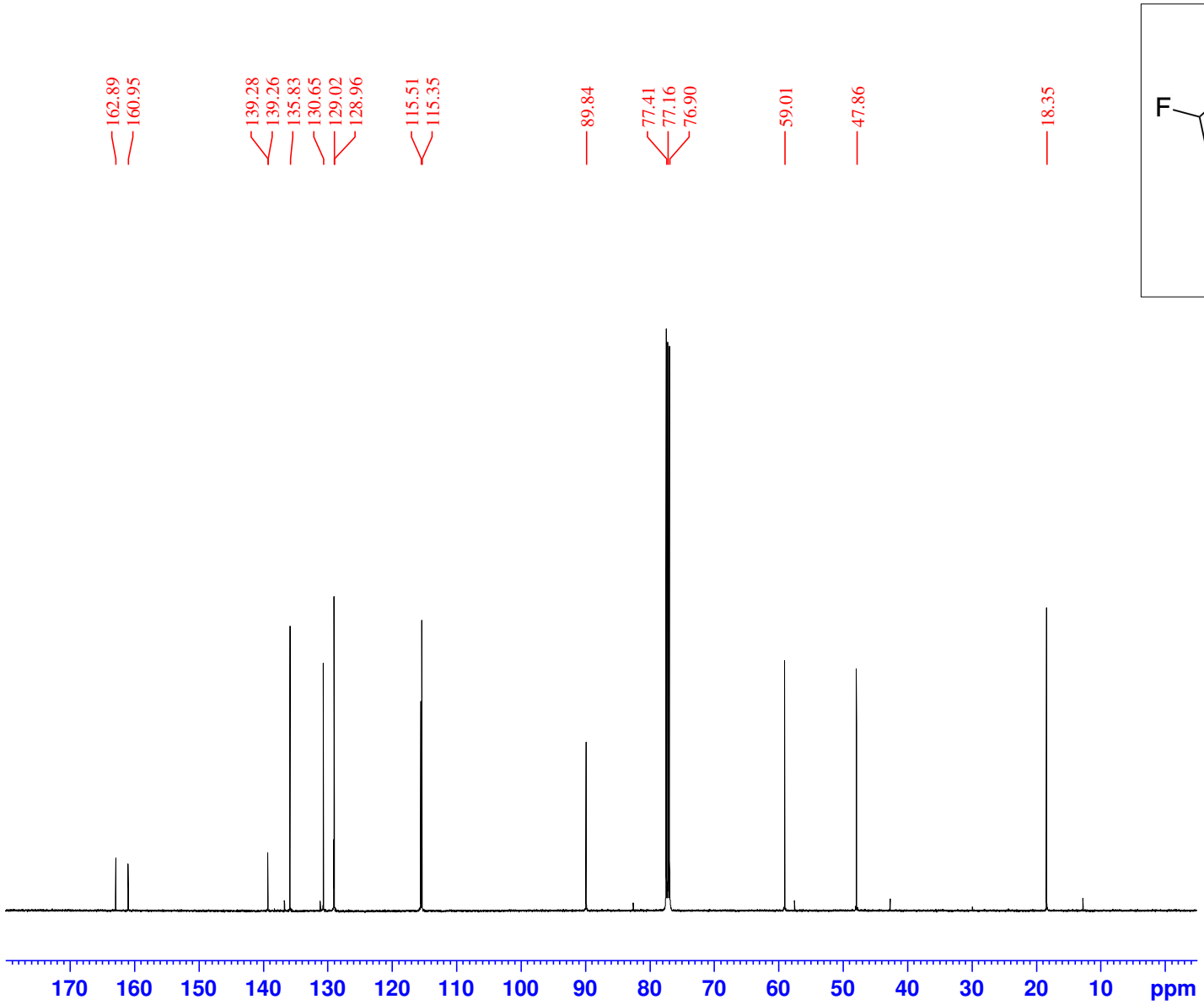


```
Current Data Parameters
NAME      KS-02-141
EXPNO                12
PROCNO                1

F2 - Acquisition Parameters
Date_          20211015
Time               14.18 h
INSTRUM            spect
PROBHD   Z125869_0055 (
PULPROG          zgpg30
TD                65536
SOLVENT           CDCl3
NS                 1024
DS                    4
SWH           29761.904 Hz
FIDRES         0.908261 Hz
AQ            1.1010048 sec
RG               190.44
DW               16.800 usec
DE               18.00 usec
TE               298.0 K
D1           2.00000000 sec
D11          0.03000000 sec
TD0                   1
SFO1        125.7955118 MHz
NUC1                13C
P0                3.33 usec
P1               10.00 usec
PLW1        56.90299988 W
SFO2        500.2320009 MHz
NUC2                1H
CPDPRG[2         waltz16
PCPD2             80.00 usec
PLW2        11.44699955 W
PLW12        0.25756001 W
PLW13        0.12955000 W

F2 - Processing parameters
SI                32768
SF          125.7829167 MHz
WDW                  EM
SSB                   0
LB                 1.00 Hz
GB                    0
PC                 1.40
```

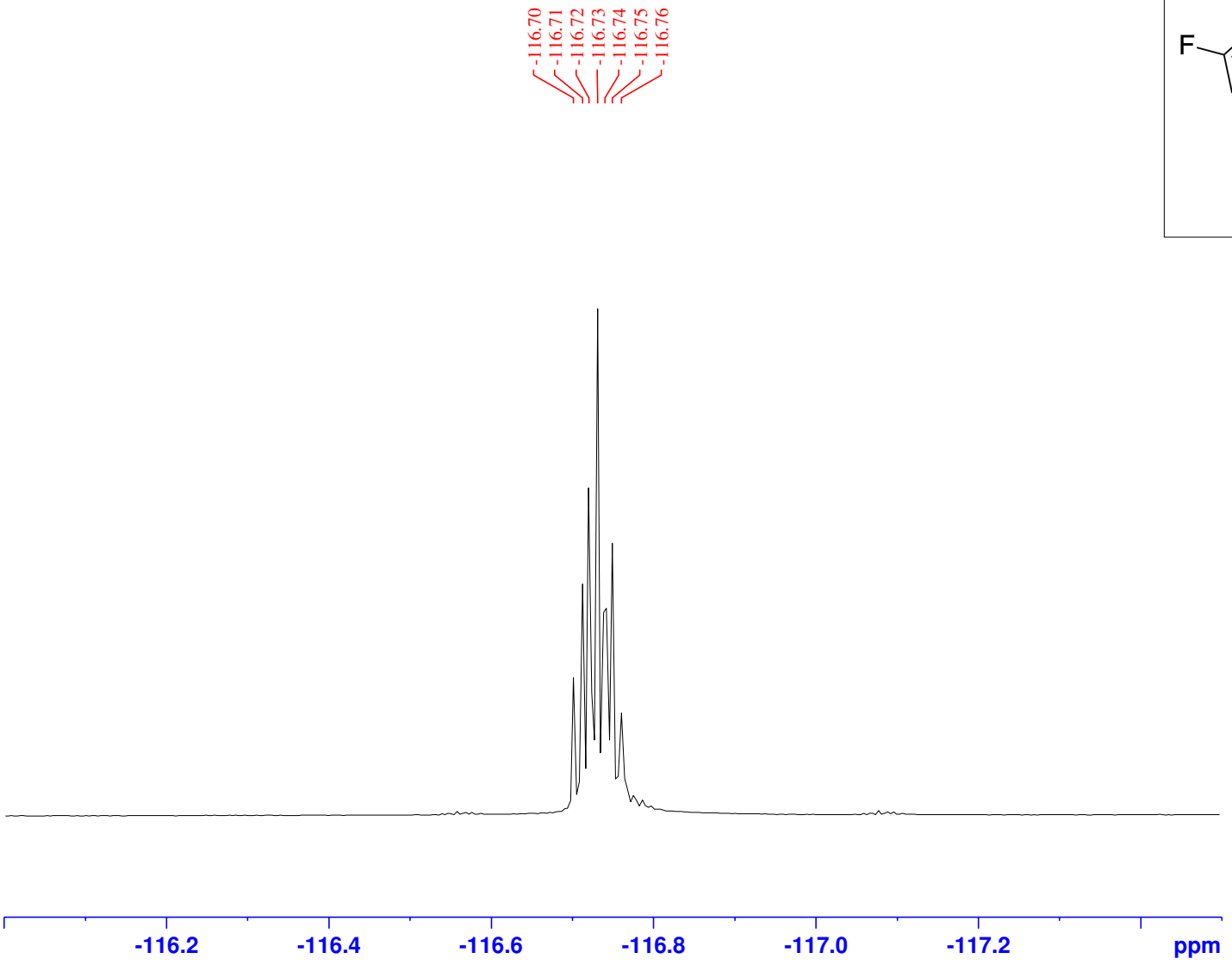

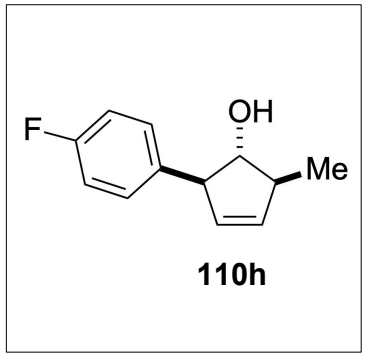

110h

```
Current Data Parameters
NAME      KS-02-141
EXPNO                11
PROCNO                1

F2 - Acquisition Parameters
Date_          20211015
Time               13.22 h
INSTRUM            spect
PROBHD   Z125869_0055 (
PULPROG           zgflqn
TD                131072
SOLVENT             CDCl3
NS                    16
DS                     4
SWH           113636.367 Hz
FIDRES          1.733953 Hz
AQ             0.5767168 sec
RG                 15.61
DW                 4.400 usec
DE                18.00 usec
TE                298.0 K
D1            1.00000000 sec
TD0                    1
SFO1         470.6394024 MHz
NUC1                 19F
P1                 15.00 usec
PLW1         11.70800018 W

F2 - Processing parameters
SI                 65536
SF           470.6864712 MHz
WDW                   EM
SSB                    0
LB                  0.30 Hz
GB                     0
PC                  1.00
```

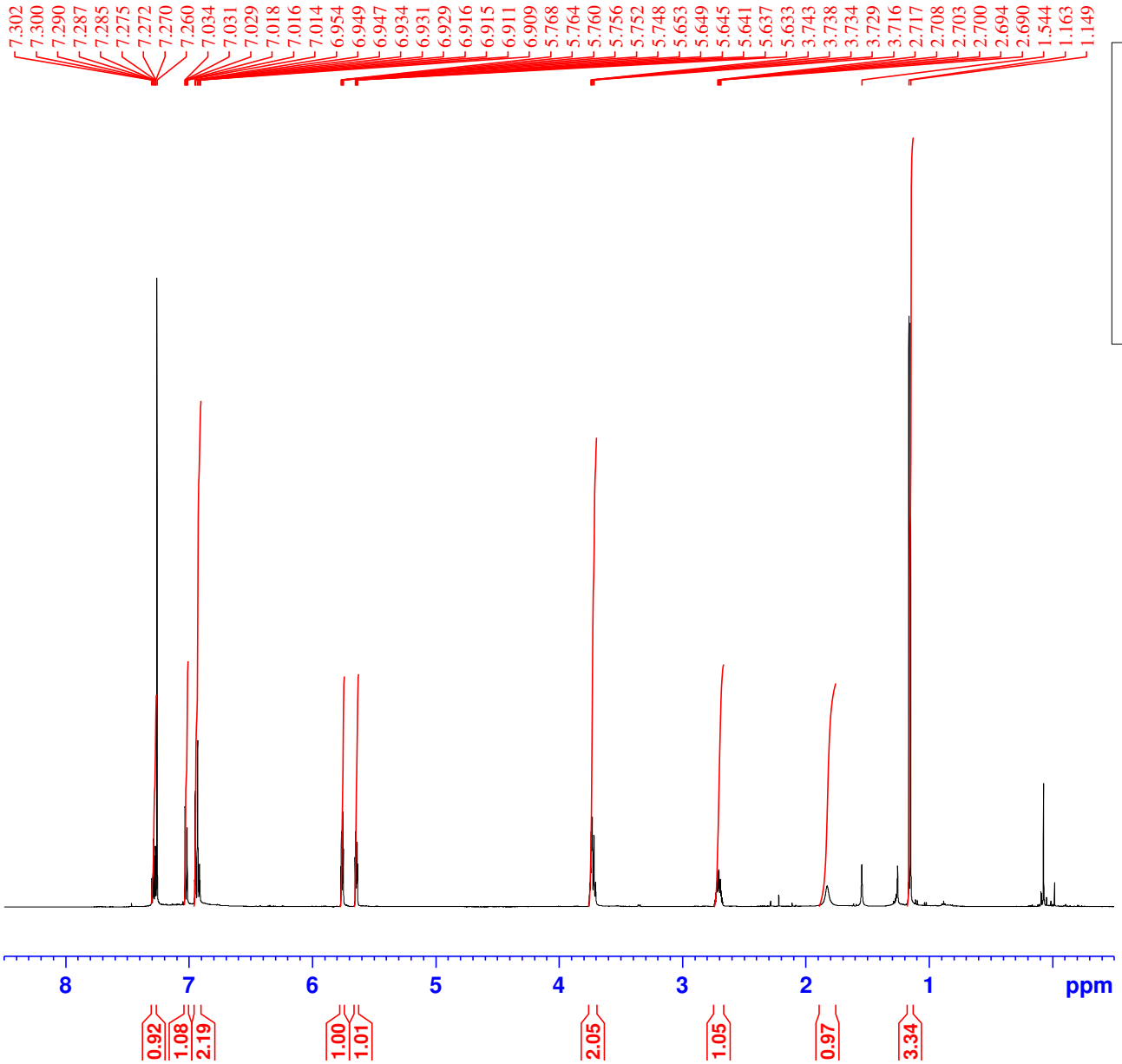

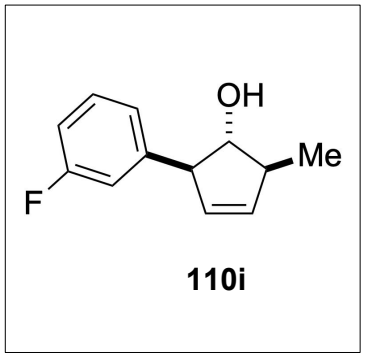

110i

```
Current Data Parameters
NAME      KS-02-210
EXPNO                10
PROCNO                1

F2 - Acquisition Parameters
Date_           20211215
Time               20.40 h
INSTRUM             spect
PROBHD    Z125869_0055 (
PULPROG             zg30
TD                 65536
SOLVENT            CDCl3
NS                    64
DS                     2
SWH            10000.000 Hz
FIDRES             0.305176 Hz
AQ             3.2767999 sec
RG                151.18
DW                 50.000 usec
DE                 16.00 usec
TE                298.0 K
D1             2.00000000 sec
TD0                    1
SFO1         500.2330889 MHz
NUC1                  1H
P0                 4.00 usec
P1                12.00 usec
PLW1         11.44699955 W

F2 - Processing parameters
SI                 65536
SF           500.2300121 MHz
WDW                   EM
SSB                    0
LB                 0.30 Hz
GB                     0
PC                 1.00
```

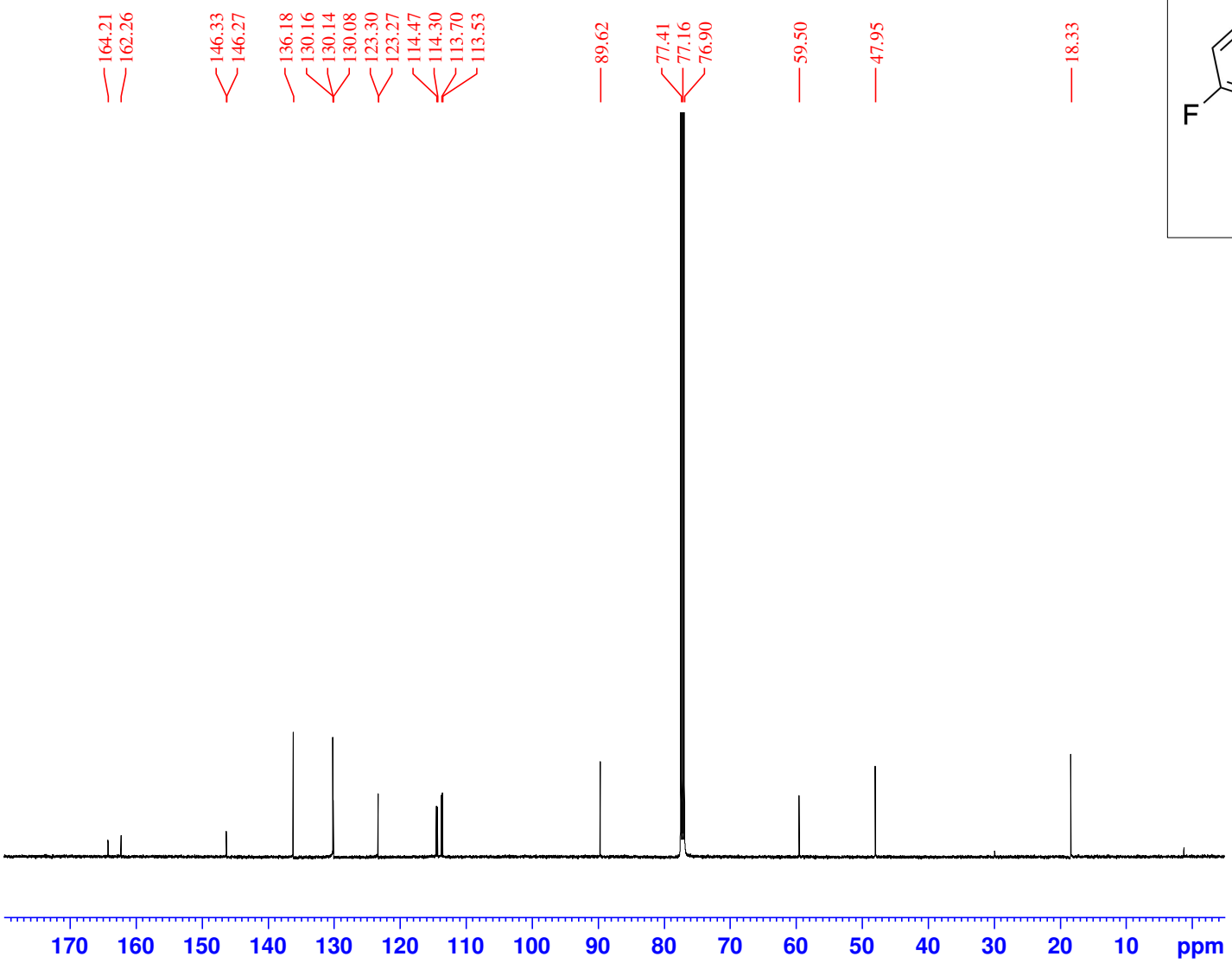

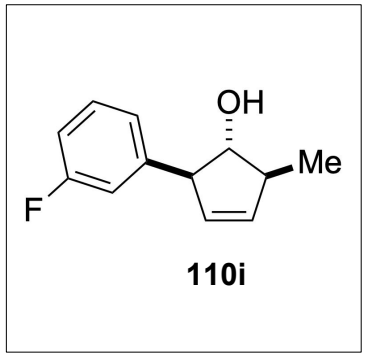

110i

```
Current Data Parameters
NAME      KS-02-210
EXPNO                12
PROCNO                1

F2 - Acquisition Parameters
Date_          20211215
Time               22.34 h
INSTRUM            spect
PROBHD    Z125869_0055 (
PULPROG          zgpg30
TD                65536
SOLVENT           CDCl3
NS                 2048
DS                    4
SWH           29761.904 Hz
FIDRES         0.908261 Hz
AQ             1.1010048 sec
RG                190.44
DW                16.800 usec
DE                18.00 usec
TE                298.0 K
D1             2.00000000 sec
D11            0.03000000 sec
TD0                   1
SFO1         125.7955118 MHz
NUC1                 13C
P0                 3.33 usec
P1                10.00 usec
PLW1         56.90299988 W
SFO2         500.2320009 MHz
NUC2                 1H
CPDPRG[2         waltz16
PCPD2             80.00 usec
PLW2         11.44699955 W
PLW12         0.25756001 W
PLW13         0.12955000 W

F2 - Processing parameters
SI                32768
SF           125.7829156 MHz
WDW                  EM
SSB                   0
LB                 1.00 Hz
GB                    0
PC                 1.40
```

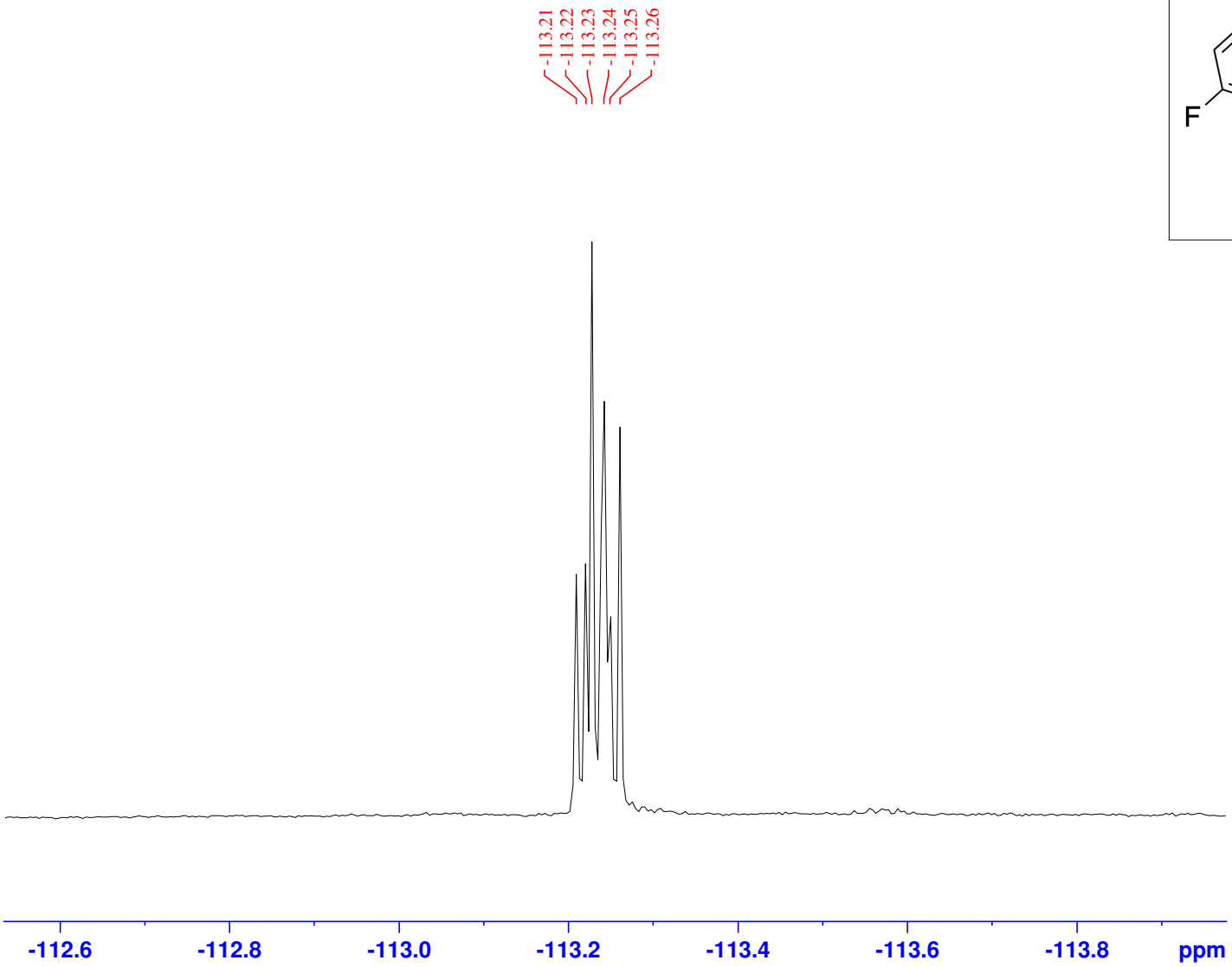

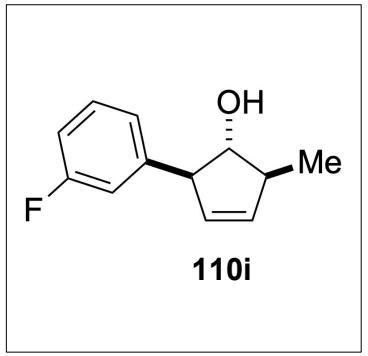


```
Current Data Parameters
NAME      KS-02-210
EXPNO                11
PROCNO                1

F2 - Acquisition Parameters
Date_          20211215
Time               20.42 h
INSTRUM            spect
PROBHD    Z125869_0055 (
PULPROG          zgflqn
TD               131072
SOLVENT             CDCl3
NS                     16
DS                      4
SWH           113636.367 Hz
FIDRES          1.733953 Hz
AQ              0.5767168 sec
RG                 14.14
DW                 4.400 usec
DE                18.00 usec
TE                298.0 K
D1             1.00000000 sec
TD0                    1
SFO1         470.6394024 MHz
NUC1                19F
P1                 15.00 usec
PLW1         11.70800018 W

F2 - Processing parameters
SI                 65536
SF           470.6864712 MHz
WDW                   EM
SSB                    0
LB                  0.30 Hz
GB                     0
PC                  1.00
```

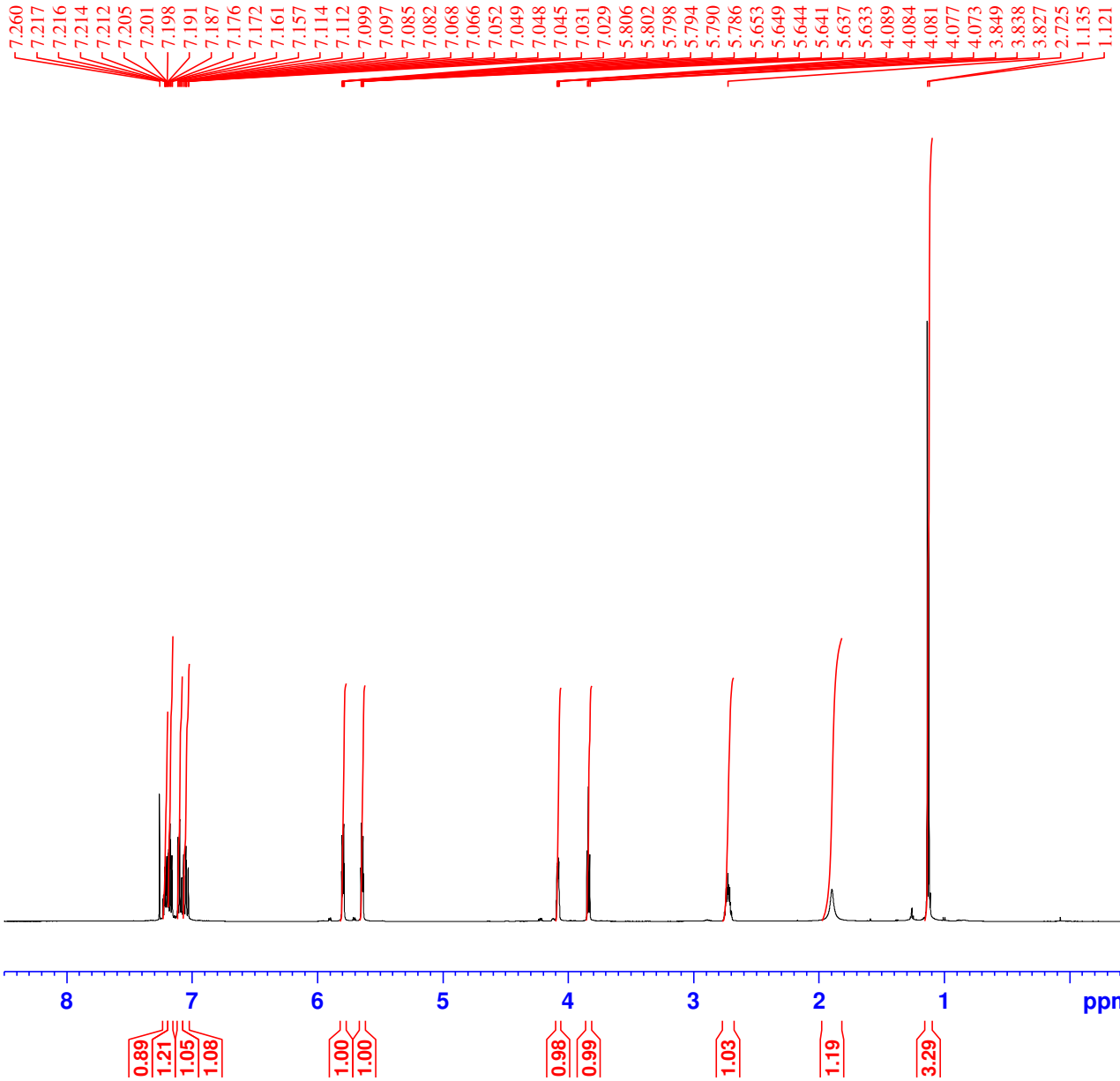

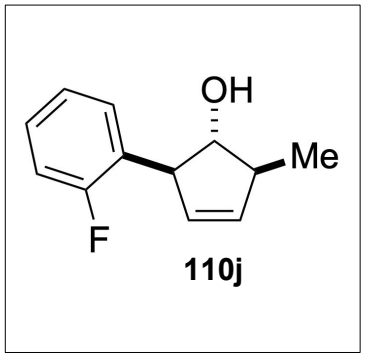


```
Current Data Parameters
NAME      KS-02-162
EXPNO                10
PROCNO                1

F2 - Acquisition Parameters
Date_           20211029
Time              16.08 h
INSTRUM             spect
PROBHD    Z125869_0055 (
PULPROG             zg30
TD                 65536
SOLVENT            CDCl3
NS                    64
DS                     2
SWH           10000.000 Hz
FIDRES            0.305176 Hz
AQ                3.2767999 sec
RG                   94.51
DW                50.000 usec
DE                16.00 usec
TE                298.0 K
D1             2.00000000 sec
TD0                    1
SFO1          500.2330889 MHz
NUC1                  1H
P0                 4.00 usec
P1                12.00 usec
PLW1          11.44699955 W

F2 - Processing parameters
SI                 65536
SF            500.2300121 MHz
WDW                   EM
SSB                    0
LB                  0.30 Hz
GB                     0
PC                  1.00
```

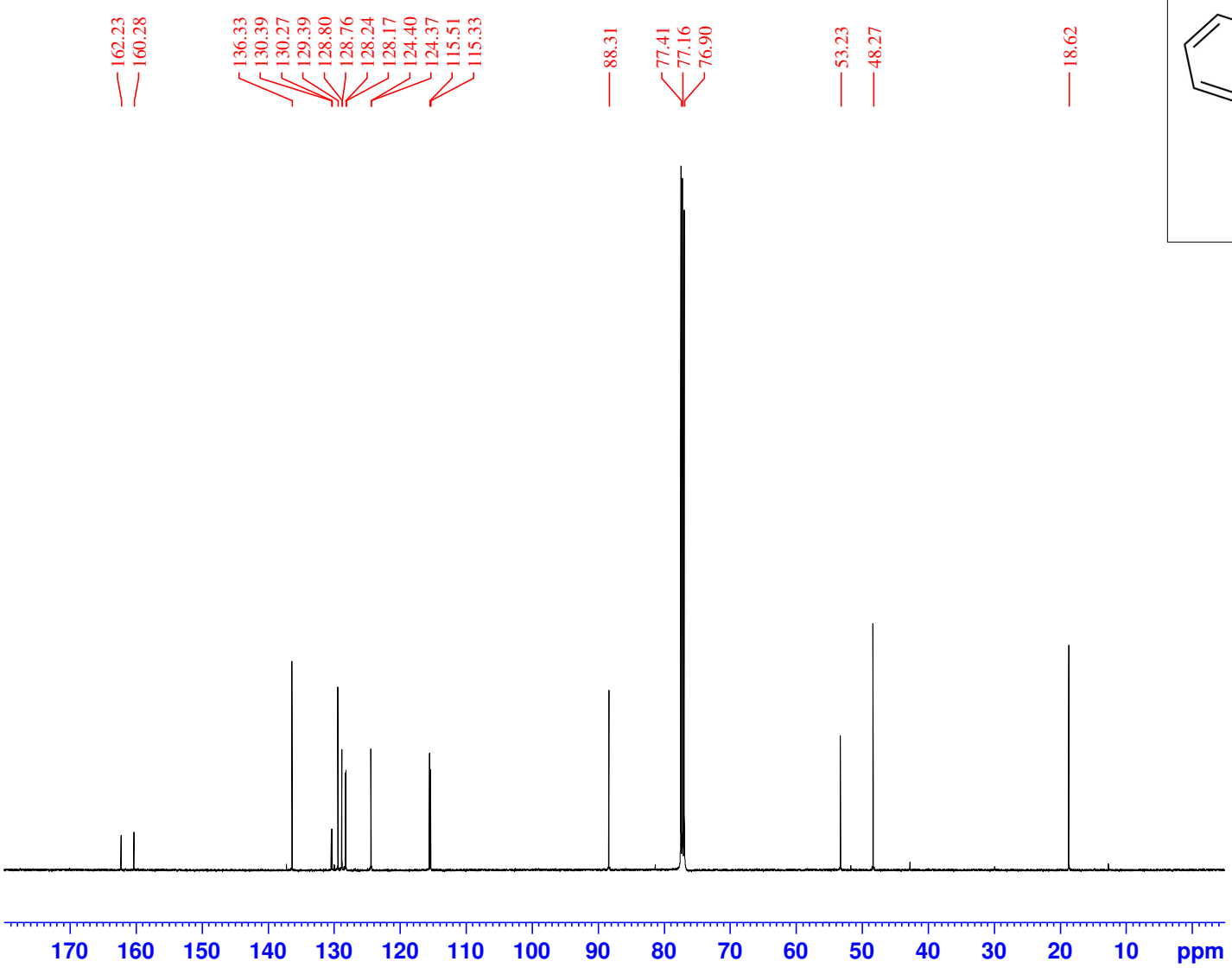

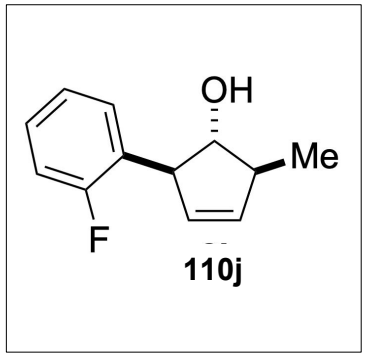


```
Current Data Parameters
NAME      KS-02-162
EXPNO                11
PROCNO                1

F2 - Acquisition Parameters
Date_          20211029
Time              17.58 h
INSTRUM           spect
PROBHD    Z125869_0055 (
PULPROG          zgpg30
TD                65536
SOLVENT           CDCl3
NS                 1024
DS                    4
SWH           29761.904 Hz
FIDRES         0.908261 Hz
AQ             1.1010048 sec
RG                190.44
DW                16.800 usec
DE                18.00 usec
TE                298.0 K
D1             2.00000000 sec
D11            0.03000000 sec
TD0                   1
SFO1         125.7955118 MHz
NUC1                 13C
P0                 3.33 usec
P1                10.00 usec
PLW1         56.90299988 W
SFO2         500.2320009 MHz
NUC2                 1H
CPDPRG[2         waltz16
PCPD2             80.00 usec
PLW2         11.44699955 W
PLW12         0.25756001 W
PLW13         0.12955000 W

F2 - Processing parameters
SI                32768
SF           125.7829171 MHz
WDW                  EM
SSB                   0
LB                 1.00 Hz
GB                    0
PC                 1.40
```

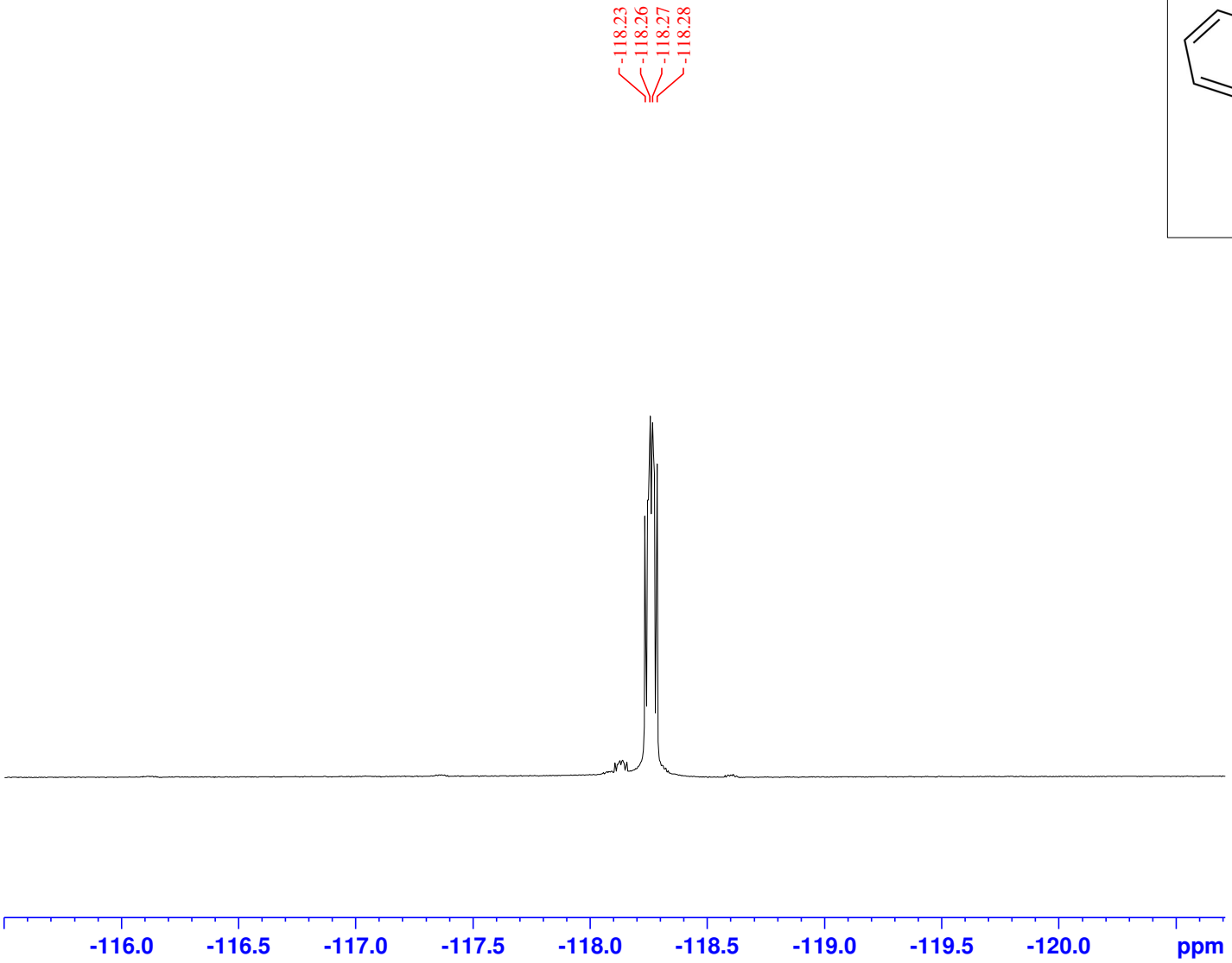

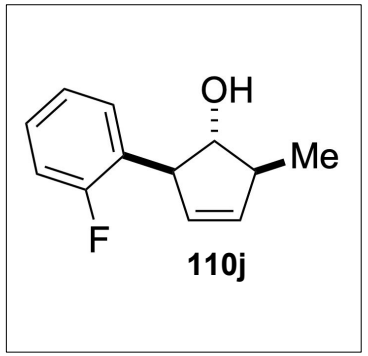


```
Current Data Parameters
NAME      KS-02-162
EXPNO                12
PROCNO                1

F2 - Acquisition Parameters
Date_          20211030
Time              11.36 h
INSTRUM           spect
PROBHD    Z125869_0055 (
PULPROG          zgflqn
TD               131072
SOLVENT             CDCl3
NS                     16
DS                      4
SWH           113636.367 Hz
FIDRES          1.733953 Hz
AQ             0.5767168 sec
RG                 14.14
DW                 4.400 usec
DE                18.00 usec
TE                298.0 K
D1            1.00000000 sec
TD0                    1
SFO1         470.6394024 MHz
NUC1                19F
P1                 15.00 usec
PLW1         11.70800018 W

F2 - Processing parameters
SI                 65536
SF           470.6864712 MHz
WDW                   EM
SSB                    0
LB                  0.30 Hz
GB                     0
PC                  1.00
```

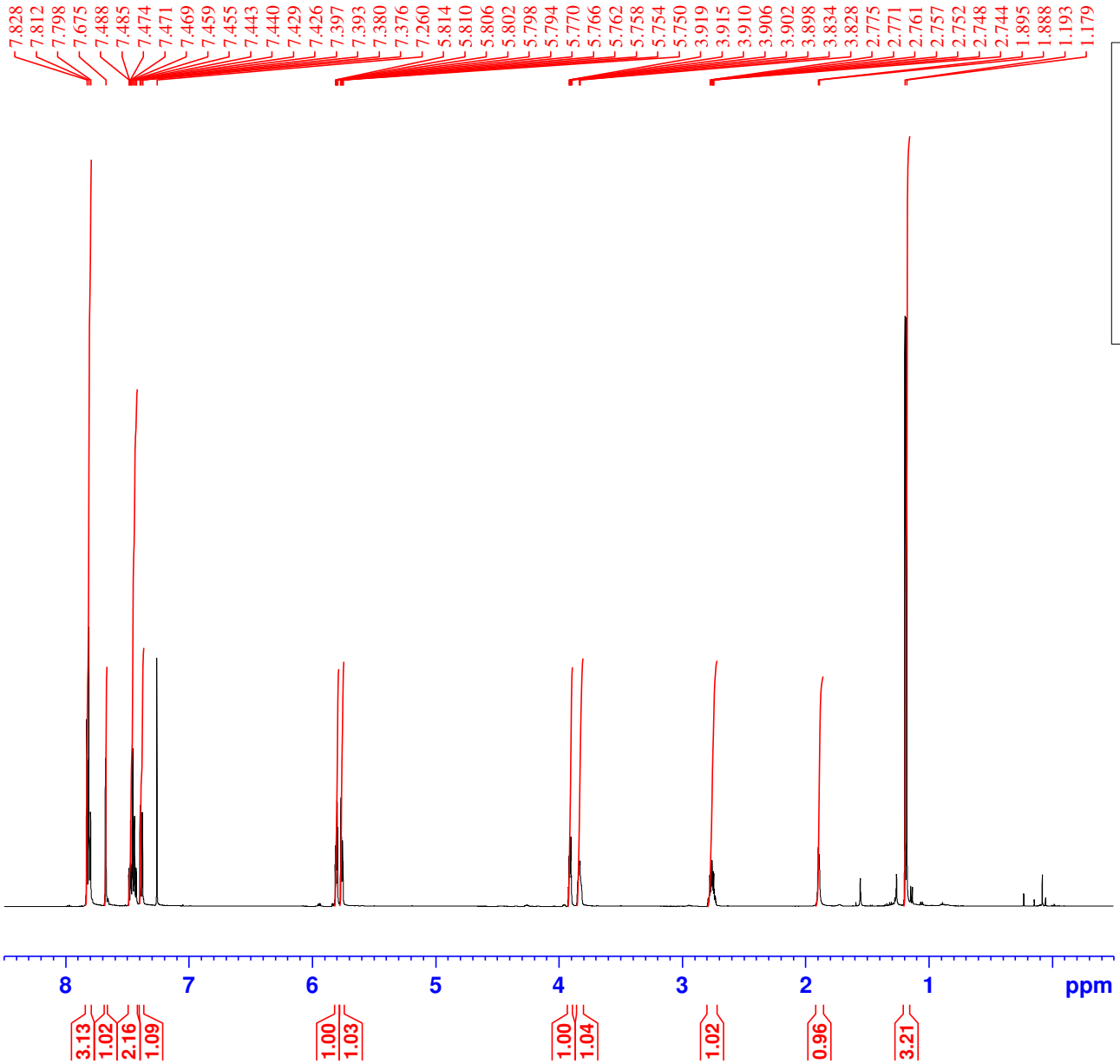

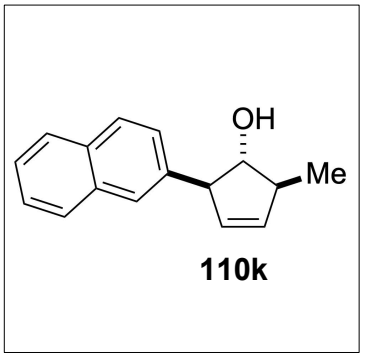


```
Current Data Parameters
NAME      KS-02-209
EXPNO                10
PROCNO                1

F2 - Acquisition Parameters
Date_           20211215
Time              18.25 h
INSTRUM             spect
PROBHD    Z125869_0055 (
PULPROG             zg30
TD                 65536
SOLVENT            CDCl3
NS                    64
DS                     2
SWH           10000.000 Hz
FIDRES            0.305176 Hz
AQ             3.2767999 sec
RG                122.05
DW                50.000 usec
DE                16.00 usec
TE                298.0 K
D1            2.00000000 sec
TD0                    1
SFO1         500.2330889 MHz
NUC1                  1H
P0                  4.00 usec
P1                 12.00 usec
PLW1         11.44699955 W

F2 - Processing parameters
SI                 65536
SF           500.2300120 MHz
WDW                   EM
SSB                    0
LB                  0.30 Hz
GB                     0
PC                  1.00
```

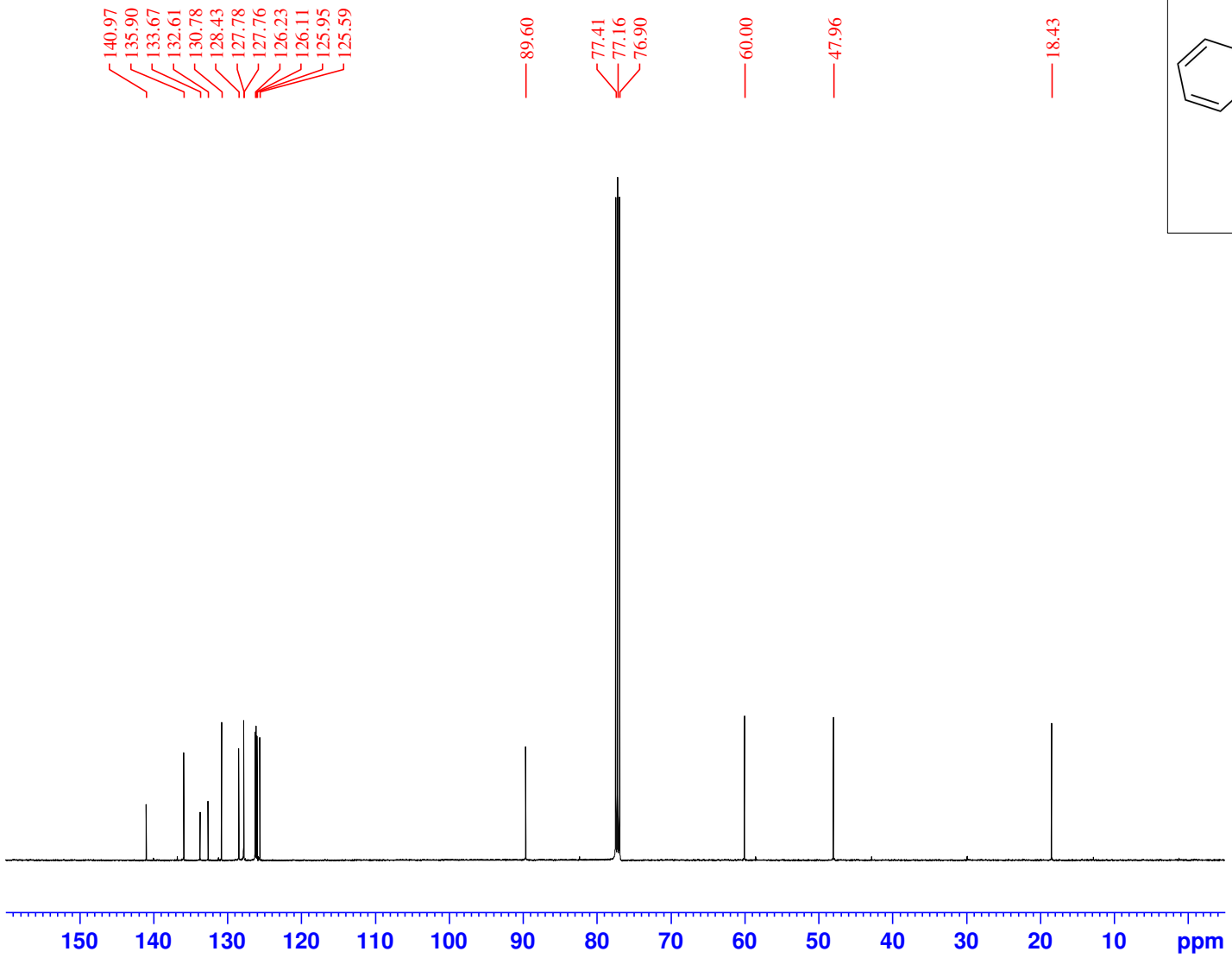

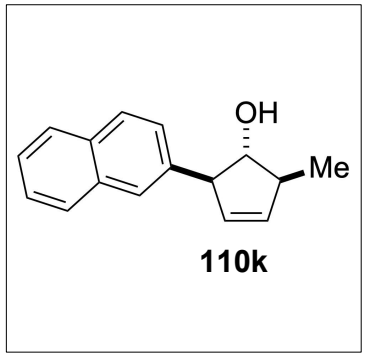

110k

```
Current Data Parameters
NAME      KS-02-209
EXPNO                11
PROCNO                1

F2 - Acquisition Parameters
Date_          20211215
Time               20.15 h
INSTRUM            spect
PROBHD    Z125869_0055 (
PULPROG          zgpg30
TD                65536
SOLVENT           CDCl3
NS                 2048
DS                    4
SWH           29761.904 Hz
FIDRES         0.908261 Hz
AQ            1.1010048 sec
RG               190.44
DW               16.800 usec
DE               18.00 usec
TE               298.0 K
D1           2.00000000 sec
D11          0.03000000 sec
TD0                   1
SFO1        125.7955118 MHz
NUC1                13C
P0                3.33 usec
P1               10.00 usec
PLW1        56.90299988 W
SFO2        500.2320009 MHz
NUC2                1H
CPDPRG[2         waltz16
PCPD2            80.00 usec
PLW2        11.44699955 W
PLW12        0.25756001 W
PLW13        0.12955000 W

F2 - Processing parameters
SI                32768
SF          125.7829173 MHz
WDW                  EM
SSB                   0
LB                 1.00 Hz
GB                    0
PC                 1.40
```

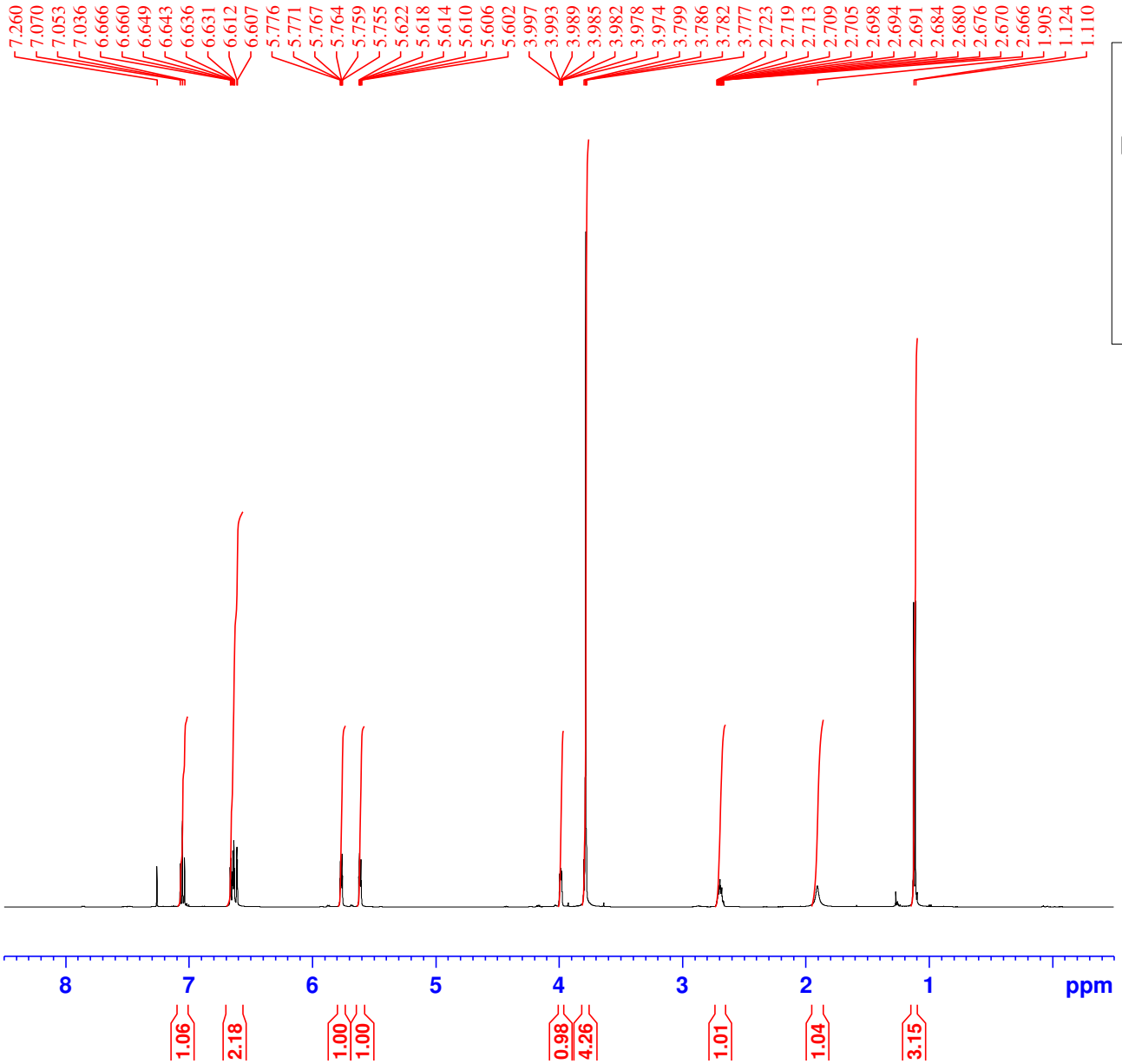

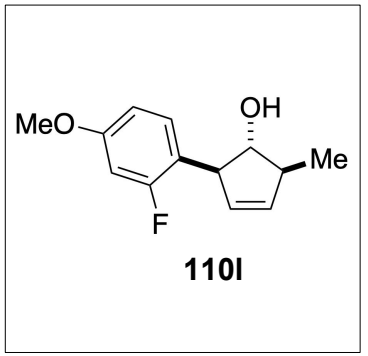

110l

```
Current Data Parameters
NAME      KS-02-163
EXPNO                10
PROCNO                1

F2 - Acquisition Parameters
Date_          20211029
Time              16.18 h
INSTRUM            spect
PROBHD   Z125869_0055 (
PULPROG            zg30
TD                65536
SOLVENT           CDCl3
NS                   64
DS                    2
SWH           10000.000 Hz
FIDRES            0.305176 Hz
AQ             3.2767999 sec
RG                 47.3
DW                50.000 usec
DE                16.00 usec
TE                298.0 K
D1             2.00000000 sec
TD0                   1
SFO1          500.2330889 MHz
NUC1                  1H
P0                 4.00 usec
P1                12.00 usec
PLW1          11.44699955 W

F2 - Processing parameters
SI                65536
SF            500.2300120 MHz
WDW                  EM
SSB                   0
LB                 0.30 Hz
GB                    0
PC                 1.00
```

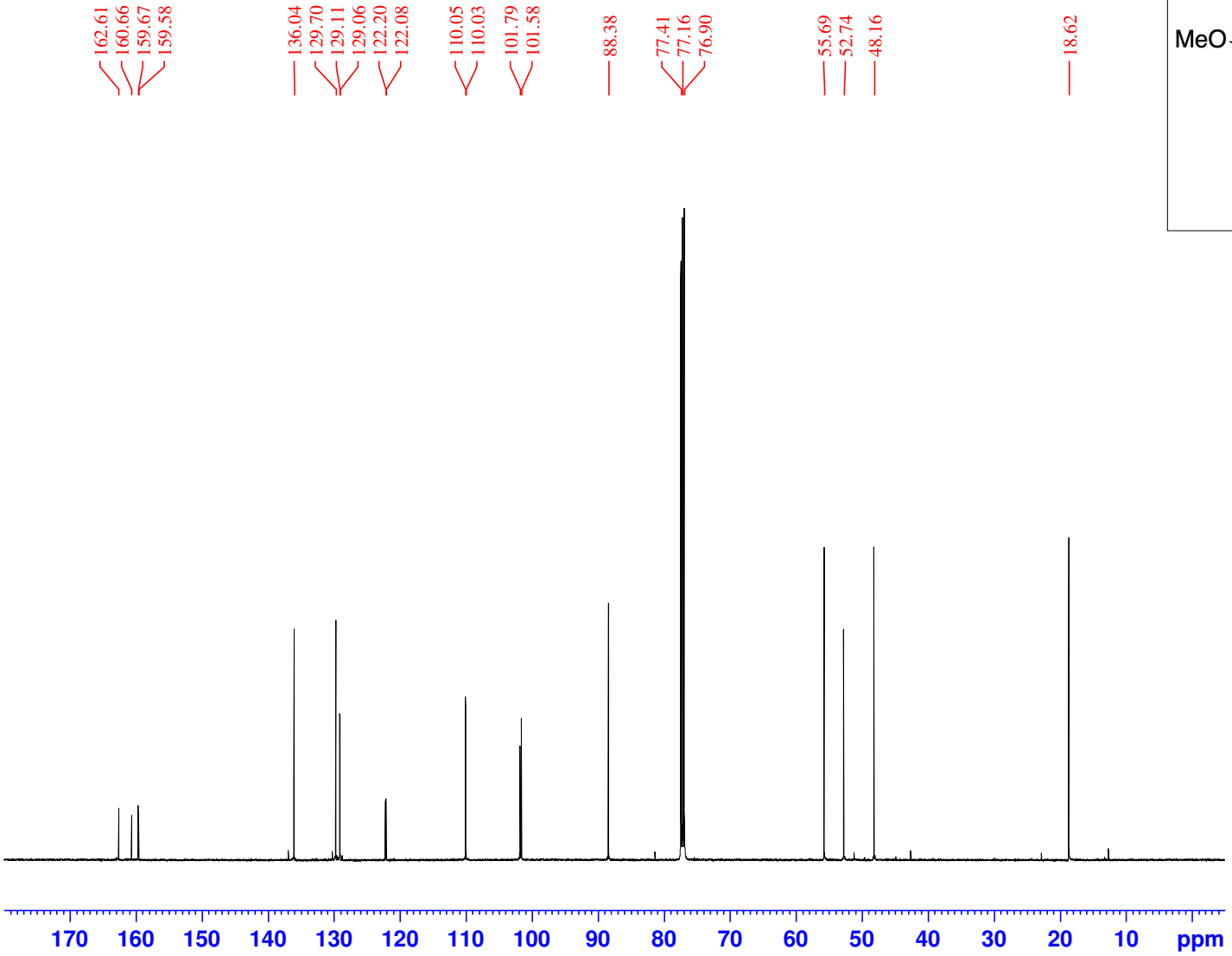

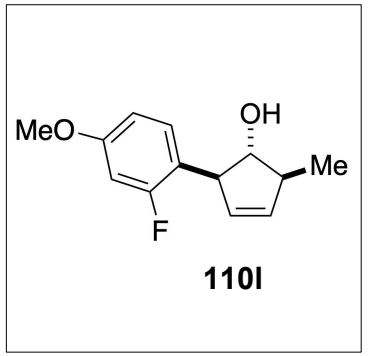

110l

```
Current Data Parameters
NAME      KS-02-163
EXPNO                11
PROCNO                1

F2 - Acquisition Parameters
Date_          20211029
Time              18.57 h
INSTRUM             spect
PROBHD   Z125869_0055 (
PULPROG          zgpg30
TD                65536
SOLVENT           CDC13
NS                 1024
DS                    4
SWH           29761.904 Hz
FIDRES         0.908261 Hz
AQ            1.1010048 sec
RG               190.44
DW               16.800 usec
DE               18.00 usec
TE               298.0 K
D1           2.00000000 sec
D11          0.03000000 sec
TD0                   1
SFO1        125.7955118 MHz
NUC1                13C
P0                3.33 usec
P1               10.00 usec
PLW1         56.90299988 W
SFO2        500.2320009 MHz
NUC2                1H
CPDPRG[2         waltz16
PCPD2            80.00 usec
PLW2         11.44699955 W
PLW12         0.25756001 W
PLW13         0.12955000 W

F2 - Processing parameters
SI                32768
SF          125.7829173 MHz
WDW                  EM
SSB                   0
LB                 1.00 Hz
GB                    0
PC                 1.40
```

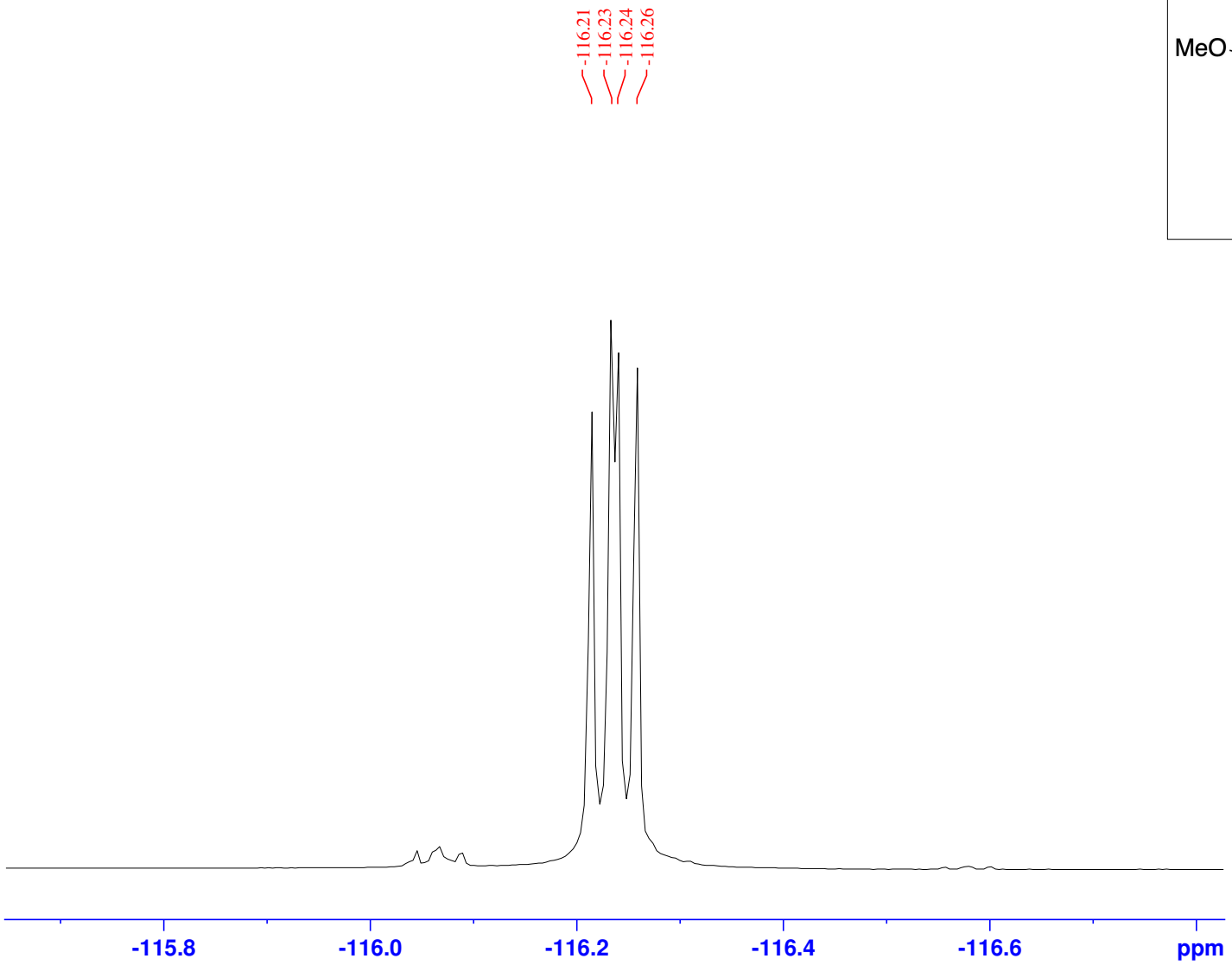

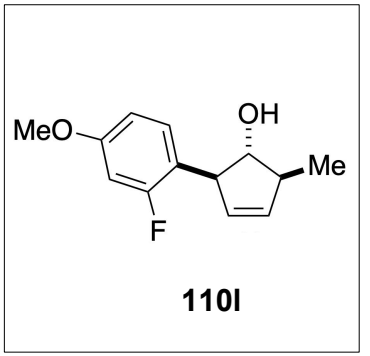

110l

```
Current Data Parameters
NAME      KS-02-163
EXPNO                12
PROCNO                1

F2 - Acquisition Parameters
Date_          20211030
Time              12.28 h
INSTRUM             spect
PROBHD   Z125869_0055 (
PULPROG          zgflqn
TD               131072
SOLVENT             CDCl3
NS                   16
DS                    4
SWH           113636.367 Hz
FIDRES          1.733953 Hz
AQ             0.5767168 sec
RG                15.61
DW                4.400 usec
DE                18.00 usec
TE                298.0 K
D1            1.00000000 sec
TD0                   1
SFO1         470.6394024 MHz
NUC1                 19F
P1                15.00 usec
PLW1         11.70800018 W

F2 - Processing parameters
SI                65536
SF           470.6864710 MHz
WDW                  EM
SSB                   0
LB                 0.30 Hz
GB                    0
PC                 1.00
```

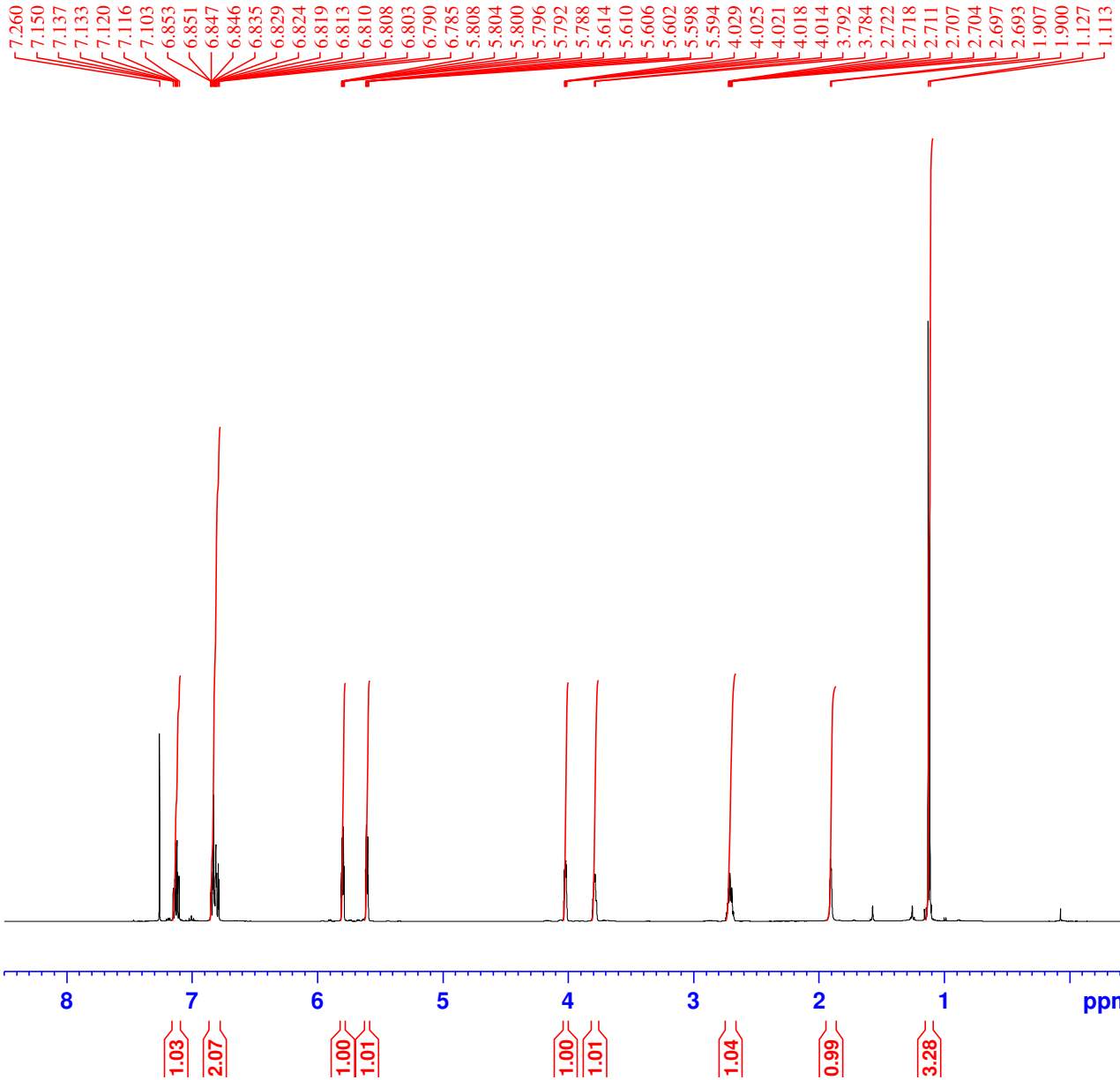

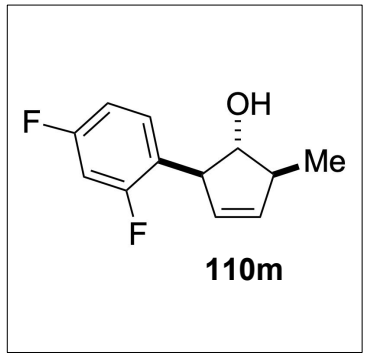


```
Current Data Parameters
NAME      KS-02-279
EXPNO                10
PROCNO                1

F2 - Acquisition Parameters
Date_          20220311
Time               17.26 h
INSTRUM            spect
PROBHD   Z125869_0055 (
PULPROG            zg30
TD                65536
SOLVENT           CDCl3
NS                   64
DS                    2
SWH           10000.000 Hz
FIDRES            0.305176 Hz
AQ             3.2767999 sec
RG                 107.7
DW                50.000 usec
DE                16.00 usec
TE                298.0 K
D1             2.00000000 sec
TD0                   1
SFO1          500.2330889 MHz
NUC1                  1H
P0                 4.00 usec
P1                12.00 usec
PLW1          11.44699955 W

F2 - Processing parameters
SI                65536
SF            500.2300120 MHz
WDW                  EM
SSB                   0
LB                 0.30 Hz
GB                    0
PC                 1.00
```

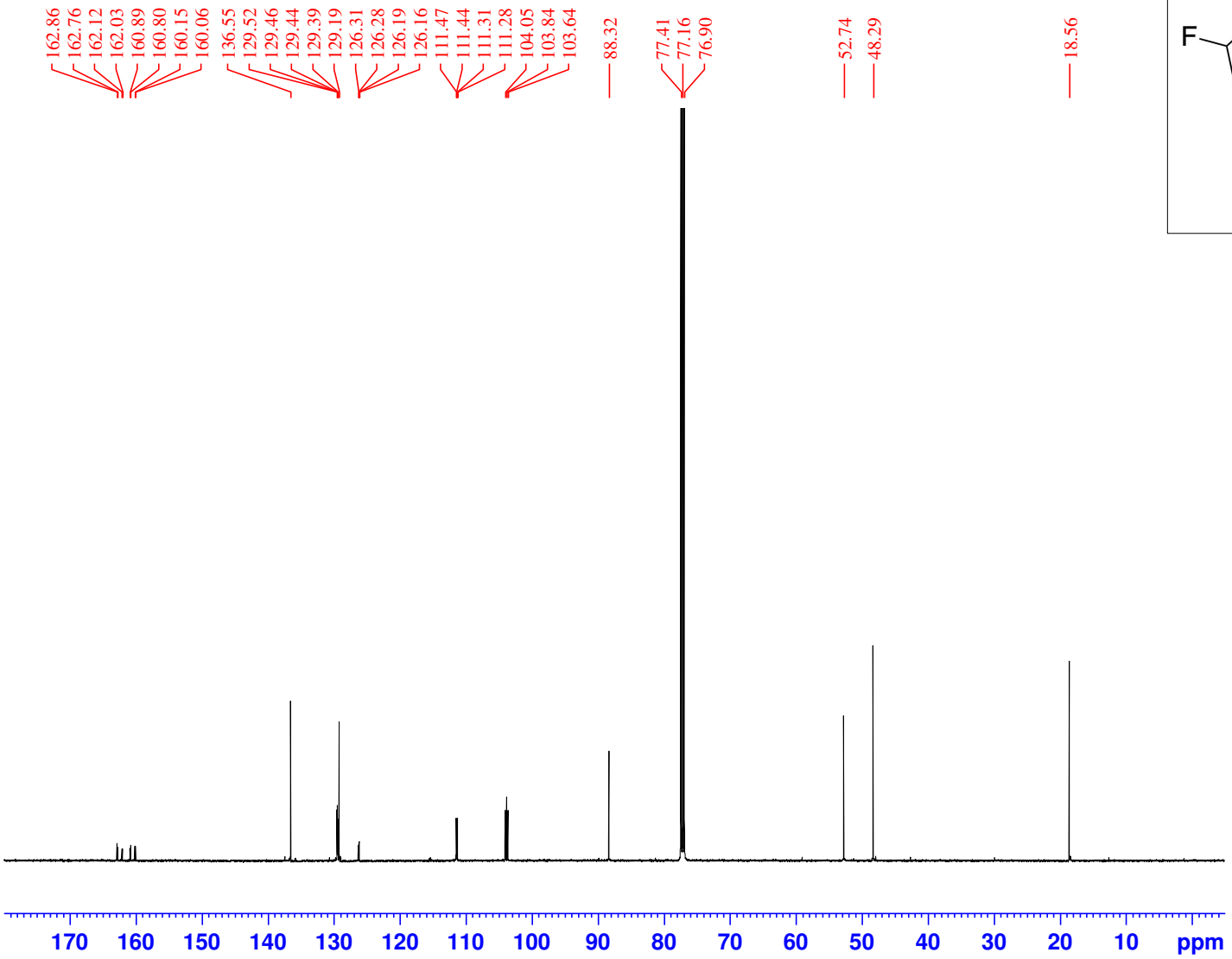

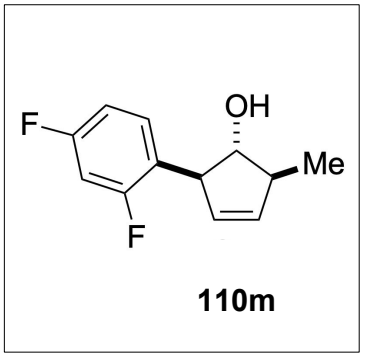


```
Current Data Parameters
NAME      KS-02-279
EXPNO                13
PROCNO                1

F2 - Acquisition Parameters
Date_          20220311
Time              19.41 h
INSTRUM             spect
PROBHD   Z125869_0055 (
PULPROG           zgpg30
TD                 65536
SOLVENT            CDCl3
NS                  1024
DS                     4
SWH            29761.904 Hz
FIDRES          0.908261 Hz
AQ             1.1010048 sec
RG                190.44
DW                16.800 usec
DE                18.00 usec
TE                298.0 K
D1           2.00000000 sec
D11          0.03000000 sec
TD0                    1
SFO1         125.7955118 MHz
NUC1                13C
P0                  3.33 usec
P1                 10.00 usec
PLW1         56.90299988 W
SFO2         500.2320009 MHz
NUC2                 1H
CPDPRG[2         waltz16
PCPD2              80.00 usec
PLW2         11.44699955 W
PLW12         0.25756001 W
PLW13         0.12955000 W

F2 - Processing parameters
SI                 32768
SF           125.7829164 MHz
WDW                   EM
SSB                    0
LB                  1.00 Hz
GB                     0
PC                  1.40
```

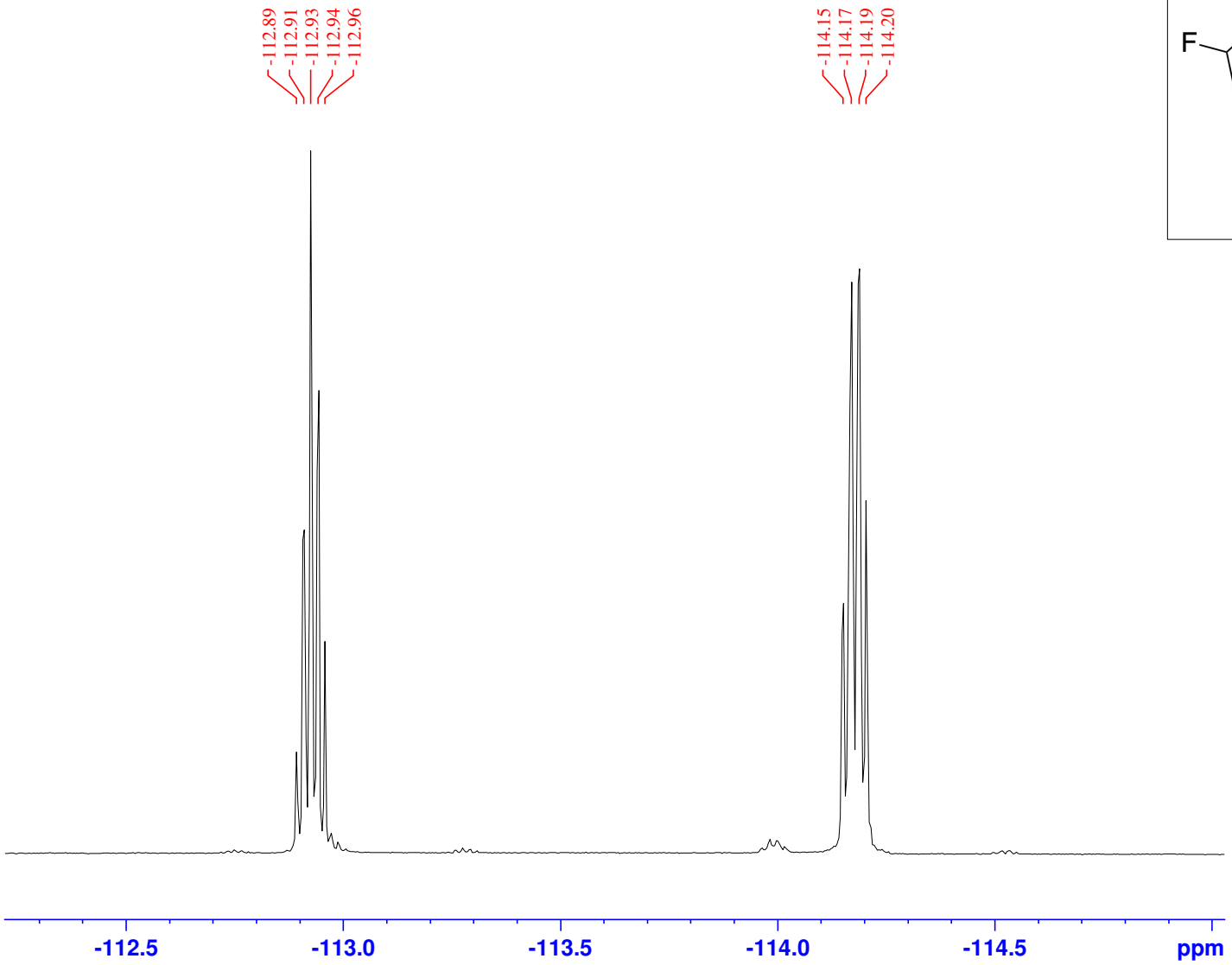

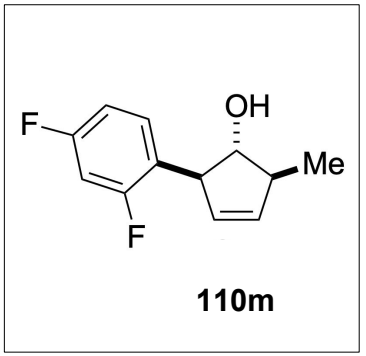


```
Current Data Parameters
NAME      KS-02-279
EXPNO                  12
PROCNO                  1

F2 - Acquisition Parameters
Date_           20220311
Time              17.28 h
INSTRUM             spect
PROBHD   Z125869_0055 (
PULPROG            zgflqn
TD                 131072
SOLVENT              CDCl3
NS                      16
DS                       4
SWH            113636.367 Hz
FIDRES           1.733953 Hz
AQ               0.5767168 sec
RG                   14.14
DW                 4.400 usec
DE                 18.00 usec
TE                 298.0 K
D1            1.00000000 sec
TD0                     1
SFO1         470.6394024 MHz
NUC1                 19F
P1                 15.00 usec
PLW1         11.70800018 W

F2 - Processing parameters
SI                  65536
SF           470.6864710 MHz
WDW                    EM
SSB                     0
LB                 0.30 Hz
GB                      0
PC                   1.00
```

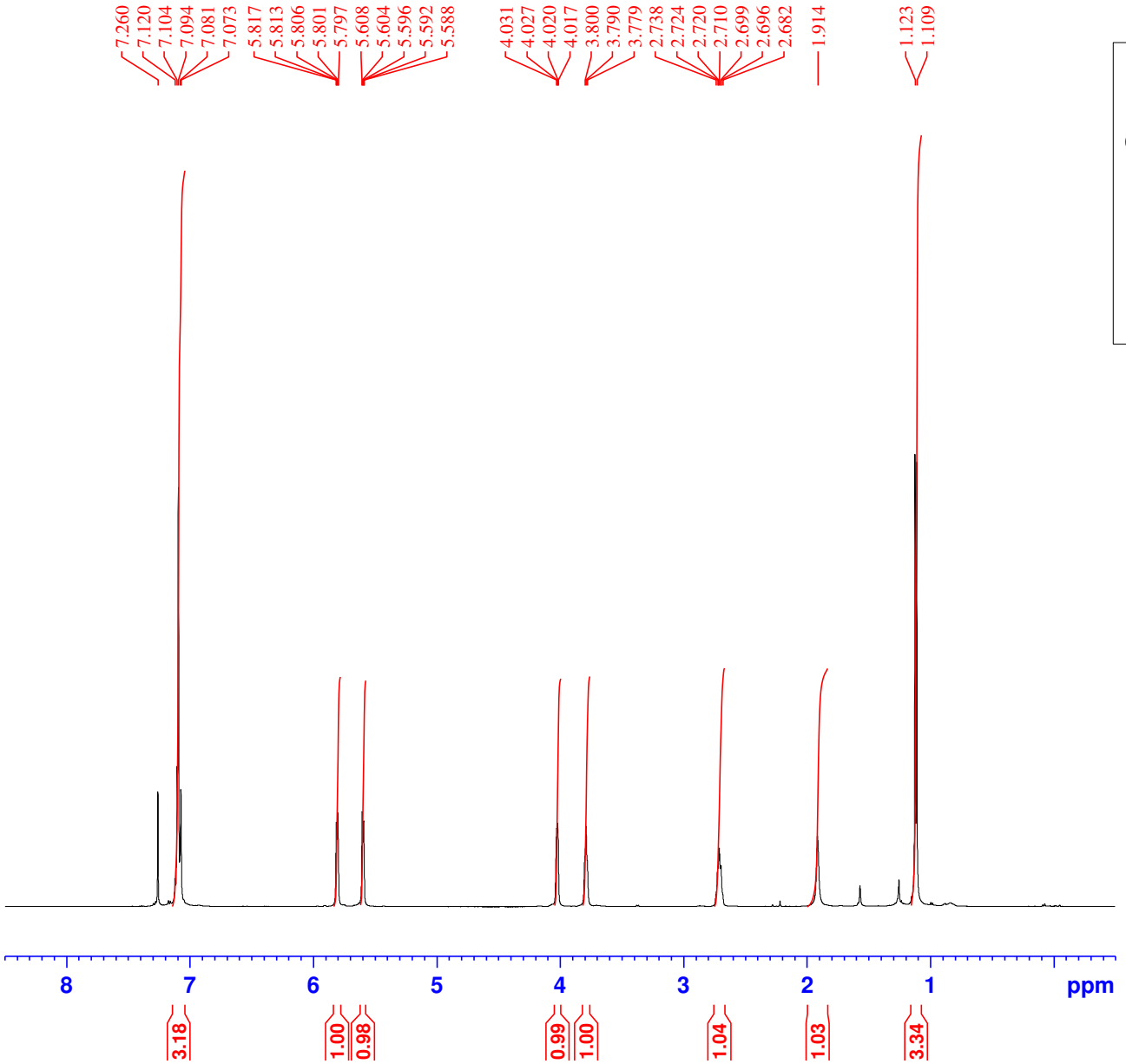

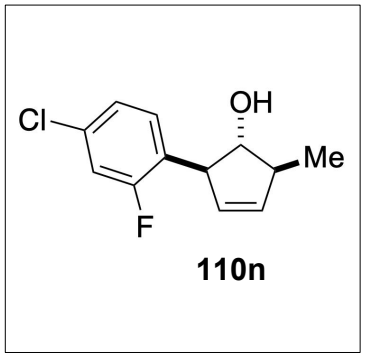

110n

```
Current Data Parameters
NAME      KS-02-285
EXPNO                10
PROCNO                1

F2 - Acquisition Parameters
Date_          20220317
Time               13.56 h
INSTRUM             spect
PROBHD   Z125869_0055 (
PULPROG             zg30
TD                 65536
SOLVENT            CDCl3
NS                    64
DS                     2
SWH            10000.000 Hz
FIDRES             0.305176 Hz
AQ              3.2767999 sec
RG                 151.18
DW                 50.000 usec
DE                 16.00 usec
TE                 298.0 K
D1             2.00000000 sec
TD0                    1
SFO1          500.2330889 MHz
NUC1                  1H
P0                 4.00 usec
P1                 12.00 usec
PLW1          11.44699955 W

F2 - Processing parameters
SI                 65536
SF            500.2300122 MHz
WDW                   EM
SSB                    0
LB                  0.30 Hz
GB                     0
PC                  1.00
```

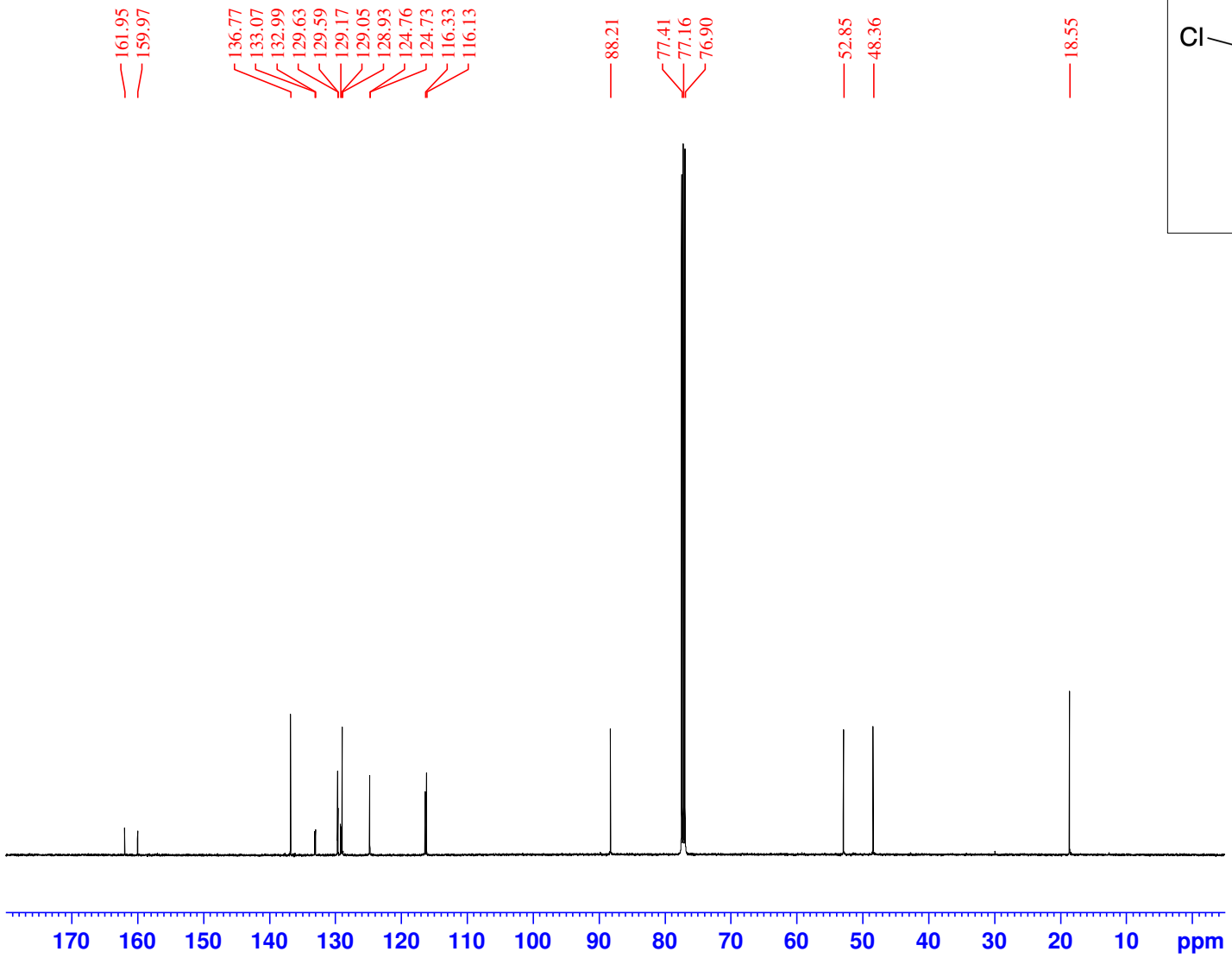

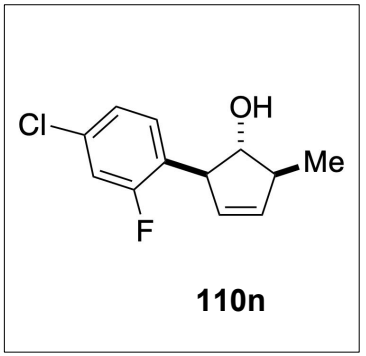


```
Current Data Parameters
NAME      KS-02-285
EXPNO                12
PROCNO                1

F2 - Acquisition Parameters
Date_          20220317
Time              14.56 h
INSTRUM             spect
PROBHD   Z125869_0055 (
PULPROG          zgpg30
TD                65536
SOLVENT           CDCl3
NS                 1024
DS                    4
SWH           29761.904 Hz
FIDRES         0.908261 Hz
AQ            1.1010048 sec
RG               190.44
DW               16.800 usec
DE               18.00 usec
TE               298.0 K
D1           2.00000000 sec
D11          0.03000000 sec
TD0                   1
SFO1        125.7955118 MHz
NUC1                13C
P0                3.33 usec
P1               10.00 usec
PLW1        56.90299988 W
SFO2        500.2320009 MHz
NUC2                1H
CPDPRG[2         waltz16
PCPD2            80.00 usec
PLW2        11.44699955 W
PLW12        0.25756001 W
PLW13        0.12955000 W

F2 - Processing parameters
SI                32768
SF          125.7829163 MHz
WDW                  EM
SSB                   0
LB                 1.00 Hz
GB                    0
PC                 1.40
```

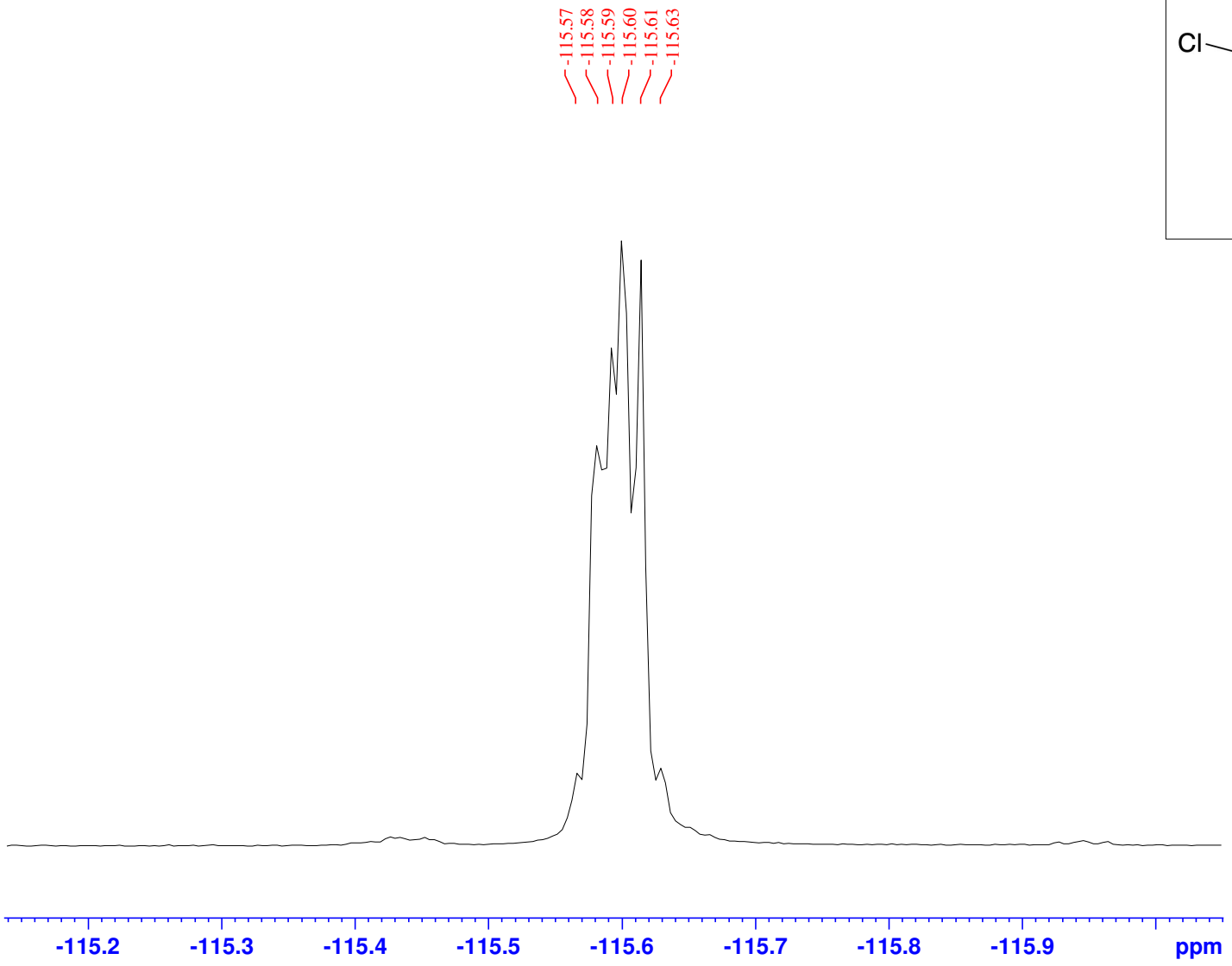

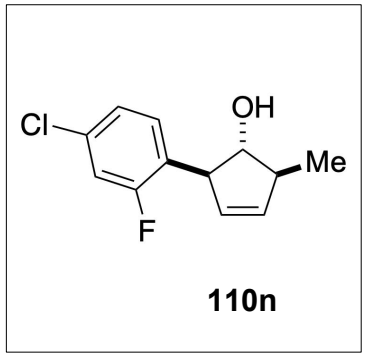


```
Current Data Parameters
NAME      KS-02-285
EXPNO                11
PROCNO                1

F2 - Acquisition Parameters
Date_          20220317
Time              13.58 h
INSTRUM            spect
PROBHD   Z125869_0055 (
PULPROG          zgflqn
TD               131072
SOLVENT            CDCl3
NS                    16
DS                     4
SWH           113636.367 Hz
FIDRES          1.733953 Hz
AQ             0.5767168 sec
RG                 15.61
DW                 4.400 usec
DE                18.00 usec
TE                298.0 K
D1            1.00000000 sec
TD0                    1
SFO1         470.6394024 MHz
NUC1                19F
P1                15.00 usec
PLW1         11.70800018 W

F2 - Processing parameters
SI                 65536
SF           470.6864710 MHz
WDW                   EM
SSB                    0
LB                  0.30 Hz
GB                     0
PC                  1.00
```

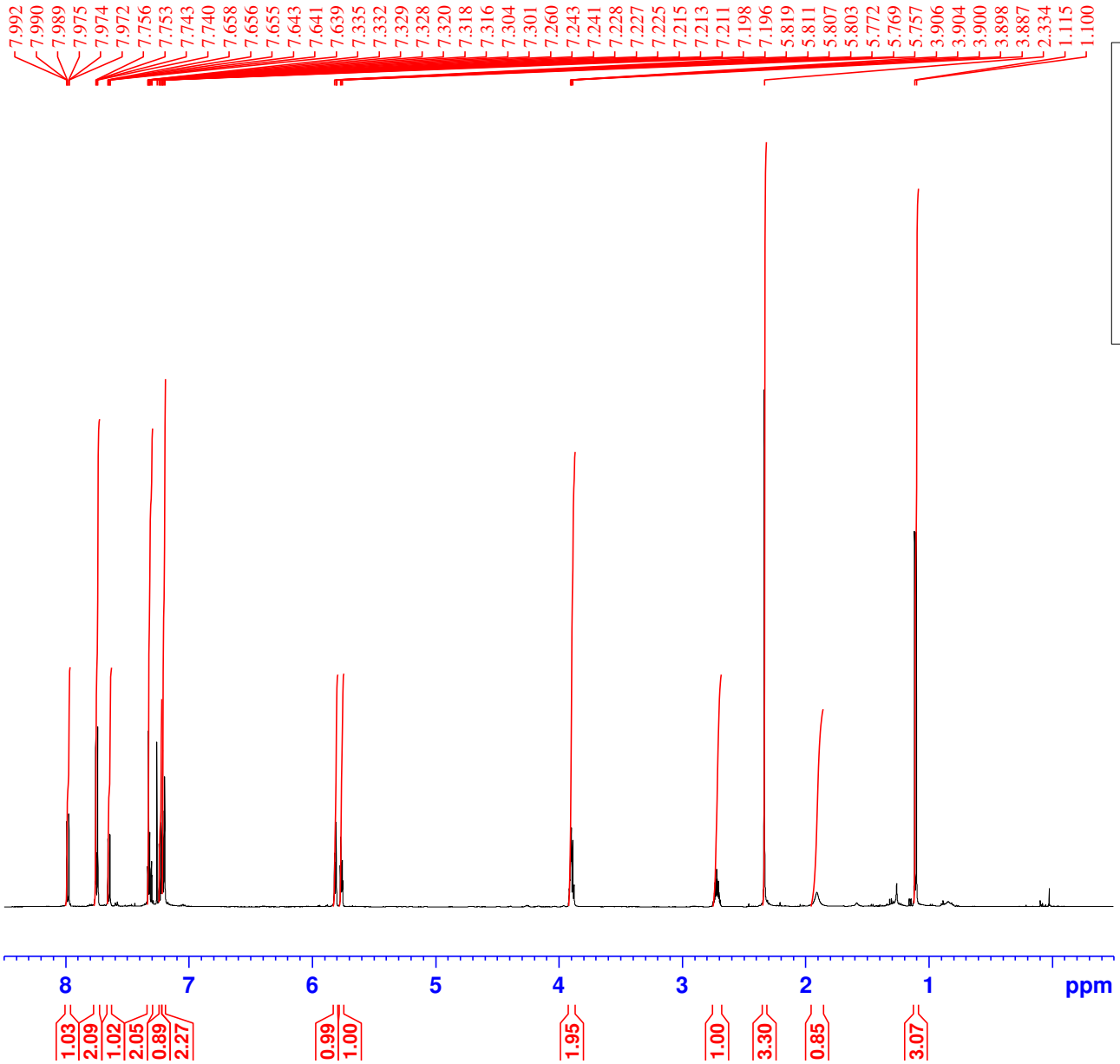

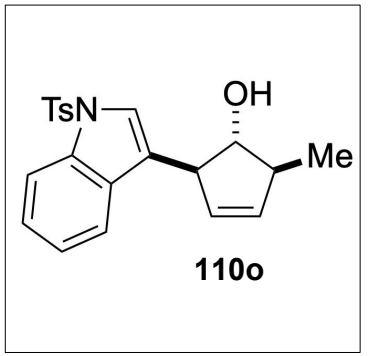


```
Current Data Parameters
NAME      KS-02-235
EXPNO                10
PROCNO                1

F2 - Acquisition Parameters
Date_          20220126
Time              17.23 h
INSTRUM             spect
PROBHD    Z125869_0055 (
PULPROG             zg30
TD                 65536
SOLVENT            CDCl3
NS                    64
DS                     2
SWH           10000.000 Hz
FIDRES            0.305176 Hz
AQ             3.2767999 sec
RG                 69.97
DW                50.000 usec
DE                16.00 usec
TE                298.0 K
D1             2.00000000 sec
TD0                    1
SFO1         500.2330889 MHz
NUC1                  1H
P0                 4.00 usec
P1                12.00 usec
PLW1         11.44699955 W

F2 - Processing parameters
SI                 65536
SF           500.2300119 MHz
WDW                   EM
SSB                    0
LB                0.30 Hz
GB                     0
PC                1.00
```

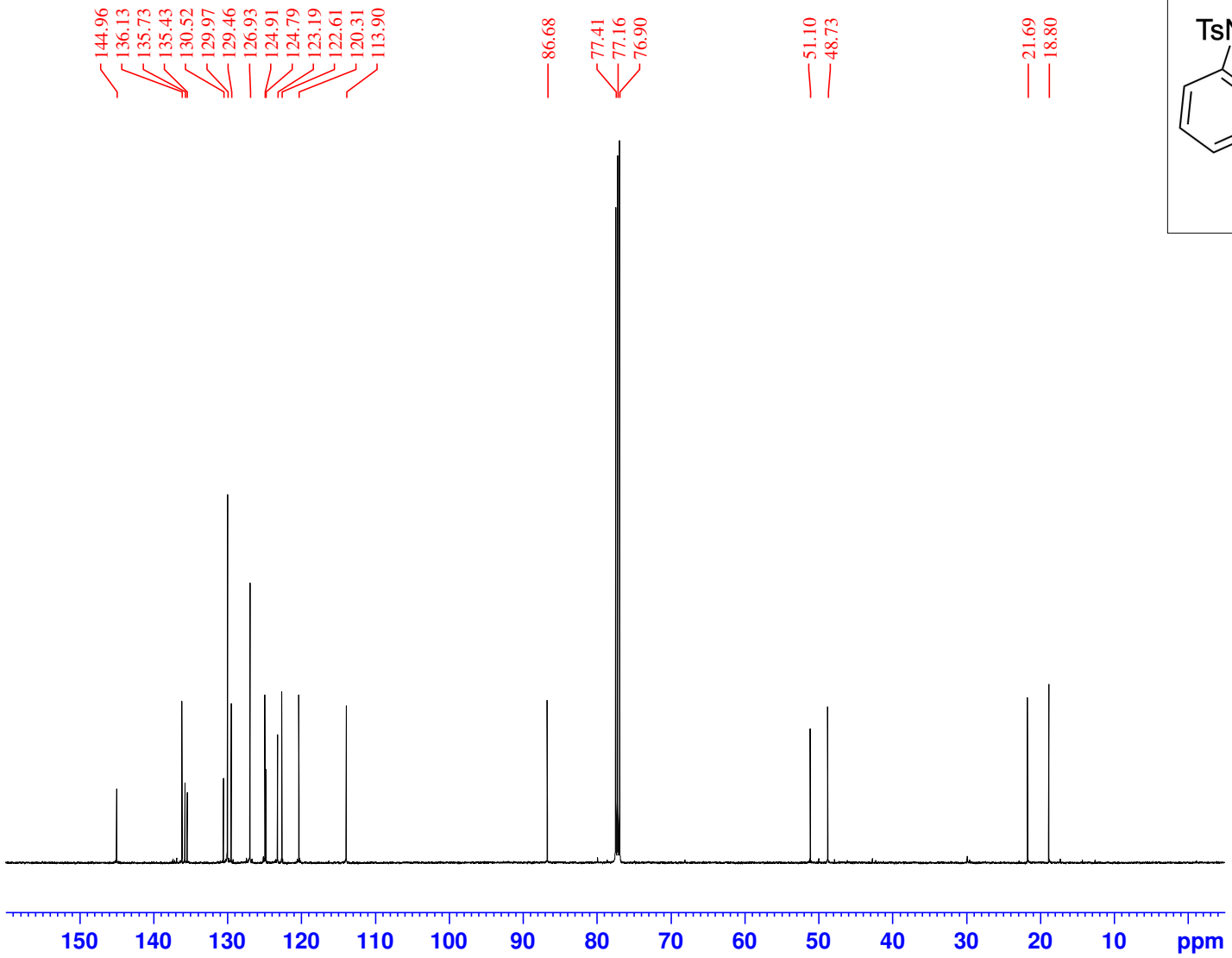

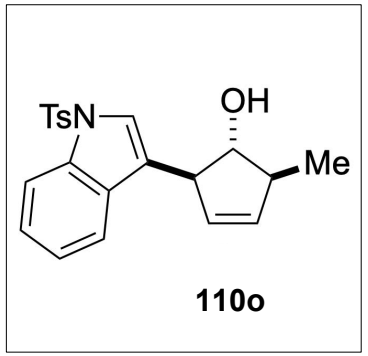


```
Current Data Parameters
NAME      KS-02-235
EXPNO                11
PROCNO                1

F2 - Acquisition Parameters
Date_          20220126
Time               18.34 h
INSTRUM            spect
PROBHD    Z125869_0055 (
PULPROG          zgpg30
TD                65536
SOLVENT           CDCl3
NS                 1024
DS                    4
SWH           29761.904 Hz
FIDRES         0.908261 Hz
AQ             1.1010048 sec
RG                190.44
DW                16.800 usec
DE                18.00 usec
TE                298.0 K
D1             2.00000000 sec
D11            0.03000000 sec
TD0                   1
SFO1         125.7955118 MHz
NUC1                 13C
P0                 3.33 usec
P1                10.00 usec
PLW1         56.90299988 W
SFO2         500.2320009 MHz
NUC2                 1H
CPDPRG[2         waltz16
PCPD2             80.00 usec
PLW2         11.44699955 W
PLW12         0.25756001 W
PLW13         0.12955000 W

F2 - Processing parameters
SI                32768
SF           125.7829182 MHz
WDW                  EM
SSB                   0
LB                 1.00 Hz
GB                    0
PC                 1.40
```

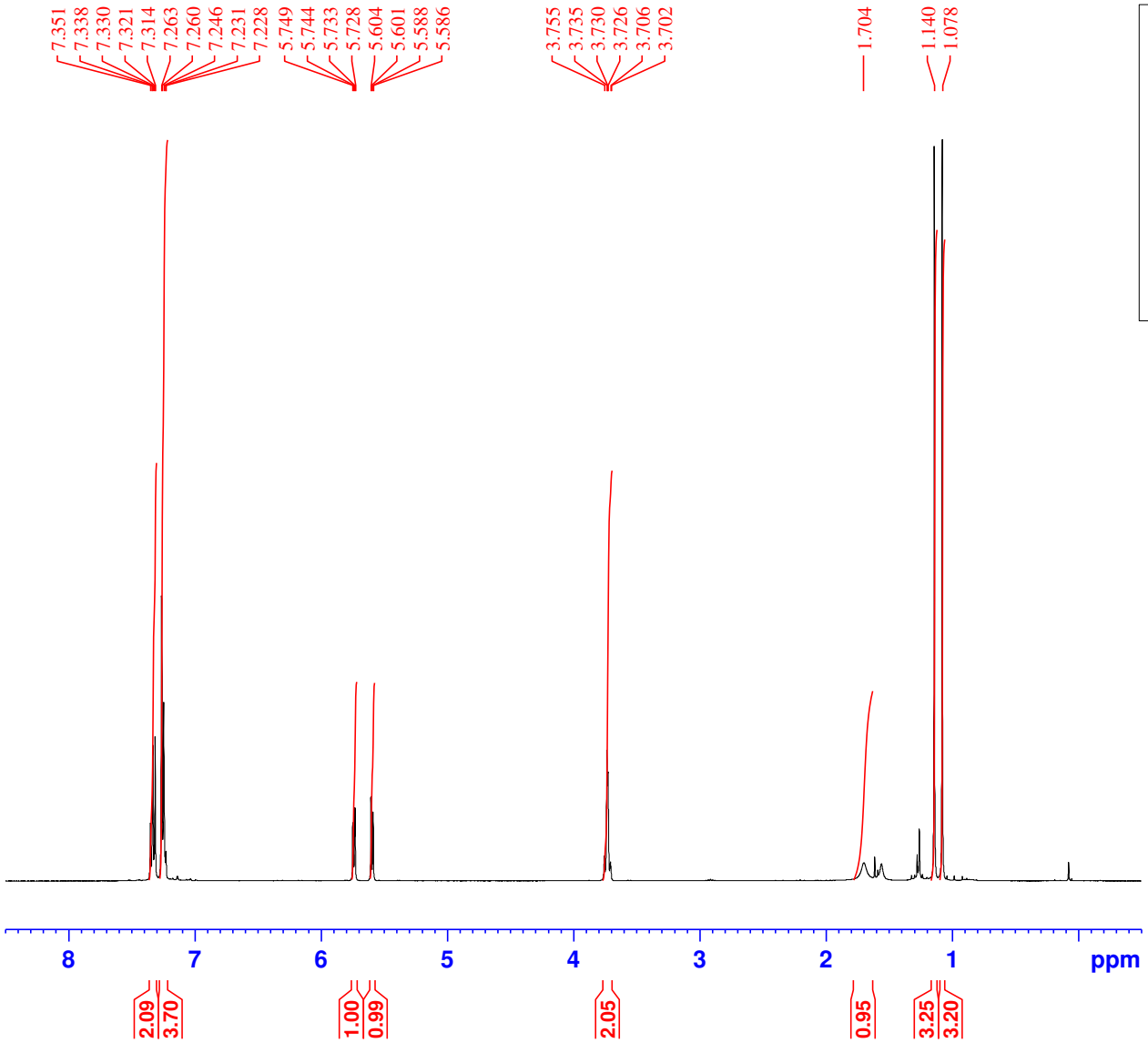

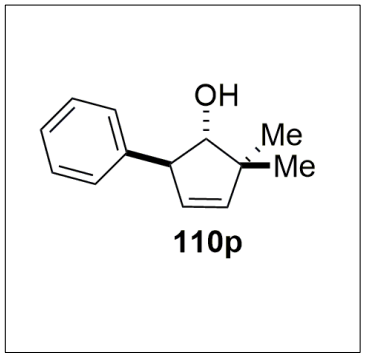

110p

```
Current Data Parameters
NAME         KS-03-97
EXPNO              10
PROCNO              1

F2 - Acquisition Parameters
Date_          20220810
Time             20.57 h
INSTRUM       Avance Neo
PROBHD   Z152088_0031 (
PULPROG            zg30
TD                65536
SOLVENT           CDCl3
NS                   32
DS                    2
SWH            8196.722 Hz
FIDRES         0.250144 Hz
AQ             3.9976959 sec
RG                  101
DW                61.000 usec
DE                13.89 usec
TE                298.0 K
D1           1.00000000 sec
TD0                   1
SFO1        400.1324708 MHz
NUC1                1H
P0                2.67 usec
P1                8.00 usec
PLW1        24.03499985 W

F2 - Processing parameters
SI                65536
SF          400.1300099 MHz
WDW                 EM
SSB       0
LB                0.30 Hz
GB        0
PC                1.00
```

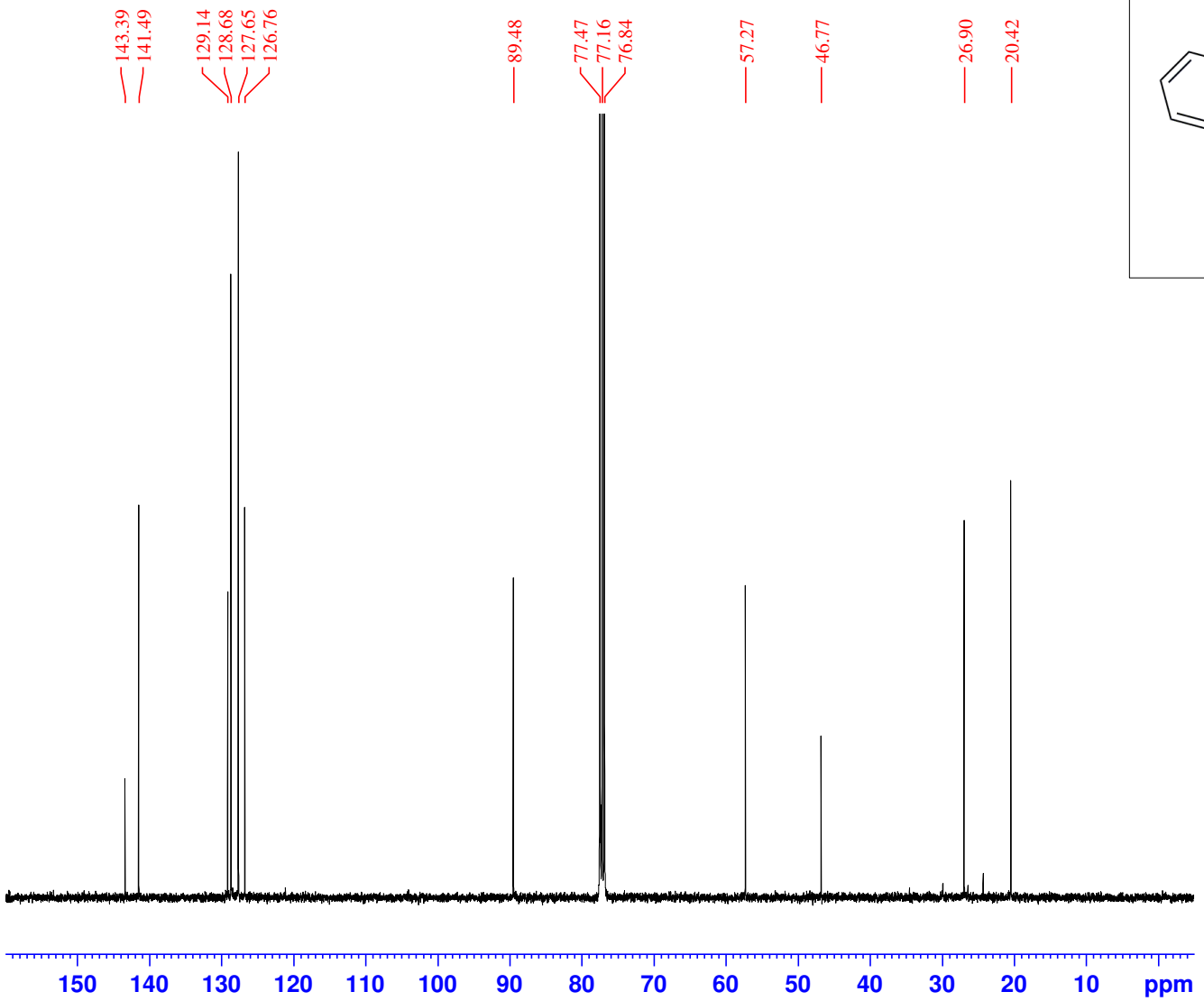

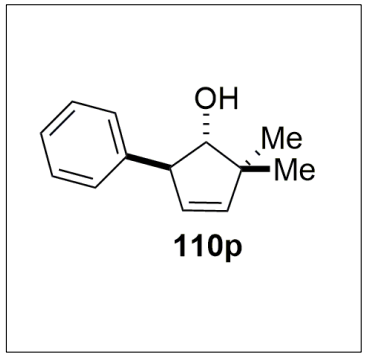


```
Current Data Parameters
NAME         KS-03-97
EXPNO              11
PROCNO              1

F2 - Acquisition Parameters
Date_         20220810
Time             22.57 h
INSTRUM      Avance Neo
PROBHD   Z152088_0031 (
PULPROG         zgpg30
TD              65536
SOLVENT          CDCl3
NS                2048
DS                   4
SWH          23809.523 Hz
FIDRES        0.726609 Hz
AQ            1.3762560 sec
RG                8.125
DW               21.000 usec
DE                6.50 usec
TE               298.0 K
D1            2.00000000 sec
D11           0.03000000 sec
TD0                  1
SFO1        100.6228298 MHz
NUC1               13C
P0                2.67 usec
P1                8.00 usec
PLW1        86.55400085 W
SFO2        400.1316005 MHz
NUC2               1H
CPDPRG[2        waltz65
PCPD2            90.00 usec
PLW2        24.03499985 W
PLW12        0.18990999 W
PLW13        0.09552100 W

F2 - Processing parameters
SI                32768
SF          100.6127551 MHz
WDW                EM
SSB      0
LB                1.00 Hz
GB       0
PC                1.40
```

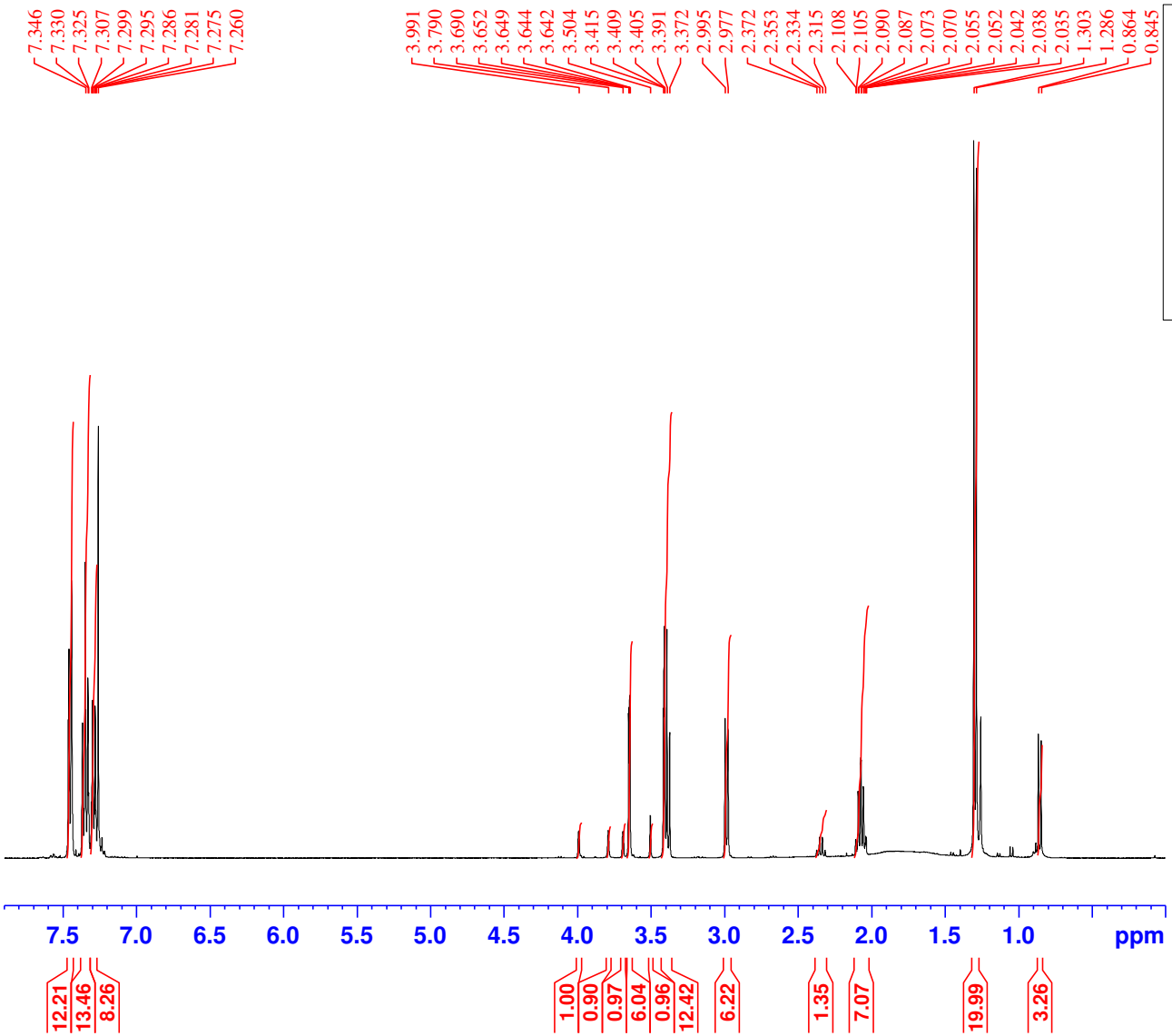

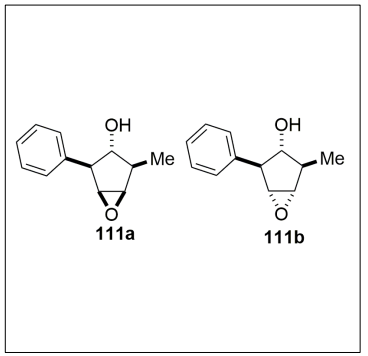


```
Current Data Parameters
NAME         KS-03-91col
EXPNO                 10
PROCNO                 1

F2 - Acquisition Parameters
Date_           20220805
Time                19.04 h
INSTRUM       Avance Neo
PROBHD    Z152088_0031 (
PULPROG             zg30
TD                 65536
SOLVENT            CDCl3
NS                    16
DS                     2
SWH             8196.722 Hz
FIDRES          0.250144 Hz
AQ              3.9976959 sec
RG                   101
DW                61.000 usec
DE                13.89 usec
TE                298.0 K
D1             1.00000000 sec
TD0                    1
SFO1         400.1324708 MHz
NUC1                  1H
P0                 2.67 usec
P1                 8.00 usec
PLW1         24.03499985 W

F2 - Processing parameters
SI                 65536
SF           400.1300096 MHz
WDW                   EM
SSB       0
LB                 0.30 Hz
GB        0
PC                 1.00
```

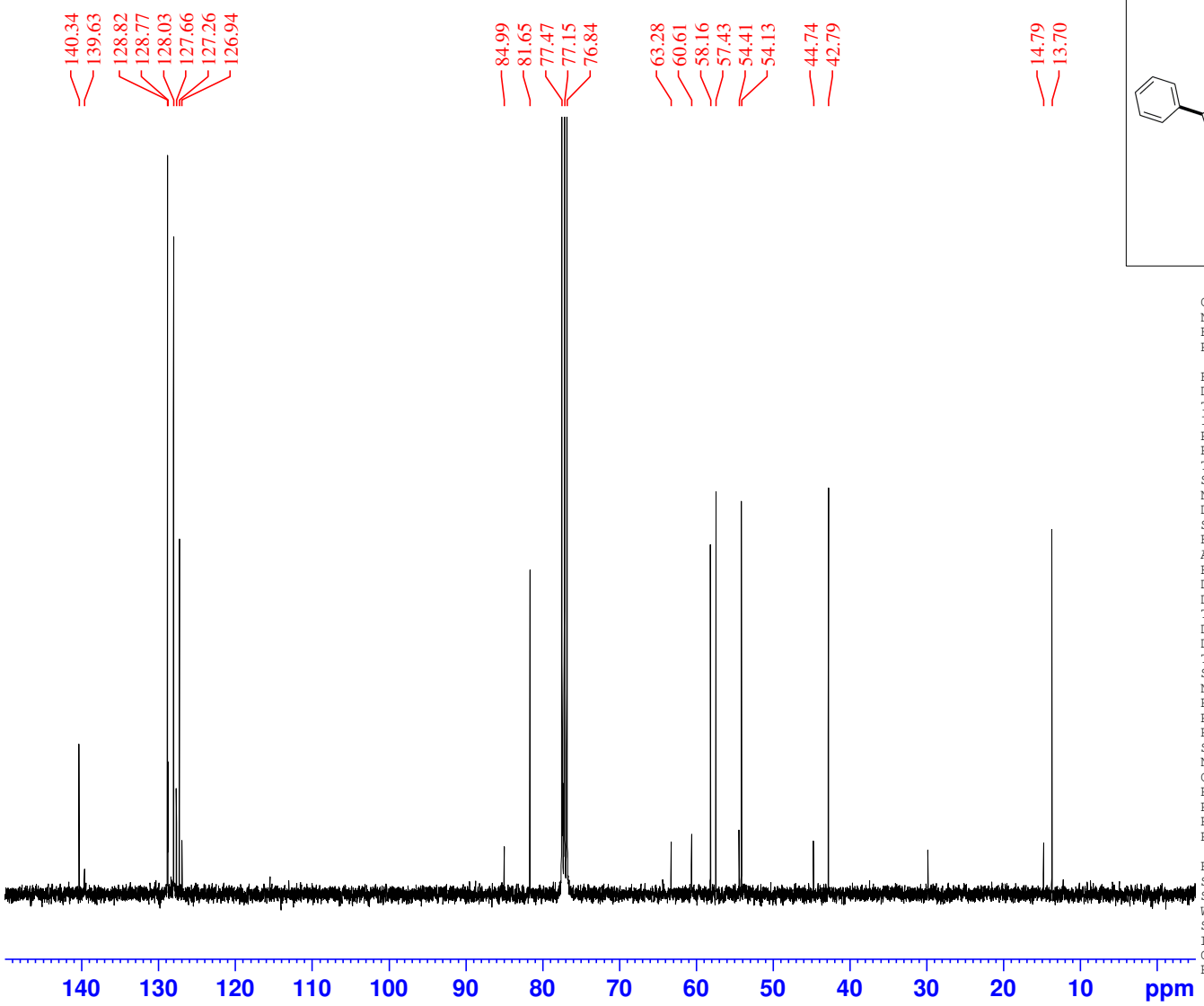

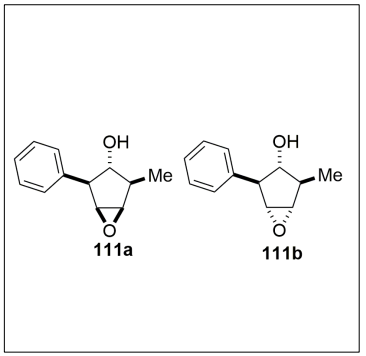


```
Current Data Parameters
NAME         KS-03-91col
EXPNO                 11
PROCNO                 1

F2 - Acquisition Parameters
Date_           20220805
Time               20.04 h
INSTRUM       Avance Neo
PROBHD    Z152088_0031 (
PULPROG          zgpg30
TD                65536
SOLVENT           CDCl3
NS                 1024
DS                    4
SWH           23809.523 Hz
FIDRES         0.726609 Hz
AQ             1.3762560 sec
RG                 8.125
DW                21.000 usec
DE                 6.50 usec
TE                298.0 K
D1             2.00000000 sec
D11            0.03000000 sec
TD0                   1
SFO1          100.6228298 MHz
NUC1                 13C
P0                 2.67 usec
P1                 8.00 usec
PLW1          86.55400085 W
SFO2          400.1316005 MHz
NUC2                 1H
CPDPRG[2          waltz65
PCPD2             90.00 usec
PLW2          24.03499985 W
PLW12          0.18990999 W
PLW13          0.09552100 W

F2 - Processing parameters
SI                32768
SF            100.6127553 MHz
WDW                  EM
SSB       0
LB                1.00 Hz
GB        0
PC                1.40
```

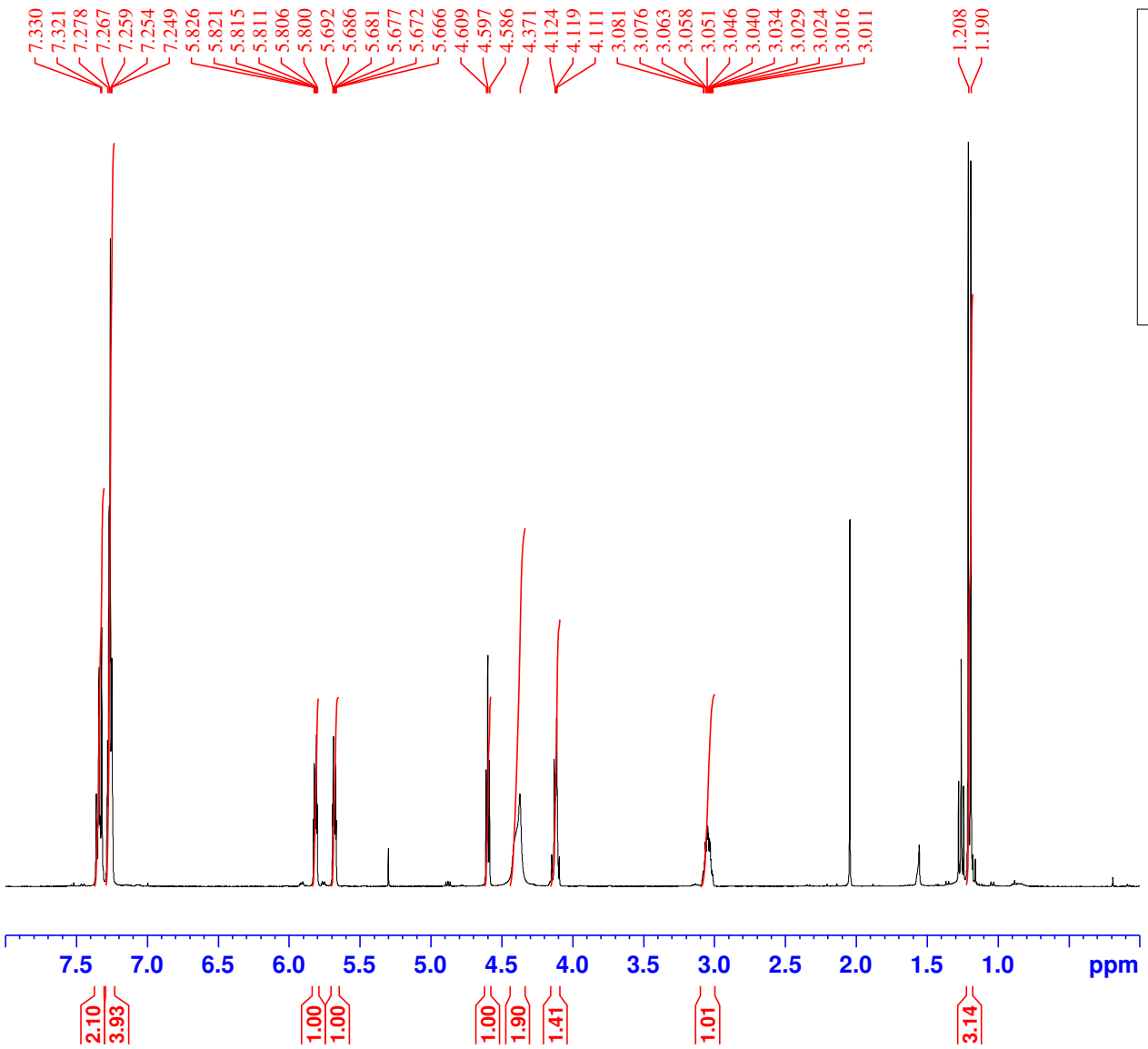

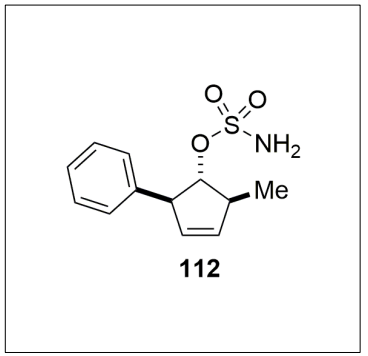

112

```
Current Data Parameters
NAME         KS-03-94col
EXPNO                 10
PROCNO                 1

F2 - Acquisition Parameters
Date_           20220809
Time              23.16 h
INSTRUM       Avance Neo
PROBHD    Z152088_0031 (
PULPROG             zg30
TD                 65536
SOLVENT            CDCl3
NS                    16
DS                     2
SWH             8196.722 Hz
FIDRES          0.250144 Hz
AQ              3.9976959 sec
RG                   101
DW                61.000 usec
DE                13.89 usec
TE                298.0 K
D1             1.00000000 sec
TD0                    1
SFO1         400.1324708 MHz
NUC1                  1H
P0                 2.67 usec
P1                 8.00 usec
PLW1         24.03499985 W

F2 - Processing parameters
SI                 65536
SF           400.1300099 MHz
WDW                   EM
SSB       0
LB                 0.30 Hz
GB        0
PC                 1.00
```

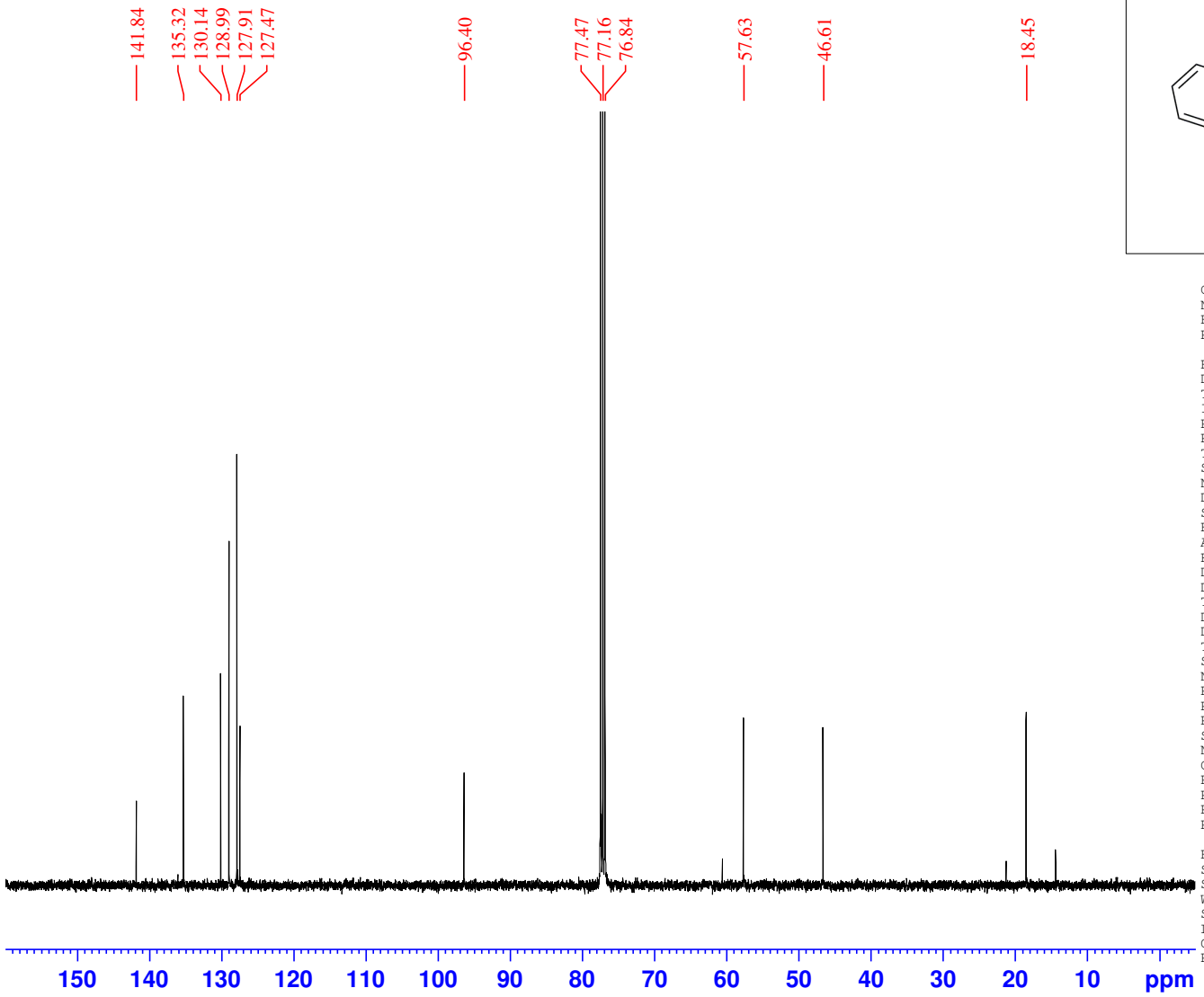

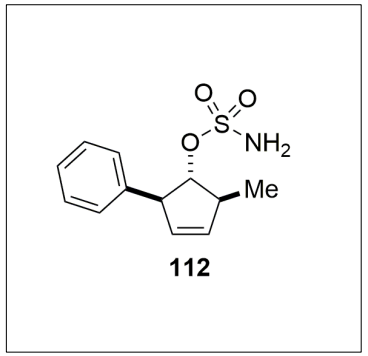

112

```
Current Data Parameters
NAME         KS-03-94col
EXPNO                 11
PROCNO                 1

F2 - Acquisition Parameters
Date_           20220810
Time                0.16 h
INSTRUM       Avance Neo
PROBHD    Z152088_0031 (
PULPROG           zgpg30
TD                65536
SOLVENT           CDCl3
NS                 1024
DS                    4
SWH           23809.523 Hz
FIDRES         0.726609 Hz
AQ             1.3762560 sec
RG                8.125
DW               21.000 usec
DE                6.50 usec
TE               298.0 K
D1            2.00000000 sec
D11           0.03000000 sec
TD0                   1
SFO1         100.6228298 MHz
NUC1                13C
P0                 2.67 usec
P1                 8.00 usec
PLW1         86.55400085 W
SFO2         400.1316005 MHz
NUC2                1H
CPDPRG[2         waltz65
PCPD2             90.00 usec
PLW2         24.03499985 W
PLW12         0.18990999 W
PLW13         0.09552100 W

F2 - Processing parameters
SI                32768
SF           100.6127551 MHz
WDW                  EM
SSB       0
LB                1.00 Hz
GB        0
PC                1.40
```

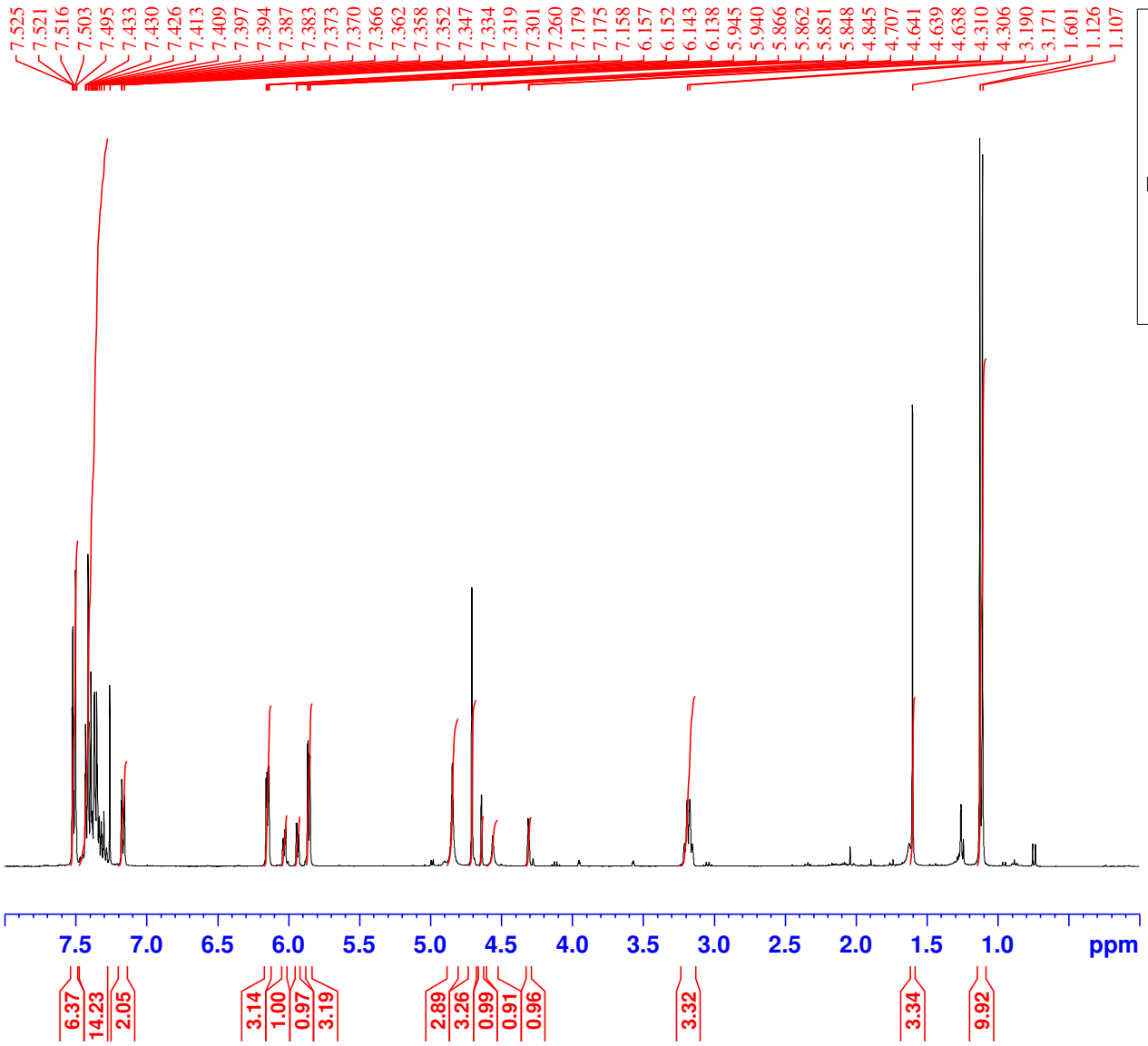

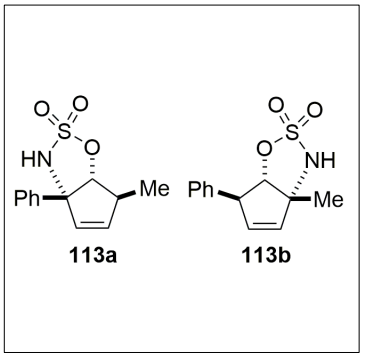


```
Current Data Parameters
NAME        KS-03-96-6-8
EXPNO                 10
PROCNO                 1

F2 - Acquisition Parameters
Date_           20220811
Time              13.29 h
INSTRUM       Avance Neo
PROBHD    Z152088_0031 (
PULPROG             zg30
TD                 65536
SOLVENT            CDCl3
NS                    16
DS                     2
SWH             8196.722 Hz
FIDRES          0.250144 Hz
AQ              3.9976959 sec
RG                   101
DW                61.000 usec
DE                13.89 usec
TE                298.0 K
D1             1.00000000 sec
TD0                    1
SFO1         400.1324708 MHz
NUC1                 1H
P0                 2.67 usec
P1                 8.00 usec
PLW1         24.03499985 W

F2 - Processing parameters
SI                 65536
SF           400.1300096 MHz
WDW                  EM
SSB       0
LB                 0.30 Hz
GB        0
PC                 1.00
```

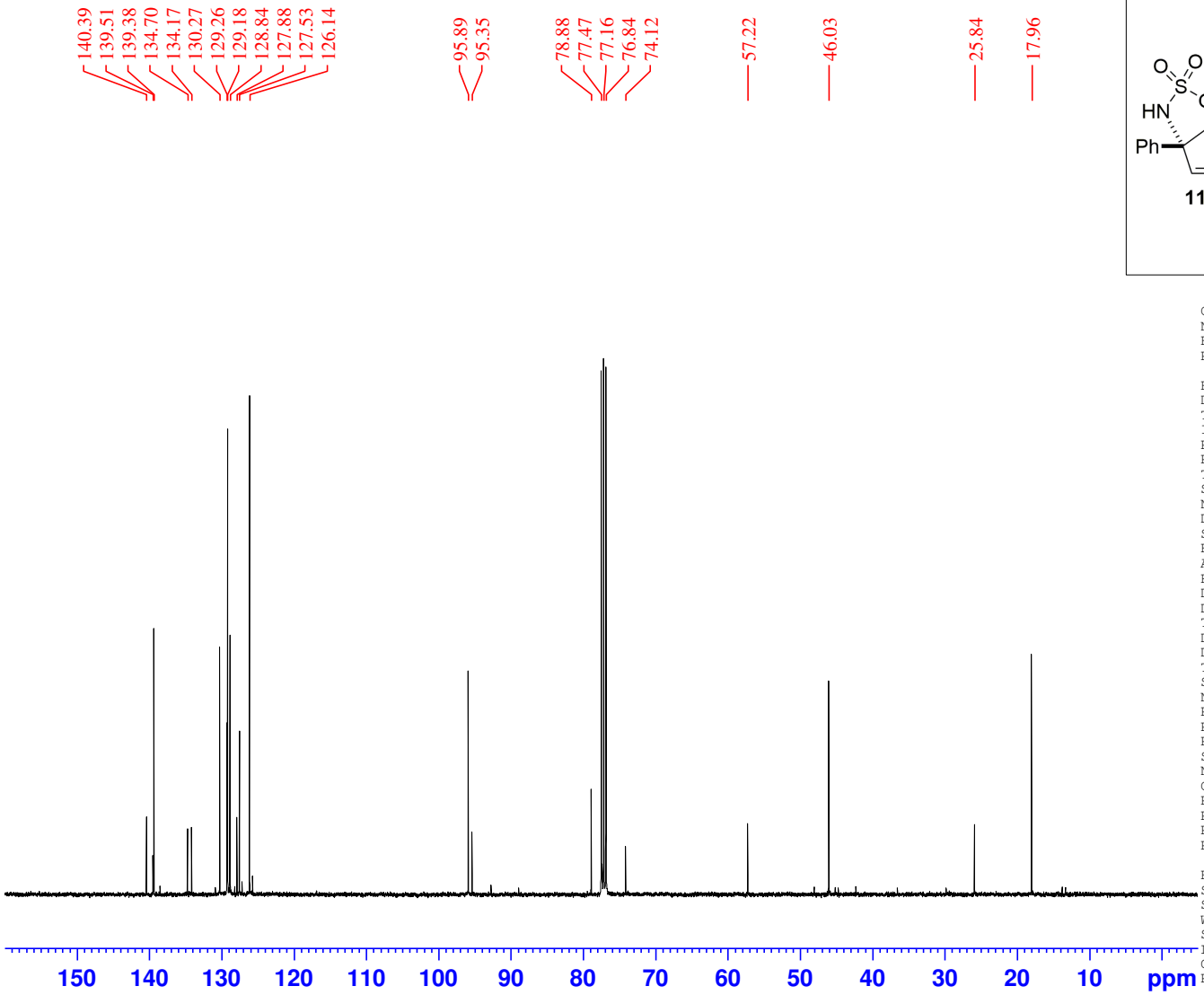

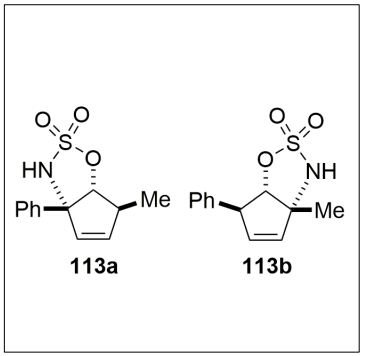


```
Current Data Parameters
NAME        KS-03-96-6-8
EXPNO                 14
PROCNO                 1

F2 - Acquisition Parameters
Date_           20220811
Time               20.16 h
INSTRUM       Avance Neo
PROBHD    Z152088_0031 (
PULPROG          zgpg30
TD                65536
SOLVENT           CDCl3
NS                 1024
DS                    4
SWH           23809.523 Hz
FIDRES         0.726609 Hz
AQ             1.3762560 sec
RG                8.125
DW               21.000 usec
DE                6.50 usec
TE               298.0 K
D1            2.00000000 sec
D11           0.03000000 sec
TD0                   1
SFO1         100.6228298 MHz
NUC1                13C
P0                 2.67 usec
P1                 8.00 usec
PLW1         86.55400085 W
SFO2         400.1316005 MHz
NUC2                1H
CPDPRG[2         waltz65
PCPD2             90.00 usec
PLW2         24.03499985 W
PLW12         0.18990999 W
PLW13         0.09552100 W

F2 - Processing parameters
SI                32768
SF           100.6127579 MHz
WDW                  EM
SSB       0
LB                1.00 Hz
GB        0
PC                1.40
```

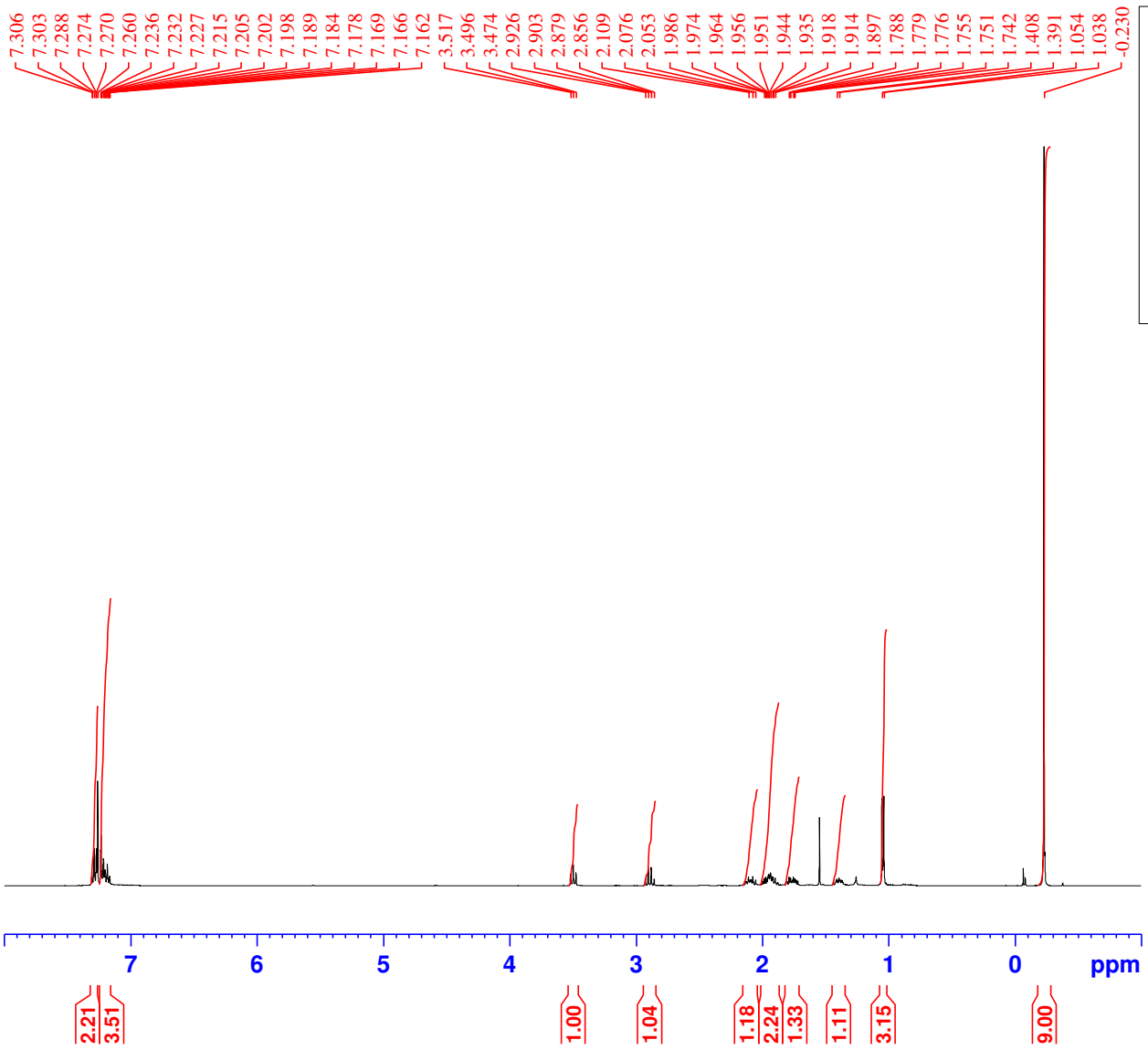

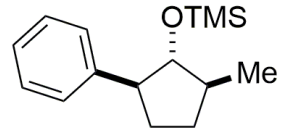

115a

```
Current Data Parameters
NAME        KS-03-98-5-9
EXPNO                 10
PROCNO                 1

F2 - Acquisition Parameters
Date_           20220811
Time              14.04 h
INSTRUM       Avance Neo
PROBHD    Z152088_0031 (
PULPROG             zg30
TD                 65536
SOLVENT            CDCl3
NS                    16
DS                     2
SWH             8196.722 Hz
FIDRES          0.250144 Hz
AQ              3.9976959 sec
RG                   101
DW                61.000 usec
DE                13.89 usec
TE                298.0 K
D1             1.00000000 sec
TD0                    1
SFO1         400.1324708 MHz
NUC1                  1H
P0                 2.67 usec
P1                 8.00 usec
PLW1         24.03499985 W

F2 - Processing parameters
SI                 65536
SF           400.1300096 MHz
WDW                   EM
SSB       0
LB                 0.30 Hz
GB        0
PC                 1.00
```

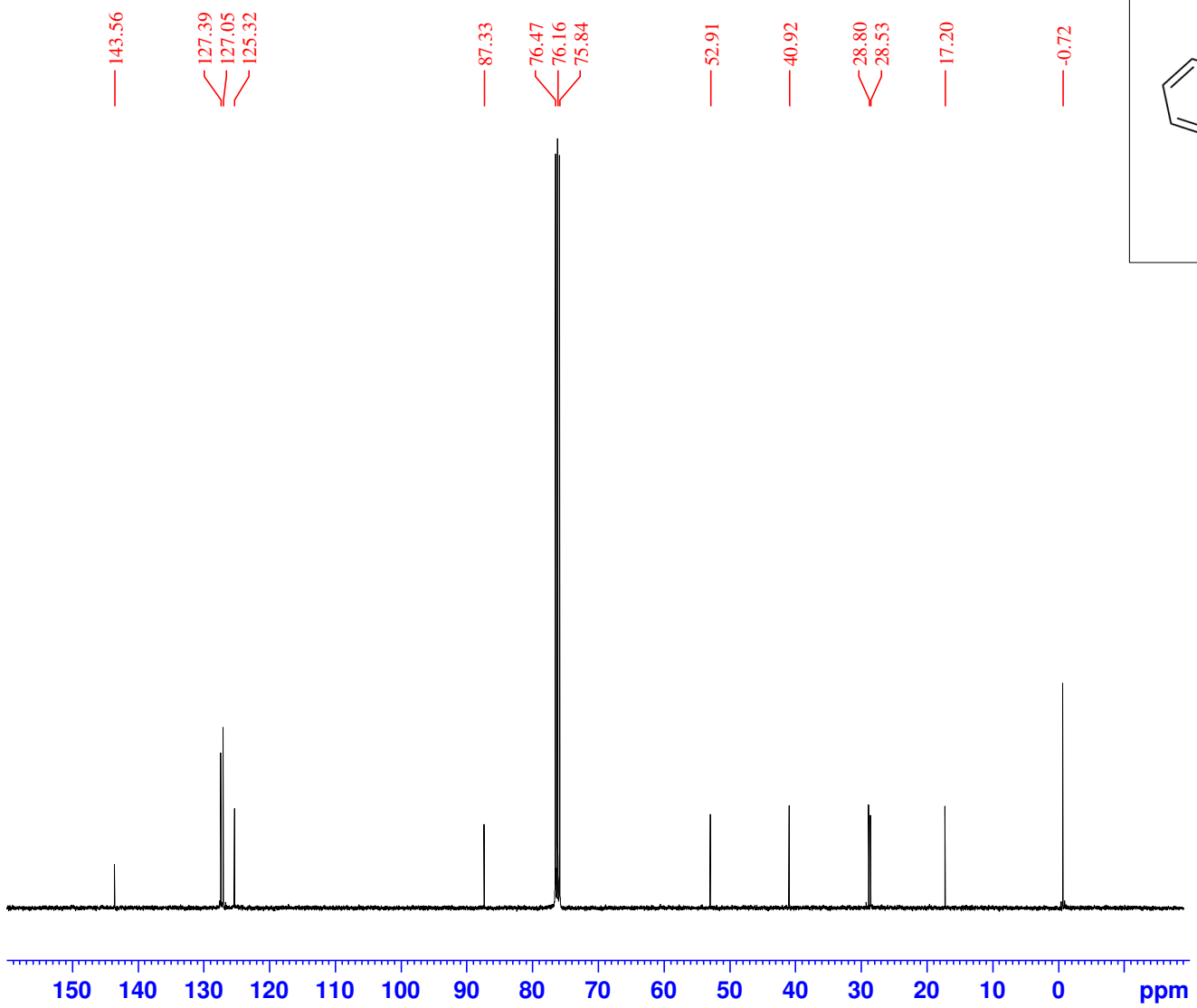

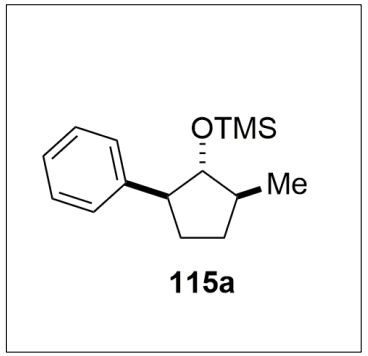

115a

```
Current Data Parameters
NAME       KS-03-98-5-9
EXPNO                11
PROCNO                1

F2 - Acquisition Parameters
Date_          20220812
Time               0.18 h
INSTRUM      Avance Neo
PROBHD   Z152088_0031 (
PULPROG          zgpg30
TD                65536
SOLVENT           CDCl3
NS                 2048
DS                    4
SWH           23809.523 Hz
FIDRES         0.726609 Hz
AQ             1.3762560 sec
RG                8.125
DW               21.000 usec
DE                6.50 usec
TE               298.0 K
D1            2.00000000 sec
D11           0.03000000 sec
TD0                   1
SFO1         100.6228298 MHz
NUC1                13C
P0                 2.67 usec
P1                 8.00 usec
PLW1         86.55400085 W
SFO2         400.1316005 MHz
NUC2                1H
CPDPRG[2         waltz65
PCPD2             90.00 usec
PLW2         24.03499985 W
PLW12         0.18990999 W
PLW13         0.09552100 W

F2 - Processing parameters
SI                32768
SF           100.6128550 MHz
WDW                  EM
SSB       0
LB                1.00 Hz
GB        0
PC                1.40
```

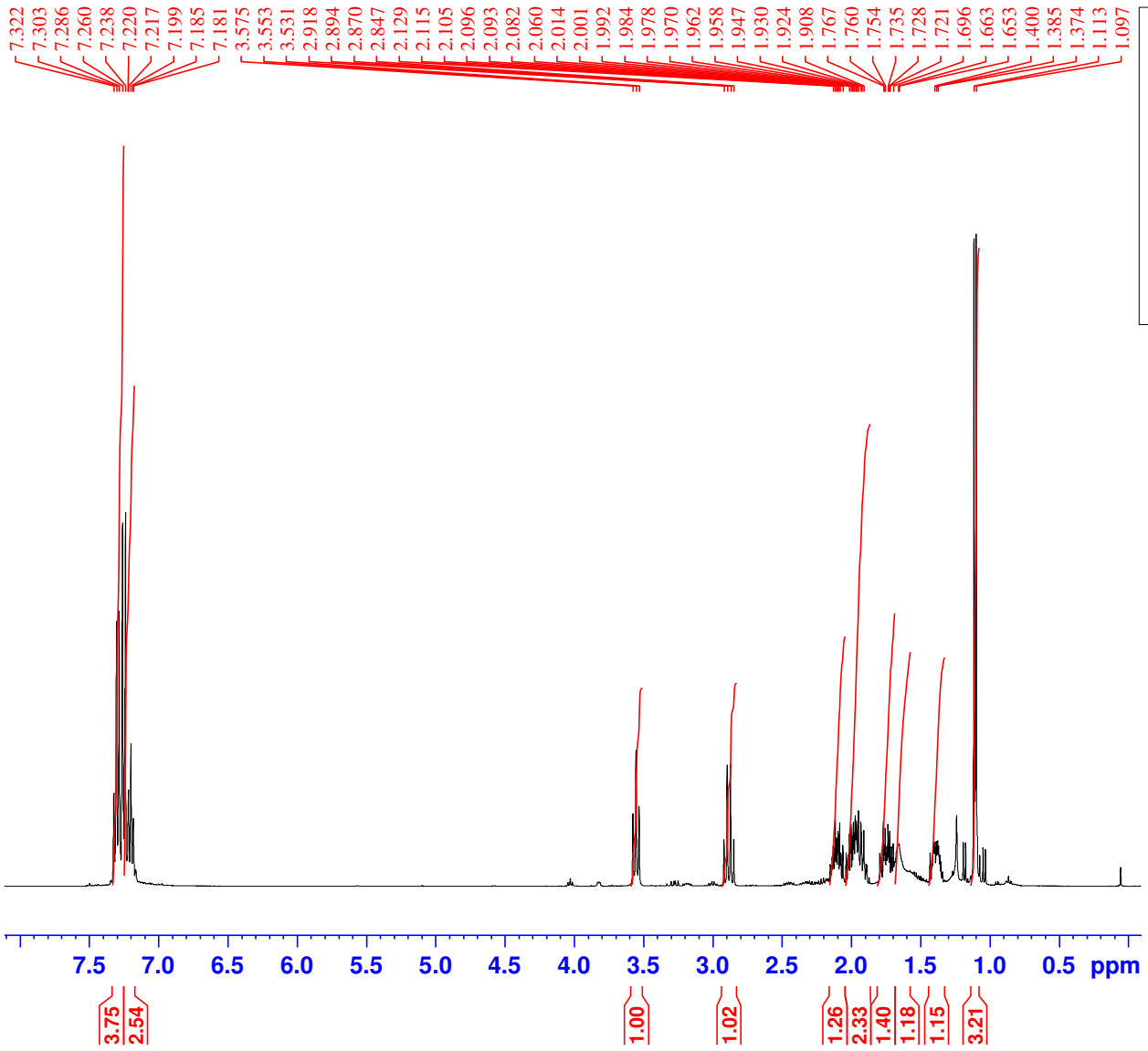

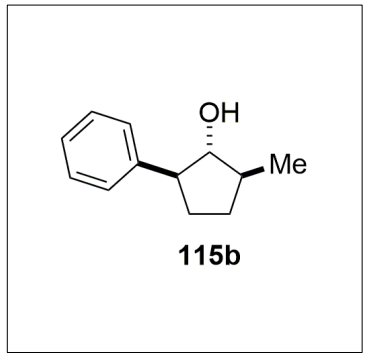


```
Current Data Parameters
NAME      KS-03-98-15-16
EXPNO                 10
PROCNO                 1

F2 - Acquisition Parameters
Date_           20220811
Time               14.13 h
INSTRUM       Avance Neo
PROBHD    Z152088_0031 (
PULPROG             zg30
TD                 65536
SOLVENT            CDCl3
NS                    16
DS                     2
SWH             8196.722 Hz
FIDRES          0.250144 Hz
AQ              3.9976959 sec
RG                   101
DW                61.000 usec
DE                13.89 usec
TE                298.0 K
D1             1.00000000 sec
TD0                    1
SFO1         400.1324708 MHz
NUC1                  1H
P0                 2.67 usec
P1                 8.00 usec
PLW1         24.03499985 W

F2 - Processing parameters
SI                 65536
SF           400.1300183 MHz
WDW                   EM
SSB       0
LB                 0.30 Hz
GB        0
PC                 1.00
```

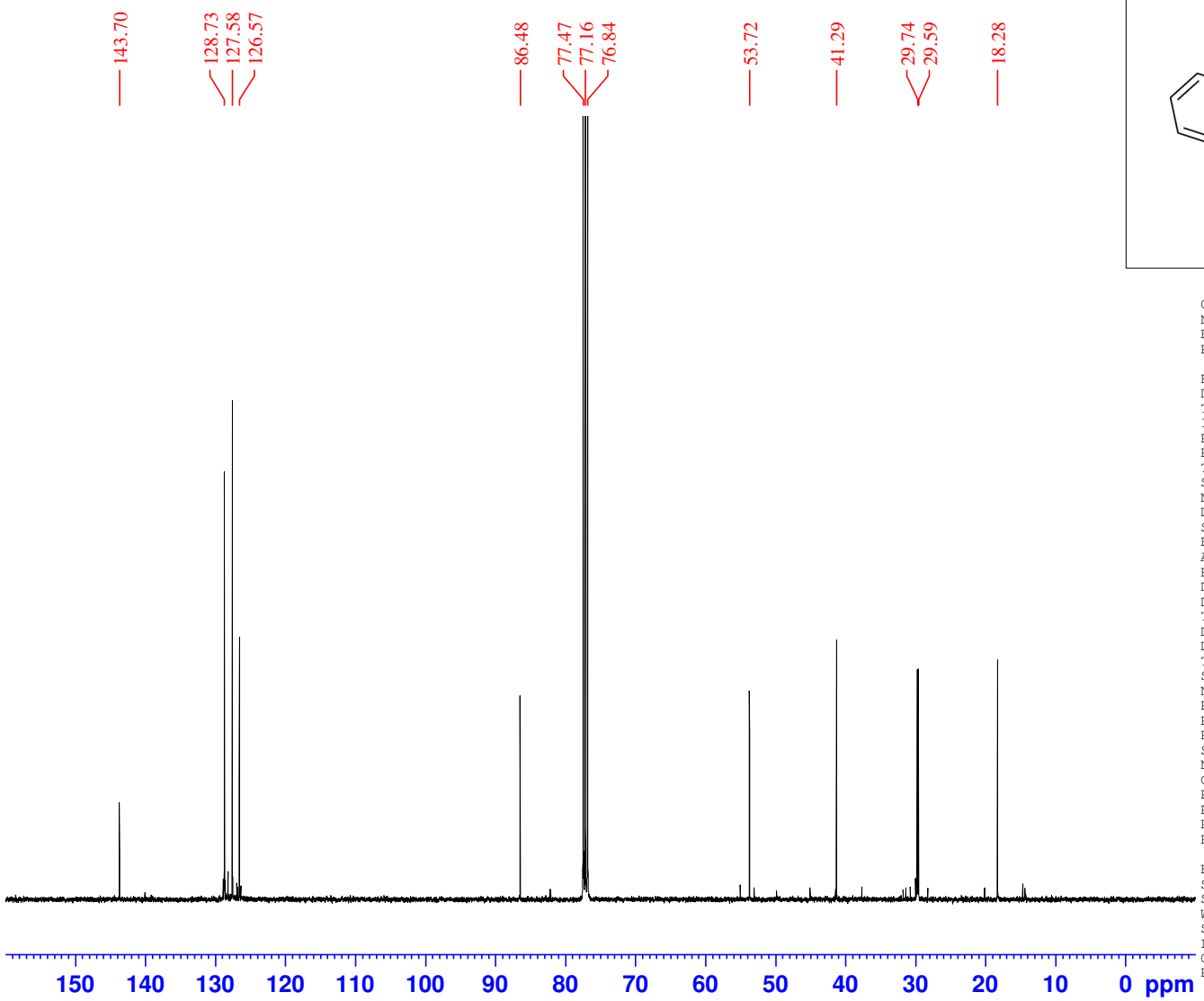

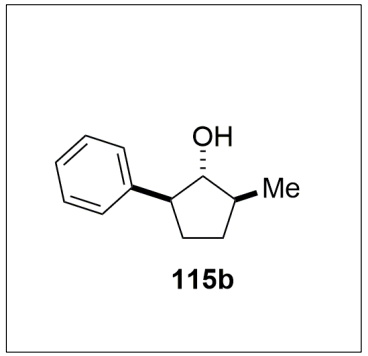


```
Current Data Parameters
NAME      KS-03-98-15-16
EXPNO                 11
PROCNO                 1

F2 - Acquisition Parameters
Date_           20220812
Time                2.21 h
INSTRUM       Avance Neo
PROBHD    Z152088_0031 (
PULPROG          zgpg30
TD                65536
SOLVENT           CDCl3
NS                 2048
DS                    4
SWH           23809.523 Hz
FIDRES         0.726609 Hz
AQ             1.3762560 sec
RG                8.125
DW               21.000 usec
DE                6.50 usec
TE               298.0 K
D1            2.00000000 sec
D11           0.03000000 sec
TD0                   1
SFO1         100.6228298 MHz
NUC1                13C
P0                 2.67 usec
P1                 8.00 usec
PLW1         86.55400085 W
SFO2         400.1316005 MHz
NUC2                1H
CPDPRG[2         waltz65
PCPD2             90.00 usec
PLW2         24.03499985 W
PLW12         0.18990999 W
PLW13         0.09552100 W

F2 - Processing parameters
SI                32768
SF           100.6127554 MHz
WDW                  EM
SSB       0
LB                1.00 Hz
GB        0
PC                1.40
```

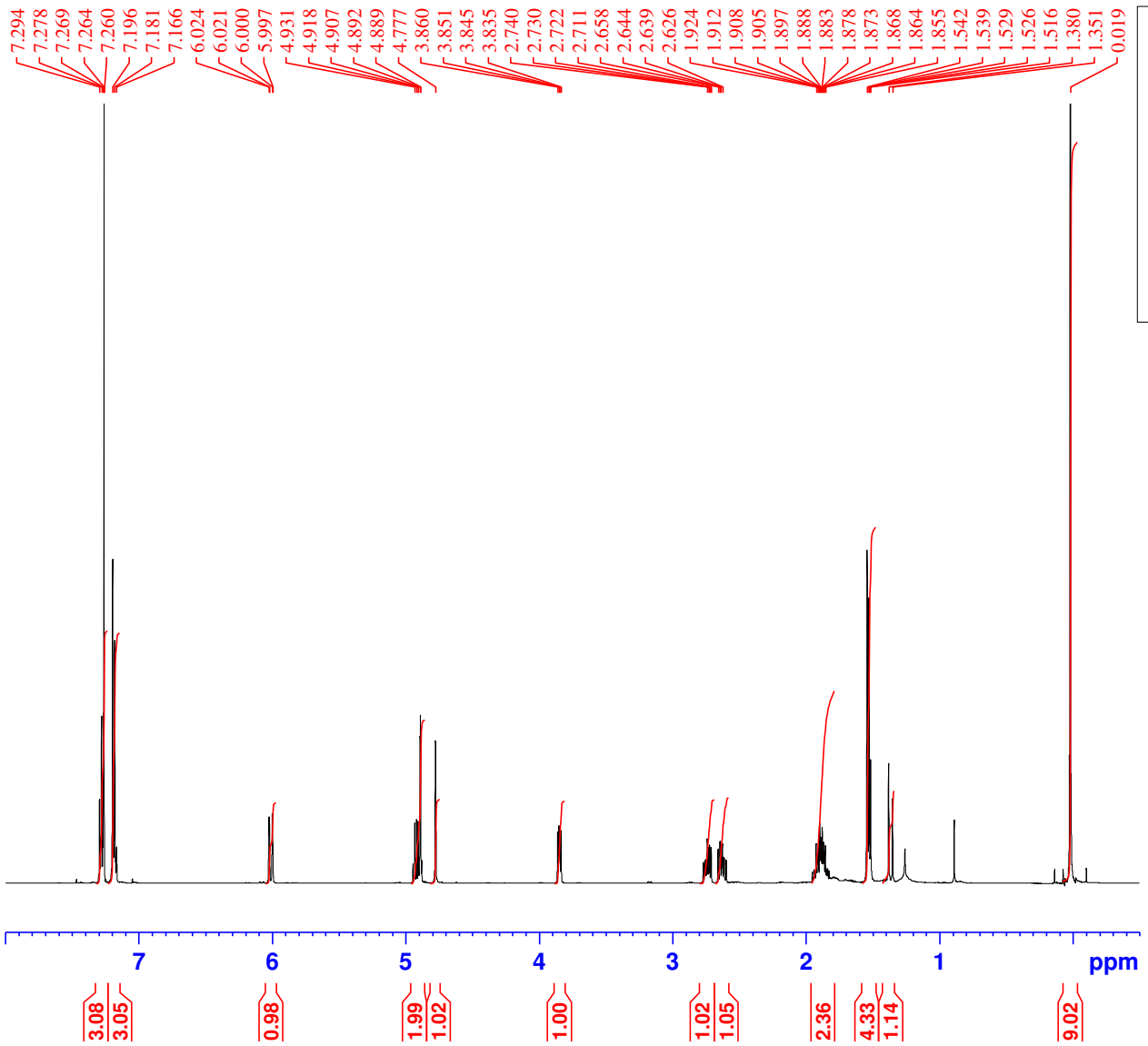

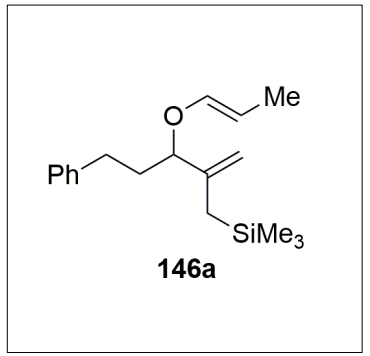

146a

```
Current Data Parameters
NAME       KS-03-103_500
EXPNO                 10
PROCNO                 1

F2 - Acquisition Parameters
Date_           20220820
Time              12.46 h
INSTRUM             spect
PROBHD   Z125869_0055 (
PULPROG             zg30
TD                 65536
SOLVENT            CDCl3
NS                    64
DS                     2
SWH           10000.000 Hz
FIDRES            0.305176 Hz
AQ             3.2767999 sec
RG                 107.7
DW                50.000 usec
DE                16.00 usec
TE                300.0 K
D1             2.00000000 sec
TD0                    1
SFO1         500.2330889 MHz
NUC1                  1H
P0                 4.00 usec
P1                12.00 usec
PLW1         11.44699955 W

F2 - Processing parameters
SI                 65536
SF           500.2300125 MHz
WDW                   EM
SSB       0
LB                 0.30 Hz
GB        0
PC                 1.00
```

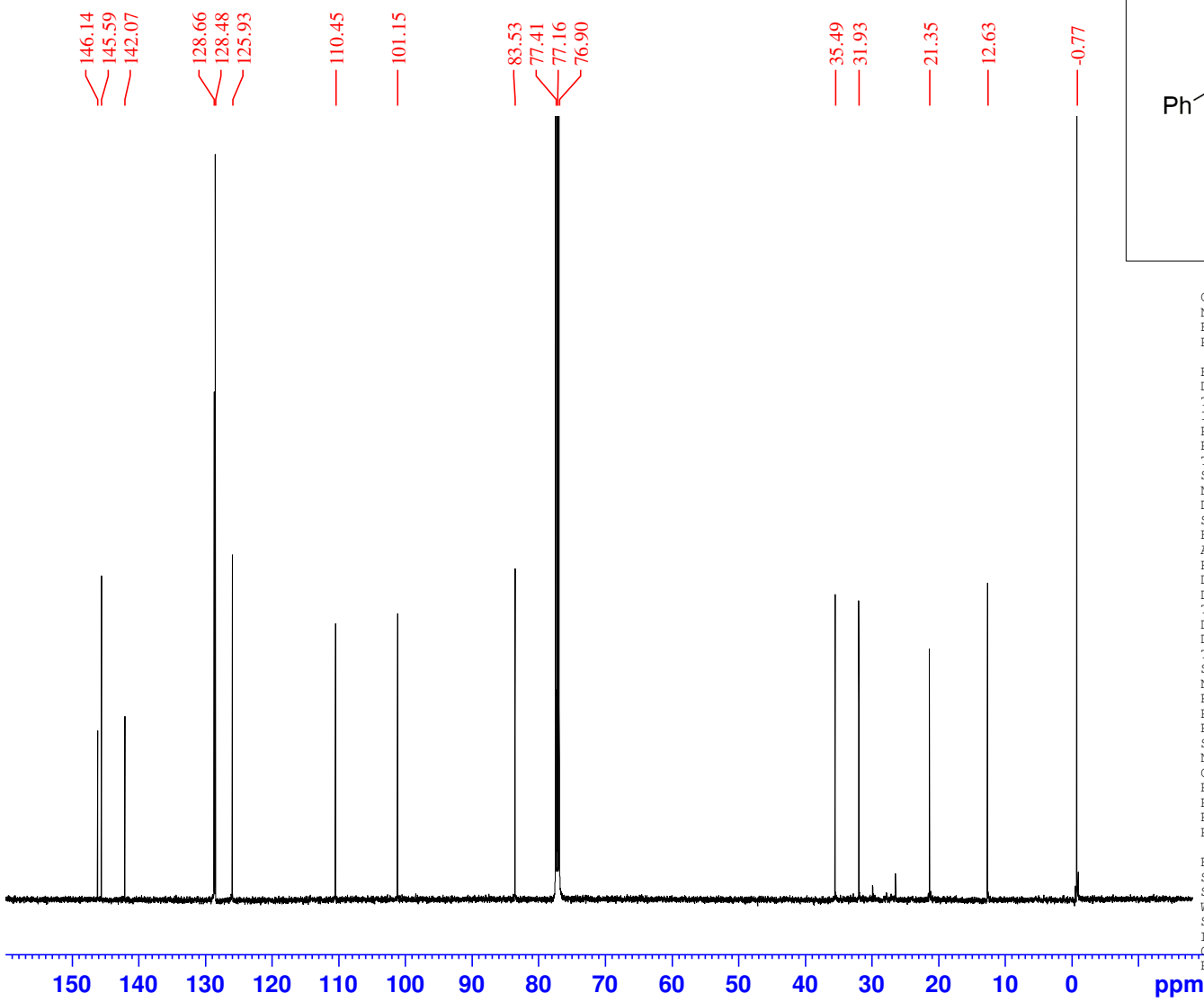

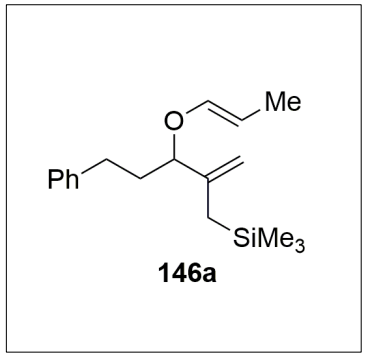

146a

```
Current Data Parameters
NAME       KS-03-103_500
EXPNO                 11
PROCNO                 1

F2 - Acquisition Parameters
Date_           20220820
Time               13.44 h
INSTRUM            spect
PROBHD    Z125869_0055 (
PULPROG          zgpg30
TD                65536
SOLVENT           CDCl3
NS                 1024
DS                    4
SWH           29761.904 Hz
FIDRES         0.908261 Hz
AQ             1.1010048 sec
RG                190.44
DW                16.800 usec
DE                18.00 usec
TE                300.0 K
D1             2.00000000 sec
D11            0.03000000 sec
TD0                   1
SFO1         125.7955118 MHz
NUC1                 13C
P0                 3.33 usec
P1                10.00 usec
PLW1         56.90299988 W
SFO2         500.2320009 MHz
NUC2                 1H
CPDPRG[2         waltz16
PCPD2             80.00 usec
PLW2         11.44699955 W
PLW12         0.25756001 W
PLW13         0.12955000 W

F2 - Processing parameters
SI                32768
SF           125.7829163 MHz
WDW                  EM
SSB       0
LB                1.00 Hz
GB        0
PC                1.40
```

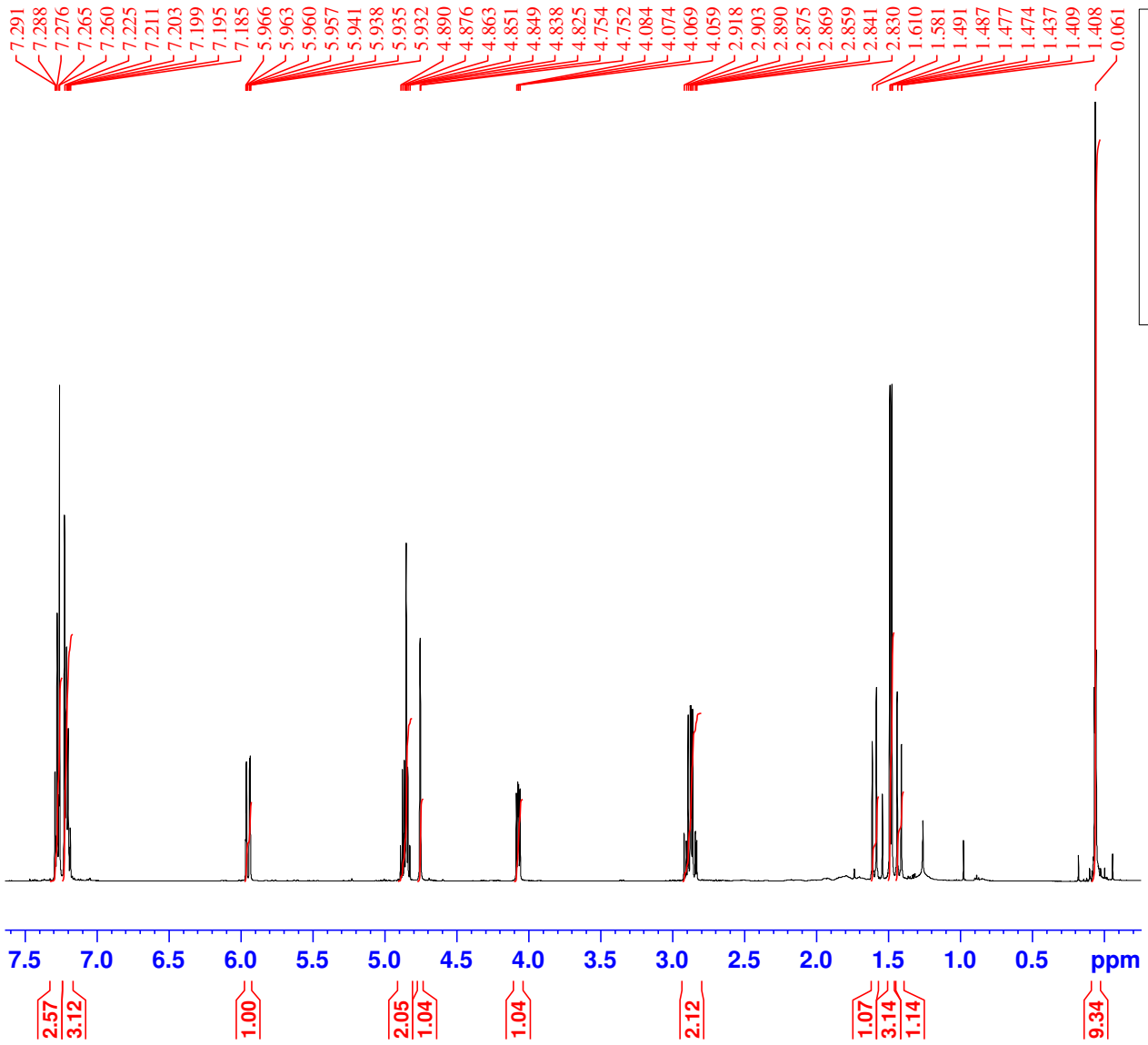

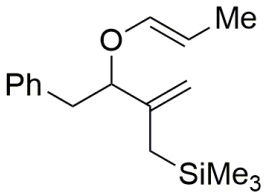

146b

```
Current Data Parameters
NAME            KS-03-56
EXPNO                 10
PROCNO                 1

F2 - Acquisition Parameters
Date_           20220629
Time              16.31 h
INSTRUM             spect
PROBHD    Z125869_0055 (
PULPROG             zg30
TD                 65536
SOLVENT            CDCl3
NS                    64
DS                     2
SWH           10000.000 Hz
FIDRES            0.305176 Hz
AQ             3.2767999 sec
RG                 53.13
DW                50.000 usec
DE                16.00 usec
TE                300.0 K
D1             2.00000000 sec
TD0                    1
SFO1         500.2330889 MHz
NUC1                  1H
P0                 4.00 usec
P1                12.00 usec
PLW1         11.44699955 W

F2 - Processing parameters
SI                 65536
SF           500.2300125 MHz
WDW                   EM
SSB       0
LB                 0.30 Hz
GB        0
PC                 1.00
```

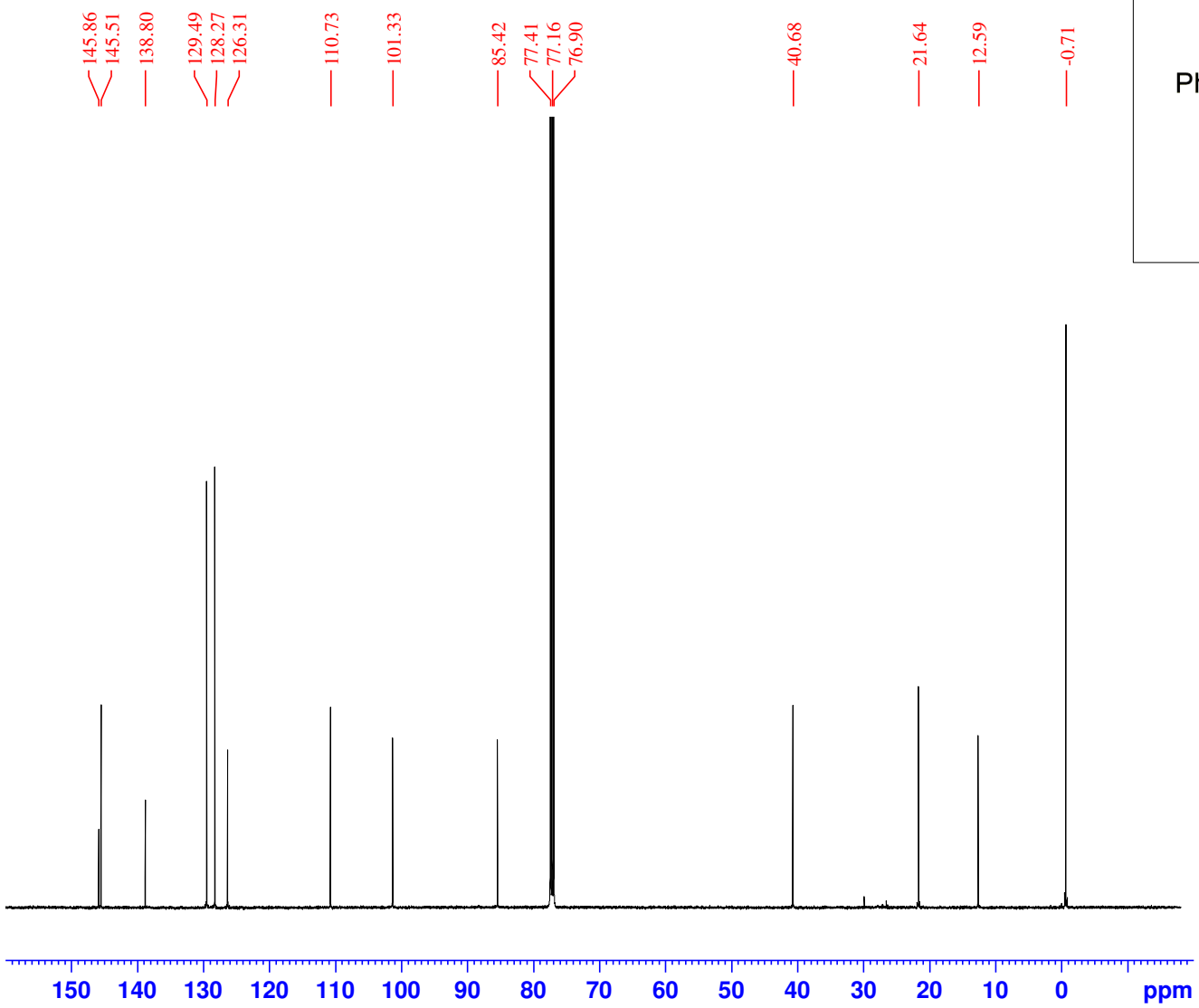

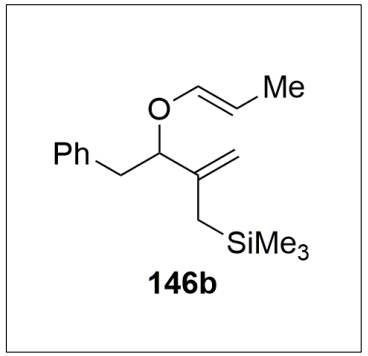

146b

```
Current Data Parameters
NAME            KS-03-56
EXPNO                 11
PROCNO                 1

F2 - Acquisition Parameters
Date_           20220629
Time              17.27 h
INSTRUM             spect
PROBHD    Z125869_0055 (
PULPROG           zgpg30
TD                 65536
SOLVENT            CDCl3
NS                  1024
DS                     4
SWH           29761.904 Hz
FIDRES         0.908261 Hz
AQ            1.1010048 sec
RG               190.44
DW               16.800 usec
DE               18.00 usec
TE               300.0 K
D1            2.00000000 sec
D11           0.03000000 sec
TD0                    1
SFO1         125.7955118 MHz
NUC1                13C
P0                3.33 usec
P1               10.00 usec
PLW1         56.90299988 W
SFO2         500.2320009 MHz
NUC2                1H
CPDPRG[2         waltz16
PCPD2            80.00 usec
PLW2         11.44699955 W
PLW12         0.25756001 W
PLW13         0.12955000 W

F2 - Processing parameters
SI                 32768
SF           125.7829163 MHz
WDW                   EM
SSB       0
LB                1.00 Hz
GB        0
PC                1.40
```

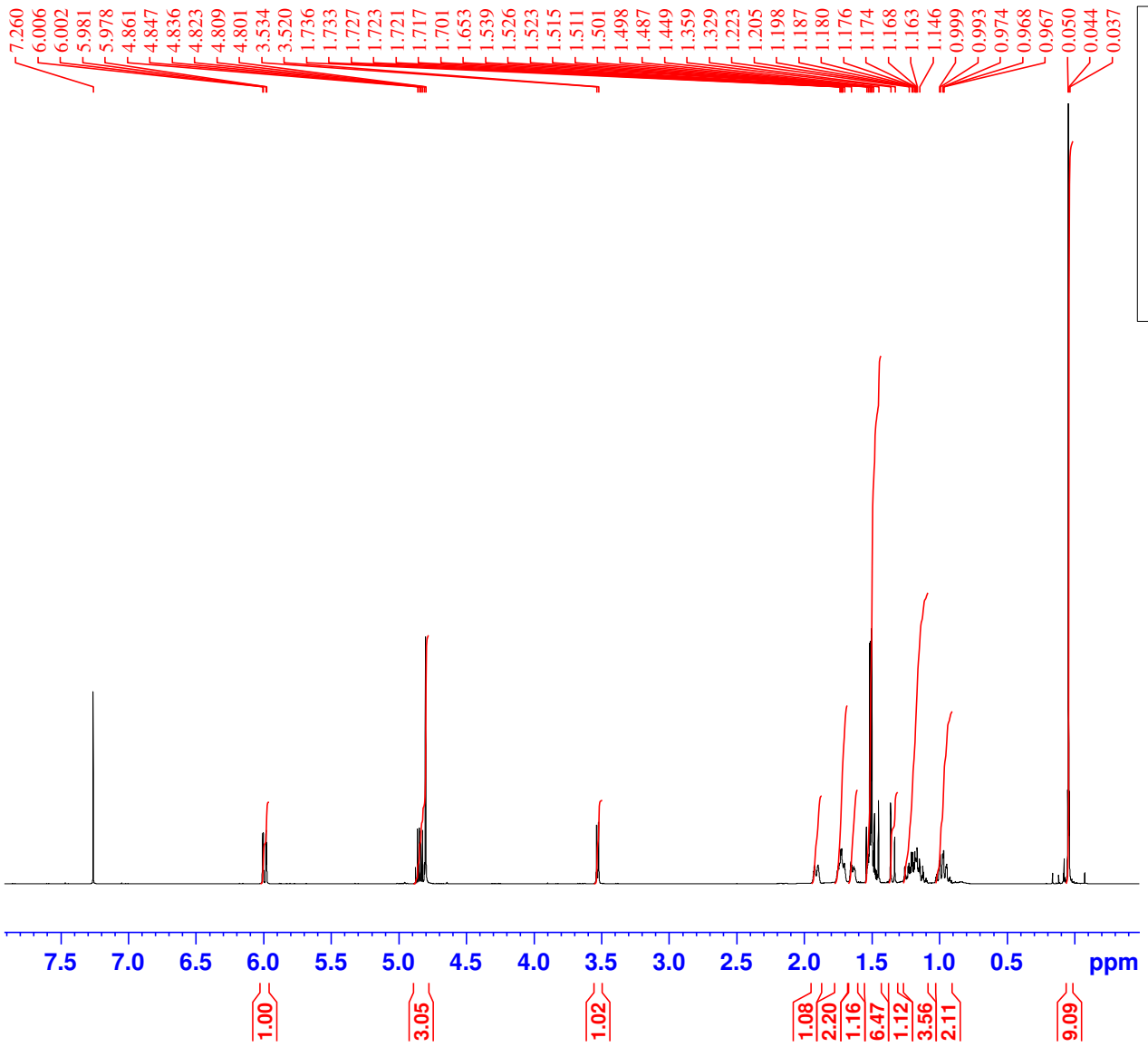

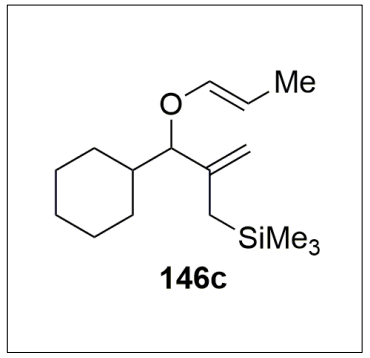

146c

```
Current Data Parameters
NAME            KS-03-70
EXPNO                 11
PROCNO                 1

F2 - Acquisition Parameters
Date_           20220711
Time              16.21 h
INSTRUM             spect
PROBHD   Z125869_0055 (
PULPROG             zg30
TD                 65536
SOLVENT            CDCl3
NS                    64
DS                     2
SWH           10000.000 Hz
FIDRES            0.305176 Hz
AQ                3.2767999 sec
RG                   53.13
DW                  50.000 usec
DE                  16.00 usec
TE                  300.0 K
D1              2.00000000 sec
TD0                    1
SFO1          500.2330889 MHz
NUC1                  1H
P0                  4.00 usec
P1                 12.00 usec
PLW1          11.44699955 W

F2 - Processing parameters
SI                 65536
SF            500.2300122 MHz
WDW                   EM
SSB       0
LB                 0.30 Hz
GB        0
PC                 1.00
```

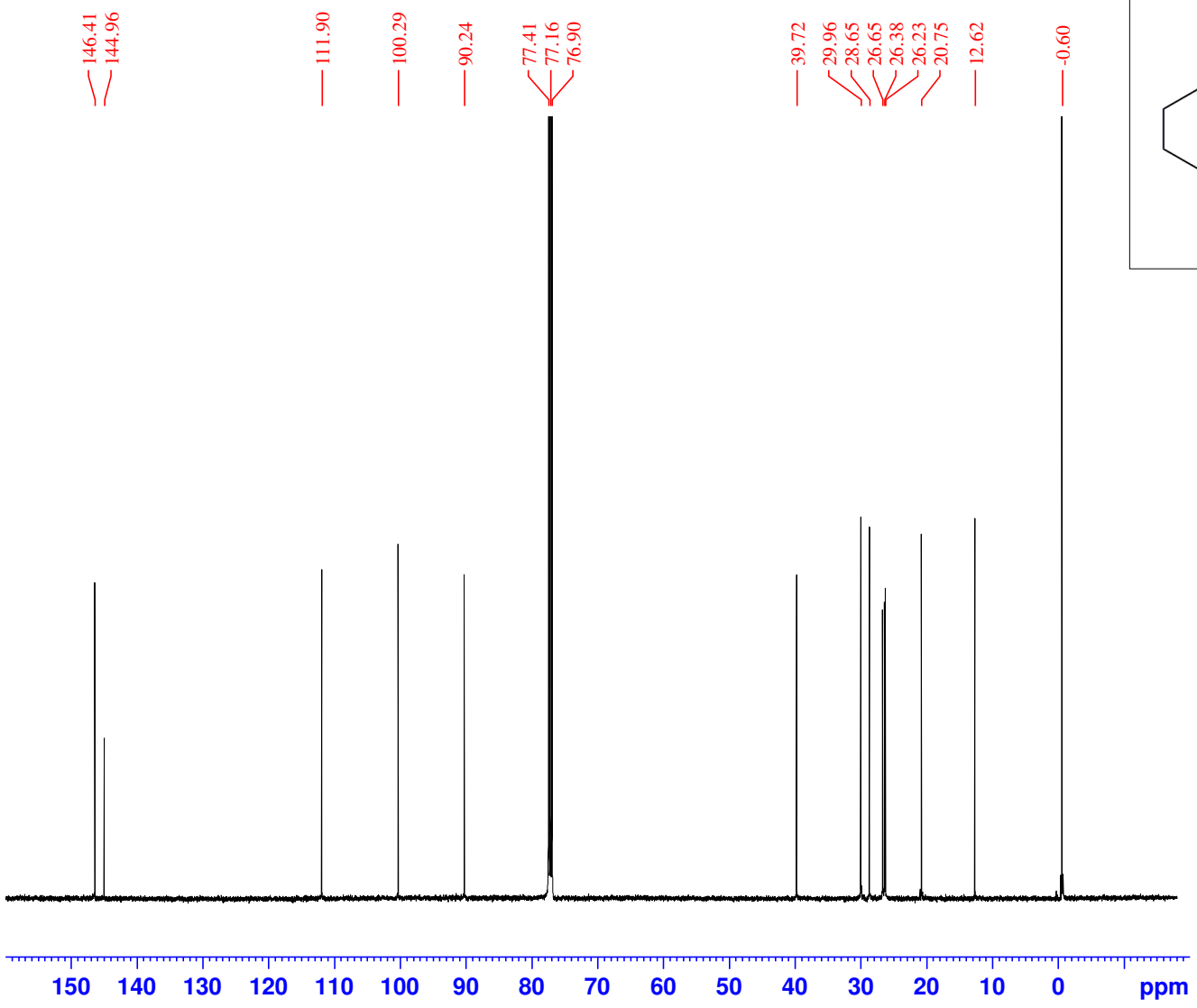

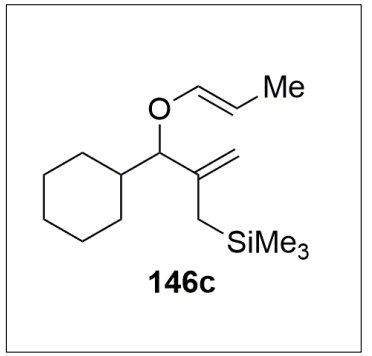

146c

```
Current Data Parameters
NAME                  KS-03-70
EXPNO                       12
PROCNO                       1

F2 - Acquisition Parameters
Date_                 20220711
Time                     17.17 h
INSTRUM                  spect
PROBHD    Z125869_0055 (
PULPROG                 zgpg30
TD                       65536
SOLVENT                  CDCl3
NS                        1024
DS                           4
SWH                  29761.904 Hz
FIDRES                0.908261 Hz
AQ                    1.1010048 sec
RG                       190.44
DW                       16.800 usec
DE                       18.00 usec
TE                       300.0 K
D1                    2.00000000 sec
D11                   0.03000000 sec
TD0                          1
SFO1                125.7955118 MHz
NUC1                        13C
P0                        3.33 usec
P1                       10.00 usec
PLW1                56.90299988 W
SFO2                500.2320009 MHz
NUC2                        1H
CPDPRG[2                waltz16
PCPD2                    80.00 usec
PLW2                11.44699955 W
PLW12                0.25756001 W
PLW13                0.12955000 W

F2 - Processing parameters
SI                       32768
SF                  125.7829154 MHz
WDW                         EM
SSB       0
LB                       1.00 Hz
GB        0
PC                       1.40
```

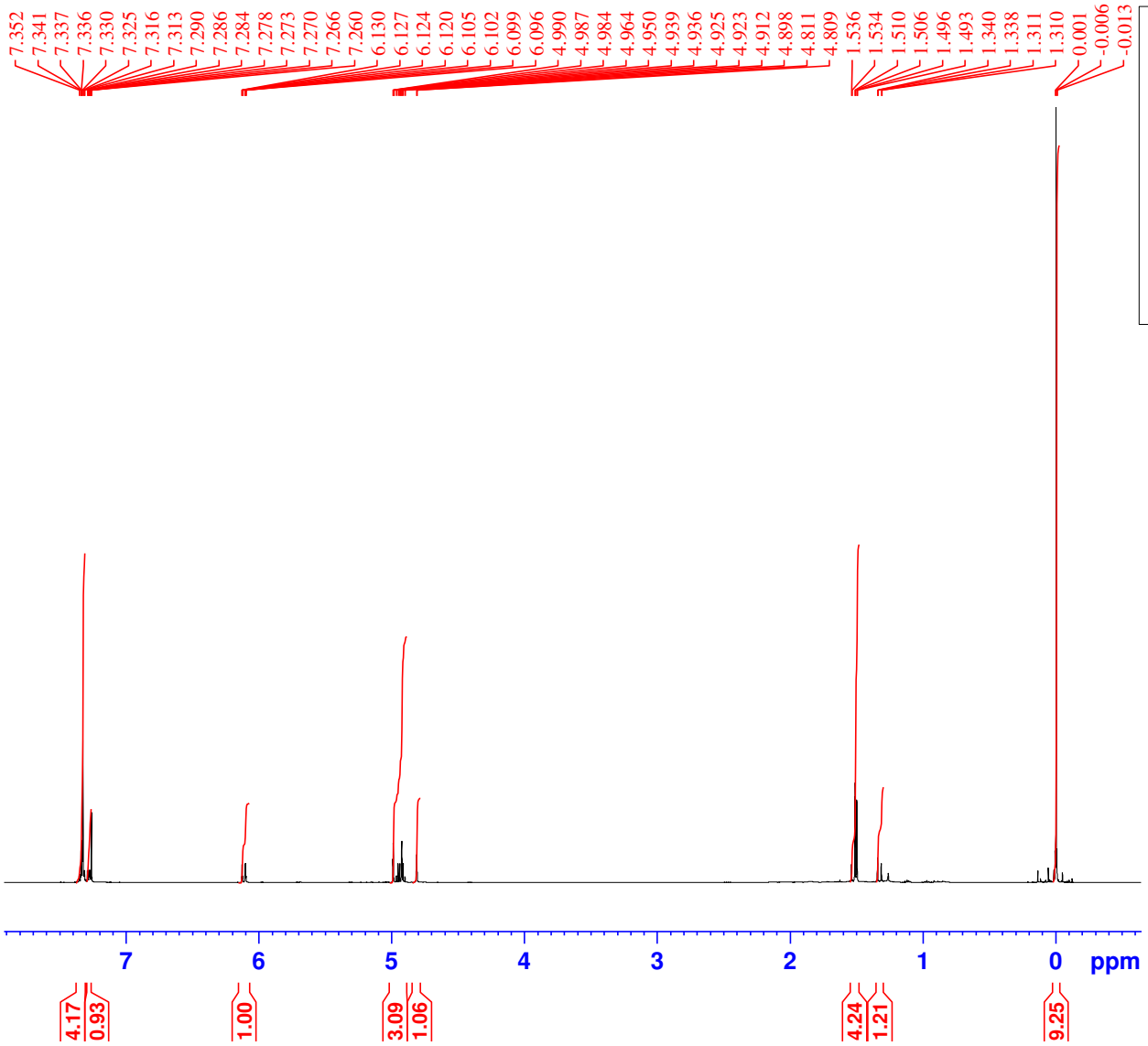

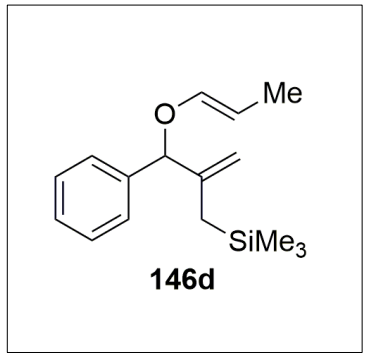

146d

```
Current Data Parameters
NAME         KS-03-31_Ph
EXPNO                 13
PROCNO                 1

F2 - Acquisition Parameters
Date_           20220613
Time              16.27 h
INSTRUM             spect
PROBHD    Z125869_0055 (
PULPROG             zg30
TD                 65536
SOLVENT            CDCl3
NS                    64
DS                     2
SWH           10000.000 Hz
FIDRES            0.305176 Hz
AQ             3.2767999 sec
RG                 86.13
DW                50.000 usec
DE                16.00 usec
TE                298.0 K
D1             2.00000000 sec
TD0                    1
SFO1          500.2330889 MHz
NUC1                  1H
P0                 4.00 usec
P1                12.00 usec
PLW1          11.44699955 W

F2 - Processing parameters
SI                 65536
SF            500.2300120 MHz
WDW                   EM
SSB       0
LB                 0.30 Hz
GB        0
PC                 1.00
```

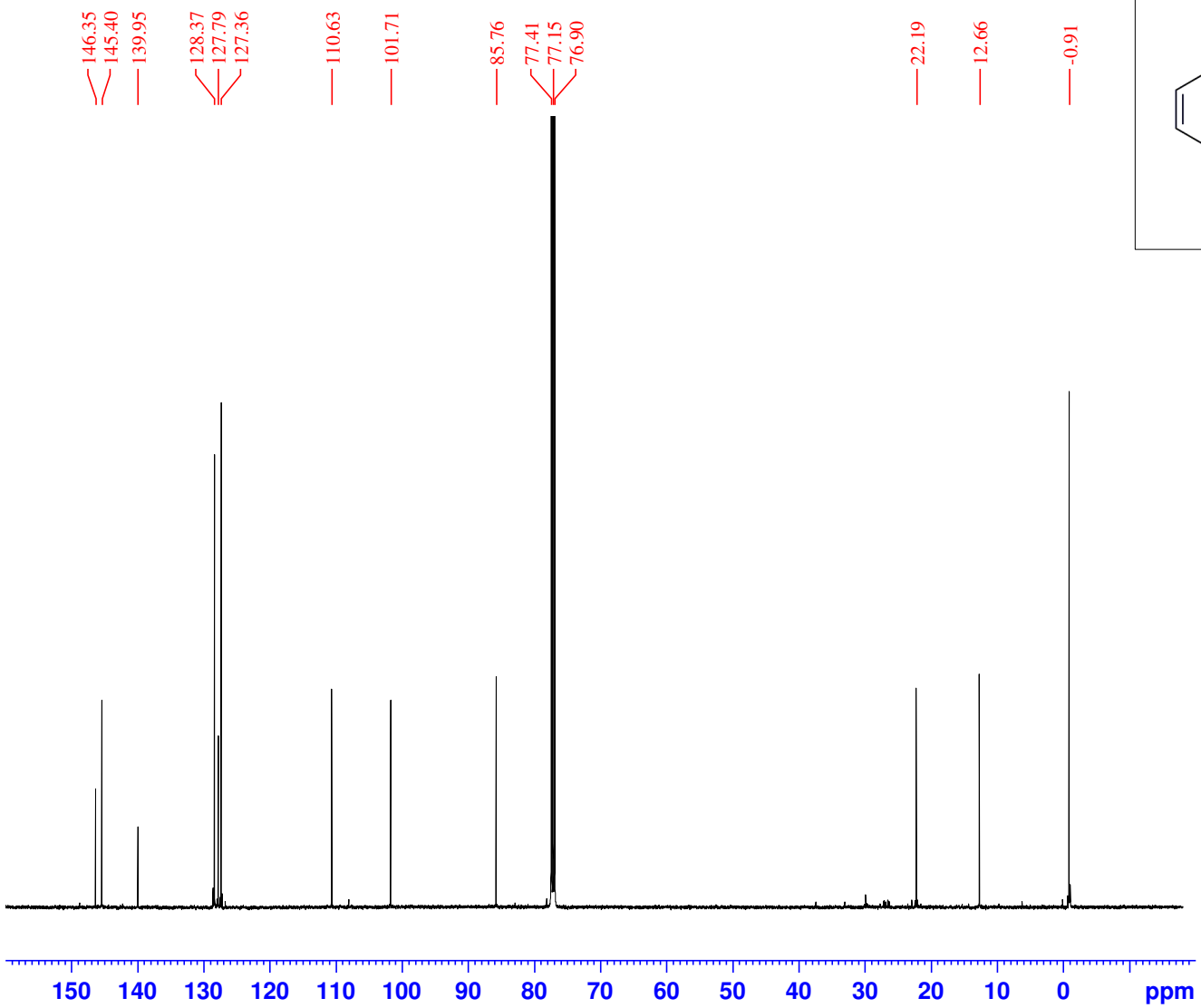

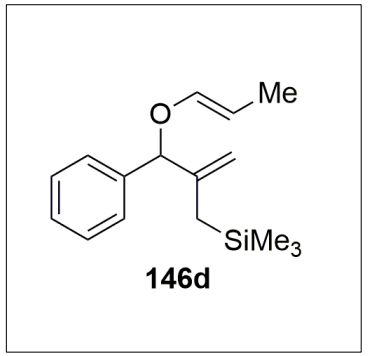

146d

```
Current Data Parameters
NAME         KS-03-31_Ph
EXPNO                 14
PROCNO                 1

F2 - Acquisition Parameters
Date_           20220613
Time              17.51 h
INSTRUM             spect
PROBHD    Z125869_0055 (
PULPROG           zgpg30
TD                65536
SOLVENT           CDCl3
NS                 1024
DS                    4
SWH           29761.904 Hz
FIDRES         0.908261 Hz
AQ             1.1010048 sec
RG                190.44
DW                16.800 usec
DE                18.00 usec
TE                298.0 K
D1             2.00000000 sec
D11            0.03000000 sec
TD0                   1
SFO1          125.7955118 MHz
NUC1                 13C
P0                 3.33 usec
P1                10.00 usec
PLW1          56.90299988 W
SFO2          500.2320009 MHz
NUC2                 1H
CPDPRG[2          waltz16
PCPD2             80.00 usec
PLW2          11.44699955 W
PLW12          0.25756001 W
PLW13          0.12955000 W

F2 - Processing parameters
SI                32768
SF            125.7829164 MHz
WDW                  EM
SSB       0
LB                1.00 Hz
GB        0
PC                1.40
```

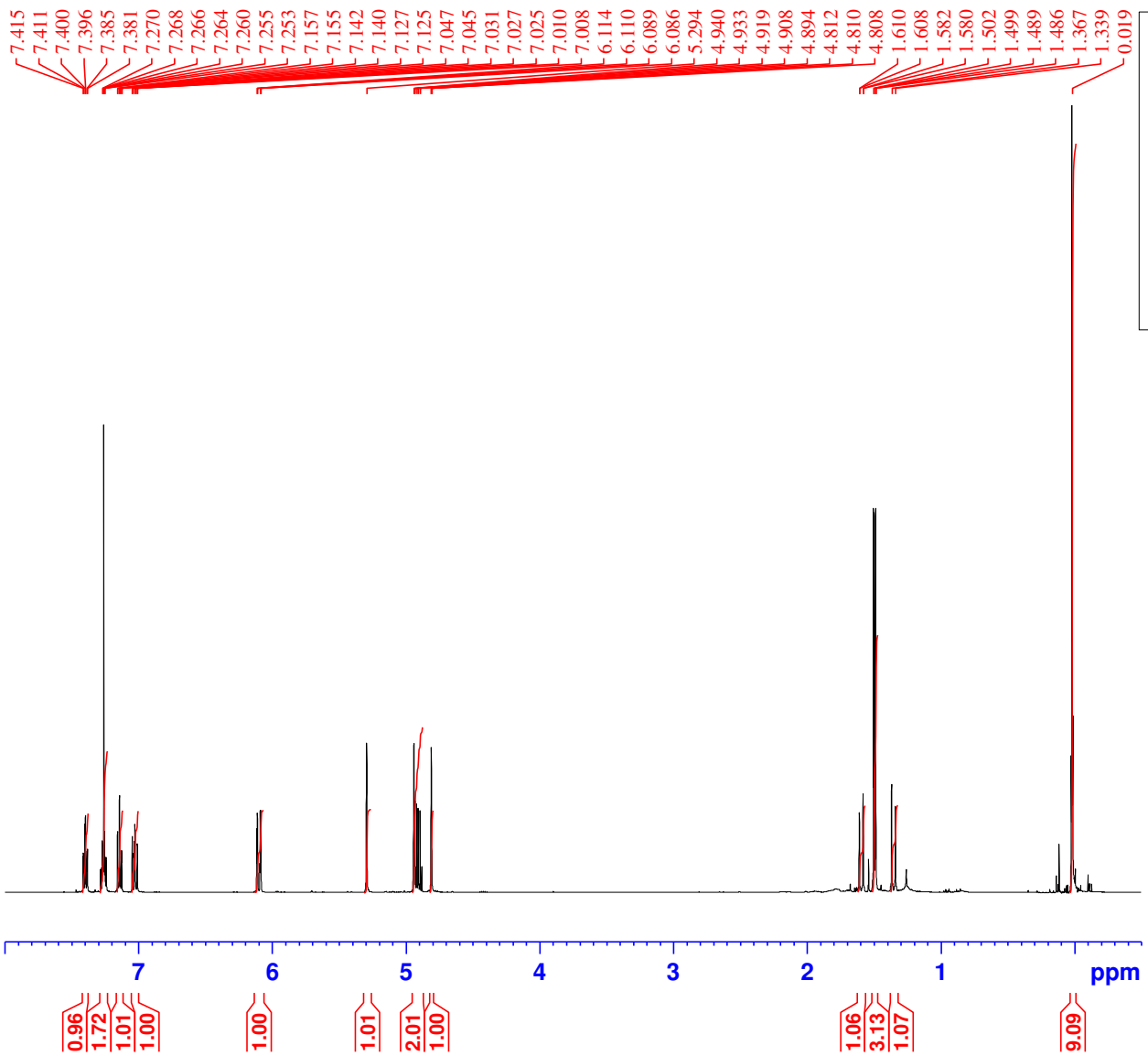

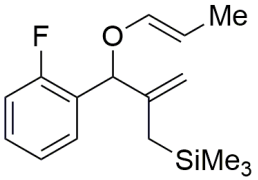

146e

```
Current Data Parameters
NAME       KS-03-104_500
EXPNO                 10
PROCNO                 1

F2 - Acquisition Parameters
Date_           20220820
Time               13.55 h
INSTRUM             spect
PROBHD    Z125869_0055 (
PULPROG             zg30
TD                 65536
SOLVENT            CDCl3
NS                    64
DS                     2
SWH            10000.000 Hz
FIDRES             0.305176 Hz
AQ             3.2767999 sec
RG                 94.51
DW                 50.000 usec
DE                 16.00 usec
TE                 300.0 K
D1              2.00000000 sec
TD0                    1
SFO1          500.2330889 MHz
NUC1                  1H
P0                  4.00 usec
P1                 12.00 usec
PLW1          11.44699955 W

F2 - Processing parameters
SI                 65536
SF            500.2300125 MHz
WDW                   EM
SSB       0
LB                  0.30 Hz
GB        0
PC                  1.00
```

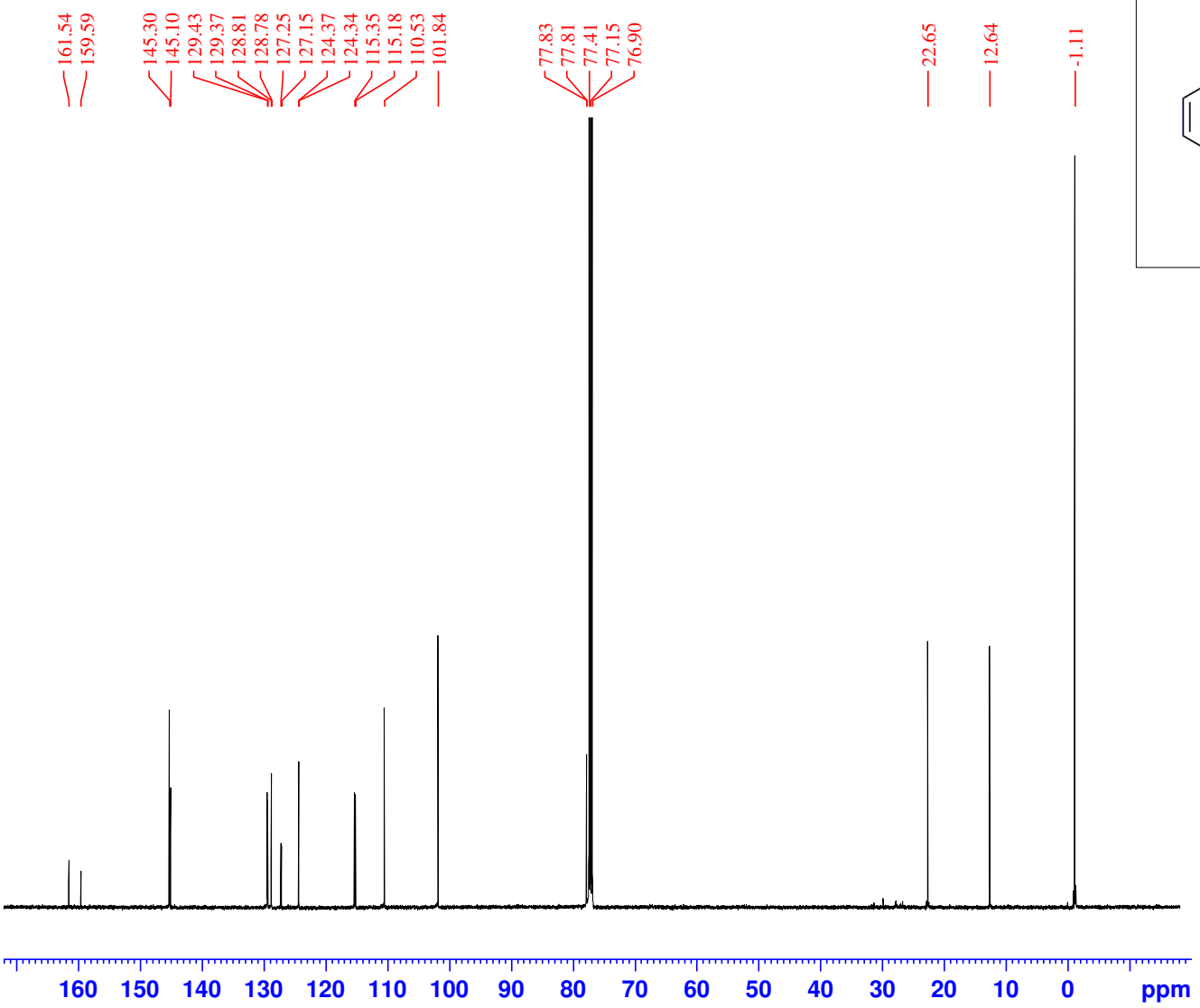

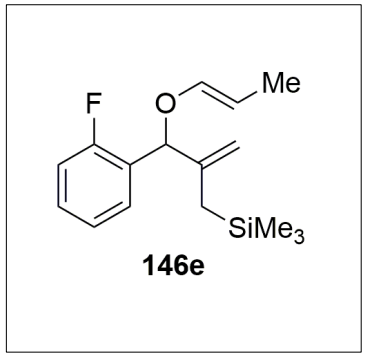

146e

```
Current Data Parameters
NAME       KS-03-104_500
EXPNO                 12
PROCNO                 1

F2 - Acquisition Parameters
Date_           20220820
Time              14.55 h
INSTRUM             spect
PROBHD   Z125869_0055 (
PULPROG           zgpg30
TD                65536
SOLVENT           CDCl3
NS                 1024
DS                    4
SWH           29761.904 Hz
FIDRES         0.908261 Hz
AQ             1.1010048 sec
RG               190.44
DW               16.800 usec
DE               18.00 usec
TE               300.0 K
D1            2.00000000 sec
D11           0.03000000 sec
TD0                   1
SFO1         125.7955118 MHz
NUC1                 13C
P0                3.33 usec
P1               10.00 usec
PLW1         56.90299988 W
SFO2         500.2320009 MHz
NUC2                 1H
CPDPRG[2         waltz16
PCPD2            80.00 usec
PLW2         11.44699955 W
PLW12         0.25756001 W
PLW13         0.12955000 W

F2 - Processing parameters
SI                32768
SF           125.7829164 MHz
WDW                  EM
SSB       0
LB                1.00 Hz
GB        0
PC                1.40
```

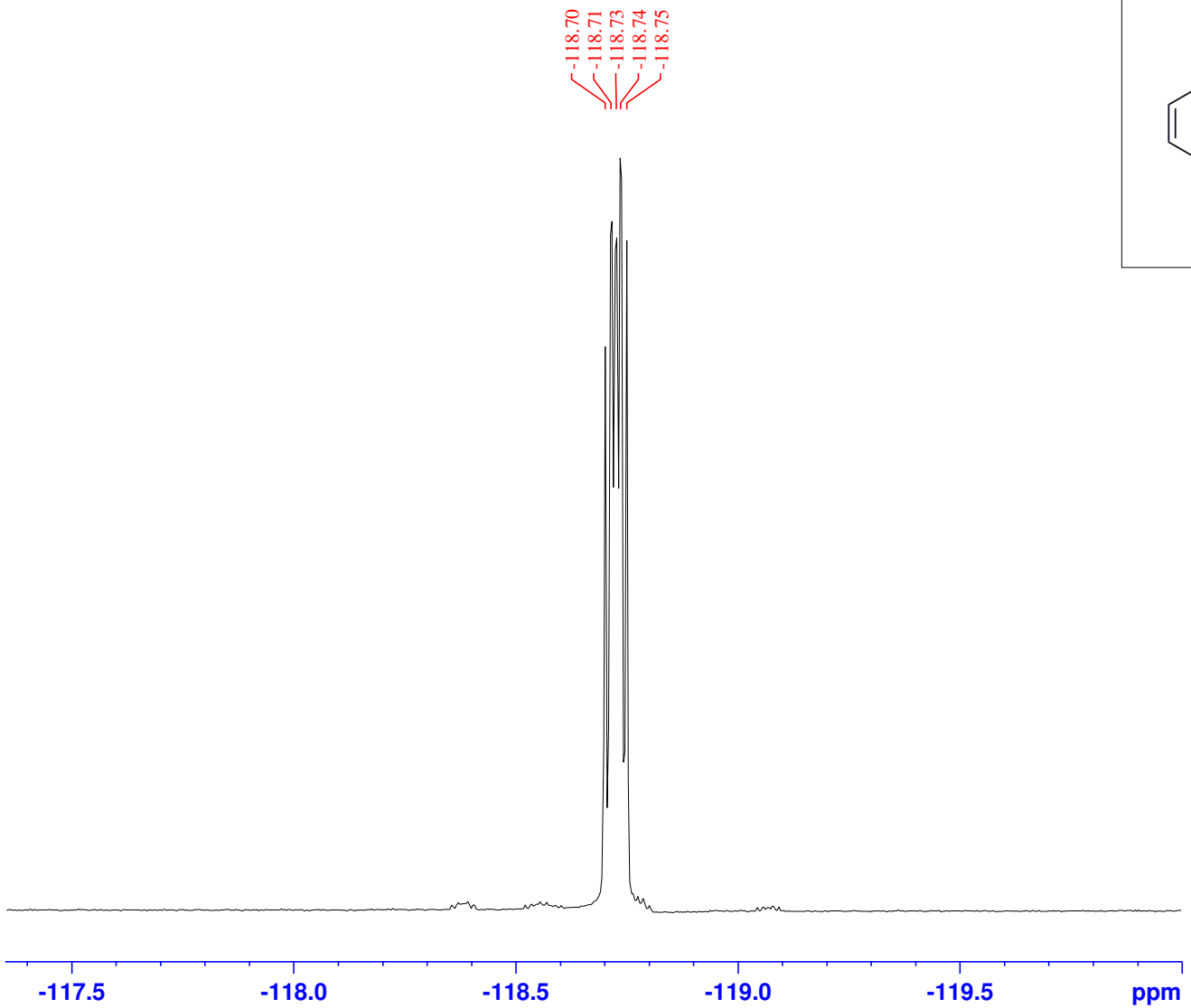

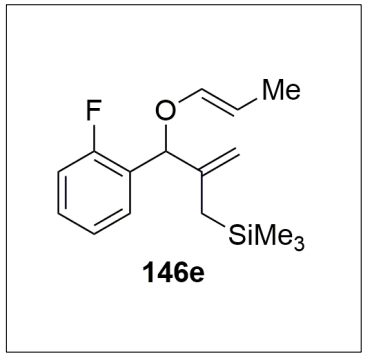

146e

```
Current Data Parameters
NAME       KS-03-104_500
EXPNO                 11
PROCNO                 1

F2 - Acquisition Parameters
Date_           20220820
Time              13.58 h
INSTRUM            spect
PROBHD    Z125869_0055 (
PULPROG           zgflqn
TD                131072
SOLVENT             CDCl3
NS                     16
DS                      4
SWH           113636.367 Hz
FIDRES          1.733953 Hz
AQ              0.5767168 sec
RG                 14.14
DW                 4.400 usec
DE                18.00 usec
TE                300.0 K
D1             1.00000000 sec
TD0                    1
SFO1         470.6394024 MHz
NUC1                19F
P1                 15.00 usec
PLW1         11.70800018 W

F2 - Processing parameters
SI                 65536
SF           470.6864710 MHz
WDW                   EM
SSB       0
LB                 0.30 Hz
GB        0
PC                 1.00
```

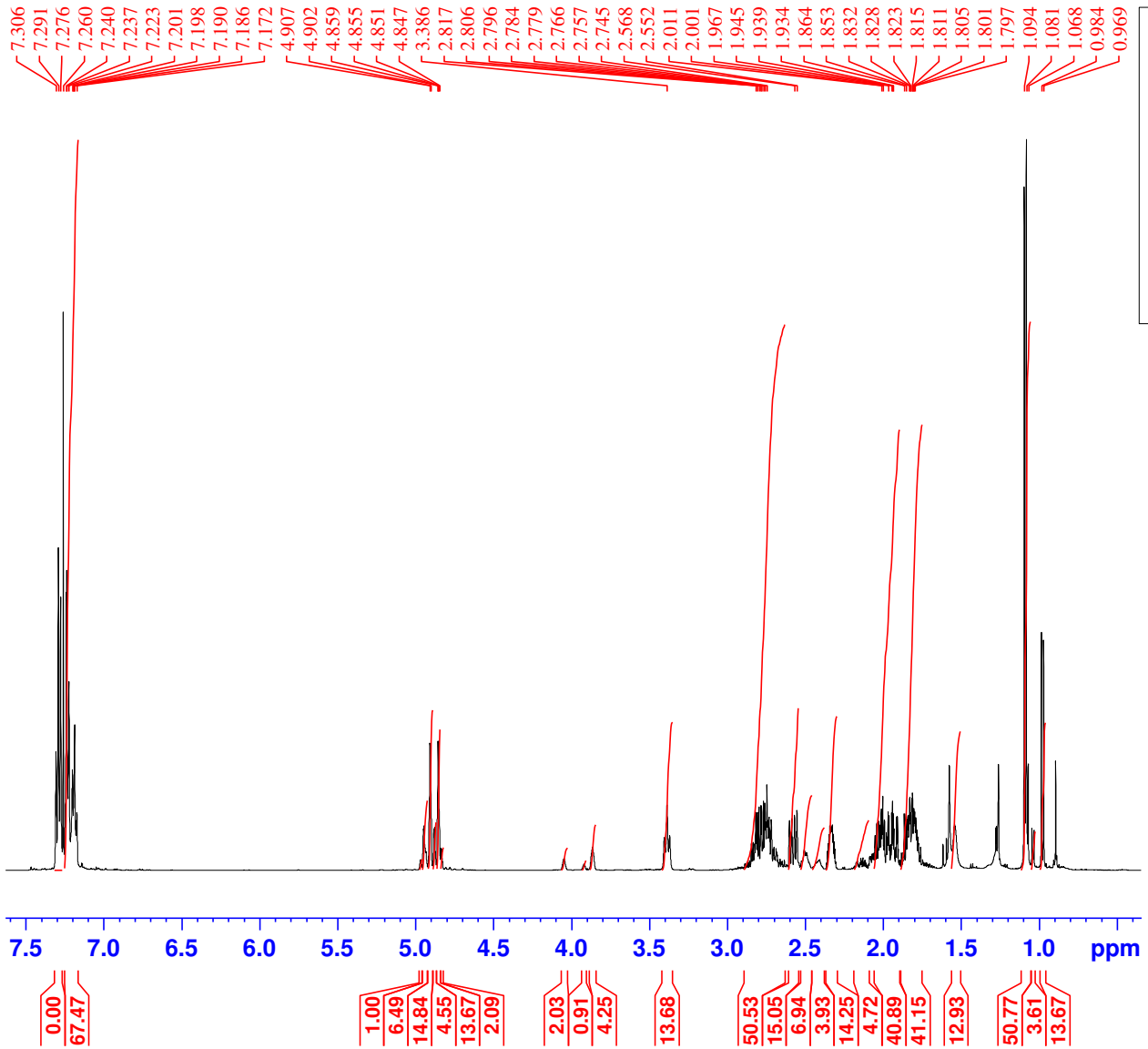

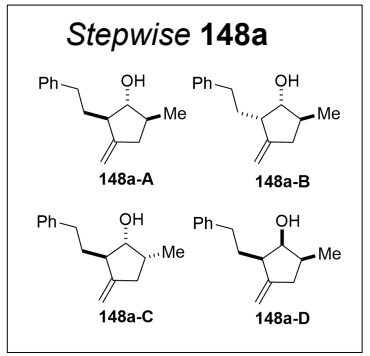


```
Current Data Parameters
NAME      KS-03-107col_500_CH2CH2Ph
EXPNO                 10
PROCNO                 1

F2 - Acquisition Parameters
Date_           20220823
Time              15.00 h
INSTRUM             spect
PROBHD   Z125869_0055 (
PULPROG             zg30
TD                 65536
SOLVENT            CDCl3
NS                    64
DS                     2
SWH           10000.000 Hz
FIDRES            0.305176 Hz
AQ             3.2767999 sec
RG                 53.13
DW                50.000 usec
DE                16.00 usec
TE                300.0 K
D1             2.00000000 sec
TD0                    1
SFO1         500.2330889 MHz
NUC1                  1H
P0                 4.00 usec
P1                12.00 usec
PLW1         11.44699955 W

F2 - Processing parameters
SI                 65536
SF           500.2300123 MHz
WDW                   EM
SSB       0
LB                 0.30 Hz
GB        0
PC                 1.00
```

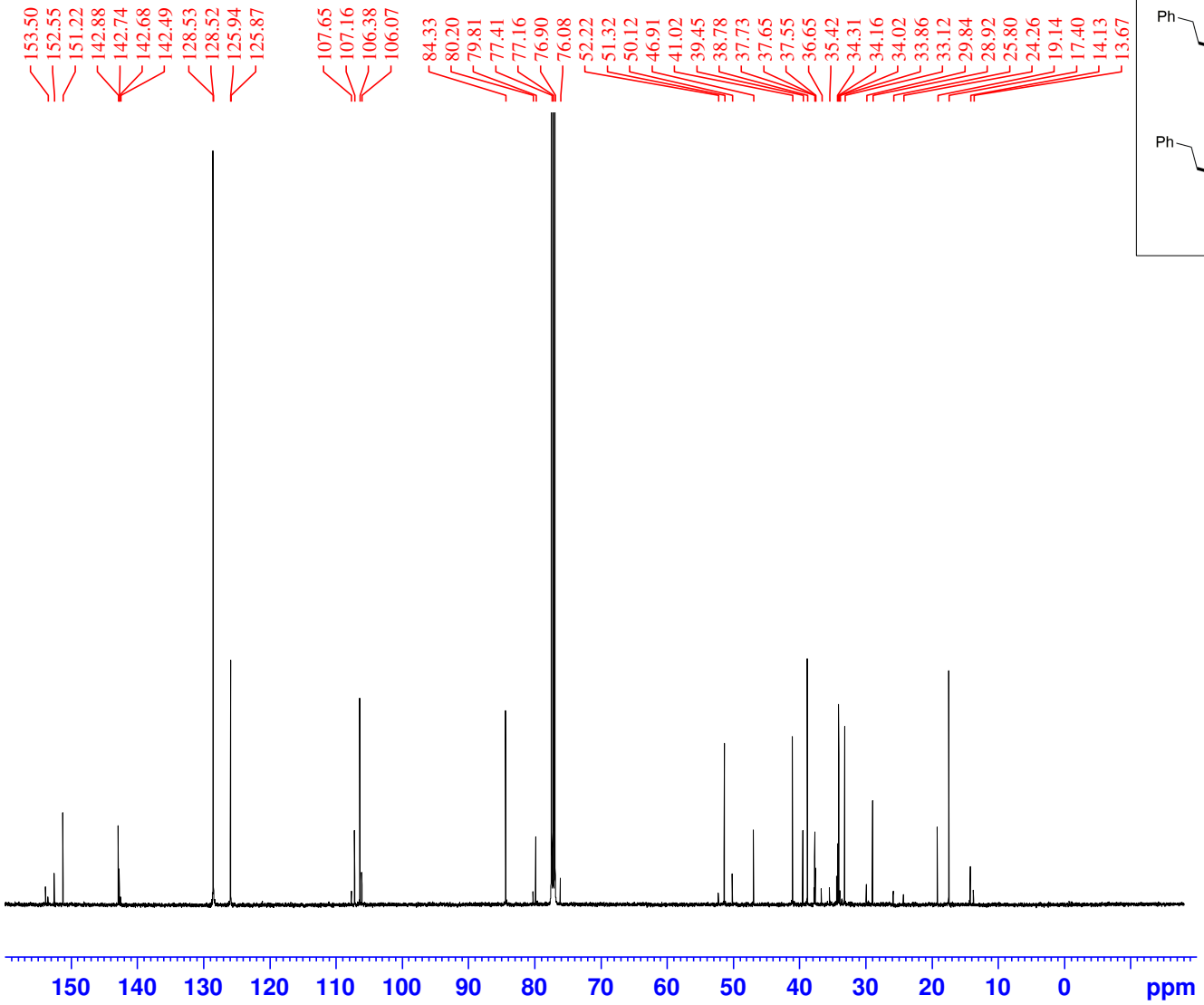

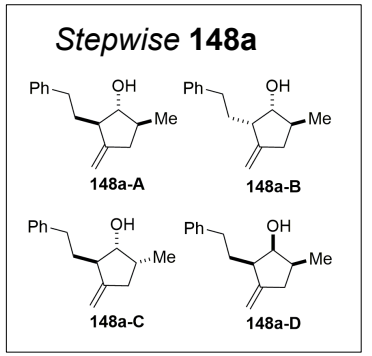


```
Current Data Parameters
NAME      KS-03-107col_500_CH2CH2Ph
EXPNO                 11
PROCNO                 1

F2 - Acquisition Parameters
Date_           20220823
Time              15.58 h
INSTRUM             spect
PROBHD   Z125869_0055 (
PULPROG           zgpg30
TD                65536
SOLVENT           CDCl3
NS                 1024
DS                    4
SWH           29761.904 Hz
FIDRES         0.908261 Hz
AQ            1.1010048 sec
RG               190.44
DW               16.800 usec
DE               18.00 usec
TE               300.0 K
D1           2.00000000 sec
D11          0.03000000 sec
TD0                   1
SFO1        125.7955118 MHz
NUC1                13C
P0                3.33 usec
P1               10.00 usec
PLW1         56.90299988 W
SFO2         500.2320009 MHz
NUC2                1H
CPDPRG[2         waltz16
PCPD2            80.00 usec
PLW2         11.44699955 W
PLW12         0.25756001 W
PLW13         0.12955000 W

F2 - Processing parameters
SI                32768
SF          125.7829173 MHz
WDW                  EM
SSB       0
LB              1.00 Hz
GB        0
PC              1.40
```

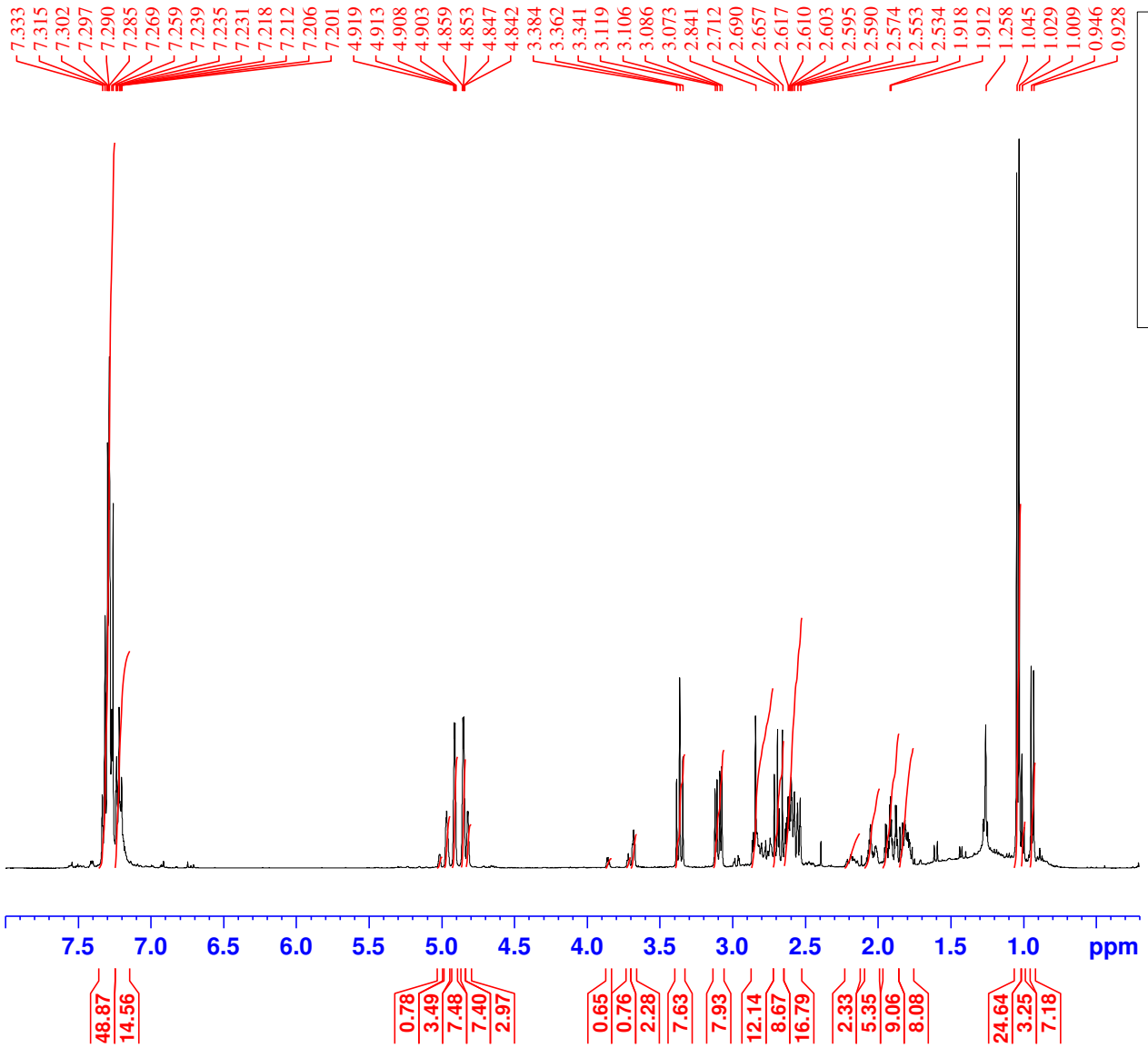

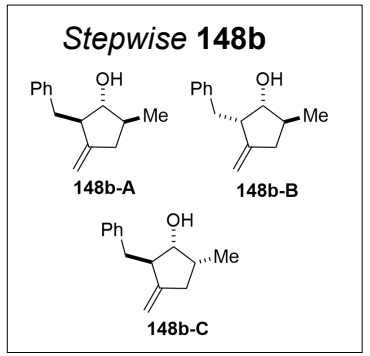


```
Current Data Parameters
NAME      KS-03-58col_Bn
EXPNO                 10
PROCNO                 1

F2 - Acquisition Parameters
Date_           20220702
Time               15.14 h
INSTRUM       Avance Neo
PROBHD    Z152088_0031 (
PULPROG             zg30
TD                 65536
SOLVENT            CDCl3
NS                    16
DS                     2
SWH             8196.722 Hz
FIDRES          0.250144 Hz
AQ              3.9976959 sec
RG                   101
DW                61.000 usec
DE                13.89 usec
TE                298.0 K
D1             1.00000000 sec
TD0                    1
SFO1         400.1324708 MHz
NUC1                  1H
P0                 2.67 usec
P1                 8.00 usec
PLW1         24.03499985 W

F2 - Processing parameters
SI                 65536
SF           400.1300098 MHz
WDW                   EM
SSB       0
LB                 0.30 Hz
GB        0
PC                 1.00
```

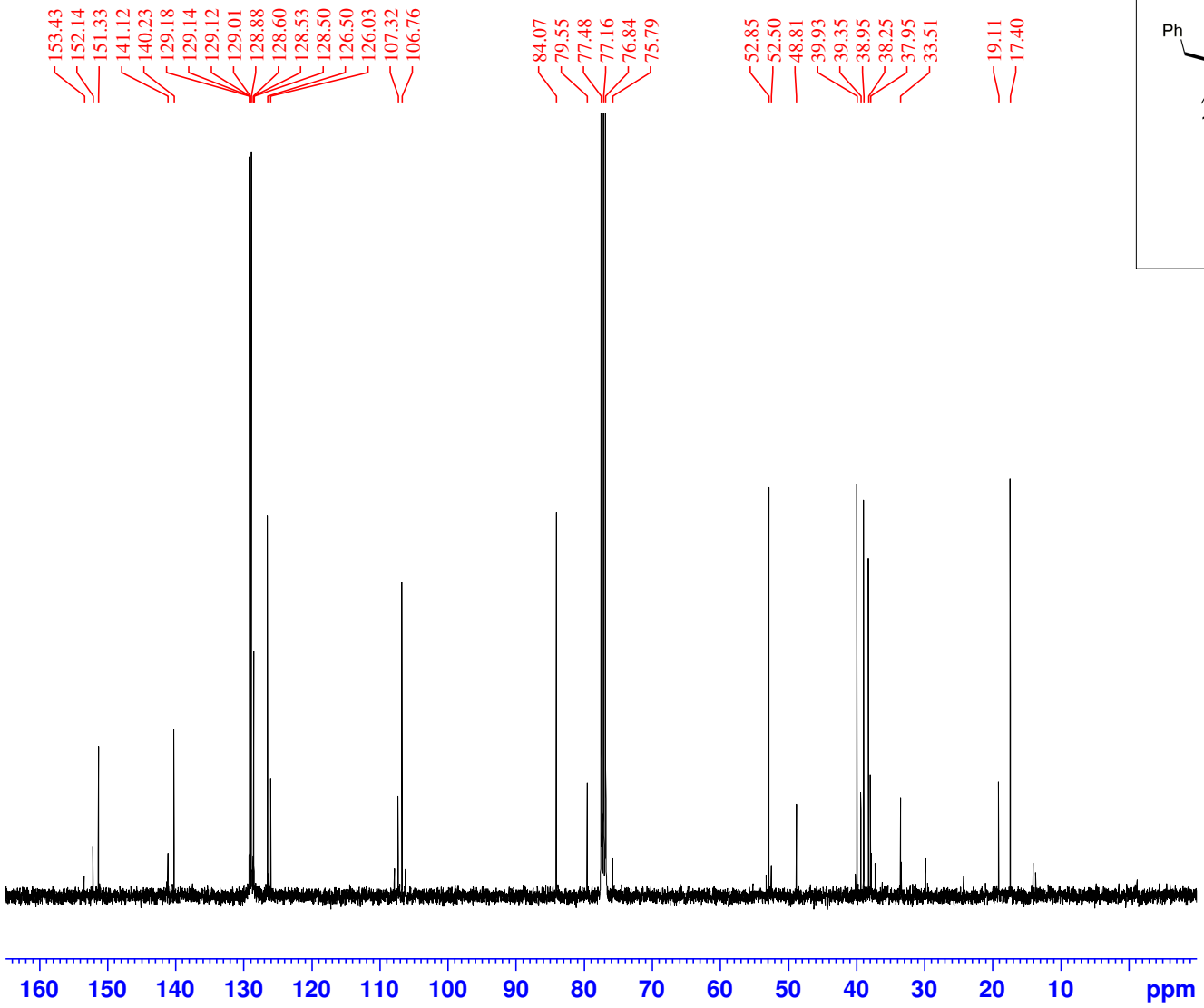

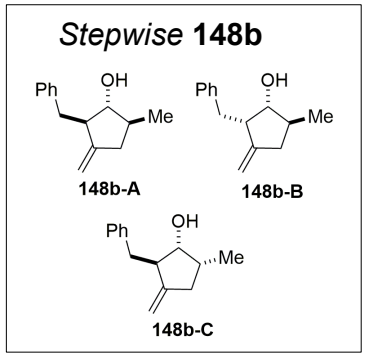


```
Current Data Parameters
NAME      KS-03-58col_Bn
EXPNO                 11
PROCNO                 1

F2 - Acquisition Parameters
Date_           20220702
Time              18.11 h
INSTRUM       Avance Neo
PROBHD    Z152088_0031 (
PULPROG           zgpg30
TD                65536
SOLVENT           CDCl3
NS                 1024
DS                    4
SWH           23809.523 Hz
FIDRES         0.726609 Hz
AQ             1.3762560 sec
RG                8.125
DW               21.000 usec
DE                6.50 usec
TE               298.0 K
D1            2.00000000 sec
D11           0.03000000 sec
TD0                   1
SFO1         100.6228298 MHz
NUC1                13C
P0                 2.67 usec
P1                 8.00 usec
PLW1         86.55400085 W
SFO2         400.1316005 MHz
NUC2                1H
CPDPRG[2         waltz65
PCPD2             90.00 usec
PLW2         24.03499985 W
PLW12         0.18990999 W
PLW13         0.09552100 W

F2 - Processing parameters
SI                32768
SF           100.6127552 MHz
WDW                  EM
SSB       0
LB                1.00 Hz
GB        0
PC                1.40
```

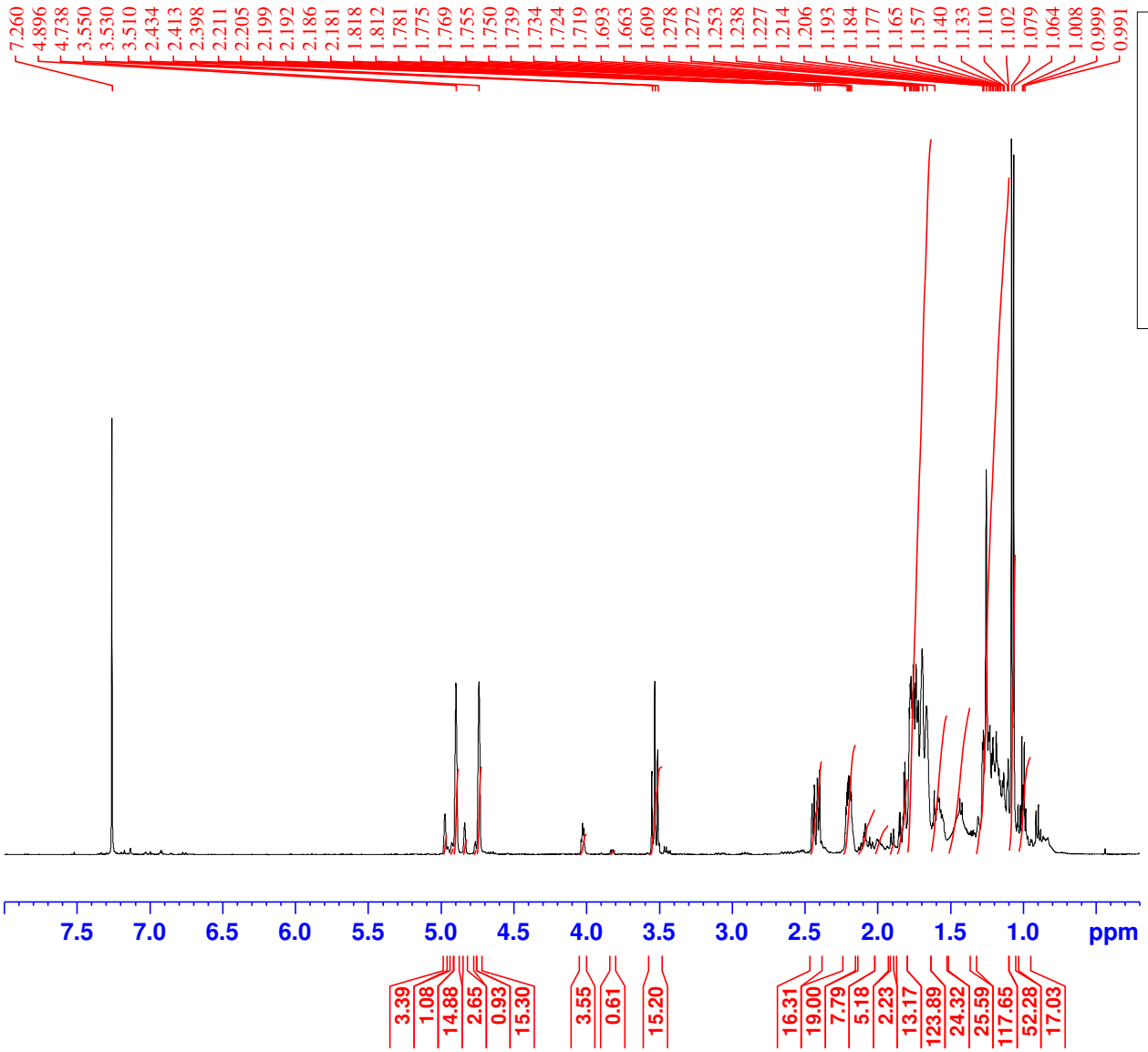

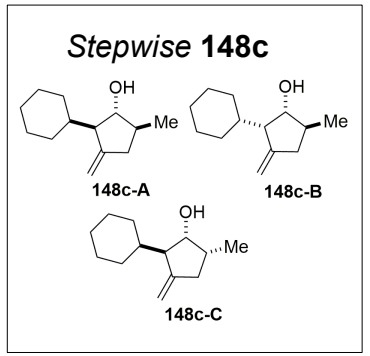


```
Current Data Parameters
NAME      KS-03-82col_Cy
EXPNO                 10
PROCNO                 1

F2 - Acquisition Parameters
Date_           20220719
Time              15.47 h
INSTRUM       Avance Neo
PROBHD    Z152088_0031 (
PULPROG             zg30
TD                 65536
SOLVENT            CDCl3
NS                    16
DS                     2
SWH             8196.722 Hz
FIDRES          0.250144 Hz
AQ              3.9976959 sec
RG                   101
DW                61.000 usec
DE                13.89 usec
TE                298.0 K
D1             1.00000000 sec
TD0                    1
SFO1         400.1324708 MHz
NUC1                  1H
P0                 2.67 usec
P1                 8.00 usec
PLW1         24.03499985 W

F2 - Processing parameters
SI                 65536
SF           400.1300096 MHz
WDW                   EM
SSB       0
LB                 0.30 Hz
GB        0
PC                 1.00
```

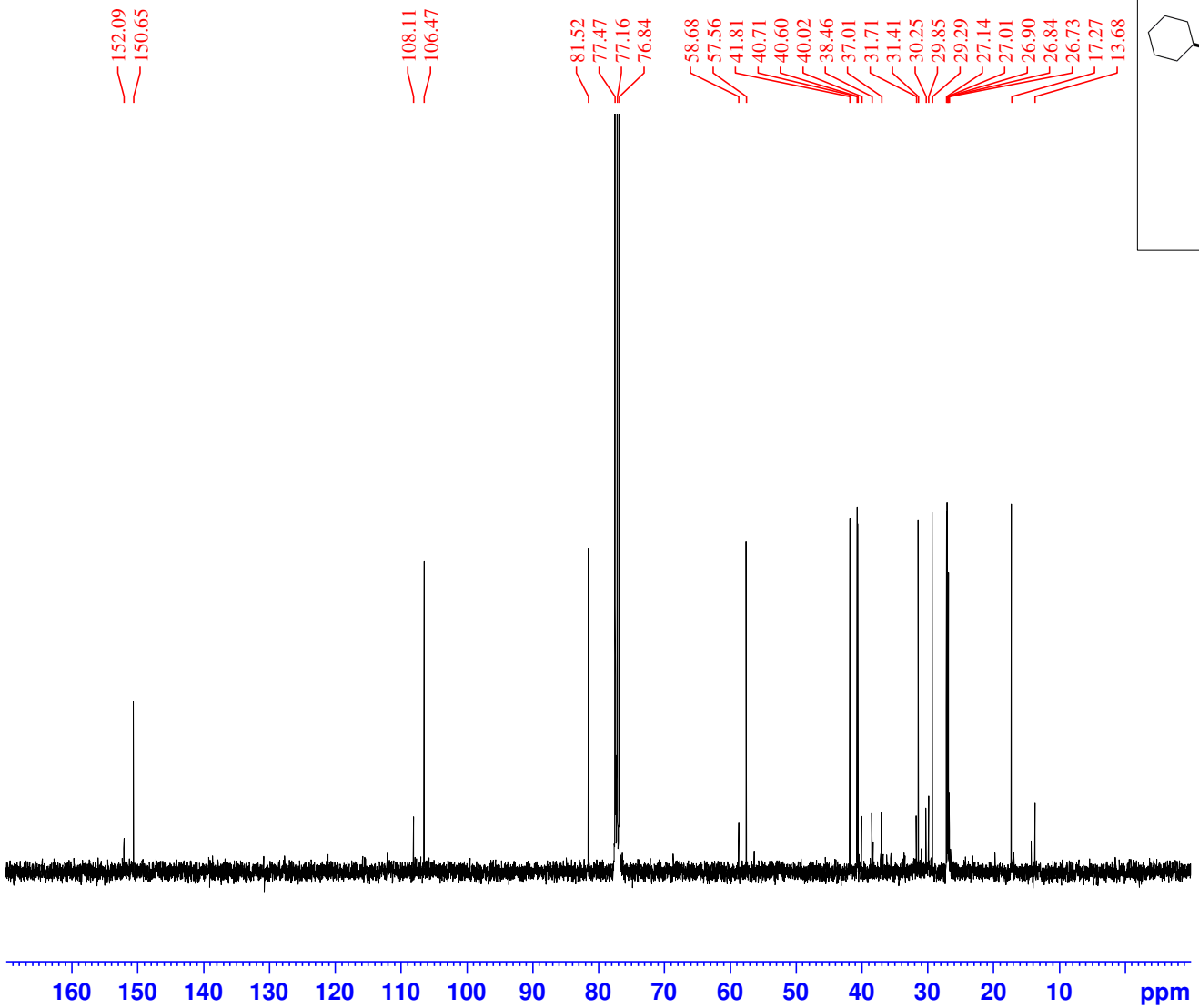

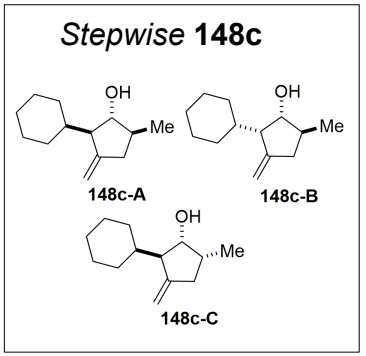


```
Current Data Parameters
NAME      KS-03-82col_Cy
EXPNO                 11
PROCNO                 1

F2 - Acquisition Parameters
Date_           20220719
Time                20.04 h
INSTRUM       Avance Neo
PROBHD    Z152088_0031 (
PULPROG           zgpg30
TD                65536
SOLVENT           CDCl3
NS                 1024
DS                    4
SWH           23809.523 Hz
FIDRES         0.726609 Hz
AQ             1.3762560 sec
RG                 8.125
DW                21.000 usec
DE                 6.50 usec
TE                298.0 K
D1             2.00000000 sec
D11            0.03000000 sec
TD0                   1
SFO1         100.6228298 MHz
NUC1                13C
P0                 2.67 usec
P1                 8.00 usec
PLW1         86.55400085 W
SFO2         400.1316005 MHz
NUC2                1H
CPDPRG[2         waltz65
PCPD2             90.00 usec
PLW2         24.03499985 W
PLW12         0.18990999 W
PLW13         0.09552100 W

F2 - Processing parameters
SI                32768
SF           100.6127545 MHz
WDW                  EM
SSB       0
LB                1.00 Hz
GB        0
PC                1.40
```

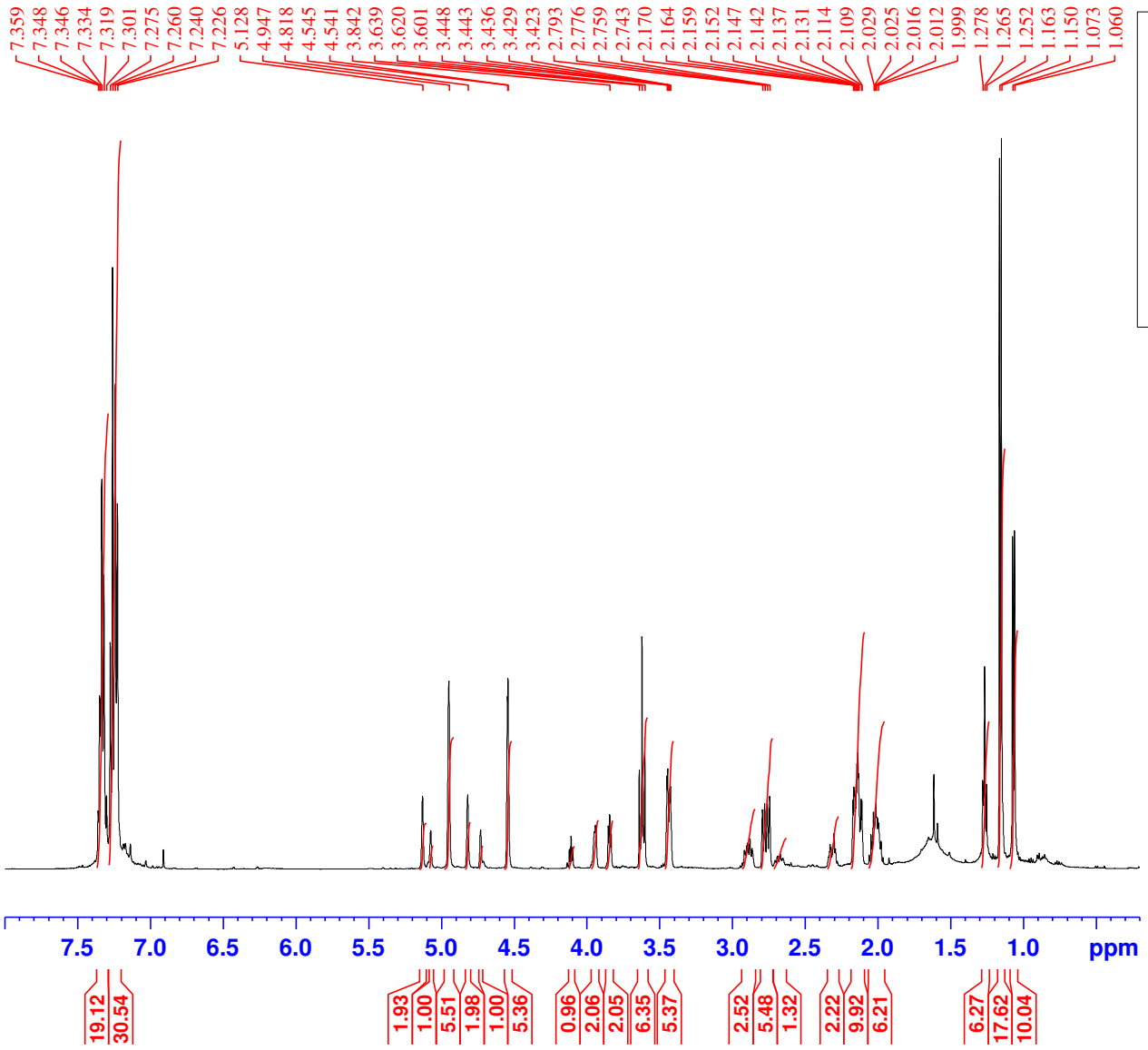

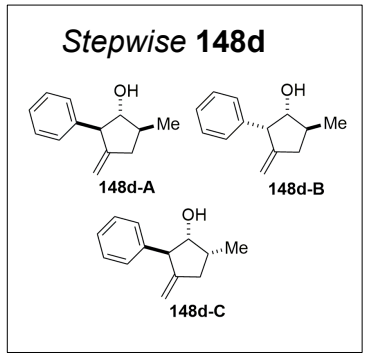


```
Current Data Parameters
NAME      KS-03-43col_comb_Ph
EXPNO                  4
PROCNO                 1

F2 - Acquisition Parameters
Date_           20220622
Time                13.16 h
INSTRUM             spect
PROBHD    Z125869_0055 (
PULPROG             zg30
TD                 65536
SOLVENT            CDCl3
NS                    16
DS                     2
SWH            10000.000 Hz
FIDRES             0.305176 Hz
AQ             3.2767999 sec
RG                 94.51
DW                 50.000 usec
DE                 16.00 usec
TE                 310.0 K
D1            2.00000000 sec
TD0                    1
SFO1          500.2330889 MHz
NUC1                  1H
P0                 4.00 usec
P1                 12.00 usec
PLW1          11.44699955 W

F2 - Processing parameters
SI                 65536
SF            500.2300121 MHz
WDW                   EM
SSB       0
LB                 0.30 Hz
GB        0
PC                 1.00
```

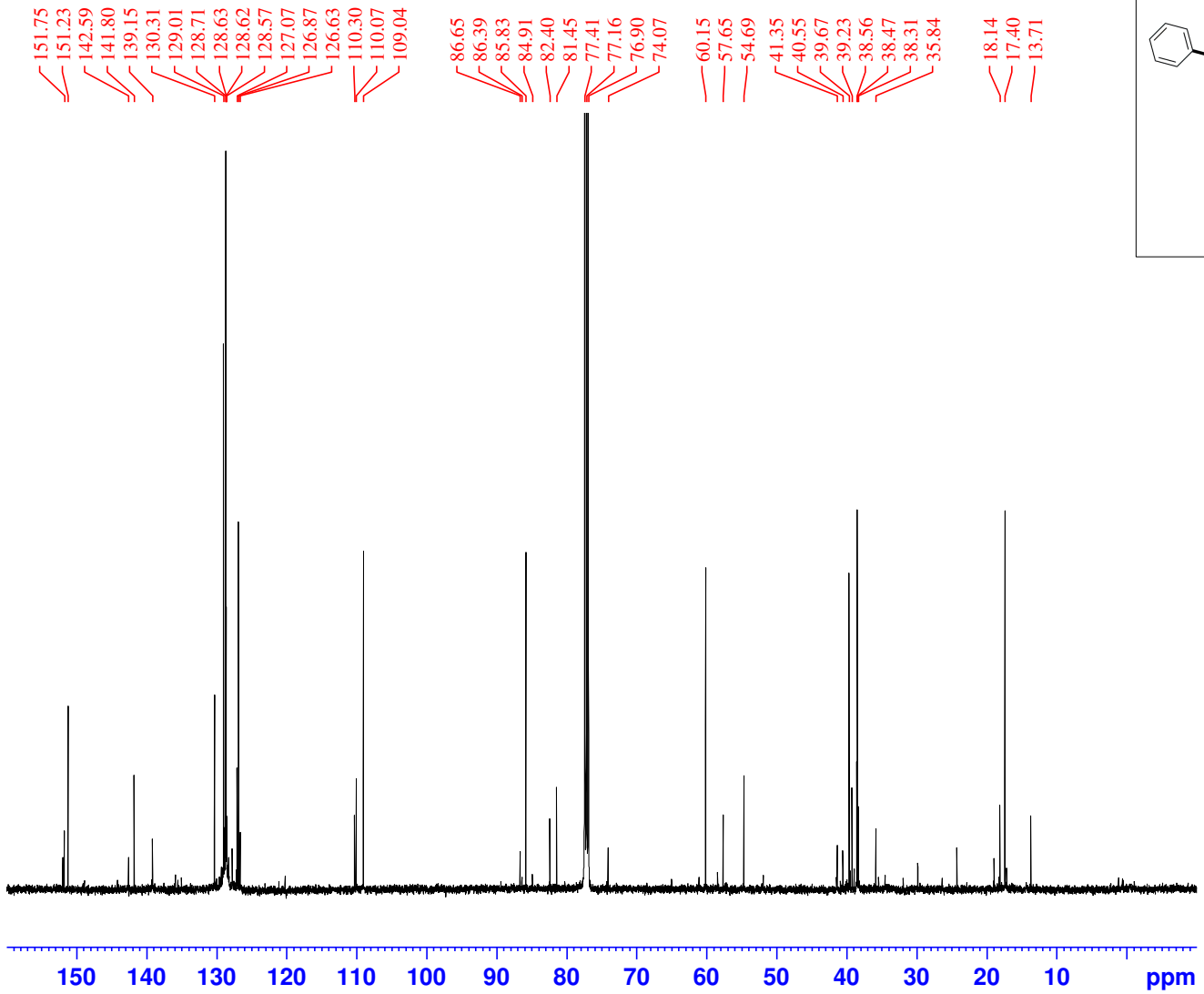

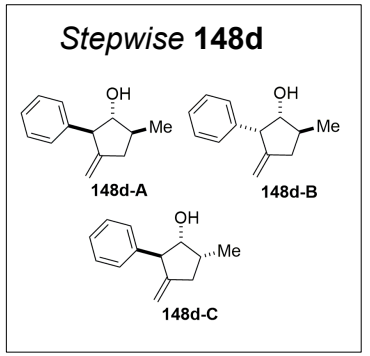


```
Current Data Parameters
NAME      KS-03-43col_comb_Ph
EXPNO                      11
PROCNO                      1

F2 - Acquisition Parameters
Date_              20220630
Time                  17.10 h
INSTRUM                spect
PROBHD    Z125869_0055 (
PULPROG               zgpg30
TD                     65536
SOLVENT                CDCl3
NS                      1024
DS                         4
SWH               29761.904 Hz
FIDRES            0.908261 Hz
AQ                1.1010048 sec
RG                   190.44
DW                   16.800 usec
DE                   18.00 usec
TE                   300.0 K
D1              2.00000000 sec
D11             0.03000000 sec
TD0                        1
SFO1           125.7955118 MHz
NUC1                    13C
P0                    3.33 usec
P1                   10.00 usec
PLW1           56.90299988 W
SFO2           500.2320009 MHz
NUC2                    1H
CPDPRG[2            waltz16
PCPD2                80.00 usec
PLW2           11.44699955 W
PLW12           0.25756001 W
PLW13           0.12955000 W

F2 - Processing parameters
SI                     32768
SF             125.7829172 MHz
WDW                       EM
SSB       0
LB                    1.00 Hz
GB        0
PC                    1.40
```

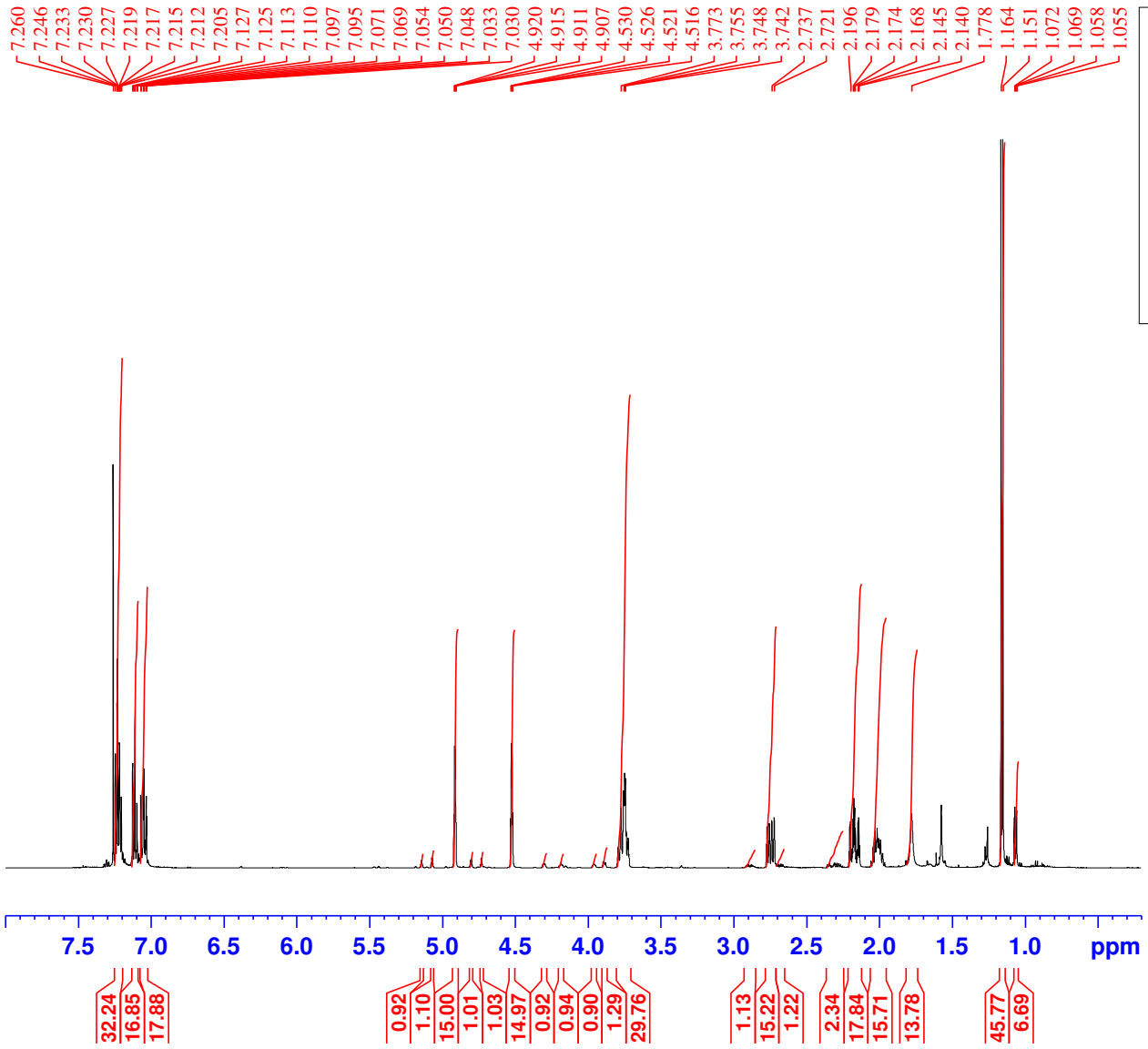

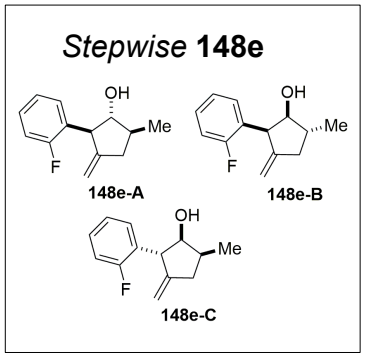


```
Current Data Parameters
NAME      KS-03-108co1_500_2FPh
EXPNO                  10
PROCNO                  1

F2 - Acquisition Parameters
Date_           20220823
Time               16.08 h
INSTRUM            spect
PROBHD    Z125869_0055 (
PULPROG             zg30
TD                 65536
SOLVENT            CDCl3
NS                    64
DS                     2
SWH            10000.000 Hz
FIDRES         0.305176 Hz
AQ             3.2767999 sec
RG                 86.13
DW                50.000 usec
DE                16.00 usec
TE                300.0 K
D1           2.00000000 sec
TD0                    1
SFO1         500.2330889 MHz
NUC1                  1H
P0                 4.00 usec
P1                12.00 usec
PLW1        11.44699955 W

F2 - Processing parameters
SI                 65536
SF           500.2300123 MHz
WDW                   EM
SSB       0
LB                 0.30 Hz
GB        0
PC                 1.00
```

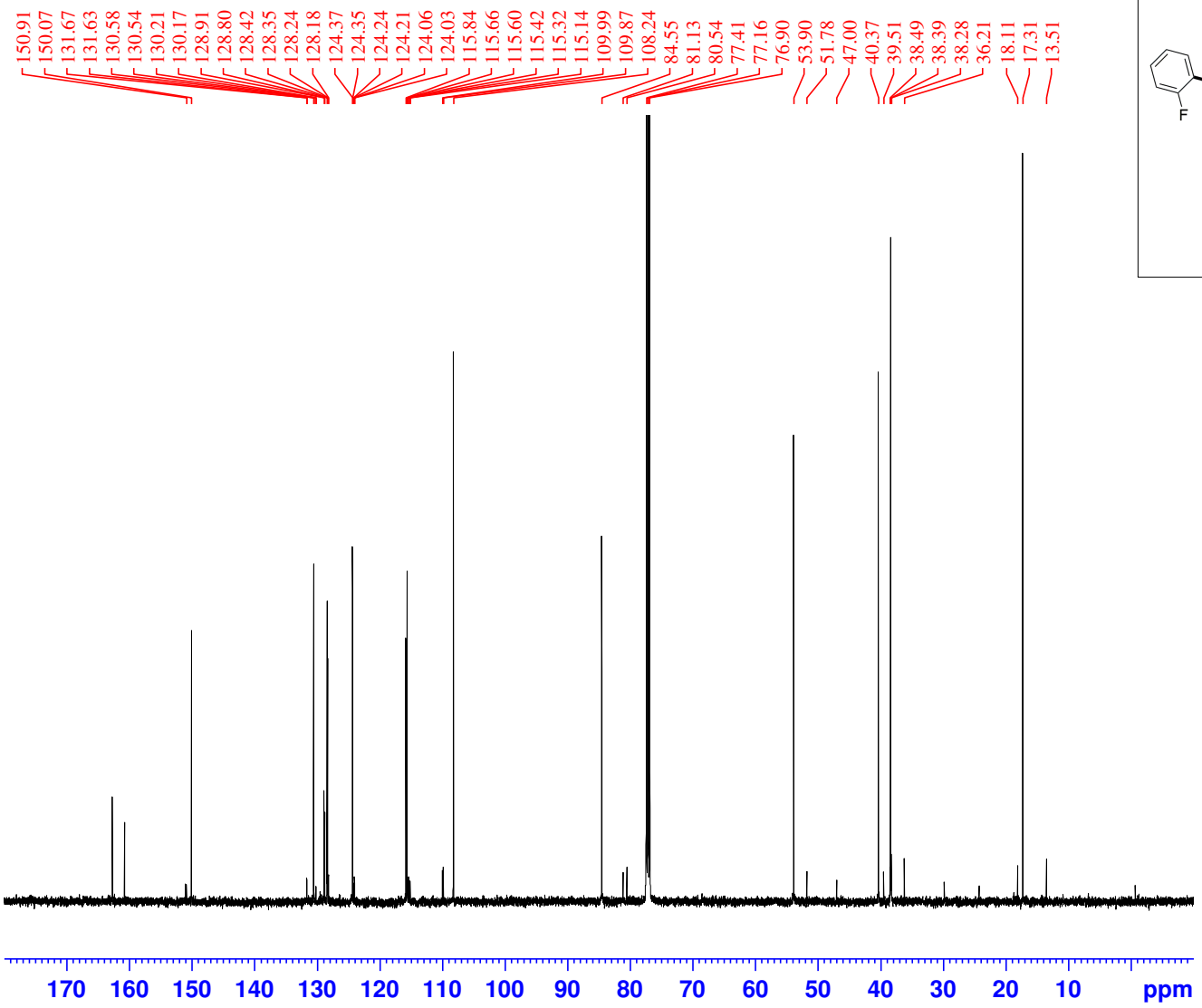

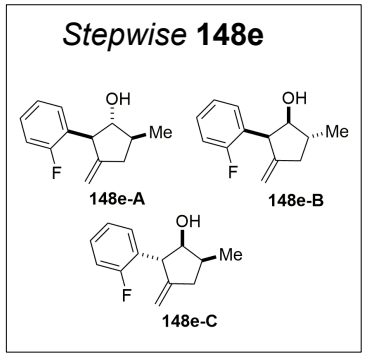


```
Current Data Parameters
NAME      KS-03-108col_500_2FPh
EXPNO                        12
PROCNO                        1

F2 - Acquisition Parameters
Date_              20220823
Time                  16.40 h
INSTRUM                spect
PROBHD    Z125869_0055 (
PULPROG              zgpg30
TD                    65536
SOLVENT               CDCl3
NS                      512
DS                        4
SWH               29761.904 Hz
FIDRES             0.908261 Hz
AQ                1.1010048 sec
RG                   190.44
DW                   16.800 usec
DE                   18.00 usec
TE                   300.0 K
D1              2.00000000 sec
D11             0.03000000 sec
TD0                       1
SFO1           125.7955118 MHz
NUC1                    13C
P0                    3.33 usec
P1                   10.00 usec
PLW1           56.90299988 W
SFO2           500.2320009 MHz
NUC2                    1H
CPDPRG[2            waltz16
PCPD2                80.00 usec
PLW2           11.44699955 W
PLW12           0.25756001 W
PLW13           0.12955000 W

F2 - Processing parameters
SI                    32768
SF             125.7829173 MHz
WDW                      EM
SSB          0
LB                    1.00 Hz
GB           0
PC                    1.40
```

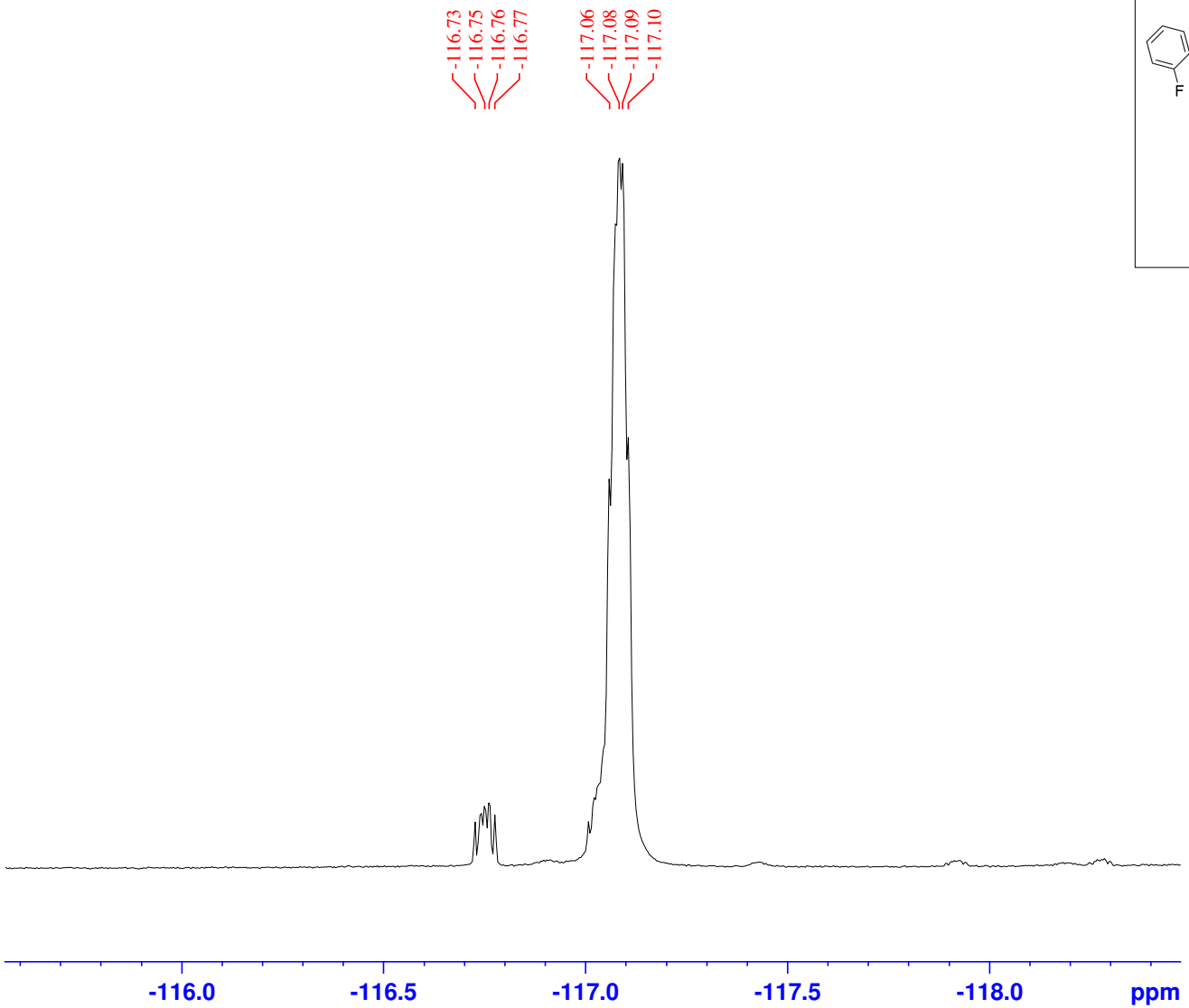

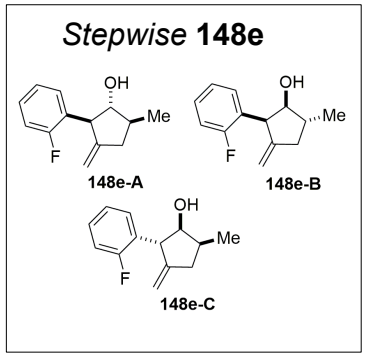


```
Current Data Parameters
NAME      KS-03-108col_500_2FPh
EXPNO                        11
PROCNO                        1

F2 - Acquisition Parameters
Date_              20220823
Time                 16.10 h
INSTRUM              spect
PROBHD    Z125869_0055 (
PULPROG              zgflqn
TD                   131072
SOLVENT              CDCl3
NS                      16
DS                       4
SWH             113636.367 Hz
FIDRES            1.733953 Hz
AQ                0.5767168 sec
RG                    14.14
DW                 4.400 usec
DE                18.00 usec
TE                 300.0 K
D1              1.00000000 sec
TD0                      1
SFO1           470.6394024 MHz
NUC1                   19F
P1                 15.00 usec
PLW1           11.70800018 W

F2 - Processing parameters
SI                    65536
SF             470.6864710 MHz
WDW                      EM
SSB       0
LB                  0.30 Hz
GB        0
PC                    1.00
```

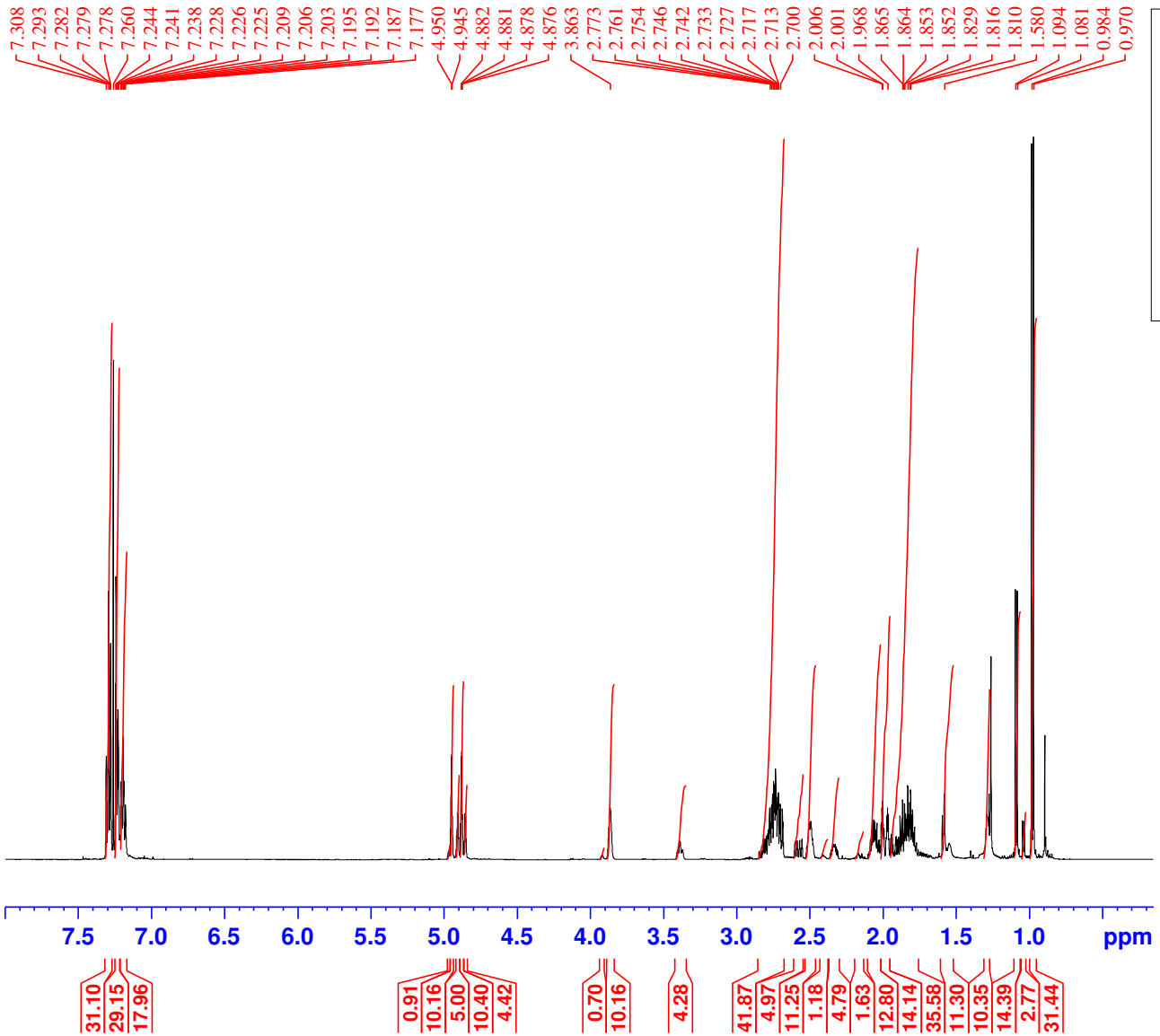

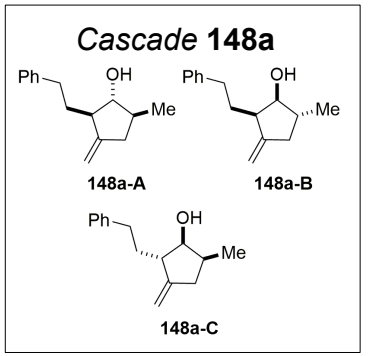


```
Current Data Parameters
NAME      KS-03-105col_500_CH2CH2Ph
EXPNO                 10
PROCNO                 1

F2 - Acquisition Parameters
Date_           20220822
Time              14.07 h
INSTRUM             spect
PROBHD   Z125869_0055 (
PULPROG             zg30
TD                 65536
SOLVENT            CDCl3
NS                    64
DS                     2
SWH           10000.000 Hz
FIDRES            0.305176 Hz
AQ             3.2767999 sec
RG                 53.13
DW                50.000 usec
DE                16.00 usec
TE                300.0 K
D1             2.00000000 sec
TD0                    1
SFO1         500.2330889 MHz
NUC1                  1H
P0                 4.00 usec
P1                12.00 usec
PLW1         11.44699955 W

F2 - Processing parameters
SI                 65536
SF           500.2300124 MHz
WDW                   EM
SSB       0
LB                 0.30 Hz
GB        0
PC                 1.00
```

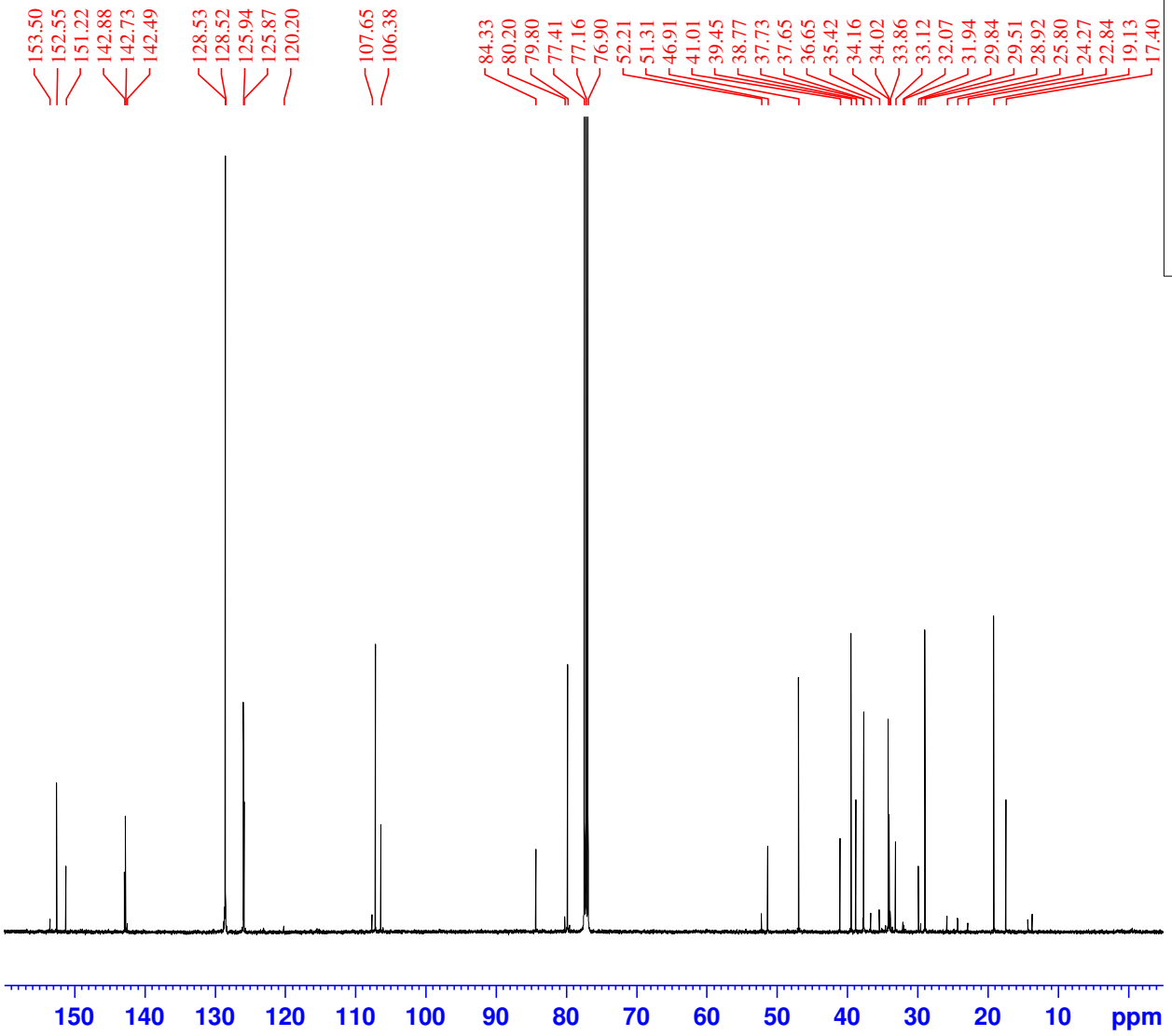

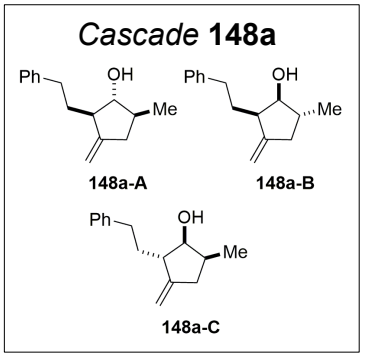


```
Current Data Parameters
NAME      KS-03-105col_500_CH2CH2Ph
EXPNO                 11
PROCNO                 1

F2 - Acquisition Parameters
Date_           20220822
Time              15.04 h
INSTRUM             spect
PROBHD   Z125869_0055 (
PULPROG           zgpg30
TD                 65536
SOLVENT            CDCl3
NS                  1024
DS                     4
SWH            29761.904 Hz
FIDRES             0.908261 Hz
AQ              1.1010048 sec
RG                190.44
DW                 16.800 usec
DE                 18.00 usec
TE                300.0 K
D1             2.00000000 sec
D11            0.03000000 sec
TD0                    1
SFO1          125.7955118 MHz
NUC1                  13C
P0                  3.33 usec
P1                 10.00 usec
PLW1          56.90299988 W
SFO2          500.2320009 MHz
NUC2                  1H
CPDPRG[2          waltz16
PCPD2              80.00 usec
PLW2          11.44699955 W
PLW12          0.25756001 W
PLW13          0.12955000 W

F2 - Processing parameters
SI                 32768
SF            125.7829176 MHz
WDW                   EM
SSB       0
LB                  1.00 Hz
GB        0
PC                  1.40
```

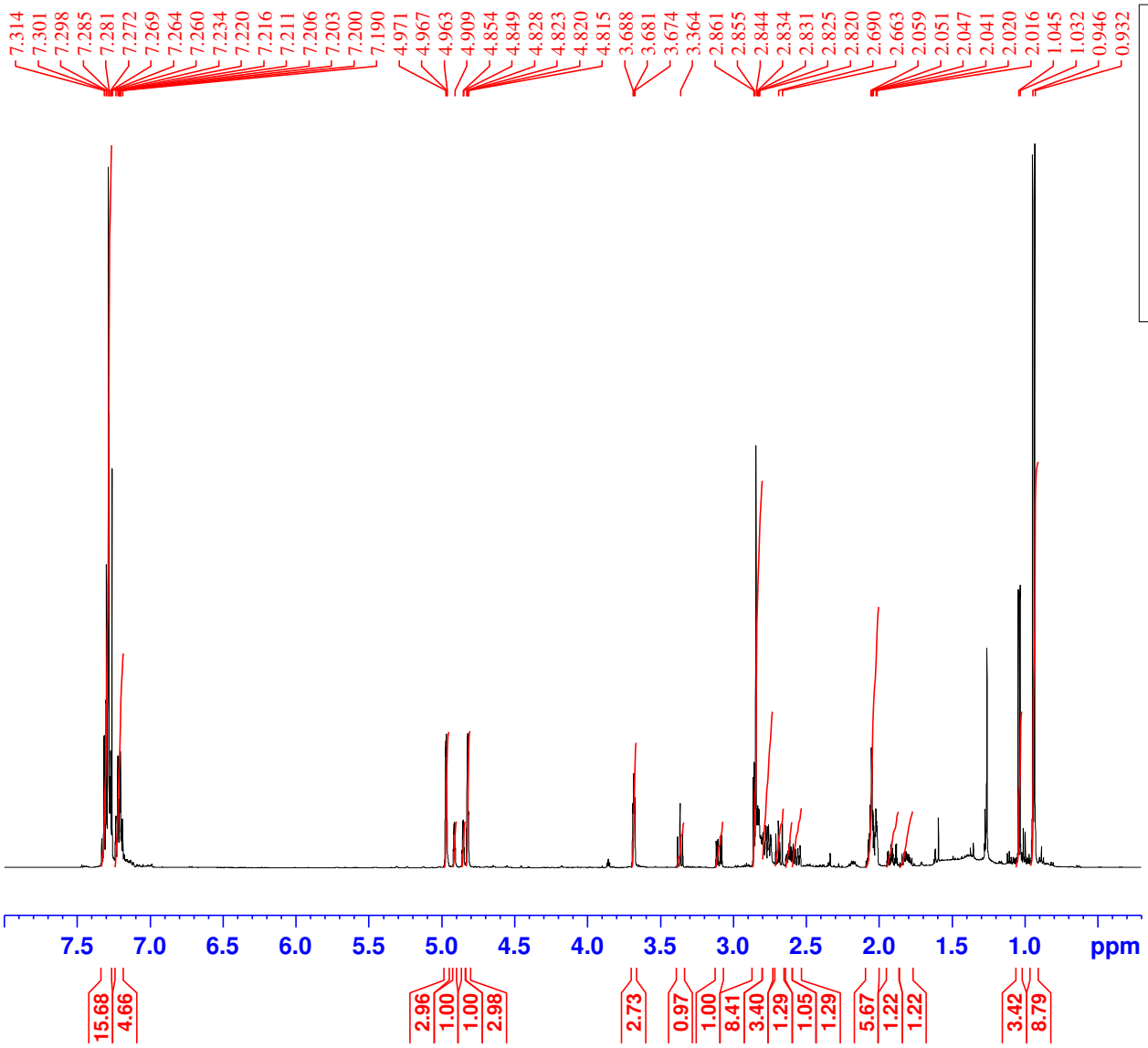

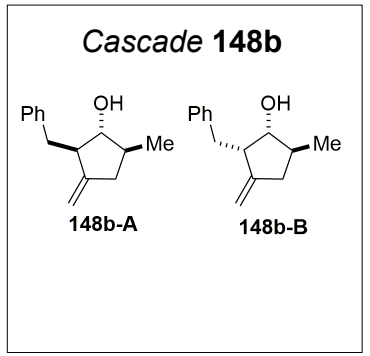


```
Current Data Parameters
NAME      KS-03-78col_Bn
EXPNO                  2
PROCNO                 1

F2 - Acquisition Parameters
Date_           20220715
Time              17.33 h
INSTRUM             spect
PROBHD    Z125869_0055 (
PULPROG             zg30
TD                 65536
SOLVENT            CDCl3
NS                    64
DS                     2
SWH           10000.000 Hz
FIDRES            0.305176 Hz
AQ                3.2767999 sec
RG                   53.13
DW                50.000 usec
DE                16.00 usec
TE                300.0 K
D1             2.00000000 sec
TD0                    1
SFO1          500.2330889 MHz
NUC1                  1H
P0                 4.00 usec
P1                12.00 usec
PLW1          11.44699955 W

F2 - Processing parameters
SI                 65536
SF            500.2300122 MHz
WDW                   EM
SSB       0
LB                 0.30 Hz
GB        0
PC                 1.00
```

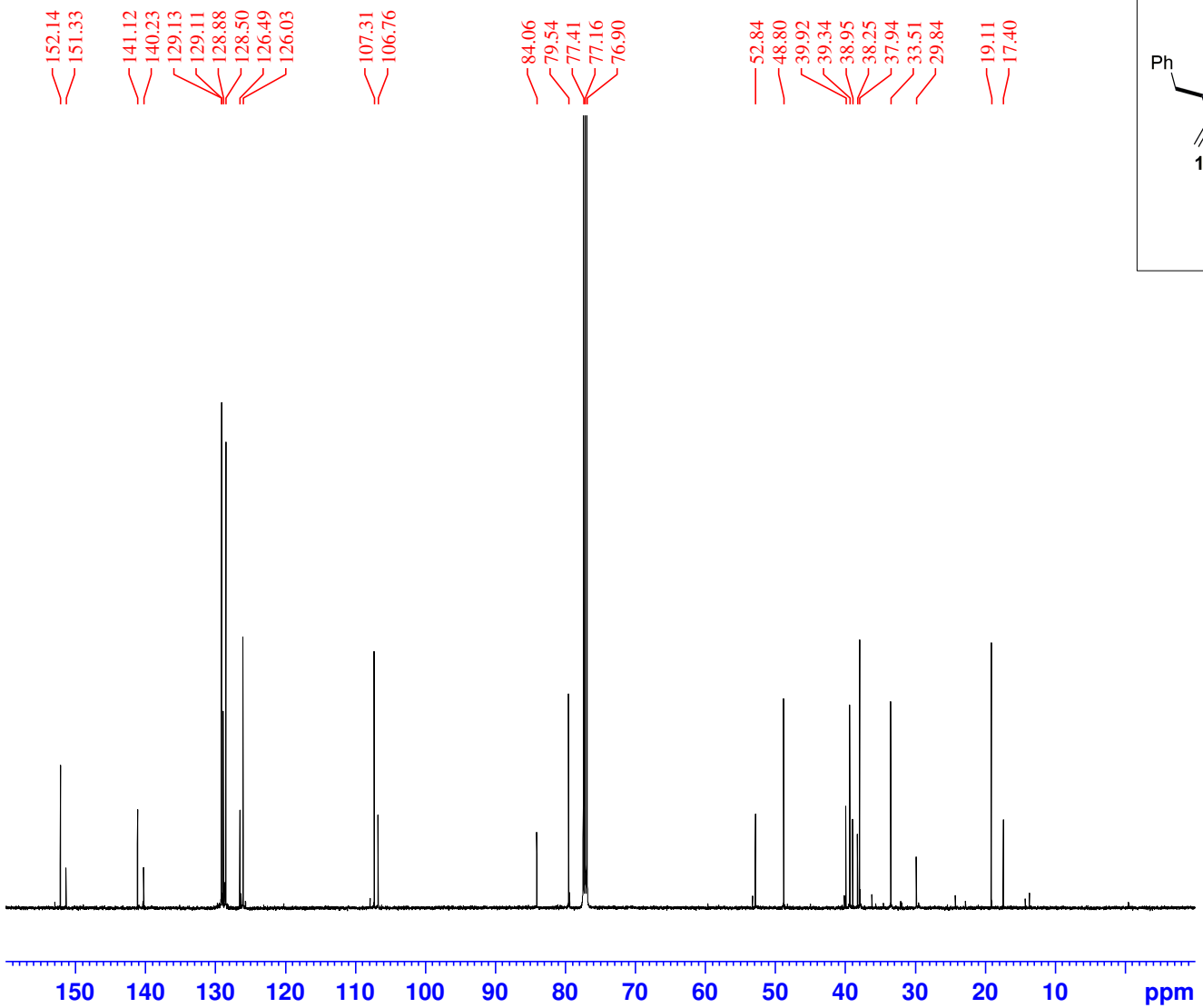

Cascade **148b**

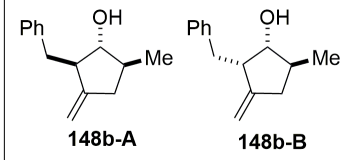

148b-A **148b-B**

```
Current Data Parameters
NAME      KS-03-78col_Bn
EXPNO                  3
PROCNO                 1

F2 - Acquisition Parameters
Date_           20220715
Time              18.29 h
INSTRUM           spect
PROBHD    Z125869_0055 (
PULPROG          zgpg30
TD                65536
SOLVENT           CDCl3
NS                 1024
DS                    4
SWH           29761.904 Hz
FIDRES         0.908261 Hz
AQ            1.1010048 sec
RG               190.44
DW               16.800 usec
DE               18.00 usec
TE               300.0 K
D1           2.00000000 sec
D11          0.03000000 sec
TD0                   1
SFO1        125.7955118 MHz
NUC1               13C
P0                3.33 usec
P1               10.00 usec
PLW1        56.90299988 W
SFO2        500.2320009 MHz
NUC2               1H
CPDPRG[2        waltz16
PCPD2            80.00 usec
PLW2        11.44699955 W
PLW12        0.25756001 W
PLW13        0.12955000 W

F2 - Processing parameters
SI                32768
SF          125.7829176 MHz
WDW                EM
SSB       0
LB               1.00 Hz
GB        0
PC               1.40
```

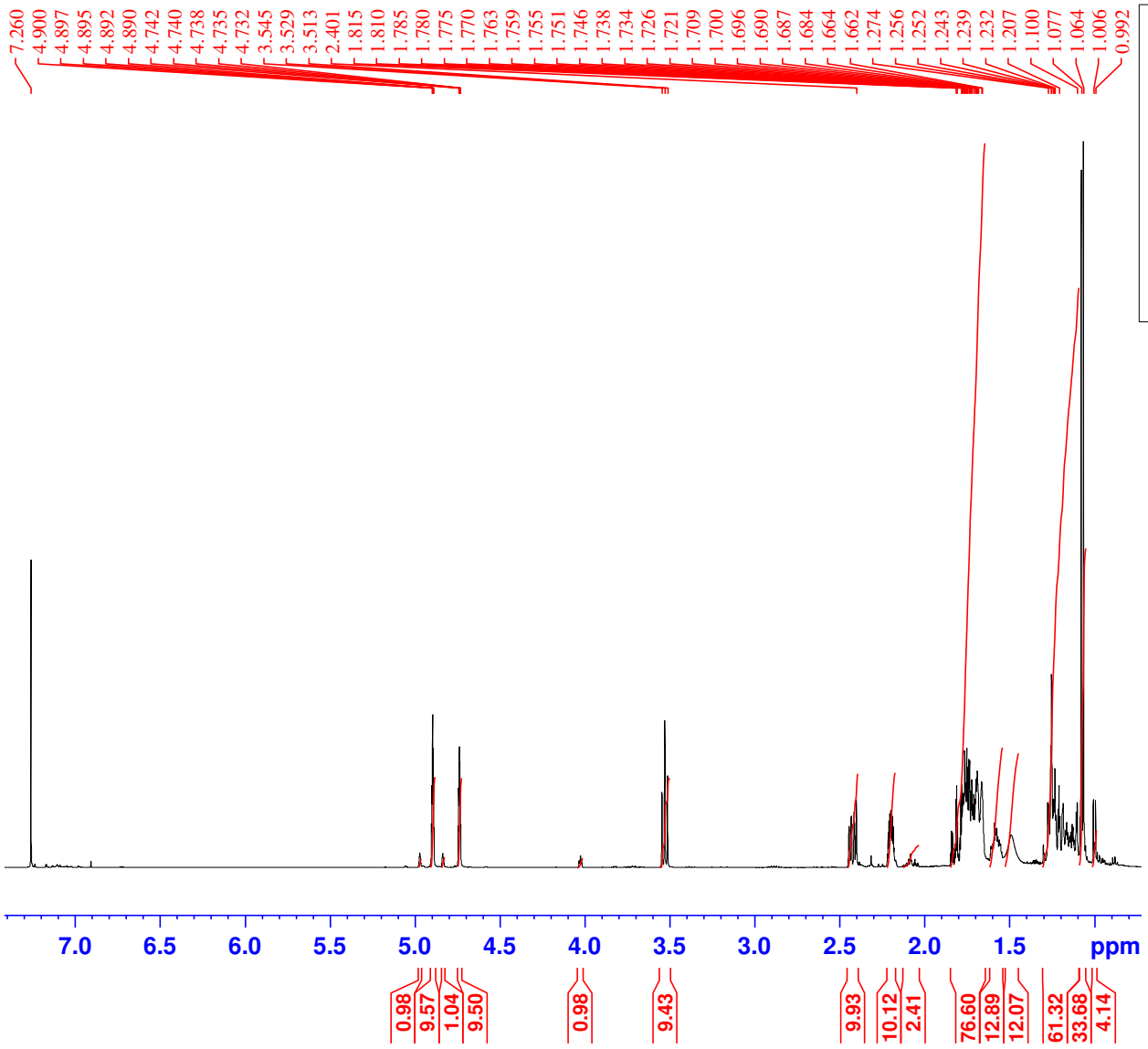

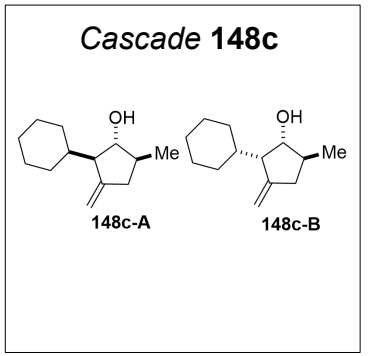


```
Current Data Parameters
NAME      KS-03-79col_Cy
EXPNO                  2
PROCNO                 1

F2 - Acquisition Parameters
Date_           20220715
Time              16.27 h
INSTRUM             spect
PROBHD    Z125869_0055 (
PULPROG             zg30
TD                 65536
SOLVENT            CDCl3
NS                    64
DS                     2
SWH           10000.000 Hz
FIDRES            0.305176 Hz
AQ             3.2767999 sec
RG                 53.13
DW                50.000 usec
DE                16.00 usec
TE                300.0 K
D1             2.00000000 sec
TD0                    1
SFO1          500.2330889 MHz
NUC1                  1H
P0                 4.00 usec
P1                12.00 usec
PLW1          11.44699955 W

F2 - Processing parameters
SI                 65536
SF            500.2300121 MHz
WDW                   EM
SSB       0
LB                 0.30 Hz
GB        0
PC                 1.00
```

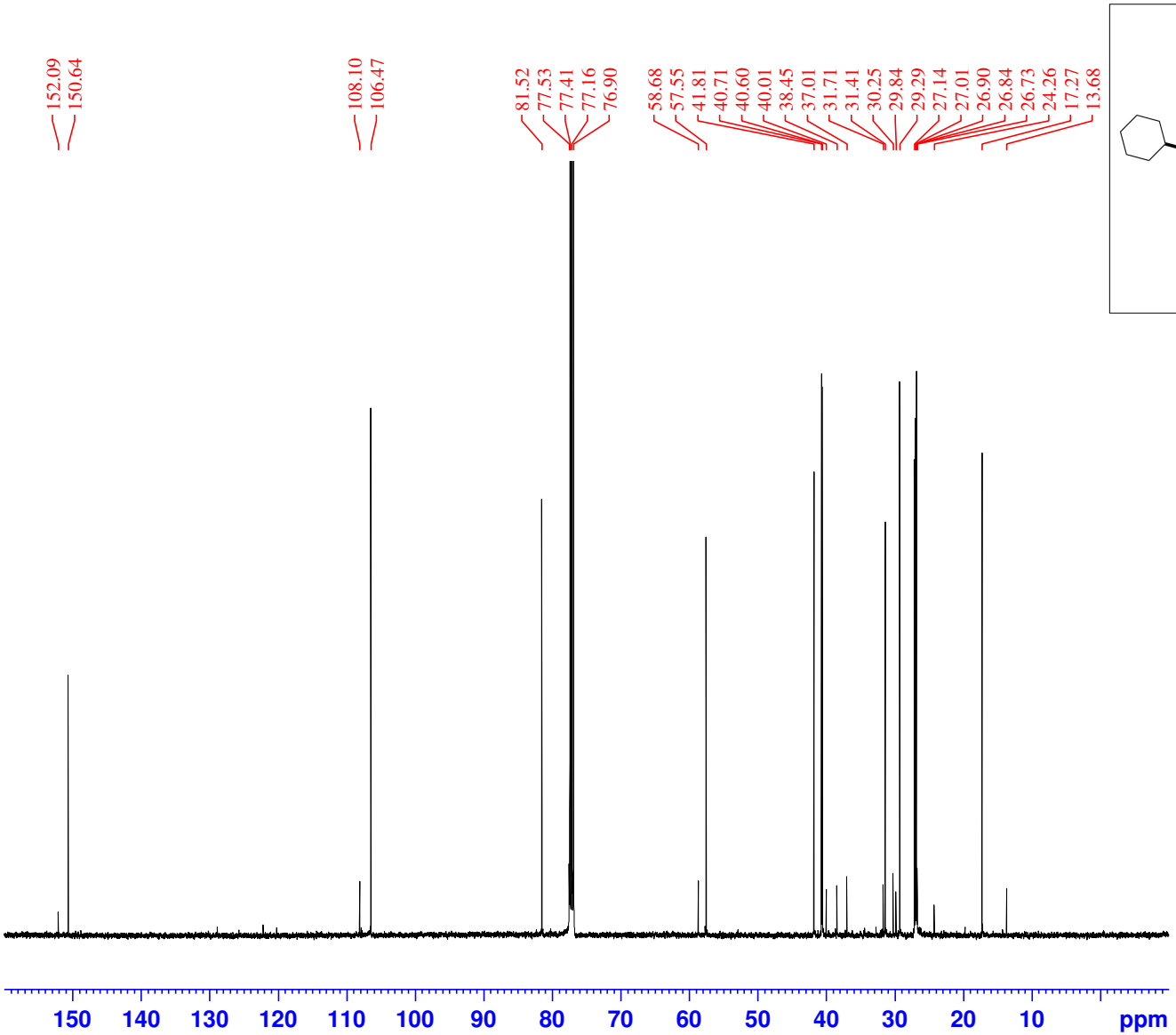

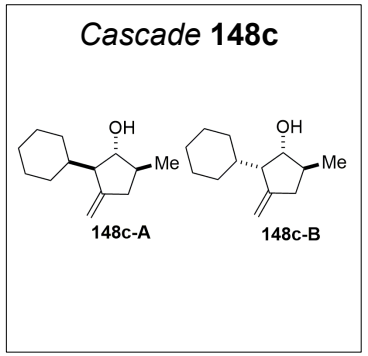


```
Current Data Parameters
NAME      KS-03-79col_Cy
EXPNO                  3
PROCNO                 1

F2 - Acquisition Parameters
Date_           20220715
Time               17.24 h
INSTRUM            spect
PROBHD    Z125869_0055 (
PULPROG          zgpg30
TD                65536
SOLVENT           CDCl3
NS                 1024
DS                    4
SWH           29761.904 Hz
FIDRES         0.908261 Hz
AQ            1.1010048 sec
RG               190.44
DW               16.800 usec
DE               18.00 usec
TE               300.0 K
D1            2.00000000 sec
D11           0.03000000 sec
TD0                   1
SFO1         125.7955118 MHz
NUC1                13C
P0                3.33 usec
P1               10.00 usec
PLW1         56.90299988 W
SFO2         500.2320009 MHz
NUC2                1H
CPDPRG[2         waltz16
PCPD2            80.00 usec
PLW2         11.44699955 W
PLW12         0.25756001 W
PLW13         0.12955000 W

F2 - Processing parameters
SI                32768
SF           125.7829164 MHz
WDW                  EM
SSB       0
LB                1.00 Hz
GB        0
PC                1.40
```

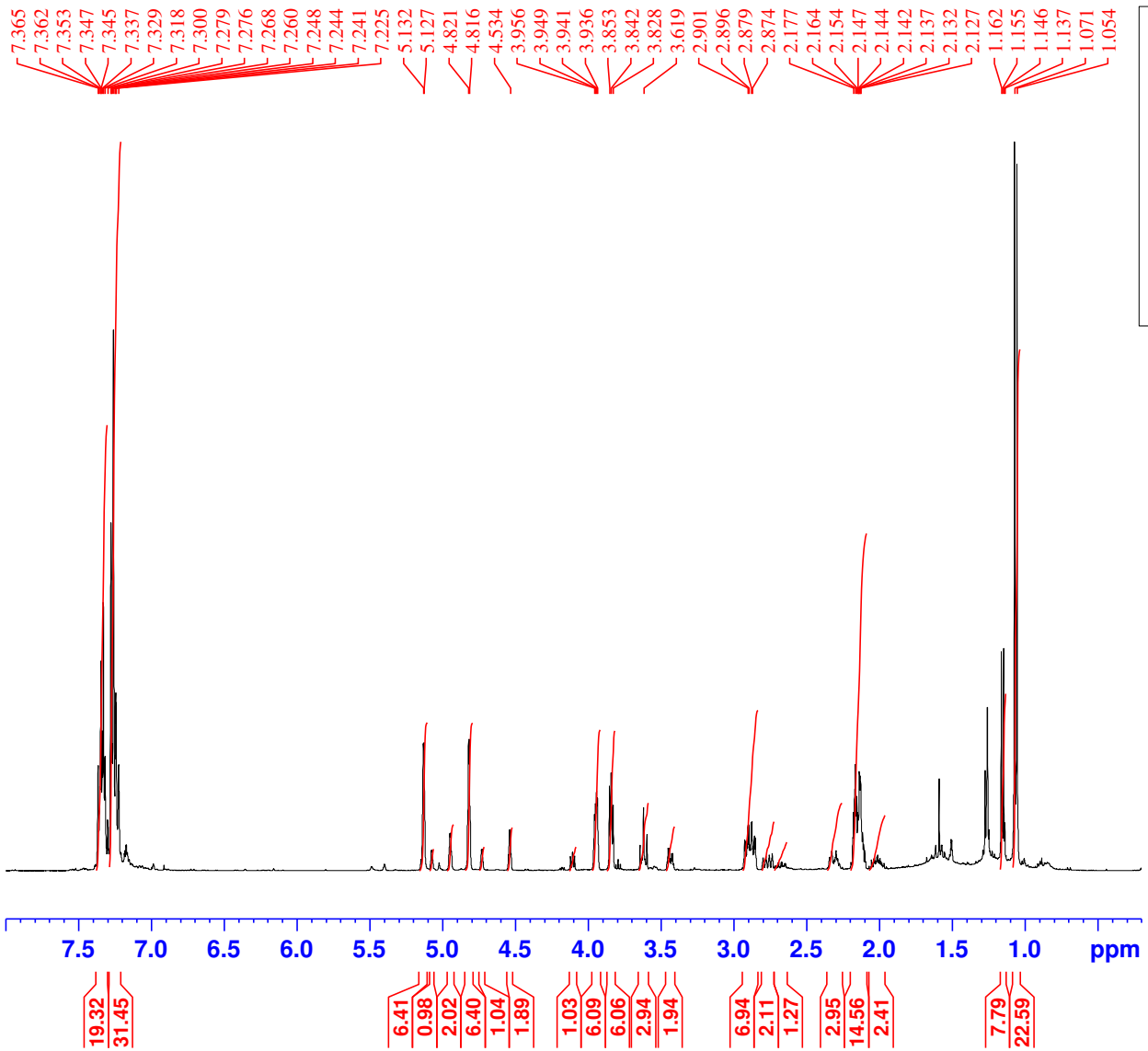

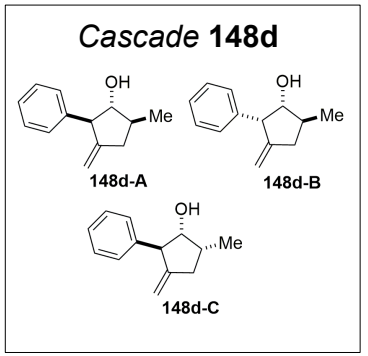


```
Current Data Parameters
NAME      KS-03-63col_Ph
EXPNO                 10
PROCNO                 1

F2 - Acquisition Parameters
Date_           20220704
Time              12.15 h
INSTRUM       Avance Neo
PROBHD    Z152088_0031 (
PULPROG             zg30
TD                 65536
SOLVENT            CDCl3
NS                    16
DS                     2
SWH             8196.722 Hz
FIDRES          0.250144 Hz
AQ              3.9976959 sec
RG                   101
DW                61.000 usec
DE                13.89 usec
TE                298.0 K
D1             1.00000000 sec
TD0                    1
SFO1         400.1324708 MHz
NUC1                  1H
P0                 2.67 usec
P1                 8.00 usec
PLW1         24.03499985 W

F2 - Processing parameters
SI                 65536
SF           400.1300097 MHz
WDW                   EM
SSB       0
LB                 0.30 Hz
GB        0
PC                 1.00
```

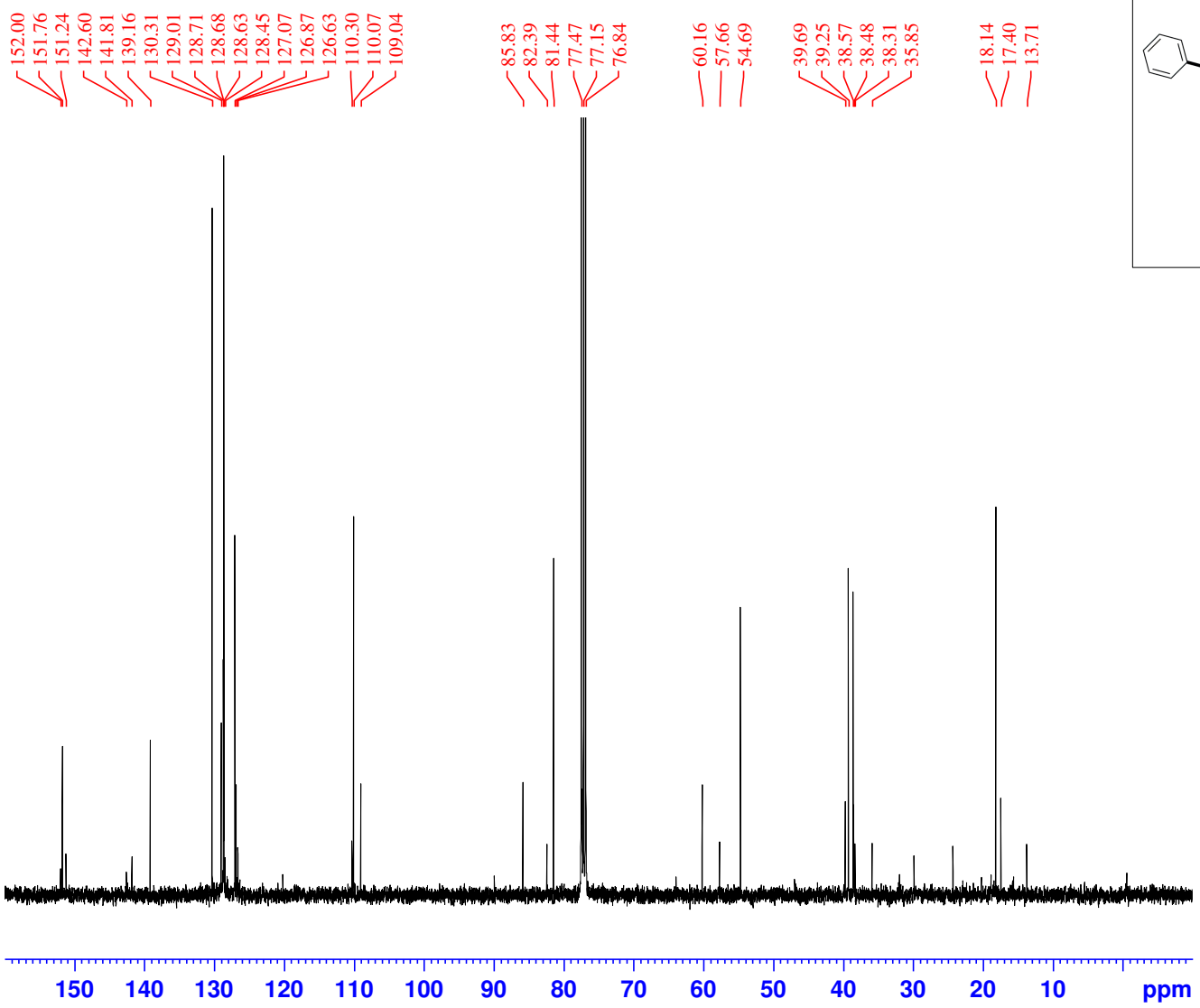

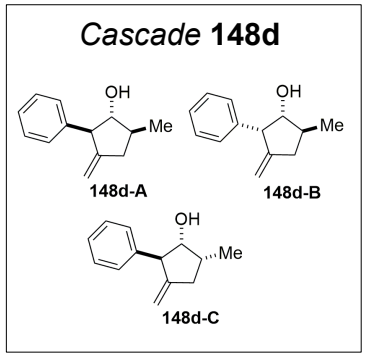


```
Current Data Parameters
NAME      KS-03-63col_Ph
EXPNO                 11
PROCNO                 1

F2 - Acquisition Parameters
Date_           20220704
Time              20.11 h
INSTRUM       Avance Neo
PROBHD    Z152088_0031 (
PULPROG          zgpg30
TD                65536
SOLVENT           CDCl3
NS                 1024
DS                    4
SWH           23809.523 Hz
FIDRES         0.726609 Hz
AQ             1.3762560 sec
RG                8.125
DW               21.000 usec
DE                6.50 usec
TE               298.0 K
D1            2.00000000 sec
D11           0.03000000 sec
TD0                   1
SFO1         100.6228298 MHz
NUC1                 13C
P0                2.67 usec
P1                8.00 usec
PLW1         86.55400085 W
SFO2         400.1316005 MHz
NUC2                 1H
CPDPRG[2         waltz65
PCPD2             90.00 usec
PLW2         24.03499985 W
PLW12         0.18990999 W
PLW13         0.09552100 W

F2 - Processing parameters
SI                32768
SF           100.6127552 MHz
WDW                  EM
SSB       0
LB                1.00 Hz
GB        0
PC                1.40
```

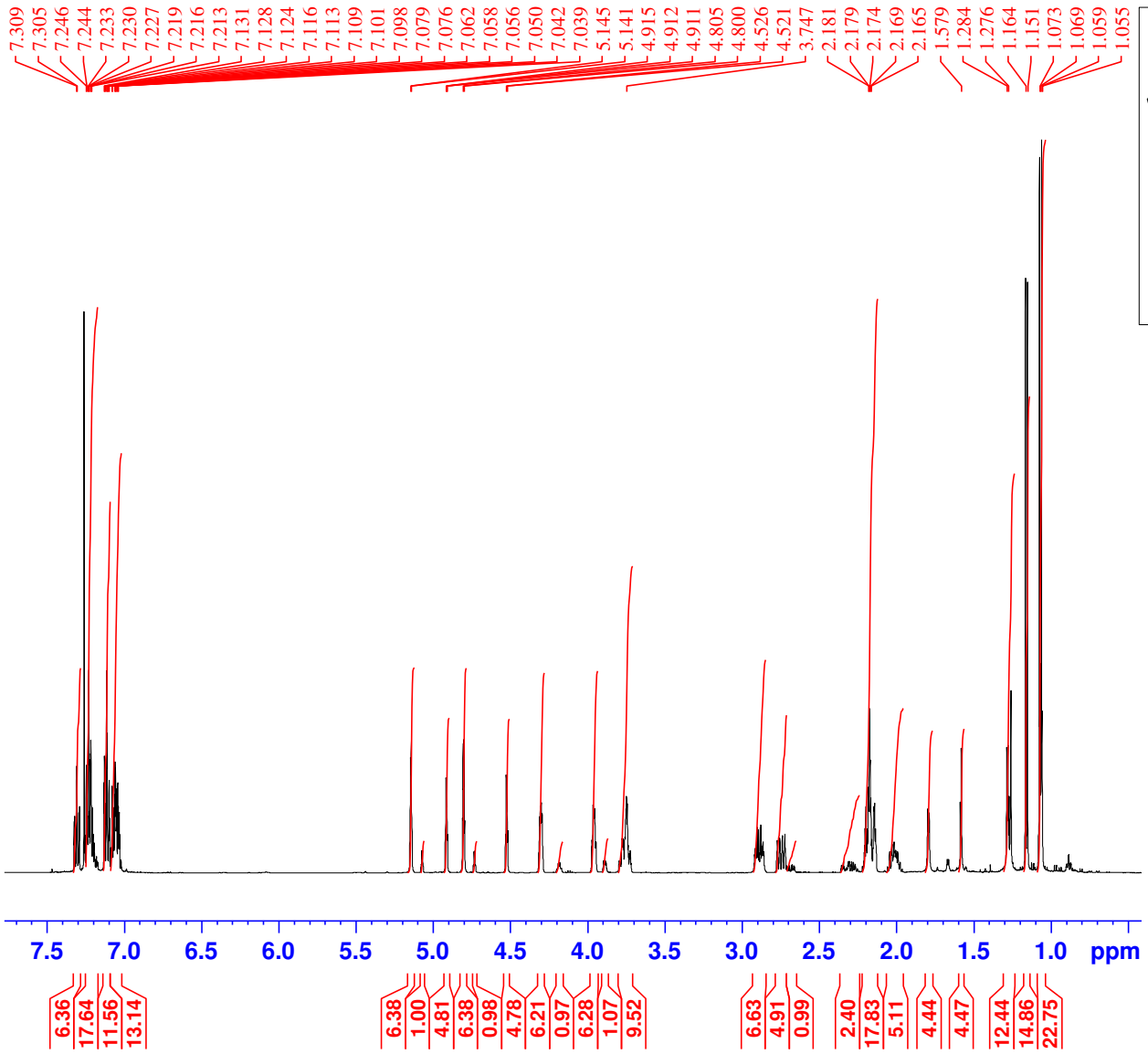

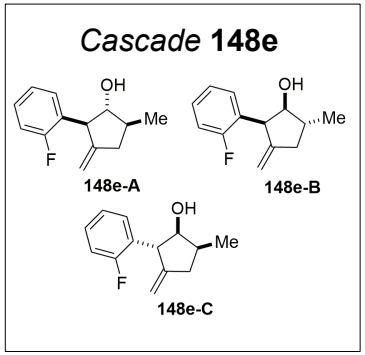


```
Current Data Parameters
NAME      KS-03-106col_500_2
EXPNO                 10
PROCNO                 1

F2 - Acquisition Parameters
Date_           20220822
Time                17.33 h
INSTRUM             spect
PROBHD    Z125869_0055 (
PULPROG             zg30
TD                  65536
SOLVENT             CDCl3
NS                    64
DS                     2
SWH             10000.000 Hz
FIDRES              0.305176 Hz
AQ              3.2767999 sec
RG                   47.3
DW                  50.000 usec
DE                  16.00 usec
TE                  300.0 K
D1             2.00000000 sec
TD0                    1
SFO1          500.2330889 MHz
NUC1                  1H
P0                  4.00 usec
P1                  12.00 usec
PLW1          11.44699955 W

F2 - Processing parameters
SI                  65536
SF            500.2300122 MHz
WDW                   EM
SSB       0
LB                  0.30 Hz
GB        0
PC                  1.00
```

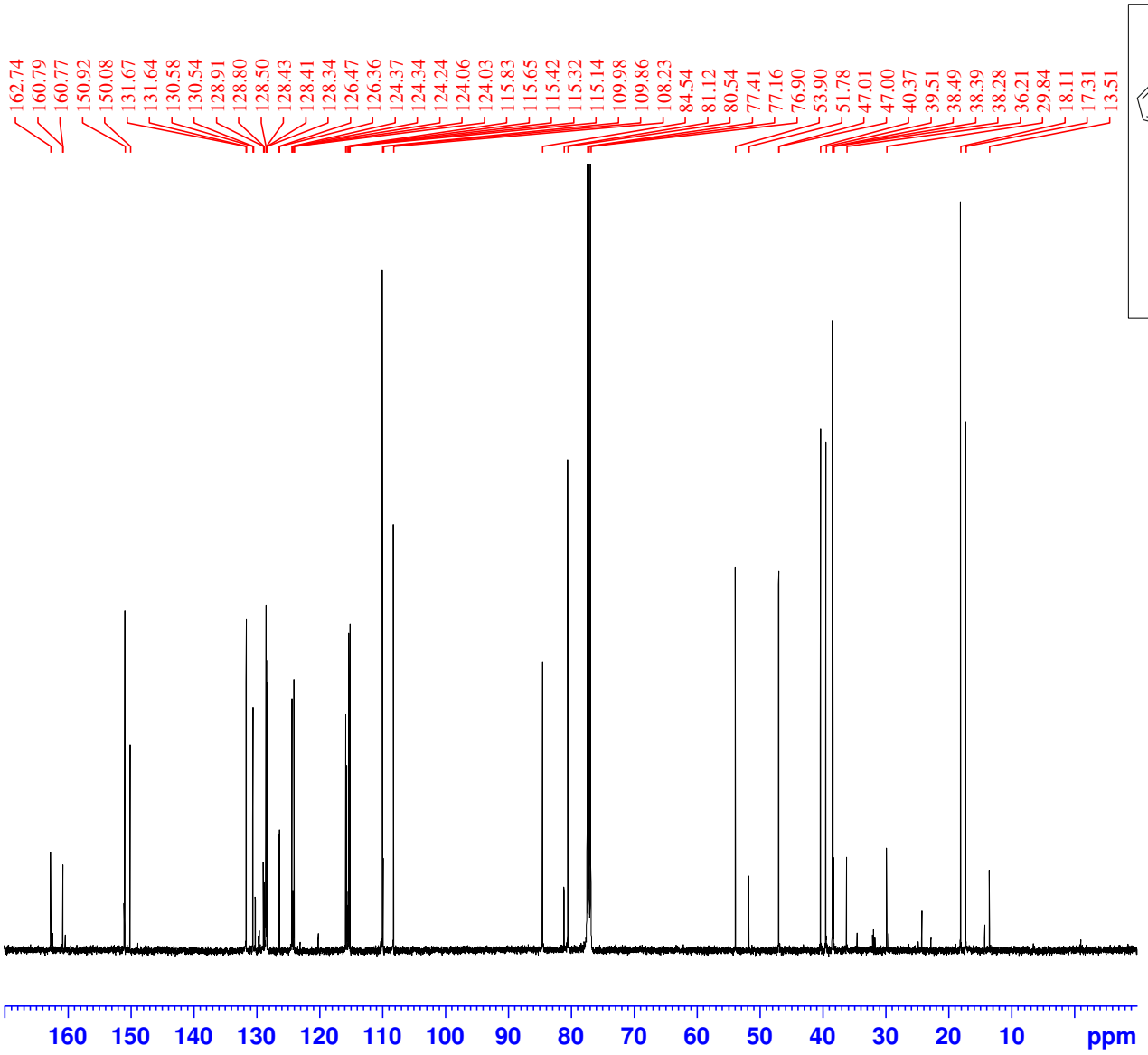

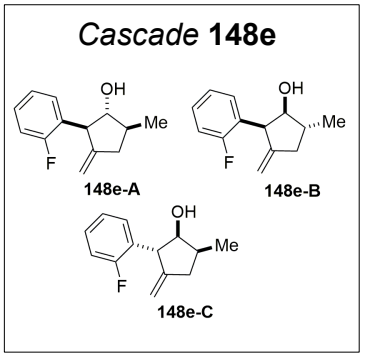


```
Current Data Parameters
NAME      KS-03-106col_500_2FPh
EXPNO                        11
PROCNO                        1

F2 - Acquisition Parameters
Date_              20220822
Time                  18.28 h
INSTRUM                 spect
PROBHD    Z125869_0055 (
PULPROG               zgpg30
TD                     65536
SOLVENT                CDCl3
NS                      1024
DS                         4
SWH               29761.904 Hz
FIDRES             0.908261 Hz
AQ                1.1010048 sec
RG                   190.44
DW                   16.800 usec
DE                   18.00 usec
TE                   300.0 K
D1                2.00000000 sec
D11               0.03000000 sec
TD0                        1
SFO1           125.7955118 MHz
NUC1                     13C
P0                    3.33 usec
P1                   10.00 usec
PLW1           56.90299988 W
SFO2           500.2320009 MHz
NUC2                     1H
CPDPRG[2            waltz16
PCPD2                80.00 usec
PLW2           11.44699955 W
PLW12           0.25756001 W
PLW13           0.12955000 W

F2 - Processing parameters
SI                     32768
SF             125.7829174 MHz
WDW                       EM
SSB          0
LB                    1.00 Hz
GB           0
PC                    1.40
```

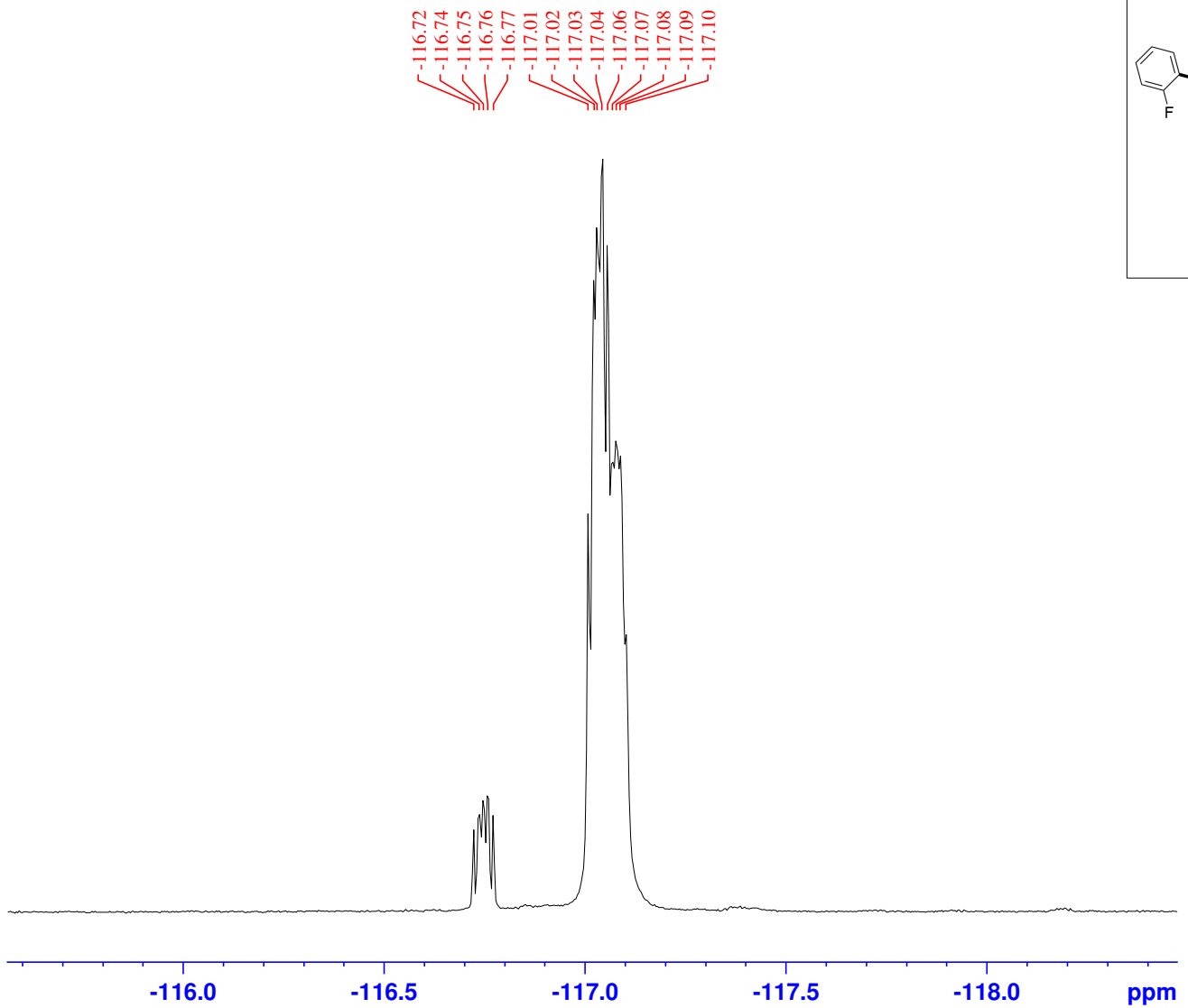

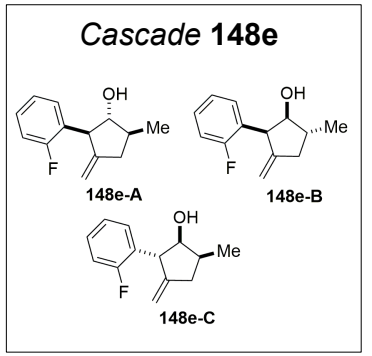


```
Current Data Parameters
NAME      KS-03-106co1_500_2FPh
EXPNO                        12
PROCNO                        1

F2 - Acquisition Parameters
Date_              20220822
Time                 18.30 h
INSTRUM                spect
PROBHD    Z125869_0055 (
PULPROG              zgflqn
TD                   131072
SOLVENT               CDCl3
NS                       16
DS                        4
SWH             113636.367 Hz
FIDRES            1.733953 Hz
AQ                0.5767168 sec
RG                    14.14
DW                 4.400 usec
DE                18.00 usec
TE                 300.0 K
D1              1.00000000 sec
TD0                       1
SFO1           470.6394024 MHz
NUC1                   19F
P1                 15.00 usec
PLW1           11.70800018 W

F2 - Processing parameters
SI                    65536
SF             470.6864710 MHz
WDW                      EM
SSB       0
LB                  0.30 Hz
GB        0
PC                    1.00
```

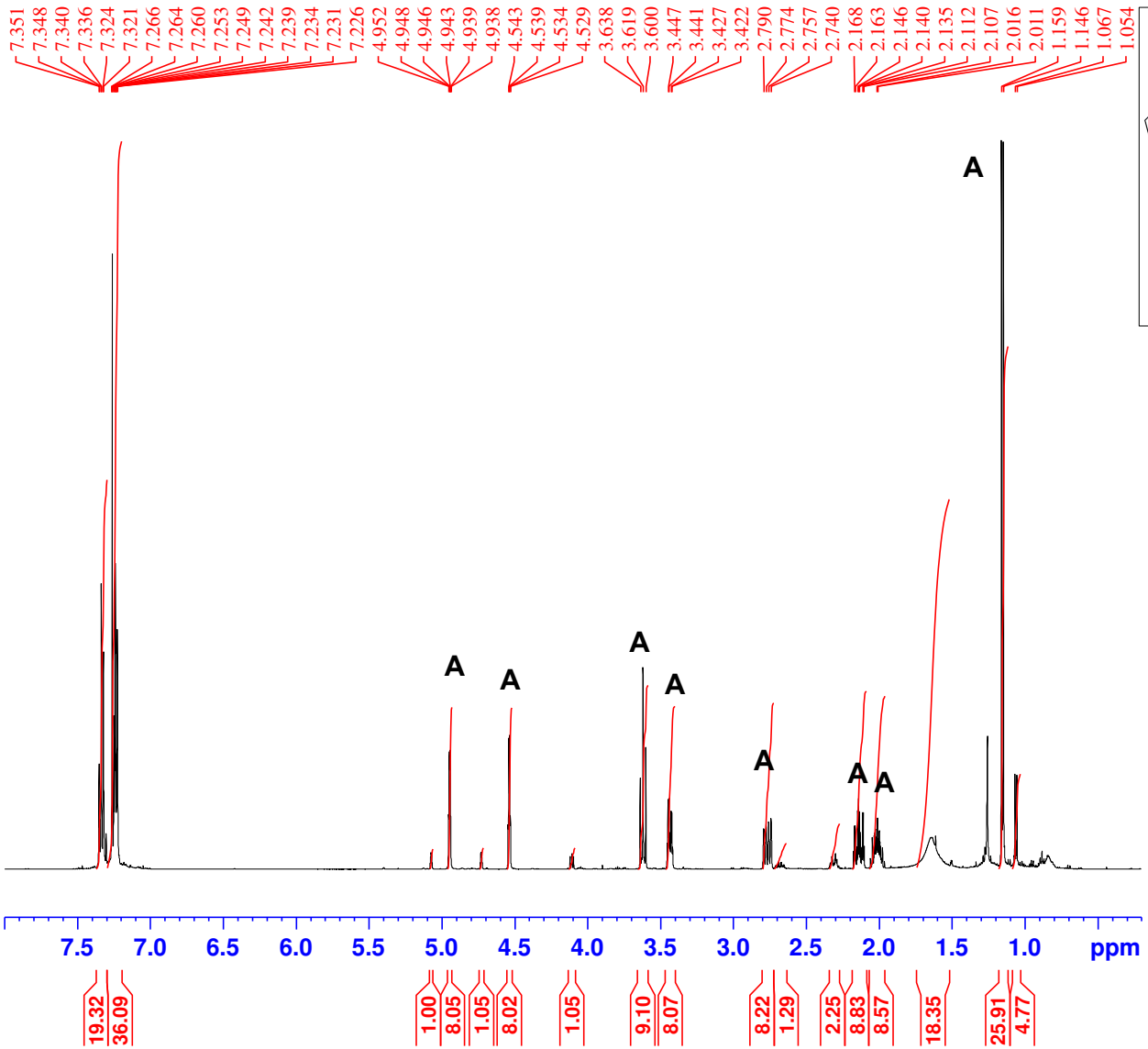

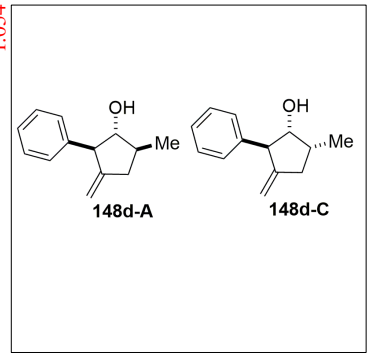


```
Current Data Parameters
NAME            KS-03-P_A
EXPNO                  12
PROCNO                  1

F2 - Acquisition Parameters
Date_            20220706
Time                18.23 h
INSTRUM              spect
PROBHD    Z125869_0055 (
PULPROG              zg30
TD                  65536
SOLVENT             CDCl3
NS                     64
DS                      2
SWH             10000.000 Hz
FIDRES              0.305176 Hz
AQ                3.2767999 sec
RG                   151.18
DW                   50.000 usec
DE                   16.00 usec
TE                   300.0 K
D1              2.00000000 sec
TD0                     1
SFO1          500.2330889 MHz
NUC1                   1H
P0                   4.00 usec
P1                   12.00 usec
PLW1         11.44699955 W

F2 - Processing parameters
SI                  65536
SF            500.2300122 MHz
WDW                    EM
SSB       0
LB                   0.30 Hz
GB        0
PC                   1.00
```

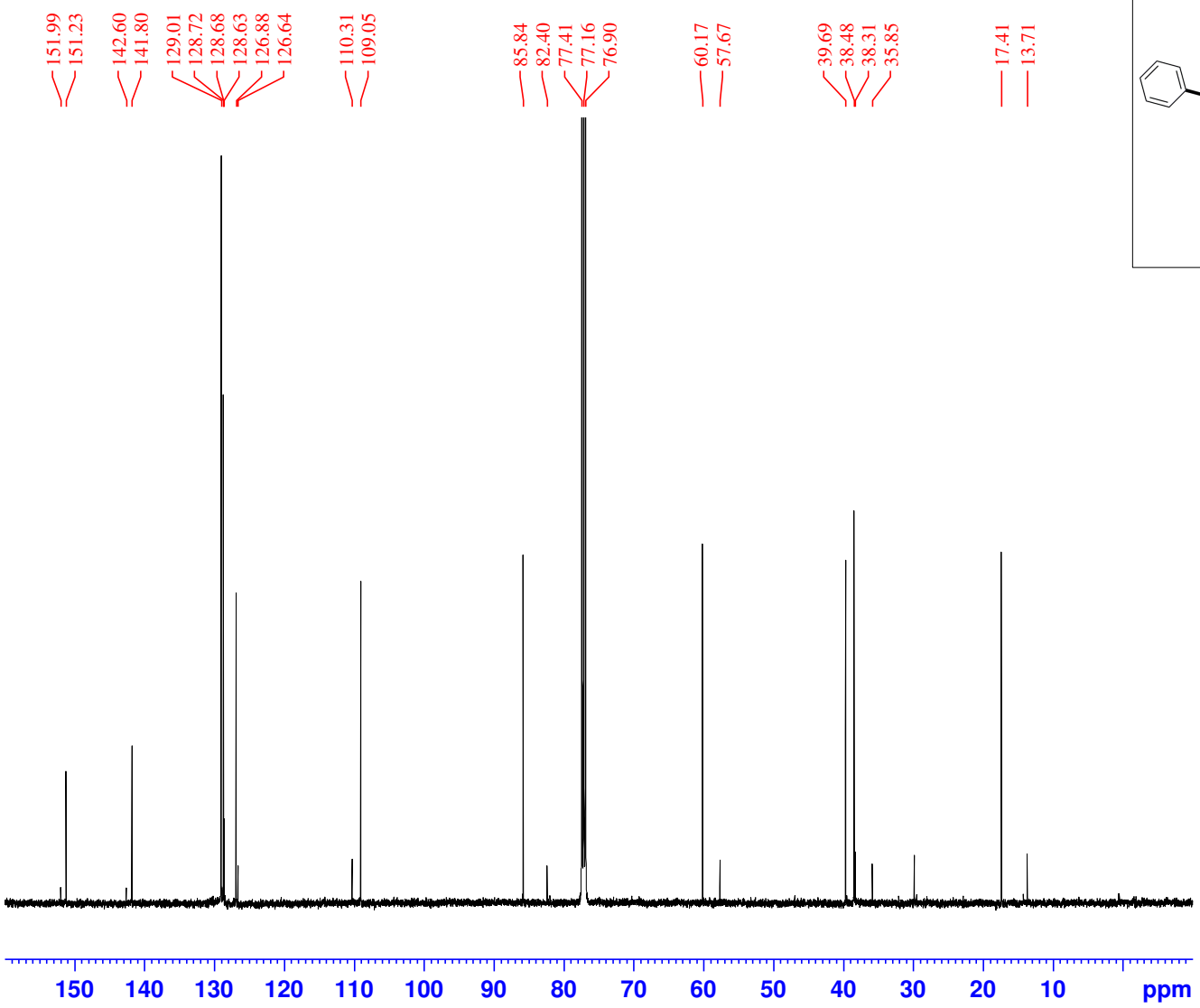

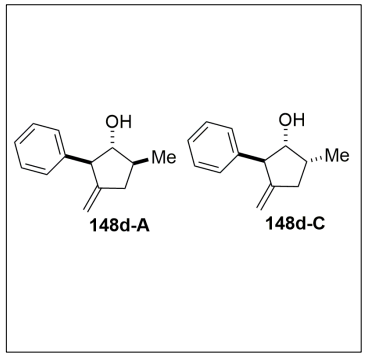


```
Current Data Parameters
NAME          KS-03-P_A
EXPNO                13
PROCNO                1

F2 - Acquisition Parameters
Date_          20220706
Time              19.20 h
INSTRUM           spect
PROBHD   Z125869_0055 (
PULPROG          zgpg30
TD                65536
SOLVENT           CDCl3
NS                 1024
DS                    4
SWH           29761.904 Hz
FIDRES         0.908261 Hz
AQ            1.1010048 sec
RG               190.44
DW               16.800 usec
DE               18.00 usec
TE               300.0 K
D1           2.00000000 sec
D11          0.03000000 sec
TD0                   1
SFO1        125.7955118 MHz
NUC1               13C
P0                3.33 usec
P1               10.00 usec
PLW1        56.90299988 W
SFO2        500.2320009 MHz
NUC2               1H
CPDPRG[2        waltz16
PCPD2            80.00 usec
PLW2        11.44699955 W
PLW12        0.25756001 W
PLW13        0.12955000 W

F2 - Processing parameters
SI                32768
SF          125.7829164 MHz
WDW                  EM
SSB      0
LB                1.00 Hz
GB       0
PC                1.40
```

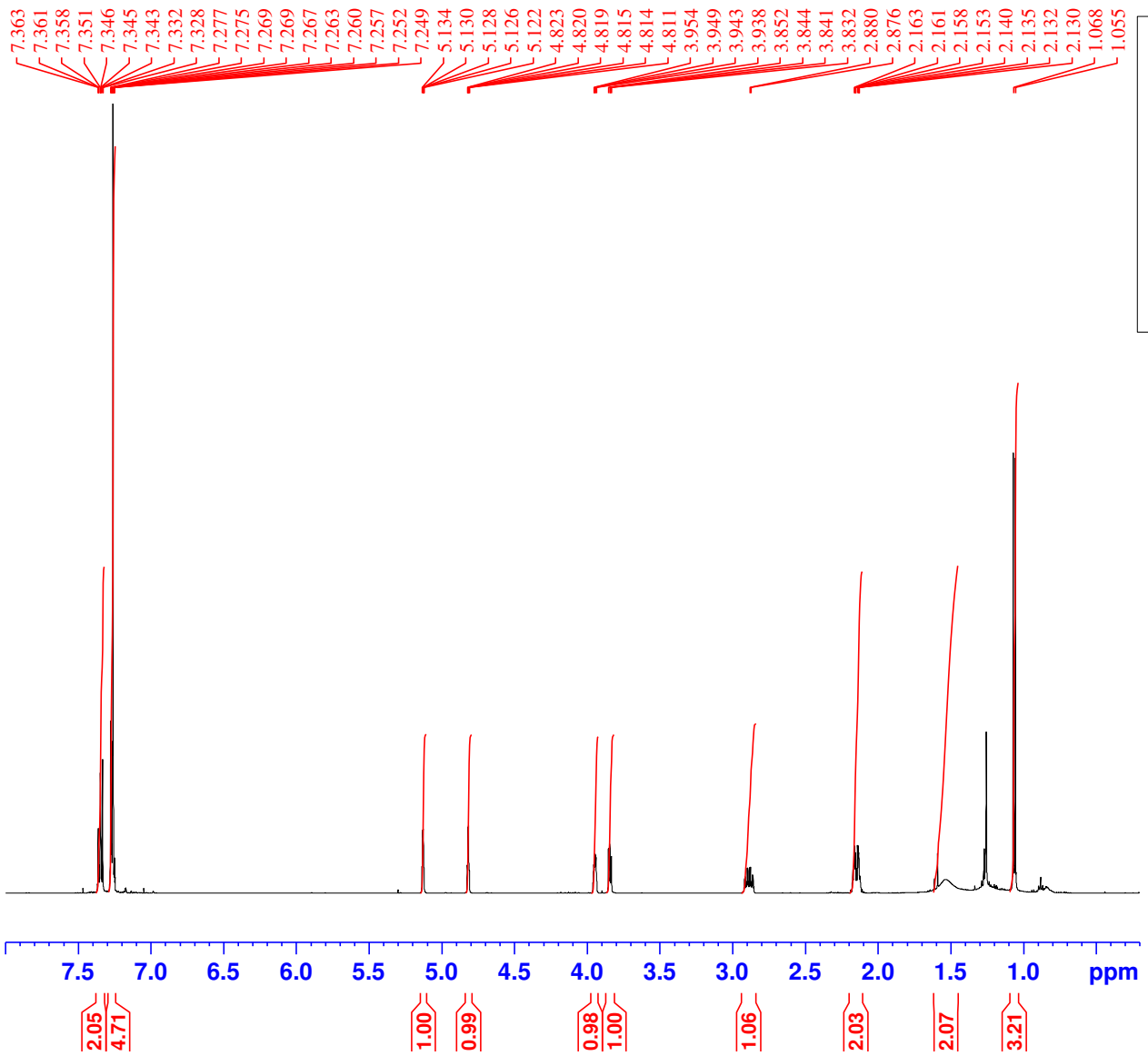

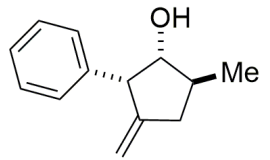

148d-B

```
Current Data Parameters
NAME          KS-03-P_B
EXPNO                10
PROCNO                1

F2 - Acquisition Parameters
Date_          20220706
Time              19.29 h
INSTRUM           spect
PROBHD   Z125869_0055 (
PULPROG           zg30
TD               65536
SOLVENT          CDCl3
NS                  64
DS                   2
SWH           10000.000 Hz
FIDRES        0.305176 Hz
AQ            3.2767999 sec
RG               151.18
DW               50.000 usec
DE               16.00 usec
TE               300.0 K
D1           2.00000000 sec
TD0                  1
SFO1        500.2330889 MHz
NUC1                1H
P0                4.00 usec
P1               12.00 usec
PLW1        11.44699955 W

F2 - Processing parameters
SI               65536
SF          500.2300122 MHz
WDW                 EM
SSB      0
LB                0.30 Hz
GB       0
PC                1.00
```

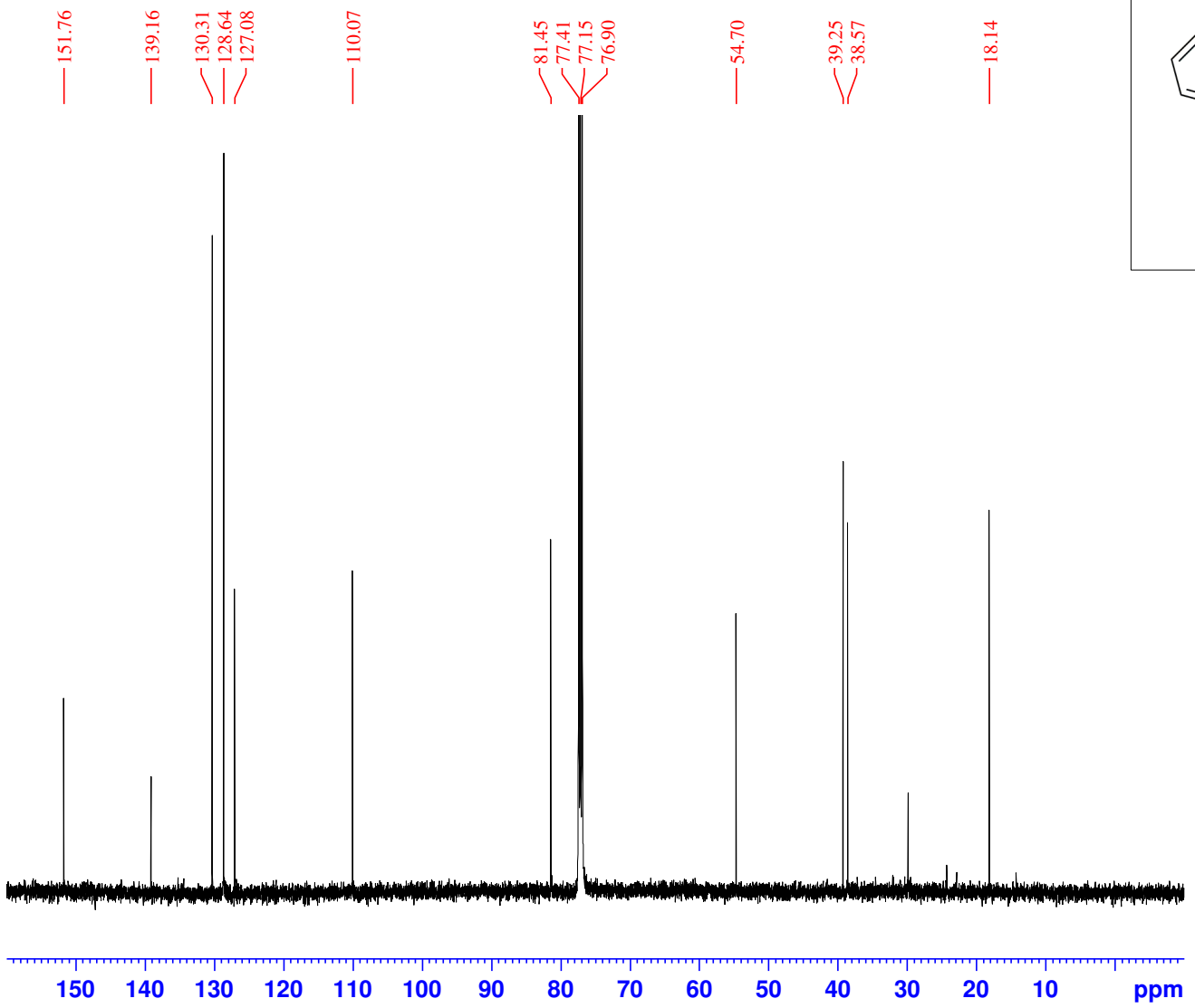

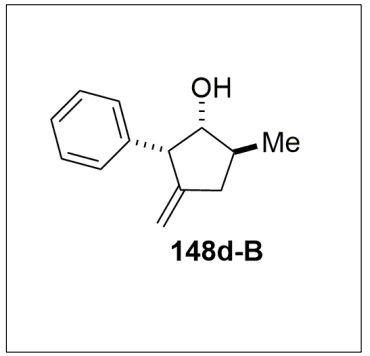


```
Current Data Parameters
NAME          KS-03-P_B
EXPNO                11
PROCNO                1

F2 - Acquisition Parameters
Date_          20220706
Time               20.25 h
INSTRUM           spect
PROBHD   Z125869_0055 (
PULPROG          zgpg30
TD                65536
SOLVENT           CDCl3
NS                 1024
DS                    4
SWH           29761.904 Hz
FIDRES         0.908261 Hz
AQ            1.1010048 sec
RG               190.44
DW               16.800 usec
DE               18.00 usec
TE               300.0 K
D1           2.00000000 sec
D11          0.03000000 sec
TD0                   1
SFO1        125.7955118 MHz
NUC1               13C
P0                3.33 usec
P1               10.00 usec
PLW1        56.90299988 W
SFO2        500.2320009 MHz
NUC2               1H
CPDPRG[2        waltz16
PCPD2            80.00 usec
PLW2        11.44699955 W
PLW12        0.25756001 W
PLW13        0.12955000 W

F2 - Processing parameters
SI                32768
SF          125.7829163 MHz
WDW                EM
SSB       0
LB                1.00 Hz
GB        0
PC                1.40
```